IMPERIAL COLLEGE OF SCIENCE, TECHNOLOGY AND MEDICINE

UNIVERSITY OF LONDON

MODELLING OF ULTRASONIC GUIDED WAVE FIELD GENERATED BY PIEZOELECTRIC TRANSDUCERS

by

Pierre Noël Marty

A thesis submitted to the University of London for the degree of

Doctor of Philosophy

Department of Mechanical Engineering
Imperial College of Science, Technology and Medicine
London SW7 2BX

March 2002

Dedication

To my dad

Steganographia, hoc est ars per occultam scrituram animi sui voluntanen absentibus aperiendi certa

Thritème

Francfort, 1606

Acknowledgements

I wish to sincerely express my thanks to Prof. Peter Cawley, Dr. Mike Lowe, and Denis Hitchings who have provided invaluable guidance, technical knowledge, support and linguistic advice throughout this project. I would also like to thank Prof. Bert Auld for his help during his two visits to Imperial College. He took a large part in the guidance of the project and enlightened it with his invaluable advice.

Welcome advice, discussions and ideas, in various forms, were often provided by other members of the non-destructive testing group at Imperial College. I enjoyed my time amongst you. They are, in approximately the order of appearance, David Alleyne, Andrew Chan, Mark Evans, Richard Monkhouse, Keith Vine, Brent Zeller, Brian Pavlakovic, Paul Wilcox, Michel Castaings, Arnaud Bernard, Rob Long, Roger Dalton, Christophe Aristégui, Stephane Baly, Jon Allen, Malcom Beard, Thomas Vogt, Alexandro Demma, Francesco Simonetti, Grzegorz Grondek and Richard Sepping.

I must thank the EPSRC and the NDT group for their financial support.

My best thanks are due to my family (you Michèle and Dominique) and Nina for their help, support and understanding during all the time I spent far from them. Nina, my warmest thanks for your enthusiasm, your confidence, and your love.

Abstract

The thesis investigates some aspects of the fundamental science necessary for the development of piezoelectric sensors for use in integral structural inspection systems based on ultrasonic Lamb waves. It is particularly concerned with the analysis of the electromechanical interaction, the process of generation of Lamb wave modes and the design of permanently attached transducers such as PVDF-based interdigital transducers (IDT) or ceramic-based piezoelectric strips.

Interdigital transducers developed for use in *smart structures* are now at the stage where practical applications on plate and pipe structures are being considered. For such a transducer to be used, it is necessary to understand exactly the electromechanical interaction and the internal scattering phenomena governing their performance. An analytical investigation into the interactions that occur between mechanical fields and electric quantities is presented. This model is developed for a simple transducer design, a single-strip transducer under plane strain conditions. A computer model for predicting the acoustic field generated by a given voltage applied to the transducer and vice-versa is presented. This model is developed on the basis of normal mode theory and perturbation methods, providing flexibility and physical insight. Intermediate calculations as well as final results are validated using the finite element model developed in parallel with this work. Since the analytical model is based on assumptions mainly related to the perturbation methods, these are discussed and limits of the model as well as its eventual extensions are drawn.

The thesis is also concerned with a numerical analysis based on the finite element method. A finite element formulation that includes the piezoelectric or electroelastic effect alongside the dynamic matrix equation of electroelasticity and its reduction to the well-known equation of structural dynamics, based on a strong analogy between electric and elastic variables, is presented. It is shown how these equations were incorporated in an already existing finite element code. In parallel with validation, results are produced to identify several important features that are not taken into account in the analytic model. Results are presented for IDTs and checked against experimental data when measuring displacement field amplitudes using a laser probe.

Contents

List of Figures

List of Tables

Chapter 1

Introduction

The aim is to model the generation of waves by piezoelectric transducers in order to optimise the design of electromechanical sensors used in what is fashionably called *smart structure* applications. Controversy has arisen over the use of these terms, which have been used to cover a broad range of related work in many disciplines, since the late 1980's. A review of work on *smart structures* can be found for example in Culshaw [1.1], [1.2] and recently my colleague R. Dalton [1.3] studied the possibility of using guided waves to monitor the structural health of an aircraft fuselage. For this thesis, we will consider a *smart structure* as being a structure that has the potential to monitor its condition repetitively. Data transport and computer technology is already sufficiently developed to meet the challenge of developing a *smart structure* for many applications, and they will undergo tremendous progress in the future, especially in the data transfer area with the *bluetooth* new technology. However sensor technology is not yet advanced enough and recent reviews state that fully adaptive systems may not be in service for several years [1.4]. In this thesis we will focus our attention on electromechanical sensors and their interaction with the structure on which they are attached.

Much research has been devoted to problems in electromagnetism and acoustics. Often the investigation runs along parallel lines, the main differences being due to the vector character of the electromagnetic field and to the scalar nature of sound waves. Some times these differences are significant because of boundary conditions but often the analysis is very similar, especially when the electromagnetic field is a simple function of time and space. For this study, we use many electromagnetic-acoustic analogies as defined by Auld [1.5]. Transducers of interest in this thesis are piezoelectric. The piezoelectric effect is basically understood to be a result of linear interaction between the mechanical and electrical systems, and studies on it are closely related to the linear response theory. The piezoelectric direct effect manifests itself

experimentally by the appearance of bound electric charges at the surface of the strained medium. The direct piezoelectric effect is always accompanied by the converse piezoelectric effect, whereby a solid becomes strained when placed in an electric field. Piezoelectricity is a fundamental process of electromechanical interaction and is representative of linear coupling in energy conversion. Obviously piezoelectricity is not the only principle on which electromechanical devices can operate but phenomena such as electrostriction, triboelectricity and Seigneto-electricity [1.6] are not covered in this thesis. Hence this analysis of electronic devices necessitates knowledge in three different fields of physics: mechanics, electromagnetism and piezoelectricity and associated mathematical developments.

1.1 ADVANTAGES OF LAMB WAVES INSPECTION TECHNIQUES

The use of ultrasonic Lamb waves for the testing of plate and pipe structures is attractive since a large area of structure can be interrogated from only a few locations. The main advantage of Lamb waves is that both sides, as well as the interior of the structure, can be sensed from only one location on one side of the structure, which makes in situ monitoring viable. Many techniques such as angle transducers or EMATs are very efficient in order to excite Lamb waves in plate or pipe structures. However, for cost and dimension reasons none of these types of transducers are suited to being permanently attached to a structure, which is a necessary requirement in a smart structure application. From a design point of view, permanently attached transducers are, by nature not reusable and thus their cost must be added to that of the structure which they are monitoring. The transducer and the structure are bonded together with an adhesive which makes consistency of the measurements easier to achieve. This means that such transducers are much more suitable for accurate condition monitoring than removable transducers for which the coupling conditions may not be consistent from one test to another. Since the thickness and the properties of each of the component of such bonded transducers is measurable, it allows us to develop a model that might be usable for any permanently attached transducer.

1.2 PERMANENTLY ATTACHED TRANSDUCER TECHNOLOGY FOR SMART STRUCTURES

Current sensor technology is well advanced in the acoustic field, but the specific application to the generation and reception of Lamb waves in non-piezoelectric structures by means of piezoelectric transducers needs some further theoretical development in order to predict accurately field parameters such as amplitude and attenuation. The generation and reception of Surface Acoustic Waves (SAW) by means of interdigital electrodes plated on piezoelectric substrates has been widely used in the electronics industry, [1.5], [1.7], [1.8], [1.9], [1.10]. This technology has made the concept of using permanently attached transducers for the generation and reception of Lamb waves in a structure for NDT purposes viable. There is a special emphasis on surface acoustic wave applications. Those waves are confined in close proximity to one surface of the substrate and are therefore efficiently excited by acoustic and electric sources on the surface. Surface acoustic wave transducer technology is not directly

applicable to smart structures because of the frequency at which these devices operate, normally in the GHz range, whereas NDT applications typically work below a frequency thickness product of 1 MHz-mm. Hence in order to inspect large structures, flexible cheap PVDF transducers have been developed for the generation and the detection of Lamb waves, [1.11], [1.12]. The geometry of these devices is similar to that of the transducers used to generate surface acoustic waves in non-piezoelectric substrates, see [1.13] and [1.14]. The plate under interrogation is overlaid by a thin piezoelectric film, itself overlaid by the interdigital electrodes. The transducer comprises the piezoelectric film and the electrodes, where the piezoelectric film is very thin and is limited in the two other dimensions to the size of the electrodes. Figure 1.1 shows this configuration for Lamb modes.

1.3 MODELLING OF FIELD GENERATED BY PIEZOELECTRIC TRANSDUCERS

From the above discussion, the main goal of this thesis appears as being to investigate the process by which permanently attached transducers can generate guided waves in structures. Our interest in this particular subject, and the particular direction we took to study it, follow from the chief objective and the main conclusions we drew from a project [1.23] founded on an EPSRC/DIG Grant which was entitled "Efficient Ultrasonic Inspection and Monitoring of Large Structures". This project linked together the combined efforts of several researchers from Strathclyde University [1.15] and Imperial College, efforts that were orientated toward a common goal: producing permanently attached sensors to monitor large structures which involved optimisation of the form of the sensors, the determination of the best mode(s) to use and the development of test strategies (e.g. pulse-echo).

The work at Imperial College concentrated on the modelling of the behaviour of the transducers, the development of inspection strategies and the refinement of PVDF based permanently attached sensors. Figure 1.2 shows a schematic diagram of such transducers, with interdigital electrodes, on a metallic plate. The aim was to produce permanently attached sensors, which could generate modes whose motion is predominantly in-plane. However it was found that this was considerably more difficult than had been anticipated. Facing these difficulties led during the growth of the project to re-direction of the work away from developing interdigital PVDF based sensors. The operation of these devices is based on the launching and the reception of wave guide modes by distributed electrodes. One of the reasons why such transducers are difficult to model is that the function that describe the charge distribution is extremely cumbersome [1.19], [1.20], [1.21], [1.22] and the number of parameters that affect the response of such a transducer is large. Solutions exist, such as those provided by Engan [1.21] and Coquin [1.22] for example, but they are valid only for SAW and not for Lamb waves and these solution still needed to be developed. Therefore we believed that we could gain in understanding and time by starting the study to a less cumbersome problem. Indeed, at first approximation each of the distributed sources (i.e. each electrode) of the IDT transducer is acting as a single transducer. Such an elementary transducer, referenced as a strip transducer by analogy with transmission line strips, is

easier to study, at least from the mathematical point of view. Figure 1.3 shows the configuration for a single element. Nonetheless if the electrostatic problem is greatly simplified for such a transducer, the mechanical problem is the same as for an IDT. The system is multilayered, limited in extend, and the guided waves generated in the structure are dependent on the mechanical and electrical waves generated inside and underneath the transducer. However we are not so much interested in what happens exactly in the transducer itself. Thus is possible to use some simplifying approximations in order to obtain information only about the fields that we are primarily interested in. This, in theory, should allow us to get the physical understanding of what is happening in the overall system.

It has also been shown during the EPSRC founded project [1.23] that satisfactory field predictions could be obtained by assuming that the analysis of the PVDF based interdigital transducer can be decoupled from that of the structure and that the action of the IDTs is essentially to apply out-of-plane forces at the locations of the fingers. Accordingly non-piezoelectric finite element or Huygens' principle based calculations [1.16] enable us to predict efficiently the field generated in the structure and a 1-D piezoelectric transmission line technique enable to analyse the electric behaviour of piezoelectric sensors [1.17]. Although these assumptions are valid in large number of circumstances, the amplitude of the acoustic wave generated by a given voltage applied to the transducer and vice-versa cannot be predicted using the models aforementioned. Moreover these approximation are fair for low acoustic impedance and weak electromechanical coupling transducer materials such as PVDF [1.11], [1.12], but it is very unlikely to remain accurate for ceramic-based transducers. It was therefore decided to develop more accurate models and this is achieved by two different means. The first one is to develop a finite element program allowing to model the full piezoelectric behaviour. The second one is to develop an analytical model that will enlighten the key factors governing the performance of the transducers.

1.3.1 FINITE ELEMENT ANALYSIS

The Strathclyde group uses a commercially available FE code, PZFlex which can perform dynamic piezoelectric analysis in the time domain, as required in this study, but, although very efficient, PZFlex is not optimized for Lamb wave work. This is a problem common to most commercially available codes and it is usually impossible to modify the source of such codes. Hence it was decided to incorporate piezoelectricity in an already existing general purpose finite element package, FE77 [1.25] developed at Imperial College by Mr. D. Hitchings for thermal and structural analysis. On previous projects [1.26], [1.27], this code has been optimized at the NDT Lab for the solution of Lamb wave propagation problems in the time domain. Unfortunately it did not allow piezoelectric equations to be solved so this feature was added. From the general formulation of finite element piezoelectric equations found in the literature, we derived a direct integration formulation based on the central difference explicit methods of integration. Although simple in its principle, implementation of a new set of equations in an already existing finite element code required lots of attention. FE77 is a research tool, constantly under development for more than 20 years, and despite the constant

help of Mr. D. Hitchings a considerable amount of time was spent on understanding the original code and tracking coding errors. Nevertheless the code is now producing piezoelectric calculations and results are systematically being validated against simple examples. Although the introduction of the piezoelectric equations in FE77 will mainly serve the purpose of validating the analytic model it is to be mentioned that it has been developed in the form of a permanent module of FE77 in order to be used by other researchers in the future.

A major drawback of the finite element technique is that this does not run quickly enough to be used as an interactive design tool. Moreover the solution provided is purely numerical, hiding most of the physical significance of the electromechanical coupling process. Hence an analytic approach of the problem was undertaken.

1.3.2 ANALYTICAL MODEL

This model was initially only concerned with PVDF based interdigital transducers (IDTs). However it is believed that the analytic work carried out for IDTs can be diverted from its initial aim to enlighten our comprehension of the physics involved in electromechanical coupling within ceramic based piezoelectric transducers. The reason for that is that basically a piezoelectric transducer always comprises a piezoelectric layer, adhesive layers and electrodes. The mathematical difficulty with the study of IDT resides entirely in the formulation of the electric charge distribution. If one compare the strip transducer geometry shown in Figure 1.3 and the geometry of the IDT transducer shown in Figure 1.2, it appears that the difference lies only in the electrode pattern. By comparison with an IDT, the electrical boundary problem is simplified for the single strip transducer but the rest of the study is identical. Therefore we decided to develop an analysis for the strip transducer bearing in mind that this study can be extended to many other transducers as long as their geometries are similar to that of the single strip transducer, that is basically a stack of layers of finite thickness and lateral dimensions. Due to the voltage applied across the electrodes, acoustic waves as well as electromagnetic waves are generated in the piezoelectric layer. However, we are not primarily interested in the exact behavior of the film so it is appropriate to make some simplifying assumptions about the piezoelectric layer/electrode structure in order to obtain a physical understanding of what is happening in the overall system. These assumptions are related to the perturbation theory and they allow keeping the model analytical. Keeping the problem analytical enable to determine appropriate transducer properties in order to generate a given mode with a given amplitude in a given structure.

1.4 THESIS OUTLINE

The thesis will investigate some aspects of the fundamental science necessary for the development of piezoelectric sensors for use in integral structural inspection systems based on the use of ultrasonic Lamb waves. It will be particularly concerned with the analysis of the electromechanical interaction and the process of generation of Lamb waves and the design of permanently attached transducers such as ceramic-based piezoelectric discs or IDT's. This work naturally fell into phases defined by the

development of the tools and theories needed to investigate the behaviour of piezoelectric transducers. These phases of work therefore form the subsequent chapters of this thesis. There are six chapters, the first being this introduction chapter.

Lamb waves, which are the guided waves of a free plate, are considered in Chapter 2, where attention focuses on their modal properties. Structures of interest in *smart structure* technologies are closely related to free plate structures and the presence of the transducers only affect the guided wave locally. As shown by Auld [1.5] modal analysis is a powerful tool for treating waveguide excitation and scattering problems. As stated by Auld, in order to apply this technique in electrodynamics, one must develop a procedure based on the reciprocity relationship and mode orthogonality, for expanding arbitrary acoustic waveguide field distributions as superposition of waveguide modes. These techniques are also presented in Chapter 2. The well-known perturbation theory is also presented since this is the approximate method used to develop the analytic model for waveguide excitation by means of piezoelectric transducer. Lastly, piezoelectric materials used in this study are presented and a short review of the piezoelectric equations is given.

A finite element formulation that includes the piezoelectric or electroelastic effect along side with the dynamical matrix equation of electroelasticity and its reduction to the well-known equation of structural dynamics, based on a strong analogy between electric and elastic variables, is developed in Chapter 3. It is shown how these equations were incorporated in an already existing finite element code [1.25]. This program has been checked against PZFlex [1.28] and the validation results are presented.

In Chapter 4, the analytical model, developed on the basis of normal mode theory and perturbation methods for predicting the acoustic field generated by a given voltage applied to a transducer and vice-versa, is presented. The sections follow naturally the three perturbation steps of the model, and insight is given on how each perturbation step can be used for various independent problems. Since the overall model is based on assumptions mainly related to the perturbation methods, these are discussed and limits of the model as well as its eventual extensions will be drawn. Throughout the development of the model, validation against the finite element program will be presented.

In Chapter 5, a full example of the structure of interest in this study is presented. Comparison between the results obtained from the analytical model and the finite element program is presented. This example serves the purpose of fully validating the analytical model presented in Chapter 4. Preliminary Results on the analysis and the experimental study of IDTs are also presented.

Lastly, Chapter 6 presents the conclusions of this thesis regarding the modelling of the generation of guided waves by piezoelectric transducers. The approach and the methods used throughout this work are also critically reviewed and a number of avenues for further work are suggested, in particular concerning the modelling of guided waves scattering at surface defects such as notches, grooves or cracks.

REFERENCES

[1.1] **Culshaw**, B., *Smart Structures Activities Worldwide*, SPIE, Vol. 2717, pp. 3-17, 1996.

[1.2] **Culshaw**, B., *Smart Structures and Materials*, Artech House, Boston and London, 1996.

[1.3] **Dalton**, R., *The Propagation of Lamb Waves Through Metallic Aircraft Fuselage Structure*, Ph.D. Thesis, University of London, (Imperial College, Mechanical engineering Department), 2000.

[1.4] **Chopra**, I., "Review of Current Status of Smart Strucutres and Integrated Systems", SPIE, Vol. 2717, pp. 20-62, 1996.

[1.5] **Auld**, B. A., *Acoustic Fields and Waves In Solids*, Vol. II, 2nd ed., Robert E. Krieger Publishing Compagny, Malabar, Florida, 1990.

[1.6] **Durand**, E., *Electrostatique III: Méthode de Calcul, Diélectriques*, Masson & C^{ie}, Paris, 1966.

[1.7] **Kino**, G. S., *Acoustic Waves: Devices, Imaging and Analog Signal Processing*, Prentice-Hall Inc., Englewood Cliffs, New Jersey, 1987.

[1.8] **Dieulesaint**, E. and Royer, D., *Elastic Waves in Solids, Application to Signal Processing*; John Wiley & Son Inc., 1980.

[1.9] **Morgan**, D. P., *Surface-Wave Devices for Signal Processing*, Elsevier, Amsterdam, Oxford, New York, Tokyo, 1991.

[1.10] **Matthews**, H., (ed.), *Surface Wave Filters*, John Wiley & Sons, New York, London, Sydney, Toronto, 1977.

[1.11] **Wilcox**, P. D., *Lamb Wave Inspection of Large Structures using Permanently Attached Transducers*, Ph.D. Thesis, University of London, (Imperial College, Mechanical engineering Department), 1998.

[1.12] **Monkhouse**, R. S. C., Wilcox, P. D., and Cawley, P., "Flexible Interdigital PVDF Transducers for the Generation of Lamb Waves in Structures', Ultrasonics, 1997.

[1.13] **Kino**, G. S. and Wagers, R. S., "Theory of Interdigital Couplers on Non-Piezoelectric Substrates", J. Appl. Phys., Vol. 44, pp. 1480-1488, 1973.

[1.14] **Dieulesaint**, E., Mattioco, F. and Royer, D., "Excitation et Détection d'Ondes de Rayleigh á l'aide d'une Feuille de Polymère Piézoéléctrique", C. R. Acad. Sc. Paris, Tome 287, Série B171, 1978.

[1.15] **Ultrasonic Research group**, Department of Electronic and Electrical Engineering, University of Strathclyde, Glasgow, U.K., G1 1XW.

[1.16] **Wilcox**, P. D., Monkhouse, R. S. C., Lowe, M. J. S. and Cawley, P., "The Use of Huygens' Principle to Model the Acoustic Field from Interdigital Transducers", Review of Progress in Quantitative NDE, eds. D.O. Thompson and D.E. Chimenti, Plenum Press, N. Y., Vol. 17, 1998.

[1.17] **Wilcox**, P. D., Monkhouse, R. S. C., Cawley, P., Lowe, M. J. S. and Auld, B. A., "Development of a Computer Model for an Ultrasonic Polymer Film Transducer System", NDT & E International, Vol. 31(1), pp. 51-64, 1998.

[1.18] **Gachagan**, A., Reynolds, P., Hayward, G. and McNab, A., "Construction and Evaluation of a New Generation of Flexible Ultrasonic Transducers", IEEE Ultrasonics Symposium, pp. 1-4, 1996.

[1.19] **Tiersten**, H. F., *Linear Piezoelectric Plate Vibrations*, Plenum Press, New York, 1969.

[1.20] **Joshi**, S. G. and Jin, Y., "Excitation of Ultrasonic Lamb Waves in Piezoelectric Plates", J. Appl. Phys., Vol. 69, pp. 8018-8024, 1991.

[1.21] **Engan**, H., "Excitation of Elastic Surface Waves by Spatial Harmonics of Interdigital Transducers", IEEE Transaction on Electron Devices, Vol. ED16, pp. 1014-1017, 1969.

[1.22] **Coquin**, G. A. and Tiersten, H. F., "Analysis of the Excitation and Detection of Piezoelectric Surface Waves in Quartz By Means of Surface Electrodes", J. Acoustic. Soc. Am., Vol. 41, pp 921-939, 1966.

[1.23] **Marty**, P. N., "Analytical Analysis of Plate Modes Generated by Interdigital Couplers on non Piezoelectric Substrates" in Efficient Ultrasonic Inspection and Monitoring of Large Structures - Progress Report on EPSRC/DIPG Grant, Appendix A, June 1997.

[1.24] **Laboratoire de Mécanique Physique**, Universté Bordeaux 1, 33405 Talence Cedex, FRANCE.

[1.25] **Hitchings**, D., "FE77 User Manual", Internal Report, Imperial College, Department of Aeronautics, 1997.

[1.26] **Alleyne**, D. and Cawley, P., "The Interaction of Lamb Waves with Defects", IEEE Transactions on Ultrasonics, Ferroelectrics, and Frequency Control, Vol. 39(3), pp 491-494, 1992.

[1.27] **Pavlakovic**, B., Alleyne, D. N., Lowe, M. J. S., and Cawley, P., "Simulation of Lamb Waves Propagation Using Pure Mode Excitation", Review of Progress in Quantitative NDE, eds. D.O. Thompson and D.E. Chimenti, American Institute of Physics, New York, Vol. 17, 1997.

[1.28] **Wojcik**, G. L., Vaughan, D. K., Abboud, N. and Mould, J. Jr., "Electromechanical Modelling using Explicit Time-Domain Finite Elements", IEEE Ultrasonic Symposium Proceedings, 1993.

FIGURES

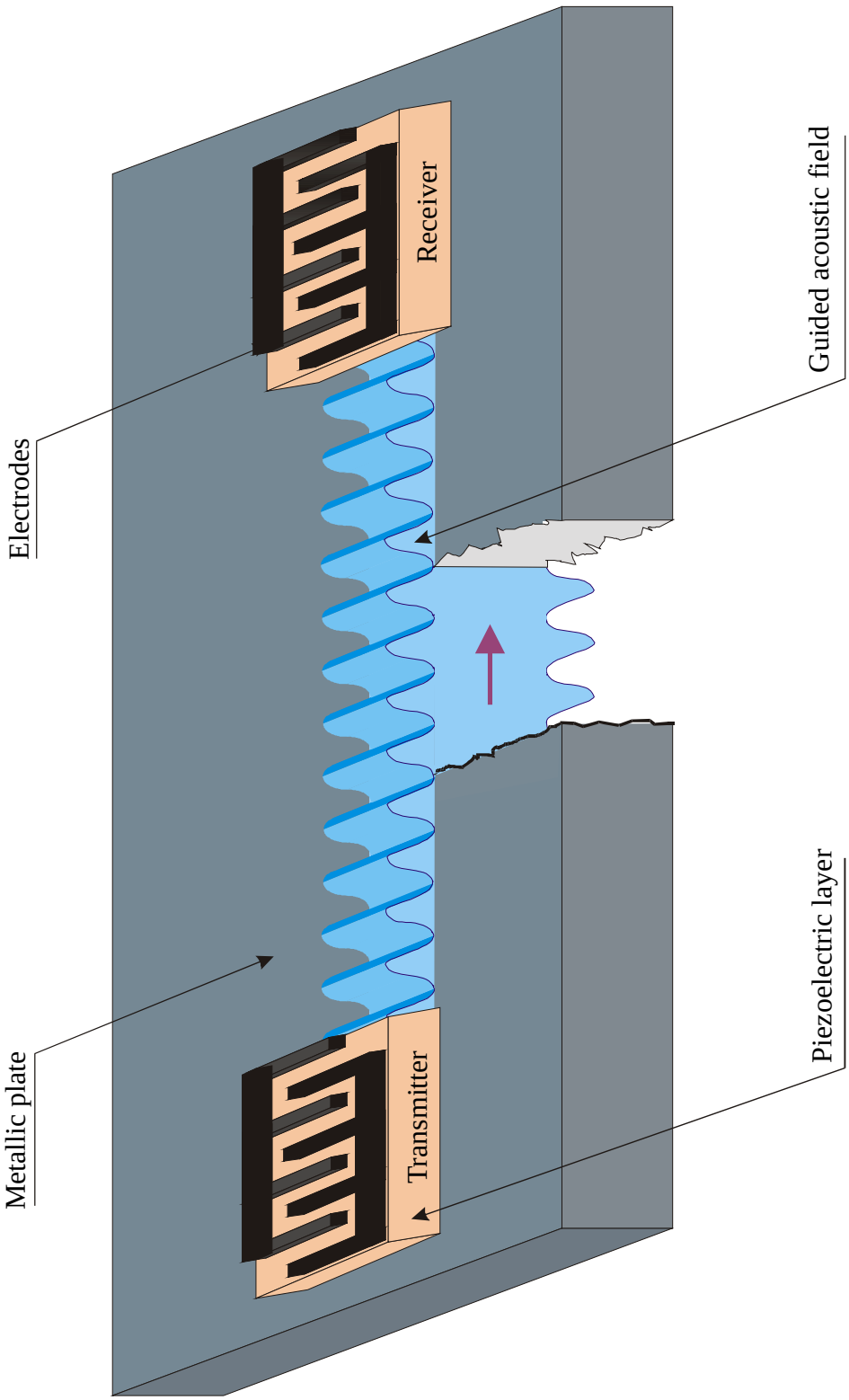

Figure 1.1 : Interdigital transmitter and receiver on a metallic plate.

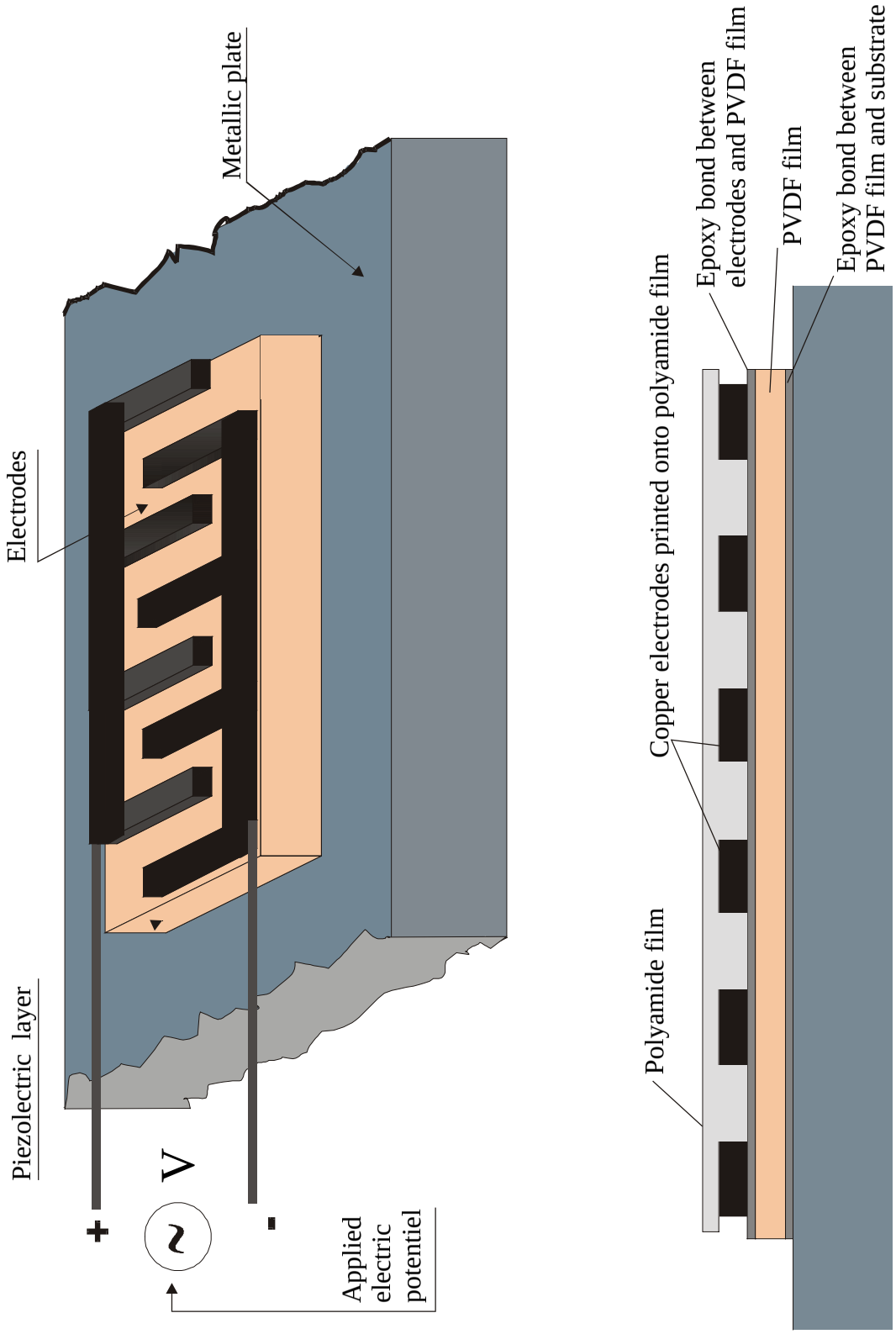

Figure 1.2 : Schematic diagram of an interdigital electrode transducer on a metallic plate.

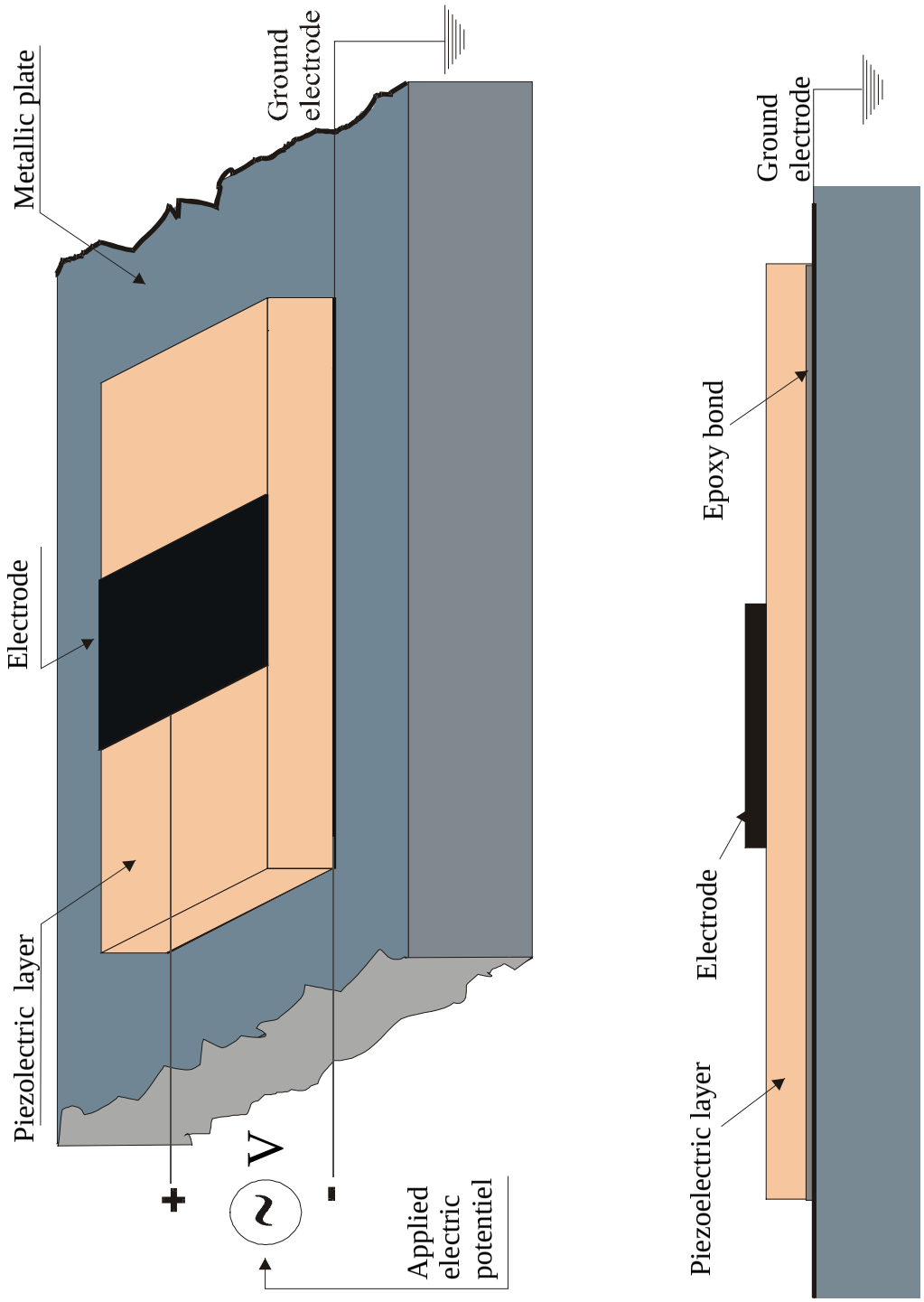

Figure 1.3 : Schematic diagram of a single strip transducer on a metallic plate.

Chapter 2

Background

The focal point of this thesis is the analysis of the generation of Lamb waves [2.1] in plate-like structures by piezoelectric transducers, with special attention given to interdigital transducers. We will concentrate our study on the interaction between thin transducers and the structure in which the Lamb waves propagate. In order to have a correct idea of the fields applied by the transducer onto the structure, any interactions between any mechanical and electrical fields in the transducer have to be quantified.

This chapter introduces the basic concepts and equations that, although well-known, are necessary for the understanding of the analysis developed in Chapters 3 to 5. The first section is concerned with a general description of the acoustic field in plate-like structures. The second section shows how the normal mode technique can be used to treat waveguide excitation problems, in conjunction with the reciprocity relationship. The third section presents the perturbation techniques which are used to quantify how the presence of a transducer influences the behaviour of the modes that propagate in that waveguide. The fourth and last section is concerned with transducers, the piezoelectric materials that constitute them and the equations of piezoelectricity.

2.1 PLATE WAVES

In this section the emphasis is on the theoretical analysis of guided waves propagating in solids. All equations and reasoning presented here can be found in more details in the selection of books [2.1] to [2.15] proposed in the reference section.

In this section, and in the rest of this thesis, it is assumed that mechanical waves suffer no attenuation due to "internal friction", i.e. material attenuation is assumed to be negligible. This condition is not too restrictive since low-loss materials are usually chosen for practical waveguides and internal friction has a negligible effect on the

velocity of propagation and other characteristics of the guided waves except for an overall reduction in amplitude.

2.1.1 PROPAGATION IN UNBOUNDED NEDIA

The general description of guided waves starts with the definition of strain and stress, and with Hooke's law, which describes the relation between stress and strain, and goes on to derive the wave equation of motion. The mathematical forms of the waves that can propagate in a solid medium (bounded or infinite), are the solution of the wave equation. If boundaries exist, these solutions must also satisfy certain conditions at the boundaries. First we shall be concerned with unbounded media of propagation, the material being homogeneous, linear elastic, non-absorbing and non-piezoelectric. Contrary to rigid body dynamics that assumes that the material of the body has infinite Young's modulus, i.e. that a resultant force sets every point in a body in motion instantaneously, we shall consider the case where a body is a sum of infinitesimally small mass elements. These masses will vibrate in the material according to Newton's law applied to each of these small masses. The motion of each particle produces changes in the equilibrium of the neighbouring particles and this cause stress, which will be transmitted through the medium [2.2].

2.1.1.1 Strain

Consider a point P(x_1, x_2, x_3) in a solid body in which a wave propagates without any loss of amplitude. This point is displaced, the components of the displacement being (u_1, u_2, u_3). Direct strains in the medium in the vicinity of P are represented by S_{11}, S_{22} and S_{33} and the shear components of strain S_{12}, S_{23} and S_{13} correspond to the rotation of the element as a rigid body. ,

The strain tensor S can be expressed in the following form, see [2.3]:

$$S_{ij} = \frac{1}{2}\left(\frac{\partial u_i}{\partial x_j} + \frac{\partial u_j}{\partial x_i} \right) \qquad i, j = 1, 2, 3 \tag{2.1}$$

The strain tensor S is symmetric and the above equation is only valid in case of small deformations, a condition that will be kept valid throughout this thesis. The velocity at which particle P is displaced is denoted as v, and in the three directions it is found from the particle displacement using formula:

$$v_i = \frac{du_i}{dt}, \qquad i = 1, 2, 3 \tag{2.2}$$

2.1.1.2 Stress

The stress is a force over a unit area, thus the net force F_i, in the direction x_i, is:

$$F_i = \frac{\partial T_{ij}}{\partial x_j} \qquad i, j = 1,2,3 \tag{2.3}$$

where T is the stress tensor. To describe the force acting on an elemental area of a body, nine stress component are required, just as for the strain. The stress tensor, alike the strain tensor is symmetric, i.e. $T_{ij} = T_{ji}$. The symmetry condition on both tensors implies that only six of the nine components are needed to fully describe the stress and strain states of the body. Therefore instead of representing the stress and strains as a tensor of rank 2, we use a 6 component vector. For example, the stress tensor T

$$\begin{pmatrix} T_{xx} & T_{xy} & T_{xz} \\ T_{yx} & T_{xx} & T_{yz} \\ T_{zx} & T_{zy} & T_{xx} \end{pmatrix} \tag{2.4}$$

is also represented by the vector

$$(T_1, T_2, T_3, T_4, T_5, T_6) \text{ with } \begin{matrix} T_1 = T_{xx}, T_2 = T_{yy}, T_3 = T_{zz} \\ T_4 = T_{yz}, T_5 = T_{xz}, T_6 = T_{xy} \end{matrix} \tag{2.5}$$

2.1.1.3 Stress-Strain Relations, Elastic Constants

The general form of Hooke's law assumes that each of the six components of the stress is a linear function of six components of the strain. Therefore 36 elastic constants, c_{ij} with i,j = 1,..,6 are needed. Love [2.3] showed that the elastic tensor must be symmetric. This property reduces the number of independent elastic constants to 21. In tensor notation, Hooke's law is given by

$$T_{ij} = c_{ijkl} S_{kl} = c_{ijkl} \frac{\partial u_l}{\partial x_k} \qquad i, j, k, l = 1,2,3 \tag{2.6}$$

and in vector notation,

$$T_I = c_{IJ} S_J \qquad I, J = 1...6 \tag{2.7}$$

The most complex crystals, of the triclinic class, require these 21 elastic constants to define the stress-strain relations, but in crystals with planes and axes of symmetry the number is reduced, as we will see it when discussing piezoelectric crystals. It is indeed very fortunate that most piezoelectric materials are either cubic, hexagonal or orthorhombic, reducing the number of independent constants to 3, 6 or 9 respectively. Metallic plate-like structures are often isotropic, for which the number of independent elastic constant is reduced to 2 Lamé's coefficients. In an isotropic solid

$$\begin{aligned} \lambda &= c_{12} = c_{13} = c_{21} = c_{23} = c_{31} = c_{32} \\ \mu &= c_{44} = c_{55} = c_{66} = , \frac{1}{2}(c_{11} - c_{12}) \\ \lambda + 2\mu &= c_{11} = c_{22} = c_{33} \end{aligned} \tag{2.8}$$

and all the other coefficients are zero. Therefore, from Eq.(2.6) Hooke's law for isotropic solids is

$$T_{ij} = \lambda \Delta \delta_{ij} + 2\mu S_{ij} \tag{2.9}$$

Lamé's constants λ and μ completely define the elastic stress-strain behaviour of the material. In engineering applications Lamé's constants are usually replaced for convenience by four related elastic constants, [2.4] and [2.5]:

$$E = \frac{\mu(3\lambda + 2\mu)}{\lambda + \mu}, \qquad \sigma = \frac{\lambda}{2(\lambda + \mu)}, \qquad B = \lambda + \frac{2\mu}{3}, \qquad G = \mu; \tag{2.10}$$

$$\lambda = \frac{\sigma E}{(1+\sigma)(1-2\sigma)}, \qquad \mu = \frac{E}{2(1+\sigma)}, \tag{2.11}$$

where E is the modulus of elasticity, ν is Poisson's ratio, B is the bulk modulus and G is the shear modulus. Lamé's constants λ and μ determine the ratio between the shear velocity and the longitudinal velocity. This ratio, for an isotropic medium, is always between 0 and 0.707.

2.1.1.4 The Equation of Motion

The equation of motion comes from the fundamental law of dynamics, F = mγ, where γ is the acceleration of the particle and F is a force given by Eq.(2.3). Neglecting the effect of gravity, stating that the force applied gives raise to the acceleration of the unit volume mass ρ and making use of Hooke's law, the equation of motion becomes:

$$\rho \frac{\partial^2 u_i}{\partial t^2} = \frac{\partial T_{ij}}{\partial x_j} \tag{2.12}$$

This equation which describes the motion in a solid is obtained by considering stress variations across an element. It can be expressed, from equations (2.1) and (2.9), in term of the stress-strain relations as [2.6]:

$$\rho \frac{\partial^2 u_i}{\partial t^2} = C_{ijkl} \frac{\partial^2 u_l}{\partial x_j \partial x_k} \tag{2.13}$$

The four-index notation for the elastic constant tensor can be contracted to the two-index notation used, for example in Eq.(2.7) in the same way the stress and strain tensors have been contracted into six-component vectors. In other words, Eq.(2.13) can be derived from Eq.(2.12) using Eq.(2.6) or (2.7). Auld [2.7] gives more details on how

the divergence of stress operation and the strain-displacement relation can be represented by a matrix in rectangular coordinates.

2.1.1.5 The Wave Equation

Further analysis of the wave equation is usually made simpler if two potential functions are introduced, a scalar and a vector potential of the displacement vector. However here we will not make use of this convenient technique. As we will see it later, to be piezoelectric a crystal must be anisotropic and it is more convenient for us to use Christoffel's equation.

In dynamic elasticity or acoustics we are interested in propagation phenomena. The equation of motion as given in Eq.(2.13) for a three-dimensional anisotropic medium, can be seen as a generalisation of the propagation equation in a fluid [2.8] which has a general solution $u(\vec{x},t)$ in the form of a progressive wave, travelling in a direction $\vec{n}$ perpendicular to the wave planes $\vec{n}.\vec{x}=\text{constant}$, where $\vec{x}$ is the position vector of the points of the wave planes. This solution,

$$u(\vec{x},t)=A\,\vec{p}\,f\left(t-\frac{\vec{n}.\vec{x}}{V}\right) \tag{2.14}$$

represents the vibration created at each position $\vec{x}$ by a wave propagating in the direction $\vec{n}$. V is the phase velocity, A is the amplitude of the vibration and $\vec{p}$ the wave polarisation (i.e. the particle displacement direction). Among all possible disturbances, harmonic vibrations about a mean position are very important since other perturbations result from the superposition of these vibrations [2.9]. The solution to Eq.(2.13), for a fluid is sought using the separation of variables techniques. The general solution is a stationary or standing harmonic wave. This solution may be put in the form of the sum of harmonic waves propagating in opposite directions. The typical form of the function f of Eq.(2.14), assuming an initial time behavior of the form $\exp(\omega t)$ is then given by $\exp(\omega t - kx)$ where ω is the frequency of the vibration and k is referred to as the wavenumber. The argument $(\omega t - kx)$ is designated as the phase and for increasing time, increasing values of x are required to maintain the phase constant. Therefore this function represent a wave propagating in the positive x direction. The propagation velocity of the planes of constant phase is the phase velocity:

$$V=\frac{k}{\omega} \tag{2.15}$$

The wavenumber is the inverse of the wavelength which is the space interval which lies, at a given time, between two identical states of the continuum, for instance two successive maxima of the vibration. Therefore the quantity (kx) measures the difference in phase at a given time between the vibration of planes separated in space by the distance x. Graff [2.9] pointed out that a solution of type $A\cos(\omega t - kx)$ has no wave front since it represents a vibration of infinite length. Therefore it is only by considering the phase that a propagation velocity can be associated with the motion. Therefore,

assuming solutions in the form of harmonic propagating waves, the equation of motion in its general form can be reduced to the Christoffel equation [2.7]

$$k^2 \Gamma_{il} u_l = \rho\omega^2 u_i \tag{2.16}$$

where the second rank tensor

$$\Gamma_{il} = c_{ijkl} n_j n_k \tag{2.17}$$

is called the Christoffel tensor. Its elements are functions only of the plane wave propagation direction and the stiffness constants of the medium. It applies to bulk waves (uniform plane waves). Generally, for a given direction of propagation of those bulk waves, there are three velocities, the three roots of the secular equation

$$\left| \Gamma_{il} - \rho V^2 \delta_{il} \right| = 0 \tag{2.18}$$

which express the compatibility of the three homogeneous equations [2.10]. Each velocity is related to an eigenvector, which defines the direction of displacement (i.e. the polarisation of the wave).

Although we are interested in the behaviour of anisotropic crystals, it is convenient first to consider a simple isotropic example. This exercise will be very useful when, in Chapter 3, we will investigate simple one-dimensional propagation along directions linked to the piezoelectric crystal axes of symmetry. The Christoffel tensor for an isotropic infinite solid, when the stiffness matrix given by Eq.(2.8) is substituted in Eq.(2.18), is

$$\Gamma_{il} = \begin{bmatrix} c_{11}n_x^2 + c_{44}(1-n_x^2) & (c_{12}+c_{44})n_x n_y & (c_{12}+c_{44})n_x n_z \\ (c_{12}+c_{44})n_x n_y & c_{11}n_y^2 + c_{44}(1-n_y^2) & (c_{12}+c_{44})n_z n_y \\ (c_{12}+c_{44})n_x n_z & (c_{12}+c_{44})n_z n_y & c_{11}n_z^2 + c_{44}(1-n_z^2) \end{bmatrix} \tag{2.19}$$

Now if we assume that the wave is propagating in a particular direction, for example the direction z, then Eq.(2.19) becomes a diagonal matrix and the Christoffel equation reduces to

$$\begin{bmatrix} c_{44} & 0 & 0 \\ 0 & c_{44} & 0 \\ 0 & 0 & c_{11} \end{bmatrix} \begin{bmatrix} u_x \\ u_y \\ u_z \end{bmatrix} = \rho\omega^2 \begin{bmatrix} u_x \\ u_y \\ u_z \end{bmatrix} \tag{2.20}$$

There are three independent solutions, i.e. three independent waves propagating in the z direction but polarised in different directions: an x-polarised wave and a y-polarised wave which both satisfy the dispersion relation

$$k^2 c_{44} = \rho\omega^2 \tag{2.21}$$

These waves are shear or transverse waves, propagating with velocity $c_T = \sqrt{c_{44}/\rho}$. The shear displacements are given by $u_s = \vec{p}\,ue^{j(\omega t - kz)}$ where $\vec{p}.\vec{z} = 0$. The third solution is a compressional wave $u_l = \vec{z}\,ue^{j(\omega t - kz)}$ propagating with velocity $c_L = \sqrt{c_{11}/\rho}$. The velocity c_L is associated with displacement components parallel to the direction of propagation, while c_T is associated with displacement components normal to the direction of propagation. The corresponding shear and longitudinal waves propagate independently of each other. Therefore, any plane wave propagating through an infinite isotropic medium must travel with a constant velocity (c_L or c_T), which is a function of material properties only. These three solutions are independent of the direction of propagation by virtue of the nature of isotropic solids. This is not true for generally anisotropic solids.

2.1.2 THE LAW OF REFRACTION OF PLANE WAVES AT AN INTERFACE

Expression of the reflection of longitudinal and shear waves incident on the boundaries is essential to the comprehension of the behaviour of guided waves. Details on this subject may, for example, be founds in Redwood [2.11] and expressions for the reflection and transmission coefficients are given in [2.9] and [2.12].

If a plane wave strikes a plane interface obliquely, reflected and transmitted waves arise, as in optics. If a longitudinal wave is incident at the boundary two waves, a longitudinal wave and a shear wave are generally reflected, the shear wave being generated by mode conversion. If only a shear wave is incident, in general there will be mode conversion to a longitudinal wave to satisfy boundary conditions. No mode conversion occurs at normal incidence, or when the shear wave is incident at 45°. The law of refraction determines the directions of the reflected and transmitted waves. For example if we assume that a wave propagates in medium "1" with velocity c_1 and is incident, at the interface between medium "1" and medium "2", with an angle $\alpha 1$, the wave transmitted in medium "2" will propagate with an angle α_2 determined by

$$\sin\alpha_2 = \frac{c_2}{c_1}\sin\alpha_1 \tag{2.22}$$

2.1.3 LAMB WAVES

If the elastic medium is made finite in the y direction then a plate results. Plates cause plane waves to be guided between their boundaries, and hence are sometimes called waveguides. The assumptions previously applied, relating to the properties of the medium, will also be employed here. The plate is assumed to extend to infinity in the x and z directions, and the origin of the y-axis is located midway through the thickness of the plate as shown in Figure 2.1. In this thesis we are only interested in plane strain problems, therefore shear horizontal (SH) waves will not been considered. Extensive details on SH waves can be found in [2.11] and [2.9].

Plate waves can be generated by exciting the plate with an obliquely incident wave. For a plate wave to travel parallel to the plate surfaces, the angle of incidence is derived from Eq.2.22 and is given by

$$\sin \alpha_1 = \frac{c_1}{c_2} \tag{2.23}$$

The transmitted waves travel unimpeded through the plate at the angle of refraction given by the law of reflection. On reaching the opposite surface the transmitted wave is reflected inside the plate at the same angle and continues its way along a zigzag path. Depending on the angle of incidence and the nature of the incident wave, either only transverse waves or both longitudinal and transverse waves travel along the plate. If the angle of incidence is chosen so that the beams cover each other in a proper phase relationship, the pattern arising in this way, composed of mutually superimposed zigzag reflected longitudinal and transverse waves is known as a Lamb wave. The simple geometrical requirement, that the reflected waves should not cancel each other, demands indeed a complicated relationship between plate thickness and the most favourable angle. The complication results from the fact that in the case of the oblique reflection of sound at surfaces of the plate, phase shifts occur which in turn depend on the angle. The relationship becomes even more complicated when one examines the velocity of these waves in the direction parallel to the surfaces of the plate. Lamb [2.13] has first published these dispersion relations. For a single plate in vacuum the solution of the Rayleigh-Lamb dispersion relationship can be expressed analytically, as shown by Viktorov [2.1] and Achenbach [2.14].

Strictly speaking the term “Lamb waves” holds only for plate waves propagating in free plates in vacuum. This is extended to plates embedded in an infinite medium, such as water, but for multilayered systems, in particular with no symmetry with respect to the z-axis, it is improper to use the term Lamb waves to depict the plate waves that propagate in such a system. In Chapter 4, plate waves in multilayered plate-like structures will be denoted with a “P” and termed acoustic plate modes (APM). Solutions in multilayered systems cannot be expressed analytically and a computer program such as DISPERSE [2.16] can be used to trace the dispersion curves for the acoustic plate modes propagating freely in the structure. Based on the geometry and the material properties of the multilayered plate system, DISPERSE determines what resonances can exist in order to satisfy the boundary conditions and the bulk wave propagation characteristics in each layer [2.17]. These resonances control how ultrasonic waves will be guided in the system and what properties each of these waves will have. The solutions to the guided wave problem lie on continuous lines called dispersion curves that must be found iteratively in frequency – wavenumber space. Once the solutions have been found, stress and displacement modeshapes can be found.

For both single plates and multilayered plate systems, these solutions form the basis for which is based our analytical model, presented in Chapter 4, for the excitation of acoustic plate modes by permanently attached piezoelectric transducers. More details on how dispersion curves are found will not be given in this thesis but extensive details can be found in [2.18].

2.2 LAMB WAVE EXCITATION IN THIN PLATES

The problem of the excitation of Lamb waves by piezoelectric transducers permanently attached to plate-like structures is the central problem that is adressed in this thesis. This problem can be formalized using the exact theory of elasticity but, in most cases it is impossible to solve the equations analytically. This limitation led researchers to find approximate theories and in particular it is well-known that most problems of forced vibrations in elastic multilayered structures, though diverse in formulation, are all amenable to solution by a uniform method that belongs to the normal mode theory. Modal analysis, basically the search for the eigenvalues of the system, is a very powerful tool for treating waveguide excitation, as shown by Rose [2.19] for a mechanical excitation. The use of this technique for dispersive plate waves has been reported only recently [2.20], [2.21], and the contribution of perturbing modes is considered in [2.22] for a simple case. None of these papers deal with piezoelectric materials however the normal mode expansion technique can also be used to solve analytically the problem of excitation of mechanical waves in piezoelectric materials driven electrically as shown by Auld [2.7].

The main idea of the normal mode method is to assume that, a priori, the sought functions, for example the particle velocity and the stresses, can be written in the form of a series with unknown amplitude

$$\begin{aligned} v(z,y) &= \sum_n a_n(z)\, v_n(y) \\ T(z,y) &= \sum_n a_n(z)\, T_n(y) \end{aligned} \tag{2.24}$$

where v_n and T_n are the particle velocity and the stress mode shapes of the n^{th} mode and a_n is the unknown amplitude. Similar expressions can be obtained for the electrical fields.

Our purpose in this thesis is to depict accurately the process by which Lamb waves can be generated in a plate by use of transducers. Therefore our primary goal is to find either a general expression for the unknown amplitudes a_n or a numerical estimate of them. In the first case when the amplitudes can be found, the expanded series should represent the exact solution to the original differential equation(s) depicting the problem. This requires the proof that the acoustic field distributions of the modes form a set of orthogonal functions, and additionally that the set of modes is complete [2.7]. Both subjects are very well documented and details can be found in both theoretical physics text books [2.23], [2.24], and in text books treating in detail about guided waves [2.7], [2.9], [2.19], [2.25], [2.26], [2.27]. However complications may be encountered when dealing with acoustic plate modes in piezoelectric layers, in which coupling between acoustic and electromagnetic fields may occur. Indeed the first step when using the normal mode theory is to make sure that the set of acoustic waveguide mode functions is complete and also that the modes are orthogonal. These two points are discussed below and will be considered as established for the remainder of the thesis.

2.2.1.1 Completeness of Normal Modes

The Lamb modes of a plate are assumed to be complete in the space of solutions of the governing equations. A set of normal modes is said to be complete in a particular space of functions if any of the functions in that space can be exactly represented in terms of a finite or infinite number of functions in the set. For example in the space of twice differentiable functions u(x) satisfying the boundary conditions u(0)=u(L)=0, it is known that the set of functions $u(x)=\sin(n\pi x)$, $n \in \{1,2,...,\infty\}$ is complete [2.28]. This means that any function which can be differentiated twice (without having singular points) and which vanishes at the boundaries can be expressed, for any x in the interval [0,L], as a series in the form $u(x)=\sum A_n \sin(n\pi x)$, for some choice of expansion coefficients, A_n. Stated alternatively, there are no twice differentiable functions, vanishing at the boundaries, which cannot be expressed in the above form. Kirrmann [2.29] treated the problem of the completeness for Lamb modes. It should be noted, however that no general proof of such completeness exists for the normal modes of even a single isotropic flat layer and in the remainder of this thesis their completeness is assumed.

2.2.1.2 Orthogonality of Normal Modes

Orthogonality of normal mode is a fundamental property of the acoustic modes. The concept of orthogonality of a set of functions is an abstraction of the notion of the orthogonality of vectors in space [2.23]. That is, for any set of functions, $U_m(x)$, $m \in \{1,2,...,\infty\}$ defined over the domain $x \in [a, b]$, the set is orthogonal over the interval [a, b], if and only if,

$$\int_a^b U_m(x)\,U_n(x)\,dx = 0 \qquad \text{for } m = n \tag{2.25}$$

The procedure to establish the orthogonality of the normal modes is similar. A pioneer text on this subject has been written by Marcuse [2.27] for optical systems and a typical example of its application to acoustics can be found in [2.30] for the study of a liquid/solid interface. The important point to remember is that if one wants to construct for a specific structure the orthogonal set of acoustic modes, one first has to derive some orthogonality relation. This means that the set of modes is intrinsic to the structure and therefore the orthogonality relation has to be built for each different system. For free waveguides, this has already been done by Auld [2.7, Chap. 10]. However, even for simple waveguides, it may be necessary to establish new orthogonality and the normalisation relations if the non-propagating modes are also considered in the analysis. It has been shown by Peach [2.31] and Kostenbauder and Siegman [2.32] that the normalisation relation used for propagating modes cannot be used for the resonant cut-off modes. In the derivation of our analytical model, see Chapter 4, it has been arbitrarily decided to omit non propagating modes and to limit the study to the two fundamental modes therefore we used directly the work done by Auld [2.7, Chap. 10] and no new orthogonality relationship has been derived.

2.2.1.3 Reciprocity Relationship

Auld [2.7] derived the orthogonality relationship, for the excitation of guide wave in free and lossless waveguides, by piezoelectric sources by means of the introduction of the complex electromechanical reciprocity relationship. This expression directly relates the electrical signal that would be received by an ultrasonic transducer to the radiation patterns of the transmitting and receiving transducers. The relationship thus provides a formalism that allows one to develop a system description of an ultrasonic measurement, which includes the influence of all aspects of the measurement system on the observed voltage. This reciprocity relationship is nonetheless useful in demonstrating the orthogonality of the Lamb modes and also is the starting point for all the perturbation calculations performed in this thesis.

Let us consider a homogeneous insulating piezoelectric material, whose behaviour is governed by the piezoelectric constitutive equations and Newton's law. Any disturbance in the material gives rise to a particle displacement velocity vector v, a stress tensor T, an electric scalar potential Φ and an electric displacement vector D, all of which are functions of the space coordinates and of time. It is assumed that these functions describe a first solution satisfying the constitutive relations of the material and they will all be assumed to be proportional to $\exp(i\omega t)$. A second solution is also assumed, described by the functions v', T', Φ' and D', and also proportional to $\exp(i\omega t)$. These two solutions are related by the complex reciprocity relation which is written

$$\nabla.\left\{-v_2^*.T_1 - v_1.T_2^* + \Phi_2^*\left(i\omega D_1\right) + \Phi_1\left(i\omega D_2^*\right)\right\} = 0 \qquad (2.26)$$

when there is no free charge and no mechanical source. This relation is not valid for lossy media and assumes the electric field to be quasi-static, E = - grad Φ.

2.2.1.4 Perturbation Theory

At this stage and for the remainder of the thesis it is considered that the completeness and the orthogonality of Lamb modes in a free plate are established. This enables us to use the normal mode expansion technique to establish expressions for the mechanical and electrical fields. To do so we will use the well-known perturbation methods [2,8], [2,23], in order to estimate the amplitude of the expansion coefficients a_n in Eq.(2.24). To solve the entire transducer problem we adopted a methodology, detailed in the introduction of Chapter 4, where each perturbation is assumed to be sufficiently weak to represent it in a linear problem and to solve it by considering each effect separately. This idea of evaluating electrical and mechanical perturbations independently has been validated by Slobdonik [2.34] and allows us to split the problem into various stages, each relatively easy to solve, and to combine them linearly.

The modes which can propagate in the entire system, transducer and structure, must be the exact solutions of the Christoffel equation for the system. Since we consider weak perturbations these solutions differ very little from the solutions for a stress-free plate and the idea to solve the problem is to start the calculations with the Lamb mode

solutions for the metallic plate in vacuum, and then to add the perturbations gradually. In other words, the problem starts with finding the Lamb modes in the structure and then we develop the calculations by gradually adding electrical and mechanical boundary conditions that represent the entire transducer plus structure system. These calculations are presented in details in Chapter 4.

The advantage of using this perturbation approach is that analytical expressions can be found. The major drawback is that the solutions found are only approximate and the solutions valid only in the limits of the assumptions used to simplify the problem.

The next section introduces the piezoelectric coupling and some notions about the transducers and piezoelectric material used in this study.

2.3 PIEZOELECTRIC MATERIALS & PIEZOELECTRICITY

Piezoelectricity is a phenomenon which allows electric polarisation to be produced by mechanical stress in certain materials. This is defined as the direct piezoelectric effect. Closely related is the converse effect, whereby a crystal becomes strained when an electrical field is applied. Both effects are manifestations of the same fundamental property of the crystal. The variables are in linear relationship to one another in both direct and indirect processes. More details can be found in the reference books by Masson [2.35] and Cady [2.36].

2.3.1 PIEZOELECTRIC MATERIALS

The piezoelectric effect is a property of a crystal structure, and a necessary condition for the existence of piezoelectricity is a certain type of asymmetry in the material: the crystal must not have a centre of symmetry. Piezoelectric materials are therefore anisotropic. In this thesis we deal with a ceramic, PZT (ferroelectrics are piezoelectric [2.37])., and a polymer, PVDF.

2.3.1.1 Piezoelectric Ceramics

Ceramics, by definition, comprise inorganic, non-metallic, non-water-soluble compounds that show ionic contributions in their chemical bonds. In this thesis we use PZT ceramics. These ceramics have originally been developed by Clevelite Corporation. They are ferroceramics based on $Pb(Zr\text{-}Ti)O_3$ compositions. Greater details are to be found in textbooks and articles by Bechmann [2.38], Jaffe [2.39], Berlincourt [2.40], [2.41], Meitzler [2.42], Cross [2.43], [2.44] and Uchino [2.45].

2.3.1.2 Piezoelectric Polymers

Polymers are another group of materials which exhibit piezoelectric effects. It is known that some natural substances such as rubber, wool, hair, etc. are piezoelectric. However in most polymers the piezoelectric effect is very weak though polyvinilidene fluoride has demonstrated promising potential. Certain polymers, such as polyvinyl

chloride (PVC), polyvinyl fluoride (PVF), and polyvinilidene fluoride (PVF_2 or PVDF) can be made piezoelectric by a combination of mechanical stretching and electric field poling at elevated temperatures. The induced anisotropy varies with the polymer and the subsequent treatment. PVDF sheet, poled along the thickness belongs to the crystal class ∞ mm (equivalent to 6mm) and uniaxial stretching or rolling converts it to orthorhombic 2mm, while biaxial stretching produces class ∞mm.

Kawai [2.46] published the first description of the piezoelectric properties of PVDF. Subsequently, it has been used in many transducer applications as reviewed by Chen and Payne [2.47]. Numerous workers among who Ohigashi [2.48], [2.49], Lovinger [2.50], Chen [2.47], Kimura [2.51] and Brown [2.52], [2.53] have made detailed investigations of the mechanical and dielectric properties, and piezoelectric coupling parameters, all of which exhibit both frequency and temperature dependence.

2.3.2 PIEZOELECTRICITY

Piezoelectricity is a fundamental process of electromechanical interaction and is representative of linear coupling in energy conversion. The piezoelectric process is adiabatic, the temperature is assumed to be constant. In linear piezoelectricity the equation of linear elasticity are coupled to the charge equation of electrostatics by means of the piezoelectric constants. However, the electric variables are not purely static, but quasistatic because of the coupling to the dynamic mechanical equations. Thus in order to provide an appropriate theoretical basis for the piezoelectric materials, the relevant electric equations are presented first in this section.

2.3.2.1 Piezoelectric Constitutive Equations

When the media are piezoelectric the problem involves not only elastic particle displacements but also the electric and magnetic fields, with the results that the applicable equations are the combination of the elastic equations of motion and the Maxwell's equations. Elastic and electromagnetic fields are coupled by the piezoelectric tensor of the media. The electromagnetic equations have two plane solutions while the acoustic equations have three. In a non-piezoelectric medium, the electromagnetic and acoustic solutions are completely independent of each other, but in the piezoelectric case, they are coupled together through the piezoelectric stress equations.

Piezoelectricity couples the mechanical stress T and strain S fields with the electric intensity E and displacement D fields. Depending on variable choice, four sets of material constitutive relations are defined for the linear case of insulating dielectric materials. The four equivalent pairs of material constitutive equations differ in their combinations of independent and dependent variables; the material constants used in the sets are interrelated. The equations relating the constitutive material values may be determined by first pairing the equations sharing common variables, then one variable is eliminated from each pair, yielding the required results, [2.55].

It must be noted that we choose a specific independent variable set that is the strain S and the electric displacement E. In many textbooks, for example [2.35], [2.36],

[2.37] and [2.56], the chosen variables are S and P the electric polarisation. We choose the electric displacement because the electric boundary conditions specified in our problems are the continuity of the electric potential and the continuity of the electric displacement. The classic thermodynamic derivation [2.7] [2.56], [2.57] of the adiabatic process leads to the fundamental relations for the selected variable set S, E as independent mixed variables:

$$T = c^E S - e^t E \qquad T_{ij} = c^E_{ijkl} S_{kl} - e_{kij} E_k \tag{2.27}$$

$$D = eS + \varepsilon^S E \qquad D_i = e_{ikl} S_{kl} + \varepsilon^S_{ij} E_k \tag{2.28}$$

The electric field E and electric displacement D are tensors of rank one. The mechanical variables T and S are tensors of rank two, which have been converted to six-dimensional vectors, see Eq.(2.5). c^E is the symmetric matrix representing the elastic stiffnesses at constant electric field. ε^S is the symmetric dielectric permittivity matrix at constant strain, while e is the piezoelectric matrix. Superscript t denotes a transposed matrix.

These relations shows that the presence of piezoelectricity modifies the elastic and dielectric constants, that the mechanical (elastic) conditions must be specified for the dielectric quantities, and that electrical conditions must be specified for elastic quantities.

2.3.3 QUASISTATIC APPROXIMATION

The piezoelectric coupling between electromagnetic and acoustic plane waves is negligible by comparison with the influence of the electric field. This is called the quasistatic approximation and it leads to a very great simplification of the analysis. In this so-called quasistatic approximation the elastic wave equations for the particle displacements are inter-coupled to the anisotropic Laplace's equation for the potential Φ by the piezoelectric tensor e. Thus the particle displacements and the potential must satisfy the following set of equations [2.54] using acoustic displacement rather than velocity,

$$c^E_{ijkl} \frac{\partial^2 u_k}{\partial x_l \partial x_i} - \rho \frac{\partial^2 u_j}{\partial t^2} + e_{kij} \frac{\partial^2 \Phi}{\partial x_k \partial x_i} = 0 \tag{2.29}$$

$$e_{ijk} \frac{\partial^2 u_j}{\partial x_k \partial x_i} - \varepsilon_{ij} \frac{\partial^2 \Phi}{\partial x_i \partial x_j} = 0 \tag{2.30}$$

Each tensor is referred to the coordinate system and the summation convention on repeated subscripts is implied.

The electric potential can be calculated from the acoustic displacement by integrating twice Eq.(2.30) and solving for the electric potential. Then substitution into

Eq.(2.29) leads to an equation of the same form as the Christoffel's equation but with a different stiffness constant. This term is called the piezoelectric stiffened elastic constant.

Eqs.(2.27) and (2.28) can be written in their developed matrix form. In general the matrices are fully populated but, considering that almost all piezoelectric crystals belong to the trigonal (3, 3m, 32), orthorhombic (222, 2mm), tetragonal (4, $\underline{4}$, 4mm, 422 ,$\underline{4}$2m), hexagonal (6, 622, 6mm, $\underline{6}$) and cubic (23, $\underline{4}$3m) systems, only a restricted number of independent constants are required.

$$\begin{bmatrix} T_I \\ D_i \end{bmatrix} = \left[\begin{array}{cccccc|ccc} C_{11} & C_{12} & C_{13} & C_{14} & -C_{25} & C_{16} & -e_{x1} & e_{y2} & -e_{z1} \\ C_{12} & C_{22} & C_{23} & -C_{14} & C_{25} & -C_{16} & e_{x1} & -e_{y2} & -e_{z2} \\ C_{13} & C_{23} & C_{33} & 0 & 0 & 0 & 0 & 0 & -e_{z3} \\ C_{14} & -C_{14} & 0 & C_{44} & 0 & 2C_{25} & -e_{x4} & -e_{y4} & -e_{z4} \\ -C_{25} & C_{25} & 0 & 0 & C_{55} & 2C_{14} & -e_{x5} & -e_{y5} & -e_{z5} \\ C_{16} & -C_{16} & 0 & 2C_{25} & 2C_{14} & C_{66} & 2e_{y2} & 2e_{x1} & -e_{z6} \\ \hline e_{x1} & -e_{x1} & 0 & e_{x4} & e_{x5} & -2e_{y2} & \varepsilon_{11}^S & 0 & 0 \\ -e_{y2} & e_{y2} & 0 & e_{y4} & e_{y5} & -2e_{x1} & 0 & \varepsilon_{22}^S & 0 \\ e_{z1} & e_{z2} & e_{z3} & e_{z4} & e_{z5} & e_{z6} & 0 & 0 & \varepsilon_{33}^S \end{array}\right] \cdot \begin{bmatrix} S_J \\ E_j \end{bmatrix} \tag{2.31}$$

In monoclinic and triclinic systems, the number of independent piezoelectric strain constants reduces to 12, and only 3 permittivity constants are required. Additionally the number of independent elastic constants is also limited to 12.

The units of the tensors in equations (2.27) and (2.28) are given in Table 1 [2.57].

2.3.3.1 Piezoelectric Forces

The volumetric force density is given by

$$F_j = \frac{\partial T_{ij}}{\partial x_i} \tag{2.32}$$

Piezoelectric force density components may be found from Eq.(2.27) as

$$\frac{\partial \left(e_{kij} E_k \right)}{\partial x_i} \tag{2.33}$$

This means that piezoelectricity forces may arise either from spatial gradients of the piezoelectric constants or from spatial gradients of the electric field. In a single crystal it is not usual that the piezoelectric constants will vary from place to place, although it is possible. Thus piezoelectricity forces arise because of spatial gradients of

the electric field. This is particularly the case when interdigital transducer electrode arrays are used to produce acoustic waves. From the electrode array placement one may find the force components and infer qualitatively if a particular type of wave motion may be driven piezoelectrically by the electrode array [2.58].

2.3.4 ELECTROMECHANICAL COUPLING FACTORS

The physical significance of various piezoelectric stress constants e_{Ij}, is illustrated in Figure 2.2. If we suppose that only one dimensional coupling occur, it is seen from the first schematic in Figure 2.2 that an electric field applied along the x-direction of the piezoelectric crystal will induce a normal stress in the x-direction via the e_{x1} coupling constant. From Eq. (2.27) the stress is given by

$$T_1 = -e_{x1}E_x \tag{2.34}$$

The piezoelectric stress constants are measured in coulomb/m^2, and values are as large as 10, meaning that at an elastic limit strain in the order of 10^{-3}, the piezoelectrically induced electrical displacement may be as large as 10^{-2} coulomb /m^2. Conversely, at break down electric field strength on the order of 10^7 volts/m, the piezoelectrically induced stress may be as large as 10^8 newtons per meter.

Electromechanical factors are dimensionless measures of the efficacy of piezoelectricity transduction and far more important than the piezoelectric constants taken by themselves. For thickness plate resonators, coupling factors have the generic form $k^2 = e^2/(\varepsilon C)$ at high frequencies. For a Z-normal sheet PVDF polymer, k_{31}=16 %, whereas k_{33} = 30-60% for Z-cut ceramics and less than 10% for AT-cut or BT-cut (k_{26}) quartz. Calculations for the electromechanical coefficients of piezoelectric elements are presented in details in Chapter 3.

2.4 CONCLUSION

In this Chapter we have introduced some basic notions on four different fields, Lamb waves, the normal mode theory, the perturbation method and the piezoelectric behaviour of piezoelectric materials. These constitute the background on which the analysis presented in Chapter 4 is based.

2.5 REFERENCES

[2.1] **Viktorov**, I., A., *Rayleigh and Lamb Waves***,** Plenum Press, New York, 1967.

[2.2] **Kolsky**, H., *Stress Waves in Solids*, Oxford, 1953.

[2.3] **Love**, A. E. H., *The Mathematical Theory of Elasticity*, 4th edition, Cambridge University Press, 1944.

[2.4] **Timoshenko**, S. P., and Godier, J. N., *Theory of Elasticity*, McGraw-Hill Book Co., New York, London, Chapters 2 & 4, 3rd edition, 1970.

[2.5] **Sommerfeld** A., *Mechanics of Deformable Bodies*, Academic Press, New York, 1950.

[2.6] **Malvern** L. E., *Introduction to the Mechanics of a Continuous Medium*, 1969.

[2.7] **Auld**, B. A., *Acoustic Fields and Waves In Solids*, Vol. II, 2nd ed., Robert E. Krieger Publishing Compagny, Malabar, Florida, 1990.

[2.8] **Morse**, P. M., *Vibration and Sound*, 2nd ed. McGraw-Hill, 1948.

[2.9] **Graff**, K. F., *Wave Motion in Elastic Solids*, Clarendon Press, Oxford, 1975

[2.10] **Dieulesaint**, E. and Royer, D., *Ondes Èlastiques dans les Solides*, Tome 1: *Propagation Libre et Guidée*, Masson, Paris, Milan, Barcelone, 1996.

[2.11] **Redwood**, M. *Mechanical Waveguides*, Pergamon Press, Oxford, 1960.

[2.12] **Brekhovskikh**, L. M., *Waves in Layered Media*, Academic Press, New York, 1980.

[2.13] **Lamb, H.**, "On Waves in Elastic Plate", Proc. Roy. Soc. London, Series A, 1917.

[2.14] **Achenbach**, J. D., *Wave Propagation in Elastic Solids*, North-Holland publishing company, Amsterdam, London, 1973.

[2.15] **Ewing**, W. M., Jardetsky, W.S. and Press, F., *Elastic Waves in Layered Media*, McGraw-Hill, 1957.

[2.16] **Lowe**, M. J. S., "Matrix Technique for Modelling Ultrasonic Waves in Multilayered Media", IEEE Transactions on Ultrasonics, Ferroelectrics, and Frequency Control, Vol. 42(4), 1995.

[2.17] **Pavlakovic**, B. N., *Leaky Guided Ultrasonic Waves in NDT*, Ph.D. Thesis, University of London, (Department of Mechanical Engineering, Imperial College), 1998.

[2.18] **Pavlakovic**, B. N., Lowe, M. J. S., Alleyne, D. N. and Cawley, P., "Disperse: A General Purpose Program for Creating Dipersion Curves", Review of Progress in Quantitative NDE, eds. D.O. Thompson and D.E. Chimenti, American Institute of Physics, New York, Vol. 16,

[2.19] **Rose**, J. L., *Ultrasonic Waves in Solid Media*, Cambridge University Press, 1999.

[2.20] **Ditri**, J. J. and Rose, J. L., "Excitation of Guided Waves in Generally Anisotropic Layers Using Finite Sources", J. Appl. Mech., Vol. 61, pp. 330–338, 1994.

[2.21] **Degertekin**, F. L. and Khuri-Yakub, B. T., "Single Mode Lamb Wave Excitation in Thin Plates by Hertzian Contacts", Appl. Phys. Lett., Vol. 69(2), pp. 146–148, 1996.

[2.22] **Jia**, X., " Modal Analysis of Lamb Wave Generation in Elastic Plates by Liquid Wedge Transducers", J. Acoust. Soc. Am., Vol. 101(2), pp. 834-842, 1997.

[2.23] **Morse**, P. M. and Feshbach, H., *Methods of Theoretical Physics*, Vol. I and Vol. II, Mc Graw-Hill Book Company Inc., New York, London, 1953.

[2.24] **Courant** R. and Hilbert, D., *Method of Mathematical Physics*, Vol.1, Interscience, NewYork, 1953.

[2.25] **Morse**, P. M. and Ingard K. U., *Theoretical Acoustics*, Chapter 2 and 5, Princeton University Press, Princeton, New Jersey, 1968.

[2.26] **Jones**, D. S., *Acoustic and Electromagnetic Waves*, Oxford Science Publications, Clarendon Press, Oxford, 1990.

[2.27] **Marcuse**, D., Light Transmission Optics, Van Nostrand Reinhold Company, 1972.

[2.28] **Friedman**, A., *Partial Differential Equations*, Huntington, New York., R. E. Krieger Pub. Co., 1976.

[2.29] **Kirrman**, P., "On the Completeness of Lamb Modes", J. Elast., Vol. 37, pp.39-69, 1994.

[2.30] **Briers**, R., Leroy, O., Shkerdin,G. N. and Gulyaev, Y. V., "Mode Theory as a Framework for the Investigation of the Generation of a Stoneley Wave at a Liquid-Solid Interface", J. Acous. Soc. Am., Vol. 95(3), pp. 1953-1966, 1994.

[2.31] **Peach**, R. C., "A Normal Mode Expansion for Piezoelectric Plates and Certain of its Applications", IEEE Transaction on Ultrasonics, Ferroelectrics, and Frequency Control, Vol. 35, pp. 593-611, 1988.

[2.32] **Kostenbauder**, A., Sun, Y. and Siegman, A. E., "Eigenmode Expansions using Biorthogonal Functions: Complex-Valued Hermite Gaussians", JOSA A, Vol. 14(8) pp. 1780-1795, 1997.

[2.33] **Thompson**, R. B., "Interpretation of Auld's Electromechanincal Reciprocity Relation via a One-Dimensional Example", Res. Nondestr. Eval., pp. 147-155, 1994.

[2.34] **Slobdonik** Jr., A. J., "Attenuation of Microwave Acoustic Waves due to Gas Loading", J. Appl. Phys. Vol.43, pp. 2565-2568, 1972.

[2.35] **Masson**, W. P., Piezoelectricity, its History and its Applications, J. Acoust. Soc. Am., Vol. 70, pp. 1561-1566, 1981.

[2.36] **Cady**, W. G., *Piezoelectricity***,** Dover Publications Inc., New York, 1964.

[2.37] **Berlincourt**, D., Curran, D. R. Jaffe, H., "Piezoelectric and Piezomagnetic Materials", Physical Acoustics, ed. Masson, W. P., New York, Academic Press New York, Vol. I(A), pp. 169, 1964.

[2.38] **Bechmann**, R., "Ceramics and some Applications of the Piezoelectric Equations", J. Acoust. Soc. Am., Vol. 28, pp. 347-350, 1956.

[2.39] **Jaffe**, B., Cook, W. R. and Jaffe, H., *Piezoelectric Ceramics*, Academic Press, New york, 1971.

[2.40] **Berlincourt**, D., "Piezoelectric ceramics: Characteristics and Applications", J. Acoust. Soc. Am., 70(6), pp. 1586-1595, 1981.

[2.41] **Berlincourt**, D., "Piezoelectric Crystals and Ceramics", In *Ultrasonic Transducer Materials*, ed, Martin, O. E., pp. 63, Plenum, New York, 1971.

[2.42] **Meitzler**, A. H., "Piezoelectric Transducer Materials and Techinques for Ultrasonic Devices Operating above 100MHz", In *Ultrasonic transducer Materials*, ed. Mattiat O. E., pp. 125, Plenum, New York, 1971.

[2.43] **Croos**, L. E. and Hardt, K. H., "Ferroelectrics**",** Encycl. Chem. Technol. Vol. I(1), 1980.

[2.44] **Cross**, L. E., "Dielectric, Piezoelectric, and Ferroelectric Components", Ceramic Bulletin, Vol. 63, pp. 586-590, 1986.

[2.45] **Uchino**, K., "Materials Issues in Design and Performance of Piezoelectric Actuators: An Overview", Acta Material, Vol. 46(11), pp. 3745-3753, 1998.

[2.46] **Kawai**, H., "The Piezoelectricity of Poly (vinylidene Fluoride)", Japanese Journal of Applied Physics **8**, pp. 975-976, 1969.

[2.47] **Chen**, Q. X. and Payne, P. A., "Industrial Applications of Piezoelectric Polymer Transducers", Meas. Sci. technol., Vol. 6, pp. 249-267, 1995.

[2.48] **Ohigashi**, H., "Electromechanical Properties of Polarized Polyvinylidene Fluoride Films Studied by the Piezoelectric Resonance Method", J. Appl. Phys., Vol. 47(3), pp. 949-955, 1976.

[2.49] **Ohigashi**, H., Koga, Suzuki, T., Nakanishi, M., Kimura, K. and Hashimoto, H., "Piezoelectric and Ferroelectric Properties of P(VDF-TrFE) Copolymers and their Application to Ultrasonic Transducers", *Ferroelectrics*, Vol. 60, pp. 263-276, 1984.

[2.50] **Lovinger**, A. J., "Ferroelectric Polymers", Science, Vol. 220, pp. 1115-1121, 1983.

[2.51] **Kimura**, K. and Ohigashi, H., "Analysis of Impulse Response Characteristics of Polymer Ultrasonic Transducers", Japanese Journal of Applied Physics, Vol. 27(4), pp. 540-546, 1988.

[2.52] **Brown**, L. F. "Ferroelectric Polymers: Current and Future Ultrasound Applications", IEEE Ultrasonics Symposium Proceedings, pp. 539-545, 1992.

[2.53] **Brown**, L., F. and Mason, J., L., "Disposable PVDF Ultrasonic Transducers for Nondestructive Testing Applications", IEEE Transactions on Ultrasonics, Ferroelectrics, and Frequency Control, Vol. 43, pp. 560-568, 1996.

[2.54] **Tiersten**, H. F., *Linear Piezoelectric Plate Vibrations*, Plenum Press, New York, 1969.

[2.55] **Ballato**, A., "Piezoelectricity: Old Effect, New Thrusts", IEEE Transactions on Ultrasonics, Ferroelectrics, and Frequency Control, Vol. 42, pp. 916-926, 1996.

[2.56] **Ikeda**, T., *Fundamentals of Piezoelectricity*, Oxford University Press, Oxford, New York, Tokyo, 1990.

[2.57] **An American National Standard** - *IEEE Standard on piezoelectricity*, ANSI / IEEE Std 176-1987, IEEE Inc., New York, USA, 1987.

[2.58] **Ballato**, A. and Gualtieri, J. G., "Shallow Bulk Acoustic Wave Progress and Prospects", IEEE Transaction on Microwave Theory Tech., Vol. 27, pp. 1004-1012, 1979.

2.6 TABLES

Field tensors		
Mechanical		
Stress, T	pascal	$Pa = N/m^2 = kg/m\ s^2$
Strain, S	dimensionless	metre/metre = m/m
Electric		
Intensity, E	volt/metre	$V/m = kg\ m^2/A\ s^3$
Displacement, D	coulomb/surface	$C/m^2 = A\ s/m^2$
Matter tensors		
Permittivity, ε^S	farad/metre	F/m = C/(Vm)
Piezo-constants e	coulomb/surface	$C/m^2 = N/(m\text{-}V)$
Elastic Stiffness, C^E	pascal	$N/m^2 = J/m^3$

Table 2.1 : SI Units for the fields and tensors used in the piezoelectric constitutive equations.

2.7 FIGURES

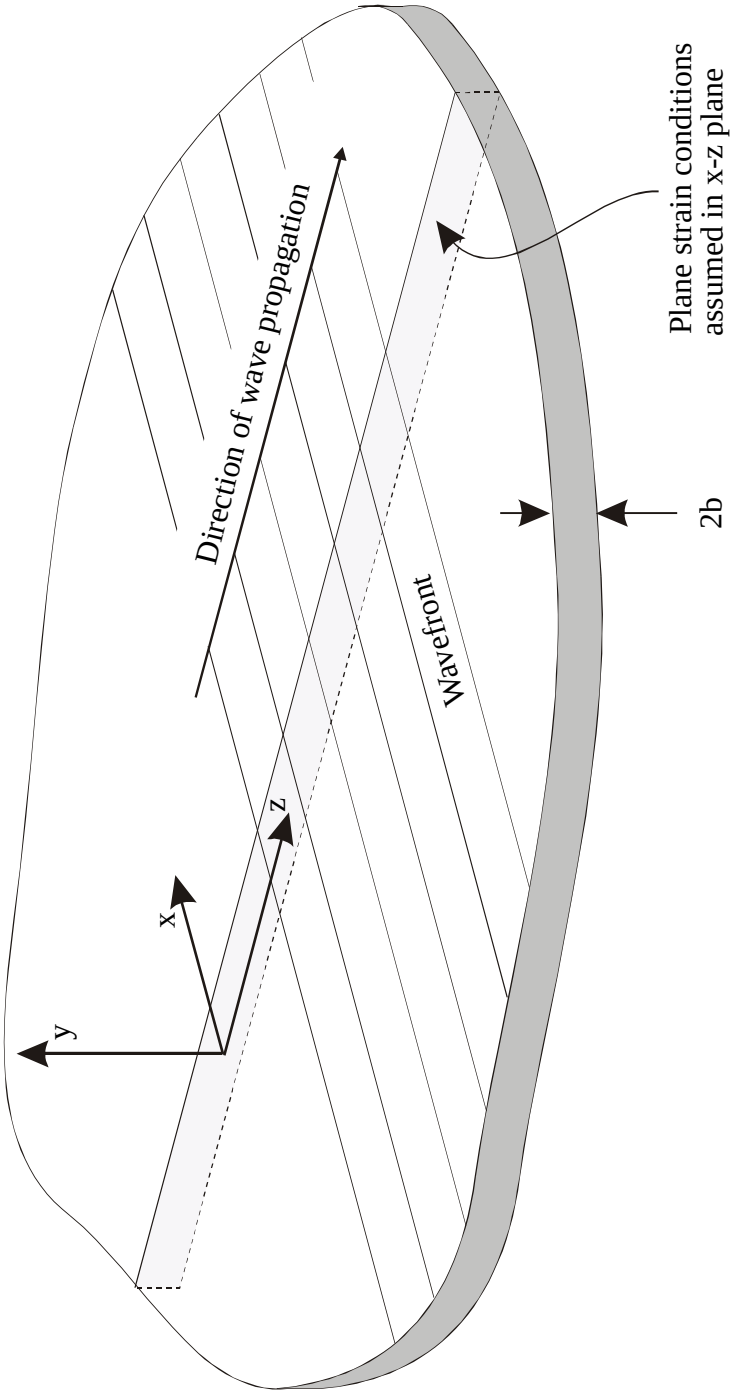

Figure 2.1 : Diagram of flat isotropic plate, showing orientation of axes, with propagation direction and wavefront.

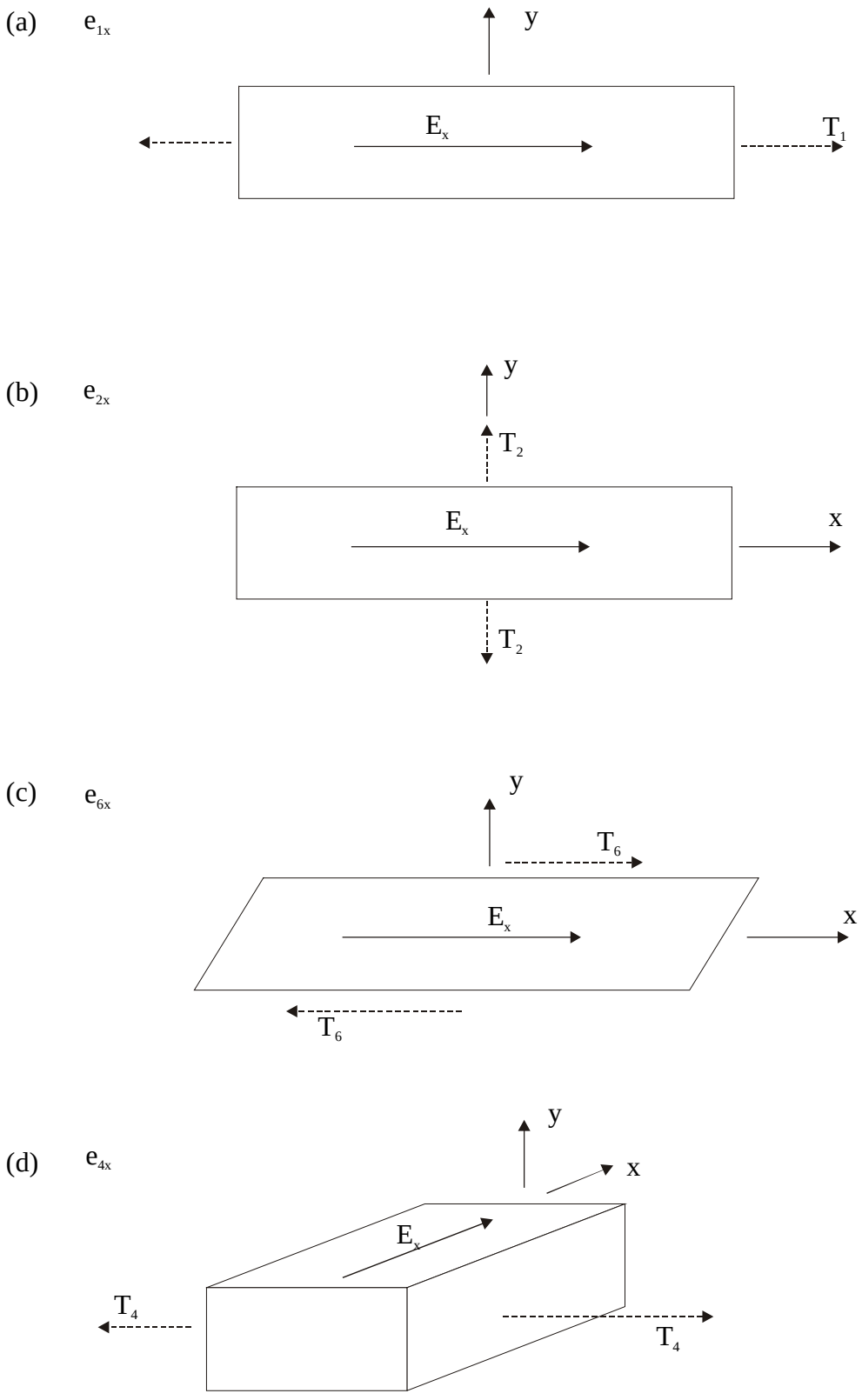

Figure 2.2 : Examples of the four basic types of piezoelectricity coupling terms (from B. Auld [2.7]).

Chapter 3

Finite Element Modelling of Piezoelectricity

The finite element method is a mathematical technique which, based on the governing constitutive differential equations of a continuum, allows the precise numerical computation of boundary value problems for arbitrary geometries. Traditionally, the finite element method is applied to mechanics and civil engineering, having its roots in these faculties as well. In electromechanical engineering, however, it has emerged over the last decade. The main reason for that delay is that for the simulation of electromechanical transducers, such as ultrasound transmitters and receivers, for example, a coupled field problem has to be solved which causes much more effort than handling a single field as is the case for purely mechanical components. In most cases, the coupling problem is twofold: first one has to describe the internal coupling mechanism of an electromechanical transducer, such as the piezoelectric effect. Secondly, the interaction of a fluid (propagation medium) and a solid (transducer) has to be considered. When the propagation of a sound wave in a huge (unbounded) domain has to be computed, further difficulties may arise, demanding special elements, such as infinite elements, or adapted procedures. However such elements will not be discussed here since this work is only concerned with propagation of plate waves in piezoelectric solids coupled or not to solid non-piezoelectric structures; coupling with fluids is beyond the scope of this thesis.

In this chapter a method for the analysis of piezoelectric structures, based on finite element calculations is presented. The implementation of these equations in an already existing finite element code, FE77, is described in some detail. Models are also presented which serve the purpose of validating this new code.

3.1 INTRODUCTION

Modelling the generation and reception of waves by piezoelectric devices requires the amplitude of the waves to be related to the voltage applied to the transducer and to its piezoelectric properties. Without a strong understanding of the electromechanical fields that can exist and propagate in the piezoelectric structure, reasonably accurate models cannot be developed to predict the amplitude and the nature of the waves generated by devices, which until recently have been empirically designed. Our main purposes in developing a computer model for simulations in transducer development are of three kinds. First the optimization of transducer design without time consuming experiments; secondly the evaluation of new materials in device design; and finally to acquire a deeper insight into the wave propagation in piezoelectric solids and coupled solid structures.

The equations of piezoelectricity are sufficiently complex to preclude closed form solution for all but the simplest cases. To overcome this limitation, since the late 1960's, variational principles have been derived which serve as the basis of approximate solution techniques such as the Rayleigh-Ritz method. From the variational principle enunciated by Holland [3.1] in 1968, a finite element formulation has been derived as early as 1970 [3.2]. Since then the industry has been slowly recognizing discrete numerical modelling on computers as a powerful alternative to conventional design methods (Masson's model or KLM model [3.3]). Today nearly all the major transducer companies are experimenting with finite element models using commercial packages like ANSYS [3.4] or by writing their own codes, [3.5]-[3.8]. However most commercially available packages are often limited to implicit algorithms for frequency-domain or time-domain analysis. In general implicit solutions are best suited to linear static problems, steady state vibrations and low frequency dynamics. A better choice for transient phenomena is an explicit time-marching algorithm [3.9] as will be demonstrated. To our knowledge other commercially available packages are available, among them PZFlex® [3.10], which are using explicit time domain solutions. However it is very unlikely that these codes are optimised for our specific problems and it would have been extremely difficult, not to say impossible, to adapt these codes to our needs. On the other hand, over the last ten years an already existing general purpose structural finite element program, FE77, developed at Imperial College by Hitchings [3.11], has been optimised for wave propagation problems [3.12]. The finite element modelling of Lamb waves presents several difficulties which have been studied in the past [3.13]-[3.17] both for mechanical structures and piezoelectric solids. Alleyne studied the interaction of Lamb waves with defects using FE77 [3.18] and developed a two dimensional Fourier transform method that enables different modes to be separated directly from the output displacements monitored within FE77 [3.19]. Pavlakovic [3.20] developed an interface between FE77 with DISPERSE [3.21], [3.22], a software for generating dispersion curves developed at Imperial college, that enables pure Lamb modes to be generated in a finite element model. In order to take advantage of these previous works, it has been decided to add piezoelectric properties to FE77 rather than purchasing a commercial code. Introduction of piezoelectricity in FE77 is done by means of matrix manipulations.

Piezoelectric transducers have been modelled using finite element analysis for more than 25 years [3.5]-[3.8], [3.23]-[3.28], however implementation of piezoelectric properties in an already working structural finite element program presents some specific difficulties [3.29] that we decided to overcome by matrix manipulations. This technique, commonly known under the names reduction or condensation [3.30]-[3.32], presents certain advantages that enabled us to incorporate the piezoelectric equations in the already existing mechanical time marching explicit algorithm without changing its structure.

Implementation of piezoelectric elements in FE77 enables selected analytical results to be checked and helps to estimate the limits of one and two-dimensional models. Selected quantitative predictions that have been made will help us to understand better the electromechanical process and to guide our analytical calculations.

3.2 ADDITION OF THE PIEZOELECTRIC EQUATIONS

This section discusses a way of generating the piezoelectric equations of motion in a method compatible with the already existing structural finite element program FE77. The electromechanical finite element matrix equations relating mechanical and electrical quantities in piezoelectric media are the basis for the derivation of the finite element model. These are derived from the piezoelectric constitutive relations [3.33]

$$\begin{aligned} T &= c^E S - e^t E \\ D &= eS + \varepsilon^S E \end{aligned} \tag{3.1}$$

In the contracted formulation T, S, E and D are vectors and c, ε and e are matrices. T contains the mechanical stresses, S the mechanical strains, E the electric fields and D the dielectric displacements. c^E represents the mechanical stiffness for constant electric field, ε^S the permittivity for constant mechanical strain and e the piezoelectric stress constants. The superscript *t* means transposed. Eq.(3.1) is just one of the possible set of piezoelectric equations and it gives the mechanical stress and electric displacement in terms of the independent variables electric field and strain. It is known as the piezoelectric stress equations. The equations of state for a piezoelectric material can be expressed in various forms by taking other pairs of variables to be independent [3.33], [3.34], [3.35]. For example, choosing the electric field *E* and the mechanical stress *T* as independent variables leads to the piezoelectric strain equations

$$\begin{aligned} S &= s^E T + d^t E \\ D &= dT + \varepsilon^S E \end{aligned} \tag{3.2}$$

where d is a matrix of the piezoelectric strain constants which expresses the magnitude of strain induced by the applied electric field, and the units are in meters per volt, or the magnitude of the electric displacement (in coulombs) per unit applied stress (Newton). The choice between the different forms of piezoelectric constitutive equations depends on the problem to be solved and the mechanical and electrical boundary conditions that

apply. However for the purpose of modelling wave propagation in piezoelectric media, the set of equations Eq.(3.1) is preferred because it is the only one which is suitable for a three-dimensional continuum when no boundaries are present [3.33]. The reason for that is that Eq.(3.1) is the only form that suits a displacement-based FE formulation, since Eq.(3.1) is directly derived from the stress equation of motion (in absence of forces) and the Poisson's equation of electrostatic for an insulator (no free charges), that is

$$\begin{aligned} T &= \rho\ddot{u} \\ \nabla.D &= 0 \end{aligned} \tag{3.3}$$

where ρ is the mass density and $\ddot{u}$ the acceleration. '$\nabla.$' is the conventional symbol for the divergence of a vector. In finite element analysis, the stresses are calculated from the strains therefore strain must be chosen as an independent variable, and as a consequence of that choice it is seen that in absence of piezoelectric coupling, Eq.(3.1) reduces directly to the generalized Hooke's law. Therefore in absence of piezoelectric material the finite element piezoelectric code will reverse simply to the original structural finite element code in which piezoelectric properties have been added.

3.2.1 FINITE ELEMENT FORMULATION OF THE PIEZOELECTRIC EQUATIONS

In electrostatics, that is when charges and current are static, the circulation of the electric field is zero, therefore E is a gradient,

$$E = -\nabla\phi \tag{3.4}$$

where ϕ is the electrostatic potential and is a scalar.

The second law of electrostatics states that the flux of the electric field from a volume is proportional to the charge inside. This is the Gauss' law

$$\nabla.E = \frac{\rho}{\varepsilon_0} \tag{3.5}$$

and in terms of the electric displacement and in the absence of charges it is given by the electrostatic charge equation:

$$\nabla.D = 0 \tag{3.6}$$

Using the symbolic notations introduced by Auld [3.34], Eq.(3.4) can be given by

$$E = -B_\phi\phi \tag{3.7}$$

where

$$B_{\phi} = \begin{bmatrix} \partial/\partial x \\ \partial/\partial y \\ \partial/\partial z \end{bmatrix} \tag{3.8}$$

The mechanical strain *S* is related to displacement through:

$$S_{ij} = \frac{1}{2}\left(\frac{\partial u_i}{\partial x_j} + \frac{\partial u_j}{\partial x_i} \right) \qquad i, j = 1, 2, 3 \tag{3.9}$$

and in Cartesian coordinates, since the strain tensor is symmetric, and using Auld's symbolic notations [3.34], this relation can be given by

$$S = Bu \tag{3.10}$$

where *u* is the vector of mechanical displacements and

$$B = \begin{bmatrix} \partial/\partial x & 0 & 0 \\ 0 & \partial/\partial y & 0 \\ 0 & 0 & \partial/\partial z \\ 0 & \partial/\partial z & \partial/\partial y \\ \partial/\partial z & 0 & \partial/\partial x \\ \partial/\partial x & \partial/\partial x & 0 \end{bmatrix} \tag{3.11}$$

The equation of motion, neglecting the effect of gravity, is given by Newton's law:

$$\rho \frac{\partial^2 u}{\partial t^2} = \nabla . T \tag{3.12}$$

where ρ is the mass density of the medium.

Equations (3.4) to (3.12) constitute a complete set of differential equations, which can be solved with the appropriate mechanical and electrical boundary conditions. The above equations can be expressed in the finite element formulation based on the Hamilton's variational principle. The variational principle which serves to incorporate the piezoelectric effect in the finite element formulation is essentially due to Holland [3.1] and is reported in details by Tiersten [3.35]. It has been formalised in finite element notation by Allik [3.2].

The finite element method reduces the electromechanical partial differential equations over the model domain to a system of ordinary differential equations in time. A problem of an infinite number of unknowns is therefore reduced to one of a finite number of unknowns by dividing the continuum (solution region) into finite elements and expressing the unknown field variables (displacements for solid mechanics problems and potential for electric problems) in terms of an assumed interpolation (shape) function within each element.

The degrees of freedom of the system are the mechanical displacements *u* and the electric potential ϕ. The prescribed quantities are defined as the body forces *F* and the charge *Q*. They are determined at the nodes of the elements. These values at any other arbitrary position on the element are given by a linear combination of polynomial interpolation functions N(x, y, z) with the nodal point values of the quantities as coefficients [3.30]. The discrete nodal values of the field variables can be used to express the continuous behaviour within each element, and the full problem for the continuum is formulated by summing the contributions from each element. For an element with n nodes (nodal coordinates: (x_i, y_i, z_i); i = 1, 2, …, n) the continuous displacement function u(x, y, z) can be evaluated from its discrete nodal point vectors as follows [3.5]

$$u(x,y,z) = N_u(x,y,z)\,\hat{u}(x_i, y_i, z_i) \tag{3.13}$$

where $\hat{u}$ is the vector of nodal point displacements and N_u is the interpolation function for the displacement. All other mechanical and electrical quantities are similarly interpolated with appropriate shape functions. With the interpolation functions for the electrical potential N_ϕ, Eq.(3.4) and Eq.(3.10) can be written:

$$\begin{aligned} E &= -\nabla\phi = \nabla(N_\phi\hat{\phi}) = -B_\phi\hat{\phi} \\ S &= Bu = B(N_u\hat{u}) = B_u\hat{u} \end{aligned} \tag{3.14}$$

Applying this formalism to the local equations yields a set of linear differential equations with a symmetric structure that describe one single piezoelectric finite element

$$m\hat{\ddot{u}} + c_{uu}\hat{\dot{u}} + k_{uu}\hat{u} + k_{u\phi}\hat{\phi} = \hat{F} \tag{3.15}$$

$$k_{u\phi}^t\hat{u} + k_{\phi\phi}\hat{\phi} = \hat{Q} \tag{3.16}$$

Subscript *u* refers to mechanical quantities whereas subscript ϕ refers to electrical quantities. The combination of the two refers to electromechanical coupling matrices, i.e. $K_{u\phi}$ is the finite element equivalent of the material piezoelectric matrix *e*. And $K_{\phi\phi}$ is the finite element equivalent of the capacitance matrix ε. On an element basis, i.e. before assembling the global matrices, the local matrices are given by

$$k_{uu} = \iiint B_u^t c^E B_u \, dV \tag{3.17}$$

$$k_{u\phi} = \iiint B_u^t e^t B_\phi \, dV \tag{3.18}$$

$$m = \iiint \rho N_u^t N_u \, dV \tag{3.19}$$

If the damping is chosen to be the Rayleigh damping [3.30], [3.31], [3.32] then the global damping matrix is given by

$$c_{uu} = \beta^{(e)} \iiint B_u^t c^E B_u \, dV + \alpha^{(e)} \iiint \rho N_u^t N_u \, dV \tag{3.20}$$

where the Rayleigh coefficients α and β are constants but can vary from element to element. α is the mass factor and this affect the low frequency damping. β is the stiffness factor and this will affect the high frequency damping. More details about the modelling of the damping is given in section 3.3.2.2.

The forces and charges are given by:

$$\begin{aligned} \hat{F} &= \int N_u^t N_f \, f^{(e)} \\ \hat{Q} &= \int N_u^t N_q \, q^{(e)} \end{aligned} \tag{3.21}$$

where the integral is a volume integral for body forces and a surface integral for surface forces and/or charges. Forces and charges can also be applied at local points; in such a case integration over the element surface or volume is not required and we have

$$\begin{aligned} \hat{F}_p &= N_u^t F_p^{(e)} \\ \hat{Q}_p &= N_\phi^t Q_p^{(e)} \end{aligned} \tag{3.22}$$

The complete finite element mesh is therefore mathematically described by a set of global differential equations

$$M\ddot{u} + C_{uu}\dot{u} + K_{uu}u + K_{u\phi}\phi = F \tag{3.23}$$

$$K_{u\phi}^t u + K_{\phi\phi}\phi = Q \tag{3.24}$$

where the quantities u, F, ϕ and Q are the global field quantities, and M, C and K are the assembled global matrices. For a three-dimensional piezoelectric mesh made of *n* nodes there are three mechanical degrees of freedom per node, the three components of the displacement vector, and one electrical degree of freedom, the electric potential. Therefore, at each time step, a coupled system of *3n* equations (3.23) and *n* equations (3.24) must be solved.

Eq.(3.23) and (3.24) can be assembled together in a single matrix equation:

$$\begin{bmatrix} M_{uu} & 0 \\ 0 & 0 \end{bmatrix} \begin{pmatrix} \ddot{u} \\ \ddot{\phi} \end{pmatrix} + \begin{bmatrix} C_{uu} & C_{u\phi}^t \\ C_{u\phi} & C_{\phi\phi} \end{bmatrix} \begin{pmatrix} \dot{u} \\ \dot{\phi} \end{pmatrix} + \begin{bmatrix} K_{uu} & K_{u\phi}^t \\ K_{u\phi} & K_{\phi\phi} \end{bmatrix} \begin{pmatrix} u \\ \phi \end{pmatrix} = \begin{pmatrix} F \\ Q \end{pmatrix} \tag{3.25}$$

Unfortunately the global mass matrix of the system of Eq.(3.25) is singular due to the zero associated with the piezoelectric terms. This means it cannot be inverted which causes problems with transient solution techniques discussed in section 3.3. The problem may be solved by reducing the electrical degrees of freedom in such a way that only one system of equations is to be solved but with no singular matrix. This method is discussed below.

3.2.2 REDUCTION OF THE MATRIX STRUCTURAL PIEZOELECTRIC PROBLEM

Reduction, which may also be called "condensation", is a way of making a few degrees of freedom (d.o.f) represent all the d.o.f of the model. Thus the size of the matrices is reduced and in some problems an analysis can be performed more cheaply and more quickly [3.30]. In mechanical problems the disadvantage of reduction is the introduction of some error and uncertainty into the analysis. However for a piezoelectric problem since we do not attempt to reduce the mass matrix of the model but only to get rid of the zeros in the lower part of the global mass matrix, errors and uncertainty should not appear.

Referring to the reduction process in stress analysis finite element models, some d.o.f are called masters which dictate the motion of other d.o.f called slaves. Slaves are discarded and masters retained. The order of matrices in the reduced problem is equal to the number of masters. The most commonly used method is the Guyan's reduction [3.36]. Its principal assumption is that inertia forces on slaves are negligible in comparison with elastic forces transmitted to slaves by the motion of masters. Transposing this method to Eq.(3.25), the electric potential d.o.f. are the slave d.o.f. of the elastic displacement d.o.f.. The slave-master relation is easily extracted and is given by

$$\phi = -K_{\phi\phi}^{-1}\left(Q - K_{u\phi}u - C_{u\phi}\dot{u}\right) \tag{3.26}$$

Hence the piezoelectric problem reduces, in absence of electric and piezoelectric damping, to:

$$M\ddot{u} + C_{uu}\dot{u} + \left[K_{uu} - K_{u\phi}^{t}K_{\phi\phi}^{-1}K_{u\phi}\right]u = F - K_{u\phi}^{t}K_{\phi\phi}^{-1}Q \tag{3.27}$$

The solution of this equation yields the mechanical displacements and the electric potentials can be obtained from Eq.(3.26). This reduction technique has been done before for reducing the size of dynamic problems, but we found no evidence that this technique has been used in the past for structural-piezoelectric problems. Articles on the implementation of piezoelectricity in time marching finite element algorithm are rare [3.2], [3.10] and none discuss the detail of the algorithm, and there are no books on the subject. It is seen that the only difficulties in solving this problem are in the inversion of the mass and the capacitance matrices. The time marching algorithm is therefore quite simple in theory and we will now discuss how it is handled in FE77.

3.3 DIRECT INTEGRATION METHODS

The equation system to be solved is the following:

$$M\ddot{u} + C\dot{u} + Ku = F \tag{3.28}$$

where u is the vector containing the generalised nodal displacements, and $\dot{u}$ and $\ddot{u}$ are the corresponding velocities and accelerations at the same time. F is the vector of applied nodal forces and can be varying with time. Matrices M, C, and K, represent the assembled mass, damping and stiffness matrices.

Eq.(3.28) is the finite element formulation of the second order differential dynamic equation of motion. For linear problems, as we are concerned with in this thesis, these matrices are invariant with time. The displacements, velocities and accelerations are assumed to be known at initial time t_0.

The problem then is to solve Eq.(3.28) for the acceleration at some later time $t_1 = t_0 + \Delta t$, where Δt is the time increment. There are two techniques to solve Eq.(3.28), the direct integration and the mode superposition. In this thesis we are only concerned with direct integration methods. In direct integration the equations in Eq.(3.28) are integrated using a numerical step-by-step procedure and "direct" means that prior to the numerical integration, no transformation of the equations in Eq.(3.28) into different form is carried out [3.30]. There are two basic iterative approaches to solving these equations directly, the implicit method where attempts are made to solve the exact equations at time t_1 and explicit methods where only an approximate form of the equation at time t_1 is solved. In both cases, successive temporal values of the displacements and forces are calculated, denoted by u_n and F_n, and correspond to the values calculated and applied at $t_1 = t_0 + n\Delta t$. This means firstly, that equilibrium is sought at discrete time points within the interval of solution and secondly, that a variation of displacements, velocities and accelerations is assumed within each time step. In the following sections we only consider the Newmark-β implicit and the central difference explicit solutions forms, since these are the two methods implemented in FE77. More details on these two methods in a general context, along with other implicit and explicit methods, may be obtained from Bathe [3.30] and Zienkiewicz [3.31].

3.3.1 THE IMPLICIT SOLUTION FORM

For the implicit solution, using the Newmark-β or other implicit method, the equations to be solved are written in the form

$$M\ddot{u}_1 = F_1 - C\dot{u}_1 + K u_1 \tag{3.29}$$

The intention is then to satisfy the complete solution at time t_1. This has to be done by some iterative technique, typically by a Newton-Raphson method. This means that the system is assumed to be at equilibrium at a given time in the future and the displacements are obtained by solving the simultaneous equations. In theory, it should be possible to solve the implicit solution form for any time step Δt. For linear problems it is used to develop unconditionally stable solution methods that give a solution for any step size. The major drawback of implicit schemes is that a matrix of the order of the number of degrees of freedom has to be inverted. This is a very restrictive condition for large models and practically, it imposes the condition for the matrix to be diagonal.

One practical implementation of the implicit solution form is the Newmark-β method in which the process of time marching uses a linear acceleration assumption combined linearly with a constant acceleration assumption. In other words the acceleration at time at time (Δt + t) is deduced from that at time t using a combination of linear and constant variation during the interval of time (Δt). By changing the parameter β the proportion of linear acceleration to constant acceleration is changed. Hence in this method pure constant acceleration or pure linear acceleration assumptions may be used. Before developing further the equations of the Newmark-β method we shall discuss the constant and linear acceleration assumptions.

3.3.1.1 Constant and Linear Accelerations

For both the explicit and implicit methods the time response has to be advanced with time. An assumption is made as to how the acceleration (or displacement or velocity) changes with time. At time t_0 the response quantities, $\ddot{u}_0$, $\dot{u}_0$ and u_0 are known. Assuming that the equations have been solved at time t_1 then, using either the implicit or explicit forms, the acceleration at the end of the step, $\ddot{u}_1$, will also be known. Assuming that the acceleration varies linearly, as shown in Figure 3.1, over the time step, then the acceleration at any time t can be written as

$$\ddot{u}(t) = \left(1 - \frac{t - t_0}{\Delta t}\right)\ddot{u}_0 + \frac{t - t_0}{\Delta t}\ddot{u}_1 \tag{3.30}$$

This can be integrated to give the velocity and integrated again to give the displacement. At the end of the step this gives

$$\dot{u}_1 = \frac{\Delta t}{2}\ddot{u}_0 + \frac{\Delta t}{2}\ddot{u}_1 + \dot{u}_0 \quad \text{and} \quad u_1 = \frac{\Delta t^2}{3}\ddot{u}_0 + \frac{\Delta t^2}{6}\ddot{u}_1 + \Delta t\,\dot{u}_0 + u_0 \tag{3.31}$$

Other assumptions can also be used since the response at all previous time steps is known. The simplest form is to assume that the acceleration is constant over the time step, so that $\ddot{u}(t) = \ddot{u}_0$, as shown in Figure 3.2. Integrating this gives the velocity and displacements at the end of the step as

$$\dot{u}_1 = \Delta t\,\ddot{u}_0 + \dot{u}_0 \quad \text{and} \quad u_1 = \frac{\Delta t^2}{2}\ddot{u}_0 + \Delta t\,\dot{u}_0 + u_0 \tag{3.32}$$

In FE77 the linear variation, or a combination of constant and linear variations, is used for the Newmark-β method.

3.3.1.2 The Newmark-β Method

The parameter β in the Newmark-β method is used to change the proportion of linear acceleration to constant acceleration. A linear combination of the constant acceleration and the linear acceleration, gives from Eq.(3.31) and Eq.(3.32), the combined velocities as :

$$\dot{u}_{t+\Delta t} = \left(a_1 \Delta t - \frac{a_2 \Delta t}{2} \right) \ddot{u}_t + \frac{a_2 \Delta t}{2} \ddot{u}_{t+\Delta t} + (a_1 + a_2) \dot{u}_t \tag{3.33}$$

where a_1 and a_2 are the constants of proportionality. Since the velocity at the start of the step must be $\dot{u}_t$ then $(a_1+a_2) = 1$ so that

$$\dot{u}_{t+\Delta t} = (2 - a_2) \frac{\Delta t}{2} \ddot{u}_t + \frac{a_2 \Delta t}{2} \ddot{u}_{t+\Delta t} + \dot{u}_t \tag{3.34}$$

Similarly the combined displacements, using values b_1 and b_2 as the constants of proportionality, become

$$u_{t+\Delta t} = \left(b_1 \frac{(\Delta t)^2}{2} + b_2 \frac{(\Delta t)^2}{2} \right) \ddot{u}_t + \frac{b_2 (\Delta t)^2}{6} \ddot{u}_{t+\Delta t} + (b_1 + b_2)(\Delta t \, \dot{u}_t + u_t) \tag{3.35}$$

and again the condition $(b_1+b_2) = 1$ must be satisfied giving,

$$u_{t+\Delta t} = (3 - b_2) \frac{(\Delta t)^2}{2} \ddot{u}_t + \frac{b_2 (\Delta t)^2}{6} \ddot{u}_{t+\Delta t} + \Delta t \, \dot{u}_t + u_t \tag{3.36}$$

With $b_2 = 1$ and $a_2 = 1$ then the basic linear acceleration interpolation form is recovered. With $a_2 = 0$ and $b_2 = 0$ the constant acceleration form is recovered.

The conventional definition for the Newmark-β [3.37] method has $b_2 = 6\beta$; $b_1 = (1-6\beta)$; $a_2 = 2\gamma$; $a_1 = (1 - 2\gamma)$, hence

$$\begin{aligned} \dot{u}_{t+\Delta t} &= (1-\gamma) \Delta t \, \ddot{u}_t + \gamma \Delta t \, \ddot{u}_{t+\Delta t} + \dot{u}_t \\ u_{t+\Delta t} &= \left(\frac{1}{2} - \beta \right) \Delta t^2 \, \ddot{u}_t + \beta \Delta t^2 \, \ddot{u}_{t+\Delta t} + \dot{u}_t + u_t \end{aligned} \tag{3.37}$$

The Newmark-β form of the implicit solution is then

$$\begin{aligned} \left(M + \gamma \, \Delta t \, C_{t+\Delta t} + \beta \Delta t^2 \, K_{t+\Delta t} \right) \ddot{u}_{t+\Delta t} = R_{t+\Delta t} &- C_{t+\Delta t} \left[(1-\gamma) \Delta t \, \ddot{u}_t + \dot{u}_t \right] \\ &- K_{t+\Delta t} \left[\left(\tfrac{1}{2} - \beta \right) \Delta t^2 \, \ddot{u}_t + \Delta t \, \dot{u}_t + u_t \right] \end{aligned} \tag{3.38}$$

3.3.1.3 Approximate Newmark-β Form in FE77

It is seen in Eq.(3.29) that the mass matrix M on the left-hand side must be inverted to solve for the acceleration at time $(\Delta t + t)$. To overcome this problem an assumption may be used stating that the changes in displacements and velocities during the time interval Δt are small enough so that Eq.(3.29) may be written at time $(\Delta t + t)$ as

$$M \ddot{u}_{t+\Delta t} = F_{t+\Delta t} - C \dot{u}_t - K u_t \tag{3.39}$$

Then since the lumped mass matrix is diagonal, the acceleration at time Δt + t is given by

$$\ddot{u}_{t+\Delta t} = M^{-1}(F_{t+\Delta t} - C\dot{u}_t - K u_t) \tag{3.40}$$

The displacement and the velocity at the end of the step are calculated by integration of the acceleration assuming the combined constant-linear acceleration assumption, that is

$$\ddot{u}_{t+\Delta t} = -\left(\frac{1}{2\beta} - 1\right)\ddot{u}_t + \frac{1}{\beta \Delta t}\ddot{u}_{tt} + \frac{1}{\beta \Delta t^2}(u_{t+\Delta t} - u_t) \tag{3.41}$$

leading to

$$\begin{aligned} \dot{u}_{t+\Delta t} - \dot{u}_t &= (1-\gamma)\Delta t\,\ddot{u}_t + \gamma \Delta t\,\ddot{u}_{t+\Delta t} \\ u_{t+\Delta t} - u_t &= \Delta t\,\dot{u}_t + \frac{\Delta t^2}{2}(1-2\beta)\ddot{u}_t + \beta \Delta t^2\,\ddot{u}_{t+\Delta t} \end{aligned} \tag{3.42}$$

The major drawback of this approximate form of the Newmark-β method is that there is no combination of a_2 and b_2 that lead to an unconditionally stable solution, hence that the algorithm needs numerical damping to stay stable [3.37]. It must be noted that this approximation of the implicit Newmark-β method assumes that the system is at equilibrium at time t to calculate the acceleration at time (Δt+t) which is the usual assumption used in the explicit algorithm.

3.3.2 THE EXPLICIT SOLUTION FORM

In the explicit method the solution for the displacement at the end of the time step is sought using the equilibrium condition at the beginning of the time step, therefore the equations to be solved are written in the form

$$M\ddot{u}_1 = F_1 - C\dot{u}_0 + K u_0 \tag{3.43}$$

The acceleration at time t_1 is determined from the known displacements and velocities at time t_0. In this case the equations to be solved are only an approximation to the true one. However, if the time step Δt tends to zero then the equations tend to the exact ones. In fact this assumption is not quite as bad as it appears at first sight. For most structural problems the damping is low and the response is largely determined by the stiffness and inertia forces, Ku and Mü respectively. In addition the displacement, being the double integral with respect to time of the acceleration, changes less rapidly than the acceleration over a small time step. It takes some time for the displacement to change but the acceleration can change immediately. This means that the assumption that the stiffness force is defined by its value at the start of the step is a much better approximation than assuming that the inertia force at the end of the step is the same as that at the start. However, the stiffness force assumption does mean that the explicit solution method can only ever be used with a small time interval Δt. This is the major

drawback of explicit solution: the solution is stable only if the growth of the disturbance is bounded. Therefore the time interval must be less than a critical time interval. Physically this restriction is that no energy may be propagated through the mesh spacing in under a time step. This condition is discussed later in more detail, for the central difference method. The major advantage of the explicit schemes is that the stiffness matrix *K* does not require factorisation in the step-by-step solution.

The only unknown in Eq.(3.43) is the acceleration, $\ddot{u}_1$, which can be found by inverting the mass matrix,

$$\ddot{u}_1 = M^{-1}(F_1 - C\dot{u}_0 + K u_0) \tag{3.44}$$

For almost all implementations of the explicit solution method the mass matrix *M*, is idealised to be a diagonal matrix, making the inversion M^{-1} trivial, although using a diagonal mass matrix is not a necessary requirement for explicit solution methods. Once the acceleration at the end of the step is known, the time step can be advanced, typically assuming linear variation of acceleration, to give the velocity and the displacement as in Eq.(3.31). The solution at the end of the step is then known and can be used as the starting conditions for the next step.

3.3.2.1 The Central Difference Explicit Method

It can be shown that most of the numerical methods of integration can be written in a similar form, the difference being in the value of coefficients affecting displacements and their derivatives. More details about the central difference method may be found in the text book by Bathe [3.30]. The characteristic of the central difference method is that velocities and accelerations are only approximated from displacements at different time positions as shown by

$$\ddot{u}(t) = \frac{1}{(\Delta t)^2}\left(u_{t-\Delta t} - 2u_t + u_{t+\Delta t}\right) \tag{3.45}$$

$$\dot{u}(t) = \frac{1}{2\Delta t}\left(u_{t-\Delta t} + u_{t+\Delta t}\right) \tag{3.46}$$

The initial condition on the velocity at time *t* is approximated, via a second order Taylor expansion, by an initial condition on the displacement at the previous time step. Substitution of Eq.(3.45) and Eq.(3.46) into Eq.(3.44) yields

$$\left(\frac{M}{(\Delta t)^2} + \frac{C}{2\Delta t}\right)u_{t+\Delta t} = R_t - \left(K - \frac{2M}{\Delta t}\right)u_t - \left(\frac{M}{(\Delta t)^2} - \frac{C}{2\Delta t}\right)u_{t-\Delta t} \tag{3.47}$$

from which we can solve for the displacement at the next time step, $u_{\Delta t+ t}$.

This method has two disadvantages. First as mentioned in the previous section, to be numerically stable this integration method must advance in time by a controlled

interval, which necessarily limits the computation speed. Secondly, when the damping matrix C is non null the inherent advantage of the explicit method disappears since a matrix (a representation of the stiffness matrix) which is not diagonal has to be factorised and inverted. Moreover, when piezoelectricity is added, the damping matrix contains also electrical and the piezoelectric damping. This means that in order to have a non singular damping matrix, electric loss must be added to the entire piezoelectric region. This problem can be overcome in theory by condensing the electric degrees of freedom, as discussed in section 3.2.2. However it then leads to a system of equations involving, at each time step, an enormous amount of matrix operations which, in practice, precludes from using such a technique when damping is to be modelled.

3.3.2.2 Modelling of Damping

In many cases, when damping is introduced in a FE model, it is ill defined and not expressed as a real damping matrix. Since the explicit solution obtains the response for all frequencies, including the highest, the computed response tends to "ring" at the high frequencies, especially for shock type loadings. To overcome this it is common to include some form of numerical damping, in the form of a damping matrix, to control this high frequency ringing. One technique for doing this is to assume the numerical damping is in the form of Rayleigh damping [3.30], [3.31], [3.32]:

$$C = \alpha M + \beta K \tag{3.48}$$

where M is the diagonal mass matrix, K is the stiffness matrix and α and β are constants to control the level of damping. α is the mass factor and this affect the low frequency damping. β is the stiffness factor and this will affect the high frequency damping. Including the numerical damping the explicit form of the equations of motion become

$$\ddot{u}_1 = M^{-1}(F_1 - C\dot{u}_0 - \alpha M\dot{u}_0 - \beta K\dot{u}_0 + K u_0) \tag{3.49}$$

Eq.(3.49) can be written in the form

$$\ddot{u}_1 = M^{-1}(F_1 - F_{C0} - F_\beta + F_{K0}) - \alpha M^{-1} M\dot{u}_0 \tag{3.50}$$

where

$F_{CO} = C\dot{u}_0$ = the damping force

$F_{KO} = K u_0$ = the stiffness force

$F_\beta = \beta K\dot{u}_0$ = the numerical stiffness damping

$\alpha M^{-1} M\dot{u}_0$ = the numerical mass damping

3.3.2.3 Choice of Time Step for the Explicit Method

One major problem with any explicit solution form, and the central difference method in particular, is the fact that it becomes unstable if the time step is above a critical value. It is necessary to use a small enough time step for the solution to be stable. For a given duration of response the computational time is directly proportional to the time step so that it is necessary to choose a time step as close to the stability limit as possible in order to minimize the computation time. A physical interpretation of the critical time step can be made by considering the propagation of a disturbance through the structure. A wave will travel between points at some velocity defined by the material properties. In many cases this is the speed of sound in the material. In the bulk of an isotropic material the quickest wave is the compression wave whose velocity is determined by the stiffness and the material density. This can be used to estimate the explicit time step [3.38]. For the explicit central difference scheme, Blake [3.13] enacted a simple rule which states that the time step must be less than the time needed by a longitudinal wave to reach the next node. When using the explicit central difference form within FE77, the time step is being defined by the relationship:

$$\Delta t = 0.8 \frac{\min(\Delta x, \Delta y, \Delta z)}{C_L} \tag{3.51}$$

where $\Delta x, \Delta y$ and Δz are the dimensions of the elements and C_L is the longitudinal phase velocity. The factor 0.8 has been determined empirically [3.12]. Eq.(3.51) implies that the time step is set to a fixed value all through the course of the calculation.

3.3.3 DISCUSSION

For linear problems, FE77 allows the user to choose between the approximated Newmark-β implicit method and the central difference explicit method. The best choice between these two methods depends on the analysis to be conducted. For wave propagation problems the central difference method is more suitable. The major drawback of the Newmark-β integration method for wave phenomena is that accurate solution requires a time step smaller than one-tenth the period of the highest frequency to be resolved. This is close to the stability limit for explicit methods and effectively removes the principal advantage of implicit integration [3.39]. Another reason to prefer the central difference algorithm for the analysis of wave phenomena is that no numerical damping is required to stabilize the integration. Therefore a wave may propagate along the structure without being artificially damped. This is of great importance for reflection coefficient prediction, for example.

When choosing which method is suitable, the efficiency of the algorithm in terms of time cost is also important. Two parameters directly affect the time of computation: the number of time steps during the solution interval and the number of equations to solve at each time step, that is the number of nodes times the number of degrees of freedom (d.o.f) at each node. Since the step length is proportional to the element size, or in other words to the time period of the highest frequency of the mesh, very many steps will be required to solve for a typical response. It is essential that the

numerous calculations per step are minimised. When dealing with high frequency (typically a few MHz) waves propagating in plate-like structures the number of degrees of freedom in the model can very easily exceed 100,000. Such analyses are very demanding in terms of memory and anything involving a disc access at each step should be eliminated, all of the required quantities being held in the fast memory of the computer. The central difference algorithm enables massive reduction in the amount of information to be accessed and stored in memory. The efficiency of the central difference method lies in considering the precise details of its implementation and coding and, in general, explicit central difference algorithm are attractive because they enable numerical integration to be performed with a minimum of information and therefore to run large models.

For these reasons, all the finite element analyses presented in this thesis have been run using the central difference algorithm without any damping, either mechanical, electric or piezoelectric. Eq.(3.47) is then reduced to

$$\frac{M}{(\Delta t)^2} u_{t+\Delta t} = F_t - \left(K - \frac{2M}{\Delta t} \right) u_t - \frac{M}{(\Delta t)^2} u_{t-\Delta t} \tag{3.52}$$

from which the displacement at the next time step is calculated from the displacement at the present time and the displacement at the previous time step. This equation can be even further reduced by calculating the displacement increment directly as:

$$2\Delta u = u_{t+\Delta t} - u_{t-\Delta t} = (\Delta t)^2 M^{-1} (F_t - K) - 2\Delta t M^{-1} u_t \tag{3.53}$$

Alleyne [3.12] carried out numerous analyses of the propagation of Lamb waves and their interaction with defects in plates using FE77 and the central difference explicit method. Results, thoroughly validated against experiments, show that the phase velocity of Lamb modes can be predicted with errors of less than 0.5%. In order to obtain accurate solutions the number of nodes per wavelength should be greater than eight. For quadrilateral 4-noded two-dimensional elements, this rule should be applied strictly. Too fine a mesh increases the number of degrees of freedom and therefore the size of the matrices and also the time step is reduced proportionally so to get to a particular future time more intermediate calculations are required. When particles of a piezoelectric material move they generate an electric field which in turn generate motion. This effect is called piezoelectric stiffening since, for static cases, it can be described as equivalent to a change in the stiffness of the material. This was discussed in great detail by Auld [3.34] and is summarized in section 3.5.1.1. Any change in the stiffness involves a change in the speed of sound travelling in such materials and therefore, when modelling piezoelectric material, particular attention must be given to the calculation of the critical time step, as given in Eq.(3.51).

3.4 TRANSIENT ALGORITHM IN FE77

FE77 is a general-purpose finite element program. It has all three aspects that are generally taken as making up a finite element program: a mesh generation facility, an analysis facility and a results presentation facility.

This program has a modular architecture, where the definition of the modules is based upon the characteristics of any finite element analysis. Typically, the solution of a finite element problem requires a mesh to be specified (module GEOMETRY), boundary conditions to be given (module SUPPORT), the finite element equations to be assembled (module ASSEMBLE), the loads to be applied (module LOAD) and the equations to be solved (module SOLVE). The user calls these modules to define the analysis that is to be conducted and gives input data to them as they are called. The modular structure of program is shown in Figure 3.3.

3.4.1 THE FE77 PROGRAM STRUCTURE

The database initialisation phase allows the user to define the basic attributes of the analysis. The executive module then calls the required modules for the analysis. Each module writes the data it generates either to the analysis database or to the output files. All modules communicate with each other via the analysis database and pass control back to the executive module when it is finished.

The input to FE77 can either be in the form of an input file for batch analysis or via menus for interactive input. In both cases the data command structure is the same, however for detailed analysis it is more efficient to use the batch analysis. See Appendix A for an example of the input data for a simple piezoelectric plate.

AWAVE is a time marching integration module which has been developed by Alleyne [3.12] in order to efficiently model the generation and the propagation of Lamb waves. For wave propagation problems the central difference algorithm is better suited than the Newmark-β method, since for proper Lamb wave analysis in non-lossy materials the amplitude of the propagating pulse must not decrease with distance. However when the analysis requires damping then the user can switch to the Newmark-β algorithm and set either the Rayleigh damping coefficients or a viscous damping matrix (which can be seen as an equivalent of the complex parts of the stiffness coefficients). Our main contribution here was to add the piezoelectric constitutive equations to the central difference algorithm in the AWAVE module.

3.4.2 SECOND ORDER TIME MARCHING INTEGRATION ALGORITHM

The structure of the algorithm is simple and is summarised in 5 steps:

1. Accessing data

2. Initialisation

3. Assembling matrices

4. Time marching integration

5. Storing and processing results

FE77 has been developed in the order of efficiency. This depends on several factors such as the use of efficient finite elements, efficient programming methods and sophisticated use of available computer hardware and software and also the use of appropriate numerical methods. The numerical procedures involved at each of the steps aforementioned are well known and only the processes specific to the implementation of piezoelectricity are discussed here and a particular attention is given to the matrix manipulations.

In FE77 the assembly of forces, as defined in Eq.(3.50) are performed such that the result of every step in the assembly is only a column vector. No element stiffness matrix, let alone the complete stiffness matrix need be formed, and since the same computation loop is involved in the assembly of each of the forces, these are performed in parallel. Such considerations are vitally important in an explicit solution program since this sequence is likely to be executed millions of times.

In FE77 matrices are stored using an inverted “sky line” scheme [3.30], which consists of storing a matrix column by column, keeping only the diagonal terms and all the non zero terms below the diagonal. Therefore the matrix is banded and only its symmetric part is stored. An additional vector must be stored to indicate how many elements stand in each column. This information is accessible before the matrix is stored and the order of the degrees of freedom can then be rearranged in order to minimize the width of the band. The fact that all non zero elements are clustered around the diagonal of the system matrices greatly reduces the total number of operations. Therefore it was imperative to implement the piezoelectric equations in FE77 without modifying the storage scheme. At the time marching integration level, the dynamic analysis of piezoelectric materials reduces to solving Eq.(3.26), what involves inverting the capacitance matrix $K_{\phi\phi}$ and assembling the charge, and to solving Eq.(3.27), what involves adding the piezoelectric contribution $K_{u\phi}^{t} K_{\phi\phi}^{-1} K_{u\phi}$ to the stiffness matrix K_{uu}, and assembling the forcing charge $K_{u\phi}^{t} K_{\phi\phi}^{-1} Q$. These operations are essentially simple when the matrices are classically stored in memory but they require more attention when the “sky line” storage technique is used.

Because it is stored using the “sky line” technique, the capacitance matrix is a banded matrix, but its inverse is not. However although the direct inversion of the capacitance matrix $K_{\phi\phi}$ is therefore not suitable, the calculation of $K_{\phi\phi}^{-1}\phi$ is possible without changing the “sky line”. This is because the vector storing the potential amplitudes ϕ can be used to decompose the matrix using the Cholesky technique [3.40] in which the capacitance matrix is expressed as the product of triangular matrices *L* obtained from the Cholesky factorisation:

$$K_{\phi\phi}^{-1}\phi = L^{-t}L^{-1}\phi \tag{3.54}$$

Then, by replacing the inverse of the capacitance matrix by its decomposition which respect the "sky line", all the other calculations for which the inversion of the capacitance matrix is required are now simplified and can be done without affecting the memory allocations.

Starting with Eq.(3.27), the first product containing the inverse of the capacitance matrix $K_{\phi\phi}$ is the piezoelectric contribution $K_{u\phi}^{t} K_{\phi\phi}^{-1} K_{u\phi}$ to the stiffness matrix K_{uu}. $K_{u\phi}^{t} K_{\phi\phi}^{-1} K_{u\phi}$ is a matrix which, in general, does not have the same structure as the capacitance matrix and when adding it to the stiffness matrix, the "sky line" format of the stiffness matrix would be modified. Moreover an extra memory space would be necessary to perform the direct assembly of $K_{u\phi}^{t} K_{\phi\phi}^{-1} K_{u\phi}$. However if $K_{\phi\phi}^{-1}$ is replaced by its Cholesky decomposition, the product $K_{u\phi}^{t} K_{\phi\phi}^{-1} K_{u\phi}$ reduces to

$$\tilde{K}_{u\phi}^{t} \tilde{K}_{u\phi} \tag{3.55}$$

with

$$\tilde{K}_{u\phi} = L^{-1} K_{u\phi} \tag{3.56}$$

$\tilde{K}_{u\phi}$ and $K_{u\phi}$ have the same shape therefore $\tilde{K}_{u\phi}$ can be stored in place of $K_{u\phi}$ and the "sky line" is preserved. Therefore the *stiffened* stiffness matrix $\left[K_{uu} - K_{u\phi}^{t} K_{\phi\phi}^{-1} K_{u\phi} \right]$ can be assembled and stored in place of the stiffness matrix K_{uu}.

Similarly, the calculus of the forcing charge $K_{u\phi}^{t} K_{\phi\phi}^{-1} Q$ on the right hand side of Eq.(3.27), is now reduced to

$$\tilde{K}_{u\phi}^{t} L^{-1} Q \tag{3.57}$$

and eventually the overall calculation of the electric potential, as given by Eq.(3.26) is now given by:

$$\phi = L^{-t} \left(L^{-1} Q - K_{u\phi} u \right) \tag{3.58}$$

This technique to implement the piezoelectric equations in the existing program by condensing the electrical degrees of freedom and without modifying the assembling technique of the matrices is very close to the *static condensation* algorithm [3.41], and is rather economical in terms of matrix manipulation. Further advantage in keeping the same structure for all the matrices is that the same storage space can be used successively. This is rather important in FORTRAN 77, language in which FE77 is written, where memory allocation is decided at the beginning. The technique described above is employed to reduce the number of nodal degrees of freedom and thus, in effect,

to perform part of the solution of the total finite element system equilibrium equations prior to solving the system of dynamic equation, that is calculating the acceleration at each time step. Finally the acceleration, once all the contributing forces have been assembled, is given by

$$\ddot{u} = M^{-1}\left(F - \tilde{K}^{t}_{u\phi}\, L^{-1} Q - C_{uu}\,\dot{u} - \left[K_{uu} - \tilde{K}^{t}_{u\phi} K^{t}_{u\phi}\right] u\right) \tag{3.59}$$

and then the central difference algorithm enables us to calculate the displacement increment as given in Eq.(3.53). This ends the time marching calculations and if it is repeated until the last time step is passed, the model is complete.

However extra calculations may prove to be very valuable for transducer characterisation, in particular the determination of the electromechanical coupling and the input impedance of the piezoelectric medium. Values of coupling and impedance given in text books or provided by manufacturers may be either experimentally measured or calculated via simple calculations that assume a one-dimensional behaviour. Using a finite element code to compute them allows better comparison with experimental data. Before developing the implementation of the electromechanical coupling coefficients and the electrical impedance it is necessary to look in some details at the electrical boundary conditions that apply to FE77.

3.4.3 ELECTRICAL BOUNDARY CONDITIONS

A finite element model is by nature limited in all its dimensions and at the outer surfaces, the appropriate boundary conditions must be satisfied. The mechanical boundary conditions are not changed by the introduction of piezoelectric properties in the structural code. At the free surface of the piezoelectric continuum they are given as follows

$$n_i T_{ij} = 0 \tag{3.60}$$

where n_i is the outward unit normal to the external surface.

Concerning the electrical boundary conditions, the difficulties arise from the fact that the outer surface of a piezoelectric body is in fact an interface between two dielectric media, and this surface can be either free or partly electroded. Problems involving electrical open boundaries in finite elements programs have been studied extensively in the past for electromagnetic waves [3.42], [3.43] and even recently for piezoelectric finite element problems [3.44].

The first important issue we must consider is the modelling of the external electrostatic field. The physics tell us that the infinite exterior region of a piezoelectric device adheres to Laplace's equation. In FE77, for the analysis of piezoelectric vibrations, the electrical field external to the crystal is neglected. In practice this is usually justified for materials with large values of relative permittivity. However for those crystals [3.45] that possess both low relative permittivity and strong piezoelectric

coupling, the electric leakage is not negligible and the vibrations in the piezoelectric device are affected. This problem was resolved, for example, by Antonova [3.44], by defining a "super element" that encircles the outer boundary. Such a procedure does not exist in FE77 and therefore no electromechanical wave can be modelled to propagate away from the model, just as it would be the case for a device in vacuum. Therefore the electrical boundary condition along a free surface is that the component of the electric displacement, normal to that surface, is zero

$$n_i D_i = 0 \tag{3.61}$$

where n_i denotes the components of the unit normal to the surface. Since there is no field in the outer region, then the potential along the outer boundary of the piezoelectric model can be set to zero. If part of the outer surface is electroded, in the general case, at an electrode some relation between the potential ϕ and the components of the electric displacement D, normal to the electrode must be found. In practice either the surface charge or the potential must be specified on the electrode:

$$n_i [D_i] = \bar{\sigma} \qquad \text{or} \qquad \phi = \bar{\phi} \tag{3.62}$$

where $[D_i]$ denotes the jump in the electric displacement at the surface, but since in FE77 the outer medium is not modelled, the jump $[D_i]$ reduces to D_i. $\bar{\sigma}$ is the applied surface charge density and $\bar{\phi}$ is the prescribed potential. If the electrode is driven by the applied surface charge density, the total charge on the electrode is given by

$$Q = -\int_S n_i D_i dS \tag{3.63}$$

Let us now consider the situation where a piezoelectric device is driven by a voltage signal applied at a very thin electrode. If its mechanical influence is considered negligible, the electrode can be modelled simply by specifying the electric potential ϕ at each node *i* of the surface and the sum of charges on the electrode is zero.

$$\phi_i = \bar{\phi} \quad \text{and} \quad \sum Q_i = 0 \tag{3.64}$$

If the electrode is grounded, all the nodes of the electrode must be set to a fixed value. This is done in FE77 by supporting the electrical degree of freedom at these nodes in the same way that mechanical boundary conditions are enforced: the relevant degrees of freedom at the fixed boundaries are simply specified to be fixed. Therefore at all nodes along the grounded electrode the potential is set to zero.

If a pair of electrodes operates, each are set to different potentials, and the difference is equal to the voltage applied between the electrodes. In real experiments the two electrodes operate into a circuit of admittance Y and the current I and the voltage V are related by the condition

$$I = \int_S n_i \frac{\partial D_i}{\partial t} ds = \pm YV \tag{3.65}$$

where n_i denotes the components of the unit normal to the electrode of area S, and the $\pm$ depends on the orientation of the coordinate axes. However FE77 does not allow us to model the effect of external electric circuits, therefore the two electrodes in FE77 are independent. This situation corresponds to that of a device operated with open-circuited electrodes.

3.4.4 ELECTROMECHANICAL COUPLING COEFFICIENTS

The piezoelectric crystal in an ultrasonic transducer behaves as an electromechanical device. It is important that the electric to acoustic energy conversion is maximised to achieve optimal performance of the transducer. The electromechanical coupling coefficient (EMCC) is widely accepted as such a measure of conversion efficiency [3.48]. The magnitude of the electromechanical coupling coefficient of a mode of vibration represents the significance of that particular mode compared with other modes, and as reported by Lerch [3.5], the larger the electromechanical coupling coefficient of the mode of interest, the lower the insertion loss and the broader the bandwidth of the transducer. In fact, the EMCC characterises a piezoelectric element better than do the sets of elastic, dielectric and piezoelectric constants since it allows materials of different levels of permittivity and/or compliance to be directly compared. Many other ways to quantify the effectiveness of a transducer can be defined, depending on the physical phenomenon to be quantified. For example Smith [3.46] defines a particular figure of merit that assesses the quality of hydrophones.

Although the literature describes several approaches, there are two main definitions for the determination of the EMCC. It can be defined either by using energy considerations [3.47], or by determining the resonant frequencies of the crystal submitted to an electrical excitation [3.33]. The method of determining the EMCC which is supported by the IEEE standards on piezoelectricity [3.33] is based on the experimental determination of the resonant frequencies of the crystal, for instance by a network analyser. On the other hand the ratio of energies lends itself easily to evaluation by numerical methods.

The general concept of the EMCC is introduced as follows [3.48]: the square of the EMCC is the ratio of the electrical energy stored in the volume of a piezoelectric body and capable of conversion, to the total mechanical energy supplied to the body. The first mathematical formulation of this concept was provided by Berlincourt [3.47]. By neglecting the thermal and magnetic terms the internal energy of a linear piezoelectric system is given by:

$$U = \tfrac{1}{2} S_I T_I + \tfrac{1}{2} D_i E_i \qquad I = 1 \text{ to } 6, i = 1 \text{ to } 3 \tag{3.66}$$

Using the set of piezoelectric equation given in Eq.(3.1), Eq.(3.66) may be written:

$$U = \tfrac{1}{2}\left(S_I c_{IJ}^E S_J\right) + \tfrac{1}{2}\left(E_i e_{iJ} S_J - S_I e_{Ji} E_j\right) + \tfrac{1}{2}\left(E_i \varepsilon_{ij}^S E_j\right) \qquad I, J = 1 \text{ to } 6, \;\; i, j = 1 \text{ to } 3 \tag{3.67}$$

This equation differs from that given in the literature [3.47] since we used the set of piezoelectric equations given by Eq.(3.1) whereas Berlincourt [3.47] used the set of equations given by Eq.(3.2). Therefore Eq.(3.67) is given here as a function of the mechanical strains and the electric field whereas Berlincourt [3.47] developed Eq.(3.66) as a function of mechanical stresses and electric field.

From the Lagrangian operator, in the Hamilton's principle, the different energies in Eq.(3.67) can be formalised in the finite element notation and are given by Lerch [3.5] as:

$$\begin{aligned} U_{strain} &= \frac{1}{2} u^t K_{uu} u \\ U_{dielectric} &= \frac{1}{2} \phi^t K_{\phi\phi} \phi \\ U_{Kinetic} &= \frac{1}{2} \dot{u}^t M_{uu} \dot{u} \\ U_{mutual} &= \frac{1}{4} \left(u^t K_{u\phi} \phi + \phi^t K_{u\phi}^t u \right) \end{aligned} \tag{3.68}$$

At each discrete time step of the simulation, to remove the time dependencies of the individual energies, we take a time average response of each term of Eq.(3.68) as given by:

$$U_{ave} = \frac{1}{N} \sum_{n=1}^{N} U(\Delta t) \tag{3.69}$$

where *E* is any of the energies calculated at each time step Δt and *N* is the total number of time steps. The electromechanical coupling is defined [3.47] by:

$$k^2 = \frac{U_{mutual}^2}{U_{strain} U_{dielectric}} \tag{3.70}$$

Eq.(3.70) is used as a general formula for the EMCC since it is suitable for both static and dynamic measurements [3.51]. Eq.(3.70) is rather simple to implement in FE77 since almost all the calculations involved are already performed at some stage of the iteration procedure. Analytical applications of Eq.(3.70) are more complicated than it first looks in the general case. However for a piezoelectric solid, having a simple shape, used dynamically as a single resonant element, the material EMCC is found as it arises naturally in analytical solutions for electrically driven electrodes. Berlincourt [3.47] derived Eq.(3.70) for simple classical problems. For all these cases, the problem is made one dimensional and the stress system is simple. Depending on the shape of the element, the stress system and the electrical boundary conditions, a particular set of piezoelectric equations may prove to be handier to use than the other ones. For example let us consider a very long, very slender piezoelectric rod of axis *z* as shown in Figure 3.4. Assuming that under the influence of a longitudinal electric field E_3, the stress system is one dimensional, then the fundamental mode of the rod is the longitudinal mode. In this

case, $T_1 = T_2 = 0$, $T_3 \neq 0$ and $S_1 = S_2 \neq S_3 \neq 0$ and since the stress system is simpler than the strain system it is better to use the set of piezoelectric equations given by Eq.(3.2). The energies can then be calculated in the same way as in Eq.(3.67), and the coupling factor for the fundamental mode is given by

$$k_{33}^2 = \frac{d_{33}^2}{\varepsilon_{33}^T s_{33}^E} \tag{3.71}$$

where d_{33} is the piezoelectric strain constant that relates the electric field along the direction z and the direct strain S_3. ε_{33}^T is the dielectric permittivity at constant stress and s_{33}^E the elastic compliance measured at constant electric field. As with other piezoelectric constants, coupling factors carry subscripts; k_{33}, for instance, is the coupling factor associated with the one dimensional fundamental longitudinal mode excited by an electric field parallel to the axis (direction 3) of the rod. Similarly k_{31} would be the coupling factor for longitudinal vibrations of a long rod under the influence of a transverse electric field and k_{15} describe the shear mode vibrations of the rod. The coupling factor, k_{33}, as given in Eq.(3.71), is usually measured statically but can also be measured in the low frequency range, as long as there are no appreciable spatial variations in the stress and electric field, in other words as long as the one dimensional assumptions remain valid. These measurements at low frequency are called quasistatic measurements [3.33].

Coupling factors can also be calculated for other modes of vibrations. For example, let us consider a thin rectangular plate electroded on the major faces, as shown in Figure 3.5. Under the thin plate assumptions the elastic boundary conditions are $S_1 = S_2 = 0$, $S_3 \neq 0$ and $T_1 = T_2 \neq 0$; $T_3 \neq 0$, and for fully electroded faces the electric field is in the direction 3. Therefore it is simpler to use the set of equations (3.1) and the internal energy is given by Eq.(3.67). Eventually one obtains

$$k_t^2 = \frac{e_{33}^2}{\varepsilon_{33}^S c_{33}^E} \tag{3.72}$$

where k_t is the piezoelectric *thickness* coupling factor and relates to as specific case of one dimensional strain parallel to the thickness axis. k_t represents the coupling between an electric field in direction 3 and mechanical vibrations in direction 3 for a planar object. Since the overall volume of the object remains constant, expansion/contraction in the thickness must always be accompanied by corresponding contraction/expansion in the transverse directions, so the strongly attenuated transverse vibrations at the higher frequency of the thickness mode tend to increase the apparent stiffness of the material. Hence k_t is lower than k_{33}, the coupling factor for longitudinal vibrations of a slender rod. For the long slender rod, the longitudinal resonant frequency is much lower than

the thickness resonant frequency of the planar object and matches more closely its transverse resonant frequency.

Therefore if the coupling factor was to be measured dynamically instead of statically, it would be found to be lower than in a static configuration because not all the elastic energy is dielectrically coupled. The difference is due to the presence of the overtones of the fundamental resonant mode as seen for the planar object. In theory for certain resonant modes which have no overtones the dynamic and static coupling factors are equal. In general however the values of the static coupling factor quoted in tables, Kino [3.3], and Berlincourt [3.47], are usually maxima based on precisely defined vibrational modes of ideal specimens of the material. Therefore in practical transducers, the coupling factors are lower. Approximate conversion formula from Eq.(3.70) to equivalent experimental representation of the EMCC have been defined by Bechman [3.52] and Naillon [3.28].

3.4.5 ELECTRIC IMPEDANCE

The electrical input impedance can also be computed in the time domain if the model is steady. This involves running the model over an unusually long time. The input impedance of the piezoelectric device is given by the ratio of the voltage to the current. Current can be calculated by summing the time rate of change of charge at the electrode nodes, but this solution involves extra operations within the time marching algorithm. A simpler technique, involving operations only at the post processing level can be used, but only in harmonic regime. For harmonic oscillations the current can be calculated from the charge:

$$I(t)=\frac{dQ(t)}{dt}=j\omega Q(t) \tag{3.73}$$

where ω is the harmonic circular frequency. Therefore, in the frequency domain, the input electric impedance is given by

$$Z(\omega)=\frac{1}{j\omega}\frac{f\{\phi_{el}\}}{f\{Q(t)\}} \tag{3.74}$$

where $f\{\phi_{el}\}$ is the Fourier transform of the electrical potential at the excited electrode. In principle the application of a delta pulse charge is superior to any other time function for the charge since the Fourier transform of a delta function is unity.

However this remark is purely theoretical since in an FE code a delta function will have to have the duration of at least 2 time steps and is therefore finite in time. Therefore the Fourier transform of this pseudo delta function has to be performed. Moreover such a spike would contain very high frequencies which are, de facto, filtered since the highest frequencies generated by a finite element code are directly linked to the size of the elements constituting the model. A better solution is to define a pseudo pulse, for instance a single cycle of a cosine wave at a frequency such that the frequency bandwidth of the pseudo pulse will be large enough to encompass the resonant

frequencies of the mode of vibration of interest. As a general matter it is necessary to bear in mind that although the FE code may produce results at high frequencies, because of the limited size of the elements, only parts of the impedance curve can be considered as being accurate.

To calculate the electrical impedance as given in Eq.(3.74), charges are applied at one electrode as given in Eq.(3.64) and the voltage variation induced is calculated at that electrode. This sounds simple enough to do but unfortunately it is not. In FE77 the electrical conductivity of the electrode is not taken into account and in fact the electrode is not modelled and is just idealised by applying the same charge load at each node of the surface that is supposed to be electroded. Electrically speaking, the electrode is usually seen as a perfect conductor which means that the electrons move freely along the surfaces of the electrode, in other words the surface of the electrode are equipotentials. This implies two things, firstly $Q(t)$ in Eq.(3.73) is for the whole electrode, that is the sum of the charge applied at all nodes and secondly, the forced electrode is an equipotential surface, hence each node on the electrode has to have the same value of electric potential to satisfy the boundary condition at a perfect conductor.

$$\phi_1 = \phi_2 = \phi_3 = \ldots = \text{unknown constant} \tag{3.75}$$

The value is not predetermined and varies at each time step. In FE77 this is done by connecting the electrical degree of freedoms of the nodes on the electrode plane in the same way as rigid mechanical connections can be set between nodes so that they undergo only rigid body translations and rotations.

The electrical impedance is a quantity that can be verified experimentally without any undue effort, since impedance measurements can easily be carried out with a network analyser by sweeping the frequency and recording the real and imaginary part of the impedance. The input impedance of the piezoelectric transducer also reveals all resonances, f_r and anti-resonances, f_a of the device. The electrical properties of a piezoelectric vibrator are dependent on the elastic, dielectric and piezoelectric constants of the vibrating material. Thus values for these constants can be obtained from resonator measurements on a suitably shaped and orientated specimen, provided the theory for the mode of motion of that specimen is known. The measurement basically consists of determining the electrical impedance of the resonator as a function of frequency. To find the material constants it is in theory necessary to obtain the resonant and anti-resonant frequencies and the capacitance and the dissipation factor. A simple calculation is that of the EMCC of each vibration mode, which requires only the knowledge of the resonant and anti-resonant frequencies. This method of determining the EMCC is supported by the IEEE Standards on piezoelectricity [3.33] and the EMCC is given using the approximate formula [3.47]:

$$k^2 = \frac{f_a^2 - f_r^2}{f_r^2} \tag{3.76}$$

where f_r and f_a are frequencies which coincide with the admittance and the impedance maxima, respectively. Eq.(3.76) can be used to calculate the coupling factor by

measuring the resonant frequency and corresponding anti-resonant frequency of the mode, although in practice it is somehow more complex than it first looks since piezoelectric materials are lossy and lossy resonators have three frequencies of interest near the maximum of admittance and three near the maximum impedance. However in FE77, piezoelectric devices are lossless and therefore resonators modelled with FE77 exhibit only f_r and f_a. The calculation of the EMCC is therefore straightforward. Naillon [3.28] applied the finite element method to a piezoelectric bar used in array transducers, and an effective piezoelectric coupling factor similar to that in Eq.(3.76) was derived to relate to the anti-resonant and resonant frequencies of the piezoelectric structure, which was then used to estimate the strength of each mode. Numerous works have been published concerning the use of finite element method and electrical impedance to understand the nature of resonant modes of piezoelectric discs [3.25], [3.27], [3.28], [3.53], [3.54] and evaluate the strength of excitation at each resonance [3.55]. Modal properties of piezoelectric discs are not of specific interest in this thesis and furthermore all our finite element calculations are performed in the time domain only.

An application of the impedance and EMCC calculations presented in this section is given in section 3.5.2 as part of the validation process.

3.5 VALIDATION OF THE ALGORITHM

The theory described above has been implemented in FORTRAN 77 routines added to FE77. In FE77 the implementation has been simplified because we had the ability to access the source code and modify it at the necessary levels. On the other hand, the limitations of the piezoelectric models are those of FE77 in general.

Alleyne [3.12] developed FE77 to model the propagation of Lamb waves in plates. His work concerned purely mechanical problems, but since the introduction of the piezoelectricity in the code does not change the integration method, the principles enacted by Alleyne remain valid for electromechanical analysis. This direct parallel with previous work is very advantageous because, since the new features have been added to a thoroughly validated code, the validation stages are greatly simplified and in fact reduced to verifying that the electromechanical coupling is accurate.

Incidentally, it is to be noted that the commercially available code PZFlex® [3.10] uses the explicit integration method for similar reasons to those described here and therefore validating FE77 against this code is helpful.

Several test cases were run using FE77 and both analytic calculations and predictions obtained using PZFlex® have been used as verification of the FE77 results. All models are two-dimensional assuming plane strain conditions. Some are also constrained mechanically to allow only plane waves to propagate.

3.5.1 FINITE ELEMENT RESULTS OF INITIAL TEST CASES

The initial validation procedure is two fold. Firstly, plane waves are modelled and their group velocity measured from the predicted displacement time histories. Secondly, Lamb waves propagating in simplified piezoelectric materials are modelled, and their predicted group velocity is compared with group velocity dispersion curves. The material properties used in both cases are listed in Table 3.1 and refer, for the mechanical part, to an isotropic material: aluminium. The physics of piezoelectricity implies that it can exist only in anisotropic materials, and the material used in these models is isotropic. However, for the purpose of the validation of the numerical calculations, these artificial material constants are satisfactory and have been chosen in order to simplify the analytic calculation and also in order to avoid matrix rotations in the finite element program.

3.5.1.1 Piezoelectrically Coupled Plane Wave

Our purpose here is to lay emphasis on the electromechanical coupling of plane waves. A simple FE model has been developed to check the predictions on velocities of plane waves obtained using FE77, when the material is artificially made to be piezoelectric.

The model is a 0.5 mm thick plate, 50 mm long, with all surface nodes pinned in one direction. The coordinate system is defined in Figure 3.6. The 'plate' is considered to be infinite in the direction normal to the plane *xy* since plane strain conditions were introduced in the code. The mesh is made of 0.25mm square 4-noded elements and the material properties are listed in Table 3.1.

In order to generate a longitudinal wave propagating in the *x* direction, the 'plate' was excited by applying initial displacements in the *x* direction to all the nodes at x = 0, with unit amplitude. Since all surface nodes are pinned in the *y* direction only the bulk longitudinal wave can propagate. The applied signal is a 1 MHz sine wave of unit amplitude modulated temporally by a 5 cycle wide Gaussian window function to limit the bandwidth, as shown in Figure 3.7.

Figure 3.8(a) shows the time history recorded at position x = 25 mm when the piezoelectric constants are set to zero. To calculate the group velocity, the transit time is measured as the arrival of the maximum of the envelope of the toneburst. The group velocity is then calculated as 6.30 mm/μs for the forward travelling wave packet. The second wave packet in Figure 3.8(a) is the first reflected wave packet from the right end of the model from which the group velocity is then measured as 6.35 mm/μs. The theoretical sound velocity for the parameters listed in Table 3.1 is C_L= 6.34 mm/μs. The error in the predicted particle velocity for the first pulse Figure 3.8(a) is 0.6 %. The error is defined as

$$\text{Error}\,(\%) = \frac{\left|V_{FE77} - V_{Theroy}\right|}{\left|V_{Theory}\right|} \times 100 \tag{3.77}$$

The model was then amended by adding the piezoelectric coupling coefficient e_{x1} with magnitude 40.46, so that the material is artificially made piezoelectric. Figure 3.8(b) shows the time history recorded at position x = 25 mm when a piezoelectricity constant e_{x1} equal to 40.46 is introduced in the model. The physical significance of piezoelectric stress constant e_{x1} can be illustrated as being the coupling term between the electric displacement in the x direction and the direct strain S_1, as discussed in Chapter 2.In this model the nodes can move only along the x direction and therefore by solving Eq.(3.1) under these boundary conditions the Christoffel equation is [3.34]

$$k^2\begin{bmatrix} C_{11}^E+\dfrac{e_{x1}^2}{\varepsilon_{xx}^S} & 0 & 0 \\ 0 & C_{66}^E & 0 \\ 0 & 0 & C_{66}^E \end{bmatrix}\begin{bmatrix} u_x \\ 0 \\ 0 \end{bmatrix}=\rho\omega^2\begin{bmatrix} u_x \\ 0 \\ 0 \end{bmatrix} \tag{3.79}$$

where k is the wavenumber, u_x is the particle displacement in the x direction and ω is the circular frequency. C_{11}, C_{12}, C_{66}, e_{x1} and ε_{xx} are material constants given in Table 3.1. Superscripts E and S indicates material constants measured, respectively, at constant electric field and constant stress. Eq.(3.79) has exactly the same form as the Christoffel equation for a non piezoelectric material, but with the C_{11} elastic constant replaced by the expression

$$C_{11}^E+\frac{e_{x1}^2}{\varepsilon_{xx}^S} \tag{3.80}$$

which is called the *piezoelectrically stiffened elastic constant.* The only non zero solution to Eq.(3.80) is a *stiffened* compressional wave with dispersion relation

$$k^2\left(C_{11}^E+\frac{e_{x1}^2}{\varepsilon_{xx}^S}\right)=\rho\omega^2 \tag{3.81}$$

The electric potential associated with this *stiffened* compressional wave is given in term of the particle displacement by

$$\Phi=\frac{e_{x1}}{\varepsilon_{xx}^S}u_x \tag{3.82}$$

From Eq.(3.80) the *stiffened* velocity is given by

$$C_L=\sqrt{\frac{C_{11}^E+\dfrac{e_{x1}^2}{\varepsilon_{xx}^S}}{\rho}} \tag{3.83}$$

Numerical application of Eq.(3.83) using the material constants given in Table 3.1, gives a theoretical *stiffened* longitudinal velocity of 8.97 mm/μs. From Figure 3.8(b) the group velocity of the wave packets is calculated as 8.94 mm/μs for the forward travelling pulse, 8.95 mm/μs for the first reflected wave packet and 8.95 for the last wave packet which was reflected at both ends of the model. The maximum error in the predicted particle velocity is 0.4 %. Compared to Figure 3.8(a), Figure 3.8(b) shows a third wave packet. this is also the S_0 mode but reflected twice, on time at each end of the plate. It is therefore propagating forward like the first wave packet. Figure 3.8(c) shows the time history of the electric potential associated to the mechanical displacements. According to Eq.(3.82) the potential time history at position x = 25 mm is proportional to the displacement at this position. Numerical application of Eq.(3.82) gives a maximum electric potential of 2.69 10^{+9} GV for the first wave packet in Figure 3.8(b). The corresponding measured electric potential in Figure 3.8(c) is 2.8 GV. The error between theoretical and predicted values is 2.8%. The value of the potential peak are in Giga Volts here since the maximum amplitude of the applied displacement is 1meter.

Figure 3.9(a) shows the envelope of the first pulse of Figure 3.8(a) when the piezoelectricity is not active in the model and Figure 3.9(b) shows the envelope of the first pulse seen in Figure 3.8(b). It is seen that both envelopes are very similar in shape and amplitude. This clearly indicates that the numerical piezoelectric routines added to FE77 do not add any dispersion to the time marching process.

The model was then amended by releasing the surface nodes in the *y* direction and pinning them in the *x* direction. Therefore nodes can only move along the *y* direction and only a shear bulk wave can propagate. Because the wavelength of the shear wave is shorter than that of a longitudinal wave the elements size was decreased to 0.166 mm in order to have enough nodes per wavelength. The overall dimensions of the model remain unchanged. To allow a pure shear wave to propagate along the direction *x*, initial displacements, in the *y* direction, as shown in Figure 3.7 are applied at each node at x = 0 with the same unit magnitude and the resulting predicted waveforms at x = 33.83 mm are shown in Figure 3.10. The group velocity for the non-piezoelectric model, Figure 3.10(a) is calculated as 3.115 mm/μs. The theoretical group velocity for the bulk shear wave is 3.132 mm/μs. The error in the velocity is less than 0.5%.

The model was then amended by adding the piezoelectric coupling coefficient e_{x6} with magnitude 20, so that the material is artificially made piezoelectric. In a two dimensional plane strain system if the particle can move only in direction *y* and if the only non zero piezoelectric stress constant is e_{x6}, the only non zero solution is a *stiffened* transverse wave with dispersion relation

$$k^2\left(C_{66}^{E}+\frac{e_{x6}^2}{\varepsilon_{xx}^{S}}\right)=\rho\omega^2 \tag{3.84}$$

where the expression in brackets is called the piezoelectrically *stiffened* elastic constant C_{66}. The electric potential associated with this *stiffened* shear wave is given in term of the particle displacement u_y as

$$\Phi = \frac{e_{x6}}{\varepsilon_{xx}^{S}} u_y \tag{3.85}$$

and the *stiffened* shear velocity is given by

$$C_S = \sqrt{\frac{C_{66}^{E} + \frac{e_{x6}^2}{\varepsilon_{xx}^{S}}}{\rho}} \tag{3.86}$$

Numerical application of Eq.(3.85) gives a theoretical stiffened transverse velocity of 4.43 mm/µs. Figure 3.10 (b) shows the time history recorded when the piezoelectricity was active in the model. The group velocity of the right propagating wave packet is calculated as 4.42 mm/µs and the group velocity for the reflected wave packet is calculated as 4.419 mm/µs. The error in the predicted particle velocity in here again less than 0.5%.

Numerical application of Eq.(3.85) gives a theoretical electric potential of 1.33 GV for the first wave packet in Figure 3.10(b). The corresponding measured electric potential in Figure 3.10(c) is 1.34 GV. The error between theoretical and predicted values is below 1%. In Figure 3.10(c) ripples are seen to occur at times earlier than that corresponding to the arrival of the first toneburst of piezoelectrically induced toneburst. The ripples are due to an interaction between the electromagnetic wave and the stiffened wave. The electromagnetic wave exists on his own since the coupled quasi-electromagnetic and the quasi-elastic waves are effectively decoupled by the large difference of their propagation velocities and become pure electromagnetic and pure elastic waves. This phenomenon has been described in great details by Auld [3.34 section F of Chapter 8, and in particular Figures 8.4 and 8.5]. To implement the piezoelectric equations in FE77 the electrical degrees of freedom are *condensed* and consequently the electrostatic wave is set instantaneously. Therefore a standing electrostatic wave exist independently of the piezoelectric coupling.

When Alleyne [3.12] validated FE77, he found that plane wave velocities could be predicted with an error less than 0.5%. In the two above cases, the finite element predictions for the piezoelectrically stiffened wave velocities differed from the theoretical value by less than 0.5% confirming the applicability of the piezoelectric routine. It must be stressed that the calculations presented here are for an isotropic material and therefore are not representative of the general behaviour of a piezoelectric solid. Eq.(3.81) and Eq.(3.84) are only valid in few particular cases where bulk waves propagate, for example, along the poling axis of a hexagonal crystal (e.g. PZT). However this remark does not affect the meaning of these calculations since the aim here was to verify that the finite element program is coupling the electrical and mechanical waves correctly.

3.5.1.2 Initial Modelling of Lamb Wave in Piezoelectric Material

Our aim here is to lay emphasis on the correct modelling of the electromechanical coupling of Lamb waves propagating in a piezoelectric plate-like structure. Two models were designed to achieve this goal. The first model is concerned with the propagation and the electromechanical coupling of the S_0 mode and the second model with the propagation and the electromechanical coupling of the A_0 mode propagating in a 1mm thick plate. In both cases the model is made of square 4-noded elements, with free boundaries assuming plane strain conditions. The plate is therefore considered as infinite in the *z* direction so that predicted velocities can be compared with the velocity dispersion curves calculated using the program DISPERSE [3.22]. The co-ordinate system is as defined in Figure 3.6 and the material properties are listed in Table 3.1. Alleyne [3.12] studied in detail the problems associated with the modelling of ultrasonic Lamb waves. First a frequency region, determined by the frequency bandwidth of the excitation signal, has been carefully chosen to avoid dispersion since we want to calculate the group velocity directly from the time histories. When selecting the frequency bandwidth of the excitation signal it is necessary to avoid cut-off frequencies since at these points in frequency, the phase velocity of that mode is infinite and the finite element program encounters great difficulties in modelling such waves. Both models presented here are only concerned with propagation below the A_1 mode cut-off frequency which, for the material properties listed in Table 3.1 and for a 1mm thick plate, is at 1.55 MHz. Therefore the higher frequency of the excitations signals must be lower that 1.55 MHz. The next step is to generate a single mode. Since at least two Lamb mode always co-exist at every frequency, generating a single mode can be achieve only by matching the initial displacements applied at the position of the nodes through the thickness of the plate, with the exact value of the displacement of the mode. For the two models designed here, the nodes at plane x = 0 are being forced with sinusoidal toneburst of amplitude the displacement components, at the centre frequency of the excitation toneburst, of the mode to be generated. This allows us to generate either the A_0 or the S_0 mode alone.

For the first model, only the e_{x1} piezoelectric stress constant is non-null. This means that a stress wave propagating in the *x* direction will generate an electric field in the same direction. For both models the aim is to generate a single Lamb wave in the piezoelectrically *stiffened* plate and measure the group velocity at the centre frequency. However the group velocity of a Lamb mode cannot easily be predicted from a simple consideration of the stiffness constants and no simple equation such as Eq.(3.86) can be used. For the first model, according to Eq.(3.79) only the bulk compressional wave is *stiffened* and its velocity is given by Eq.(3.83). All other elastic constants and the density remain unchanged. The *stiffened* dispersion curves can therefore be deduced from those for the *non-stiffened* material (i.e. when the piezoelectric constant e_{x1} is equal to zero) by just replacing the C_{11} elastic constant by its stiffened value as given in Eq.(3.80). The group velocity dispersion curves for the 1mm thick plate *stiffened* only through the piezoelectric constant e_{x1} are shown in Figure 3.11. It is seen that the group velocity of the S_0 mode is greatly increased at low frequency whereas the group velocity of the A_0 mode is only slightly changed, as expected since only the e_{x1} piezoelectric constant is active in this model. Indeed, the piezoelectric coupling can only be activated

by the T_{11} direct stress component, that is the compressional stress and the bending stress have no influence. When propagating, the compressional wave components generate an electric field in the x direction, which in turn increases the compressional strain. Therefore the solid appears to be stiffer in compression and all compressional wave components propagate at a higher velocity. It is seen in Figure 3.11 that the group velocity of the A_1 mode is also increased by the piezoelectric stiffening. This is due to the high proportion of compressional displacement in the A_1 mode stress mode shapes. However its cut-off frequency is unchanged since this corresponds to a shear wave, unaffected by the stiffening, travelling between the free surfaces of the plate with no transmission of energy along the *x* direction. This wave is unaffected by the piezoelectric stiffening, its velocity is unchanged and therefore the frequency at which it resonates between the free surfaces of the plate is also unchanged.

With this first model the attempt is to model the propagation of the S_0 mode alone. All nodes at x = 0 are therefore forced in the *x* and *y* directions with amplitude corresponding to the particle displacement mode shapes of the S_0 mode, calculated with DISPERSE [3.22]. The input signal is a sinusoidal toneburst at 0.505 MHz modulated in a 5-cycle wide Gaussian window function. Its frequency spectrum is shown in Figure 3.11. It is seen that within the input frequency bandwidth, the S_0 mode, propagating in a 1mm thick plate, is weakly dispersive. It is also seen that the excitation frequency bandwidth ends before the A1 mode cut-off frequency therefore only the S_0 and A_0 mode are can propagate in the plate, but in fact only the S_0 mode is being excited since the plate is being excited with displacement components, at 0.505 MHz of the S_0 mode. At this frequency, the S_0 mode behaves like a compressional mode, hence its velocity is highly affected by the piezoelectric stiffening.

The model is first run without any piezoelectricity. At 0.505 MHz in a 1mm thick plate the theoretical group velocity of the S_0 mode is 5.38 mm/μs. Figure 3.12(a) shows the time history recorded at position x = 25 mm in the *x* direction when the plate in non piezoelectric (i.e. $e_{x1} = 0$). The group velocity is measured as 5.38 mm/μs. The error is therefore negligible in this purely mechanical case. Figure 3.12(b) shows the time history recorded at position x = 25 mm in the *x* direction when the plate is piezoelectric (i.e. e_{x1}= 40.46 coulomb/m^2). The group velocity is measured as 8.3 mm/μs. Numerical application of Eq.(3.80) shows when the plate is piezoelectrically active, (i.e. e_{x1} = 40.46 coulomb/m^2), the *stiffened* C_{11} elastic constant is in fact the double of the original C_{11} elastic constant. Figure 3.12(c) shows the time history recorded at x = 25 mm in the x direction when the plate is non piezoelectric but when the value of the C_{11} elastic constant has been doubled, i.e. C_{11} = 217.6 GPa. It is seen that Figure 3.12(b) and Figure 3.12(c) are indeed very similar which demonstrates clearly that the dispersion curves, for the piezoelectrically coupled material, can be deduced from those of a purely mechanical system by just adapting the value of the elastic constant to their *stiffened* equivalent value. From the dispersion curves shown in Figure 3.11 the group velocity at 0.505 MHz for the S_0 mode in the *stiffened* plate is calculated as 8.32 mm/μs. The error between the predicted FE value of the group velocity and the calculated value given by the dispersion curve is less than 0.15%.

The model was then amended by changing the forcing amplitudes at the nodes on plane x = 0. The input was designed to reproduce the particle displacement mode shape of the mode A_0 propagating in a 1mm thick plate. In order to minimise the dispersion effect a 10-cycle toneburst at 1.5 MHz was used. As shown in Figure 3.13, the mode A_0 is almost non dispersive within the frequency bandwidth of this toneburst. The A_0 mode has large transverse displacements at these frequencies and therefore we chose to only set the e_{x6} piezoelectric coupling constant for this test case. Therefore the coupling will occur between the shear stress T_6 and the electric field in direction of propagation E_x, and the equivalent *stiffened* elastic constant is given by the expression in the bracket in Eq.(3.84). The dispersion curves for the *stiffened* equivalent material, traced by DISPERSE, are shown in Figure 3.13. As expected, it is seen that, at low frequency, the S_0 mode is almost unaffected whereas the A_0 mode is highly affected by the stiffening due to the piezoelectric coupling. It is also seen that the cut-off frequency of the A_1 mode is changed to a higher frequency, which corresponds to the resonant frequency of the *stiffened* shear wave in the thickness of the plate. From Eq.(3.86), the *stiffened* shear wave velocity is given as 4.43 mm/μs and for a 1mm thick plate the cut-off frequency is 2.215 MHz instead of 1.56 MHz for the non-piezoelectric plate.

The group velocity in the non piezoelectric model is measured as 3.14 mm/μs from Figure 3.14(a). From the dispersion curves the group velocity for the mode A_0 at 1.5 MHz is found as 3.16 mm/μs. The error is 0.7%. After the second wave packet on the right of Figure 3.14(a) there is a third packet that has a long 'tail'. This shows that this signal is dispersive. This wave packet that spreads in time is the A1 mode which is also generated in the non-piezoelectric plate. In Figure 3.13 it is seen that the excitation bandwidth has been chosen so that the A_0 mode in the piezoelectric plate would be generated alone and in a non dispersive region since the cut-off of the A1 mode has been shifted to 2.215 MHz. Therefore, in the piezoelectric plate, the input signal cannot generate the A1 mode. However when the plate is not piezoelectric, the A_1 cut-off frequency is 1.56 MHz and this mode, very dispersive in this frequency region, is excited along with the A_0 mode. When the piezoelectricity is turned on in the model (i.e. e_{x6} = 20 coulomb/m^2), the group velocity is measured from Figure 3.14(b) as 4.12 mm/μs. The theoretical group velocity for a material with a *stiffened* C_{66} constant is 4.15 mm/μs. The error between the predicted FE value of the group velocity and the calculated value given by the dispersion curve is less than 0.7%.

Alleyne [3.18] proved the capability of FE77 to model accurately Lamb waves in plates. The same accuracy in the group velocity is found here for piezoelectric plates what clearly demonstrates that the piezoelectric coupling is correctly modelled in the two directions.

Alleyne [3.19] also demonstrated that the two dimensional Fourier transform method can be used to measure both the velocity and the amplitude of propagating Lamb waves when more than one mode is present and the 2D-FFT method has been used to determine mode purity very accurately in FE77 modelling studies. It is therefore necessary to verify that the piezoelectric routine retains those capabilities. To do so the first model (for the S_0 mode with e_{x1} = 40.46 and e_{x6} = 0 coulomb/m2) is amended so that the modes are launched by superposing the displacement components, at 1 MHz, of

the S_0 and A_0 modes, as shown in Figure 3.15(a) and (b). The input at x = 0 is a 5-cycle 1.0 MHz toneburst of the form shown in Figure 3.7(a). The normalised time history, at position x = 18 mm, of the response of the plate to the excitation at x = 0, is shown in Figure 3.16. The first toneburst correspond to the fastest forward travelling mode, the S_0 mode. The following, slower, wave packet corresponds to the A_0 mode forward propagating away from the excitation zone. The last toneburst on the right corresponds to the first reflection of the S_0 mode at the right end side of the plate (x = 50 mm). Figure 3.17 shows the results of carrying out a two dimensional Fourier transform (2-D FFT) on the time histories of 100 equally spaced points between x = 0 mm and x = 50 mm. This technique involves two Fourier transform stages. Firstly, the time domain traces from each individual monitoring point are Fourier transformed into the frequency domain, yielding the frequency spectrum for each monitoring point. For each frequency component, a spatial Fourier transform is carried out encompassing all consecutive monitoring points; this yields the wavenumber components present at each frequency. The resulting two-dimensional array contains the amplitudes of the different frequency and wavenumber components of the signal. The Lamb modes present have different wavenumbers (owing to their different phase velocities), and therefore appear at different locations on the wavenumber axis, allowing their amplitudes to be measured independently. It is seen that the maximum amplitude of the response of the plate is at 1 MHz, the centre frequency of the excitation toneburst. At each discrete frequency in Figure 3.17, the maximum amplitude is seen at the wavenumbers corresponding to the A_0 and S_0 modes. The negative range of wavenumbers correspond to the S_0 mode travelling backward after reflection at the right end side of the plate. The theoretically predicted wavenumber dispersion curves are overlaid on Figure 3.17. The agreement with the theoretical curves is excellent, the maximum error in wavenumber being less than 0.5%. The response is dominated by the S_0 mode, the amplitude of the A_0 mode being always less than 50% of S_0 mode.

These results show that the 2-D FFT method may also be used to measure both the velocity and the wavenumber of Lamb modes propagating in piezoelectric plates, when more than one mode is present.

3.5.2 TWO-DIMENSIONAL VALIDATION CASE

Two transducer problems are presented here, a clamped strip alone and a strip mounted on a plate (see section 3.5.3). For these models the excitation signal is an alternating electric potential applied between two electrodes on either side of the piezoelectric device. For the clamped piezoelectric strip an approximate analytical solution can found but for the piezoelectric strip mounted on an aluminium plate, there are no analytical solutions. Therefore the predicted displacements for the two models presented here have been compared to the displacement predicted using PZFlex® [3.10], a commercially available finite element program.

3.5.2.1 Clamped Piezoelectric Strip

The first model represents a thin piezoelectric platelet, of thickness h, with one face (perpendicular to z) rigidly bonded to a fixed support and the other face free as shown in Figure 3.18. For this problem it is assumed that the metal electrode deposited on the free face has no mechanical influence. Therefore it is only modelled in FE77 by applying the prescribed voltage at all the nodes of the free surface. The excitation signal is an alternating voltage of amplitude V applied between the two faces: one electroded (z = h) and the other grounded (z = 0). This electromechanical problem can be solved analytically and the mechanical displacements at the upper surface calculated with very little approximation. These results are then compared with the displacements predicted along the upper surface, using the finite element program FE77.

Because the displacements in the x and y directions, at the clamped face z = 0, are null, the strains in the xy plane are also zero :

$$S_1(z=0)=S_2(z=0)=S_6(z=0)=0. \tag{3.87}$$

where S_1 and S_2 are the direct strains in the x and y directions and S_6 the shear strain in the xy plane. Eq.(3.87) is valid only at z=0. However in this problem the frequency of the excitation signal is chosen to be much lower than the thickness resonant frequency so that the wavelength of the alternating voltage is much bigger than the thickness of the layer. Therefore, under the thin plate approximations Eq.(3.87) remains valid at all points through the thickness:

$$S_1=S_2=S_6=0 \quad \forall z \tag{3.88}$$

At the free face, z = h, the stresses in the yz and xz planes are zero,

$$T_3(z=0)=T_4(z=0)=T_5(z=0)=0 \tag{3.89}$$

and with the wavelength much greater than the thickness, these stresses are also assumed to remain null within the layer,

$$T_3=T_4=T_5=0 \quad \forall z \tag{3.90}$$

In this problem we try to relate the strains and the stresses to the electric field. Therefore the most suitable set of piezoelectric equation is the so-called piezoelectric strain equations [3.34], which use the stresses and the electric field as independent variables. This constitutive relation is given as:

$$S=s^E : T + d.E \tag{3.91}$$

where S and T are the strain and stress tensors, E is the electric field vector, s^E is the compliance tensor and d is the third rank tensor containing the piezoelectric strain constants. The units of these constants are meters per volt. The colon sign indicates a tensor product. In matrix notation and using Eq.(3.90), the strains are given by:

$$S_\alpha = s^E_{\alpha 1} T_1 + s^E_{\alpha 2} T_2 + s^E_{\alpha 6} T_6 + d_{3\alpha} E_3 \tag{3.92}$$

where $\alpha = 1..6$. The last term $d_{3\alpha} E_3$ gives the piezoelectrically induced strains. For a lithium niobate, LiNbO3 (trigonal class 3m) piezoelectric layer, only four piezoelectric strain constants, d_{15}, d_{24}, d_{31} and d_{33} are non-null. Neglecting the edge effects, the electric field is supposed to be along the *z* direction only. Therefore, using conditions given in Eq.(3.88), the relation between the direct in-plane stresses and the electric field is

$$T_1 = T_2 = -\frac{d_{31}}{s^E_{11} + s^E_{12}} E_3, \qquad T_6 = 0 \tag{3.93}$$

Then the strain along the *z* axis is given by:

$$S_3 = \left(d_{33} - \frac{d_{31} s^E_{13}}{s^E_{11} + s^E_{12}} \right) E_3 = \bar{d}_{33} E_3 \tag{3.94}$$

By integrating Eq.(3.94) through the layer thickness, the displacements at the top surface $z = h$ are found to be:

$$u_z(h) = \bar{d}_{33} V \tag{3.95}$$

where *V* is the voltage applied between the electrodes. From the material properties of lithium niobate given in Table 3.2, the displacement, per unit voltage, at the top electrode, in the direction normal to the electrode is given by:

$$u_z(h) = 5.69 \text{ pm} \tag{3.96}$$

A pure 1-Dimensional problem would have given the displacement to be:

$$u_z(h) = \bar{d}_{33} V = 6.00 \text{ pm} \tag{3.97}$$

The difference between Eq.(3.96) and (3.97) is a direct, although simplified, quantification of the lateral effects.

A piezoelectric layer, 0.5 mm thick and 10mm long, is modelled using two dimensional square four-noded elements, with a nodal spacing of 0.1mm. All nodes at $z = 0$ are clamped in all directions and maintained at zero potential. The row of nodes at $z = h$ are forced with an alternating potential. The excitation signal is a sinusoidal wave of frequency 50 kHz. The thickness, h, of the layer is 0.5mm, and the bulk longitudinal wave velocity is 6500 m/s for LiNbO3, the first thickness resonance occurs around 3.25 MHz. Therefore the piezoelectric layer is driven well away from resonance. The displacements are monitored at the top surface ($z = h$) in the normal direction (*z*). Figure 3.19(a) shows the profile of the maximum displacements predicted at each nodes along the 10mm long top surface. The theoretical value given by Eq.(3.96) for a voltage of unit amplitude is plotted as a straight line. The value of the displacements in a pure one-

dimensional case are also plotted, from Eq.(3.97). The error between the one-dimensional theoretical results and the two-dimensional FE77 predicted values is less than 4%. In order to better verify whether these 4% error are inherent to FE77 or due to the approximations in the theoretical calculation, the same model was run using PZFlex™. Figure 3.18(a) also shows the comparison between the displacement amplitudes in the *z* direction predicted by FE77 and PZFlex™. Figure 3.19 shows the comparison of the displacement amplitudes in the *x* direction. In both cases the error is less than 1%.

3.5.2.2 Electric Impedance and Electromechanical Coupling Coefficient

This model was amended in order to trace the impedance plot of the LiNbO3 piezoelectric strip. This is done by releasing the nodes at the back face in order to avoid ringing. A pseudo impulse charge is applied at the top electrode and the bottom electrode is grounded. At first approximation the through thickness resonance occurs for a wavelength equal to twice the thickness of the layer, that is at 6.5 MHz. The bandwidth of the impulse is chosen to be as broad as possible that is a single cycle of sine wave at 20MHz which has a frequency bandwidth that encompasses the resonant frequencies of the mode of vibration of interest.

The impedance calculations performed by FE77 are described in section 3.4.4 and the electromechanical coupling coefficient, as given in Eq.(3.70) is also calculated. The transient voltage response across the strip is shown in Figure 3.20. It is seen that the induced voltage vibration is not decaying to zero. This is due to the fact that in FE77 the piezoelectric material is lossless, therefore the applied charge does not decay to zero and consequently the piezoelectrically induced voltage does not decay to zero. To avoid leakage [3.57], that is the consequence of truncating the time history, associated with the assumption of periodicity when performing the Fourier transform, a decaying exponential window is applied to the charge time history and to the voltage time history prior to performing their Fourier transform. The spectrum of the voltage response, as shown in Figure 3.21 shows the vibration modes which have been excited by the pseudo pulse. Each peak represents a mode in the response, and the value of the frequency corresponds to the resonant frequency of the mode. However, although Figure 3.21 shows the response of the strip up 40 MHz, the predictions above a certain frequency are subjected to large errors since this frequency response results from a time domain analysis which, because of the limited size of the elements and therefore of the time step, de facto filters the highest frequencies. From Eq.(3.74) the impedance is calculated and is shown in Figure 3.22 in a range of frequency where the FE code is accurate. The same model was run with PZFlex® and the electrical input impedance predicted by FE77 is compared with that predicted with PZFlex®.

The plots in Figure 3.22 also reveal the resonance and antiresonance of the thickness vibration mode of the strip. Impedance calculations are described in detail in section 3.4.5. The resonance (f_r) is the natural frequency of the short-circuited electrodes and corresponds to the maximum admittance, while the antiresonance (f_a) is that of the open-circuit conditions and corresponds to the maximum impedance. The antiresonance is excited by a pulse of the electric charge thus it is represented by the

maximum of the electric input impedance predicted by FE77. The resonance and anti-resonance of the thickness mode predicted by FE77 and those predicted by PZFlex® are given in Table 3.3. The difference between the predictions is approximately equal to 0.1 MHz, that is a relative difference of 1.1%.

When exposed to an alternating electric field, a piezoelectric element oscillates and if the frequency lies in the vicinity of its series resonant frequency, its behaviour can be described by an equivalent circuit. Equivalent circuits for unloaded piezoelectric resonators can be found in the literature [3.47] and it can be shown that the series resonant frequency, or resonant frequency f_r, lies in the vicinity of the minimum of impedance, and the parallel resonant frequency, or anti-resonant frequency f_a, lies in the vicinity of the maximum impedance. Below the resonant frequency and above the anti-resonant frequency, in Figure 3.22, the piezoelectric strip behaves capacitively between f_r and f_a.

The electromechanical coupling coefficient can be deduced for these resonant frequencies, for both FE77 and PZFlex® using Eq.(3.76). The results are compared in Table 3.3. The difference between the predicted EMCC by FE77 and PZFlex® is approximately equal to 0.6%.

Here it must be stressed that in order to calculate the electric input impedance with FE77, the lower face of the strip has been unconstrained and that the thickness of the strip, 0.5 mm, is much smaller than its lateral dimension in the *x* direction, 10 mm. Therefore, if at first approximation the electric field is considered to be only along the *z* axis, the stress system in the strip approximates a one-dimensional stress parallel to the *z* axis and the theoretical static coupling coefficient is found as Eq.(3.72):

$$k_t^2 = \frac{e_{z3}^2}{\varepsilon_{zz}^S c_{33}^E}$$

This coupling coefficient corresponds to the thickness vibration of the strip electroded on the major faces and poled along the z axis.

The dynamic electromechanical coupling coefficient has also been predicted by FE77 using Eq.(3.70).

These three coupling factors, $k_{33,}$ the static coupling factor, k, the coupling factor determined by the resonant frequencies and the dynamic coupling factor predicted by FE77 are compared in Table 3.4. As expected they are very close to each other since the strip is very slender and is even infinite in one direction. Nevertheless it is noted that the dynamic coupling coefficient k is lower than k_{33} the static coupling coefficient as expected.

3.5.2.3 Discussion

This model of a piezoelectric strip driven electrically proved the capability of FE77 to model accurately the piezoelectric effect. Under the action of the applied

electric field the particles move and the magnitude of their displacements in both directions have been predicted accurately. Moreover, the calculation of the electrical impedance and of the dynamic electromechanical coupling coefficient when charges are applied at the top electrode of the piezoelectric strip proved also to be accurate.

Transducers are in general more sophisticated than the simple strip studied here, having backing materials on either side of the piezoelectric element, but their piezoelectric behaviour is not different from that of the clamped strip, and FE77 already proved its capability to predict reflection coefficients for mechanical waves. Therefore the predictions performed for the strip prove the capability of FE77 to characterise piezoelectric transducers.

3.5.3 GENERATION OF LAMB WAVES BY A PIEZOELECTRIC STRIP MOUNTED ON A PLATE

The previous model emphases the capability of FE77 to characterise piezoelectric transducers but in this thesis we are interested in the generation and propagation of Lamb waves by piezoelectric elements. Therefore a last model is designed to investigate how accurately FE77 can predict the generation of Lamb waves by a simple piezoelectric strip mounted on an aluminium plate. Figure 3.23 shows a schematic diagram of the mesh and the associated coordinate system. Such a problem can hardly be studied analytically and therefore the predictions from FE77 have been validated against the results obtained, for the same model, from PZFlex®.

The plate is 100mm long and 1mm thick and is made of aluminium. The strip is mounted at the middle of the plate. It is 2mm thick and 5mm long so that there is 47.5 mm of free plate on either side of the strip. The piezoelectric strip is made of PZT-5H whose properties are listed in Table 3.5. The top face of the strip and the interface with aluminium plate are electroded but the electrodes are assumed to have no mechanical influence and are not modelled. Moreover, no adhesive bond being modelled, the piezoelectric strip is in direct contact with the plate. The model uses two-dimensional 4-noded square elements in plane strain conditions, and free external boundary conditions are assumed. The piezoelectric strip is driven electrically by an alternating voltage applied at the top electrode (top nodes of the strip) and the strip-plate interface is grounded. The applied signal is a 5-cycle sine wave at 0.9 MHz in a rectangular window. It is in general better to use a smoothly varying window function such as a Gaussian or a Hanning function but the version of PZFlex® that we used did not offer us that possibilty. Figure 3.24(a) shows the applied toneburst. The signal is not modulated and therefore the frequency spectrum has numerous side lobes as shown in Figure 3.24(b). The bandwith of the main lobe is 400 kHz. The centre frequency and the number of cycles have been chosen in order to generate non dispersive Lamb modes. Unlike the example discussed in 3.5.1.2, the modes are not generated by carefully selected displacement profiles applied through the thickness of the plate but by applying an electric field across the thickness of the piezoelectric strip. Exposed to this alternating electric field the size of the piezoelectric strip changes periodically in accordance with the frequency of the electric field and motion is transmitted to the plate

at the interface. The stress and displacement profiles at the interface are not known a priori and both shear and compressional stresses are transmitted. Therefore it is not possible to know a priori which modes will be generated and propagate in the plate. However only the modes that exist within the excitation frequency bandwidth can propagate away from the strip region. The group velocity dispersion curves for the aluminium plate alone are shown in Figure 3.25. The frequency spectrum of the excitation electric signal is overlaid on the dispersion curves and the frequency bandwidth (20 dB down points) is shown as a shaded zone. It is seen that the only Lamb modes that can be generated with significant amplitude in the plate away from the strip region are the S_0 and A_0 modes.

The first step of the comparison of the results obtained from FE77 and PZFlex® is to extract time histories of displacements at nodes located at the plane z =1mm and from x = 50mm to x = 99.8mm. This monitoring line, as shown in Figure 3.23, starts at the middle of the strip and finishes at the end of the top surface of the aluminium plate. Every other node along this line as been monitored so that a total of 249 time histories were extracted from each code and compared. Figure 3.26(a) and (b) show the time histories predicted by FE77 and PZFlex®, at the same position, x = 50 mm, for the displacements in the *z* direction over 13 μs. This position corresponds to the node at the middle of the interface between the plate and the strip. It is seen that the time history starts at zero as expected, and this is verified for all the interface nodes. Figure 3.26(c) and (d) show the time histories predicted by FE77 and PZFlex®, at the next to last node of the plate, x = 99.8 mm. It is seen that the wave front reaches that position after 9.09 μs which corresponds to a Lamb mode travelling at 5.2 mm/μs. From the group velocity dispersion curves, this mode is identified as the S_0 mode.

From these time histories it seems that both codes are producing very similar results although the time traces from PZFlex® exhibit some high frequency components that are not present in the traces from FE77. To quantify the differences the maximum absolute displacement amplitude in both directions, at each node along the monitoring line have extracted and maximum displacement profiles for this line of nodes, in each direction, are shown in Figure 3.27. The comparison between the displacement profile in the *z* direction predicted by FE77 and that predicted PZFlex® is shown in Figure 3.27(a). The averages of these maximum displacements have been calculated for both profiles and are shown as horizontal lines. The average difference in the predicted amplitudes is 1.08 % for a maximum displacement of 1.20 μm, PZFlex® predicting higher amplitudes than FE77. The same calculation was carried out for the displacements in the *x* direction and the predicted profiles from FE77 and PZFlex® are shown in Figure 3.27(b). The average difference is equal to 1.7%, FE77 predicting higher amplitudes than PZFlex® in this case.

From the surface out-of-plane displacement monitored along a top line of nodes along the plate, a two-dimensional Fourier transform has been performed. This method is described in section 3.5.1.2. Figure 3.28(a) shows the results of carrying out a two dimensional Fourier transform on the time histories of 223 equally spaced points between x = 52.5 mm and x = 99.8 mm. It is seen that the maximum amplitude of the response of the plate is at 900 kHz, the centre frequency of the excitation toneburst. At

each discrete frequency, the maximum amplitude is seen at the wavenumbers corresponding to the A_0 and S_0 modes. The theoretically predicted wavenumber dispersion curves are overlaid on the plot. The agreement with the theoretical curves is excellent, the maximum error in wavenumber being less than 0.5%. It is seen that the A_0 mode is present over almost all the frequency range shown in Figure 3.28; this is due to the broadband of the input signal which excited the strip over a very large frequency bandwidth as shown in Figure 3.24(b). A direct consequence is that the A_0 mode is excited even in its dispersive region and therefore the A_0 signal is spreading in time what, in the frequency domain, is represented as leakage of energy over all the frequency window, as seen in Figure 3.28. This problem is also affecting the S_0 mode. This problem of leakage is well known in signal processing [3.56] and it is a serious limitation when trying to generate Lamb modes selectively. It is even more problematic in finite element analysis since it is necessary to shorten as much as possible the duration of the calculations. This is typically one of the reasons that lead us to develop our own code. In FE77 one can choose between several windows, among which the Gaussian window as illustrated in Figure 3.7.

3.6 CONCLUSION

Although the predictions obtained from the test cases studied in sections 3.5.1 and 3.5.2 agree very closely with the theory, they have two limitations. Firstly they are uni-directional and the piezoelectric matrix is over simplified in order to simplify the analytic calculations. Therefore, these results, on their own, cannot fully validate the capability of FE77 to model electromechanical systems. However from these models it is seen that the *stiffened* velocity of plane and Lamb waves are accurately predicted by FE77. Two other models, two-dimensional this time, have also been designed to model real transducer problems. These models were driven electrically by either alternating electric potential applied between two electrodes on either side of the piezoelectric device, or by application of electric charges at one electrode. The predictions from FE77 could not be validated analytically for such problems and therefore have been compared with the predictions obtained using PZFlex® [3.10], a commercially available FE program.

The results of the comparisons show that the predicted displacements and the electric input impedance match very closely with those predicted by PZFLex®. Moreover the predicted dynamic electromechanical coupling coefficients and group velocities of the generated Lamb modes have been compared with analytic values and once again the agreement is good. It is therefore believed that FE77 can accurately model electromechanical problems. Added to the already-acknowledged performances of FE77 [3.12], [3.18], [3.19], [3.20], the piezoelectric routines makes it a very general tool for transducer design and wave propagation problems.

REFERENCES

[3.1] **Holland**, R. and EerNisse, E. P., "Variational Evaluation of Admittances of Multielectroded Three-dimensional Piezoelectric Structures", IEEE Transactions on Sonics and Ultrasonics, SU-15, pp. 119-132, 1968.

[3.2] **Allik**, H. and Hughes, T. J. R., "Finite Element Method for Piezoelectric Vibration", Interntional Journal for Numerical Methods in Engineering, Vol. 2, pp. 151-157, 1970.

[3.3] **Kino**, G. S., *Acoustic Waves: Devices, Imaging and Analog Signal Processing*, Prentice Hall Inc., Englewood Cliffs, New Jersey, 1987.

[3.4] **Kohnke** P.C., ANSYS ® "Engineering Analysis System Theoretical Manual", Swanson Analysis Systems Inc., P. O. Box 65, Houston, Pennsylvania 15342

[3.5] **Lerch**, R., "Simulation of Piezoelectric Devices by Two- and Three-Dimensional Finite Elements", IEEE Transaction on Ultrasonics, Ferroelectrics, and Frequency Control, Vol. 37, pp. 233-247, 1990.

[3.6] **Lerch**, R., "Finite Element Analysis of Piezoelectric Transducers", IEEE Ultrasonic Symposium Proceedings. 2, pp. 643-654, 1988.

[3.7] **Dobrucki** A., Pruchnicki P. and Szmal C., "Modelling of Piezoelectric Circular Bending Sensor by Finite- Element Method", J. Acoust. Soc. Am., Vol. 82, 1992.

[3.8] **Hwang,** W. and Park, H., "Finite-Element Modelling of Piezoelectric Sensors and Actuators", IEEE transaction on Ultrasonics, Ferroelectrics, and Frequency Control, Vol.31(5), pp. 930-937, 1993.

[3.9] **Belytschko** T. and Hughes T.J.R, (Eds), *Computational Methods for Transient Analysis*, Elsevier Science Publishers B. V., 1983.

[3.10] **Wojcik**, G. L., Vaughan, D. K., Abboud, N. and Mould, J. Jr., "Electromechanical Modelling using Explicit Time-Domain Finite Elements", IEEE Ultrasonic Symposium Proceedings, 1993.

[3.11] **Hitchings**, D., "FE77 User Manual", Imperial College Internal Report, Imperial College, Department of Aeronautics, 1997.

[3.12] **Alleyne**, D. N., "The Nondestructive Testing of Plates using Ultrasonic Lamb waves", PhD Thesis, University of London (Imperial College), 1990.

[3.13] **Blake**, R. J., "Numerical Models of Rayleigh Wave Scattering from Surface Features", Ph.D. Thesis, University of London (University College, Department of Electronic and Electrical Engineering), 1988.

[3.14] **Hasegawa**, K. and Koshiba M., "Finite-Element Analysis of Periodic Surface Acoustic Wave Guides", IEEE transaction on Ultrasonics, Ferroelectrics, and Frequency Control, Vol. 34(5b), pp. 2642-2645, 1995.

[3.15] **Moulin**, E., Assaad, J., Delebarre, C., Kaczmarek, H. and Balageas, D., "Piezoelectric Transducer Embedded in Composite Plate: Application to Lamb Wave Generation", J. Appl. Phys., Vol. 82, pp. 2049–2055, 1997.

[3.16] **Friedrich** W., Lerch R., Prestele K., and Soldner R, "Simulations of Piezoelectric Lamb Wave Delay-Lines using a Finite-Element Method", IEEE Transactions on Ultrasonics, Ferroelectrics, and Frequency Control, Vol. 37(3), pp. 248-254, 1990.

[3.17] **Lerch**, R., "Acoustic Wave Propagation in Surface Acoustic Wave Devices", IEEE Transactions on Ultrasonics, Ferroelectrics, and Frequency Control, Vol. 44(4), pp. 317-327, 1990.

[3.18] **Alleyne**, D. and Cawley, P., "The Interaction of Lamb Waves with Defects" IEEE Transactions on Ultrasonics, Ferroelectrics, and Frequency Control, Vol. 39(3), pp. 487-494, 1992.

[3.19] **Alleyne**, D. and Cawley, P., "A Two-Dimensional Fourier Transform Method for the Measurement of Propagating Multimode Signals", J. Acoust. Soc. Am., Vol. 89, pp. 1159-1168, 1990.

[3.20] **Pavlakovic**, B., Alleyne, D. N., Lowe, M. J. S., and Cawley, P., "Simulation of Lamb Waves Propagation Using Pure Mode Excitation", Review of Progress in Quantitative NDE, eds. D.O. Thompson and D.E. Chimenti, American Institute of Physics, New York, Vol. 17, 1997.

[3.21] **Lowe**, M. J. S., "Matrix Technique for Modelling Ultrasonic Waves in Multilayered Media", IEEE Transactions on Ultrasonics, Ferroelectrics, and Frequency Control, Vol. 42(4), 1995.

[3.22] **Pavlakovic**, B., Lowe, M. J. S., Alleyne, D. N. and Cawley, P., "Disperse: A General Purpose Program for Creating Dipersion Curves", Review of Progress in Quantitative NDE, eds. D.O. Thompson and D.E. Chimenti, American Institute of Physics, New York, Vol. 16, pp. 185-192, 1996.

[3.23] **Allik**, H., Webman, K. M. and Hunt, J. T., "Vibrational Response of Sonar Transducers using Piezoelectric Finite Elements", J. Acous. Soc. Am., Vol. 56, pp. 1782-1792, 1974.

[3.24] **Kagawa**, Y. and Yamabuchi, T., "A Finite Element Approach to Electromechanical Problems with an Application to Energy Trapped and Surface-Wave Devices", IEEE Transactions on Sonics and Ultrasonics, Vol. 23, pp. 263-272, 1976.

[3.25] **Kagawa**, Y. and Yamabuchi, T., "Finite Element Simulation of two-dimensional Electromechanical Resonators", IEEE Transactions on Sonics and Ultrasonics, Vol. 21, 1979.

[3.26] **Kagawa**, Y. and Yamabuchi, T., "Finite Element Simulation of Composite Piezoelectric Ultrasonic Transducers", IEEE Transactions on Sonics and Ultrasonics, Vol. 26, pp. 81-88, 1981.

[3.27] **Boucher**, D., Lagier, M. and Maerfeld, C., "Computation of the Vibrational Modes for Piezoelectric Array Transducers using a Mixed Finite Element-Perturbation Method", IEEE Transactions on Sonics and Ultrasonics, Vol. 28, pp. 318-330, 1981.

[3.28] **Naillon**, N., Coursant, R. and Besnier, F., "Analysis of Piezoelectric Structures by a Finite Element Method", Acta Electronica, Vol. 25(4), pp. 341-362, 1983.

[3.29] **McDearmon** G.F., "The Addition of Piezoelectric Properties to Stuctural Finite Element Programs by Matrix Manipulations", J. Acous. Soc. Am., Vol. 76, 1984.

[3.30] **Bathe**, H. J., *Finite Element Procedures in Engineering Analysis*, Prentice Hall Inc., New York, 1982.

[3.31] **Zienkiewicz**, O. C., *The Finite Element Method in Engineering Science*, Second Edition, McGraw-Hill, New York, 1971.

[3.32] **Cook**, R. D., *Finite Element Modelling for Stress Analysis*, John Wiley, 1995.

[3.33] **An American National Standard** - *IEEE Standard on Piezoelectricity*, ANSI / IEEE Std 176-1987, IEEE Inc., New York, USA, 1987.

[3.34] **Auld**, B. A., *Acoustic Fields and Waves in Solids*, First Edition, Vol. I Chapter 8 & Appendix 2, Robert E. Krieger Publishing Compagny, Malabar, Florida, 1971.

[3.35] **Tiersten**, H. F., *Linear Piezoelectric Plate Vibrations*, Plenum Press, New York, 1969.

[3.36] **Guyan**, R. J., "Reduction of Stiffness and Mass Matrices," AIAA Journal, Vol. 3(2), pp. 380, 1965.

[3.37] **Newmark**, N. M., "A Method of Computation for Structural Dynamics", A.S.C.E., Journal of Engineering Mechanics Division, Vol. 85, pp. 67-94, 1959.

[3.38] **Alterman**, Z. and Loewental, D., "Computer Generated Seismograms," Methods in Computational Physics, Vol. 12, 1972.

[3.39] **Courant**, R., Friedrichs, K. an Lewy, H., "On the Partial Differential Equations of Mathematical Physics", IBM J. Res. and Dev., Vol. 11, pp. 215-234, 1967.

[3.40] **Wilkinson**, J. H., *The Algebraic Eigenvalue Problem*, Oxford University Press Inc., London, 1965.

[3.41] **Wilson**, E. L., "The Static Condensation Algorithm", International Journal for Numerical Methods in Engineering, Vol. 8, pp. 199-203, 1974.

[3.42] **Silvester**, P. P. and Pelosi, G., *Finite Elements for Waves Electromagnetics, Methods and Techniques*. IEEE Press, New York, 1994.

[3.43] **Emson**, C. R. I., "Methods for the Solution of Open-Boundary Electromagnetic Field Problems", IEE Proceedings-A, Vol. 135(3), pp. 151-158, 1988.

[3.44] **Antonova**, E. E. and Silvester, P. P., "Finite Elements for Piezoelectric Vibrations with Open Electric Boundaries", IEEE Transactions on Ultrasonics, Ferroelectrics, and Frequency Control, Vol. 44(3), pp. 548-556, 1997.

[3.45] **Gualtieri**, Jj. G., Kosinski, J. A. and Ballato, A., "Piezoelectricity Materials for Acoustic Wave Applications", IEEE Transactions on Ultrasonics, Ferroelectrics, and Frequency Control, Vol. 41(1), pp. 53-58, 1994.

[3.46] **Smith**, W., "Modelling 1-3 Composite Piezoelectric Hydrostatic Response", IEEE Transactions on Ultrasonics, Ferroelectrics, and Frequency Control, Vol. 40(1), pp. 41-48, 1993.

[3.47] **Berlincourt**, D., Curran, D. R. Jaffe, H., "Piezoelectric and Piezomagnetic Materials", Physical Acoustics, Vol. I(A), ed. Masson, W. P., New York, Academic Press New York, pp. 169, 1964.

[3.48] **Chang**, S. H., Rogacheva, N. N. and Chou, C. C., "Analysis of Methods for Determining Electromechanical Coupling Coefficients of Piezoelectric Elements", IEEE Transactions on Ultrasonics, Ferroelectrics, and Frequency Control, Vol. 42, pp. 630-640, 1995.

[3.49] **Nair**, V. K. and Ludwig, R., "Electromechanical Coupling Coefficient in Piezoelectric Transducers", Review of Progress in Quantitative NDE, eds. D.O. Thompson and D.E. Chimenti, American Institute of Physics, New York, Vol. 13, pp. 1031-1038, 1994.

[3.50] **Masson**, W. P., *Crystal Physics of Interaction Processes*, Academic Press, 1966.

[3.51] **Brissaud**, M., "Characterisation of Piezoceramic", IEEE Transactions on Ultrasonics, Ferroelectrics, and Frequency Control, Vol 38(6), 1991.

[3.52] **Bechmann**, R., "Ceramics and some Applications of the Piezoelectric Equations", J. Acoust. Soc. Am., Vol. 28, pp. 347-350, 1956.

[3.53] **Locke**, S., Kunkel, H. A. and Pikeroen, B., "Finite Element Modelling of Piezoelectric Ceramic Disks", Proc. IEEE. Ultrasonic Symposium, pp. 853-858, 1987.

[3.54] **Meeker**, T. R., "Thickness Mode Piezoelectric Transducer", Ultrasonics, Vol. 10, pp. 26-36, 1972.

[3.55] **Guo**, N., "The Vibration Characteristics of Piezoelectric Discs", Ph.D. Thesis, University of London (Department of Mechanical Engineering, Imperial College), 1989.

[3.56] **Ewings**, D. J., *Modal Testing Theory and Practice*, Research Studied Press Ltd., John Wiley & Sons Inc., 1984.

TABLES

Stiffness (Gpa)		Relative Permittivity Constants	
C11	108.8	ε_{xx}^{S}	1700
C12	55.8	ε_{zz}^{S}	1700
C66	26.5	Piezoelectric Stress Constants (coulomb/m^2)	
Density (Kg/m^3)		e_{x1}	40.46
ρ	2700	e_{x6}	20

Table 3.1: Material parameters.

Stiffness (Gpa)		Relative Permittivity Constants	
C33	245	ε_{xx}^{S}	44
C11	203	ε_{zz}^{S}	29
C13	75	Piezoelectric Stress Constants (coulomb/m^2)	
C14	9	e_{x5}	3.7
C44	60	e_{y2}	2.5
Density (Kg/m^3)		e_{z1}	0.2
ρ	4700	e_{z3}	1.3

Table 3.2: Material parameters for lithium niobate - LiNbO3.

	FE77	PZFlex®	Difference
Resonance (MHz)	7.19 ± 0.01	7.27 ± 0.01	1.1% ± 0.3
Anti-resonance (MHZ)	7.29 ± 0.01	7.37 ± 0.01	1.1% ± 0.3
$k_d = \sqrt{\frac{f_a^2 - f_r^2}{f_r^2}}$	0.167	0.164	0.6 %

Table 3.3: Comparison of the predicted resonance and anti-resonance frequencies of the FE77 for the first mode of the LiNbO3 free strip shown in Figure 3.22.

Electromechanical coupling coefficients	$k = \sqrt{\frac{f_a^2 - f_r^2}{f_r^2}}$ from FE77	Static EMCC $k_{33} = \sqrt{\frac{e_{z3}^2}{\varepsilon_{zz}^S C_{33}^E}}$	$k = \sqrt{\frac{E_m^2}{E_{st} E_d}}$ from FE77
	0.167	0.164	0.163

Table 3.4: Comparison of the electromechanical coupling coefficient predicted by FE77 for the first mode shown in Figure 3.22 and the electromechanical coupling coefficients calculated using one-dimensional approximations.

Stiffness (Gpa)		Relative Permittivity Constants	
C33	117.4	ε_{xx}^S	1700
C11	127.2	ε_{zz}^S	1470
C13	84.7e9	Piezoelectric Stress Constants (coulomb/m^2)	
C44	23.5e9	e_{x5}	17
Density (Kg/m^3)		e_{z1}	-6.5
ρ	7500	e_{z3}	23.3

Table 3.5: Material parameters for PZT 5H.

Density	Longitudinal velocity	Shear velocity
2700 Kg/m^3	6.41 mm/μs	3.04 mm/μs

Table 3.6: Material parameters for the aluminium plate.

FIGURES

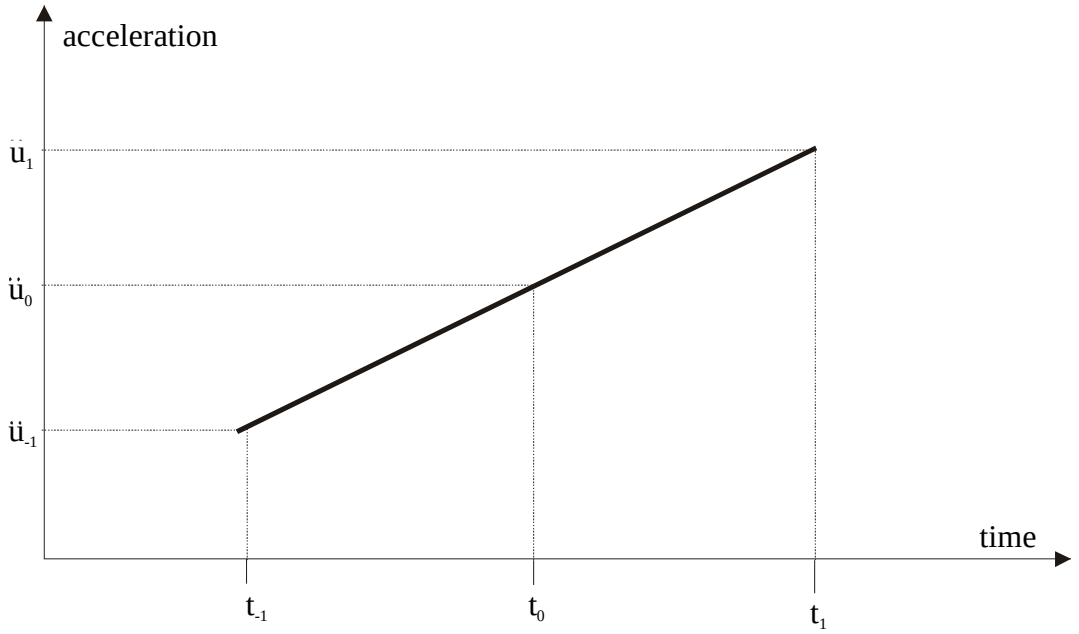

Figure 3.1 : Linear acceleration

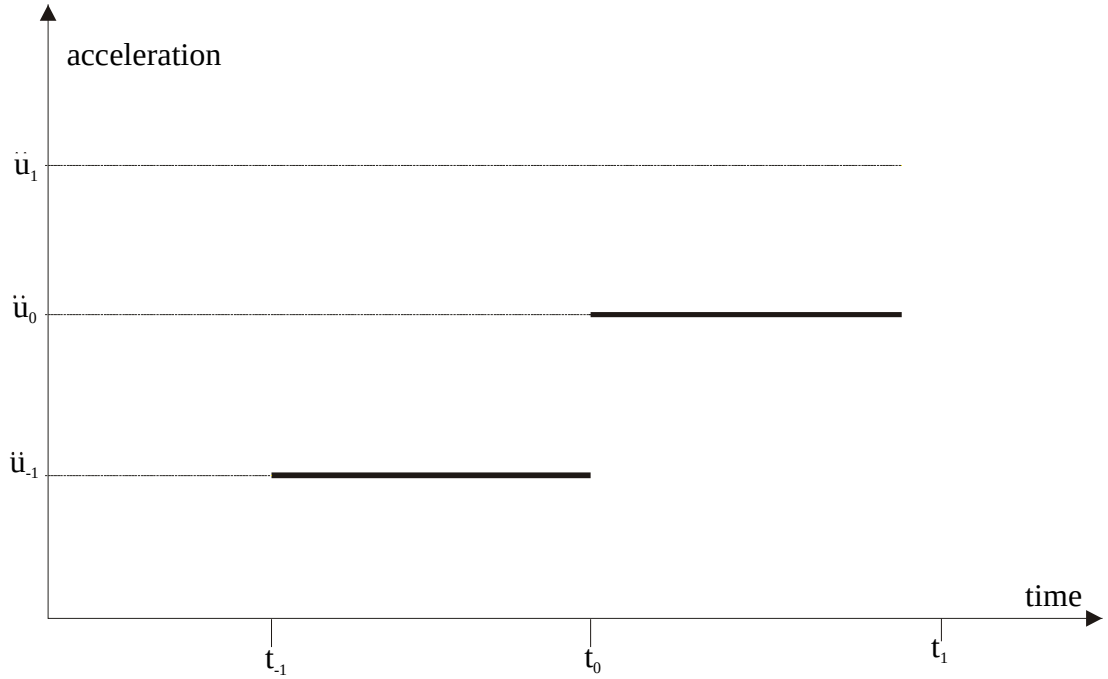

Figure 3.2 : Constant acceleration

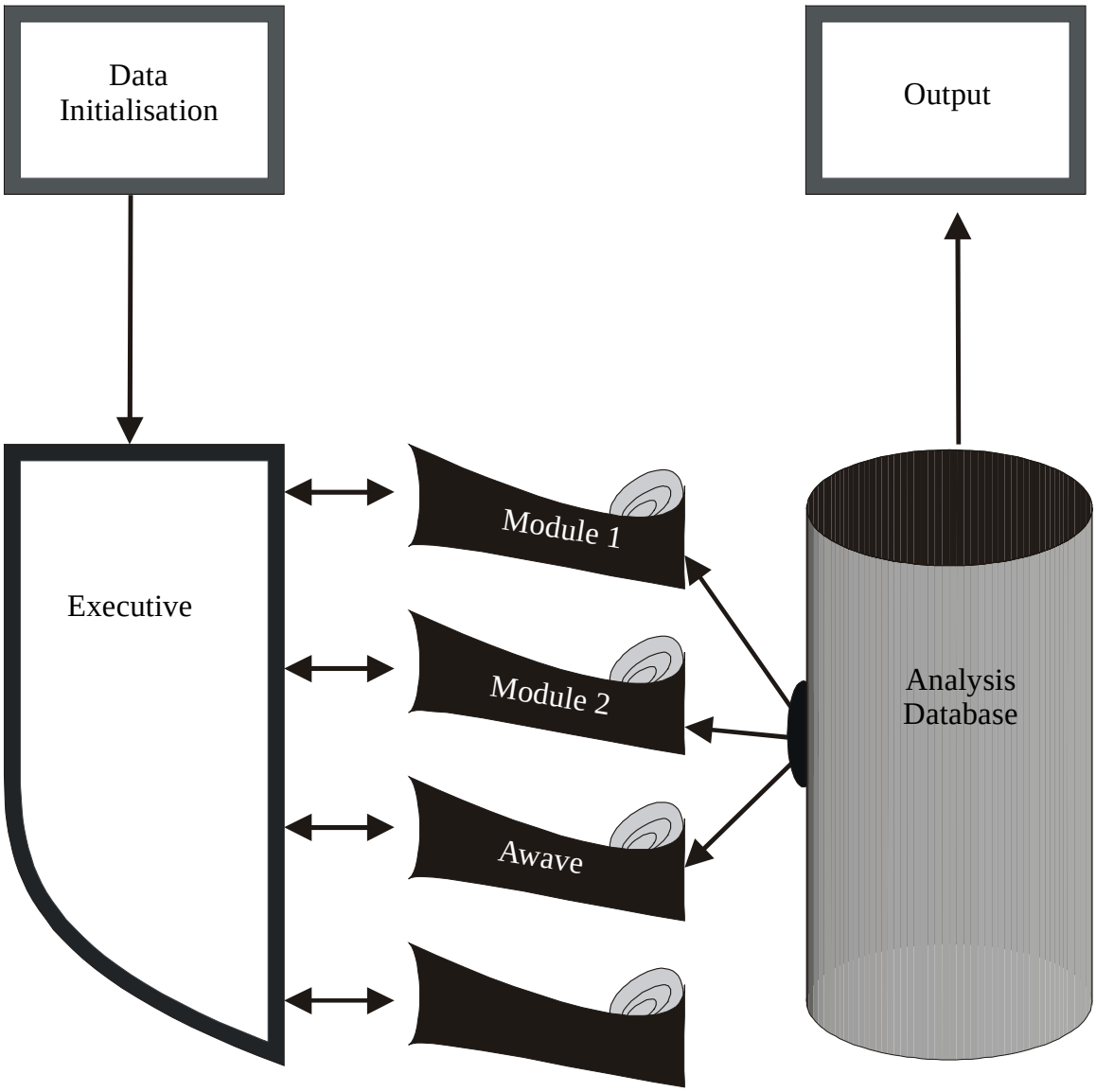

Figure 3.3 : FE77 program architecture

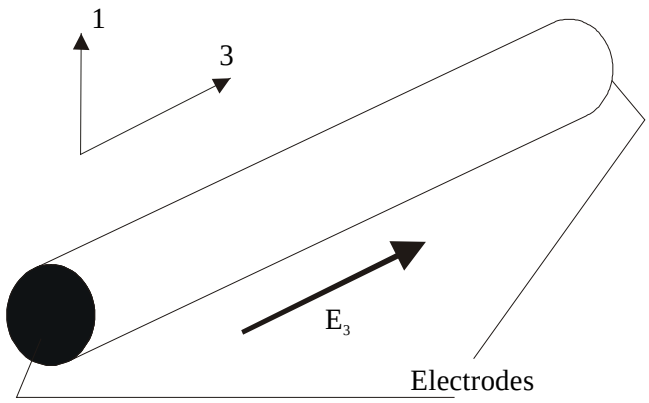

Figure 3.4 : Schematic representation of a long slender rod submitted to an axial electric field, E_3. Elastic conditions for the calculation of fundamental mode coupling factor are: $T_1 = T_2 = 0$, $T_3 \neq 0$ and $S_1 = S_2 \neq S_3 \neq 0$.

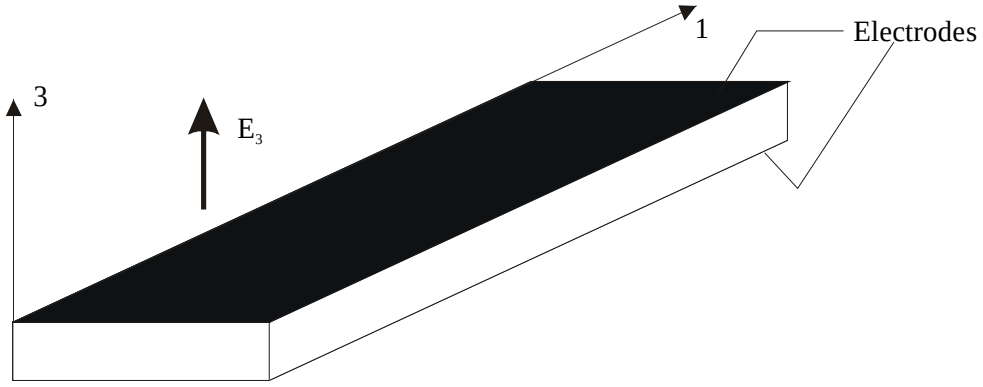

Figure 3.5 : Schematic representation of a thin plate submitted to a through thickness electric field, E_3. Elastic conditions for the calculation of thickness mode coupling factor are: $S_1 = S_2 = 0$; $S_3 \neq 0$ and $T_1 = T_2 \neq 0$; $T_3 \neq 0$.

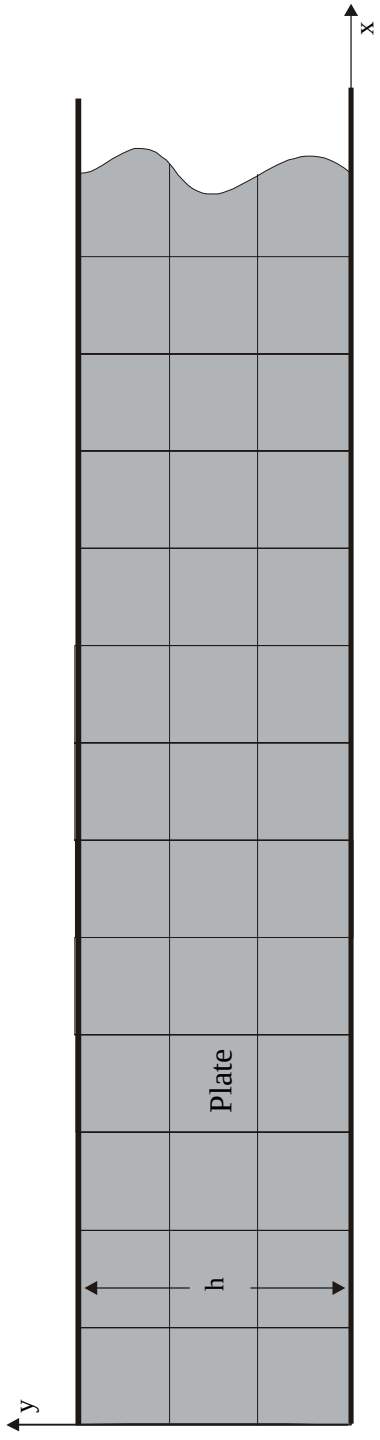

Figure 3.6 : Schematic representation of the geometry and the coordinate system used.

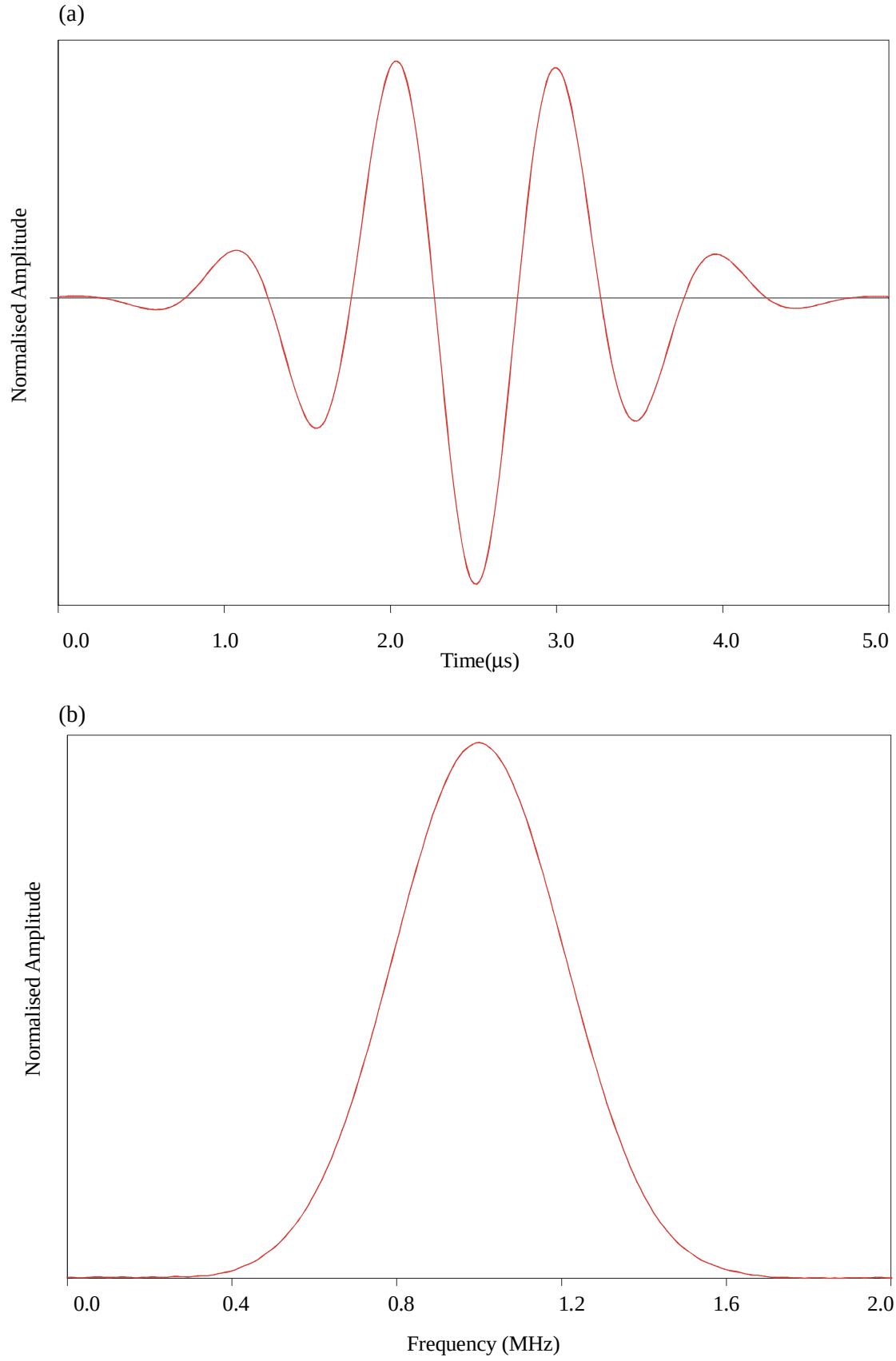

Figure 3.7 : Time history and corresponding amplitude spectrum of the 5-cycle toneburst applied at all nodes on plane x = 0.

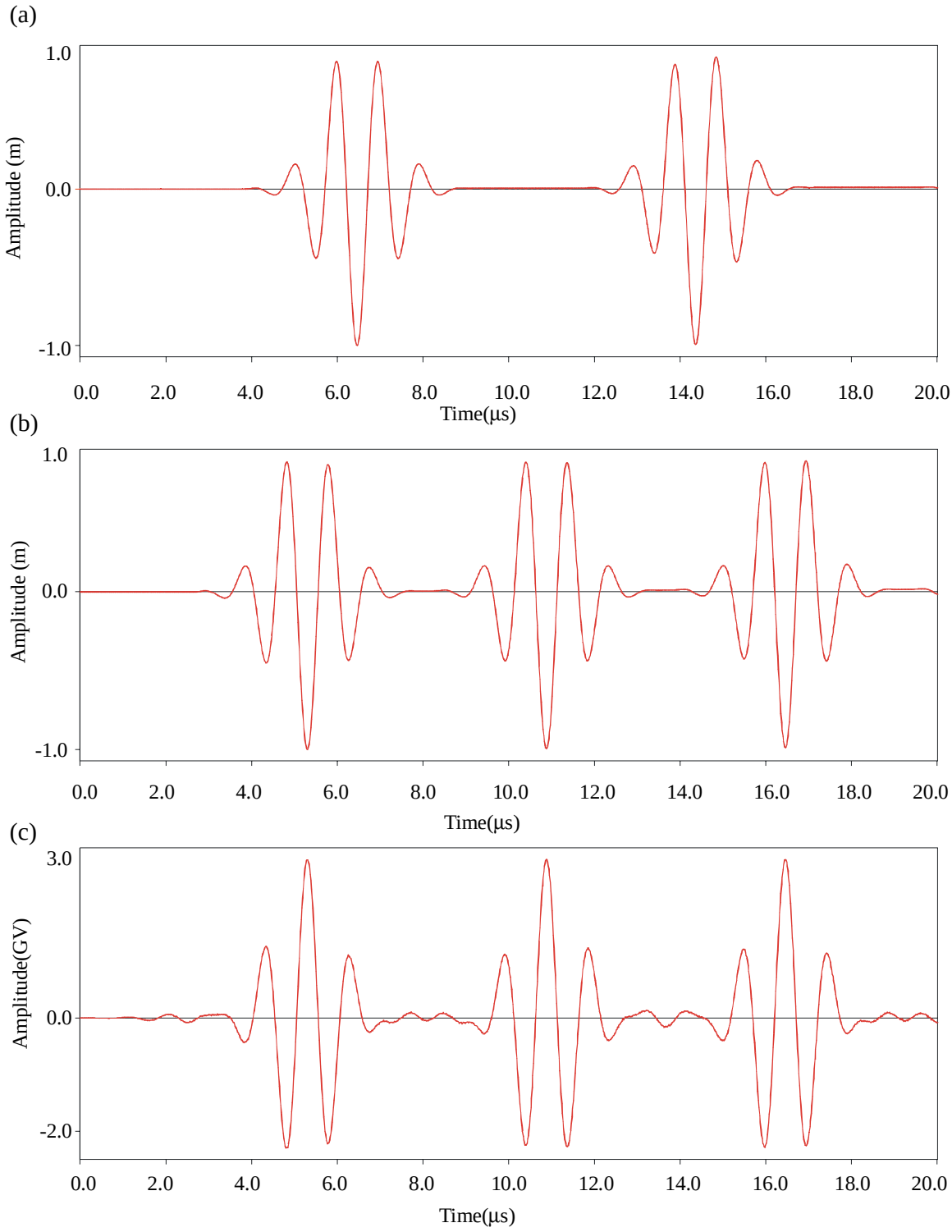

Figure 3.8 : Predicted time history at x = 25 mm, when the input was designed to excite only the longitudinal wave, (a) displacement in the x direction with no piezoelectricity, (b) displacement in the x direction with piezoelectricity and (c) corresponding electric potential.

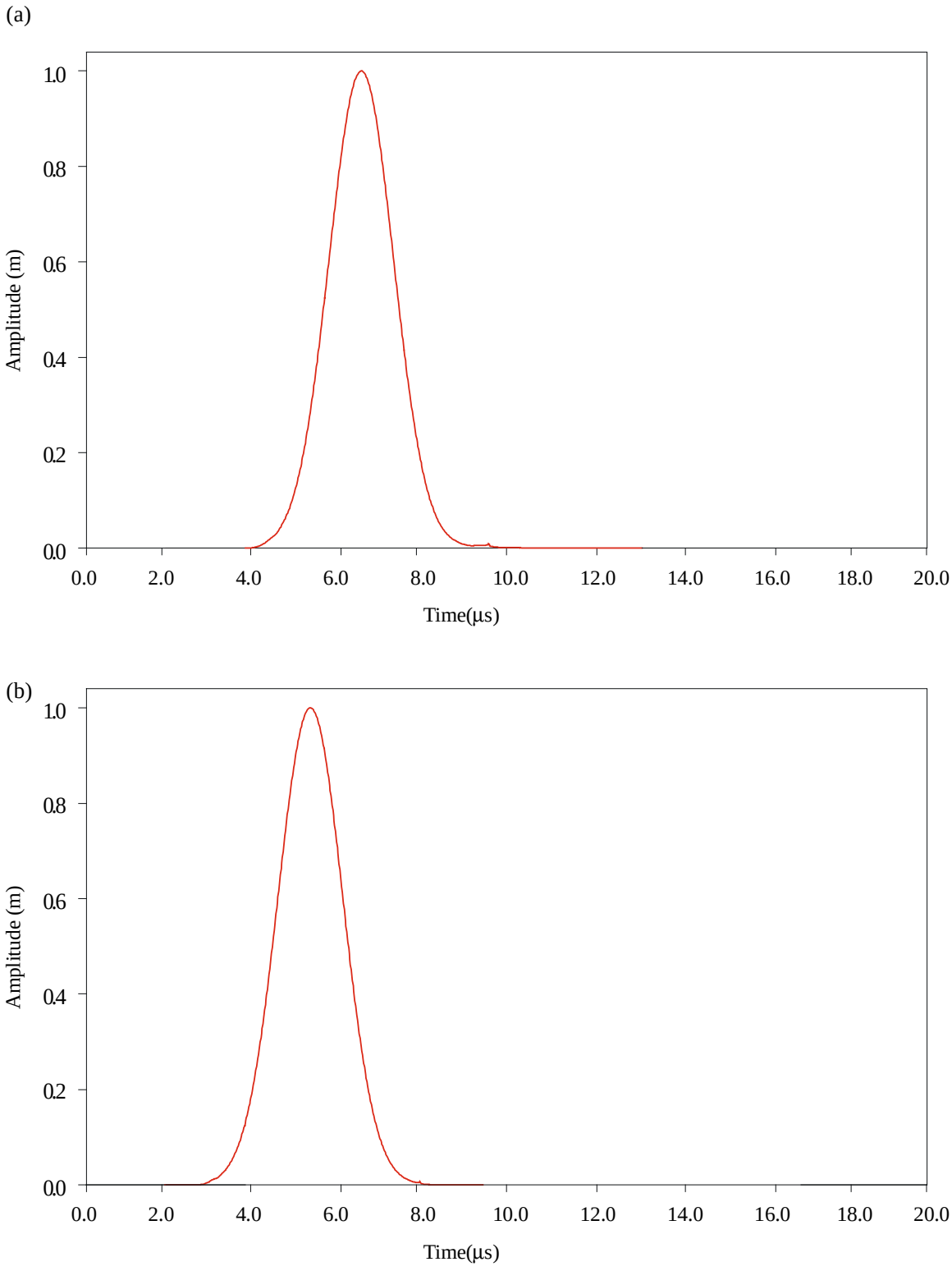

Figure 3.9 : Envelopes of the first wave packets taken from (a) Figure 3.8(a) and (b) Figure 3.8(b).

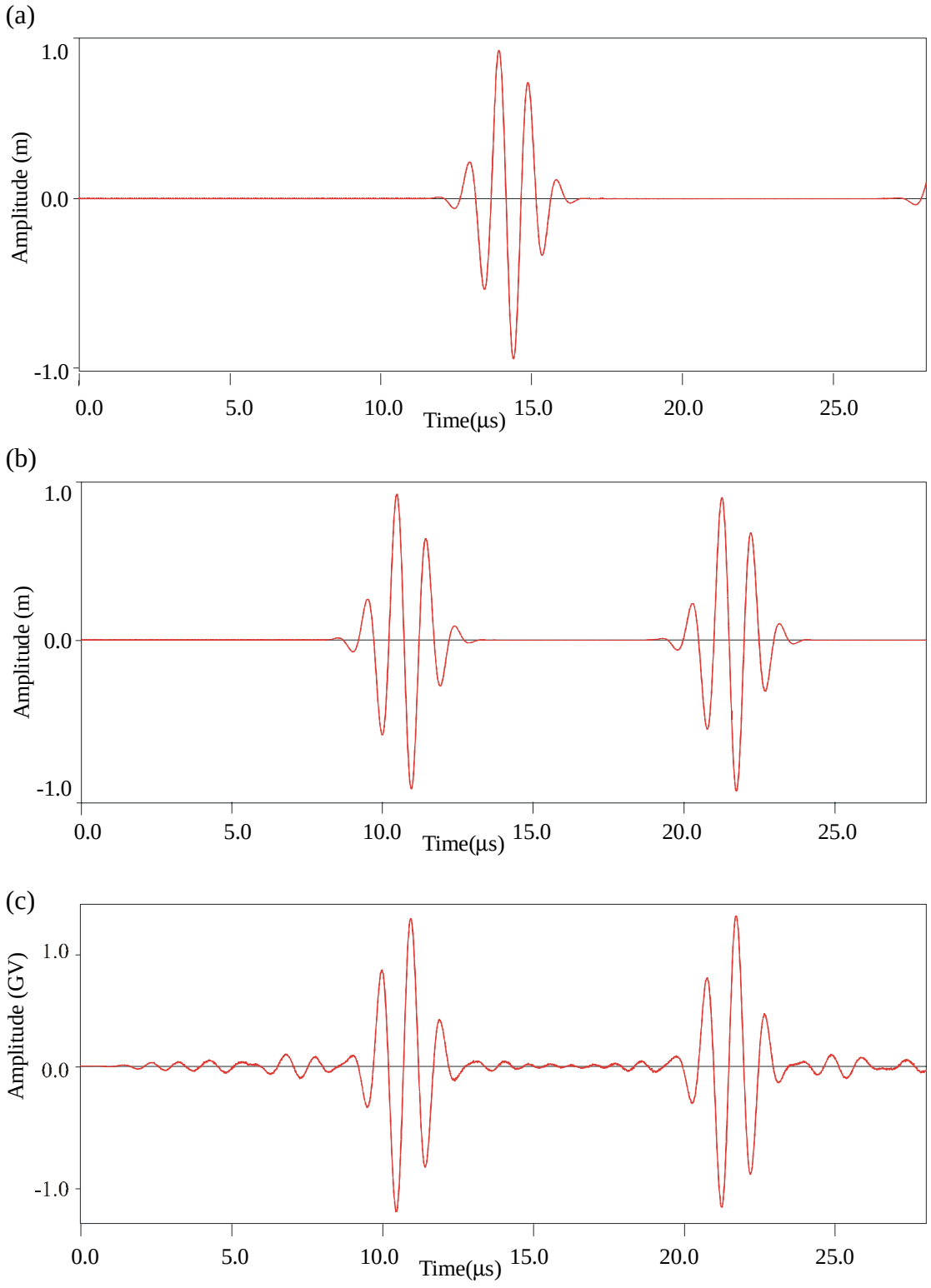

Figure 3.10 : Predicted time history at x = 25 mm, when the input was designed to excite only a shear wave, (a) displacement along *x* with no piezoelectricity, (b) displacement along *x* with piezoelectricity, and (c) corresponding electric potential.

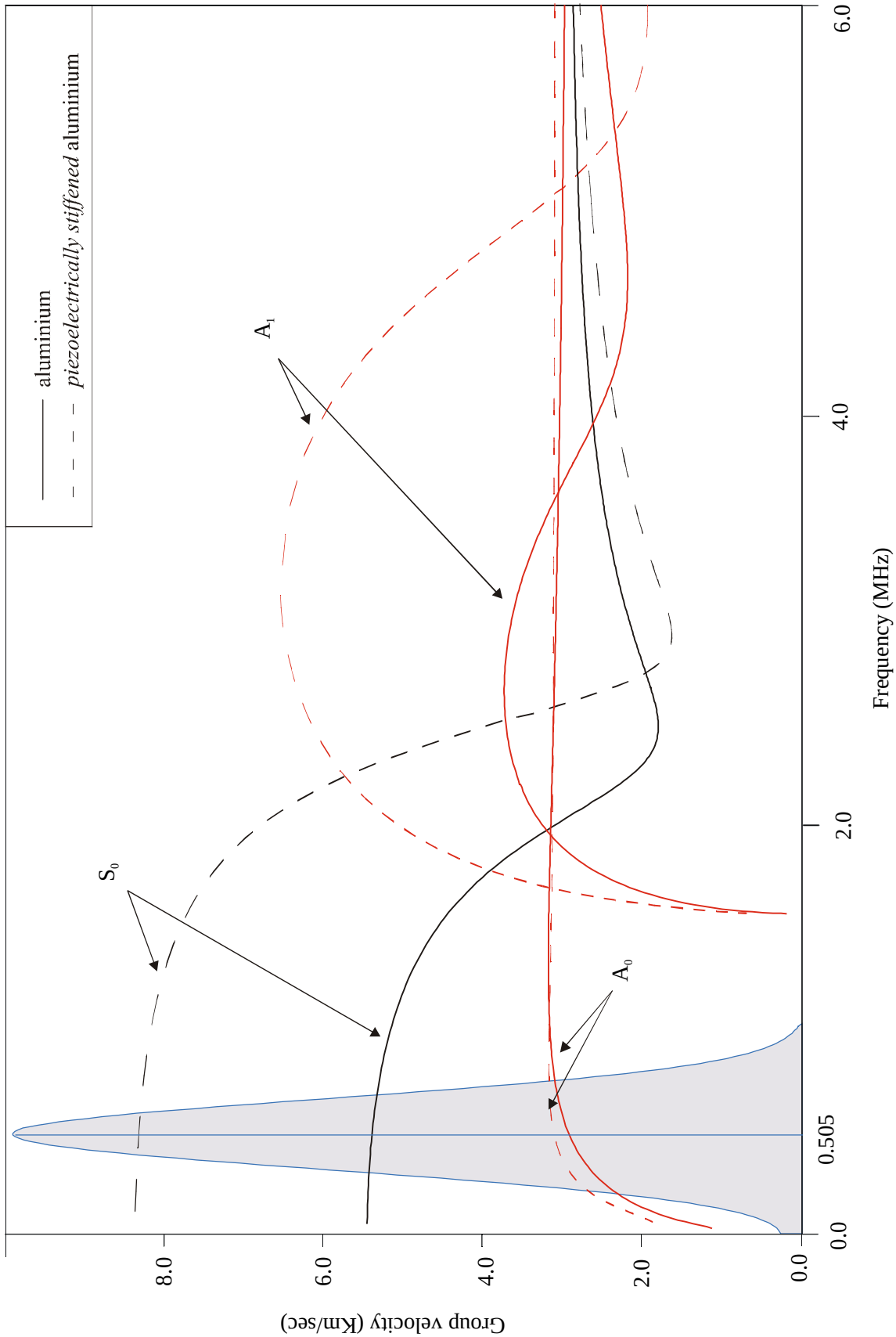

Figure 3.11 : Comparison between the group velocity dispersion curves for aluminium and for aluminium with the C_{11} stiffness constant piezoelectrically *stiffened* (e_{x1} = 40.46).

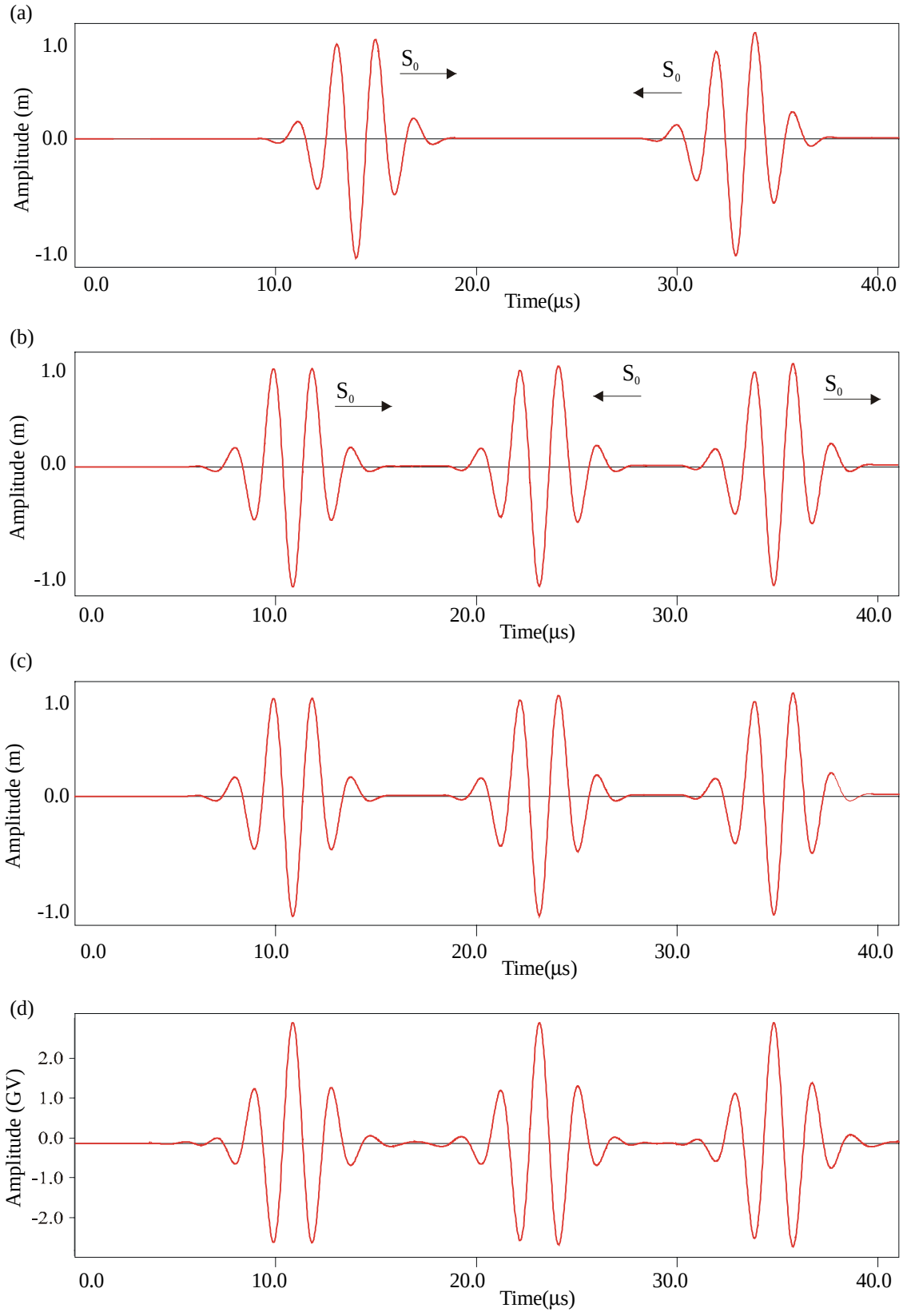

Figure 3.12 : Predicted time history when the input was designed to excite only the S_0 mode, (a) displacement in the aluminium plate, (b) displacement in aluminium with the C_{11} stiffness constant piezoelectrically *stiffened* (e_{x1} = 40.46), (c) displacement in an aluminium plate with the stiffness constant C_{11} doubled, (d) electric potential corresponding to (b).

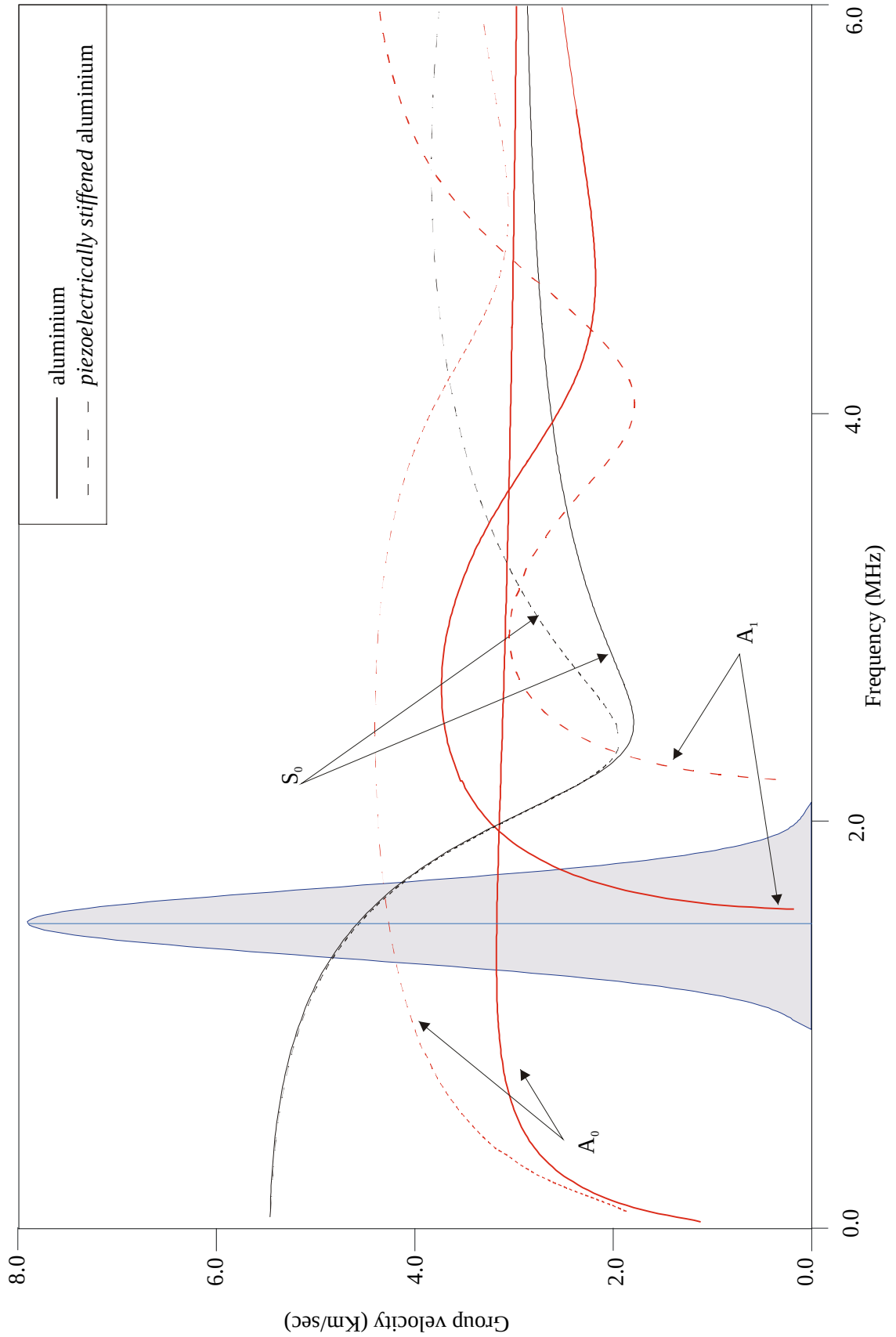

Figure 3.13 : Comparison between the group velocity dispersion curves for aluminium and for aluminium with the C_{66} stiffness constant piezoelectrically *stiffened* (e_{x6} = 20).

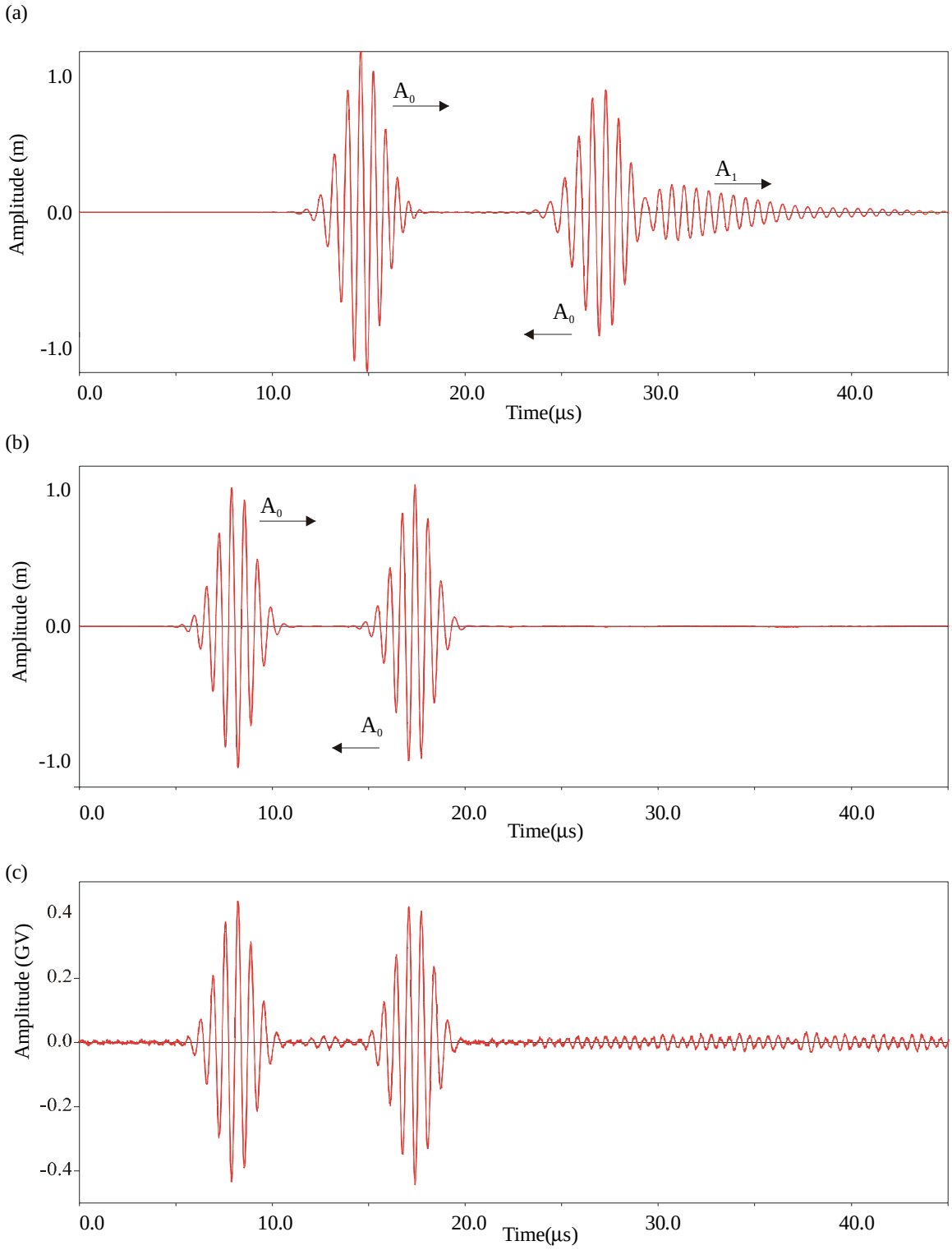

Figure 3.14 : Predicted time history when the input was designed to excite only the A_0 mode, (a) displacement in the aluminium plate, (b) displacement in aluminium with the C_{66} stiffness constant piezoelectrically *stiffened* (e_{x6} = 20), and (c) corresponding electric potential.

(a)

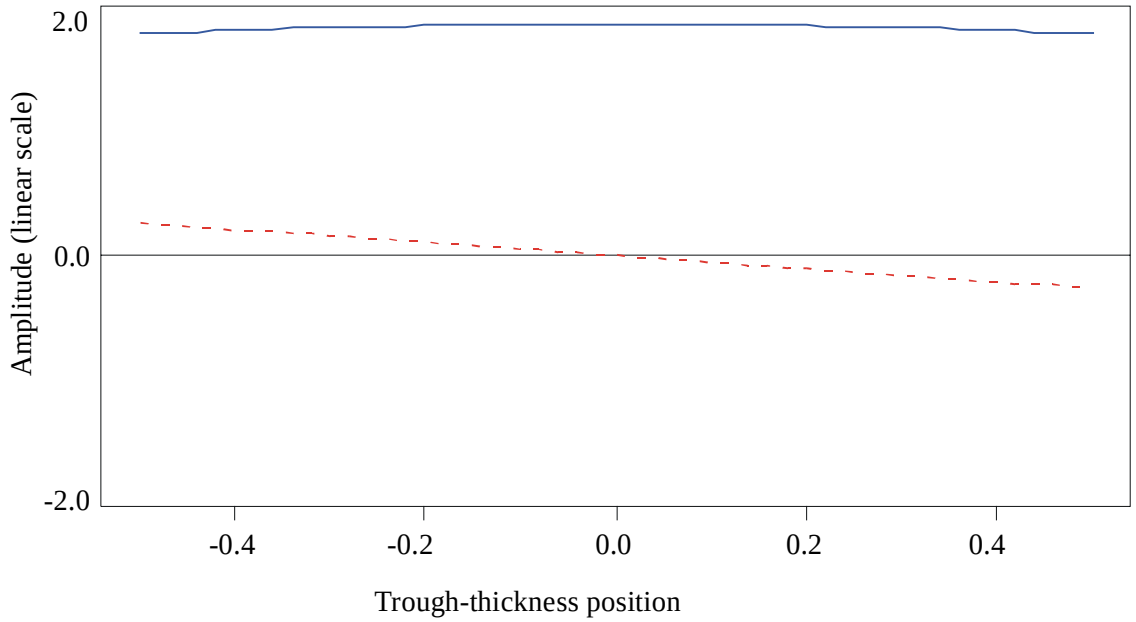

(b)

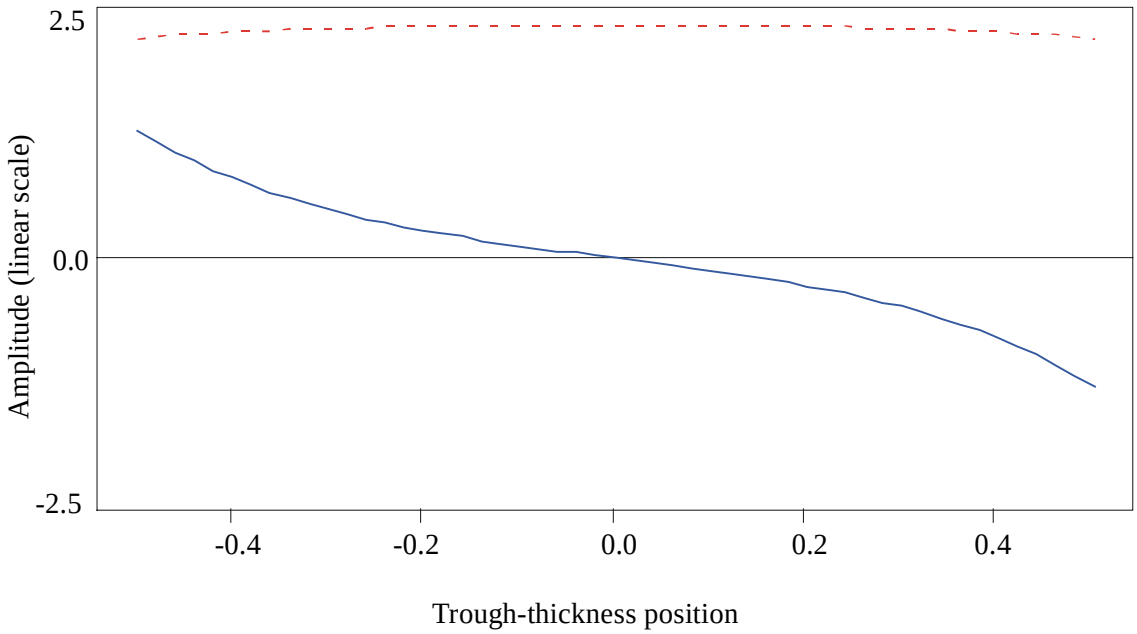

Figure 3.15 : The through-thickness deflected mode shapes of Lamb waves in a 1 mm thick plate with material properties are as given in Table 3.1 and where the longitudinal wave is *stiffened* with ex1 = 40.46: _____ x direction displacements, ---------- y direction displacements. (a) S_0 mode at 1 MHzmm (b) A_0 mode at 1MHzmm.

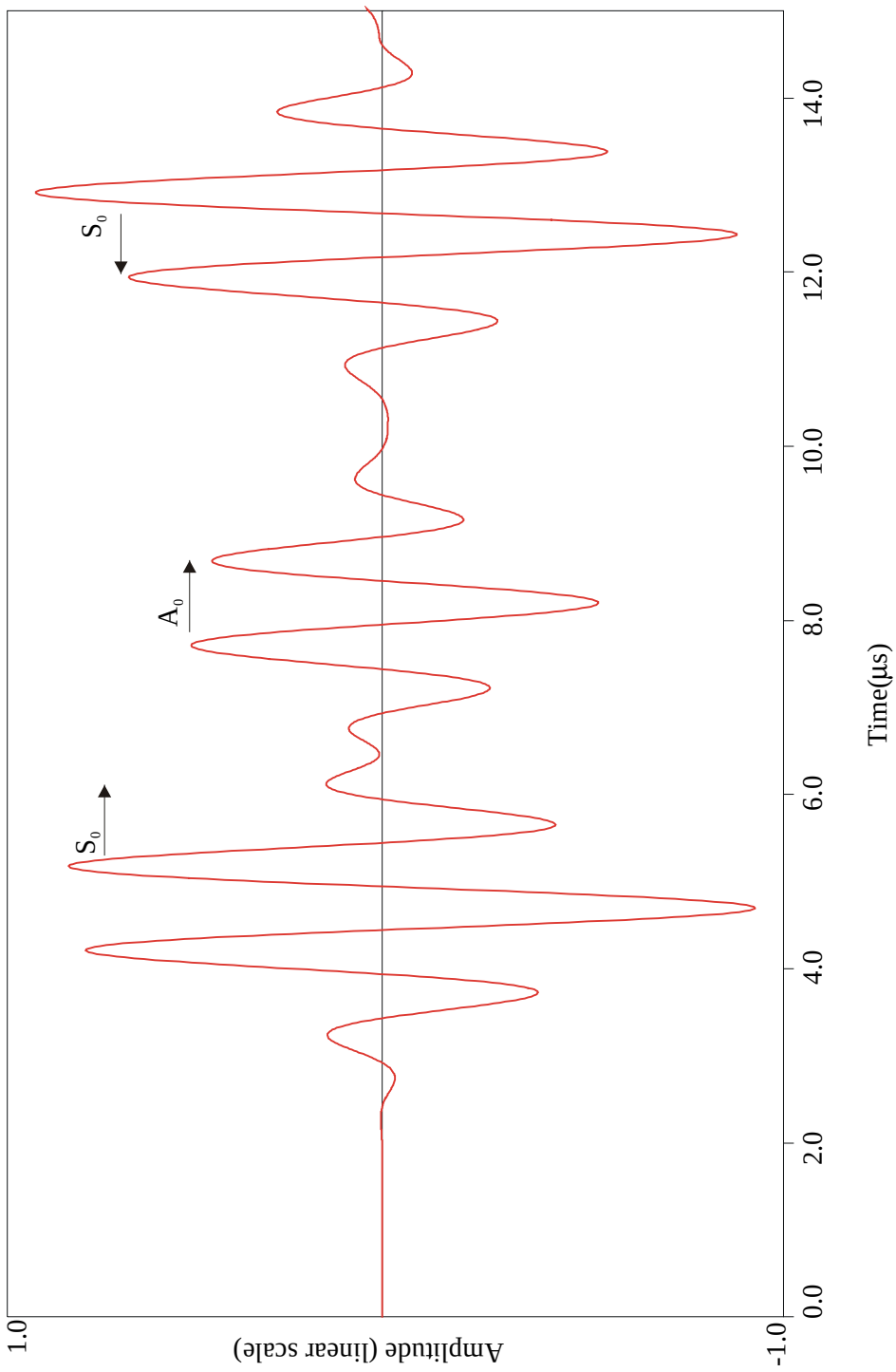

Figure 3.16 : Predicted time history, for x-direction displacements, at x = 18mm in a 1mm plate when the input is designed to excite both the A_0 and the S_0 modes at 1 MHz.

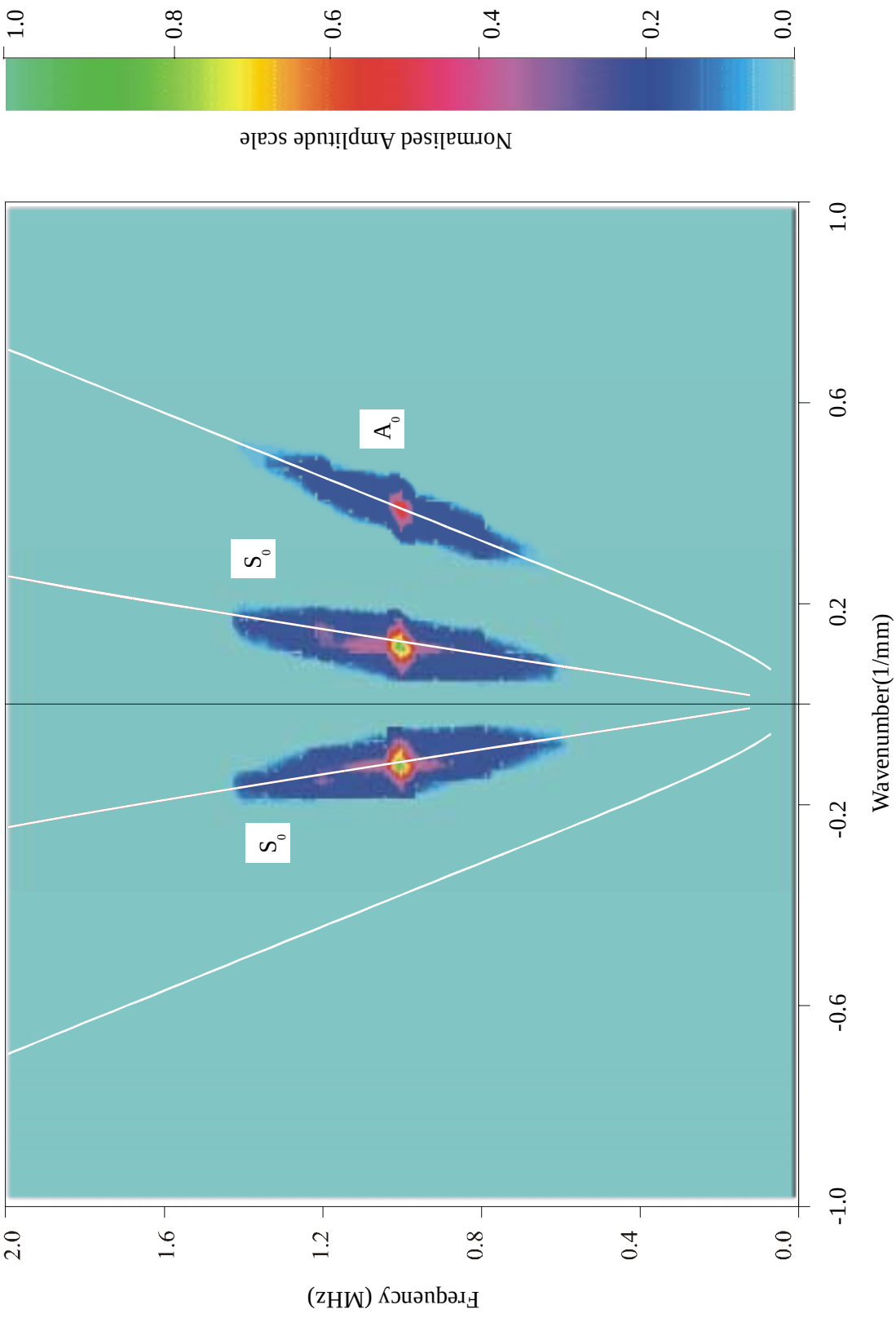

Figure 3.17 : Surface plot of the 2-D FFT results of the case given in Figure 3.16. Reflected waves are plotted with negative wavenumbers. Wavenumber dispersion curves are overlaid.

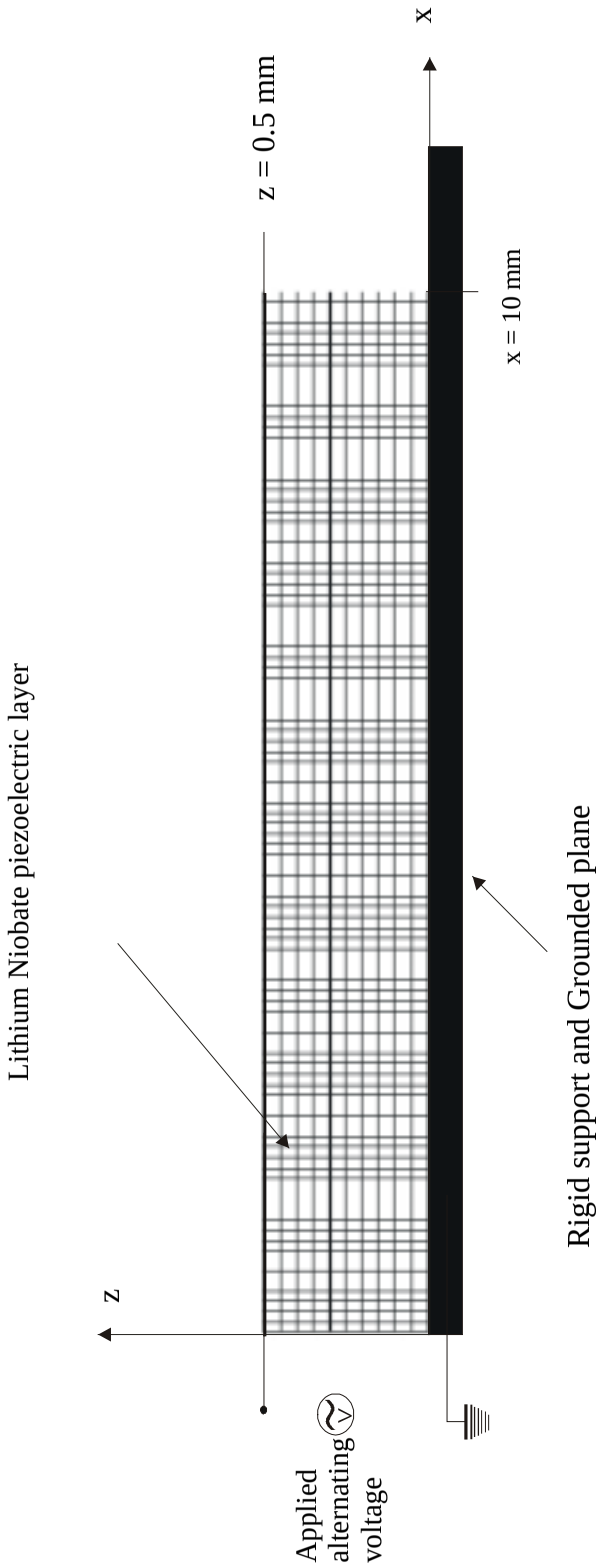

Figure 3.18 : Schematic diagram of the clamped piezoelectric strip model.

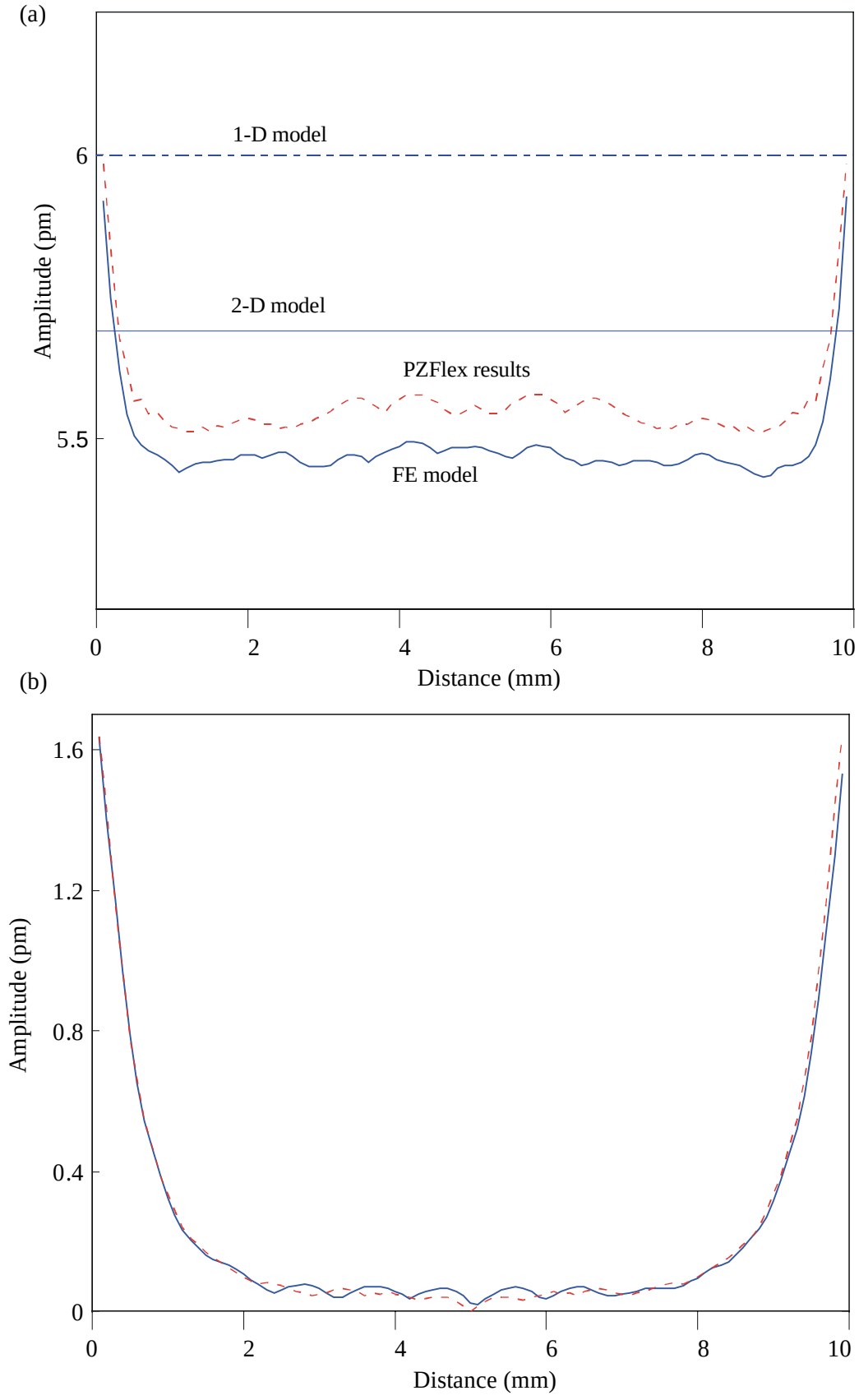

Figure 3.19 : Displacement profile at the free face. (a) Comparison between theoretical results and displacements, in the z direction, predicted using FE77 and PZFlex® (b) Comparison between FE77 and PZFlex® in the *x* direction.

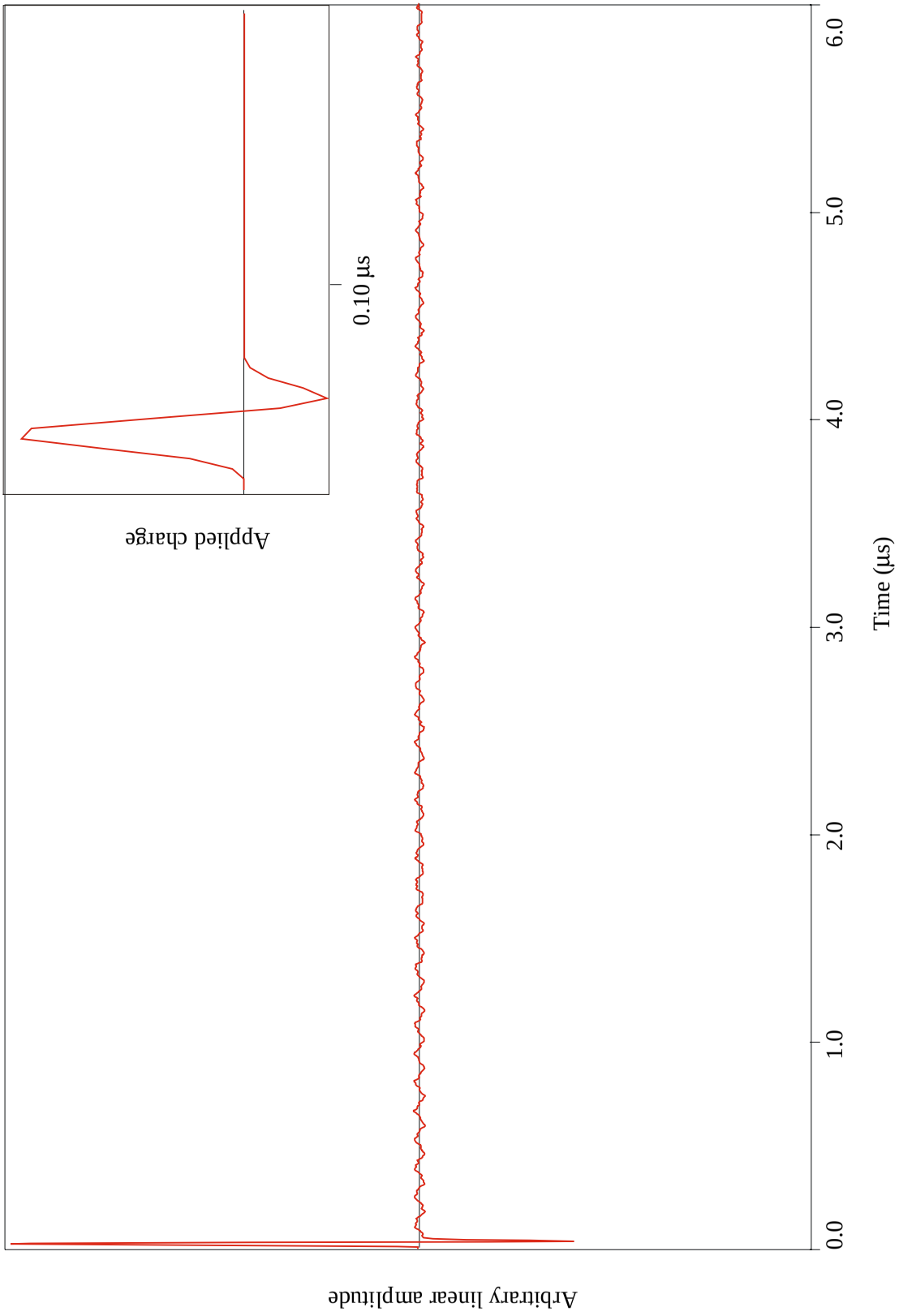

Figure 3.20 : The induced transient voltage response across the LiNbO3 free strip to the charge pulse of 0.0525 µs.

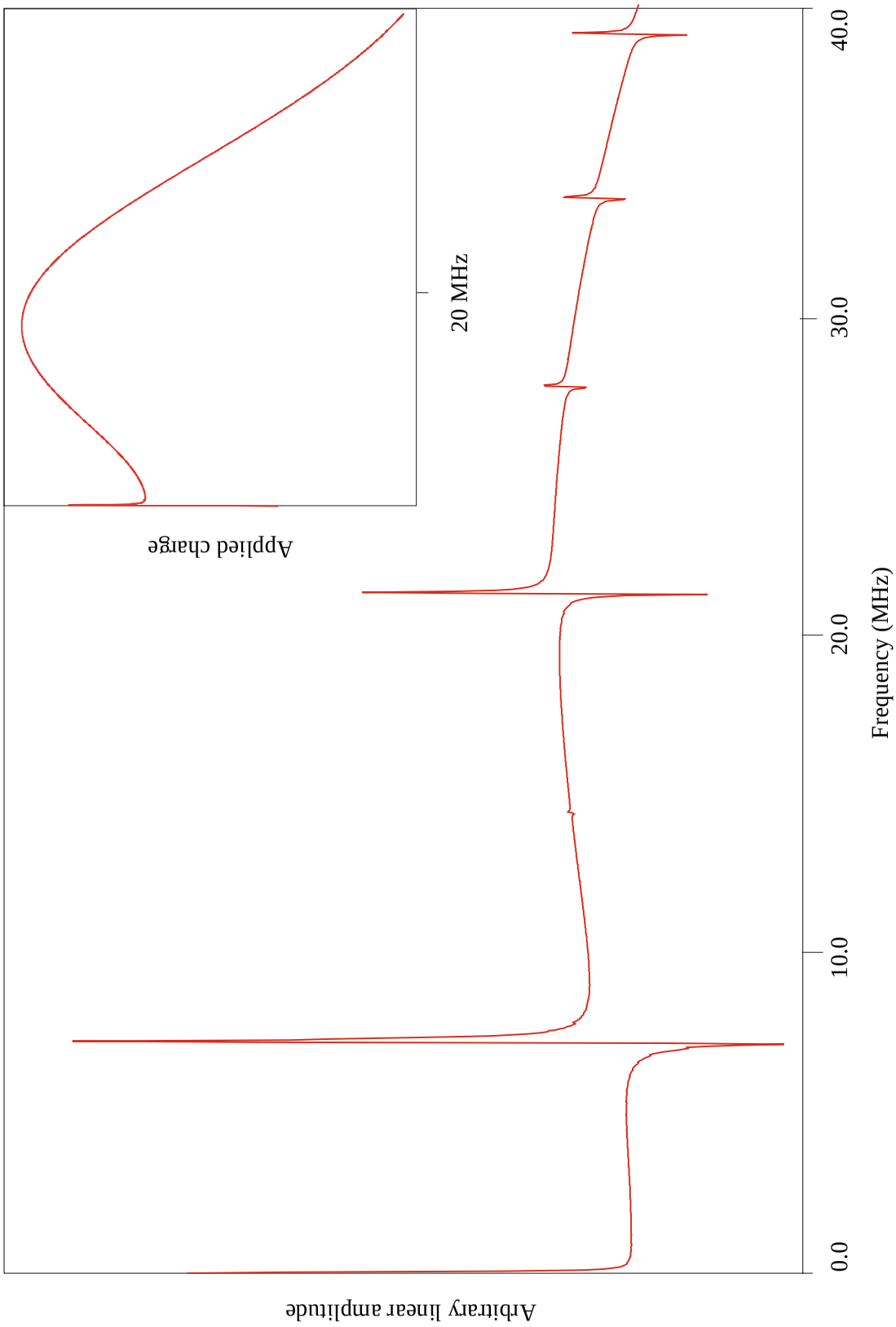

Figure 3.21 : Frequency spectrum of the charge impulse (1 cycle at 20 MHz) and frequency spectrum of the predicted voltage response at the surface top electrode of the LiNbO3 free strip.

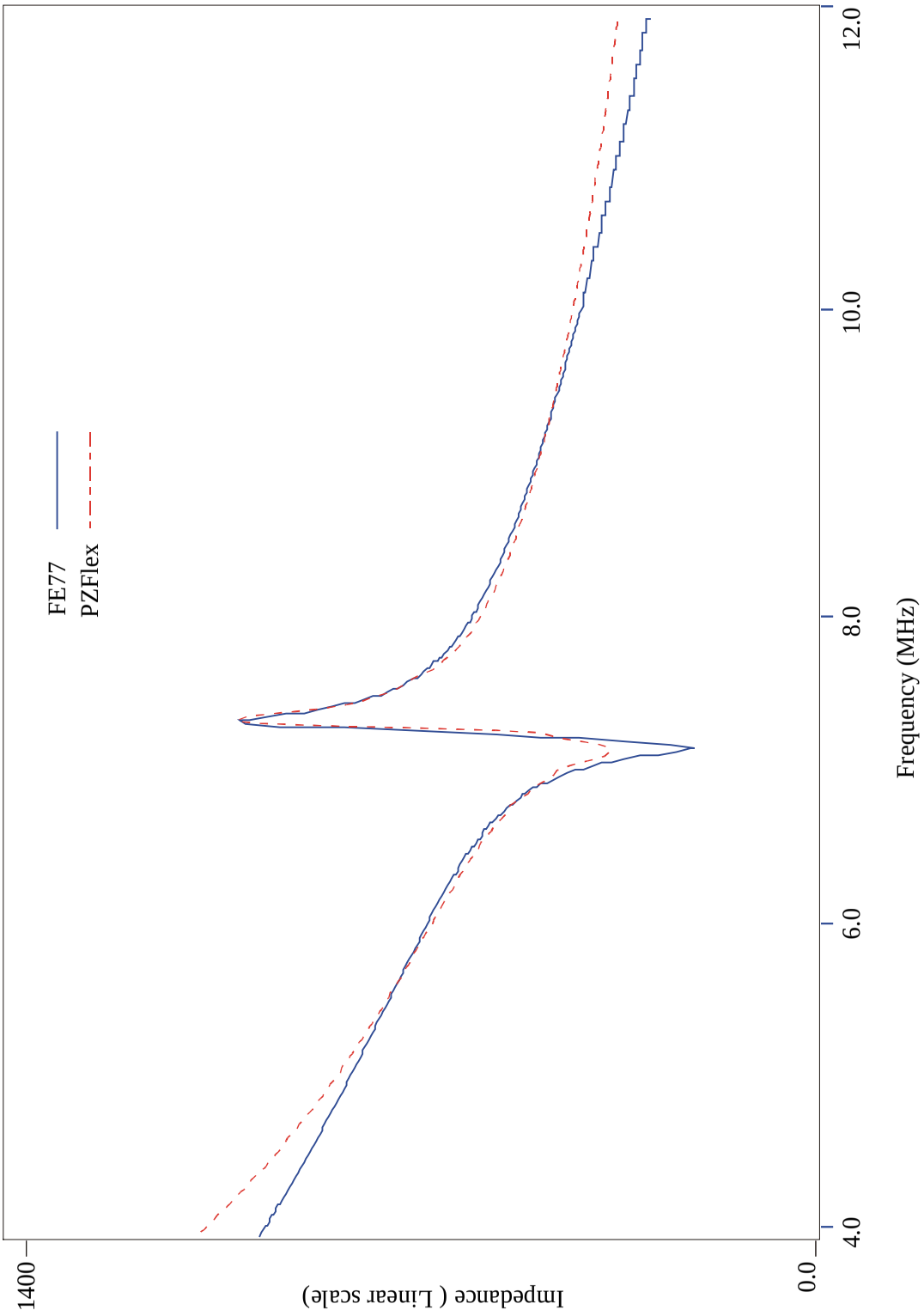

Figure 3.22 : Comparison of the predicted electrical input impedance of the LiNbO3 free strip by FE77(_____) and PZFlex® (-------). Only the first mode of vibration is shown.

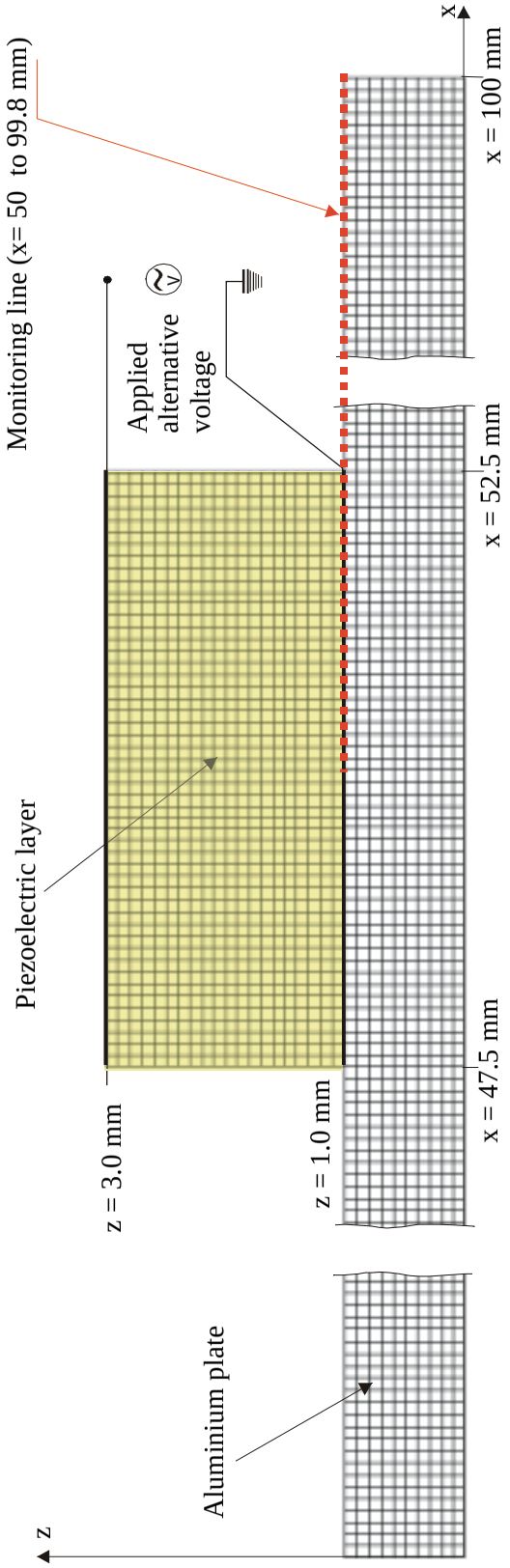

Figure 3.23 : Schematic diagram of the model, of a piezoelectric strip mounted on a plate, used in FE77.

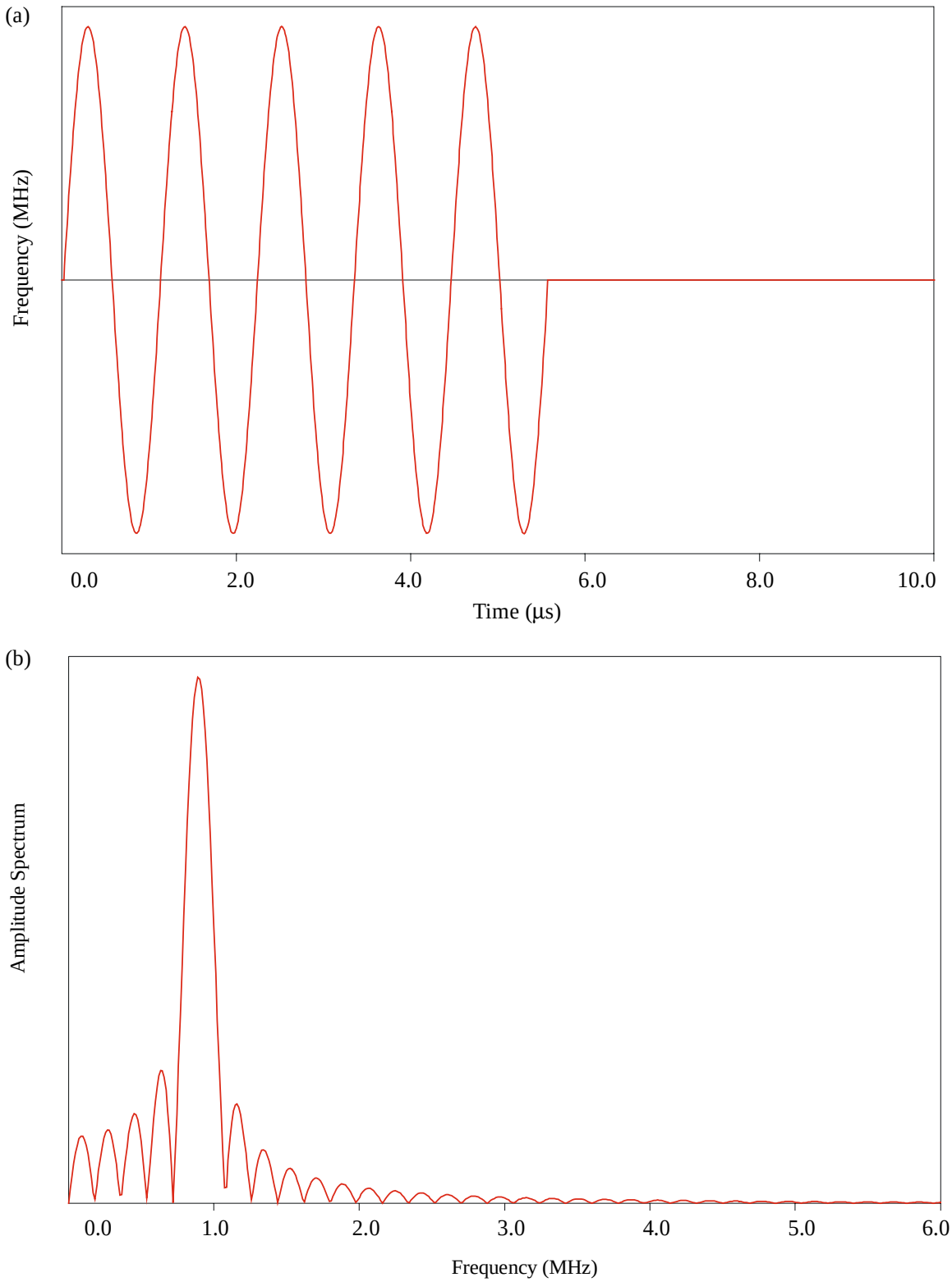

Figure 3.24 : (a) Time trace of the input signal, a 5 cycle toneburst in square window at 900 kHz, (b) frequency bandwith of the input toneburst.

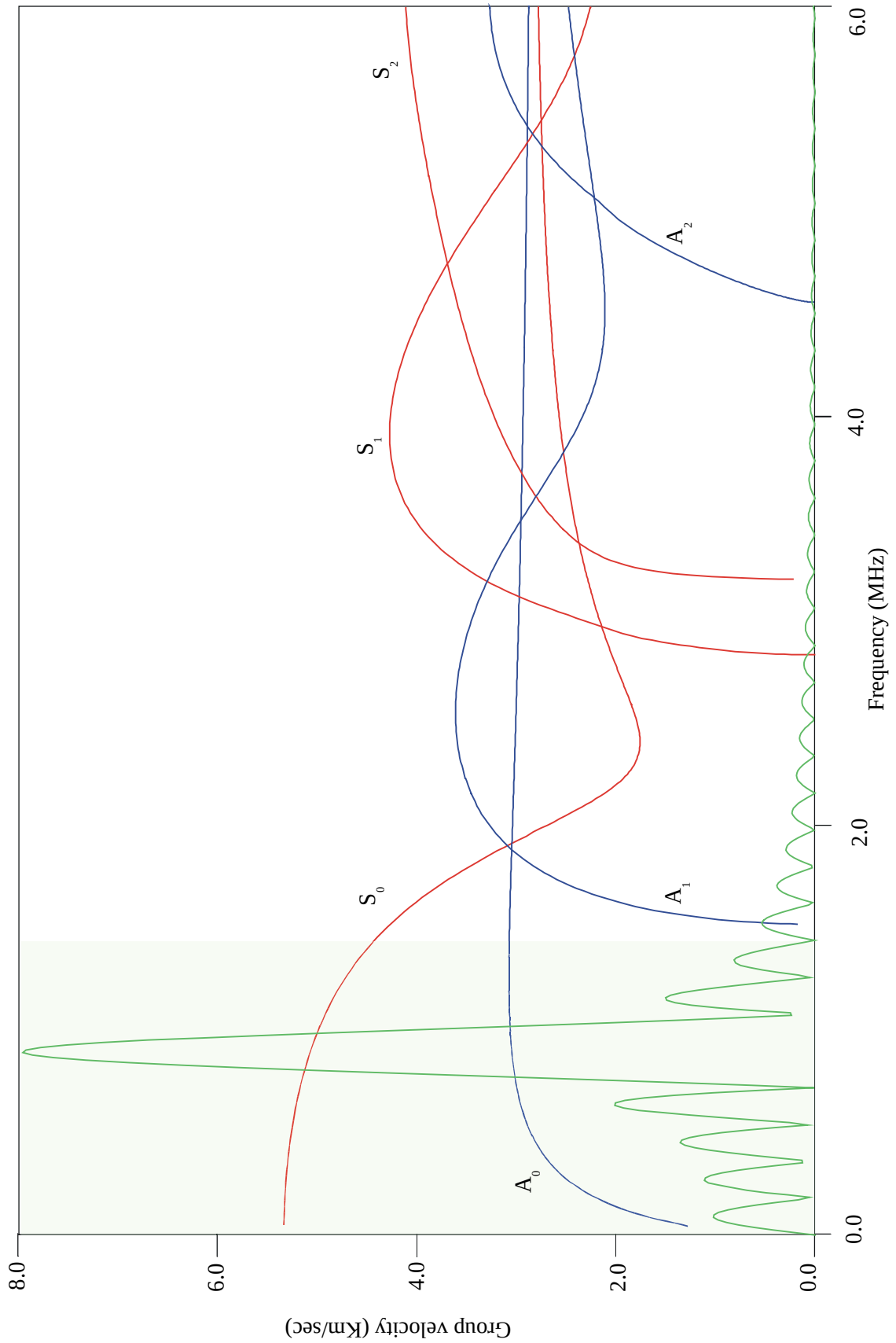

Figure 3.25 : Group velocity dispersion curves of the Lamb modes in a 1mm thick aluminium plate with, overlaid, the frequency spectrum of the excitation signal.

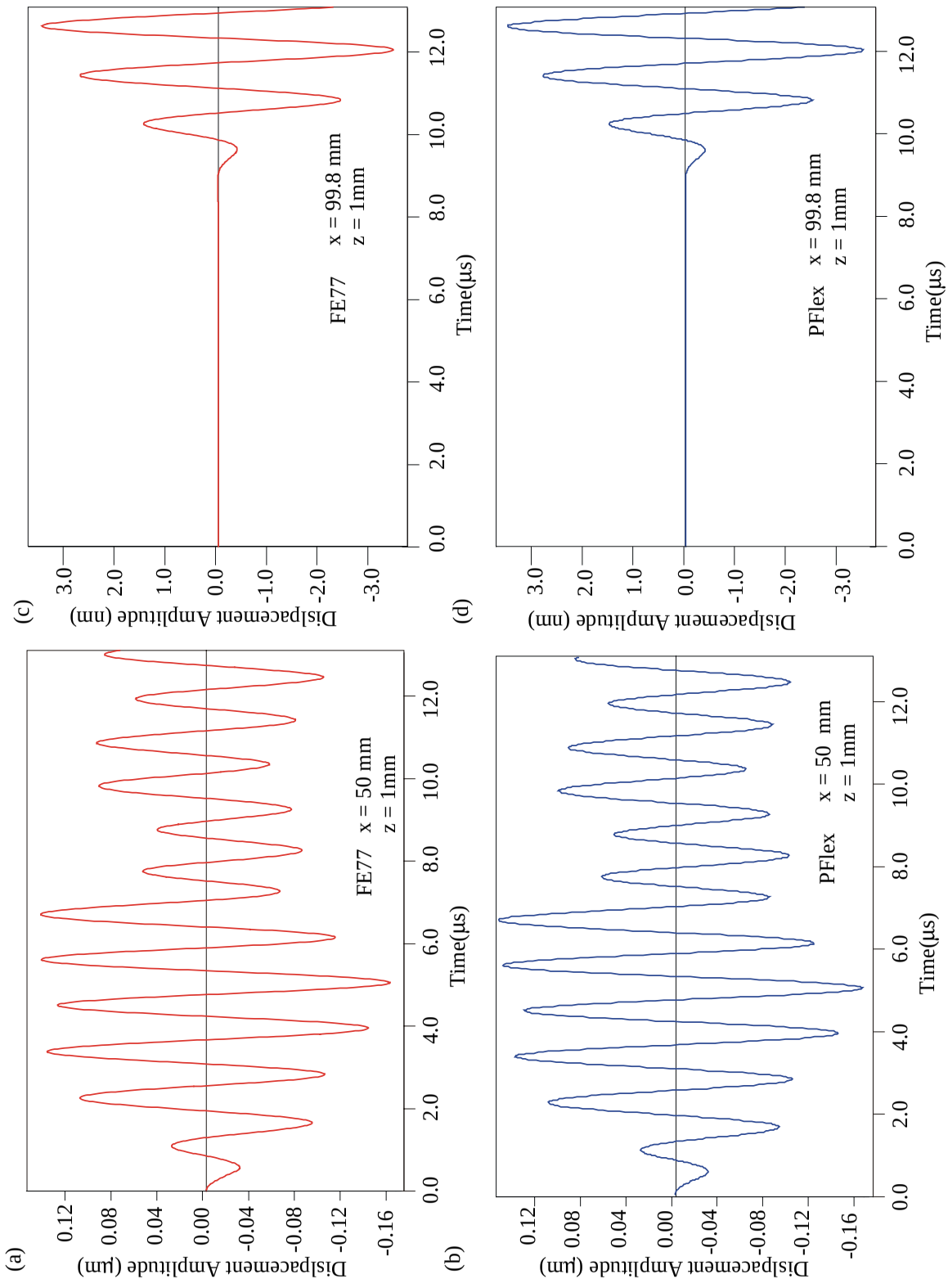

Figure 3.26 : Time history of the displacement in the *z* direction predicted by (a) FE77 at x = 50mm, (b) PZFlex at x = 50 mm, (c) FE77 at x = 99.8 mm and (d) PZFlex at x = 99.8 mm.

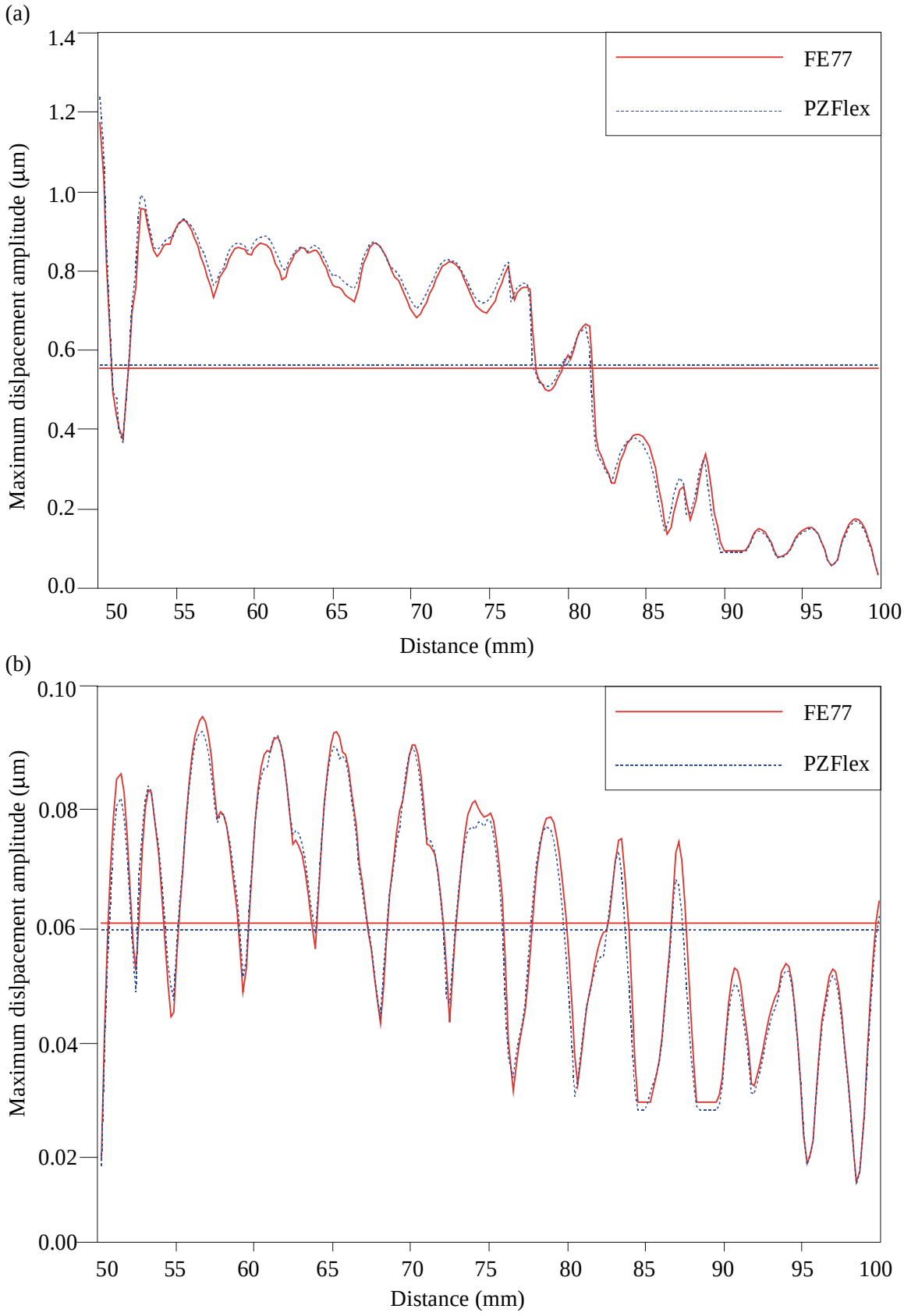

Figure 3.27 : Maximum displacement profiles. Comparison between the displacements predicted by FE77 and PZFlex (a) in the *z* direction, (b) in the *x* direction. Horizontal lines show the average value over the distance.

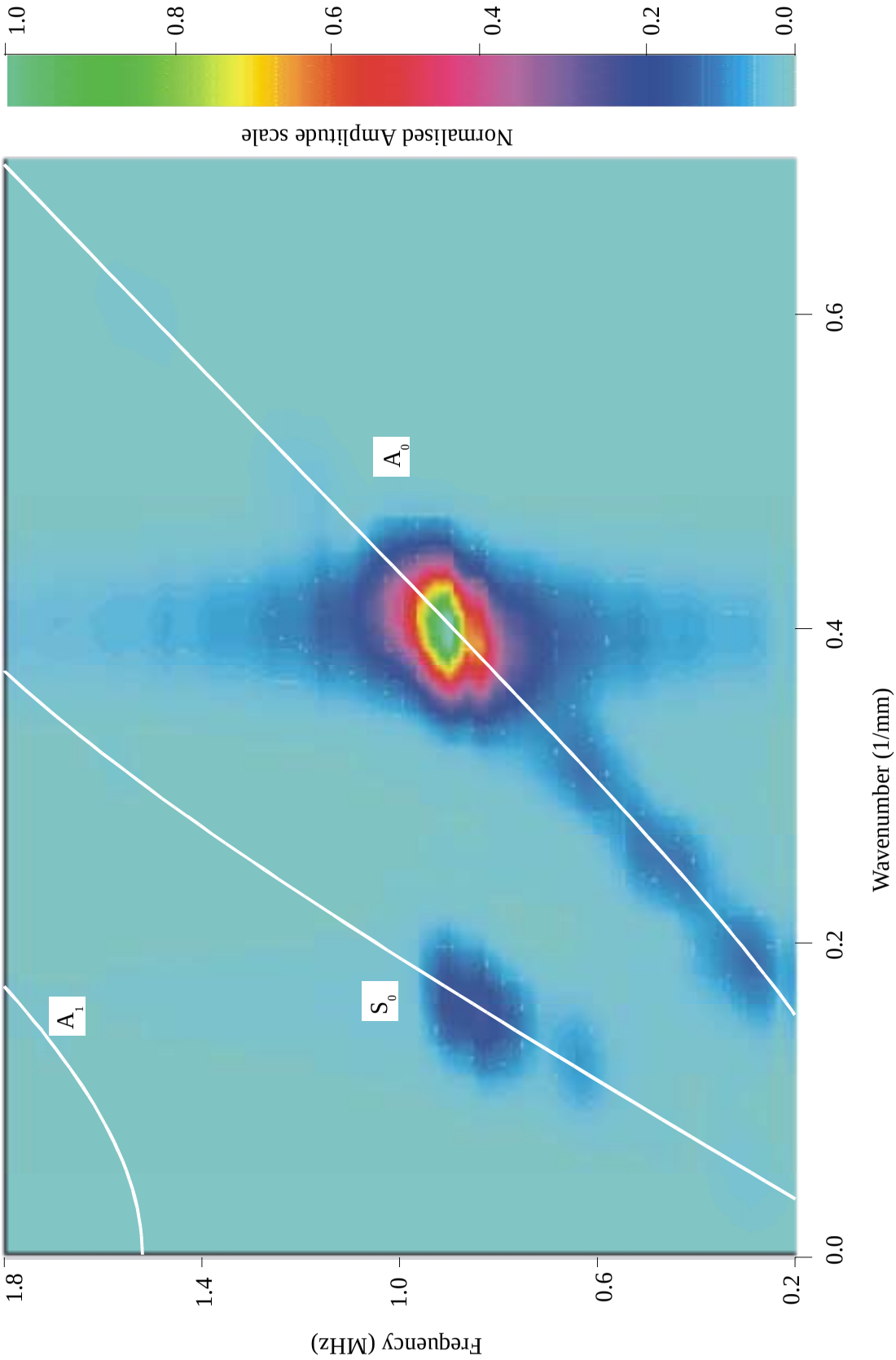

Figure 3.28 : Surface plot of the 2D-FFT results of the displacements in the *y* direction at the top surface of the plate. Wavenumber dispersion curves overlaid.

Chapter 4

Analytical Model

4.1 INTRODUCTION

This chapter is concerned with the development of an analytical model of the generation of Lamb waves by permanently attached sensors. As described in Chapter 1, the motivation for this model is the analysis of IDTs developed for use in *smart structures*. To do so we start with a simpler transducer design, the strip transducer. A strip transducer is simpler to model than an IDT because the electrical charge distribution under the single electrode of the strip transducer is much more simple to model than the charge distribution under the interdigital electrodes of an IDT. Simplifying the electrode pattern simplifies some of the mathematics associated with the model without diminishing the physical insights we draw from it, and lessons learned from this model will remain valid in most cases and in particular for IDTs.

A transducer structure is basically a simple stack of layers, the piezoelectric layer(s), electrodes, adhesive bonds and possibly other layers acting as backing or delay lines. Obviously each layer is of limited size in the three directions, however we perform a two-dimensional analysis assuming, with reference to many works on IDTs [4.1], [4.2], [4.3], [4.4], that the strip is long enough so that plain strain conditions are fulfilled. This not only simplifies the study but also allows us to use the classical Lamb wave solutions in rectangular two-dimensional coordinates. To model the interaction between the transducer and the structure it is necessary to understand both the mechanical and electromechanical interactions and also the internal scattering phenomena, and it is important to propose a model that will offer the necessary flexibility to design new transducers without having to redevelop a complete theory. Therefore this work not only aims to predict the amplitude of the Lamb wave generated

in the structure by a given voltage applied to the transmitter, but it also aims to do it in such a way that different designs can be modelled without having to change the model significantly. We also tried to keep the model analytical in order to provide physical understanding of the key processes. Keeping the problem analytical also enables us to determine appropriate transducer properties in order to generate a given mode with a given amplitude in a given structure. In that respect, an analytical model is superior to a finite element analysis.

4.2 PERTURBATION STRATEGY

To solve our problem, there exist various possible techniques, such as Green's functions to solve directly the field equations [4.5], and the variational method [4.6] to quantify the transducer admittance. They are very attractive in many respects but they both present some serious disadvantages regarding the desired flexibility of the model and moreover they require heavy numerical calculations. These techniques have in common that the solution is found by calculating the electromechanical coupling coefficient of the transducer, then the power radiated into the plate is calculated and eventually the amplitudes of the modes that propagate in that plate is derived. The disadvantages of such techniques come from their complexity and also from the fact that right from the beginning the calculations are intimately linked to the shape of the transducer and in particular to the shape of the electrode(s) which determines the distribution of the electric field within the piezoelectric layer, and therefore the nature of the piezoelectric coupling. In order to overcome this inconvenience we propose a totally opposite approach based on the normal mode theory [4.7] and the perturbation method [4.8]. We start by calculating the fields of the modes that can exist in the plate and then we perturb them by adding layers and boundary conditions that represent the layers and the boundary conditions inside the transducer. The main reason that justifies such a choice is that only modes that can physically exist in the plate can be generated by the transducer and since the system of the transducer with the plate differs only very little from the plate alone, the perturbation induced by adding the transducer onto the plate is weak, the action of the transducer being mainly to generate waves that are very similar to those that are calculated for a free plate. The drawback in such a technique is linked to the main assumption of the perturbation method, that is that the changes induced in the free wave fields by the presence of the transducer are assumed to be weak. This condition limits the study to thin transducers by comparison with the thickness of the structure. Assuming that this condition is respected, the weak perturbation assumption [4.7] allows us to separate the problem into different stages, each adding linearly. We split the problem into three steps: mechanical perturbation, piezoelectric perturbation, and scattering calculations. Figure 4.1(a) and (b) show schematic diagrams of how the real transducer structure is idealised as a stack of three layers. The first layer is the metallic plate itself; the second layer is the piezoelectric layer and the third layer is the electrode layer. The piezoelectric layer plays a double role in this problem; firstly it has a mechanical influence because of its material properties and its geometry. Secondly, the electromechanical coupling occurs in this layer; because the electric fields are quasistatic in such a problem, the mechanical influence of this layer can be dissociated from its electromechanical influence. This point is essential in the sense that it allows us

to split the problem into the mechanical stage and the electromechanical (or piezoelectric) stages.

The flexibility and the simplicity of the model derive directly from this series of stages since each can be performed independently from the others and can then be changed if necessary. The transmitter problem that relates the voltage applied at the electrode to the amplitude of the waves generated in the metallic plate differs from the receiver case where the voltage at the electrical ports of the receiver is calculated as a function of the amplitude of the waves reaching the receiving transducer. The difference, however, lies only in the electrical boundary conditions at the electrodes. Therefore the two problems are treated in parallel. Prior to the perturbation stages we first need to find the analytic solutions for Lamb waves. These are the starting equations on which the three perturbations are gradually added in order to represent the real system. Starting from the analytic form of the Lamb waves in a free plate, the first perturbation stage yields the calculation of guided wave fields in a layered structure consisting of the waveguide and the piezoelectric layer. The second step concerns the introduction of the piezoelectric coupling within the transducer. The third step consists in approximating the scattering coefficients of the generated modes at the edges of the transducer. At this third stage the calculations are mechanical only and use most of the calculations made at the first stage.

4.2.1 LAMB WAVE SOLUTIONS

First we have to calculate the solutions for the free plate. The formulation of the Lamb wave problem has been introduced in Chapter 2. The roots of the Rayleigh-Lamb frequency equations, the transcendental equations for Lamb waves, are obtained from the program DISPERSE [4.9], written in the NDT lab. However for a free plate in vacuum the dispersion relations have an analytical formulation and we used the form proposed by Achenbach [4.10] to express the displacement fields or any other fields. Although these dispersion curves can be directly obtained from DISPERSE we prefer to work with the analytical form of the fields rather than with a series of numerical values. Moreover solutions provided by DISPERSE are all normalised to unit power flow in the direction of propagation. This is advantageous in most situations but unfortunately it is important in our calculations to have access to the power flow function at various stages. This point is particularly important when calculating the scattering coefficients at the limits of the transducer when mode conversion occurs. This will be developed in more detail in section 4.7.

In this study we limit ourselves to a single and simple structure, that is a 1mm thick aluminium plate. However it is important to appreciate that the remainder of the model is completely independent of the choice of the structure. This is certainly one of the main advantages of this technique. For example even if the structure is a complex multi-layered composite plate, pipe or any other possible waveguide, provided that the dispersion curves can be obtained, the model still provides solutions.

4.2.2 MECHANICAL SURFACE PERTURBATION BY AN OVERLAY

The first stage in the perturbation calculation is to consider a simple model where the plate is entirely covered by a thin piezoelectric layer, as presented in Figure 4.1(c). Following the early work by Slobodnick [4.14] and Auld [4.7], a perturbation formula is derived which expresses analytically the perturbation in the wavenumber of each mode due to the presence of the coating layer. The changes in the boundary conditions at the interface are discussed as well as the stress field in the plating layer. In our simplified transducer description, see Figure 4.1(b), this overlay is simply the piezoelectric layer, with the piezoelectric coupling considered as being "turned off". However it is possible to add extra layers such as an adhesive bond layer. This just requires the perturbation calculation to be run a second time with the material parameters of that new layer, as shown in section 4.3.6. The limit to the addition of extra layers is that the overall perturbation must remain weak. Another limit concerns the frequency regions near the cut-off frequencies of high-order modes. All modes, except the two fundamental modes have cut-off frequencies at which they do not propagate along the plate but instead are resonant thickness modes. The orthogonality relationship of non-propagating modes, that is high-order modes near their cut-off frequency, is not the same as that for propagating modes and therefore the perturbation formula is not valid near cut-off frequencies [4.7]. Therefore the perturbation calculations for these high-order modes is subject to large errors near their cut-off frequencies.

4.2.3 PIEZOELECTRIC PERTURBATIONS

The fields obtained in the first step are now perturbed by the electromechanical coupling within the piezoelectric layer, the piezoelectricity being "turned on". The piezoelectric effect within the piezoelectric layer is triggered by the presence of charges at the upper free surface of the layer. Assuming that the electrode in Figure 4.1(d) is so thin that it has no mechanical influence, its influence is purely electrical and can be expressed as a change in the electric boundary conditions at the surfaces of the piezoelectric layer. In the transmitter case when a voltage is applied at the electrodes, charges appear at the surface and the electrical boundary conditions are changed in a similar way to which the velocities and stresses were changed at the mechanical perturbation stage. Therefore a perturbation formula is derived that allows us to calculate the electrostatic potential associated with each mode propagating in the layered structure.

4.2.4 INFINITE LAYERS PROBLEM

At this stage of the model, the dispersion curves and the potential for each mode propagating in the transducer are known. However so far the calculations have been eased by the fact that the mode has been considered to propagate freely and to be independent of other modes. This results from having implicitly assumed that the two layers are infinite in the direction of propagation. This is not a very realistic problem but

it has the advantage of keeping the problem simple and giving a simple relationship between the potential associated with the waves and their frequency-wavenumber characteristics. If we assume that a thin electrode (having no mechanical influence) of finite length is deposited on top of the piezoelectric layer then a transmitter or a receiver problem can be treated. The relative simplicity of the equations so far is suitable to make a first attempt to solve the normal mode excitation equations introduced in Chapter 2, and to calculate the amplitudes of the different modes for a given voltage applied at the electrode, or conversely, the magnitude of the voltage at the electrode when a given mode of unit amplitude propagates underneath the electrode.

4.2.5 SCATTERING COEFFICIENTS

This is the final stage of the calculations, which is concerned with the effect of the limited size of the thin layer(s) overlay. When the piezoelectric layer is of limited size in the direction of propagation, the modes that propagate underneath the layer are scattered at the edges of the layer. Mode conversion occurs and the energy is then shared between different modes. It is therefore necessary to estimate the amount of energy that is converted from one mode to another. This is done by calculating the amplitude of the wave scattered at the edges of the overlay, which is modelled as a rectangular thin strip. We show how the boundary conditions at the strip surfaces act as secondary sources and how the amplitude of the scattered waves is related to the geometrical parameters and the material constants of the "obstacle". The so-called S-parameters are calculated for the fundamental Lamb modes. Obviously this calculation can be immediately extended to the study of the scattering of Lamb waves at defects. Although this is not the purpose of this thesis, it is shown how these calculations are amenable to the calculation of the scattering coefficients of Lamb waves incident at surface and interior (volume) defects.

4.2.6 FINITE TRANSDUCER MODEL

The linear combination of the two perturbation stages and the scattering calculations, as shown in Figure 4.2, leads to the entire model that describes the electromechanical interaction between the electric potential and the amplitude of the guided waves in the structure. Particular applications are discussed in Chapter 5 for the transmitter case where guided waves are generated as a result of an electrical signal applied at the transducer.

4.3 FIRST STAGE: MECHANICAL SURFACE PERTURBATION

The first stage is concerned with the calculation of the mechanical fields of guided waves propagating in a plate covered by a thin anisotropic layer, as presented in Figure 4.1(c). The piezoelectric layer is, at this stage, considered as a passive elastic material. This is achieved using perturbation calculations. The perturbation formulae, for an elastic waveguide, are a natural extension of the normal mode theory, which has been presented in Chapter 2. The details of the derivation of the perturbation formulae

are not repeated here and can be found in Chapter 10 of [4.7]. The perturbation formulae for boundary perturbations are based on the reciprocity relation, which defines the relationship between two solutions of the same field equations. When considering the particular problem of the perturbation induced by an overlay on a metallic plate, the reciprocity relationship is used to relate the fields in the plate without the overlay to those in the plate/overlay bi-layer system. These two solutions are related by the complex reciprocity relation which is written [4.7] as:

$$\nabla.\left\{-v_2^*.T_1 - v_1.T_2^*\right\} = 0 \tag{4.1}$$

The first solution describes the particle velocity vector v and the stress tensor T of the Lamb waves propagating in the metallic plate alone; see Figure 4.3(b). These are the fields of unperturbed waveguide modes. For the particle velocity field, solution "1" is

$$v_1 = v_n(z)\, e^{j(\omega t - \beta_n x)} \tag{4.2}$$

This solution is assumed to be for lossless and propagating waves only, i.e. the wavenumber β_n is pure real. The second solution is the corresponding perturbed modes

$$v_2 = v'_n(z)\, e^{j(\omega t - \beta'_n x)} \tag{4.3}$$

4.3.1 MECHANICAL SURFACE PERTURBATIONS

If only the upper surface, z = 0 in Figure 4.3, of the metallic plate is perturbed by the addition of a thin layer, the change in the propagation factors, expressed as a wavenumber shift is given [4.7] by

$$\Delta\beta_n = \beta'_n - \beta_n = \frac{i\left(\left\{-v_n^*.T'_n\right\}.z\right)_{z=0}}{4P_n} \tag{4.4}$$

where β_n is the wavenumber, T_n is the stress tensor and v_n is the particle velocity vector of the n^{th} unperturbed mode. These fields are all functions of time and frequency. β', T' and v' are the corresponding perturbed fields, that is those in the bi-layer system, as shown in Figure 4.3(c). The unit vector *z* is in the direction normal to the plate surfaces and a superscript * denotes the complex conjugate vector. The denominator P_n is the average power flow per unit width along direction *x* of the unperturbed mode *n*. The co-ordinate system in Figure 4.3(b) differs from that for the bi-layered plate, Figure 4.3(c), because when solving the Lamb wave problem it is wise to take advantage of the symmetry of the geometry. However the bi-layer system breaks this symmetry and in this case it simplifies the analytical formulation of the stress boundary conditions if the upper surface is at the z = 0 plane. However it is perfectly valid to use different co-ordinate systems since the unperturbed Lamb wave solutions are not dependent on the co-ordinate system. It is assumed that the solutions for the unperturbed waveguide are well known. In order to use the perturbation formula given by Eq.(4.4) it is necessary to

estimate the perturbed stress field. The perturbed surface traction force, $-T_n^{'}.y$, can be defined in terms of an acoustic surface impedance $Z_A^{'}$ [4.7],

$$-T_n^{'}.z = Z_A^{'}.v_n^{'} \tag{4.5}$$

by analogy with the shear and longitudinal acoustic impedances in isotropic materials. The concept has been extended, see Chapter 7 of [4.7], to plane waves propagating in any direction of a anisotropic material. From Eq.(4.5) the perturbation formula is

$$\Delta\beta_n = \frac{i\left(\left\{v_n^{*}.Z_a^{'}.v'_n\right\}\right)_{z=0}}{4P_n} \tag{4.6}$$

4.3.2 USE OF THE PERTURBATION FORMULA

To evaluate the integral in the numerator of Eq.(4.6) it is necessary to calculate both the perturbed and the unperturbed fields. This usually involves solving a boundary value problem. Fields have to be determined which, added to the unperturbed fields, enable the boundary conditions to be satisfied on the surfaces of the perturbed domain. These additional fields must satisfy the boundary conditions on the bounding surface of the unperturbed domain. Once the perturbed fields have been calculated or estimated, the calculation of the perturbation in wavenumber is straightforward, although it may be tedious. Simple examples of the kind of problem to which the perturbation formula is applicable are [4.7], [4.11], [4.12], [4.13]:

1) A waveguide consists of a two-layered composite material. The fields in the medium A are found. These are the unperturbed fields. The perturbation consists now in adding material B. In the perturbed state all fields can exist but are modified, denoted by a prime, and the problem is to choose the perturbed fields in the material B so that the boundary conditions are satisfied at the interface between A and B.

2) One of the materials is anisotropic with an elastic-constant tensor where one of the constants, say C'_{11} is approximately but not exactly equal to $C_{12}+2\,C_{44} = C_{11}$. Then C'_{11} may be replaced by $C_{12} + 2\,C_{44}$, corresponding to an isotropic material and the fields are obtained for this model. The perturbation is then the change of C_{11} from the assumed value to the actual value.

3) If a waveguide contains a material that is slightly lossy, the loss may be ignored at first, and the fields evaluated for the lossless case. The loss terms due to imaginary parts of the elastic constants then constitute the perturbation and this case is similar to the previous case.

4) Refinements can be made by adding the effects of thermoelastic coupling on the propagation of Lamb wave in a piezoelectric rectangular plate. It is well known that application of high voltage will produce heating of the electrode fingers and of the piezoelectric plate. This can be analysed by considering the thermoelastic and

thermoelectric effects as perturbations and calculating an attenuation coefficient, which will be the imaginary part of the induced frequency shift.

5) The problem that consists in calculating the characteristics of the guided waves propagating along a tapered structure is certainly not an easy problem to solve. However if we consider the case of a plate covered by a thin overlay whose thickness is a slowly varying function in x (the direction of propagation), it is possible to approximate the boundary conditions within this layer and therefore to estimate the variation induced in the wavenumber. The boundary conditions for such a problem are equivalent to the Brekhovskikh boundary conditions [4.13].

This list is not exhaustive but presents the major cases relevant to this study, where the piezoelectric layer is always anisotropic. In this study, because we use the complex reciprocity relationship, the material of the substrate cannot be attenuative and only loss-less materials are considered. However the attenuation can still be added as a perturbation if needed.

Prior to the complex transducer case that we eventually want to model, we present examples in order to establish the limits within which our perturbation approach is valid. The first example concerns the calculation of the attenuation of Lamb waves due to energy leakage into a surrounding fluid, treated as a perturbation for the plate wave guide. Later we consider the perturbations induced on the guided modes of an isotropic plate by, firstly a thin isotropic overlay, and secondly a thin anisotropic overlay. These preliminary examples first establish the necessary equations but also point up the limits of the perturbation method for such problems involving Lamb waves. Lessons learned from these examples are used to modify the perturbation formula in order to obtain more accurate results for the transducer problem we want to solve, that is a plate overlaid with an anisotropic layer and possibly other layers representing the adhesive bonds and the electrodes.

4.3.3 FIRST VALIDATION EXAMPLE : ISOTROPIC IMMERSED PLATE

In this section our aim is to validate the perturbation method for Lamb waves rather than a particular formula. To do so a simple problem such as a plate loaded on one side by a fluid represents an ideal case because it is simpler than the transducer problem and solutions are already available. When a plate is loaded with water, each mode that propagates within the plate leaks energy into the fluid and the loss of energy is expressed as an attenuation factor which we want to estimate using the perturbation method. Even if it is a rather specialised case, no extra assumptions being made about the plate material or the loading medium, it enables us to test the limits of the assumptions we will use in our transducer problem. The starting points are the Lamb solutions in the plate, in terms of the phase velocities and the particle velocities at the surface of the plate. The perturbation calculations relevant to a plate loaded by a gas have been done by Slobdonick [4.14], and Jia [4.15] developed similar calculations for a fluid loaded plate, adding in the input exciting force the contribution of the waves reaching the plate after having been first reflected at the plate and then again at the

surface of the transducer. In these works, the acoustic surface impedance $Z_A^{'}$ in Eq.(4.6) is given as

$$Z_a^{'} = \frac{p}{v_y} = -\frac{\rho\ V_C}{\cos\theta_n} = -\frac{\rho V_C V_n}{\sqrt{V_n^2 - V_C{}^2}^{'}} \tag{4.7}$$

where p is the pressure on the plate, ρ is the density of the fluid, V_C and V_n are the phase velocities of the plane wave in the fluid and the Lamb modes in the plate. θ_n is the angle of incidence of the wave in the fluid, calculated to excite the n^{th} mode, and v_y is the particle velocity in the fluid. If the attenuation is small it is permissible to assume that the velocity of the perturbed mode is similar to that of the unperturbed mode and thus that the perturbed wavenumber is equal to the unperturbed one since the frequency remains unchanged. The remaining assumption is that the Lamb modes in the immersed plate are the same as those in a free plate. This is reasonable in all cases when the plate is loaded with gas, but is only valid with a liquid when the impedance of the liquid is much smaller than that of the elastic waveguide [4.7]. The attenuation of the n^{th} Lamb mode is related to the wavenumber variation as [4.14], [4.15],

$$\Delta\beta_n = -i\alpha_n \qquad \text{with} \qquad \alpha_n = \frac{\left|v_{ny}\right|^2_{z=b/2}}{4P_n} Z_a^{'} \tag{4.8}$$

where α_n is the attenuation constant per unit width along the propagation direction *x*, and is implicitly frequency dependent. Since the propagation constant β_n is real for a propagating mode, the leakage of energy is represented by the imaginary part of the wavenumber, which is a well-known concept.

The attenuation of the four first Lamb modes have been computed for a 1.2mm thick aluminium plate loaded with water. In parallel, exact calculations have been done using DISPERSE for the same system. Figure 4.4 shows the approximate solutions and the exact solutions. The curves are seen to be very similar at low frequency but separate at higher frequency as was expected from the assumptions made. However for the two fundamental modes, the curves do not have the same shape above 4.0 MHz. These differences are not due to the approximations made but to the fact that, for this particular system, a plate loaded by a fluid on only one face, these modes both tend to become two surface waves, one propagating along the free boundary of the plate and the other propagating at the plate-fluid interface. This change in the nature of the modes cannot be taken into account with the perturbation method where it is expected that the perturbed solutions are weakly different from the unperturbed solutions. In the unperturbed system, the Mode A0 and S0 combine at high frequency to become a Rayleigh wave. The mode shape grids plotted in Figure 4.4 show that at high frequency, the mode S_0 behaves as an interface wave propagating along the plate-fluid interface yielding a very high attenuation, while the mode A_0 behaves as a surface wave propagating along the bottom surface of the plate, there is no power located near the fluid interface leading to less and less leakage of energy in the fluid as the wavelength decreases.

Therefore numerical calculations show that the weak perturbation approximation can be used for Lamb waves. It appears though that the frequency range of validity is limited and different for each particular mode, depending on how it is affected by the perturbation. It is shown that in an non-symmetric system where the two fundamental modes separate at high frequencies, the perturbation method cannot predict the changes. These limits hold for other systems and in particular for plates perturbed by the addition of thin layers.

4.3.4 THIN ISOTROPIC LAYER OVERLAY

The problem here is to extend the metal plate structure to the metal/isotropic layer composite structure, so as to calculate the stress and the displacement at the interface between the overlay and the plate; the co-ordinate system is shown in Figure 4.3(a). To estimate the change in propagation factor for the bi-layer from that of the single plate, the perturbed fields v' and T' or an approximation of them, must be known. For a thin isotropic overlay, this problem is usually solved in the constant field approximation, which states that the mechanical displacements have negligible *z* variation within the thin film. Practically this means that the particle velocity fields at the interface between the plate and the overlay are assumed to be equal to those at the free surface of the overlay and those fields are taken to be the same as those at the free surface of a free plate. Accordingly Eq.(4.6) becomes, [4.7]:

$$\Delta\beta_n = \frac{i\left(\left\{v_n^*.Z_a^{'}.v_n\right\}\right)_{z=0}}{4P_n} \tag{4.9}$$

No variation of the displacements or velocities through the layer thickness implies that the variation of the stress field is linear and the first order terms of the stress in the perturbed system, for Lamb modes with displacements in the sagittal plane *yz*, are given by:

$$\begin{aligned}(T_n^{'})_{zz} &= -i\omega h\rho^{'}\left(v_n^{'}\right)_z \\ (T_n^{'})_{zx} &= -i\omega h\left[\rho^{'} - \frac{S_{11}^{'}}{V_n^2\left(S_{11}^{2'} + S_{12}^{2'}\right)}\right]\left(v_n^{'}\right)_x\end{aligned} \tag{4.10}$$

at z = 0, where the approximation $\beta_n^{'} = \beta_n$ has been used. These are the *Tiersten boundary conditions* [4.17] for a thin isotropic film overlay. Eq.(4.10) has been established by expanding stress to only first order. Stresses at first order are the derivatives of stresses at zero order, zero order stresses representing forces and first order stresses representing moments. This expansion to only first order is justified by the fact that because the layer is very thin, only its extensional resistance needs to be considered [4.18]. However since the thin layer is attached to the plate, we must impose the conditions of continuity of surface traction and mechanical displacement across the interface [4.19], which means that the inertia of the layer must also be included, i.e. the

traction force at the face of the plate is balanced by the traction at the outer face of the layer due to the applied surface forces and the inertia force due to the mass of the layer. The particle velocity fields in the layer have been expanded to zero order which means taking the velocity field in the layer to be that at the free surface of the plate alone. This also means that the free thickness-stretch motion (first order normal displacement) which accompanies the extensional motion of the layer is ignored, as well as the extensional motion that accompanies the thickness-stretch motion of the layer. From Eq.(4.6) and Eq.(4.10) the perturbation formula for a very thin isotropic overlay is derived as:

$$\frac{\Delta\beta_n}{\beta_n} = \frac{V_n}{4P_n}\left[\left(\rho' h\right)\left|v_{nz}\right|^2 + \left(\rho' h\right)\left(1 - \frac{E'}{\rho'\left(1-\nu'^2\right)V_n^2}\right)\left|v_{nx}\right|^2\right]_{z=0} \tag{4.11}$$

This formula differs from that given in [4.7] because it is expressed in terms of the Young's modulus E' and the Poisson's ratio ν' rather than in terms of the Lamé coefficients of the thin overlay. v_{nx} and v_{ny} are the particle velocity fields, in the sagittal plane, of the n^{th} Lamb mode propagating in the plate *alone*. From Eq.(4.11) it can be seen that at first order only the mass loading and the extensional resistance of the layer have been considered. The mass loading per unit area is introduced via the parameter $\Delta m = h\rho'$ that appears as a multiplier of each of the particle velocities, and the extensional resistance is introduced only as a factor of the inplane particle velocity, via a sensitivity factor $(1 - \alpha)$ with

$$\alpha = \frac{E'}{\rho'\left(1-\nu'^2\right)V_n^2} = \left(\frac{V'_{S_0}}{V_n}\right)^2 \tag{4.12}$$

where V'_{S_0} is the phase velocity, at very low frequency, of the lower extensional mode (S_0) of the layer [4.20]. In practical analysis of the acoustic plate modes (APM) of a bi-layered system, the layer thickness *h* is fixed and all the material parameters are known. Therefore the wavenumber variation, for each mode, only depends on the dispersion characteristics of the mode of interest. Considering first the S_0 Lamb mode, if the layer has similar density and Young's modulus to the plate substrate, then the sensitivity parameter tends to zero, the term in $\left|v_{nx}\right|^2$ cancels and the variation in wavenumber is only due to the mass loading. When the material properties of the layer are different from those of the substrate, the sensitivity factor is either positive or negative. Considering a particular mode *n*, if its phase velocity V_n is lower than that of the S_0 mode at low frequency in the layer (V'_{S_0}) than the sensitivity factor is negative and the inplane motion in the layer acts as to reduce the wavenumber variation. Conversely if $V_n > V'_{S_0}$ then the effect of the mass loading and of the extensional resistance add to increase the wavenumber variation.

Since the phase velocity can be calculated from the frequency and the wavenumber, i.e. $V_n = \omega/\beta_n$, the variation induced by the addition of the thin overlay can be also expressed in term of a phase velocity relative variation using

$$\frac{-\Delta V_n}{V'_n} = \frac{\Delta\beta_n}{\beta_n} \tag{4.13}$$

where V_n and V'_n are the unperturbed and the perturbed phase velocities of the mode "n". Therefore an increase in the wavenumber leads to a reduction of the phase velocity.

In theory, expanding the stresses to higher order should lead to an increase of accuracy of the perturbation formula. Following the demonstration given by Auld [4.7] for first order expansion, we derived the stress fields to second order as:

$$\begin{aligned}
(T'_n)_{zz} &= -i\omega h\rho'\left(v'_n\right)_z + \frac{\beta_n h(\omega h)}{2V_n^2}\left[\rho' V_n^2 \frac{S'_{11}}{S'_{11}+S'_{12}} - \frac{S'_{11}}{S_{11}^{2'}+S_{12}^{2'}}\right]\left(v'_n\right)_x \\
(T'_n)_{xz} &= -i\omega h\left[\rho' - \frac{S'_{11}}{V_n^2\left(S_{11}^{2'}+S_{12}^{2'}\right)}\right]\left(v'_n\right)_x + \\
&\qquad \frac{\beta_n h(\omega h)}{2V_n^2}\left[\rho' V_n^2 \frac{S'_{11}}{S'_{11}+S'_{12}} - \frac{S'_{11}}{S_{11}^{2'}+S_{12}^{2'}}\right]\left(v'_n\right)_z
\end{aligned} \tag{4.14}$$

which shows that the second order normal stress depends on the extension of the layer and that the second order shear stress depends on the thickness-stretch motion of the layer. While deriving the stress expressions it is possible to show that the stress in the inplane direction (T_{xx}) is a function of the shear stress at first order and the inplane stress at zero order which is another way of showing that second order derivations take into account shearing effects that first order derivations do not consider. Similarly, it is possible to show that third order expansion is required to take into account the rotary inertia effect. From these new boundary conditions the wavenumber variation induced by the overlay is:

$$\frac{\Delta\beta_n}{\beta_n} = \frac{V_n\left(\rho' h\right)}{4P_n}\left[\begin{array}{l} |v_{nz}|^2 + \\ \left(1 - \dfrac{S'_{11}}{\rho'\left(S_{11}^{2'}+S_{12}^{2'}\right)V_n^2}\right)|v_{nx}|^2 + \\ \omega h\left(\dfrac{S'_{11}}{S'_{11}+S'_{12}} - \dfrac{S'_{11}}{\rho'\left(S_{11}^{2'}+S_{12}^{2'}\right)V_n^2}\right)|v_{nx}||v_{nz}| \end{array}\right]_{z=0} \tag{4.15}$$

where $S_{ij}^{'}$ are the compliance coefficients of the thin layer. The improvement in the formula comes directly from the fact that at second-order the stresses are assumed to vary as quadratic functions. Therefore in the frequency range where the stresses do not vary linearly throughout the thickness of the layer, the wavenumber variation might better approximated using Eq.(4.15) than the first order perturbation formula. However for thin layers it is only at high frequencies that the stresses do not vary linearly throughout the thickness of the layer and at high frequencies the assumption that the wave is not significantly altered by the addition of the layer is no longer valid. Therefore, because the velocities enter recursively into the calculations, any error in the particle velocities would lead to higher error in the second-order formula than in the first order formula. Consequently no general improvement may be obtained by going to higher-order approximations and first-order predictions may be more accurate than higher-order ones when unperturbed free-surface particle velocities are assumed.

4.3.4.1 Limitations of the Perturbation Formula

The perturbation formula given in Eq.(4.4) is simple to understand but is not general since it can only be used when the wave functions are real functions of position in the cross section of the waveguide multiplied by $\exp(i\omega t - i\beta x)$, β being real. This condition is satisfied in non-attenuative waveguides. Furthermore for a waveguide at cut-off, $\partial\beta/\partial\omega$ becomes infinite and remains large for a limited frequency range in the neighbourhood of cut-off. Then the variation $\partial\beta/\beta$ is large and the perturbation formula is invalid since it has been derived on the assumption that $\partial\beta/\beta$ is small.

The perturbation formula given in Eq.(4.11) is a classic solution that can be found, for example in Auld [4.7] and which is derived from the so-called *Tiersten boundary conditions* [4.17]. It has been used widely and an extensive literature can be found for SH and Lamb waves applications [4.21], [4.22], [4.23], [4.12] with a special emphasis on mass sensitivity sensors [4.24], [4.25], multisensing oscillators [4.26], [4.27] and biological applications such as gas or solution concentration sensors [4.28], [4.29]. In the transducer model Eq.(4.11) is used with great accuracy when the layers are either the adhesive bond, considered as isotropic, and the electrode layer, made of copper and also considered as isotropic. The two layers are very thin, of the order of 20 microns or less and Eq.(4.11) gives results that are very close to the exact solutions, as shown below in the validation examples. However Eq.(4.11) it is not sufficient for describing the influence of an anisotropic overlay. In our problem, the mechanical perturbation is principally used to obtain the fields of the guided waves that propagate in a system made of a metallic plate overlaid by a piezoelectric layer, both being infinite, and the piezoelectric effect being neglected at this stage. A physical condition for the existence of piezoelectricity in a material is that this material must be anisotropic [4.32]. A formulation for an anisotropic overlay has been given by Wolkerstorfer [4.30] but it was reported [personal communication by B. A. Auld] that the formula, as given in Auld [4.7], might be inaccurate. Moreover in the derivation of Eq.(4.11) as provided by Auld, only the three stresses that vanish at the free surface of the layer are expanded to first order. However, in our plane strain problem, the stress tensor contains four non-zero components which are T_{xx}, T_{yy}, T_{zz} and T_{xz}. Therefore we are missing information

about two stress components, T_{yy}, the stress in the direction normal to the sagittal plane and T_{xx} the stress in the direction of propagation. This remark is not relevant to the perturbation problem treated by Auld but is nonetheless extremely pertinent to the development of the next perturbation stage, where the electric potential is calculated from the stress fields within the piezoelectric layer. For these reasons it was decided not to use the stress fields provided in Eq.(4.10) or Eq.(4.14) but to develop the stress fields for an anisotropic medium.

4.3.5 SECOND EXAMPLE : PZT-5H OVERLAY

In this section the bi-layered system is made of a 1mm thick aluminium substrate on top of which a PZT-5H piezoelectric layer is rigidly bonded. PZT-5H is a crystal of hexagonal symmetry of class 6mm. In this study we assume that the PZT strips are Z-cut, that is that the 6-fold axis of symmetry is the Z-crystal axis. In this problem, to simplify the calculations we chose to have a co-ordinate system parallel to the crystal axis as shown in Figure 4.5.

4.3.5.1 Anisotropic perturbation formula.

The analysis of the stresses in the layer for a general orthorhombic crystal, shows that they can be written in terms of the particle velocities at the top of the overlay. This is done in Appendix B using a method which differs slightly from than that used originally by Tiersten. The Tiersten perturbation series for the stress is not a Taylor or MacLauren series, with the n^{th} term of the form

$$\frac{1}{n!}\left(\frac{\partial^n F}{\partial x^n}\right)_{x=0} \quad \text{Taylor Series} \tag{4.16}$$

and

$$\frac{1}{n!}\left(\frac{\partial^n F}{\partial x^n}\right)_{x=x_0} \quad \text{MacLauren Series} \tag{4.17}$$

Rather, the various orders are calculated directly from the differential equation and/or the boundary conditions. In Appendix B, a classic power series technique is used, and the zero and first order coefficients are directly calculated by successive derivations. The results, to first order only, and for an hexagonal material are

$$T_{nxx} = \frac{-s'_{11}}{\left(s'^2_{11} - s'^2_{12}\right)V_n}\left[\begin{array}{l} v_{nx}(h) \\ +\left\{ j\beta_n \left(1+\rho' V_n^2 s'_{13} \dfrac{s'_{11}-s'_{12}}{s'_{11}} \right)(z-h) \right\} v_{nz}(h) \end{array}\right] \tag{4.18}$$

$$T_{nzz} = \left\{ j\rho'\omega(z-h) \right\} v_{nz}(h) \tag{4.19}$$

$$T_{nyy} = \frac{s'_{12}}{\left(s'^2_{11} - s'^2_{12}\right)V_n}\left[\begin{array}{l} v_{nx}(h) + \\ \left\{ j\beta_n \left(1 + \rho' V_n^2 s'_{13} \left(\frac{\left(s'_{11} - s'_{13} + s'_{12}\right)}{s'_{11}} - \frac{s'_{11}}{s'_{12}} \right) \right)(z-h) \right\} v_{nz}(h) \end{array}\right] \tag{4.20}$$

$$T_{nyz} = \left\{ j\omega \left(\rho' - \frac{1}{V_n^2} \frac{s'_{11}}{s'^2_{11} - s'^2_{12}} \right)(z-h) \right\} v_{nx}(h) \tag{4.21}$$

where $v_{nx}(h)$ is the particle velocity in the direction of propagation, calculated at the top of the layer and $v_{nz}(h)$ is the normal particle velocity at the top of the layer for the mode "n". β_n and V_n are the wavenumber and phase velocity of the unperturbed modes. The s'_{ij} are the compliances of the PZT-5H material. The linear approximations are written out explicitly for later examination of their influence on the electric potential. It is noted that T_{nyy} and T_{nyz} vanish at the free surface as required by the boundary conditions. Because only lower order terms of the power series have been kept, the validity of the analysis will be limited to small values of the layer thickness *h*, where the stress variations in the film are easily approximated by a power series. From these stress expressions we derive the perturbation formula as

$$\beta'_n = \beta_n \left\{ 1 + \frac{V_n h}{4P_n} \left[\left| v_{nz}(h) \right|^2 + \left(\rho' - \frac{s'_{11}}{s'^2_{11} - s'^2_{12} V_n^2} \right) \left| v_{nx}(h) \right|^2 \right]_{z=0} \right\} \tag{4.22}$$

where β'_n is the wavenumber of the perturbed modes propagating in the bi-layered system and P_n is the power flow of the unperturbed modes, that is the Lamb modes in the aluminium plate. Material properties of PZT-5H are given in Table 4.1 in the crystal co-ordinate system so that, for example, the compliance S_{33} refers to the relation between a stress applied in the Z crystal axis and the strain in the Z crystal direction. $S'_{23} = S'_{13}$ since the plane XY is a plane of isotropy for a Z-cut hexagonal crystal. Material properties of Aluminium are given in Table 4.2.

4.3.5.2 Aluminium-PZT-5H

The system we will study in this section is a 1mm aluminium plate overlaid by a 100μm thick PZT-5H layer. Figure 4.6 shows the comparison between the exact dispersion curves (plain lines) for this system, calculated using DISPERSE, and the dispersion curves for a single aluminium plate (in dashed lines). This emphasises the differences between the dispersion curves in the two systems. Because the bi-layer system is not symmetric, the modes cannot be labelled using the classical "A" and "S" letters representing respectively the anti-symmetric and symmetric Lamb modes. Here it has been arbitrarily decided to label the exact modes of the bi-layer system by a "P". Figure 4.6 shows that the addition of the PZT-5H layer induces important changes in the

Lamb modes of the substrate alone, among which we can notice a decrease in the phase velocity of the lowest extensional mode (P_2) at low frequency. We also notice an inflection of the phase velocity of the lowest bending mode (P_1) above 1MHz. This is emphasised in Figure 4.7 which shows the spatial distribution of power flow for both modes. The power flow for a mode is a quantity for the whole structure which is calculated by integrating the power flow density along the direction of propagation, over the thickness of the structure. To produce the curves shown in Figure 4.7 we separated the integral over the structure thickness into a first integral over the layer thickness and a second integral over the substrate thickness, and calculated the ratio of the two integrals. The trend of the P_1 curves in Figure 4.7 shows that when the frequency increases, more power for mode P_1 is located within the layer. This indicates that, as the frequency increases, the mode P_1 tends to behave as a surface wave propagating at the free boundary of the PZT-5H. Concerning the mode P_2, Figure 4.7 shows that above 2MHz more than 90% of the power is located in the substrate. The influence of the overlay is therefore very weak. At higher frequencies, mode P_2 will therefore behave as a surface wave propagating along the free boundary of the substrate at the Rayleigh wave velocity of aluminium.

If the material properties of PZT-5H are fed into Eq.(4.22) the approximate phase velocities for the modes that propagate in the aluminium(1mm)/PZT(100μm) system are calculated using Eq.(4.13). Figure 4.8 shows the comparison between these approximate curves and the exact dispersions curves, obtained using DISPERSE, for the aluminium(1mm)/PZT(100μm) system. The approximate modes are labelled with the letters “F” and “L” where the “L” modes are derived from the symmetric Lamb modes and the “F” modes are derived from the anti-symmetric Lamb modes. This labelling is made by analogy with the characteristics of the S_0 and A_0 lamb waves at low frequency. S_0 mode is predominantly longitudinal and the A_0 mode is predominantly flexural.

The first striking feature in Figure 4.8 is that the perturbation formula as given in Eq.(4.22) does not work for the cut-off modes. Very poor agreement is found between the exact and the approximate curves for the cut-off modes P_3 and P_4 at high phase velocities in Figure 4.8. This is expected since Eq.(4.4) is derived from the complex reciprocity relationship, see Chapter 2, on the basis of an orthogonality relationship that does not account for the nature of evanescent modes. Auld [4.7] and Peach [4.33] showed that the normalisation relation used in the development of the orthogonality relationship of the propagating modes cannot be used for the resonant cut-off modes. This problem is particularly inconvenient when considering the problem of mode conversion at the edges of the transducers, for example, since non-propagating modes are generated along with propagating modes. These modes are said to be bi-orthogonal [4.31] and a new orthogonality relationship must be developed for these modes. Several attempts have been made in optics following the work from Marcuse [4.34], and also in acoustics, in particular for Stoneley waves [4.35] and more recently for fluid loaded plates containing defects [4.36]. However the reciprocity relationship for propagating modes already exists and since we are mainly interested in the two fundamental modes, it was not a priority to develop a new reciprocity relationship for the non-propagating modes.

The second striking point from Figure 4.8 is that the approximate curves for the modes L_0 and F_0 match correctly the exact curves for the modes P_2 and P_1 below, respectively 1 MHz and 2 MHz, but differ significantly from the exact curves above those frequencies. Let us first consider the case of F_0, the lowest bending mode, below 2MHz. There are two reasons why the match is reasonably good. Firstly, at very low frequency (below 300KHz) the dispersion curve of the mode P_1 is the same than that of the A_0 mode in the aluminium plate as shown in Figure 4.6. Secondly, the perturbation formula induces a reduction of the phase velocity of the mode A_0. The reason for this is that below 2 MHz, the normal particle velocity of the A_0 mode is larger than its inplane particle velocity, therefore the wavenumber variation (given in Eq.(4.22)), is positive and from Eq.(4.13) the phase velocity variation is negative. Since it is seen from Figure 4.6 that the phase velocity of the mode P_1 is lower than that of the mode A_0, a negative phase velocity variation is correct. Physically this means that the phase velocity of the mode A_0 depends upon the mass loading effect of the layer. At low frequency the loading is reactive, that is not much energy is radiated into the layer. At higher frequencies, the loading is dissipative and as the frequency increases, more and more energy radiates into the layer, and eventually when the frequency is such that the wavelength of this mode is much smaller than the layer thickness, the mode P_1 becomes a surface wave at the free surface of the overlay. The dispersion characteristics of such a surface wave are very different from that of the A_0 mode and these differences cannot be accounted for by the perturbation formula.

Concerning L_0, the approximated fundamental extensional mode, the agreement below 1MHz is good. To understand why the decrease in phase velocity is well predicted at low frequencies we must refer to the discussion in section 4.3.4 about the significance of the mass loading term and the extensional resistance term that compose the wavenumber perturbation formula for isotropic overlays (Eq.(4.11)). Although we are dealing here with an anisotropic layer the principle remains the same and to emphasise the relative importance of these two terms, we computed Eq.(4.22) in two different partial forms. Figure 4.9 shows the comparison between the exact dispersion curves for the S_0 mode and the P_2 mode (dashed lines) and three approximate dispersion curves for the L_0 mode. Firstly we computed Eq.(4.22) ignoring the term in v_y, that is keeping only the extensional resistance term. The second L_0 curve has been computed from Eq.(4.22) but ignoring the term in v_z, that is keeping only the mass loading term. Lastly the full formula has been computed. It shows that at low frequency the phase velocity decrease is entirely due to the mass loading term, whereas as the frequency increases, the extensional resistance term takes over from the mass loading term. At high frequency it is seen that the extensional resistance term over-estimates the phase velocity decrease and the approximate L_0 curve is lower than the exact P_2 curve.

It is seen that above a certain frequency, which varies for each mode, the perturbation formula does not predict the correct dispersion curves. The reason for that is that, above those frequencies, the aluminium(1mm)/PZT-5H(100μm) system reaches the limits of the weak perturbation assumption, but it is not clear whether the limits are reached because the thickness of the PZT layer represents as much as 10% of that of the aluminium plate, which is already a large perturbation, or because of the material properties of PZT-5H for which the shear and longitudinal acoustic impedances of PZT-

5H are close to those of aluminium. Our aim in investigating this problem is to find a way to improve the results shown in Figure 4.8.

To understand what is really driving the limits of this system we applied Eq.(4.22) to a closely related system, a 1mm steel plate overlaid by a 100μm thick epoxy layer. This new system presents a large difference between the shear and longitudinal acoustic impedances of the two materials but the substrate and layer thicknesses are kept the same as in the aluminium(1mm)/PZT-5H(100μm). The comparison between the exact dispersion curves and the approximate dispersion curves for the steel(1mm)/epoxy(100μm) system is shown in Figure 4.10, for the phase velocity. It is seen that the approximate curves (F_0 and L_0 modes) match very closely the exact dispersion curves up to 3MHz. It is obvious that the accuracy of the perturbation calculation is greatly improved by increasing the acoustic impedance mismatch between the two materials. From this comparison we can conclude that for the two fundamental Lamb modes, the principal factor that determines the accuracy is the ratio between the acoustic impedances of the layer and the substrate. The physics behind this statement, in line with the curves shown in Figure 4.7, is that the key phenomenon, for the two fundamental modes, is the facility with which energy can be radiated and later trapped within the layer. If the impedance mismatch is high, most of the energy carried by the partial waves is reflected at the interface between the layer and the substrate and the modes for the bi-layered system remain close to those of the substrate alone. This statement does not hold for higher-order modes. As a direct consequence, by choosing a piezoelectric material with lower acoustic impedances, the perturbation formula would be accurate over a broader frequency range. A material such as PVDF, whose properties are close to those of epoxy could be a good choice but such a piezoelectric material also has a very low piezoelectric coupling coefficient and a transducer made of PVDF would radiate much less energy within the substrate than a transducer made of PZT-5H. The amplitude of the waves generated in the substrate would therefore be smaller than that generated by a PZT-5H based transducer. An example of the use of PVDF is give in Chapter 5

To produce the approximate curves shown in Figure 4.8 and in Figure 4.10, Eq.(4.22) has been developed on the assumption that the velocity fields are those of the aluminium plate alone (referred to as zero order velocity), and that the stress fields vary linearly across the overlay (expansion to first order). Therefore the model could be improved by modifying these assumptions.

4.3.5.3 Stress and Particle Velocity Fields for the Aluminium/PZT System

Figure 4.11 shows the stress mode shapes for the modes P_1 and P_2, produced using DISPERSE, across the 100μm PZT-5H layer at 0.5 MHz and 2 MHz. It appears clearly that most of the mode shapes have linear variation of stresses across the layer. Only the shear stress mode-shape at 2 MHz for the mode P_2, in Figure 4.11(f), shows a significant non-linear variation. Therefore developing the stress to second order as given in Eq.(4.15) for the isotropic case would not lead to any major improvement and the calculations that led to Eq.(4.10) are not to be reconsidered for the sake of improving the accuracy of Eq.(4.22). Another reason why developing the stress fields to higher-

orders does not lead to any major improvement is that the phase velocity and particularly the particle velocities enter recursively into the calculations so that any error in the first-order coefficients will be increased in the second- and higher-order stress terms. Consequently first-order predictions are more accurate than any higher-order ones when unperturbed free-surface particle velocities are assumed which is the case for the curves shown in Figure 4.8. Figure 4.12 and Figure 4.13 show the exact particle velocity dispersion curves for the fundamental modes P_1 and P_2 of the aluminium (1mm)/PZT(100μm) system. Particle velocity dispersion curves are not unique like group velocity or phase velocity dispersion curves since the particle velocity depends on the mode amplitude. The particle velocities of Figure 4.12 and Figure 4.13 are calculated for a mode with unit power flow. Figure 4.12 shows the comparison between the normal particle velocity dispersion curves at the interface between the aluminium plate and the PZT layer, and the normal particle velocity dispersion curves at the upper surface of the PZT overlay. Figure 4.13 shows the same curves as Figure 4.12 but for the particle velocities in the direction of propagation (inplane particle velocities). From both Figure 4.12 and Figure 4.13 it is seen that neither the normal nor the in-plane particle velocities vary much across the layer thickness, the solid and dashed lines for the modes P_1 and P_2 being very close. This is in agreement with the assumption made to expand the stress to first order only and was expected from the above discussion on the linear variation of the stress mode shapes. However Figure 4.12 and Figure 4.13 also show the particle velocity fields of the Lamb modes at the free surface and it appears clearly that they do not match the exact particle velocity fields, either at the interface or at the top PZT surface. This clearly shows that the use of the Lamb modes particle velocities, for the unperturbed substrate in Eq.(4.22) is not suitable for the system we want to study here.

4.3.5.4 Stress Fields for the Exact Particle Velocity Fields

To derive Eq.(4.22) the surface traction forces in Eq.(4.5) have been evaluated assuming that the particle velocity field at the surface is unchanged by the perturbation; that is

$$(v'_n)\big|_{z=h} = (v'_n)\big|_{z=0} = (v_n)\big|_{z=0} \tag{4.23}$$

However such an approximation is not needed if the exact particle velocity field can be obtained. In such a case the perturbation formula is given by Eq.(4.6) and the perturbed surface impedance Z'_a is obtained through the calculation of the surface traction forces but using the exact particle velocities. The stress fields are given in Eq.(4.18) to Eq.(4.21). Figure 4.14 shows the comparison between the exact stress dispersion curves for the mode P_1 and the approximated stress dispersion curves for the F_0 mode obtained from the exact particle velocities. Figure 4.15 shows the same but for the exact P_2 mode and the approximate L_0 mode. The stress dispersion curves were extracted from the stress mode shapes of each mode, and calculated assuming a power flow in the mode of 1 Watt. It is seen that in most cases the agreement is very good, at least below 2 MHz. Therefore the exact particle velocity fields, obtained form DISPERSE have been introduced in place of the Lamb wave fields in Eq.(4.22). The approximate phase velocity dispersion curves for the aluminium (1mm)/PZT (100μm)

are shown in Figure 4.16. It is seen that the agreement between the exact "P" modes and the approximate F_0 and L_0 modes is much better than in Figure 4.10. The agreement is excellent up to 3 to 4 MHz, and therefore at frequencies below the first cut-off, the approximate wavenumber functions can be used in place of the exact wavenumber functions. It also appears that none of the attempts to improve the accuracy of the perturbation calculations has led to a significant improvement for the higher-order modes. Therefore in the remainder of this thesis we will only concentrate on the two fundamental modes, F_0 and L_0.

To emphasise the efficiency of this technique, the wavenumber dispersion curves for two systems are presented in Figure 4.17 to Figure 4.20. Figure 4.17 and Figure 4.18 show the wavenumber dispersion curves for a 50 μm PZT-5H layer overlaying a 1mm aluminium plate. In Figure 4.17 the perturbations calculations were obtained by using the particle velocities of the unperturbed substrate whereas in Figure 4.18 the particle velocities at the top of the PZT-5H layer have been used. Figure 4.17 shows good agreement between the exact modes (P_1 and P_2) and the perturbation calculations (F_0 and L_0) up to 2-3 MHz, i.e. $\beta h = 0.3$ whereas Figure 4.18 shows a good agreement up to 3-4 MHz, i.e $\beta h = 0.5$. The product layer thickness-wavenumber βh is a parameter traditionally used to quantify the range of validity of perturbation formulae [4.11]. Figure 4.19 and Figure 4.20 show the wavenumber dispersion curves for a 100 μm PZT-5H layer overlaying a 1mm aluminium plate. In Figure 4.19 the perturbations calculations obtained by using the particle velocities of the unperturbed substrate whereas in Figure 4.20 the particle velocities at the top of the PZT-5H layer have been used. Figure 4.19 shows a good agreement between the exact modes (P_1 and P_2) and the perturbation calculations (F_0 and L_0) up to 2 MHz, i.e. $\beta h = 0.5$ whereas Figure 4.20 shows a good agreement up $\beta h = 0.8$ which corresponds to 3 MHz for the F_0 mode (derived from the A_0 mode in the aluminium plate) and 3.6 MHz for the L_0 mode (derived from the S_0 mode in the aluminium plate). Overall it is clear that using the particle velocities at the free boundary of the PZT-5H layer rather than those at the free boundary of the aluminium substrate considered alone increases the frequency range (or thickness-wavenumber product) over which the perturbation calculations are in good agreement with the exact curves.

4.3.6 A MULTI-LAYERED SYSTEM TO MODEL A TRANSDUCER

Adding more than one perturbing layer is possible since the weak perturbation assumption makes the problem linear. Here we are interested in a four-layered system, which is basically the same as the bi-layered system studied before but to which we added an epoxy layer between the PZT layer and the aluminium plate, and a copper layer on top of the PZT layer. The epoxy layer represents the adhesive layer that bonds the transducer to the plate, and the copper layer represents the electrode. Figure 4.5(a) shows the bi-layered structure and Figure 4.5(b) shows its extension to a four-layered structure. Permanently attached transducers are rigidly bonded to the structure using an adhesive. Here we assume the properties of the adhesive bond to be those of epoxy. A bond thickness can vary from few microns to a few hundreds of microns but if the transducer is glued to the structure and pressure is applied on the transducer during the curing of the bond, the bond may be fairly thin. For the sake of this demonstration we

will assume that the bond is 10 microns thick. Therefore we intend to model the complete transducer-structure system as a 4-layer system, the structure layer, the bond layer, the piezoelectric layer and the electrode layer. Material properties of epoxy and copper are given Table 4.2.

An iterative use of Eq.(4.22) allows us to calculate the approximate wavenumber of the modes propagating in the four-layered system. First the influence of the epoxy layer is calculated. The results are then used as unperturbed solutions from which, again using Eq.(4.22), we calculate the approximate fields for the aluminium/epoxy/PZT system. Another iteration yields the approximate fields within the four-layered system. The comparison between the approximate and the exact wavenumber dispersion curves are shown in Figure 4.21. It is seen that the agreement is excellent up to $\beta h = 0.5$ where h is the thickness of the PZT layer. Above this, we notice that there is a large deflection for the lowest bending mode that is not correctly predicted. Redoing the calculations for the same system but without the epoxy layer shows that the large deflection is due to the presence of the epoxy layer. As noticed in the study of the steel(1mm)/epoxy (100μm) system, when the mismatch of acoustic impedance between the substrate material and the epoxy is large, the unperturbed Lamb modes of the substrate are not noticeably affected by the presence of the epoxy layer (it is noted that it was assumed that the epoxy layer was not attenuative). However this conclusion holds only because the upper surface of the epoxy is free. Here the epoxy layer is sandwiched by two thicker and stiffer materials. Therefore, this soft thin layer acts as a spring in between two masses and large displacement variations occur across the epoxy layer which cannot be predicted in the weak perturbation approximation. Figure 4.22(a) shows the group velocity dispersion curves for an aluminium(1mm)/epoxy(10μm) system and Figure 4.22(b) shows the group velocity dispersion curves for aluminium(1mm)/epoxy (10μm)/PZT(100μm) system. It clearly appears that the dispersion curve characteristics for the P_1 mode are very different. For this particular system, the stress must certainly be expanded to second or higher-order and the exact value of phase velocity must be introduced in the formula in order to obtain a better result. Results obtained in this section will be used in Chapter 5 when modeling an IDT.

4.3.7 CONCLUSION

A simple divergence relation between the perturbed and the unperturbed fields has been obtained for an anisotropic layer, in terms of wavenumber, via a formal manipulation of the fundamental acoustic field equations. We showed that the first-order stress fields derived from the zero-order particle velocity fields, (i.e. the particle velocities at the free boundary of the plate alone) are accurate only over a narrow frequency range and only for the fundamental modes. To improve the frequency range over which the agreement between the exact dispersion curves and the approximate dispersion curves is good, explicit analytical formulations for the stress fields and the wavenumbers have been derived. The exact free-surface particle velocity amplitudes and the exact phase velocities for the aluminium(1mm)/PZT (100μm) bi-layered system have been entered in the calculation of approximate fields. Finally we have analytic formulations for the stress fields within the layer which only require the knowledge of the dispersion characteristics of the substrate, which is available analytically, and of the

particle velocity amplitudes at the free-surface of the layer which may be obtained using DISPERSE or may even be obtained experimentally, at each frequency.

Because only lower order terms of the power series have been kept, the validity of the analysis will be limited to small values of the film thickness h, where the stress variations in the film are limited and are easily approximated by truncated power series. Detailed studies on the stress fields in zinc oxide films on fused silica substrates show that the approximation should be quite valid for layer thickness of $\beta h \leq 0.5$ and still be reasonable for films with $\beta h \leq 1$ [4.6]. However these studies concern surface acoustic waves (SAW) and not acoustic plate modes (APM). For APMs in an aluminium (1mm)/PZT-5H(100μm) structure, the agreement between the approximate and the exact values is excellent up to $\beta h=0.5$. It is clear that the dominant effects that control the stress mode shapes are contained in the analysis. It was clearly shown that the perturbation formula, as derived here, does not provide good results for the higher-order modes and in the next sections we will study only the two fundamental modes F_0 and L_0 between 0 and 1.5 MHz.

4.4 SECOND STAGE: PIEZOELECTRIC PERTURBATION

The problem is to extend the aluminium plate-like structure to a composite substrate/PZT-5H structure so as to calculate the electrostatic fields within the piezoelectric layer and in particular at the interface between the plate and the layer (z = 0) and at the upper surface of the layer (z = h). The selected approach consists of successive mechanical and piezoelectric perturbation calculations. The mechanical perturbation analysis carried out in the preceding section has enabled us to establish explicit polynomial expressions for the variation of the stresses across the layer. The remaining task is then to introduce a piezoelectric perturbation into this system. This problem is treated as a perturbation problem in the sense that we assume that the stresses within the layer remain unchanged when “switching on” the piezoelectric coupling. This is the weak perturbation approximation. From the piezoelectric constitutive equation

$$D = \varepsilon^T . E + d : T \tag{4.24}$$

where ε^T is the permittivity of the piezoelectric layer, d is the strain piezoelectric constants, and T is the stress of the mechanical waves traveling in the piezoelectric layer. More details about this equation are given in Chapter 2. If the piezoelectric constants d are set to zero, then the piezoelectric coupling is “switched off” and by setting the constants d to a nonzero value, the piezoelectricity is “switched on”. In the mechanical problem, the constants d were equal to zero. In this section we set them to their effective value for a PZT-5H material which are given in Table 4.1. The coupling between the stresses in the layer and the electric fields is then established and the knowledge of the mechanical field amplitudes yields the electrical fields.

This piezoelectric perturbation problem is very close to some electrical perturbation problems solved in the past for SAW in piezoelectric media, [4.37], [4.38],

[4.39] which consisted in evaluating the effect of a boundary condition change, for example predicting the phase velocity change of a mode travelling from an electroded region to a free region. The same principles apply to our problem and basically we follow the main lines of the analysis carried out in these works.

In this section our primary interest is to calculate the electric potential associated with the freely propagating acoustic modes, meaning that the electric potential is generated by the acoustic disturbances and not by some applied electric field or charges. It was proved in a detailed theory about the excitation of SAW by interdigital transducers shorted at the top surface [4.6], that the magnitude of the bandwidth of the transducer is controlled by the strength of the electrical potential of the freely propagating acoustic surface wave at the position where the transducer would be placed. Therefore the electric potential at the interface and its dependence on the parameters of the layer media are important parameters for designing optimum transducer configurations. If the free boundary of the piezoelectric layer is unelectroded and open-circuit boundary conditions assumed, than the amplitude of the electrical potential at the free surface (z = h) is needed to determine the amplitude of the waveguide modes generated by applied electrical sources. One of the most important applications of modal analysis is for analysing waveguide mode excitation by sources placed, in our case, on the surface of the plate waveguide. The principles of these calculations are given by Auld [4.7] and will be developed to some extent in section 4.6 which is concerned with the transducer problem.

4.4.1 STRESS FIELDS AS DRIVING TERMS FOR THE POISSON EQUATION

When considering piezoelectricity in a dielectric, it is a fair assumption to consider the electric fields to be quasistatic, and therefore the first Maxwell's equation [4.40] take the form

$$\mathrm{E} = -\nabla\Phi \tag{4.25}$$

and we have the auxiliary equation

$$\nabla.\mathrm{D} = 0 \tag{4.26}$$

where Φ is the electric potential and is a scalar quantity while E is the electric field vector. The quasistatic approximation is discussed in more detail in section 4.5. Eq.(4.26) defines the divergence of the flux density. The divergence of the vector D is nonzero if electric free charges are present in the volume considered, i.e. the piezoelectric layer. It is important to note that charges present at the surface of an electrode at which a voltage is applied (transmitter case) are not free charges and therefore the divergence is still null in such a case. A simple combination of equations(4.24), (4.25) and (4.26) yields the well-known Poisson equation for the electric potential in the layer [4.3],

$$\nabla.\varepsilon^{T}.\nabla\Phi=\nabla.(d:T) \tag{4.27}$$

In the system of coordinates chosen, according to the hexagonal symmetry of the film, and to the plane strain assumption, Poisson's equation reduces to

$$\varepsilon_{33}^{T}\frac{\partial^2\Phi}{\partial z^2}+\varepsilon_{11}^{T}\frac{\partial^2\Phi}{\partial x^2}=-\frac{1}{\varepsilon_{33}^{T}}\nabla.d:T \tag{4.28}$$

Assuming propagation as $e^{j(\omega t-\beta x)}$, the partial derivative with respect to the propagation direction x is simplified as $\partial^2/\partial x^2=-\beta^2$ and Eq.(4.28) simplifies to

$$\frac{\partial^2\Phi}{\partial z^2}-\beta^2\gamma^2=-\frac{1}{\varepsilon_{33}^{T}}\nabla.(d:T) \tag{4.29}$$

where

$$\gamma^2=\frac{\varepsilon_{11}^{T}}{\varepsilon_{33}^{T}} \tag{4.30}$$

In Eq.(4.29) T are the stress fields in the piezoelectric layer. Eq.(4.29) is the mathematical expression of the piezoelectric perturbation calculation and its solution is the electric potential induced, through the piezoelectric coupling d, by the mechanical waves travelling in the layer. In the weak coupling approximation T are the stress fields in the layer calculated at the mechanical perturbation step. These are now considered as the unperturbed stress fields and define the polarisation source for the electric potential in the piezoelectric layer. Because of the dominance of mechanical energy over electrical energy, the reaction of the electric potential on the waves is neglected. The general solution of the differential equation (4.29) is

$$\Phi=\Phi_g(z)e^{-j\beta x}=\left(F_1e^{-\gamma z}+F_2e^{+\gamma z}\right)e^{-j\beta x} \tag{4.31}$$

where γ is a constant obtained by a separation of variables with the right hand side equal to zero. Let

$$\Phi=\Phi_p(y)e^{-j\beta x} \tag{4.32}$$

be a particular solution to Eq.(4.29). The combination

$$\Phi_n(y,z)=\left(\Phi_g(z)+\Phi_p(z)\right)e^{-j\beta x} \tag{4.33}$$

that satisfies the boundary conditions is the solution of the Poisson's equation. The problem is correctly conditioned since there are two boundary conditions for the two unknowns F_1 and F_2. The coupling parameter, by analogy with the SAW problems can be found using the normalized potential $\tilde{\Phi}_n$

$$\tilde{\Phi}_n = \frac{\Phi_n(-h)}{\sqrt{p_n}} \tag{4.34}$$

where P_n is the power flow of the n^{th} mode. The interactions of acoustic waves with a transducer are controlled by the strength of the electrical potential of the freely propagating waves at the position where the electrodes would be placed.

4.4.2 BOUNDARY CONDITIONS

This piezoelectric perturbation problem we have to solve is a boundary value problem which is mathematically described by the Poisson's equation (Eq.(4.29)) and the relevant boundary conditions. In the general solution given in Eq.(4.31) there are two unknowns and since the piezoelectric layer has two boundaries, we can set two boundary conditions to make the problem well conditioned. The choice of the boundary conditions controls the validity of the results. In the general case, the boundary conditions depend on the electrical connections that are made and the surrounding media. However in this problem we will consider only the simplest terminations. We consider the structure to be metallic (aluminium) and we assume that in practical experiments this structure will be grounded. Therefore at the interface z = 0 the electrical boundary condition is

$$\Phi(z=0)=0 \tag{4.35}$$

At the upper surface, which is mechanically free, two cases can be considered. In the first case the space above the surface is vacuum and conductors are excluded, so that there are no bound charges. This is known as the free-surface case and is shown in Figure 4.23(a). In general there will be a potential in the vacuum above the surface and many different boundary conditions can be used, including capacitance loading and also short-circuit ($\Phi = 0$) and open-circuit boundary conditions ($D.\vec{n} = 0$). In the second case the surface is assumed to be covered with a thin metal layer with infinite conductivity, which shorts out the horizontal component of the electric field at the surface but does not affect the free mechanical boundary conditions. This corresponds to the case where the electrode is purely passive and short-circuited, as shown in Figure 4.23(b). If electrical connections are made with a reactive circuit, for example a wave generator or an oscilloscope, the boundary conditions are complex. The simplest terminations to be considered in this case are short-circuit and open-circuit.

It is well known in SAW technologies that the free-surface and the metallised surface give different velocities and that the velocity difference gives a measure of the coupling between the wave and the electric perturbations at the surface. This is a crucial point in the performance of surface wave transducers.

For the free surface case, the potential in vacuum satisfies Laplace's equation

$$\nabla^2\Phi = 0 \tag{4.36}$$

If the wavenumber of the mode is β, the potential Φ in the vacuum can be written

$$\Phi = f(z)e^{j(\omega t-\beta x)} \tag{4.37}$$

Using Laplace's equation shows that the function f(z) has the form $e^{(\pm\beta(z-h))}$ and since the potential must vanish at infinity the potential is given for z ≥ h by

$$\Phi = \Phi_0 e^{(-|\beta|(z-h))} e^{j(\omega t-\beta x)} \tag{4.38}$$

where Φ_0 is a constant. Since there are no free charges the normal component of the electric displacement D_z must be continuous, so that in both the piezoelectric and the vacuum we have

$$D_z = \varepsilon_0 |\beta| \Phi \text{, at } z = h \tag{4.39}$$

If the piezoelectric medium has very high dielectric constants, then it is a fair assumption to consider that at the interface

$$D_z (z = h) = 0 \tag{4.40}$$

and the boundary condition can therefore be written as

$$\frac{\partial \Phi}{\partial z} = 0 \text{, at } z = h \tag{4.41}$$

For the metallised case the boundary conditions are

$$\Phi(z = h) = 0 \tag{4.42}$$

If the metallised surface is used as an electrode, i.e. not short-circuited but wired to an electrical generator, the boundary conditions, for the simplest terminations are

$$\Phi(z = h) = \text{constant} \tag{4.43}$$

$$I = \frac{\partial Q}{\partial t} = -\int_S \frac{\partial (D.n)}{\partial t} dS \text{, at } z = h \tag{4.44}$$

where S is the surface of the electrode, I the current, Q the charge, and n the vector normal to the electrode.

4.4.3 SOLUTION OF THE POISSON EQUATION

The analytical solution of the Poisson's equation is done in Appendix C using a polynomial method. More details on that method can be found in [4.41]. The solution is however simplified from the first order mechanical perturbation analysis. The stresses have been developed in the form of linear polynomials, which can be written as

$$\begin{aligned} T_5 &= A_5(z-h) \\ T_I &= A_I(z-h) + B_I \qquad I=1,2\,\text{or}\,3 \end{aligned} \tag{4.45}$$

The coefficients A_1, A_2, A_3, B_1, B_2, B_3 and A_5 are obtained from equations (B.31) to (B.34) in Appendix B, and the Poisson's equation simplifies to

$$\frac{\partial^2\Phi}{\partial z^2} - \beta^2\gamma^2\Phi = \frac{1}{\varepsilon_{33}^T}(-j\beta d_{x5}[A_5(z-h)] + d_{zI}A_I) \tag{4.46}$$

where summation over repeated indice I is assumed. The particular solution to Eq.(4.46) is given by Eq.(C.11) and the solution to the homogeneous equation is given by Eq.(4.31). Any linear combination of the general and particular solutions gives a unique solution to Eq.(4.47). The solution can then be written as

$$\Phi(z) = \left(F_1 e^{-\gamma z} + F_2 e^{+\gamma z}\right) - \frac{1}{\gamma^2\varepsilon_{33}^T}(-j\beta d_{x5}[A_5(z-h)] + d_{zI}A_I) \quad 1 \le I \le 3 \tag{4.48}$$

where summation over repeated indices *I* is assumed. It remains only to identify the coefficients F_1 and F_2 from two boundary conditions. The first boundary condition is that at the interface between the substrate and the layer. In this thesis we are interested in modelling transducers for smart structures. In most of the cases the structure is a metal, and therefore we assume that the substrate is a perfect conductor (i.e. infinite conductivity) which shorts out the horizontal component of the electric field at the surface. The boundary condition at the interface between the substrate and the piezoelectric layer is therefore given by Eq.(4.42).

The second boundary condition is that at the upper surface of the PZT-5H layer. We define 2 particular cases, the so-called open-circuit case and the so-called short-circuit case, as shown in Figure 4.23.

4.4.3.1 Metallised Top Surface

Using the boundary condition $\Phi(z=h)=0$, the solution is given by

$$\Phi(z) = \frac{e^{-z\beta\gamma}}{\beta^2\gamma^2\varepsilon_{33}^T\left(-1+e^{2\gamma\beta h}\right)}\left[\begin{array}{c} \left(-1+e^{h\gamma\beta}\right)\left(-1+e^{z\gamma\beta}\right)\left(e^{z\gamma\beta}-e^{h\gamma\beta}\right)d_{zI}A_I \\ +j\beta\left(\begin{array}{c} h\left(e^{2\gamma\beta h}-e^{2\gamma\beta z}\right)+e^{z\gamma\beta}\left(h-z\right) \\ +e^{(2h+z)\gamma\beta}\left(h-z\right) \end{array}\right)A_5 d_{x5} \end{array}\right] \quad 1\le I\le 3 \tag{4.49}$$

where summation over repeated indices *I* is assumed.

4.4.3.2 Free-Surface Case

If the upper surface of the layer is electrically free, then because electromagnetic wave propagate in vacuum or in air, the electrical potential at the layer/vacuum (air) interface must be continuous. This condition is given by Eq.(4.38) and the solution is given as a function of the constant Φ_0

$$\Phi(z)=\frac{e^{-z\beta\gamma}}{\beta^2\gamma^2\varepsilon_{33}^{T}\left(e^{2\gamma\beta h}-1\right)}\begin{bmatrix}\left(e^{h\gamma\beta}-1\right)\left(e^{z\gamma\beta}-1\right)\left(e^{z\gamma\beta}-e^{h\gamma\beta}\right)d_{zI}A_I\\ +j\beta\begin{pmatrix}h\left(e^{2\gamma\beta h}-e^{2\gamma\beta z}\right)\\ +e^{z\gamma\beta}\left(h-z\right)\\ +e^{(2h+z)\gamma\beta}\left(z-h\right)\end{pmatrix}A_5d_{x5}\\ +\Phi_0\beta^2\gamma^2\varepsilon_{33}^{T}\left(e^{2\gamma\beta h}-1\right)e^{h\gamma\beta}\end{bmatrix}\quad 1\le I\le 3 \quad (4.50)$$

where summation over repeated indices I is assumed. This potential constant is found using Eq.(4.39) as

$$\Phi_0=\frac{1}{\beta^2\gamma^2\varepsilon_{33}^{T}\left(\gamma+\gamma e^{2\gamma\beta h}+\varepsilon_0-\varepsilon_0e^{2\gamma\beta h}\right)}*\begin{bmatrix}\left(e^{h\gamma\beta}-1\right)^2\gamma d_{zI}A_I\\ +j\beta\left(e^{2\gamma\beta h}-2e^{\gamma\beta h}\gamma\beta h-1\right)A_5d_{x5}\end{bmatrix}\quad 1\le I\le 3 \quad (4.51)$$

and the solution for the potential within the layer is

$$\Phi(z)=\frac{e^{-z\beta\gamma}}{\beta^2\gamma^2\varepsilon_{33}^{T}\left(\gamma+\gamma e^{2\gamma\beta h}+\varepsilon_0-\varepsilon_0e^{2\gamma\beta h}\right)}*\begin{bmatrix}\left(e^{z\gamma\beta}-1\right)\begin{pmatrix}-\varepsilon_0e^{h\gamma\beta}\left(1+e^{z\gamma\beta}\right)+\\ e^{2\gamma\beta h}\left(\varepsilon_0-\gamma\right)+e^{z\gamma\beta}\left(\varepsilon_0+\gamma\right)\end{pmatrix}d_{zI}A_I\\ +j\begin{pmatrix}e^{h\gamma\beta}\left(1-e^{2z\gamma\beta}\right)+\\ \left(h-e^{z\gamma\beta}\left(h-z\right)\right)e^{2\gamma\beta h}\beta\left(\gamma-\varepsilon_0\right)\\ +\left(e^{\gamma\beta z}h+\left(z-h\right)\right)\beta e^{z\gamma\beta}\left(\varepsilon_0+\gamma\right)\end{pmatrix}A_5d_{x5}\end{bmatrix}\quad 1\le I\le 3 \quad (4.52)$$

If the relative dielectric constants of the piezoelectric layer are high, then it is reasonable to assume that the potential in the vacuum half space is negligible and the boundary condition simplifies into Eq.(4.41) and the solution is given by

$$\Phi(z)=\frac{e^{-z\beta\gamma}}{\beta^2\gamma^2\varepsilon_{33}^T}\left[\begin{array}{l}\left[-e^{z\gamma\beta}\,d_{zI}A_I+j\beta A_5 d_{x5}\left(e^{z\beta\gamma}(z-h)\right)\right]+\\ -\dfrac{e^{2z\beta\gamma}}{\gamma\beta\left(e^{2\gamma\beta h}+1\right)}\left[\begin{array}{l}-je^{h\gamma\beta}\beta A_5 d_{x5}+\\ \gamma\beta\left(d_{zI}A_I+jh\beta A_5 d_{x5}\right)\end{array}\right]\\ +\dfrac{e^{\beta\gamma h}}{\gamma\beta\left(e^{2\gamma\beta h}+1\right)}\left[\begin{array}{l}j\beta A_5 d_{x5}+\\ e^{h\gamma\beta}\gamma\beta\left(d_{zI}A_I+jh\beta A_5 d_{x5}\right)\end{array}\right]\end{array}\right] \qquad 1\le I\le 3 \quad (4.53)$$

This solution applies to PZT-5H since it has a dielectric constant in the normal direction that is 1700 times larger than the dielectric constant of vacuum. In most cases this assumption is not very restrictive and the solution will remain representative of many practical cases as long as the relative dielectric constant of the piezoelectric layer is large. In the remainder of this Chapter, this solution is preferred to that given by Eq.(4.52) firstly because of its simplicity, but also because it is derived from a boundary condition at the upper surface that matches the electrical boundary condition available in the piezoelectric finite element module developed in Chapter 3. In this FE model, no external infinite element to model vacuum has been developed so far and therefore the FE programs acts as if no wave can radiate outside the limits of the model. Therefore validating Eq.(4.52) with the FE code would lead to errors than can be avoided by using Eq.(4.53).

From Eq.(4.53) the electrical potential at the upper surface is given by:

$$\Phi(h)=\frac{1}{\beta^2\gamma^3\varepsilon_{33}^T\left(e^{2\gamma\beta h}+1\right)}\left[\begin{array}{l}\left(1-e^{2\gamma\beta h}+2h\gamma\beta e^{h\gamma\beta}\right)jA_5 d_{x5}\\ \left(e^{h\gamma\beta}-1\right)^2\gamma\left(-d_{z1}A_1-d_{z2}A_2-d_{z3}A_3\right)\end{array}\right] \qquad (4.54)$$

with $\gamma=\sqrt{\dfrac{\varepsilon_{11}^T}{\varepsilon_{33}^T}}$ and where the summation over the indices *I* has been developed.

$$\Phi(h)=-C_1\left(d_{z1}A_1+d_{z2}A_2+d_{z3}A_3\right)+jC_2\,d_{x5}A_5 \qquad (4.55)$$

where C_1 and C_2 are constants depending only on the geometric, elastic and piezoelectric constants of the thin layer and on the wavenumber of the mode under consideration.

$$C_1=\frac{(e^{h\gamma\beta}-1)^2\gamma}{\gamma^3\beta^2\varepsilon_{33}^T(1+e^{2h\gamma\beta})} \qquad (4.56)$$

$$C_2=\frac{(1+2\beta\gamma h e^{h\gamma\beta}-e^{2h\gamma\beta})}{\gamma^3\beta^2\varepsilon_{33}^T(1+e^{2h\gamma\beta})} \qquad (4.57)$$

It is noted that the term in A_5 is 90 degrees out of phase with the other terms. Constants A_1, A_2, A_3 and A_5 are the slope of the stresses in the piezoelectric layer, which are given by the first order terms in the power series expansion. The potential is then given by

$$\Phi(h) = -C_1 (d_{z1} T_1^{(1)} + d_{z2} T_2^{(1)} + d_{z3} T_3^{(1)}) + jC_2 d_{x5} T_5^{(1)} \tag{4.58}$$

The first order stress coefficients are functions of the particle velocities at the upper surface, and we can rearrange Eq.(4.58) so that the particle velocity functions appear explicitly

$$\begin{aligned} \Phi(h) = &- jC_1 \left[d_{z1} D_1 + d_{z2} D_2 + d_{z3} D_3 \right] v_3(h) \\ &- C_2 \left[d_{x5} D_5 \right] v_1(h) \end{aligned} \tag{4.59}$$

with, from equations (4.18) to (4.21)

$$D_1 = \frac{-s_{11}}{s_{11}^2 - s_{12}^2} \frac{\beta_n}{V_n} \left\{ 1 + \rho V_n^2 \frac{s_{13}(s_{11} - s_{12})}{s_{11}} \right\} \tag{4.60}$$

$$D_2 = \frac{s_{12}}{\left(s_{11}^2 - s_{12}^2\right)} \frac{\beta_n}{V_n} \left\{ 1 + \rho V_n^2 s_{13} \left(\frac{\left(s_{11} - s_{13} + s_{12}\right)}{s_{11}} - \frac{s_{11}}{s_{12}} \right) \right\} \tag{4.61}$$

$$D_3 = \omega\rho \tag{4.62}$$

$$D_5 = \omega\rho - \frac{s_{11}}{s_{11}^2 - s_{12}^2} \frac{\beta_n}{V_n} \tag{4.63}$$

It is seen that for z = 0, both constants C_1 and C_2 vanish which is in line with the boundary condition for electric potential at the grounded interface. Eventually the solution is explicitly given by

$$\begin{aligned} \Phi(h) = \frac{-j(e^{h\gamma\beta} - 1)^2 \gamma}{\gamma^3 \beta^2 \varepsilon_{33}^T (1 + e^{2h\gamma\beta})} &\left[\begin{array}{l} d_{z1} \left\{ \dfrac{-s_{11}'}{s_{11}'^2 - s_{12}'^2} \dfrac{\beta_n}{V_n} \left(1 + \rho' V_n^2 \left(\dfrac{s_{13}' \left(s_{11}' - s_{12}' \right)}{s_{11}'} \right) \right) \right\} + \\ d_{z2} \left\{ \dfrac{s_{12}'}{s_{11}'^2 - s_{12}'^2} \dfrac{\beta_n}{V_n} \left(1 + \rho' V_n^2 \left(\dfrac{s_{13}' \left(s_{11}' - s_{12}' \right)}{s_{11}'} \right) \right) \right\} + \\ d_{z3} \{ \omega\rho' \} \end{array} \right] v_3(h) \\ - \frac{(1 + 2\beta\gamma h e^{h\gamma\beta} - e^{2h\gamma\beta})}{\gamma^3 \beta^2 \varepsilon_{33}^T (1 + e^{2h\gamma\beta})} &\left[d_{x5} \left\{ \omega\rho - \frac{s_{11}'}{s_{11}'^2 - s_{12}'^2} \frac{\beta_n}{V_n} \right\} \right] v_1(h) \end{aligned} \tag{4.64}$$

By using Eq.(4.64) the electric potential was computed for the two fundamental modes of the bi-layered system aluminium(1mm)/PZT-5H(0.1mm) and the results are shown in Figure 4.24. The electric potential has been calculated using the particle velocities of the modes P_1 and P_2 at the top surface of the PZT-5H layer.

Eq.(4.64) is the sum of 4 terms, each being a multiple of the piezoelectric constants d. These terms arise from the integrated effect of the $\nabla.(d:T)$ term in the Poisson's equation. The term in d_{z5} is derived from the shear stress and the terms in d_{zI} derive from the direct stresses T_I where I can take the values 1, 2 or 3. For this reason none of them can play an important part in generating the electric potential until the layer is thick enough to have a significant integration volume. Such an effect is directly dependent on the electrical boundary conditions chosen. Because the substrate is a grounded metallic plate there is no potential within the substrate, and the potential develops from zero at the interface to its maximum value at the top surface. When each term in Eq.(4.64) is computed separately, it appears that the coupling, for the two modes, is dominated by the terms arising from the normal stress. This is due to the fact that the slope of the normal stress within the layer is the steepest one. From Figure 4.14 and Figure 4.15, it is seen that the magnitude of the normal (T_3) and inplane (T_1) stresses are similar at the interface but whereas T_1 varies only slightly through the thickness of the layer, the normal stress must be zero at the top surface. Therefore its spatial derivative is higher than that of T_1 and the term arising from the normal stress dominates the coupling. For example, at 1MHz for the mode P_2, the term in d_{z3} represents 66% of the sum of the 4 terms.

4.4.4 FINITE ELEMENT VALIDATION

At the mechanical stage, we used the program Disperse to validate our mechanical perturbation formulae. However Disperse does not model piezoelectric materials, therefore to validate the analytical formula for the electrical potential, two series of finite element models were designed in order to predict the amount of electrical potential associated with a given mode propagating along the model. To do so we used the finite element code presented in Chapter 3. The FE models comprised a piezoelectric layer (PZT-5H) rigidly attached to an aluminium plate. The PZT-5H layer is 100μm thick and 100 mm long and is modelled with 2 elements through its thickness and 1000 elements along its length. The aluminium plate is 1mm thick and 100mm long. It is made of 10 by 1000 square elements as shown in Figure 4.25. The elements used are two-dimensional, four noded quadrilaterals and the calculations are done assuming axi-symmetry and free boundary conditions for all cases. Within the aluminium plate, square elements, 100μm by 100μm, elements are used whereas in the PZT-5H layer, two rectangular elements are used through the thickness of the layer. Using only one quadrilateral element would "force" the fields to vary linearly through the thickness of the layer. This may be convenient to validate our model but can still be too coarse to model accurately the real behaviour of the system. Therefore 2 elements were used through the thickness of the layer in order to make sure that the real behaviour of the fields could be modelled more accurately than in the approximation analysis. The models vary from each other in the centre frequency and the magnitude of

the excitation signal applied at the nodes along the left-hand edge of the model. In all models, the excitation signal was a 6 cycle Hanning windowed toneburst. The bandwidth (40dB down points) of such a signal depends upon its the centre frequency.

The first series of models were designed to generate the mode P_1 at various frequencies within the range 0 to 2.5MHz. At each particular frequency, the amplitude of the excitation signals, applied in each directions at each node along the edge of the model, match the magnitude of the displacement mode shapes in the normal and the inplane directions. However these mode shapes have been calculated with Disperse what implies that they are exact but have been calculated for non-piezoelectric materials. This procedure was repeated at several frequencies for the mode P_1 and then for the mode P_2 at the same frequencies. Below 500 kHz, models have been run at every 50 kHz and above 500 kHz, models have been designed at every 250 kHz up to 2.5 MHz. This results in 19 models for each of the two modes.

The results are presented in Figure 4.26 and are compared with the perturbation calculations obtained from Eq.(4.64). The electrical potential was monitored along the top surface at 500 nodes. When the modes are dispersive, the signal in the time domain looses the shape of the original 6 cycle toneburst and spreads in time. Therefore a direct reading of the amplitude of the signals in the time domain would be erroneous at frequencies where the modes are dispersive. Therefore the results obtained were processed using the two-dimensional Fourier transform method (2-D FFT [4.16]). This technique involves two Fourier transform stages. Firstly, the time domain traces from each individual monitoring point are Fourier transformed into the frequency domain, yielding the frequency spectrum for each monitoring point. For each frequency component, a spatial Fourier transform is carried out encompassing all consecutive monitoring points; this yields the wavenumber components present at each frequency. The resulting two-dimensional array contains the amplitudes of the different frequency and wavenumber components of the signal. The Lamb modes present have different wavenumbers, owing to their different phase velocities, and therefore appear at different locations on the wavenumber axis, allowing their amplitudes to be measured independently. The electrical potential has been calculated by integrating the magnitude of the 2D-FFT for each mode along its dispersion curve and the magnitude as a function of frequency is shown with '+' marker in Figure 4.26. The perturbation calculations are plotted as lines in Figure 4.26 and have been obtained from Eq.(4.64). The plain lines represents the electrical potential obtained from Eq.(4.64) when the particle velocities at the top of the PZT-5H layer are used. The dashed lines represent the electrical potential calculated from Eq.(4.64) when the particle velocities at the top surface of the aluminium plate considered alone are used. To compare FE predictions and the perturbation calculations both quantities have been normalised to a common quantity. The electrical potential given in Eq.(4.64) depends upon the particle velocities and in general such quantities are normalised to unit power flow in the direction of propagation but the power flow is not a quantity easily accessible from the finite element model because of the inaccuracies in the stress field of the finite element model. Finite element analysis using displacement elements enforces displacement continuity at the nodes, but there are no constraints on the continuity of the stresses across elements [4.42]. Unless the element can exactly model the required stress distributions, which is very rarely the

case for guided waves, there will be discontinuities in the stresses. The power flow formula depends on the stresses in the same way as the orthogonality relationship and it was shown by Pavlakovic [4.43] that the inaccuracy in the stress profile of guided modes can be large enough to render the mode orthogonality relationship useless. Therefore instead of normalising the finite element results to unit power flow they have been normalised to a more accurately predicted field, the particle displacements at the top surface of the plate. Therefore the electrical potential in Figure 4.26 are given for modes having, at the top of the PZT-5H layer, a displacement amplitude, in the direction of propagation, equal to one nanometer.

It is seen that below 1.5 MHz, better agreement between the FE predictions and the perturbations calculations is obtained when the exact particle velocities are used in Eq.(4.64). Thus, in maximizing the coupling the proper values of particle displacements at the top of the layer should be sought. However, at least up to 500 kHz in Figure 4.26, the electrical potential is well approximated using the particle velocities at the top of the aluminium plate (the dashed lines).

Although the agreement between FE predictions and perturbation calculations are good up to 1.25 MHz, it deteriorates above 1.5 MHz and the problem comes from the method used to extract the FE points. As mentioned above, to generate the modes in the models, excitation signals matching the displacement mode shapes have been applied at one edge of the model. However this technique is inaccurate for two reasons. Firstly the mode shapes have been calculated for a non-piezoelectric layer and not for an active PZT-5H layer, therefore the mode shapes are inaccurate. Secondly the mode shape magnitudes have been matched only at the centre frequency of the 6 cycle excitation toneburst. Therefore the modes are excited over the whole bandwidth of the toneburst and not only at the centre frequency but the excitation displacement profile matches only the mode shapes at the centre frequency and not at the other frequencies of the excitation bandwith. Therefore the displacements applied at the edge of the model are not exactly those that would be needed to generate one mode only. When the modes are well separated, as it is the case for the two fundamental modes below 1.25 MHz as seen in Figure 4.27(a), the modeshapes are very different and only one mode is excited although the excitation profile is not exactly matching the mode shape of the mode that is generated.

However, above 1.25 MHz, not only the two fundamental modes but also the cut-off modes can be generated. If the mode shapes are not perfectly reproduced by the applied excitation then the modes present at that frequency can be generated. Figure 4.27(b) shows that the first cut-off mode appears at 1.25 MHz for the aluminium(1mm)/PZT-5H(0.1mm) system, without considering the piezoelectric coupling. Above 1.25 MHz, this mode is a propagating mode and can be generated. Figure 4.28(a) shows the electrical potential associated with the mode P_2 (lowest extensional mode) after it has propagated over 67.5 mm. The shape of the signal is that of at least two signals interfering with each other. The first signal arrival is the mode P_2 and it is believed that the second is the cut-off mode P_3. Figure 4.28(b) shows the signal that would be monitored at the same location if the mode P_2 was the only one to propagate. This signal has been obtained from the program DISPERSE and takes into

account the dispersion of the mode and the shape of the 6 cycle Hanning windowed excitation toneburst. If now we suppose that both the modes P_2 and P_3 are generated at the same time in the model and assuming that the mode P_3 has an amplitude equal to 20% of that of the mode P_2, then after having propagated over 67.5 mm, the overall signal, for at the 6 cycle Hanning windowed toneburst, with centre frequency 1.5MHz, would look like that shown in Figure 4.28(c). This time trace is also a simulation obtained from DISPERSE, from the dispersion curves of the aluminium(1mm)/PZT-5(0.1mm) system. Although the piezoelectric coupling is not taken into account in the simulated signal shown in Figure 4.28(c) it is seen that it is very similar to that in Figure 4.28(a). This indicates clearly that at 1.5 MHz the mode P_2 has not been generated alone in the FE models but the cut-off mode P_3 has also been generated. Part of the energy is carried by this mode and less energy is carried by the mode P_2. Therefore when performing the integration in the wavenumber-frequency plane along the dispersion line of the mode P_2, the energy carried by the cut-off mode P_3 was not taken into account and therefore the magnitude of the electric potential associated with the mode P_2 has been underestimated leading to the large mismatch between the FE prediction and the perturbation calculations. This phenomenon applies at all the frequencies above the first cut-off frequency and also to the predictions made for the mode P_1. Therefore the FE points above 1.5 MHz cannot be trusted and the predictions and the perturbation calculations can be compared only in the range 0 to 1.25 MHz where it is seen that the agreement is very good.

The perturbation calculations for the electrical potential have been validated for one simple case and before proceeding with the more complex cases, it is necessary to review the assumptions and the approximations that have been used both in the mechanical perturbation stage and in this piezoelectric perturbation stage.

4.5 DISCUSSION ABOUT THE VARIOUS ASSUMPTIONS AND APPROXIMATIONS USED

In the two first stages, we made use of various approximations and we made a number of assumptions which all contribute to limit to some extent the validity of the analysis. It might have appeared to the reader that we made use of numerous approximations and we think it is important to regroup them all here in order to explain in some detail the ground on which each of them hold, and how each contributes to limit the analysis. All the items listed below are not necessarily independent but they must be consistent if the final perturbation expression is to have any meaning. Basically six hypothesis have been made throughout the development of the perturbation analysis:

1 The electrostatic approximation (but using full dynamic equations).

2 The assumption of small perturbations.

3 Most of the power flow is contained in the mechanical system.

4 Acoustic stress defines the polarisation source for the potential, through the piezoelectric strain constants *d*.

5 The electrical boundary conditions are independent of the direction of propagation.

6 The total power flow is unchanged by the addition of a shorting plane.

Item (1) is essentially assumed in treating all problems dealing with acoustic waves in piezoelectric ceramics because the propagation constant of the acoustic waves is 10^5 times larger than the value for an electro-magnetic wave. These five orders of magnitude arise from the ratio of the velocity of electro-magnetic waves to the velocity of acoustic waves and permit use of the quasistatic approximation for the electric potential, while using the full dynamic format for the elastic terms. Details on the development of Maxwell's equations and the piezoelectric equations under the quasistatic approximation are given in chapter 8 of [4.7]. Obviously such an assumption has other consequences as well as conveniently simplifying the Maxwell's equations. If this approximation is valid it means that the magnetic portion of the electrical Poynting vector is negligible compared to the electric portion and a degenerate form of the Poynting energy flux may be used, which is the case in all this thesis and is implicitly used in the mode amplitude equations derived from the modal analysis. In addition the condition must also hold in the vacuum (or air) immediately outside the piezoelectric body to satisfy the electric boundary conditions at the interface and consequently, the electric equation in the vacuum in the immediate vicinity of the piezoelectric body is Laplace's equation (Eq.(4.36)).

Item (2) is based partly on empirical results. Numerical results for a two-layered mechanical problem show that the stresses are weakly perturbed by the addition of a thin layer as long as the thickness of the layer remains small compared to the wavelength of the considered wave. This has been proved for surface acoustic waves where it can be easily understood since the wavelength of those waves is inversely proportional to the frequency (constant phase velocity). For plate modes however the phase velocity changes with frequency so that the thickness to wavelength ratio can vary significantly over a narrow frequency range. This is especially obvious near cut-off frequencies for high-order modes but also for the fundamental modes in frequency ranges where their group velocity is undergoing steep variations. For the aluminium(1mm)/PZT-5H(100mm) system the wavelength to layer thickness ratio is always above 50 below 5 MHz for both fundamental modes and is therefore high enough to consider the small perturbation assumption valid.

Item (3) is not independent of item (2). Since the electromagnetic fields are weakly coupled to the acoustic fields one may be tempted to assume that the majority of the power flow is contained within the acoustic wave and hence the mechanical fields are little affected by changes in the electromagnetic fields. For SAW it has been proved by Lakin [4.38] that this assumption is safe even for strongly coupled materials like $LiNBO_3$. In Chapter 3 we derived the solutions for longitudinal and shear vertical waves propagating in PZT-5H. We found that for quasistatic waves the elastic energy density is much greater than the electric energy density. The assumption is that this conclusion holds for acoustic plate modes in the bi-layered system aluminium/PZT-5H.

Item (4) is correct as long as the acoustic stress, which creates the polarization, is that resulting from a solution of the coupled acoustic and electromagnetic equations.

Item (5) was required to simplify the integrations leading to Poisson's equation but can be relaxed if the electrical impedance is varying slowly in terms of wavelengths along the propagation direction. However this case is not considered in this study.

Based on the assumption that the stresses are the same when the top surface is short-circuited or not, the total power flow is assumed to be unchanged by the addition of a shorting plane. Because the total power flow of the wave is the addition of a mechanical power flow and an electrical power flow the assumption that the total power flow is unchanged by the addition of a shorting plane is dependent on items (1) and (3).

4.6 TRANSDUCER PROBLEM

At this stage of the development of our transducer model, approximate solutions for the dispersion curves and for the potential have been found for the two fundamental modes propagating in a substrate/piezoelectric layer system. The two layers are still considered as being infinite in the direction of propagation so the modes propagate in the system without being scattered. If we now assume that a thin electrode (having no mechanical influence) of finite length is deposited on top of the piezoelectric layer, as shown in Figure 4.29(a), then we have a transducer problem. Figure 4.29(b) shows the new electrical boundary conditions. A voltage V is applied across the electrode attached to the top surface of the piezoelectric layer and the interface between the piezoelectric layer and the grounded metallic substrate. Our aim in this section is to calculate the amplitude of the modes, generated by the electrical source, that propagate in the system away from the electrode.

The specific problem of the excitation of Lamb waves by external sources, being electrical or mechanical, has been extensively studied. One of the pioneering studies has been performed by Viktorov [4.20], who established the analytical expressions for wedge transducers emitting in isotropic plates. In the late eighties there was much interest in multisensing oscillators and sensors using IDTs to generate plate waves and detect variations of their properties [4.26], [4.27], [4.44]. These works made great use of the perturbation theory and are recommended for their detailed review of experimental set-ups. In the nineties, the excitation of ultrasonic Lamb waves and shear-horizontal waves in piezoelectric plates by SAW devices (IDTs in most cases) has been studied both theoretically and experimentally. Joshi [4.5] and Jin [4.45] have studied the excitation of Lamb waves by IDTs deposited on piezoelectric plates, using the Greens function technique. Using the same technique the wave propagating at the interface between a piezoelectric plate and a viscous [4.46] or dielectric liquid has been studied by Josse [4.47]. Guided modes in loaded piezoelectric plate have been studied by Yang and Chimenti [4.48]. Laurent [4.49] used two pairs of IDTs deposited on both sides of the piezoelectric plate to generate selectively either the lower symmetric or the lower anti-symmetric Lamb modes. These works, from Joshi to Laurent, use various techniques, none of which we decided to use in this study. More recently, works have been published on solid [4.50] and liquid [4.15] wedge transducers as well as air

coupled transducers [4.51]. Other, more atypical excitation techniques, have also been theoretically studied including comb transducers [4.52], buffers [4.53] and Hertzian contacts [4.54]. The problem of piezoelectric transducers embedded in the waveguide has been studied by Moulin [4.55] using a finite element technique. Most of these recent works are making use of the normal mode expansion technique.

This quick review shows that the problem involving forced loading of plate-like waveguides can be tackled using many different techniques. The most general and powerful technique is to treat the source function as a combination of point loads and solve the problem for a point load. Then assuming that the governing equations are linear the overall solution is given by the linear superposition of the Green's function of the governing equation. This technique, which usually involves integral transform techniques and integration in a complex plane, is cumbersome, and an example of its complexity is given by Morgan [4.3]. Moreover it is not a versatile technique and for each different transducer design a new solution must be sought. A more attractive technique is the normal mode expansion technique used by Jia [4.15], Ditri [4.50] and Degertekin [4.56]. Recent work by Moulin [4.57] emphasises the versatility of the technique by using finite element predictions of the mechanical fields generated by a piezoelectric transducer to predict the amplitudes of the normal modes generated by the transducer.

The normal mode expansion technique is analogous to the eigenfunction expansion methods discussed in many theoretical physics books [4.8], [4.58], [4.59]. Since Lamb modes are eigenmodes of a solid, infinite and stress free plate, the normal mode expansion technique is particularly suited to predict Lamb waves as a function of the plate excitation and the goal of this technique is to find a general expression for the unknown amplitudes of the modes in which the fields have been expanded. The general principles along with the main advantages of this technique are described in textbooks by Auld [4.7], Kino [4.1], Jones [4.60] and more recently by Rose [4.61]. The details of the derivations are given in publications made in the early seventies when many researchers all around the word paid a considerable amount of attention to the problems of the excitation and the reception of surface acoustic waves (SAW) and the design of suitable excitation and reception devices. Auld derived the reciprocity relationship [4.62], and normal mode theory [4.63] for acoustic wave guide problems to determine a variational expression for the input admittance of an IDT. Kino [4.64] developed the perturbation theory on the basis of the normal mode theory to study the properties of a piezoelectric-semiconductor system in terms of a small perturbation of the unperturbed defined as one with the semiconductor absent. Many other works followed among them Wagers [4.65] who expanded the fields of the transducers in short-circuited modes by contrast with the open-circuited modes used by Auld [4.7, Chapter 10]. These works are important to our analysis since they present the theoretical basis of the normal mode expansion technique. However they are only concerned with surface acoustic waves (SAW) and not with Lamb waves and the important problem that constitutes the focal point of the work presented in this chapter is the generation of Lamb waves. However the reciprocity relationship is by no means limited to a particular mode and as pointed out by Wagers [4.66] and Laurent [4.49], the excitation of plate modes can be solved in the same way as surface acoustic waves.

The efficacy of normal mode expansion depends directly on two main considerations: completeness and orthogonality of the eigenfunctions. The question of the completeness of the expansion is a delicate question since, to our knowledge, there exists no proof of it even for the Lamb wave modes. However the completeness of the set of modes is always assumed in practical problems since if the set of modes were not complete then the solution of the governing equation might not be expressible. A definition of completeness is given in Chapter 2. Establishing orthogonality of the modes is essential since it is the tool by which the expansion amplitudes are determined. In practice this means that a new orthogonality relationship (and a new normalisation formula) must be found for each new system. Peach [4.33] derived a normal mode for piezoelectric plates of limited extent and applied it to the prediction of the amplitude of energy trapped resonator modes. Briers [4.35], [4.67] showed in great detail how a new orthogonality relation can be derived for Stoneley waves. These works show that the normal mode expansion technique can also present some difficulties despite its apparent simplicity. However, this is a not a problem that we have to face here since the modes that propagate in our system are Lamb modes, or perturbed Lamb modes. Therefore we can use the orthogonality relationship for Lamb modes presented in Chapter 2.

The perturbation theory and the normal mode expansion technique are based on similar considerations and the starting point for both theories is the reciprocity relationship. In the following section we present a perturbation theory based on the idea that total field of a single mode in a perturbed waveguide can be expressed as a weighted sum of the original modes in the unperturbed medium. If we assume that the effect of the applied excitation can be expressed as a change in the boundary condition of an originally free waveguide, then the perturbation is a change of boundary conditions and the amplitude of the perturbed modes can be expressed as a function of the new boundary conditions.

4.6.1 NORMAL MODE EXPANSION

The normal mode excitation equations have been posed by Auld [4.7] and here we only present an heuristic derivation of them, stressing the assumptions made in the derivation. More detailed and rigorous derivation can be found in [4.62] and [4.63].

Since Lamb waves are eigenmodes of a solid infinite and stress-free plate, the normal mode expansion method is suitable for this application. If the plate is anisotropic, the dispersion characteristics of the normal modes are dependent on the orientation between the wavevector of the mode and the crystallographic coordinate system of the medium. In this section, following the example treated in the previous section, the piezoelectric crystal is Z-cut, and the modes propagate along the x-direction. Figure 4.30 shows the coordinate axes and the geometry of the system. In this coordinate system, the fields of any mode propagating in the system are uniform in the y-direction; the problem is therefore one of plane strain in the plane (x, z). The fields propagating in the waveguide can therefore be written in the following form

$$f(x,z,t) = g(z)\, e^{j(\omega t \pm \beta x)} \tag{4.65}$$

where g(z) represents the modal distribution, or the z-variation of the field f, and β is the wavenumber of the mode, determined at the frequency ω, by the dispersion equation. The frequency is real and positive but the wavenumber, which is real for the propagating modes, can be complex for non-propagating modes.

Let us assume that the plate-like waveguide is only mechanically excited by either an internal force field F or a surface traction field T_S and let us consider two different volume and surface excitations **(**F_1, Ts_1) and **(**F_2, T_{S2}) of the waveguide, considered temporarily non-piezoelectric. In the case of harmonic excitation and assuming a lossless material, there exists a relation, called complex reciprocity relation [4.7], between the acoustic fields **(**v_1, T_1) and **(**v_2, T_2) generated by the two excitation sources

$$\frac{\partial}{\partial x}(v_1^*.T_2 + v_2.T_1^*).x + \frac{\partial}{\partial z}(v_1^*.T_2 + v_2.T_1^*).z = -v_1^*.F_2 - v_2.F_1^* \tag{4.66}$$

where the asterisk * denotes complex conjugation. By applying it to two distinct eigenmodes of the waveguide, with wavenumbers β_n and β_m and associated acoustic fields **(**v_n ,T_n) and **(**v_m ,T_m), following Auld [4.7], the orthogonality relation is given by

$$P_{nm} = 0 \quad \text{for} \quad \beta_n \neq \beta_m \tag{4.67}$$

with

$$P_{nm} = \frac{1}{4}\int_{-d}^{d}\left(-v_m^*.T_n - v_n.T_m^*\right).x\,dz \tag{4.68}$$

where x is the unit vector for the x-direction. Thus, the plate modes in the waveguide are demonstrated to form a set of normal modes. Therefore, the acoustic fields (v, T) created in the waveguide by the arbitrary excitation fields **(**F, T_S), can be expanded into a summation over the normal modes:

$$\begin{aligned} v(x,z) &= \sum_m a_m(x) v_m(z) \\ T(x,z) &= \sum_m a_m(x) T_m(z) \end{aligned} \tag{4.69}$$

where $v_m(z)$ and $T_m(z)$ are the acoustic field of the m^{th} plate mode, and $a_m(x)$ is the modal amplitude, generally complex and x-dependent. The perturbation is incorporated in the formalism by this non-trivial x-dependency of the modal amplitude. For an unperturbed mode, i.e. a mode propagating freely in the free waveguide, $a_m(x) = \exp(-i\beta_m x)$. A perturbed mode is a mode that exists in the waveguide plus source system. For example if the excitation are forces applied along a finite length, the system of waveguide plus forces is different from the waveguide without the forces and the applied forces changes the boundary conditions. Therefore in the forced region the waveguide is different and this difference is dependent on the length of the forced region. It is in that sense that the x-dependence of the modal amplitude incorporates the perturbation introduced by the excitation.

The solution of the transducer problem is then reduced to the determination of each modal amplitude $a_m(x)$ since away from the transducer only Lamb modes can propagate in the plate and the fields of these modes are already known. To determine their amplitudes, we consider two solutions and apply the reciprocity relationship. The first solution is taken to be the fields in the system perturbed by the applied source and this first solution is expanded in terms of the original modes of the unperturbed system.

$$\begin{aligned} v_1(x,z) &= v(x,z) \\ T_1(x,z) &= T(x,z) \end{aligned} \tag{4.70}$$

The second solution is taken to be one particular mode of the unperturbed system, for example the n^{th} normal mode of the unperturbed system

$$\begin{aligned} v_2(x,z) &= e^{(-i\beta x)} v_n(z) \\ T_2(x,z) &= e^{(-i\beta x)} T_n(z) \end{aligned} \tag{4.71}$$

Solution "1" is a disturbance and the boundary conditions at the surface are unspecified at this stage. Setting $F_2 = F_1 = 0$ in Eq.(4.66) eliminates the volume sources and the integral over the thickness of the waveguide vanishes for all modes unless m = n due to the orthogonality relationship. Thus from Eq.(4.66) the amplitude of the n^{th} normal mode is given by

$$4P_{nn}\left(\frac{\partial}{\partial x} + j\beta_n\right) a_n(x) = f_{Sn}(x) \tag{4.72}$$

with

$$f_{Sn}(x) = \left\{ v_n^*(x).T_S(x) + v_S.T_n^*(x) \right\}.z \tag{4.73}$$

The second solution has been chosen to correspond to modes propagating in a free waveguide. This implies that these modes satisfy the free surface boundary condition, $T_n.z = 0$. Therefore Eq.(4.73) reduces to

$$f_{Sn}(x) = \left\{ v_n^*(x).T_S(x) \right\}.z \tag{4.74}$$

which indeed is the formulation of a very well-know fact, i.e. a traction force drive corresponds to the modal boundary condition $T_n.z = 0$. The other possibility is obviously to consider a clamped waveguide, in which the modes must satisfy the boundary conditions $v_n = 0$, and the only possibility to drive a clamped waveguide at its boundaries, is to apply a velocity field.

Assuming that there is no excitation source outside an interval $-L/2 < x < L/2$ (see Figure 4.30(a)), the solution of this differential equation Eq.(4.72) for propagating modes traveling rightward (in the positive x-direction) is given by

$$a_n(x) = \frac{e^{-j\beta_n x}}{4P_{nn}} \int_{-L/2}^{L/2} f_{Sn}(\eta) e^{-j\beta_n \eta} \, d\eta \tag{4.75}$$

We then write the forcing function explicitly in terms of the applied tractions and the velocity components of the propagating mode at the plate surface as:

$$\int_{-L/2}^{L/2} f_{Sn}(\eta) e^{-j\beta_n \eta} \, d\eta = v_{nx}^*(d) \int_{-L/2}^{L/2} T_{xz}(x,d) e^{j\beta_n x} dx + v_{nz}^*(d) \int_{-L/2}^{L/2} T_{zz}(x,d) e^{j\beta_n x} dx \tag{4.76}$$

where T_{xz} and T_{zz} are the lateral and normal components of the applied traction T_S. Assuming that Eq.(4.75) can be solved for each mode, the total fields in the waveguide can be determined. However the total field can be obtained only from an infinite summation of all modes, including the non-propagating modes. Non propagating modes (with complex wavenumbers) will not be taken into account in this study. The error introduced by taking only the propagating modes into consideration is only significant near the source. The amplitude of the evanescent modes decreases exponentially in the *x*-direction, so their influence decreases exponentially away from the source.

To use the formulation for the modal amplitude, the stress and velocity fields of the unperturbed waves must be known. In the present problem, these fields are those of the modes propagating in the bi-layered system. These fields have been determined approximately at the previous mechanical perturbation stage. Therefore if the applied source, i.e. the applied traction in Eq.(4.75), is known then the amplitude of the modes is also known. The problem we want to solve in this section is a transducer problem where the applied source is electrical and not mechanical as presented above.

This transmitter problem is in fact the combination of two problems. One problem is the wave generation in the piezoelectric layer by a specified electrical source (charge distribution or potential source), and the other is the electrostatic problem of determining the charge distribution (or the electric field) on the electrode due to the applied voltage. These problems may be treated separately and then combined by means of an integral equation. The next section derives a relationship between the mode amplitudes and the applied electric source. Then, section 4.6.3 presents some important transducer characteristics and emphasises the differences between SAW devices and our bi-layered system designed to generate plate modes. Section 4.6.4 shows how to solve the electrostatic problem and formulae for the electrical charge distribution are derived for a single strip. Eventually, in section 4.6.5, the amplitudes of the modes S_0 and A_0 generated by the applied voltage at the electrode are calculated and validated using the finite element program.

The originality of our work is that we coupled the perturbation theory with the normal mode expansion technique to calculate the amplitude of Lamb waves.

4.6.2 TRANSMITTER PROBLEM

The waveguide is excited via an electrical voltage applied to an infinitely thin electrode whose effect is only to modify the electrical boundary conditions at the upper surface of the piezoelectric layer. The modes propagating in the piezoelectric layer are not only described by their velocity and stress fields but also by their electrical potential and their normal electrical displacement. The electrical fields can also be expanded in a sum of normal modes

$$\begin{aligned}\Phi(x,z) &= \sum_m a_m(x)\Phi_m(z) \\ D_z(x,z) &= \sum_m a_m(x)D_{zm}(z)\end{aligned} \tag{4.77}$$

In the transmitter case, the sources are electrical. The electrode can be either driven by an applied potential Φ_S or an applied normal electrical displacement D_{Sz} in the same way that the mechanical source can be either forces or velocities. Therefore the forcing function in Eq.(4.72) is replaced by electrical fields, yielding

$$4P_{nn}\left(\frac{\partial}{\partial x}+j\beta_n\right)a_n(x) = -\left\{\Phi_n^*(x)\left(i\omega D_S(x)\right)+\Phi_S(x)\left(i\omega D_n^*(x)\right)\right\}.z\Big|_{z=h} \tag{4.78}$$

where, as seen in Figure 4.29(b), the electrical drive is applied at z = h, the upper surface of the piezoelectric layer and the thickness "t" of the electrode is considered to be zero. Φ_n is the potential associated with the elastic waves propagating in the piezoelectric layer, and D_n is the strain-induced electric displacement These quantities correspond to the modes propagating in the bi-layered waveguide before the electrical source is applied, i.e. the unperturbed modes. The fields of the modes in the waveguide being known, Eq.(4.78) provides a complete formulation of the excitation problem.

4.6.2.1 Boundary Conditions

In the same way that the modal boundary conditions and the nature of the drive are connected in the purely mechanical case, choosing the electrical boundary condition of the unperturbed modes to be short-circuit or open-circuit determines implicitly whether the modes are driven by the potential or the charges. Because the normal modes must satisfy the boundary conditions, one of the two source terms on the right-hand side of Eq.(4.78) will vanish. If we assume that the electrical boundary condition of the unperturbed system is short-circuit at the upper surface of the piezoelectric layer, than the normal modes must satisfy the boundary condition

$$\left(\Phi_n\right)_{z=h} = 0 \tag{4.79}$$

and the potential distribution through the thickness of the piezoelectric layer of the short-circuited unperturbed modes is given by Eq.(4.49). Therefore the amplitude of the modes excited by the potential drive is given by

$$4P_{nn}\left(\frac{\partial}{\partial x}+j\beta_n\right)a_n(x)=-\Phi_S(x)\left(i\omega D_n^*(x)\right).z\Big|_{z=h} \tag{4.80}$$

This corresponds to the situation where the initial boundary condition, $\Phi_n = 0$ is perturbed to make the potential finite, which occurs, for example if a gap is cut in a metal film placed on the substrate. This condition can also be used in other situations when it is more convenient to use a potential drive than a charge drive. Indeed finding the distribution of the charges on a forced electrode is not always very easy depending on the shape of the electrode, and in any case the charge has singularities at the edges of the electrode. When seeking for a mathematically simple formulation of the admittance of the transducer, Wagers [4.65] found it more suitable to chose the electric potential as the function that determines the admittance, and therefore to employ short-circuited normal modes. In general though this is not the boundary condition that is chosen. It was customary in most of the analysis of IDTs for SAW to chose open-circuit boundary conditions [4.63], [4.64], [4.66]. In this case the potential associated with the n^{th} mode is Φ_n, given by Eq.(4.64), and the electrical boundary condition at the surface is that of continuity of electrical displacement density $D_n.z$. Then if a surface charge distribution $\rho_S(x)$ is introduced, as would be the case if electrodes were placed on the substrate, the boundary conditions at the upper surface are perturbed to become

$$D_z^+ - D_z^-\Big|_{z=h} = \rho_S(x) \tag{4.81}$$

The source function therefore must represent the effect of the applied charges on the propagating modes and the differential equation for the amplitude of the modes is given by

$$4P_{nn}\left(\frac{\partial}{\partial x}+j\beta_n\right)a_n(x)=-\Phi_n^*(x)\left(i\omega D_S(x)\right).z\Big|_{z=h} \tag{4.82}$$

4.6.2.2 Amplitude of the Radiated Modes

Here we attempt to find the amplitude of the plate modes generated in the bi-layered system aluminium(1mm)/PZT-5H(0.1mm), when an AC voltage is applied across the electrodes. The region beneath the electrode is the excitation region in which the forward and backward travelling waves are co-existing but on each side of the excitation region only one wave propagates as shown in Figure 4.30(b). The amplitudes of the forward and backward normal modes outside of the excitation zone are given by two differential equations similar to Eq.(4.82)

$$\left(\frac{\partial}{\partial x}+j\beta_n\right)a_{n+}(x)=-\frac{i\omega}{4P_{nn}}\left\{\Phi_{n+}^*(h)D_S(x,h)\right\}.z \tag{4.83}$$

$$\left(\frac{\partial}{\partial x}-j\beta_n\right)a_{n-}(x)=\frac{i\omega}{4P_{nn}}\left\{\Phi_{n-}^*(h)D_S(x,h)\right\}.z \tag{4.84}$$

for positive and negative traveling modes respectively. P_{nn} is the magnitude of the total power flow per meter of acoustic beam, $D_S(x, h)$ is the electric displacement at the location of the electrode and $\Phi^*_{n+}(h)$ is the complex conjugate of the electrical potential associated with the n^{th} mode propagating freely in the positive direction, and is given by Eq.(4.64). The electrical potential is not a function of the x-coordinate. Eq.(4.83) and Eq.(4.84) can be integrated to obtain explicit representations for the normal mode amplitudes. In carrying out the integration use is made of the boundary conditions at the ends of the electrode. If the ends of the electrode are $x = \pm L/2$ the positive wave is zero at the end $x = -L/2$ and the negative wave is zero at the end $x = L/2$. Direct integration of the mode amplitude equations, following [4.7 Vol. I Chapter 6] yields

$$a_{n+}(x) = -\frac{i\omega e^{-j\beta_n x}}{4P_{nn}} \int_{-L/2}^{+L/2} e^{j\beta_n \xi} \left\{ \Phi^*_{n+}(h) D_S(\xi, h) \right\}.z \, d\xi, \qquad z > \frac{L}{2} \quad (4.85)$$

$$a_{n-}(x) = \frac{i\omega e^{j\beta_n x}}{4P_{nn}} \int_{-L/2}^{+L/2} e^{-j\beta_n \xi} \left\{ \Phi^*_{n-}(h) D_S(\xi, h) \right\}.z \, d\xi, \qquad z < -\frac{L}{2} \quad (4.86)$$

and the amplitudes of the modes are thus

$$|a_{n+}| = \frac{\left|\Phi^*_{n+}\right|_{z=h}}{4P_{nn}} \left| \int_{-L/2}^{+L/2} e^{j\beta_n \xi} \left(i\omega D_{Sz}(\xi, h) \right) d\xi \right| \quad (4.87)$$

$$|a_{n-}| = \frac{\left|\Phi^*_{n-}\right|_{z=h}}{4P_{nn}} \left| \int_{-L/2}^{+L/2} e^{-j\beta_n \xi} \left(i\omega D_{Sz}(\xi, h) \right) d\xi \right| \quad (4.88)$$

Eq.(4.83) and Eq.(4.84) give the amplitude of the modes throughout the transducer region. To evaluate the integrals it is necessary to relate D_{Sz} to known quantities such as the applied voltage and current.

4.6.3 TRANSDUCER ANALYSIS.

The analysis of a thin disk piezoelectric bulk wave transducer [4.70], and its extension to normal modes [4.7], shows that it is not sufficient to calculate the amplitude of the radiated acoustic wave in terms of the electric current or voltage applied at the input terminals of the transducer because the acoustic field reacts back on the electrical source and, in this way, affects the level of excitation. Back reactions always occur when the electrical source has a finite electrical admittance and their importance depends on the relationship between the source impedance and the input impedance of the transducer. Therefore the calculation of the input admittance is of crucial importance in transducer analysis. This applies directly to waveguide transducers.

4.6.3.1 Quasi-Static Analysis for the Transducer Admittance.

A global description of a bulk wave transducer is usually provided in terms of radiation conductance G_a. A dielectric layer between two electrodes is a capacitor with admittance $Y_{in} = j\omega C$. When the medium is piezoelectric the direct piezoelectric effect excites acoustic waves which carry energy away and that can be expressed in terms of radiating conductance. The eventual mechanical and electrical losses are represented by the loss conductances, G_m and G_e respectively. The radiation conductance, G_a, is the useful power and from it the efficiency of the transducer is deduced. The technique used to maximize this power is to add an inductance in parallel with the capacitance to cancel the term $j\omega C$, and to add a transformer to change the impedance of the input to match it with the transducer impedance. Basically, the bulk wave transducer can be described as shown in Figure 4.31.

Analogously, the conversion efficiency of the interdigital electrode transmitter is determined by its radiation admittance Y_a into a non reflecting acoustic waveguide. This radiation admittance is in parallel with the static capacitance of the transducer. Electric circuit theory allows us to model the receiving transducer as a constant current source I in parallel with the input admittance ($Y_a + i\omega C$) of the same transducer when used as a transmitter. When a voltage V is applied to an isolated transducer, i.e. when there is no incident acoustic wave and the charge density is not affected by the presence of any other electrodes on the surface (Figure 4.32), the transducer generates a current I, and the ratio I/V is the transducer admittance, Y. A major part of the current is due to the electrostatic charge density $\rho_e(z,\omega)$, which is in phase with V and gives the capacitance contribution to Y. This contribution is usually written explicitly, denoting the capacitance by C, so that

$$Y(\omega) = Y_a(\omega) + j\omega C \tag{4.89}$$

with

$$Y_a(\omega) = G_a(\omega) + jB_a(\omega) \tag{4.90}$$

Here $G_a(\omega)$ and $jB_a(\omega)$ are the real and imaginary contributions due to $\rho_a(z,\omega)$, the acoustic charge density, i.e. the charge density induced by the strains. G_a is the acoustic conductance and B_a is the acoustic susceptance. The admittance may be represented as an electrical equivalent circuit with these three contributions in parallel, as in Figure 4.33.

From Eq.(4.87) and Eq.(4.88), using Eq.(4.64) for the potential associated with the n^{th} mode and if the charge density function is known, the amplitude of the modes can be calculated. It is the acoustic modes which carry energy away from the transducer; for a particular mode, the power radiated is the sum of the power radiated by the forward and the backward travelling waves

$$P_{RAD} = \left(\left|a_n^+\right|^2 + \left|a_n^-\right|^2 \right) P_n = 2\left|a_n^+\right|^2 P_n \tag{4.91}$$

and since we assume plane-strain boundary condition, this is the power per unit width. The average power supplied by the source is

$$P_{AV} = \frac{1}{2} G_a \left| V \right|^2 \tag{4.92}$$

where G_a is the input conductance of the transducer per unit width (the subscript a stands for acoustic). The power balance requires that the average power of the mode radiated equals the average electrical power input (in a non lossy case), $P_{AV} = P_{RAD}$ [4.7]. From Eq.(4.87) and Eq.(4.88), the radiation conductance for the n^{th} mode is given by

$$\left(G_a\right)_n = S\left(\beta_n\right) \frac{\omega^2}{4} \frac{\left|\Phi_n\right|^2}{P_{nn}} \tag{4.93}$$

where

$$S\left(\beta_n\right) = \left| \int_{-L/2}^{+L/2} e^{-j\beta_n \xi} \frac{D_{Sz}\left(\xi, h\right)}{V} d\xi \right|^2 \tag{4.94}$$

Eq.(4.93) shows that the radiation conductance for a mode is dependent only on the applied frequency, the spectrum function S(β) and on its wave impedance defined as follows by Auld and Kino [4.63]:

$$Z_n = \frac{\Phi_n^* \Phi_n}{2P_{nn}} = \frac{\left|\Phi_n\right|^2}{2P_{nn}} \tag{4.95}$$

The distribution of energy between the modes is obtained from the relative magnitude of the power flow of the modes and in Eq.(4.94) this is controlled by the power flow term in the modal impedance.

The spectrum function S(β) is the Fourier transform of the applied charges and it is the same for all modes. As pointed out by Wagers [4.66], this is a very interesting property of the normal mode excitation equations since if S(β) can be measured experimentally for one mode well separated from the others, then we do not need to derive an expression for D_{Sz} to integrate Eq.(4.94). However it is important to stress that although S(β) is the same for all modes, formulations derived for SAW do not apply to this problem since the charge distribution D_{Sz} on strips at the interface between two semi-infinite media (SAW case) is not the same as that on strips deposited at the surface of a thin and grounded piezoelectric layer. This point will be discussed in more detail in the following sections. Therefore if the propagation constant β_n of the n^{th} normal mode is within the bandwidth of an interdigital transducer, the mode receives the same array (charge distribution on the fingers) effect as all other modes. The differences in energy radiation into modes come only through the impedance. The frequency in Eq.(4.94) is not independent of the wavenumber of the mode since they constitute a solution pair of the dispersion relation. For one given mode, there correspond only one wavenumber at a

particular frequency. However at least two modes correspond to one single frequency (below the first cut-off frequency).

The imaginary part of the admittance of the modes $B_a(\omega)$ can be expressed easily from $G_a(\omega)$ using an Hilbert transform [4.3]. In the case where the piezoelectric coupling of the crystal is very weak, all the modal susceptances are negligible compared to that of the static capacitance. Therefore once the capacitance and the conductance of the modes have been calculated, the transducer performance can be determined in terms of its admittance.

4.6.3.2 Effective Permittivity

For problems concerning electrical excitation at the surface, the variables of interest are the potential and the normal electrical displacement. In the vacuum above the transducer, the potential must satisfy Laplace's equation and must also vanish when *z* approaches infinity, so

$$\Phi = \Phi_n(z)\, e^{-j\beta x} = e^{\beta_n z} e^{-j\beta_n x} \qquad z > h \tag{4.96}$$

and the normal component of the electric displacement is

$$D_z = D_{nz}(z)\, e^{-j\beta x} = -\beta_n \varepsilon_0\, e^{\beta_n z} e^{-j\beta_n x} \qquad z > h \tag{4.97}$$

At the interface between the vacuum and the layer, the potential must of course be the same on both sides but the electric displacement can be different. The discontinuity is related to the potential by the *effective permittivity* defined by

$$\varepsilon_S(\beta) = \frac{\tilde{D}_z^{vac} - \tilde{D}_z^{pze}}{|\beta|\,\tilde{\Phi}} \tag{4.98}$$

in the wavenumber domain. Thus the effective permittivity gives the electrical behaviour of the interface between the vacuum and the piezoelectric layer. If the electric displacements are not the same at the interface this is due to the presence of electrodes. $\tilde{D}_z^{vac}$ is then equal to the charge density on the vacuum side of the electrode and $\tilde{D}_z^{pze}$ to the charge density on the layer side of the electrode. The total charge density, for both sides, is denoted ρ_S and thus we have

$$\varepsilon_S(\beta) = \frac{\tilde{\rho}_S}{|\beta|\,\tilde{\Phi}} \tag{4.99}$$

where the charge and the potential are proportional to $e^{j(\omega t - \beta x)}$. In the absence of charges (which occurs when there are no electrodes, i.e. when the modes propagate along free surfaces), the effective permittivity $\varepsilon_S(\beta)$ is equal to zero. In general ε_S is a complicated function of the wavenumber. It will be seen that the method to evaluate ε_S using a Fourier synthesis allows us to unify the single strip transducer problem with

the IDT problem and that the method is the same as in the electrostatic problem of determining the charge distribution due to the applied voltage.

4.6.3.3 Electromechanical Coupling of Lamb Waves

Eq.(4.93) is given as a function of the modal impedance Z_n whereas the more common measure of coupling is $\Delta V / V$. It is well known that the electromechanical coupling coefficient K plays an important role in the analysis of the surface wave IDT, and similarly the coupling coefficient of a given Lamb mode provides a useful measure of the relative efficiency with which that mode can be excited by the transducer. Generally, the electromechanical coupling coefficient is defined to be the ratio of the stored electrical energy to the stored mechanical energy. This holds for bulk wave transducers but the fields are not uniform within the guided wave transducers, and thus this definition of K is not suitable [4.1]. An important result of perturbation theory is a relationship giving the change in the velocity ΔV of a Rayleigh wave, travelling in an isotropic substrate, due to electrical loading. The idea here is to evaluate the change of velocity induced by the application of a conducting film to the transducer which eliminates the storage of electrostatic energy outside the plate. Unlike acoustic waves, electromagnetic waves can propagate in vacuum and a conducting film avoids this leakage of energy. The magnitude of the leakage is a direct measure of the piezoelectric coupling. It has been shown by Ingebringsten [4.68], [4.69] that

$$K^2 = 2\frac{\Delta V}{V} = 2\frac{V_0 - V}{V} \tag{4.100}$$

where V is the unperturbed phase velocity (without metallisation) and V_0 is the phase velocity of the wave perturbed by the addition of the conducting film. This formulation is based on the so-called Ingebringsten approximation for Rayleigh waves which provides an approximate formula for the effective permittivity $\varepsilon_S(\beta)$ assuming that $\varepsilon_S(\beta)$ is proportional to the wavenumber perturbation induced by short circuiting the free surface along which the Rayleigh propagates. This approximation implies implicitly that the analysis is carried out at constant frequencies.

4.6.3.4 Specific Formulation for APM

The important point here is that the modal impedance Z_n can be formulated as a function of $\Delta V / V$ and since $\Delta V / V$ can be measured experimentally, it is a very practical and simple way to access the modal impedance without having to solve the Poisson equation in order to obtain the associated modal potentials Φ_n. Therefore it is extremely desirable to use the same technique for Lamb wave transducers. For SAW Kino and Reeder [4.64] showed that the relationship between the velocity change and the wave impedance Z_n is

$$Z_n = \frac{2}{\omega\left(\varepsilon_0 + \varepsilon_p^T\right)}\left|\frac{\Delta V_n}{V_n}\right| \tag{4.101}$$

It is shown in Appendix D that the formula for plate modes is

$$Z_n = \frac{2}{\omega\left(\varepsilon_0 + \varepsilon_p^T \coth\left(\gamma h\right)\right)}\left|\frac{\Delta V_n}{V_n}\right| \tag{4.102}$$

where

$$\gamma = \beta_n \sqrt{\frac{\varepsilon_{xx}^T}{\varepsilon_{zz}^T}} \tag{4.103}$$

There are two differences between Eq.(4.101) and Eq.(4.102). Firstly the surface permittivity ε_p is multiplied by the factor $\varepsilon_p^T \coth\left(\gamma h\right)$ which depends on the wavenumber-thickness product and which comes from the fact that the lower boundary of the layer is grounded. This term, here an hyperbolic cotangent of the wavenumber-thickness product, will not be the same for other boundary conditions at the lower surface of the layer. Secondly each Lamb wave has different modal parameters, which are different from Rayleigh wave modal parameter, and they are dispersive, so that the wavenumber is not proportional to the frequency ω. Thus it is clear that the relationship for the wave's impedance in term of $\Delta V / V$ is not the same for acoustic plate waves as for the traditional case of Rayleigh waves. The same conclusion holds for the relationship between the input conductance of the transducer and $\Delta V / V$, which can be derived from Eq.(4.93), using Eq.(4.95) and Eq.(4.102).

The relationship (4.100) between the electromechanical coefficient K and $\Delta V / V$ for Rayleigh waves is not valid for Lamb waves since it is based on the assumption that

$$\varepsilon_S\left(\beta\right) \approx \left(\varepsilon_0 + \varepsilon_p^T\right)\left|\frac{\Delta\beta_n}{\beta_n}\right| \tag{4.104}$$

which implies that the effective permitivity is directly proportional to the perturbation. From Eq.(D.20) this appears to be clearly not a valid approximation for plate modes and it is clear that the frequency dependence has to be explicitly formulated.

In general in previous works on the coupling of Lamb waves in piezoelectric plates, the SAW relationship based on Ingebrigsten approximation has been used. In [4.47] Josse expanded Ingebringsten formula to plate modes propagating in a piezoelectric layer loaded by a conductive liquid. In his derivation, Josse expresses the perturbed fields $D_n^{'}$ and $\Phi_n^{'}$ as a function of the unperturbed fields using the formula proposed by Auld for surface waves. This clearly does not take into account the influence of the electrical boundary conditions. Wagers in [4.66] also ignored the influence of the bottom boundary and used the SAW formulation given by Eq.(4.101). More recently Laurent [4.49] also directly used Eq.(4.100) to evaluate the coupling coefficients of plate modes generated in thin piezoelectric plates and noted a strong

disagreement between computed and experimental values but did not provide any explanation for the discrepancies.

Eq.(4.101) and Eq.(4.102) have been computed for the two fundamental modes. Figure 4.34 shows the curves from Eq.(4.101) in dashed lines and the results from Eq.(4.102) in plain lines. As expected it is seen that the formula for plate modes (Eq.(4.102)) leads to a higher coupling. It is important to keep in mind that these curves are concerned with a piezoelectric layer which is grounded on the bottom electrode. The results would be different in the absence of the ground plane, for example if the substrate was another piezoelectric material or even just a dielectric material. For SAW, Kino and Wagers showed the importance of the effect of the ground plane. In general $\Delta V / V$ curves for SAW exhibit a single peak. In the presence of a ground plane, they observed a second peak. In Figure 4.34 a peak occurs near $h/\lambda = 0.05$ for the mode P_2, where h is the thickness of the piezoelectric layer and λ the wavelength. This is essentially due to a sharp peak in the partial potential term depending on the shear stress (coupling with d_{x5} in Eq.(4.64)). Indeed it is seen from Eq.(4.102) that $\Delta V / V$ has the same variation with film thickness as does the wave impedance. Therefore the study of the potential at the free surface carried out in section 4.4.3 reveals how $\Delta V / V$ behaves. Figure 4.34 shows results only up to $h/\lambda = 0.15$ since it is the limit beyond which the perturbation calculations are not accurate as shown in Figure 4.20. Therefore, even by extending the range of h/λ to higher values it is only possible to *estimate* that the mode P1 has a peak around $h/\lambda = 0.30$ and such an estimate may be subject to large errors. This nonetheless shows clearly that each plate mode has a different $\Delta V / V$ and this must be taken into account when designing a transducer even though the calculation of $\Delta V / V$ does not take into account the position of the electrode(s) but only the coupling of electric field and strain for a mode propagating in the electrically unperturbed waveguide.

4.6.4 SURFACE CHARGE DISTRIBUTION ON A SINGLE STRIP

In this section we formulate the electrostatic problem as finding the charge distribution on the electrode on the upper surface of the piezoelectric (but represented as a simple dielectric) layer. A common approximation when calculating D_{Sz} in SAW problems is to neglect the acoustic response [4.7] of the piezoelectric layer. This called the *weak-coupling* approximation in which the stress field is assumed to be unchanged by the perturbation, as described in item 3 of section 4.5. When the acoustic response is ignored, the problem reduces to an electrostatic problem similar to the analysis of a transmission line made of a single strip and a ground plane on opposite faces of a sheet of dielectric material as seen in Figure 4.35(a). The metallic substrate only plays the role of the ground electrode and is ignored in the electrostatic problem since there is no electric field. The most important dimensional parameters are the electrode width L and the thickness h of the dielectric sheet, as well as the permittivity ε of the dielectric. On the grounds that the electrode is a perfect, lossless conductor the electrical influence of its thickness is negligible and is assumed to be zero, which is in line with the assumption that the electrode has no mechanical influence.

If the electrodes and the piezoelectric layer were all of the same width, and with no fringing of the electric field, the problem would be one-dimensional. However this microstrip configuration is certainly not a parallel plate and does involve the appearance of fringing electrical fields. This enhances the effect of the anisotropy of the piezoelectric layer. Solutions for the microstrip configuration and for the simple parallel plate capacitor are treated separately.

4.6.4.1 Isolated Strip Capacitor Solution

The piezoelectric layer is very thin compared to the wavelength of the two fundamental modes below the first cut-off frequency. Therefore it is a good approximation to assume that the region under the electrode acts as an isolated strip capacitor and that the piezoelectric layer is subjected to a thickness electric field excitation. In this case, as shown in Figure 4.35(b) the electric lines are perfectly perpendicular to electrode. A uniform time-dependent voltage is applied uniformly over traction free faces by means of a thin perfectly conducting film,

$$\Phi(h,t) = Ve^{iwt} \qquad -L/2 \le x \le L/2 \tag{4.105}$$

where V is the constant voltage drop across the thickness. At the interface between the layer and the substrate we have

$$\Phi(0) = 0 \tag{4.106}$$

and because the lateral dimensions of the electrode are greater than the thickness of the layer, the potential is independent of x and y and increases linearly from the ground plane to the driven electrode

$$\Phi(z) = V\frac{z}{h} \quad 0 \le z \le h, \qquad -L/2 \le x \le L/2 \tag{4.107}$$

In the case where the acoustic response is omitted, the electric field is given by

$$E_z = -\operatorname{grad}(\Phi) = -\frac{d\Phi}{dz} = -\frac{V}{h} \tag{4.108}$$

Therefore the electric field is uniform between the plates and for a medium which has a diagonal dielectric matrix,

$$D_z = \varepsilon_{zz} E_z = -\varepsilon_{zz}\frac{V}{h} \tag{4.109}$$

and the plate at z = h has a uniform surface charge density given by

$$Q = \int \rho dS = \int D_z \, dS = -\varepsilon_{zz}\frac{V}{h}L \tag{4.110}$$

there being an equal and opposite distribution on the plate at z = 0. Such a solution is well-known. However it is a coarse solution in the sense that it ignores the fringing field. In the case where the piezoelectric layer is of finite extent, the fringing field can be neglected because dielectric constants of the layer are much higher than that of the vacuum outside of the layer. However at this stage of the single strip transducer design, the piezoelectric layer is infinite and therefore on either side of the electroded region, the dielectric constants are the same as in the electroded region and the fringing field must be taken into account. This is usually done using the Schwarz transformation and the solution for a thin and long parallel plate capacitor is given by

$$C = \frac{\varepsilon_{zz} L}{h}\left(1 + \frac{\ln(\pi L/h)}{\pi L/h}\right) \tag{4.111}$$

Application of Eq.(4.111) to a 10 mm long electrode and a layer thickness equal to 0.1 mm, gives an increase of 1.8% in the capacitance value due to the fringing field. It must be noted that this value is rather high since in some text books [4.71] it is mentioned that a good approximation of the capacitance of a finite length capacitor is to calculate the capacitance considering that the length of the electrode is in fact extended artificially by a distance equal to 3/8 of the thickness. This rule would lead to an increase of only 0.375%.

4.6.4.2 Strip Capacitor Solution Including the Piezoelectric Effect

For vibrational modes with long wavelengths and since the surface potential is assumed to be uniform over the electrode, we may ignore the spatial variation of field variables by setting their derivatives with respect to the x-coordinate equal to zero. Because the problem assumes plane strain conditions (i.e. the electrodes are infinite in the y-direction), the derivative with respect to the y-coordinate is also equal to zero. Thus from the second piezoelectric equation

$$D = e : S + \varepsilon^S . E \tag{4.112}$$

we have, in the normal direction,

$$D_z = e_{z3} S_3 - \varepsilon_{zz}^S \frac{\partial \Phi}{\partial z} \tag{4.113}$$

and in absence of free charges the divergence of D is null, so

$$e_{z3} \frac{\partial^2 u_z}{\partial z^2} - \varepsilon_{zz}^S \frac{\partial^2 \Phi}{\partial z^2} = 0 \tag{4.114}$$

The potential is then given by

$$\Phi = \frac{e_{z3} u_z}{\varepsilon_{zz}^S} + A(t) z + B(t) \tag{4.115}$$

where A and B are integration constants. Substituting Φ into Eq.(4.113) leads to

$$D_z = -\varepsilon_{zz}^S A(t) \tag{4.116}$$

The integration function A(t) can be obtained by substituting Eq.(4.115) and Eq.(4.116) into the boundary conditions given in Eq.(4.105) and Eq.(4.106), yielding

$$A(t) = \frac{Ve^{i\omega t}}{h} - \frac{e_{z3}}{h\varepsilon_{zz}^S}\left(u_z(h,t) - u_z(0,t)\right) \tag{4.117}$$

Then the electric displacement is given as a function of the applied potential and the displacements at the electrodes,

$$D_z = -\frac{\varepsilon_{zz}^S Ve^{i\omega t}}{h} + \frac{e_{z3}}{h}\left(u_z(h,t) - u_z(0,t)\right) \tag{4.118}$$

and the electrostatic potential at all positions in the piezoelectric layer is given by

$$\Phi(z,t) = \frac{e_{z3}u_z(z,t)}{\varepsilon_{zz}^S} - \frac{e_{z3}u_z(0,t)}{\varepsilon_{zz}^S} - \frac{e_{z3}\left(u_z(h,t) - u_z(0,t)\right)}{h\varepsilon_{zz}^S}z + \frac{Ve^{i\omega t}z}{h} \tag{4.119}$$

The current through the layer is equal to the time derivative of the integral surface charge Q, over the whole area of a face, where

$$Q = \int_S D_z\big|_{z=h}\, dS \tag{4.120}$$

Substituting from the two-dimensional equation of electrostatics, the surface charge is given as

$$Q = V\frac{L}{h}\left(-\varepsilon_{zz}^S e^{i\omega t} + \frac{e_{z3}}{V}\left(u_z(h,t) - u_z(0,t)\right)\right) \tag{4.121}$$

with the capacitor dimension factored out. The formula (4.121) for the total surface charge on the electrode takes account of the action of the piezoelectric crystal both as a capacitor and as a charge generator. If the piezoelectric coupling is “turned off”, the total charge is then that given in Eq.(4.110) for a simple dielectric capacitor. Formula (4.121)does not take into account the finite dimension of the piezoelectric plate. In fact this formula is wrong is all cases. If the plate is limited in size, as it will be the case in real experiment, lateral effects must be taken into account. Tiersten [4.17] developed a complete theory for rectangular piezoelectric plates. We are not interested in the study of piezoelectric resonators but it is desirable to take into account, to a certain extent, the finite dimensions of the piezoelectric plate by artificially changing some factors in the same way that we did for the dielectric capacitor to account for the fringing field. Following Tiersten we can replace ε_{zz}^S in Eq.(4.121) by

$$\varepsilon_{zz}^{S} = \frac{1}{2}\varepsilon_{zz}^{S} + \varepsilon_{zz}^{S} + \frac{e_{z3}^{2}}{C_{33}} \tag{4.122}$$

where firstly the dielectric constants are artificially increased by a factor 3/2 to take into account the fact that the capacitance is increased if the piezoelectric layer is effectively limited in size. Secondly an additional term is added, the ratio of the square of the piezoelectric stress constant e_{z3} to the stiffness constant C_{33}. e_{z3} is a measure of the piezoelectric coupling between the normal stress and the normal electric field. This term, e_{z3}^{2}/C_{33}, has been added to take into account the fact that the dielectric constant, relevant to static measurement, is that measured at zero stress and not that measured at zero strain since when an electric field is applied the piezoelectric coupling is activated and strains are generated in the material. This can be demonstrated easily by drawing a parallel with the demonstration posed by Auld to show the relationship between the stiffness constant relevant to short-circuited problems and the stiffness constant relevant to open-circuited problems [4.7 Chap. 8, Vol. I]. In the quasistatic approximation, the first piezoelectric stress equation is given by

$$T = -e.E + c^{E} : S \tag{4.123}$$

from which the strain can be expressed as

$$S = \left(c^{E}\right)^{-1} : T + \left(c^{E}\right)^{-1} : e.E \tag{4.124}$$

Substitution into Eq.(4.112) leads to

$$D = e : \left(c^{E}\right)^{-1} : T + \left(e : \left(c^{E}\right)^{-1} : e + \varepsilon^{S}\right).E \tag{4.125}$$

and by analogy with the second equation of the piezoelectric strain equations, setting

$$D = d : T + \varepsilon^{T}.E \tag{4.126}$$

we find

$$\varepsilon^{T} = \varepsilon^{S} + e : \left(c^{E}\right)^{-1} : e \tag{4.127}$$

which in a one-dimensional case takes the form

$$\varepsilon_{zz}^{T} = \varepsilon_{zz}^{S} + \frac{e_{z3}^{2}}{C_{33}} \tag{4.128}$$

Another reason why formula (4.121) is inaccurate is that the piezoelectric layer is infinite but not the electrode, as shown in Figure 4.35(a), so there are fringing fields on both sides of the electroded region is in the piezoelectric layer, as shown in Figure 4.35(c). The strength of these fringing fields benefiting from the strength of the

dielectric constant of the piezoelectric layer. A first possibility to take into account these fields is to use Eq.(4.111). Another possibility is to solve the two-dimensional electrostatic problem, what involves solving a two-dimensional Poisson's equation with boundary conditions, at the upper surface, which are aperiodic functions of the position, i.e. the electrode is of limited size which mean that the electrical boundary condition at the upper boundary is not homogeneous. Fortunately solutions are available in the literature, since such a problem has raised great interest in the domain of microstrip transmission lines. Such solutions are available only for dielectric slabs, and not for piezoelectric layers. Though, in the weak coupling approximation this limitation should not be too restricting.

4.6.4.3 Analytical Solution to the Electrostatic Problem

Solving the electrostatic problem for the two-dimensional system shown in Figure 4.35(a) can be done using the eigenfunction expansion technique. This technique is discussed in detail in [4.8] and a solution is provided for the short-circuited case, where the potential at the top surface is zero everywhere except at the position of the electrode where the potential is V. However there is very little point in developing a new solution for this problem, based on this eigenfunction method, since very similar problems have already been solved for microstrip transmission lines problems and a solution to our problem can easily be derived from the solution provided for similar configurations. Microstrip line problems have received considerable amount of attention in the fifties and the sixties and many solutions have been found and published for many different microstrip configurations [4.72]. However as Wheeler [4.73] pointed out even the simple "microstrip" configuration shown in Figure 4.35(a) is resistant to solutions in simple and easy to use forms and requires elaborate mathematical treatment, [4.74], [4.75]. The most common technique used to solve microstrip problems is the conformal mapping technique [4.76], [4.77] and in particular the Schwartz-Christoffel transformation which provides a formalism for transforming a relatively complex geometry into a simpler one where solutions of the two-dimensional Laplace's equation can be more easily obtained. To our knowledge no simple formulation of the capacitance is provided in the literature for a single stripline. A complete study has been carried out by Coquin and Tiersten [4.77] for an electrode array. They also calculated the capacitance per unit length per electrode. However the derivation of their calculus is extremely cumbersome and the problem can be approached by a more simple technique. Let us consider a single stripline in a shielded box as shown in Figure 4.36(a). Cohn [4.81] derived an analytical solution for this configuration, which is expressed in a simple form of the ratio of two elliptic integrals,

$$C = 2(\varepsilon_1 + \varepsilon_2)\frac{K(k)}{K(k')} \tag{4.129}$$

where K(k) is the complete elliptic integral of first kind and k its modulus [4.82]. The form of Eq.(4.129) is very general and the capacitance for similar configurations can always be expressed in a similar form. Tables of elliptic integrals such as [4.83] allow us to evaluate the capacitance without having to compute directly the elliptic integrals. From Eq.(4.129) it is then straight forward to derive a solution for a single stripline

between two parallel ground planes, as shown in Figure 4.36(b), just by extending the lateral sides of the rectangular shielded box to infinity. Then we can imagine the case where the dielectric constant ε_2 is much larger than the dielectric constant ε_1 so that all the flux is in the stronger dielectric medium. If no flux is in the upper dielectric, the effect of the upper ground plane is negligible. This is representative of the system shown in Figure 4.35(c) where a single strip line is suspended over a dielectric layer grounded at its lower surface, and where the upper medium is vacuum. The difference between all the solutions available is in the modulus *k* of the elliptic integrals. Adapting Eq.(4.129) to our problem can then be done by taking the modulus derived by Coquin and Tiersten [4.77].

For a 10 mm long electrode over a 0.1mm thick PZT-5H layer, the static capacitance at constant strain given by Eq.(4.111) is 1.24 micro-farad per meter of electrode in the y-direction. It is increased to 1.26 micro-farad per meter of electrode in the y-direction if the fringing field is taken into account. If the piezoelectric effect is taken into account, the capacitance calculated from Eq.(4.121) is then equal to 1.29 μf for the mode P_1 and 1.30 μf for the mode P_2. These values are given at 500 kHz, and vary very little with frequency. They are also given without considering any fringing field. Direct computation of the capacitance derived by Coquin and Tiersten [4.77] leads to the capacitance values of 1.29 μf for the mode P_1 and 1.31 μf for the mode P_2. It is clear that the main effects are taken into accounts in the simple static formula with less than 5% errors. However the error depends on the ratio of the electrode length to the thickness of the dielectric layer, and in IDTs the electrode length is likely to be much less than 10mm. The fringing field is increased as the electrode length is decreased, as shown by Eq.(4.111), and it is necessary, for IDTs, to have an electrostatic solution as exact as possible.

4.6.5 FINITE ELEMENT VALIDATION

In order to validate the amplitudes $|a_n|$ calculated from direct integration of Eq.(4.87), we compared them with finite element predictions. The magnitudes of displacements in the x- and in the z-directions have been monitored at the top surface of a finite element model reproducing the design of the problem, as shown in Figure 4.37. In the model, the modes P_1 and the mode P_2 are generated simultaneously when a voltage is applied to a single 10mm long electrode deposited at the upper surface of the infinite bi-layered system PZT-5H(0.1mm)/Aluminium(1mm). The models are similar to those designed in section 4.4.4, with the same mesh density and the same through thickness dimensions. However in this case, the applied signals are not mechanical displacements applied along one edge of the models, but a series of voltage tonebursts applied at the location of the electrode. The electrode is exactly in the middle of the model so that the model is perfectly symmetrical and the magnitudes of the displacements are identical at the left and at the right of the electrode. The electrode has not been modelled as an extra layer but has been replaced by connecting together all nodes along 10 mm (101 nodes) at the position where the electrode should be. Therefore in the model the electrode has no mechanical effect and the electrical and mechanical boundary conditions are exactly those used to derive Eq.(4.64). The potential at the

location of the electrode varies accordingly to the toneburst window for the duration of the input signal and zero after. A series of 10 models was run in steps of 100 kHz between 100 kHz and 1MHz. These frequencies correspond to the centre frequency of the input voltage toneburst which was made up of at least 5-cycles in the non dispersive regions and up to 10 cycles in the regions where at least one of the modes is dispersive. The dimensions of the model and the duration of the calculations have been adjusted for each case in order to avoid multiple reflections of the modes.

The mechanical displacements at the top surface of the piezoelectric layer have been monitored in the x- and in the z-directions at evenly spaced positions, along a distance at least equal to 10 times the longest wavelength, i.e. that of the mode P_2 at the lowest frequency of the input frequency bandwidth. Close to the electrode, the two modes are interfering with each other and a direct reading of the amplitude of each mode is not possible in the time domain. Separating the two modes in the time domain to measure their amplitudes would have been achievable only at a prohibitive cost in computational time and in any case, a direct reading of the amplitude of the signals in the time domain would be erroneous at frequencies where the modes are dispersive. Therefore the results were processed using the two-dimensional Fourier transform method (2-D FFT [4.16]), procedure which is the same as that used earlier in section 4.4.4. The magnitude at each frequency is shown in Figure 4.38 for the mode P_1 and in Figure 4.39 for the mode P_2. The amplitudes of the normal modes have been calculated by integrating Eq.(4.87). This integration is extremely simple in the case where the electric displacement is not a function of position. Therefore the integral leads to a term in $\sin(\beta_n L/2)$. When the wavelength of the mode is an integer multiple of half of the electrode length, there is a cancelling effect which is modelled by the sine term going to zero. Once the modal amplitudes have been obtained from Eq.(4.87), the amplitude of the particular field at any location through the thickness of the system is obtained from the normal mode expansion formalism given by Eq.(4.70). In Figure 4.38 the amplitude of the normal particle displacement for the mode P_1, and in Figure 4.39, the amplitude of the inplane particle displacement for the mode P_2, at the top surface of the PZT-5H layer, is shown as functions of frequency. Changing the electrode length will change the curves since the frequencies at which the zeros in amplitude occur will change.

Figure 4.38 and Figure 4.39 shows very good agreement between the normal mode theory and the FE predictions. Therefore the amplitude of any field associated with the mode P_1 and P_2 can be predicted accurately using our analysis.

4.6.6 ALTERNATIVE CALCULATIONS

Another way to calculate the amplitude of the modes is to use the second source term of Eq.(4.78) and to model the strip transducer as being driven by the applied potential. From Eq.(4.49) we computed the electrical displacement field associated with each mode and we computed the source function

$$f_{sn} = \left\{ \Phi_S(x) \left(i\omega D_n^*(x) \right) \right\} . z \Big|_{z=h}$$

for the short-circuited normal modes. However no improvement was achieved using this source function. Some other possibilities to formulate the surface excitation have not been investigated. In particular a “secondary source” concept may be likely to be valid. The idea is to formulate the source function as being a that a volume source and to integrate it over the thickness of the piezoelectric layer. The equation is given by Auld [4.7, page 162, Eq. 10.136] with the free charge density replaced by the piezoelectrically induced "bound" charge density. This secondary source concept is detailed in the following section on scattering parameters and the methodology of this equivalent volume source approach is given in the papers from Bowler [4.99], [4.100] for indent cracks and volumetric flaws detection by Eddy current.

4.6.7 CONCLUSION

The above finite element validation shows clearly that the perturbation analysis developed to predict the amplitude of plate waves generated when applying a AC voltage at the strip electrode, yields very good results. At this stage the piezoelectric layer is infinite and the plate modes propagate freely in the bi-layered system aluminium/PZT-5H.

The problem of a strip transducer on an aluminium substrate can be derived from the problem just treated above by evaluating the scattering coefficients at both sides of the strip. In the following section these scattering coefficients are evaluated approximately by using a perturbation approach. This is only an approximation and by no mean an exact solution to the scattering problem since only the mode conversion from propagating mode into propagating modes is considered. It is however well-known that at the scatterer, not only propagating modes are generated but also a set of evanescent modes are generated and their presence must be taken into account in the energy balance. The approximation we are making in the following section is that, since far from the scatterer only propagating modes can remain, it may be a fair approximation to neglect the effect of evanescent modes. It is beyond the scope of this thesis to discuss the validity of this approximation. We are only aiming to obtain an approximation of the main effects due to the reflections at the end of the strip.

4.7 SCATTERING

At this stage, the piezoelectric layer is still infinite which is not a very realistic situation. A much more probable design for the transducer is that the piezoelectric layer and the electrode are of similar lateral extent, as shown in Figure 4.40. The amplitude of the modes generated by the transducer when the piezoelectric layer is infinite have been calculated in the previous section. When the layer is finite, the modes generated under the electrode are scattered at the edges of the electrode and they convert into other modes. Therefore the amplitude of the modes propagating away for the transducer are not correctly approximated by the formula derived in Eq.(4.87) and Eq.(4.88). It is necessary to take into account the scattering effects. In this section these scattering coefficients are evaluated by using a perturbation approach based on the S-parameter formalism.

The method presented here is only an approximation and by no mean an exact solution to the full scattering problem since only the mode conversion from propagating mode into propagating modes is considered. It is well known that the reflection of a Lamb wave from the end of a plate is very often accompanied by the generation of additional localized disturbances. For example, the mode of A_0 normally incident at the perfectly square edge of a plate do not convert and reflects in A_0, with a reflection coefficient amplitude of unity. Close examination shows that there are additional motions near the edge of the plate as the reflection takes place and that phase delays occur in the reflections. This is due to the presence of non-propagating modes, which exist solely in the material near the end of the plate, and which are present only during the time it takes for the Lamb wave to reflect. The role of the non-propagating modes can usually be explained by the fact that, at the surface of the scatterer, there is no linear combination of incident and reflected modes which can satisfy the boundary conditions. For example at the end of the plate, the requirement that both the normal and the shear component of the stress are zero across the end of the plate is not matched by the linear combination of incident and reflected A_0 modes. It is then of course the presence of non-propagating modes which help in satisfying the boundary conditions. Therefore when applying normal mode superposition techniques, it is necessary to consider these modes in order to properly account for all contributions to the field around a discontinuity. Such problems have been studied and reported quite extensively, see for example [4.7], [4.85], [4.86], [4.87]. The approximation we are making in this section is that, since far from the scatterer only propagating modes remain and since non propagating modes have a null power, it may be a fair approximation to neglect the presence of the evanescent modes in the normal mode expansion.

The usual method to solve scattering problems is to consider problems described over a domain extending to infinity, as a consequence of which the eigenvalues form a continuous spectrum. It is the relationship between the behaviour of the wave function near infinity and the properties of the medium in which the wave propagates which is of greatest interest. At large distances from the scattering region we observe both scattered and incident waves as shown in Figure 4.41. The general formulation of the problem, in term of an inhomogeneous scalar Helmholtz equation for a wave decomposed into incident and scattered fields and satisfying the boundary conditions [4.8], is cumbersome. However the result to keep in mind is fairly simple and can be summarized as follows: a wave function which satisfies the boundary condition at infinity incidentally gives a value for the scattering amplitude. In other words when considering the particular case where a wave is partially reflected, the volume (or the surface) of the defect can be treated as a source term for the scattered waves and thus we can calculate the amplitude of the scattered wave. This important observation allows us to use a much more simple approach to calculate the scattering coefficients, based on the normal mode expansion. This method is referenced later as the *secondary source method*. The main advantage in using this technique at this stage of our analysis is that the most of calculations required have already been performed in the preceding sections. It is only a matter of reformulating the problem to express the scattering parameters.

4.7.1 THEORETICAL BASIS

The starting point of the derivation is once again the reciprocity relationship which provides a rigorous starting point to derive the scattering theory in terms of the fields produced by the transducer. The derivation of the scattering matrix from the complex reciprocity relationship is detailed by Auld in his book [4.7] and also in [4.88]. Other important papers on the subject have been written by Kino [4.89] and Qu and Achenbach [4.90], among many others. The paper by Thompson [4.91] is particularly recommended since it presents a clear and simple interpretation of the reciprocity relationship via a one-dimensional example.

4.7.1.1 Reciprocity Relationship for Ultrasonic Scattering

Following Ditri [4.92] and Auld [4.7], let us assume that we want to calculate the scattering coefficients of waves propagating in a planar waveguide in which there is a defect as shown in Figure 4.42 and consider the reciprocity relationship

$$\nabla.\left(v_1.T_2 - v_2.T_1\right) = 0 \tag{4.130}$$

Solution "1" is the incident mode from the left, with the flaw removed in Figure 4.42(a) and solution "2" is an incident mode from the right with the flaw present in Figure 4.42(b). As described by Ditri [4.92], expressions for the scattering parameters are obtained by integrating Eq.(4.130) over the volume enclosed between the outer dashed surface

$$S_l + S_{B1} + S_r + S_{B2} \tag{4.131}$$

and the inner dashed surface S_F in Figure 4.42(b). One difference between this description and that made by Ditri [4.92] is that the defect is not restricted to a crack but is taken to be generalised flaw, including cracks, voids, inclusions, strips, grooves, corrosion, etc. Therefore the inner surface in Figure 4.42(b) is labelled S_F. Following Ditri [4.92] again, the volume integral of Eq.(4.130) is converted to a surface integral over the inner and outer surfaces in Figure 4.42(b). The integrals over S_{B1} and S_{B2} are zero so the result of the integration relates the incident and scattered wave amplitudes at the planes S_l and S_r to the fields near the flaw at S_F. In this way the scattering amplitudes are found to be proportional to

$$S \cong \int_{S_F} \left\{v_1.T_2 - v_2.T_1\right\}.\vec{n}\, dS \tag{4.132}$$

where different scattering parameters are obtained by suitably choosing solutions "1" and "2" in Eq.(4.132). The above treatment is particularly suited to defects in the form of cracks. For volumetric flaws (inclusions) it is appropriate to reformulate Eq.(4.132) as a volume integral by using the reciprocity theorem [4.88] in the inverse sense. Thus the scattering amplitudes are proportional to

$$S \cong \int_{V_F} \nabla.\{v_1.T_2 - v_2.T_1\}.\vec{n}\, dV \tag{4.133}$$

4.7.1.2 S-Parameter Formalism

The general principle is that the change in the transmission induced by the presence of the scatterer is given as a function of the fields propagating in the waveguide in the absence of the flaw and the fields propagating in the waveguide in presence of the flaw. The S-parameters of a scatterer are coefficients that relate the scattered mode amplitudes to the incident mode amplitudes, at referenced planes on either sides of the scatterer. Therefore they clearly depend on the modes involved but also the direction (positive or negative) in which they propagate and the location (reference plane) at which the S-parameter is calculated. Therefore one difficulty in the use of S-parameter formulation from the normal modes propagating in a waveguide is the formal nature of the derivation. Thorough derivation of the S-parameter formalism can be found in the second edition of [4.7]. Ditri [4.92] also provides a very detailed development of the formalism and gives extended explanations on the notations. Instead of reproducing their derivations, let us imagine a simple situation such as that shown in Figure 4.42. We define two planes at the left and the right of the scatterer and we label them “l” for left and “r” for right. These planes are far away enough from the flaw so that the non propagating modes have vanished before reaching the planes. The fields propagating in the waveguide can be expanded in a complete set of orthogonal modes as shown in section 4.6.1. Let us imagine that only the mode “m” is incident at the left plane. If the velocity and stress fields (v_m, T_m) of that mode are know, the fields of any other mode generated by mode conversion at the scatterer are given from the incident fields (v_m,T_m) and the scattering parameters S. For example if we assume that the mode A_0 is incident at the left plane, the amplitude of the converted mode S_0 at the left plane is given by

$$b_{S_0 l} = S_{S_0 l, A_0 l}\, a_{A_0 l} \tag{4.134}$$

The amplitude of the S-parameter is given from the reciprocity relationship between the two modes. If, for example, the flaw is a vertical notch, and assuming that the surfaces of the notch are traction free, the stresses in the presence of the notch, T_2, are zero at the surface S_F and the S parameter is given by,

$$S_{S_0 l, A_0 l} = \frac{j\omega}{4P_{A_0}} \int_S \{[\![u_2]\!].T_{A_0}\}\, z\, dS \tag{4.135}$$

where T_{A0} is the stress of the mode A_0 propagating in the waveguide in absence of the crack. $[\![u_2]\!]$ is the difference of the displacements of the left and right faces of the notch. In general, the term P_{A0} at the denominator is ignored since it is set to unity. However it is important to understand that the fields are power normalised upon the incident mode, that is the mode in the unperturbed waveguide and propagating rightward (here we introduce the idea that the flaw can be seen as a perturbation of an *unflawed* waveguide as we will discuss later).

The subscripts of the S-parameter are important. In Eq.(4.135) this S-parameter is a measure of the reflection coefficient of the A_0 mode into the S_0 mode. Changing S_0 for A_0 would give the reflection coefficient of the A_0 mode into itself. Changing the subscript l associated with the mode S_0 for r, leads to the transmission coefficient, calculated at the *right* plane, of the mode A_0 into the mode S_0, etc. The general formalism is therefore given by,

$$S_{M\lambda,N\lambda} = \frac{1}{4P_{NN}} \int_{S_F} \{ v_N . T_M - v_M . T_N \} . z \, dS \tag{4.136}$$

where M is the incident mode, N the scattered mode, and "λ" indicates the plane at which the S-parameter is calculated, either "l" or "r". In the analysis, the modal fields are normalized to unit average power flow through the cross-section of the waveguide. However, non-propagating and inhomogeneous modes do not carry power. Therefore they cannot be normalized in the same manner. Some researchers used the complex power flow instead, noting that non-propagating modes can be normalized to the imaginary unit [4.93]. In this section, the propagating modes which have purely real wavenumbers are normalized, to unit power flow. Eq.(4.136) provides the *surface integral format* of the S-parameter formula where integration of the fields in the curved brackets has been performed over the surface of the flaw. A *volume integral format* can be derived from the surface integral format. For more detailed treatment of the mathematical development the reader should refer to Auld's book, [4.7 Vol2, pp. 190-201], and to Ditri's paper [4.92].

4.7.1.3 Methods of Solution

So far we have a very elegant and concise formula to calculate the transmission and reflection coefficients of the waveguide modes, but the most important information is still missing. Indeed, to evaluate Eq.(4.135) we need to know what the displacements at the crack faces are. In the general case, the velocity and stress fields at the surface of the flaw must be known to calculate the S-parameters. There are basically two methods of solution.

The first method is based on the reciprocity relationship. If the flaw is a crack for example, the *surface integral format* must be used and the quasistatic approximation [4.94], [4.88] is used for the crack opening displacements. Tables of COD under given stress are available and this method has been used recently with success by Lowe [4.97], [4.98]. If the flaws are considerably larger than the wavelength of the incident mode, the Kirschoff approximation can be used to compute the scattering parameters [4.95], [4.96]. If the flaw is an inclusion, the *volume integral format* is used and the perturbed fields can be approximated by the Born approximation, which allows us to approximate the perturbed fields by the unperturbed fields if the compliances of the unperturbed and the perturbed media are not too different.

The second method of solution, which we will use in this section, is based on the *secondary source concept*. In the *volume integral format* the scattering parameters, normalized to unit power are given by,

$$S_{Ml,Nr} = \frac{-i\omega}{4P} \int_{V_F} \nabla.\{v_1.T_2 - v_2.T_1\}.\vec{n}\, dV \tag{4.137}$$

This result can be made more physical by using the identity

$$\nabla.(v.T) = v.\nabla.T + T : \nabla_S v \tag{4.138}$$

and applying the acoustic field equations, which for $e^{i\omega t}$ time dependence are given by

$$\nabla.T = i\omega\rho v \qquad \text{and} \qquad \nabla_S v = i\omega S = i\omega(s : T) \tag{4.139}$$

to solutions "1" and "2" in Eq.(4.137), yielding

$$S_{Ml,Nr} = \frac{-i\omega}{4P} \int_{V_F} \{ v_2.(\rho_2 - \rho_1).v_1 - T_2 : (s_2 - s_1) : T_1 \}\, dV \tag{4.140}$$

where the solution "1" corresponds to the mode "N" incident from the left in absence of the flaw, and solution "2" to the mode "M" propagating in the waveguide with a flaw. In Eq.(4.140) $(\rho_2 - \rho_1).v_1$ and $(s_2 - s_1) : T_1$ are taken to be the secondary sources. The normal mode amplitude equation Eq.(4.72) can then be applied with $f_{vn} = (\rho_2 - \rho_1).v_n$ as the secondary body force source and $f_{sn} = (s_2 - s_1) : T_n$ as the secondary strain source. The development and position of a strain source in the field equations is sketched in Eq.12.65 page 303 of [4.7 Vol.2]. In this approach the modes radiated by the *secondary* source are calculated for a given assumed incident mode. By varying the incident mode a set of coupled mode equations is obtained. These in turn are converted into a set of S-parameter equations by normalising the mode field distribution function to unit transmitted power. The methodology of the equivalent source approach is given by Bowler [4.99], [4.100] both for volumetric or indent cracks. The advantage of the *secondary source* method is that it works for any shape of the flaw, in contrast to with the method based on the reciprocity relationship under the quasistatic approximation, where the opening of the crack must be small.

4.7.2 PROBLEM STATEMENT AND SOLUTION

The theoretical analysis above shows how the S-parameter can be calculated, using the mode equations, from simple considerations of the boundary conditions at the interface between the transducer and the substrate. It is also shown how the strip can be treated as a volume source. Both method are shown to be identical. The S-parameters will be computed for the two fundamental modes A_0 and S_0. The results are then compared to FE predictions.

A 10mm long PZT-5H strip, 100 mm thick, is deposited at the top surface of an infinitely long aluminium plate. A propagating waveguide mode is incident from the left section of the waveguide and will be scattered and mode converted at the edge of the

PZT-5H strip, as shown in Figure 4.43. Two different approaches to solving the problem will be taken in the following both using the S-parameter formalism, and it will be shown that both lead to the same scattering results.

Once again, we use the perturbation theory to evaluate the so-called perturbed fields. If the fields in the perturbed waveguide were known, the perturbation feature being a thin layer as in section 4.3, or piezoelectrically induced charges as in section 4.4 or a strip as we discuss here, then the equations derived from the complex reciprocity relationships would lead to exact results. The equations to solve in this problem are given by Eq.(4.136) and Eq.(4.140). In these, the fields in the waveguide with the strip are labelled "N". We use the Born approximation to approximate the fields of the mode "N" by those of the mode "M".

4.7.2.1 Datta-Hunsinger Boundary Conditions

The problem we want to solve is indeed very similar to that of Rayleigh waves propagating at the surface of a piezoelectric medium and scattered at metallic strip electrodes. The problem of mechanically (and also electrically) induced surface acoustic wave reflections has been tackled in many different ways. Solie [4.39] reviewed reflection filters and Blotekjaer [4.101] using the effective permittivity method developed by Ingebringsten [4.68], proposed a theory that allows the calculation of the amplitude and the phase of the scattered Rayleigh waves at periodic metal strips. Chen and Haus [4.102] utilized the variational principle to derive expressions of the reflection coefficients. The technique we use in this section is based on that presented by Datta and Hunsinger [4.103] for SAW. Datta and Hunsinger derived the mechanical reflection coefficients for an isotropic overlay on an arbitrary substrate using first order perturbation theory. This method is based on a former one proposed by Auld [4.7 1st ed., Chap. 12], in which the normal and tangential stresses generated by the strip at the interface between the substrate and the strip, are used as source terms in normal mode amplitude equations. In his development, Auld used the *Tiersten boundary conditions* given by Eq.(4.10), which provide an approximate but analytical expression for the stresses at the interface between a substrate and a thin isotropic overlay. In other words, the stresses of the mode propagating in the waveguide with a strip, in Figure 4.43(a) are now known as a function of the particle velocity fields of the modes propagating in the waveguide without the flaw, just as explicitly shown by Eq.(4.10). This simplification, i.e. expressing the perturbed field in terms of the unperturbed fields, is allowed in the Born approximation. Therefore in solving the scattering problem of the waves incident at the strip, the problem reduces to that shown in Figure 4.43(b) where the stress fields replace the strip. The task is then to find the amplitudes of the modes generated by these stress fields. If we assume that the fields in the strip-less waveguide are known, under the small perturbation assumption we also know the fields of the modes in the waveguide with the strip. Therefore the amplitudes of the modes generated by the presence of the stresses can be calculated in the same way that the amplitude of the modes due to the presence of charges has been calculated in section 4.6.2.2 but replacing the electrical source function by its mechanical equivalent given by Eq.(4.73), yielding

$$\left(\frac{\partial}{\partial x}+j\beta_n\right)a_{n+}(z)=\frac{1}{4P_{nn}}\left\{-v_{n+}^{*}(0).T_S(z,0)\right\}.y \tag{4.141}$$

$$\left(\frac{\partial}{\partial x}-j\beta_n\right)a_{n-}(z)=-\frac{1}{4P_{nn}}\left\{-v_{n-}^{*}(0).T_S(z,0)\right\}.y \tag{4.142}$$

in the region -a/2 < z <a/2 in Figure 4.43(b). This uses the stress free boundary condition of the unperturbed modes, i.e. the second term ($v_S.T_n$) in Eq.(4.73) is zero. The unperturbed wave has been chosen to be a positive travelling mode with unit amplitude, $v = v_{n+}(y)e^{-j\beta_n z}$, and therefore $v_{n-}(y)e^{j\beta_n z}$ is the particle velocity field of a negative travelling mode with unit amplitude, and the relationship between the negative and positive travelling mode is given by

$$v_{n-}(y)=-\left(v_{n+}(y)\right)^{*} \tag{4.143}$$

Therefore, knowing the stresses at the interface, the mode amplitude equations can be integrated and the amplitudes of the positive and negative travelling modes calculated. Thereafter simple ratios of amplitudes lead to the scattering coefficients. Despite its simplicity, this method cannot be used as it is since by using the *Tiersten boundary conditions* as an approximation for the stress fields in the perturbed waveguide, it is implicitly assumed that the strip is modelled only by a mass and a stiffness change. This means that the limited size of the strip is not explicitly formulated, which has the advantage of not introducing in the source term a function of the position along the x-axis and therefore simplifying greatly the integral. However this simplification that assumes that the stresses under the strip are the same as those under an infinite overlay is however inaccurate. Datta and Hunsinger [4.103] showed that in addition to these uniform stress components, shear stresses are generated at the edges of the strip. These discontinuities can be mathematically modelled and introduced in the source term T_S in Eq.(4.142) and Eq.(4.141). This is done by introducing two *delta-function* shear stresses. Datta and Hunsinger [4.103] gave the boundary conditions for an isotropic strip.

However for two reasons we cannot use the Datta-Hunsinger boundary conditions exactly as they are given in [4.103]. Firstly, Datta and Hunsinger considered only strips of constant thickness. Here we introduce a normalised function g(x) which defines the strip geometry as a function of the x-direction,

$$g(x) = \pm\begin{cases} x/\varepsilon, & 0 < x < \varepsilon \\ 1, & l \le x \le L \\ (L+\varepsilon-x)/l, & L < x < L+\varepsilon \end{cases} \tag{4.144}$$

The strip shape is defined by h.g(x) where h is the thickness of the strip, and as the slope parameter $\varepsilon \rightarrow 0$ the strip geometry approaches a rectangular shape. The sign of the function g(x) is positive if we want to define a strip but can be defined as negative if we want to define a filled groove. Secondly, in our problem the strip is made of PZT-5H

which is anisotropic, and the Datta-Hunsinger boundary conditions have been established for an isotropic strip. In Appendix B, we already established expressions for the interfacial stresses between an aluminium plate and a PZT-5H strip, so amending the Datta-Hunsinger boundary conditions is straight forward and eventually the normal and shear component of the interface traction forces between the PZT-5H strip and the aluminium plate are given by,

$$\left(T'.z\right)_{z=0} \equiv T^{(1)}.z \tag{4.145}$$

with

$$T_{zz}^{(1)} = j\omega\rho' hg(x)\left(v_z\right)_{n+} e^{-j\beta_n x} \tag{4.146}$$

$$T_{xz}^{(1)} = j\omega hg(x)\left(\rho' - \alpha_n(x)\right)\left(v_x\right)_{n+} e^{-j\beta_n x} \tag{4.147}$$

where

$$\alpha_n(x) = \frac{1}{V_n^2}\left(\frac{s_{11}}{s_{11}^2 - s_{12}^2}\right) + \frac{d(x)}{\beta_n V_n^2}\left(\frac{s_{11}}{s_{11}^2 - s_{12}^2}\right) \tag{4.148}$$

and

$$d(x) = \delta(x + a/2) - \delta(x - a/2) \tag{4.149}$$

where the stresses are expressed in the coordinate system shown in Figure 4.43(a). In general the solution for the boundary conditions is not be affected by the coordinate system in which it is calculated but because the strip is a piezoelectric material, attention must be paid to which stiffness constants must be used in Eq.(4.147) which have been developed for a Z-cut hexagonal crystal.

Finally, from the above, the mechanical term in the integrand of Eq.(4.136) can be written, following Auld,

$$\left\{-v_M.T_N\right\}.z = -v_{M+}.B(x).v_N e^{-j2\beta_N x} \tag{4.150}$$

where, for Lamb waves,

$$B(x) = \begin{bmatrix} \rho' - \alpha_n(x) & 0 & 0 \\ 0 & 0 & 0 \\ 0 & 0 & \rho' \end{bmatrix} \tag{4.151}$$

The scattering parameters are then given by,

$$S_{M\lambda,N\lambda} = \frac{1}{4}\int_{-a/2}^{a/2} \left(-(v_x)_{M+} . B_{xx}(x) . (v_x)_N - (v_z)_{M+} . B_{zz}(x) . (v_z)_N \right) e^{-j2\beta_N x} dx \quad (4.152)$$

where the incident mode is the mode M travelling in the positive x-direction, and the mode N is the scattered mode.

In this section we made use of the *surface integral format* assuming that the strip can be modelled as a surface disturbance. But a strip can also be considered as an inhomogeneity in the plate waveguide and the S-parameters are derived assuming the inhomogeneity is in the bulk of the material and leaves the boundary conditions on the two surfaces of the plate waveguide unaffected. Such perturbations are called volume or interior perturbations and are not limited to a flaw with a clearly defined surface and can be used to approximate the influence of global quantities such as, for example viscosity. The volume perturbation approach is derived in Appendix E.

Integrating Eq.(4.152) gives the S-parameters. The velocity fields do not depend on the x-direction so if g(x) = 1 over the strip length, the integral is reduced to that of exponential and delta function terms, which both lead to sine functions. Example of the details of the integration is given in Appendix E.

4.7.3 FINITE ELEMENT VALIDATION

Finite element models provide only raw data, basically absolute displacement amplitudes at local positions, and because displacement is a vector, the displacements have to be monitored in a given direction. Therefore the displacement amplitude monitored in the FE models, and hence the scattering coefficients calculated from these displacements depend on the position in the thickness at which the displacements have been monitored and on the direction in which they have been monitored. In other words the ratio of the displacements of two different modes monitored at the top of the plate is not equal to the ratio of the displacements monitored in the middle of the plate. The reason for this is that the mode shapes are not constant through the thickness and are different for each mode. The normal mode amplitudes come from the normal mode expansion formalism where each field associated with the waves is decomposed into the product of a x-dependent amplitude by a z-dependent field, for example for the particle displacement,

$$u(x,z) = a_n(x)\, u_n(z) \quad (4.153)$$

Therefore the modal amplitudes $a_n(x)$ are independent of the direction and the position in the thickness. Therefore the ratio of displacement monitored in the FE models cannot be compared, in the general case, with the ratio of normal mode amplitudes and mode shape information must be taken into account.

The validating example used in this section is shown in Figure 4.44. By applying along the left hand edge of the model displacement profiles that match the mode shape of a particular mode, this mode propagates alone toward the 10 mm long, 0.1 mm thick,

PZT-5H strip. This mode is then scattered a first time at the left edge of the strip and the part that is transmitted is reflected again at the right edge of the strip. Displacements have been monitored in both directions in the region between the forced edge and the left corner of the strip. This allowed us to monitor both the amplitude of the incident mode and the amplitude of the reflected modes generated by mode conversion at the strip. Two models were designed, one with the mode A_0 incident and the other with the mode S_0 incident. The first model gives the reflection coefficient for the A_0 mode incident and the A_0 mode reflected, and also the reflection coefficient for the A_0 mode incident and the S_0 mode reflected. The second model provides also two reflection coefficients but this time for the S_0 mode incident. These models were then run at different frequencies. As already explained in the previous FE validation (see section 4.6.5) what we mean by frequency here is the central frequency of the applied toneburst. The FE models provide only discreet values for the reflection coefficients whereas the theory provides a continuous function of frequency. The same technique (integration in the wavenumber-frequency domain) as discussed in section 4.6.5, has been used to process the FE results. Comparison between the FE predictions and the S-parameter theory are shown in Figure 4.45(a) for the S_0 mode incident and the S_0 mode reflected. Figure 4.45(b) shows the comparison for the S_0 mode incident and the A_0 mode reflected. Figure 4.45(c) shows the comparison for the A_0 mode incident and the S_0 mode reflected and Figure 4.45(d) shows the comparison for the A_0 mode incident and the S_0 mode reflected. It is seen that agreement between the theory and FE predictions is good. Therefore it is believed that the S-parameter calculations (in the Born approximation) provide accurate approximations for the scattering coefficients and mode conversion of the two fundamental modes at an anisotropic thin strip.

4.8 CONCLUSION

In this Chapter, a method has been presented that allows us to model the amplitude of the fields generated by a single strip transducer when a voltage is applied across the electrodes of the transducer. This method based on the normal mode expansion technique has been derived analytically step by step. Each step has been validated so that each step on its own provides reliable results. The mechanical perturbation technique developed in section 4.3 allows us to obtain accurate analytical dispersion curves for a multilayered system. In section 4.4 a technique has been derived that allows the potential associated with plate modes travelling in piezoelectric layers to be calculated. In section 4.6 it has been shown how the amplitude of modes generated by a piezoelectric transducer can be calculated with very good precision. Finally in section 4.7 we showed how the classical S-parameter technique can be simplified to provide accurate analytical formulations for the scattering coefficients of Lamb waves, including mode conversion. Only the mechanical effect of the strip has been modelled in section 4.7, however it is easily extended to calculate the reflection coefficient due to a change in the electrical boundary conditions by using Eq.(D.21) and the electrical surface impedance concept introduced in section4.6.3.

It is the combination of these steps that leads to the final results. In the next Chapter, this method is applied to the particular case of a single PZT transducer on an

aluminium plate. This straight forward application of all the results presented in the present Chapter, provides a “unit cell” solution that is later used to analyse the behaviour of interdigital transducers.

REFERENCES

[4.1] **Kino**, G. S., *Acoustic Waves: Devices, Imaging and Analog Signal Processing*, Prentice Hall Inc., Englewood Cliffs, New Jersey, 1987.

[4.2] **Dieulesaint**, E. and Royer, D., *Elastic Waves in Solids, Application to Signal Processing*; John Wiley & Son, 1980.

[4.3] **Morgan**, D. P., *Surface-Wave Devices for Signal Processing*, Elsevier, Amsterdam, Oxford, New York, Tokyo, 1991.

[4.4] **Matthews**, H., (ed.) *Surface Wave Filters*, John Wiley & Sons, New York, 1977.

[4.5] **Joshi**, S. G. and Jin, Y., "Excitation of Ultrasonic Lamb Waves in Piezoelectric Plates", J. Appl. Phys., Vol. 69, pp. 8018-8024, 1991.

[4.6] **Kino**, G. S. and Wagers, R. S., "Theory of Interdigital Couplers on Non-Piezoelectric Substrates", J. Appl. Phys., Vol. 44, pp. 1480-1488, 1973.

[4.7] **Auld**, B. A., *Acoustic Fields and Waves In Solids*, Vol. II, 2nd ed., Robert E. Krieger Publishing Compagny, Malabar, Florida, 1990.

[4.8] **Morse**, P. M., and Feshbach, H., *Methods of Theoretical Physics* Vol. I & II, Mc Graw-Hill Book company Inc., New York, London, 1953.

[4.9] **Pavlakovic**, B., Lowe, M. J. S., Alleyne, D. N., and Cawley, P., "Disperse: A General Purpose Program for Creating Dipersion Curves", Review of Progress in Quantitative NDE, eds. D.O. Thompson and D.E. Chimenti, American Institute of Physics, New York, Vol. 16, pp. 185-192, 1996.

[4.10] **Achenbach**, J. D., *Wave Propagation in Elastic Solids*, North-Holland Publishing Company, 1973.

[4.11] **Waldron**, R., A., *Theory of Waveguides and Cavities*, MacLaren, London, 1967.

[4.12] **Waldron**, R., A., *Theory of Guided Electromagnetic Waves*, Van Nostrand, N. J., 1970.

[4.13] **Brekhovskikh**, L. M., "Propagation of Surface Rayleigh Waves along the Uneven Boundary of an Elastic Body", Sov. Phys. Acous., Vol.5, pp. 288-295, 1959.

[4.14] **Slobdonik** Jr., A. J., "Attenuation of Microwave Acoustic Waves due to Gas Loading", J. Appl. Phys. Vol.43, pp. 2565-2568, 1972.

[4.15] **Jia**, X., "Modal Analysis of Lamb Wave Generation in Elastic Plates by Liquid Wedge Transducers", J. Acoust. Soc. Am., Vol. 101(2), pp. 834-842, 1997.

[4.16] **Alleyne**, D. and Cawley, P., "A Two-Dimensional Fourier Transform Method for the Measurement of Propagating Multimode Signals", J. Acoust. Soc. Am., Vol. 89, pp. 1159-1168, 1990.

[4.17] **Tiersten**, H. F., *Linear Piezoelectric Plate Vibrations*, Plenum Press - New York, 1969.

[4.18] **Timoshenko**, S., *Theory of Plates and Shells*, McGraw-Hill Book Co., Chap. 2-4 1940.

[4.19] **Mindlin**, R. D., "High Frequency Vibrations of Plated, Crystal Plates", Progress in Applied Mechanics, MacMillan Co., New York, pp. 73-84, 1963.

[4.20] **Viktorov**, I., A., *Rayleigh and Lamb Waves***,** Plenum Press, New York, 1967.

[4.21] **Wang**, Z., David, J. Cheeke, N. and Jen, C. K., "Perturbation Method for Analysing Mass Sensitivity of Planar Multilayer Acoustic Sensors", IEEE Transactions on Ultrasonics, Ferroelectrics and Frequency Control, Vol. 43, pp. 844-851, 1996.

[4.22] **Wang**, Z., Jen, C. K. and Cheeke,J. D. N., "Analytical Solutions for Sagittal Plate Waves in Three-Layer Composites", IEEE Transaction on Ultrasonics, Ferroelectrics, and Frequency Control, Vol. 40, pp. 293-301, 1996.

[4.23] **Josse**, F., Andle, J. C., Vetelino, J. F., Dahint, R. and Grunze, M., "Theoretical and experimental study of mass sensitivity of PSAWs on ZX-$LiNbO_3$", IEEE Transaction on Ultrasonics, Ferroelectrics, and Frequency Control, Vol. 42, pp. 517-524, 1995.

[4.24] **Wang**, Z., David, J. Cheeke, N. and Jen, C. K., "Mass Sensitivity Analysis for Planar Acoustic Sensors by the Perturbation Method", IEEE Ultrasonics Symposium Proceedings, pp. 411-415, 1993.

[4.25] **Teston**, F., Feuillard, G., Tessier, L., and Lethiecq, M., "Mass Sensitivity of Acoustic plate mode in Liquids", IEEE Transaction on Ultrasonics, Ferroelectrics, and Frequency Control, Vol. 45, pp. 218-228, 1998.

[4.26] **White**, R. M., Wicher, P. J., Wenzel, S. W. and Zellers, E. T., "Plate-Mode Ultrasonic Oscillator Sensors", IEEE Transaction on Ultrasonics, Ferroelectrics, and Frequency Control, Vol. 34, pp. 162-171, 1987.

[4.27] **Wenzel**, S. W. and White, R., "A Multisensor Employing an Ultrasonic Lamb-Wave Oscillator", IEEE Transactions on Electron Devices, Vol. ED-40, pp. 735-743, 1998.

[4.28] **Andle**, J. C., Weaver, J. T., Vetelino, J. F. and McAllister, D. J., "Application of Unidirectional Transducers in Acoustic Plate Mode Biosensors", IEEE Ultrasonics Symposium Proceedings, pp. 331-335, 1993.

[4.29] **Esteban**, I., *Ètude et Integration de Capteurs Acoustiques à Modes de Plaque Transverse orizontaux (SH-APM). Application à la détection de Gaz Organophosphore*, Ph.D. Thesis, Université Bordeaux 1, 1999.

[4.30] **Wolkerstorfer**, D. C., *Methods for Measuring the Acoustic and Optical Properties of Organic Crystals*, PhD Thesis, Dept. of Applied Physics, Stanford University, 1971.

[4.31] **Kostenbauder**, A., Sun, Y. and Siegman, A. E., "Eigenmode Expansions using Biorthogonal Functions: Complex-Valued Hermite Gaussians", JOSA A, Vol. 14(8) pp. 1780-1795, 1997.

[4.32] **Cady**, W. G., *Piezoelectricity*, Dover Publications Inc., New York, 1964.

[4.33] **Peach**, R. C., "A Normal Mode Expansion for Piezoelectric Plates and Certain of its Applications", IEEE Transaction on Ultrasonics, Ferroelectrics, and Frequency Control, Vol. 35, pp. 593-611, 1988.

[4.34] **Marcuse**, D., *Light Transmission Optics*, Van Nostrand Reinhold Company, 1972.

[4.35] **Briers**, R., Leroy, O., Shkerdin,G. N. and Gulyaev, Y. V., "Mode Theory as a Framework for the Investigation of the Generation of a Stoneley Wave at a Liquid-Solid Interface", J. Acous. Soc. Am., Vol. 95(3), pp. 1953-1966, 1994.

[4.36] **Crasters**, R. V., Williams, D. P., "A Reciprocity Relation for Fluid-Loaded Elastic Plates that Contain Rigids Deffects", Journal of Sound and Vibration, Vol. 235(4), pp. 655-670, 2000.

[4.37] **Skeie**, H., " Electrical and Mechanical Loading of a Piezoelectric Surface Supporting Surface waves", J. Acous. Soc. Am., Vol. 48(2), pp. 1098-1109, 1970.

[4.38] **Lakin**, K. M., "Perturbation Theory for Electromagnetic Coupling to Elastic Surface Waves on Piezoelectric Substrates", J. of Appl. Phys. Vol. 42(3), pp. 899-906, 1971.

[4.39] **Solie**, L. P., "Piezoelectric Effects in Layered Structures", J. App. Phys, Vol.44(2), pp. 619-627, 1973.

[4.40] **Straton**, J. A., *Electromagnetic Theory***,** McGraw-Hill Book Co., 1941.

[4.41] **Slater**, J. C., and Frank, N. H., *Introduction to Theoretical Physics*, Mc. Graw-Hill Book Company Inc., New York and London, 1933.

[4.42] **Bathe**, H. J., *Finite Element Procedures in Engineering Analysis* Prentice Hall Inc., New York, 1982.

[4.43] **Pavlakovic**, B. N., Leaky Guided Ultrasonic Waves in NDT, Ph.D. Thesis, University of London, (Imperial College, Mechanical engineering Department), 1998.

[4.44] **Vellekoop**, M., J., "All-Silicon Plate Wave Oscillator System for Sensors", Sensors and Actuators, Vol. A-25, pp. 699-703, 1991.

[4.45] **Jin**, Y. and Joshi, S. G., "Excitation of High Order Ultrasonic Lamb Wave Modes in Piezoelectric Plates", J. Acoust. Soc. Am., Vol. 92, pp. 914-919, 1992.

[4.46] **Josse**, F. and Shana, Z. A., "Analysis of Shear Horizontal Surface Waves at The Boundary Between a Piezoelectric Crystal and a Viscous Fluid Medium", J. Acoust. Soc. Am., Vol. 84(3), pp. 978-984, 1988.

[4.47] **Josse**, F. and Shana, Z. A., "Electrical Surface Perturbation of a Piezoelectric Acoustic Plate Mode by a Conductive Liquid Loading", IEEE Transaction on Ultrasonics, Ferroelectrics, and Frequency Control, Vol. 39, pp. 512-518, 1992.

[4.48] **Yang**, C. H. and Chimenti, D. E., "Guided Plate Waves in Piezoelectrics Immersed in a Dielectric Fluid", J. Acoust. Soc. Am., Vol. 97, pp. 2103-2115, 1994.

[4.49] **Laurent**, T. and Bastien, F., "Lamb and Shear-Horizontal Wave Production by Interdigital Transducers Deposited on Both Sides of a Piezoelectric Plate", J. Acoust. Soc. Am., Vol. 99(5), pp. 2876-2882, 1996.

[4.50] **Ditri**, J. J. and Rose, J. L., "Excitation of Guided Waves in Generally Anisotropic Layers Using Finite Sources", J. Appl. Mech., Vol. 61, pp. 330–338, 1994.

[4.51] **Castaings**, M. and Cawley, P., "The Generation, Propagation, and Detection of Lamb Waves in Plates Using Air-Coupled Ultrasonic Transducers", J. Acoust. Soc. Am., Vol. 100, pp. 3070–3077, 1996.

[4.52] **Rose**, J. L., Pelts, S. P. and Quarry, M. J., "A Comb Transducer Model for Guided Wave NDE", Ultrasonics, Vol.36, pp. 163–169, 1998.

[4.53] **Degertekin**, F. L., Honein, B. V. and Khuri-Yakub, B. T., "Efficient Excitation and Detection of Lamb Waves for Process Monitoring and NDE", IEEE Ultrasonics Symposium 1995, pp. 787-790, 1995.

[4.54] **Degertekin**, F. L. and Khuri-Yakub, B. T., "Single Mode Lamb Wave Excitation in Thin Plates by Hertzian Contacts", Appl. Phys. Lett., Vol. 69(2), pp. 146–148, 1996.

[4.55] **Moulin**, E., Assaad, J., Delebarre, C., Kaczmarek, H., and Balageas, D., "Piezoelectric Transducer Embedded in Composite Plate: Application to Lamb Wave Generation", J. Appl. Phys., Vol. 82, pp. 2049–2055, 1997.

[4.56] **Degertekin**, F. L. and Khuri-Yakub, B. T., "Lamb Wave Excitation by Hertzian Contacts with Applications in NDE", IEEE Transactions on Ultrasonics, Ferroelectrics and Frequency Control, Vol. 44, pp. 769–778, 1997.

[4.57] **Moulin**, E., Assaad, J. and Delebarre, C., "Modelling of Lamb Waves Generated by Interdigital Transducers in Composite Plates using a coupled Finite Element-Normal Mode Expansion Method", J. Acoust. Soc. Am., Vol. 107(1), pp. 87-94, 2000.

[4.58] **Courant**, R. and Hilbert, D., *Method of Mathematical Physics*, Vol.1, Interscience, New York1953.

[4.59] **Roseau**, M., *Vibrations in Mechanical Systems*, Springer-Verlag, Berlin, Heidelberg, New York, 1983.

[4.60] **Jones**, D. S., *Acoustic and Electromagnetic Waves*, Oxford Science Publications, Clarendon Press, Oxford, 1990.

[4.61] **Rose**, J. L., *Ultrasonic Waves in Solid Media*, Cambridge University Press, 1999.

[4.62] **Auld**, B. A., "Application of Microwave Concepts to the Theory of Acoustic Fields and Waves in Solids", IEEE Transaction on Microwave Theory and Techniques, Vol. MTT17, pp. 800-811, 1969.

[4.63] **Auld**, B. A. and Kino, G. S., "Normal Mode Theory for Acoustic Waves and its Application to the Interdigital Transducer", IEEE Transaction on Electron Devices, Vol. ED18, pp. 898-908, 1971.

[4.64] **Kino**, G. S. and Reeder, T., "A Normal Mode Theory for the Rayleigh Wave Amplifier", IEEE Transaction on Electron Devices, Vol. ED-18, pp. 909-919, 1971.

[4.65] **Wagers**, R. S., "Evaluation of the Finger Withdrawal Transducer Admittance by Normal Mode Analysis", IEEE Transactions on Sonics and Ultrasonics, Vol. SU-25, pp. 85-91, 1978.

[4.66] **Wagers**, R. S., "Plate Modes in Surface Acoustic Wave Devices", Physical acoustics, W. P. Masson and R. N. Thurston (Ed.) Vol. 13, pp. 49-78, 1979.

[4.67] **Briers**, R., Leroy, O. and Shkerdin, G. N., "The Generation of a Stoneley Wave at the End of a Fluid Loaded by an Incident Bounded Beam", J. Acoust. Soc. Am., Vol. 101, pp. 1366-1372, 1997.

[4.68] **Ingebrigtsen**, K. A., "Elastic Surface Saves in Piezoelectrics and their Coupling to Carriers in an Adjoining Semiconductor", ELAB REPORT TE-94, Electronics Research Laboratory, The Norwegian Institut of technology, Trondheim, (copy at the British Museum Library), 1967.

[4.69] **Ingebrigtsen**, K. A., "Surface Waves in Piezoelectrics", J. Appl. Phys., Vol. 40, pp. 2681-2686, 1969.

[4.70] **Wilcox**, P., D., Monkhouse, R. S. C., Cawley, P., Lowe, M. J. S. and Auld, B. A., "Development of a Computer Model for an Ultrasonic Polymer Film Transducer System", NDT & E International, Vol. 31(1), pp. 51-64, 1998.

[4.71] **Feynman**, R. P., *The Feynman Lectures on Physics: Commemorative Issue*, Redwood City, Wokingham, Addison-Wesley, 1989.

[4.72] **IEEE Standard** Definitions of Planar Transmission Lines, ANSI/IEEE std 1004-1987

[4.73] **Wheeler**, H. A., "Transmission-Line Properties of Parallel Wide Strip by Conformal Mapping Approximation", IEEE Transactions on Microwave Theory and Techniques, Vol. MTT-12, pp. 280-289, 1964.

[4.74] **Harrington**, R. F., *Time-Harmonic Electromagnetic Fields*, McGraw-Hill, 1961.

[4.75] **Edwards**, T. C., *Fondations for Microstrip Circuit Design*, John Wiley & Sons, 1991.

[4.76] **Wheeler**, H. A., "Transmission-Line Properties of Parallel Strip Separated by a Dielectric Sheet", IEEE Transactions on Microwave Theory and Techniques, Vol. MTT-13, pp. 172-185, 1965.

[4.77] **Coquin**, G. A. and Tiersten, H. F., "Analysis of the Excitation and Detection of Piezoelectric Surface Waves in Quartz By Means of Surface Electrodes", J. Acoustic. Soc. Am., Vol. 41, pp 921-939, 1966.

[4.78] **Tseng**, C, and White, R. M., "Propagation of Piezoelectric and Elastic Surface Waves on the Basal Plane of Hexagonal Piezoelectric Crystals", Journal of Applied Physics, Vol. 38(11), pp. 4274-4280, 1967.

[4.79] **De Cicco**, G., "Elastic Surface Wave Devices Based on Piezoelectric Thick Films", Ultrasonic Symposium Proceeding, pp. 281-285, 1993.

[4.80] **Peach**, R. C., "A General Approach to the Electrostatic Problem of SAW interdigital Transducer", IEEE Transaction on Ultrasonics, Ferroelectrics, and Frequency Control, Vol. 28(2), pp. 96-105, 1981.

[4.81] **Cohn**, S. B., "Characteristic Impedance of the Shielded-Strip Transmission Line", IRE Transactions on Microwave Theory and Techniques, Vol. MTT-2, pp. 52-57, 1954.

[4.82] **Ederlyi**, A., *Higher Transcendental Fuctions*, McGraw-Hill Book Company Inc., New York and London, 1953.

[4.83] **Abramovitch**, M. and Stegun, I. A., (Eds.), *HandBook of Mathematical Functions*, Dover Publications Inc., New York. 1973.

[4.84] **Maxwell**, J. C., *A Treatise on Electricity and Magnetism*, New York, Dover Publications, 1954

[4.85] **Mindlin**, R.D., in *Structural Mechanics*, edited by J.N. Goodier, Pergamon, New York, pp. 199-232, 1960.

[4.86] **Torvik**, P.J., "Reflection of Wave Trains in Semi-infinite Plates", J. Acoust. Soc. Am., Vol. 41, pp. 346-353, 1967.

[4.87] **Cho**, Y., and Rose, J. L., "A Boundary Element Solution for a Mode Conversion Study on the Reflection of Lamb Waves", J. Acoust. Soc. Am., Vol. 99, pp. 2097-2109, 1996.

[4.88] **Auld**, B. A., "General Electromechanical Reciprocity Relations Applied to the Calculations of Elastic Wave Scattering Coefficients", Wave Motion, Vol. 1, pp. 3-10, 1979.

[4.89] **Kino**, G. S., "The Application of Reciprocity Theory to Scattering of Acoutic Waves by Flaws", J. App. Phys., Vol. 49, pp. 3190-3199, 1978.

[4.90] **Qu**, J., Achenbach, J. D. and Roberts, R. A., "eciprocal Relations for Transmission Coefficients Theory and Applications", IEEE Transactions on Ultrasonics, Ferroelectrics, and Frequency Control, Vol. 36(2), pp.280-286, 1989.

[4.91] **Thompson**, R. B., "Interpretation of Auld's Electromechanincal Reciprocity Relation via a One-Dimensional Example", Res. Nondestr. Eval., pp. 147-155, 1994.

[4.92] **Ditri**, J. J., "Utilization of Guided Elastic Waves for the Characterisation of Cicunferential Cracks in Hollow Cylinders", J. Acoust. Soc. Am., Vol. 96(6), pp. 3769-3770, 1994.

[4.93] **Engan**, H. E., "Torsional Wave Scattering from a Diameter Step in a Rod", J. Accoust. Soc. Am., Vol. 104, pp. 2015-2024, 1998.

[4.94] **Eshelby**, J. D., " The Determination of the Elastic Field of an Ellipsoidal Inclusion and Related Problems", Proc. Roy. Soc., Vol. A-241, pp. 376-396, 1957.

[4.95] **Deutsch, W. A. K, "**Wave Scattering from Surface-Breaking Cracks Sonified by a Linear Phased Array", Review of Progress in Quantitative NDE, eds. D.O. Thompson and D.E. Chimenti, American Institute of Physics, New York, Vol. 18, pp. 71-78, 1998.

[4.96] **Roberts**, R. A., "Recent Developments in Kirschoff Crack Tip Diffraction Correction", Review of Progress in Quantitative NDE, eds. D.O. Thompson and D.E. Chimenti, American Institute of Physics, New York, Vol. 18, pp. 53-61, 1998.

[4.97] **Lowe**, M. J. S., and Diligent, O., "Low-Frequency Reflection Characteristics of the S_0 Lamb Wave from a Rectangular Notch in a Plate", J. Acoust. Soc. Am., Vol. 111, 2002

[4.98] **Lowe**, M. J. S., "Reflection of the Fundamental Lamb Modes from the Ends of Plates", Review of Progress in Quantitative NDE, eds. D.O. Thompson and D.E. Chimenti, American Institute of Physics, New York, Vol. 20, pp. 89-96, 2001.

[4.99] **Bowler**, J. R. and Jenkins, S. A., "Eddy-Current Probe Impedance Due to Volumetric Flaw", J. App. Phys., Vol. 70(3), pp. 1107-1114, 1991.

[4.100] **Bowler**, J. R, "Eddy-Current Interaction with an Ideal Crack, I: The Forward Problem", J. App. Phys., Vol. 75(12), pp. 8128-8137, 1995.

[4.101] **Blotekjaer**, K., Ingebrigtsen, K. A. and Skeie, H., "Acoustic Surface Waves in Piezoelectric Materials with Periodic Metal strips on the Surface", IEEE Transaction on Electron Devices, Vol. Ed-20, pp. 1139-1146, 1973.

[4.102] **Chen**, Q. X. and Haus, H. A., "Analysis of Metal-Strip SAW Gratings and Transducers", IEEE Transactions on Sonics and Ultrasonics, Vol. 32, pp. 395-408, 1985.

[4.103] **Datta**, S. K. and Hunsinger, B. J., "First Order Reflection Coefficient of Surface Acoustic Waves from Thin-Strip Overlays", J. Appl. Phys. Vol. 50, pp. 5561-5565, 1979.

TABLES

Compliances (10^{-12} m^2/newton)				Stiffness (10^{10} newton/ m^2)			
S_{11}	16.66	S_{33}	20.7	C_{11}	12.6	C_{33}	11.7
S_{12}	-4.78	S_{44}	43.5	C_{12}	7.95	C_{44}	2.3
S_{13}	-8.45	S_{55}	43.5	C_{13}	8.41	C_{55}	2.3
S_{23}	-8.45	S_{66}	42.88	C_{23}	8.41	C_{66}	2.35
Piezoelectric Strain Constants (10^{-10} coulomb/newton)		Piezoelectric Stress Constants (coulomb/m^2)		Relative Permittivity Constant Stress $\varepsilon_0 = 8.854\ 10^{-12}$ farads/m		Relative Permittivity Constant Strain $\varepsilon_0 = 8.854\ 10^{-12}$ farads/m	
d_{x5}	7.41	e_{x5}	17	ε_{xx}^S	3130	ε_{xx}^T	1700
d_{y4}	7.41	e_{y4}	17	ε_{yy}^S	3130	ε_{yy}^T	1700
d_{z1}	-2.74	e_{z1}	-6.5	ε_{zz}^S	3400	ε_{zz}^T	1470
d_{z2}	-2.74	e_{z2}	-6.5	Density (Kg/m^3)			
d_{z3}	5.93	e_{z3}	23.3	7500			

Table 4.1: Material parameters for Z-cut PZT-5H.

	Density (Kg/m^3)	Longitudinal velocity (m/s)	Shear velocity (m/s)
Aluminium	2800	6370	3100
Epoxy	1100	2700	1100
Copper	8930	5010	2200

Table 4.2: Material parameters.

FIGURES

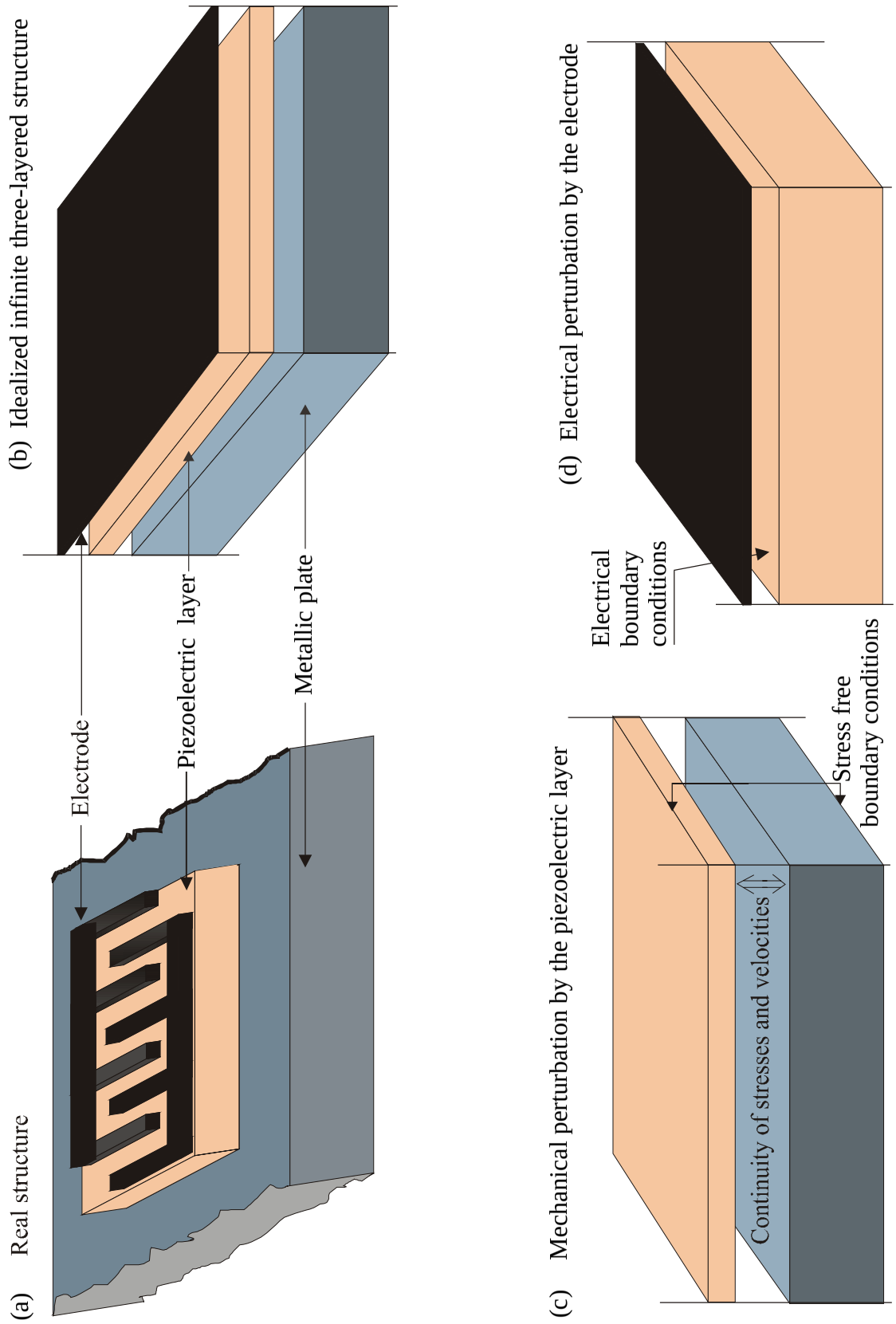

Figure 4.1 : Modelling of the transducer (a) by an infinite three-layered plate (b). (c) Shows the purely mechanical system, while the purely electrical system is shown in (d).

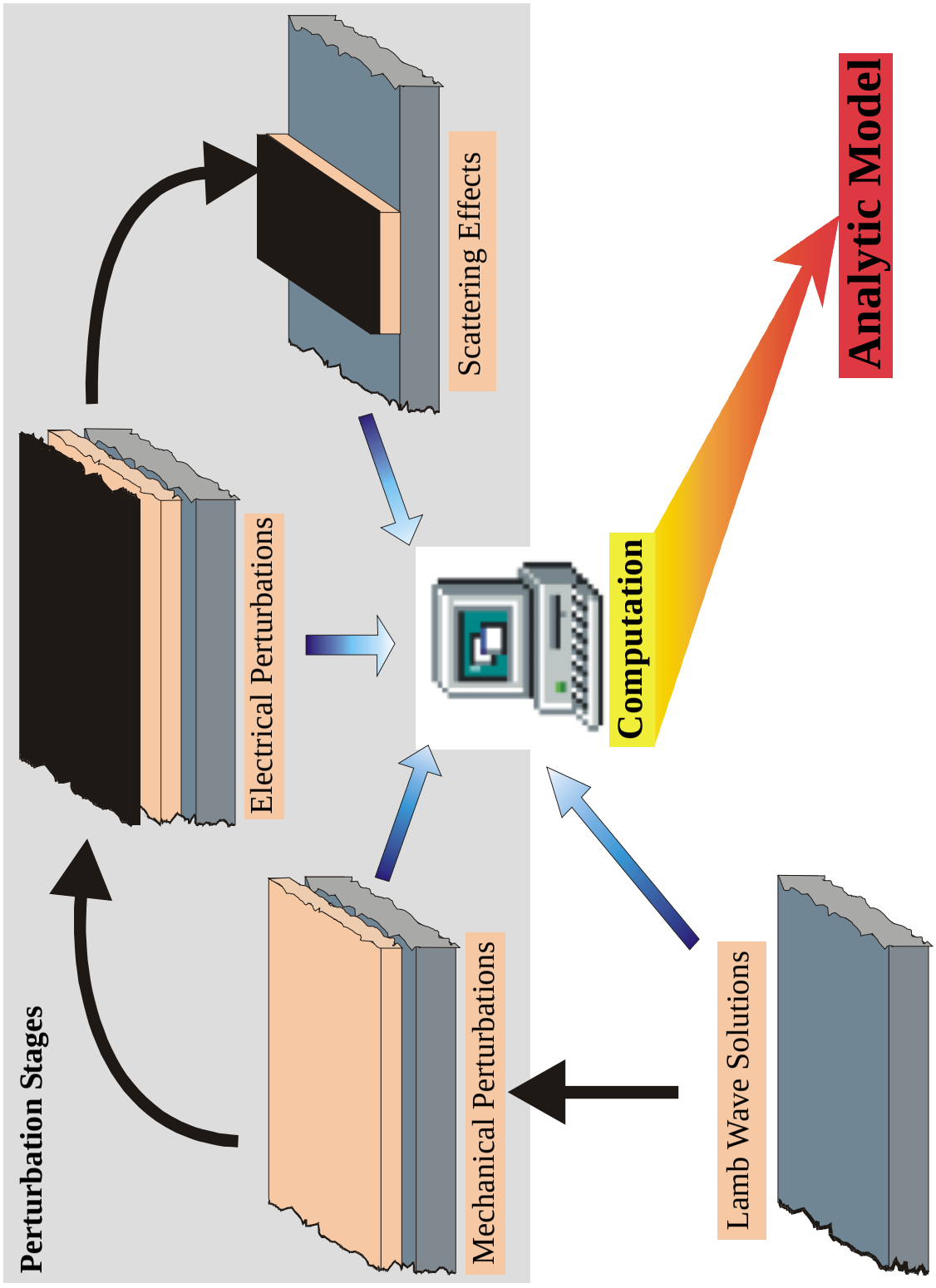

Figure 4.2 : Schematic diagram showing the progression of the analysis.

(a)

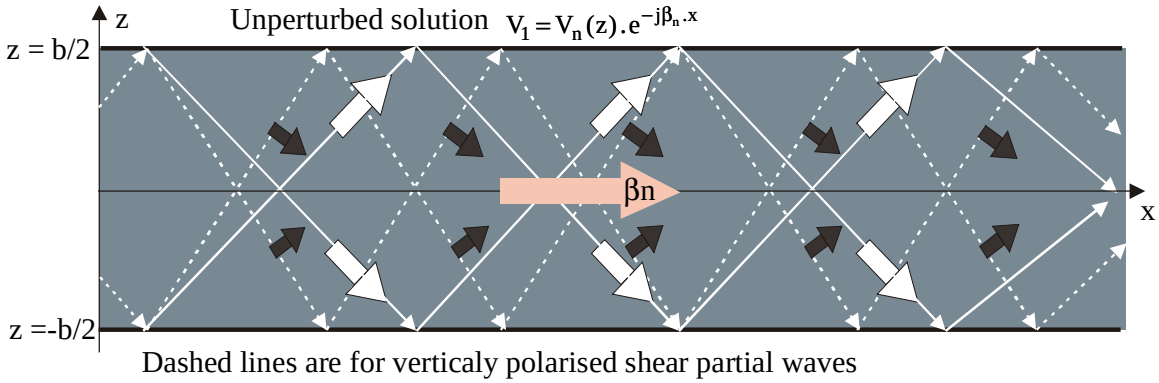

Dashed lines are for verticaly polarised shear partial waves
Plain lines are for longitudinal partial waves
In a free plate, L-waves and SV-waves are coupled in Lamb modes.

(b)

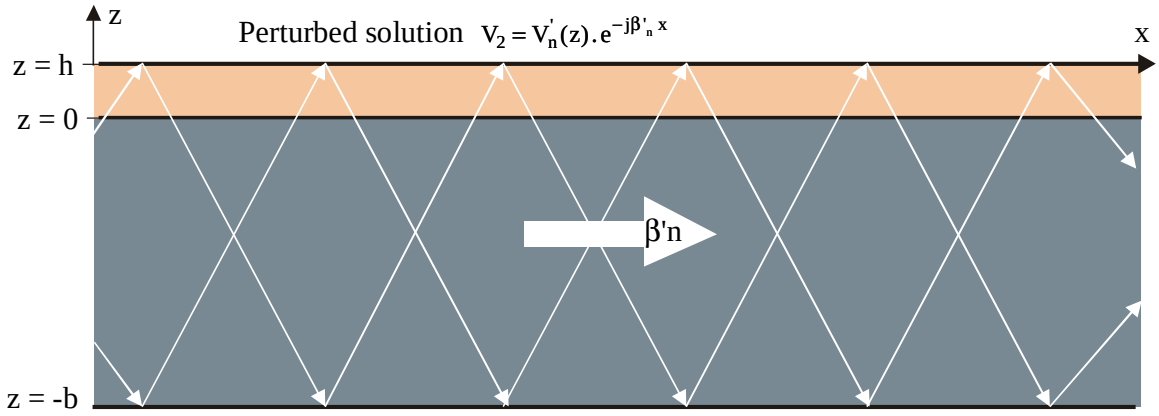

(c)

Figure 4.3 : Perturbation of the upper mechanical surface (y = 0) by a thin film isotropic overlay, (a) the infinite perturbed structure, (b) coordinate system and modes propagating in the unperturbed plate, (c) coordinate system and modes propagating in the perturbed system.

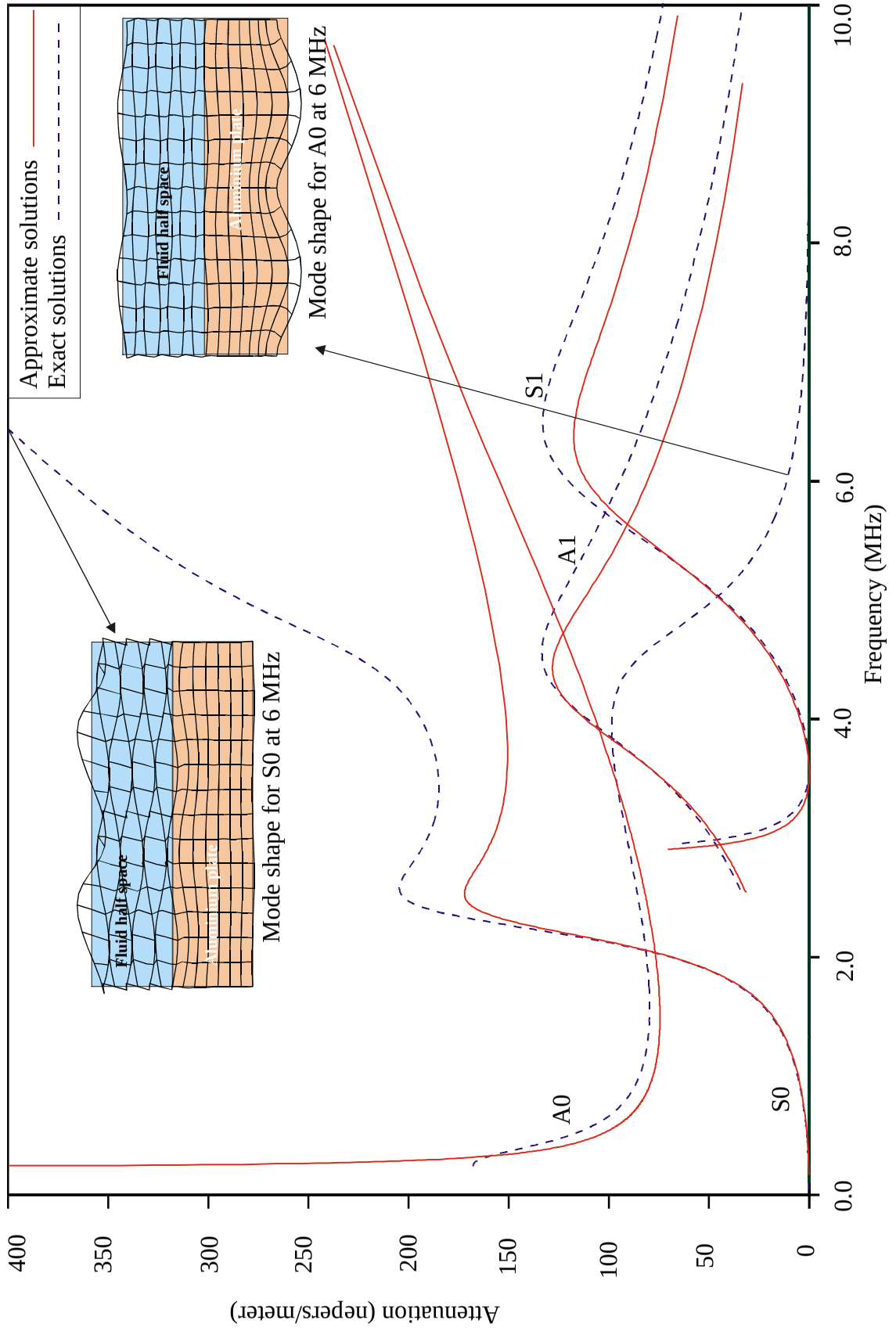

Figure 4.4 : Comparison between the exact attenuation dispersion curves and the approximate wavenumber dispersion curves for the 1.2mm thick aluminium plate loaded with water on one face.

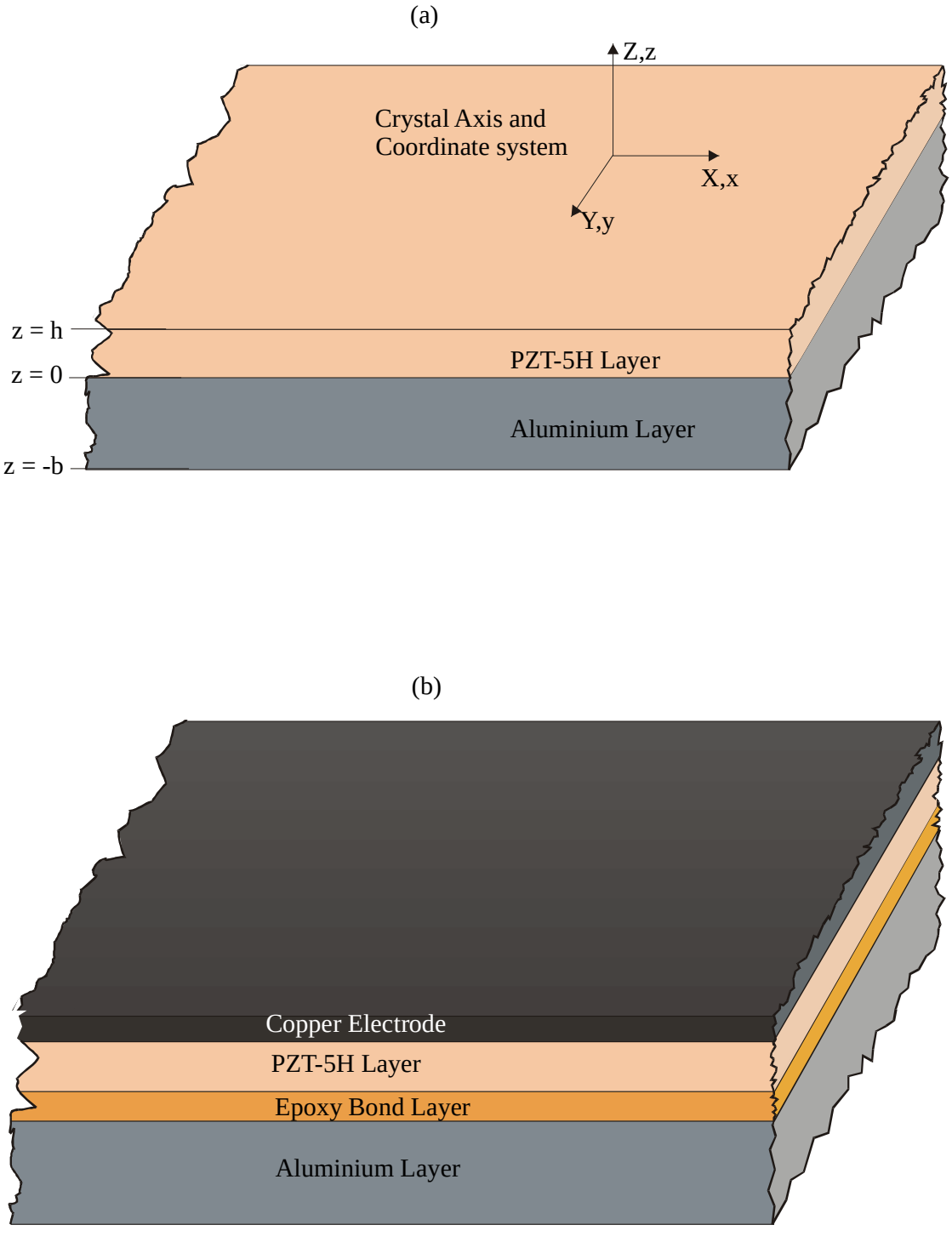

Figure 4.5 : (a) Bi-layer system Aluminium(1mm)/PZT-5H(100µm) with coordinate system and crystal axis. (b) Four-layered system Aluminium(1mm)/Epoxy(10µm)/PZT-5H(100µm)/Copper(10µm). The propagation direction is x.

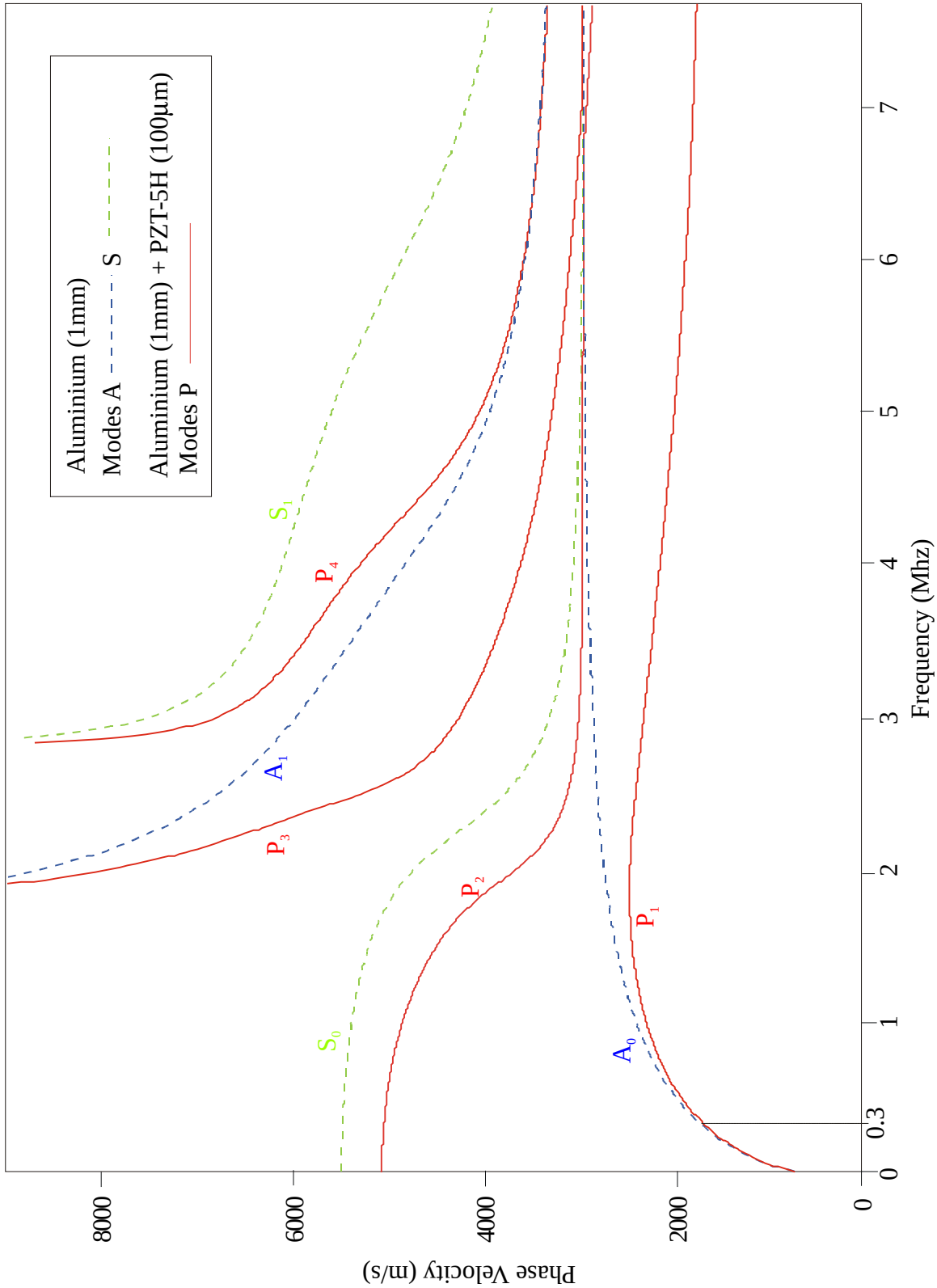

Figure 4.6 : Comparison between the exact dispersion curves for an aluminium plate (1mm thick) and the exact dispersion curves for the aluminium(1mm)/PZT(0.1mm) system.

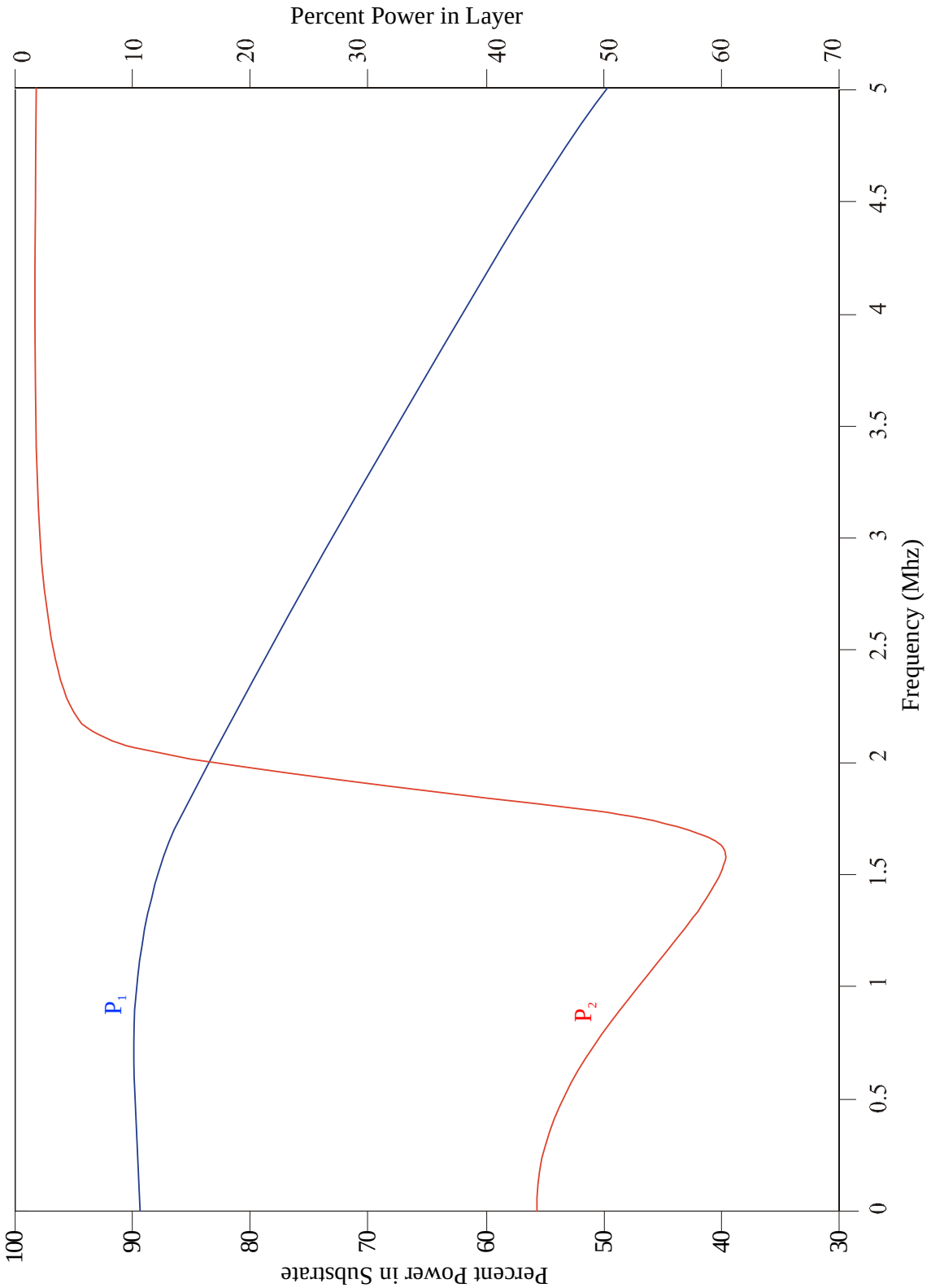

Figure 4.7 : Spatial distribution of the power flow, for the two fundamental modes, in the bi-layered structure aluminium(1mm)/PZT(100µm).

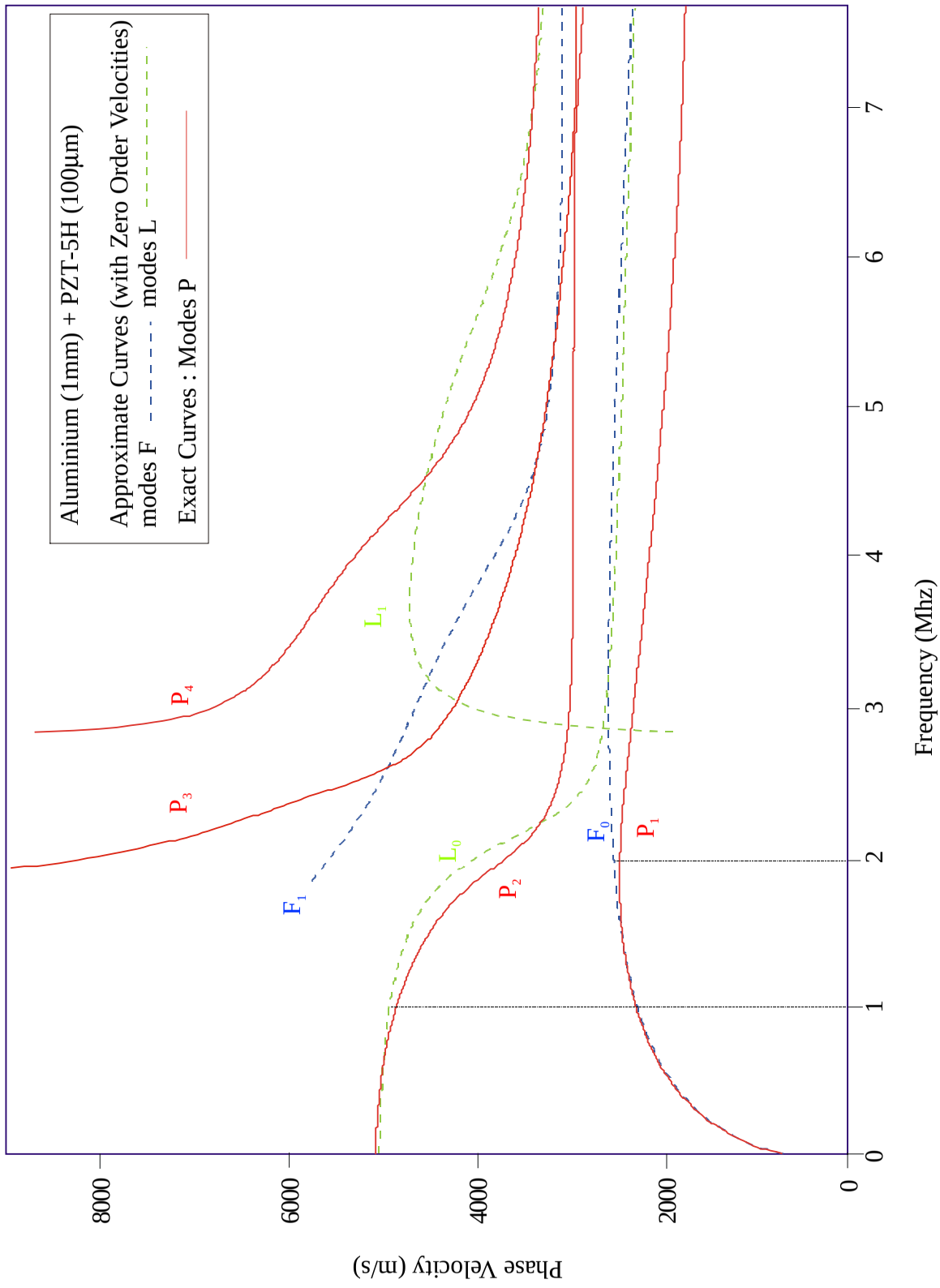

Figure 4.8 : Comparison between the exact dispersion curves and the approximate dispersion curves for the aluminium(1mm)/PZT(0.1mm) system.

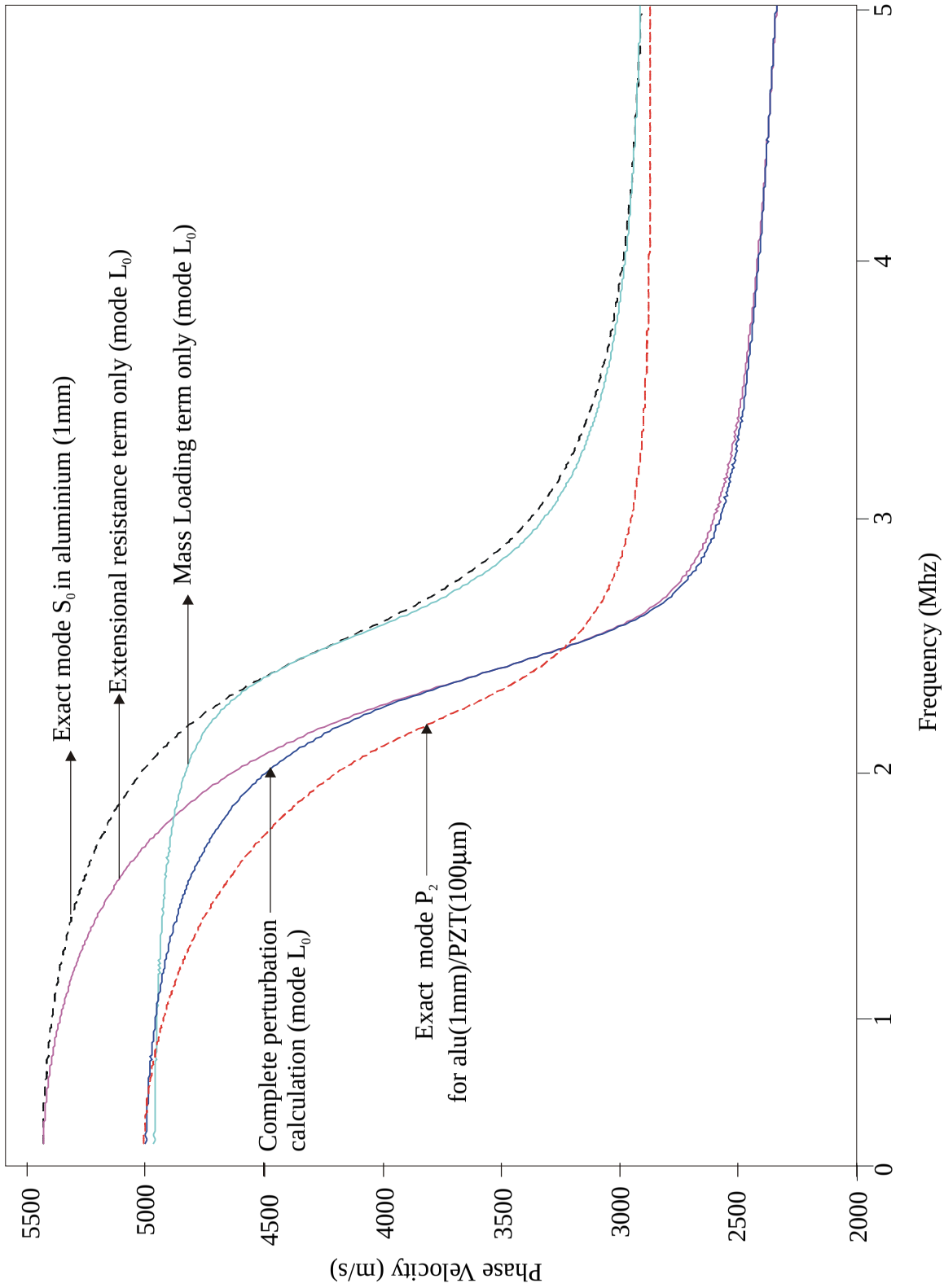

Figure 4.9 : Comparison between different approximate dispersion curves for the lowest extensional mode (L_0) of the system aluminium(1mm)/PZT(0.1mm). The exact dispersion curves for the aluminium plate (S_0) alone and for the bi-layer system (P_2) are represented by dashed lines.

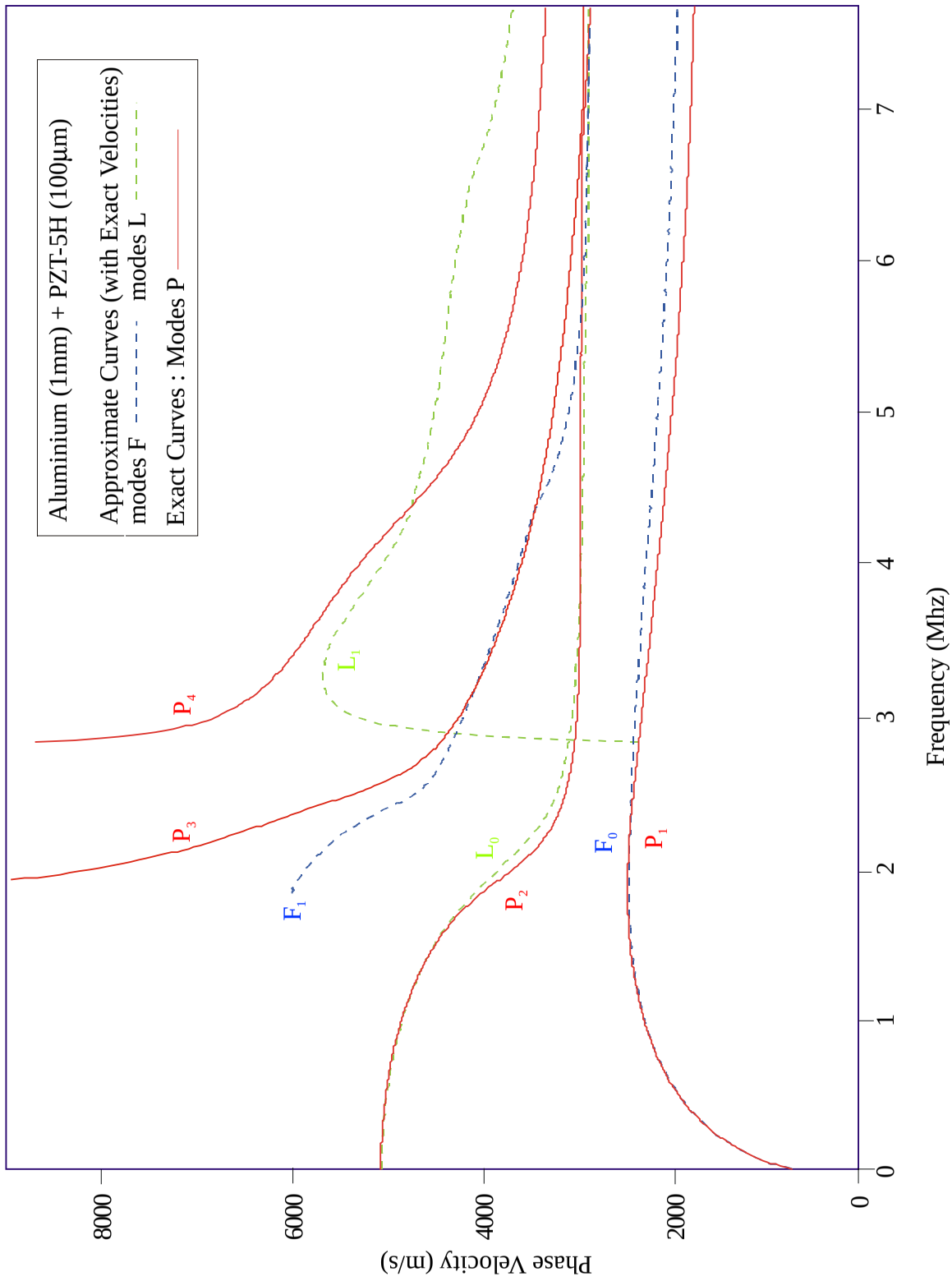

Figure 4.10 : Comparison between the exact dispersion curves and the approximate dispersion curves for the steel(1mm)/epoxy(0.1mm) system.

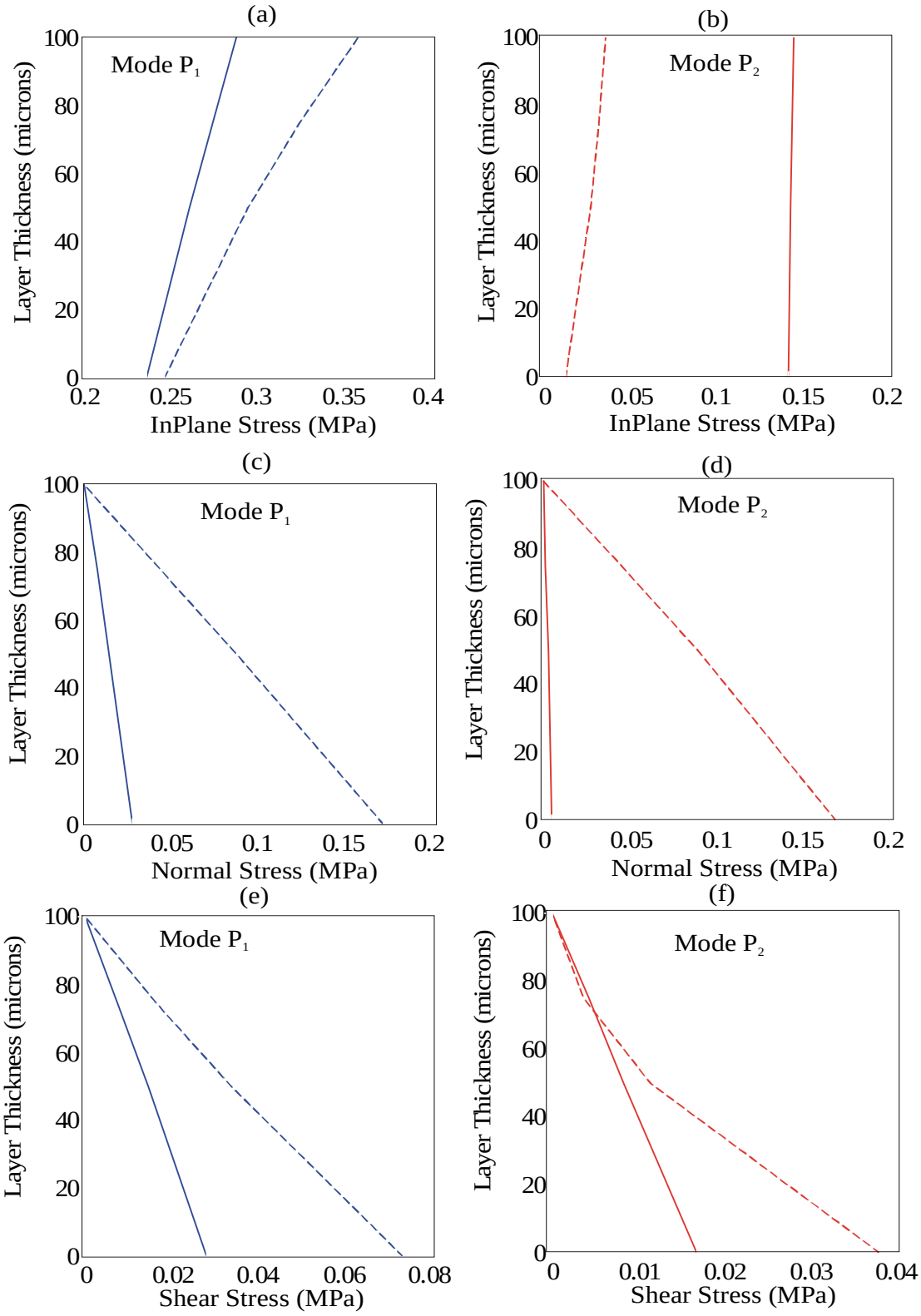

Figure 4.11 : Stress mode shapes in 100µm the PZT-5H layer. (a),(c) and (e) show the mode shapes for the mode P1, (b), (d), (f) show the mode shapes for the mode P2. (a) and (b) inplane stress mode shapes, (c) and (d) normal stress mode shapes and (e) and (f) shear stress mode shapes. Plain lines represent the stress at 0.5 MHz and dashed lines represents the stress at 2MHz.

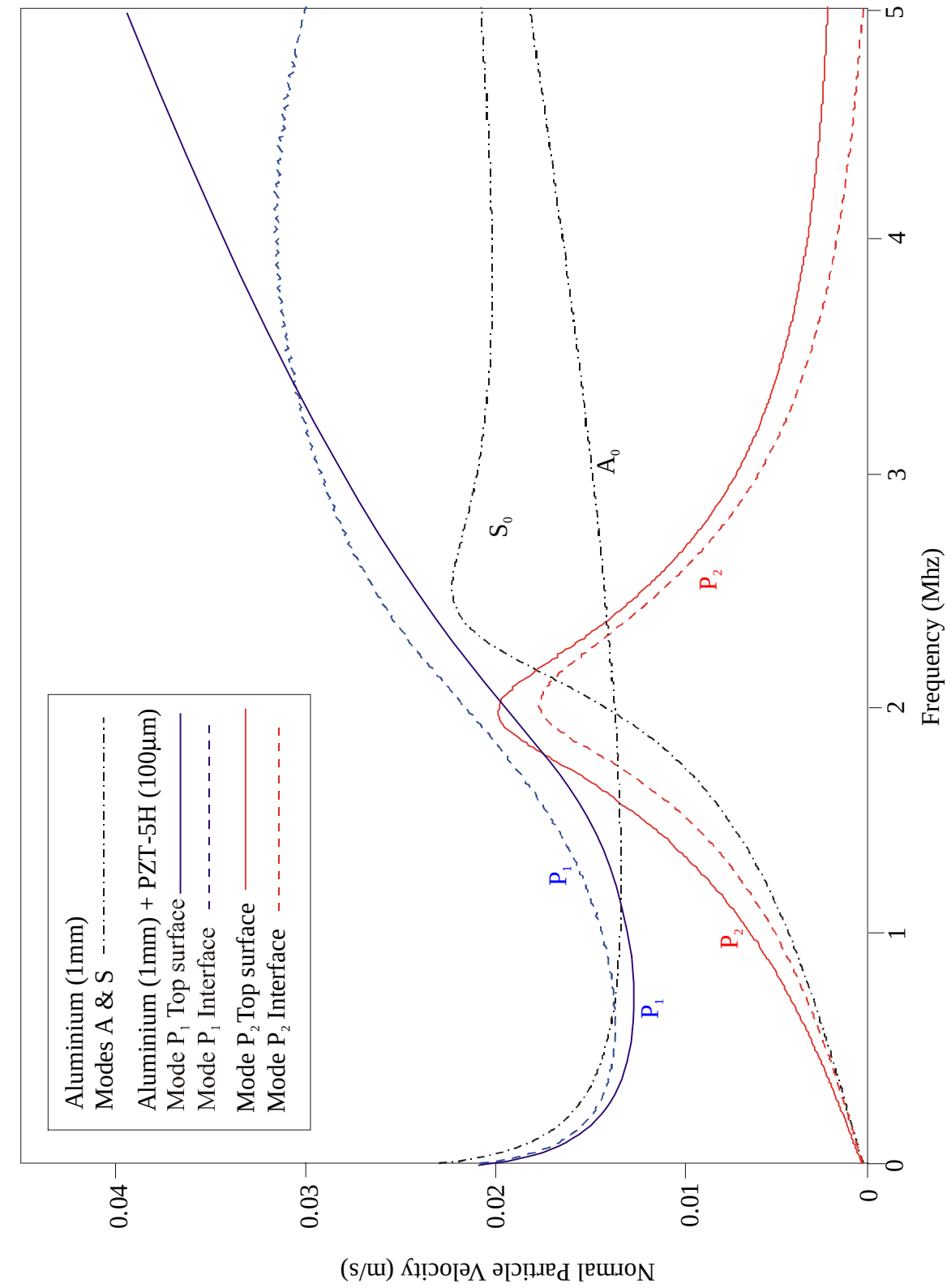

Figure 4.12 : Normal particle velocity dispersion curves for the aluminium(1mm)/PZT(100µm) system. Comparison between dispersion curves at the top surface of the PZT layer and the dispersion curves at the interface between the aluminium and the PZT layer. The dispersion curves for the single 1mm aluminium plate are also shown. All curves have been calculated for a mode with unit power flow.

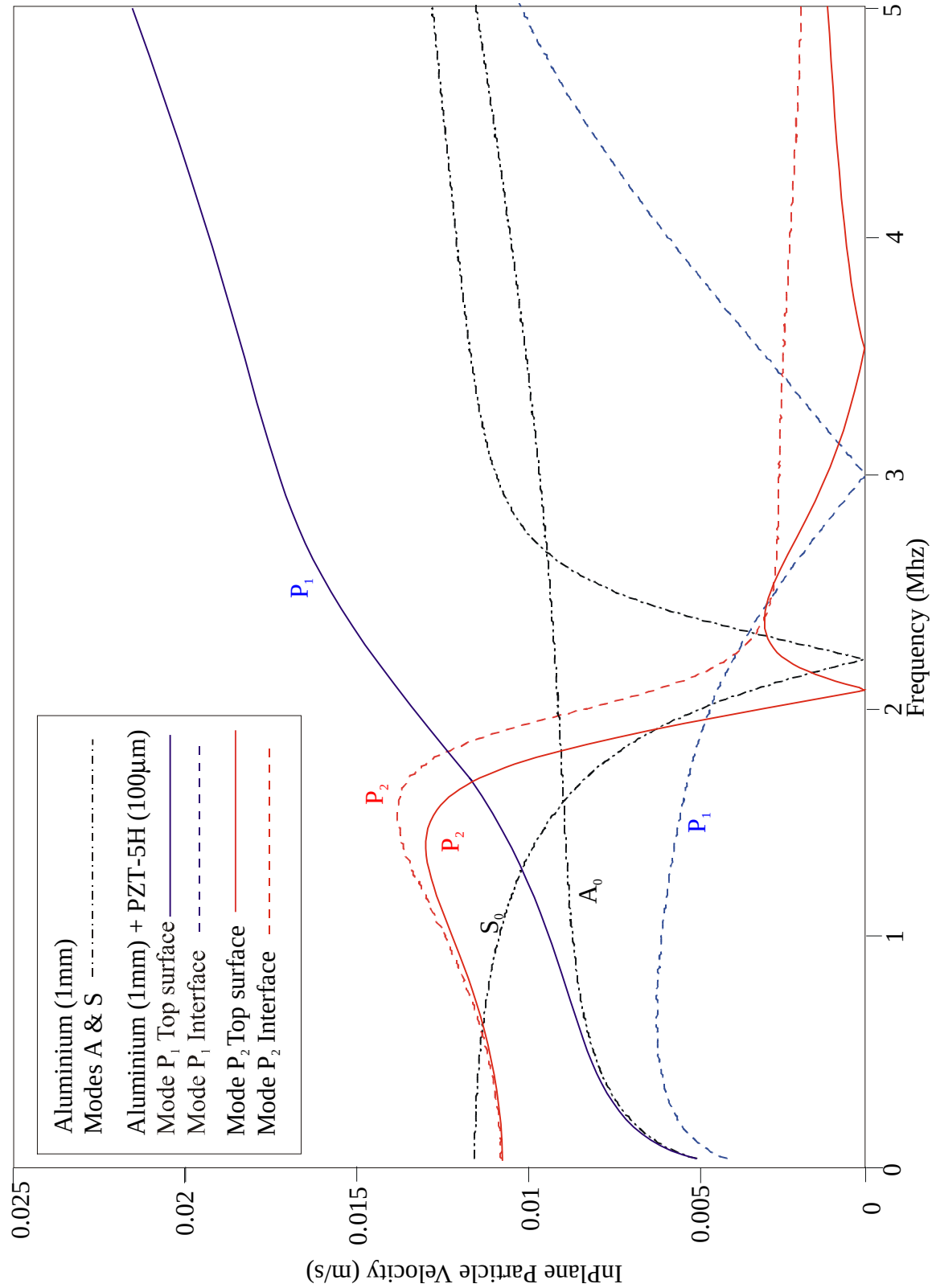

Figure 4.13 : Inplane particle velocity dispersion curves for the aluminium(1mm)/PZT(100µm) system. Comparison between dispersion curves at the top surface of the PZT layer and the dispersion curves at the interface between the aluminium and the PZT layer. The dispersion curves for the single 1mm aluminium plate are also shown. All curves have been calculated for a mode with unit power flow.

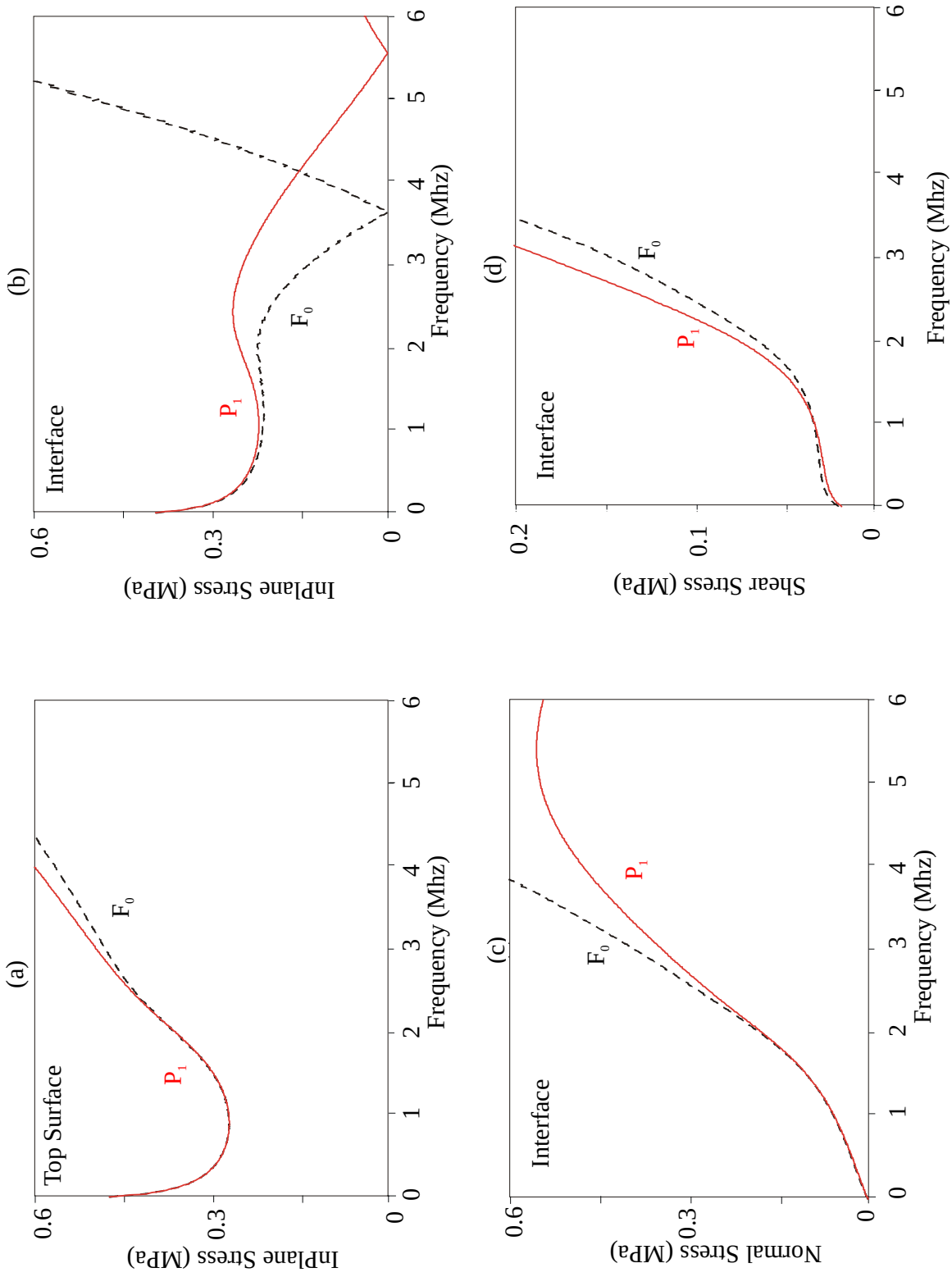

Figure 4.14 : Stress dispersion curves for the modes F_0 and P_1. Comparison between the exact stress dispersion curves and the approximate stress dispersion curves for the aluminium(1mm)/PZT(100µm) system. The approximate dispersions curves have been obtained using the exact velocity fields. (a) Inplane stress at the top surface of the PZT layer, (b) inplane stress at the interface between the aluminium plate and the PZT layer. (c) normal stress at the interface and (d) shear stress at the interface. All curves have been calculated for a mode with unit power flow.

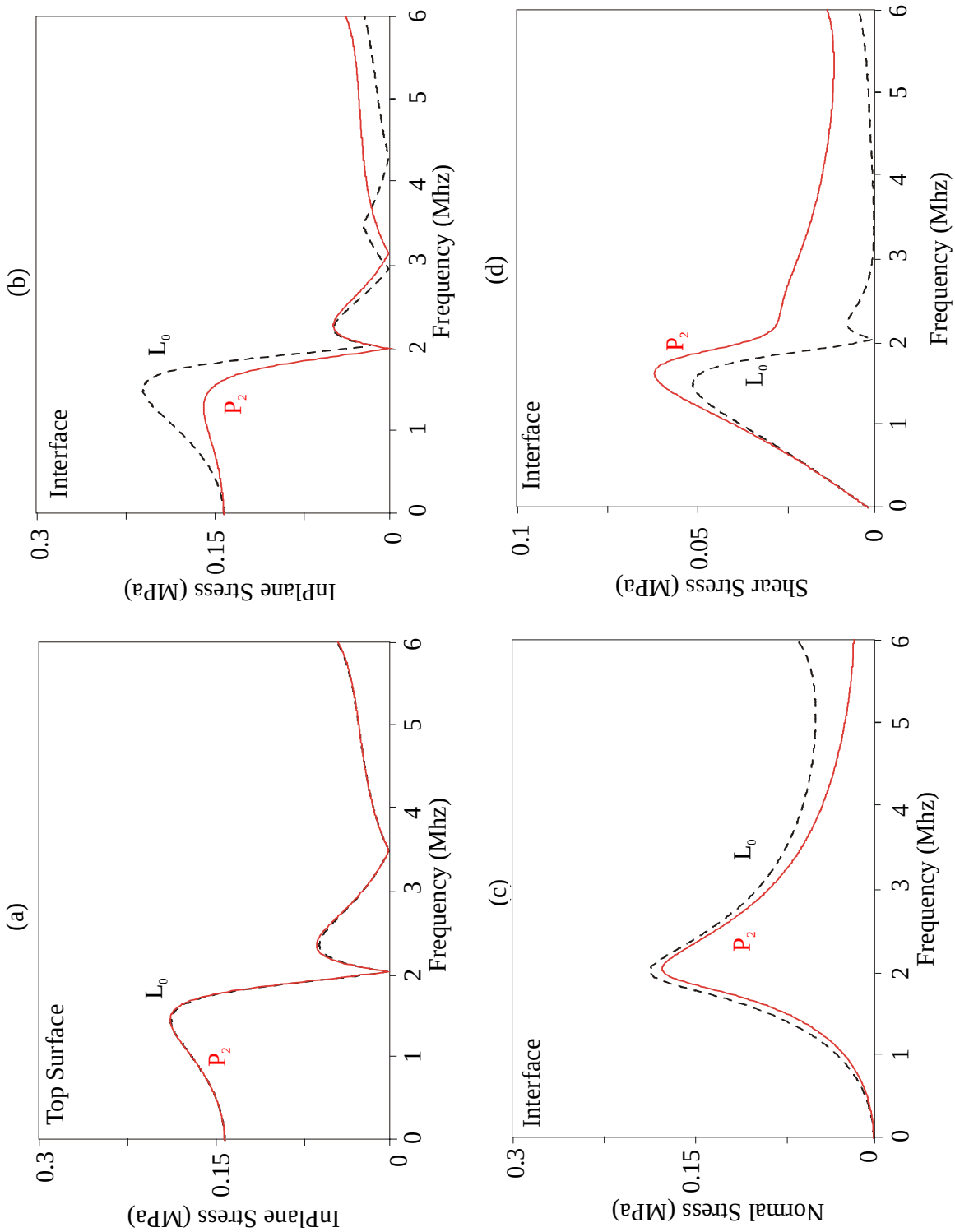

Figure 4.15 : Stress dispersion curves for the modes L_0 and P_2. Comparison between the exact stress dispersion curves and the approximate stress dispersion curves for the aluminium (1mm)/PZT(100µm) system. The approximate dispersions curves have been obtained using the exact velocity fields. (a) Inplane stress at the top surface of the PZT layer, (b) inplane stress at the interface between the aluminium plate and the PZT layer. (c) normal stress at the interface and (d) shear stress at the interface. All curves have been calculated for a mode with unit power flow.

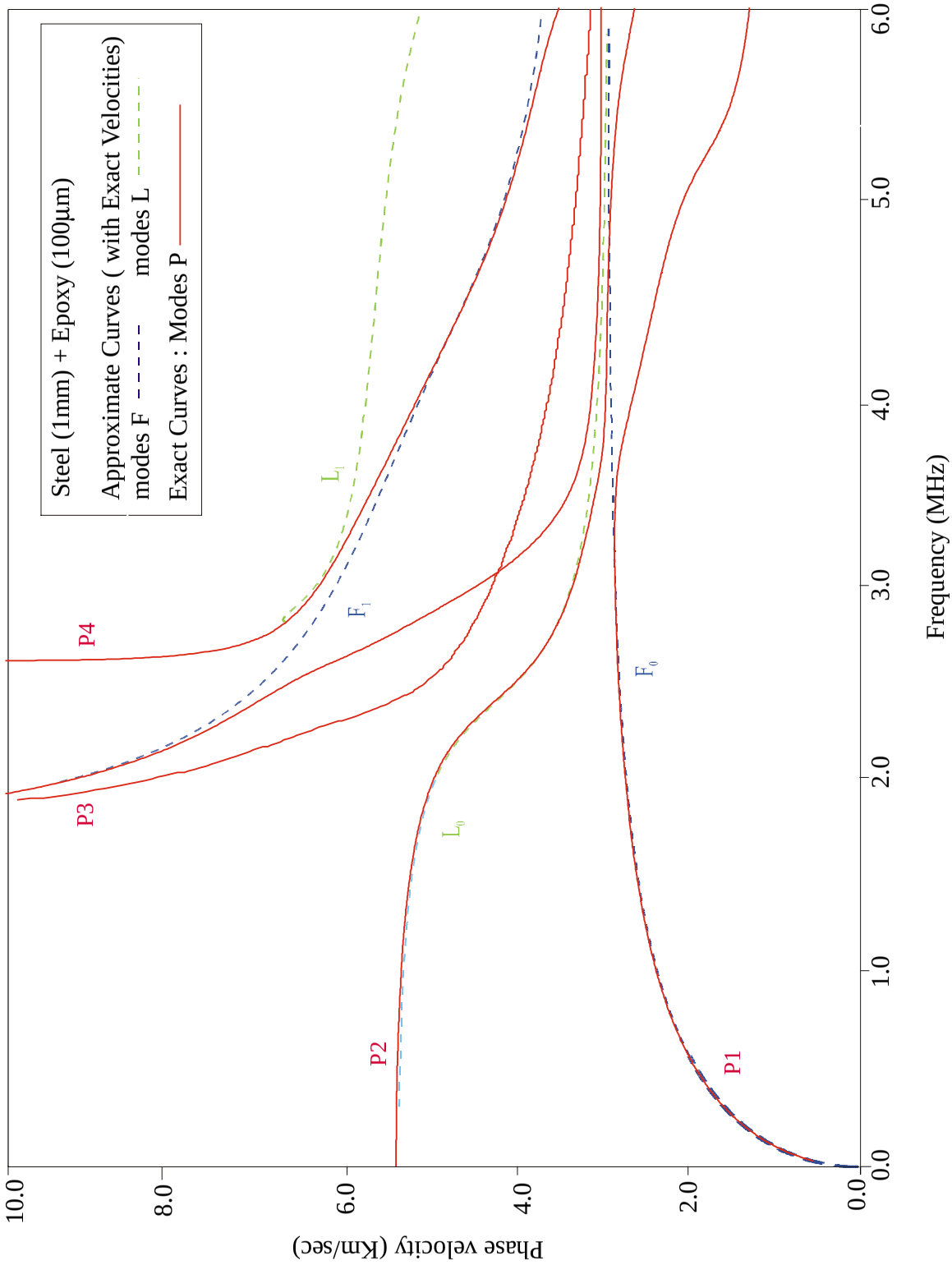

Figure 4.16 : Comparison between the exact dispersion curves and the approximate dispersion curves using the exact velocity fields for the steel(1mm)/epoxy(100µm) system.

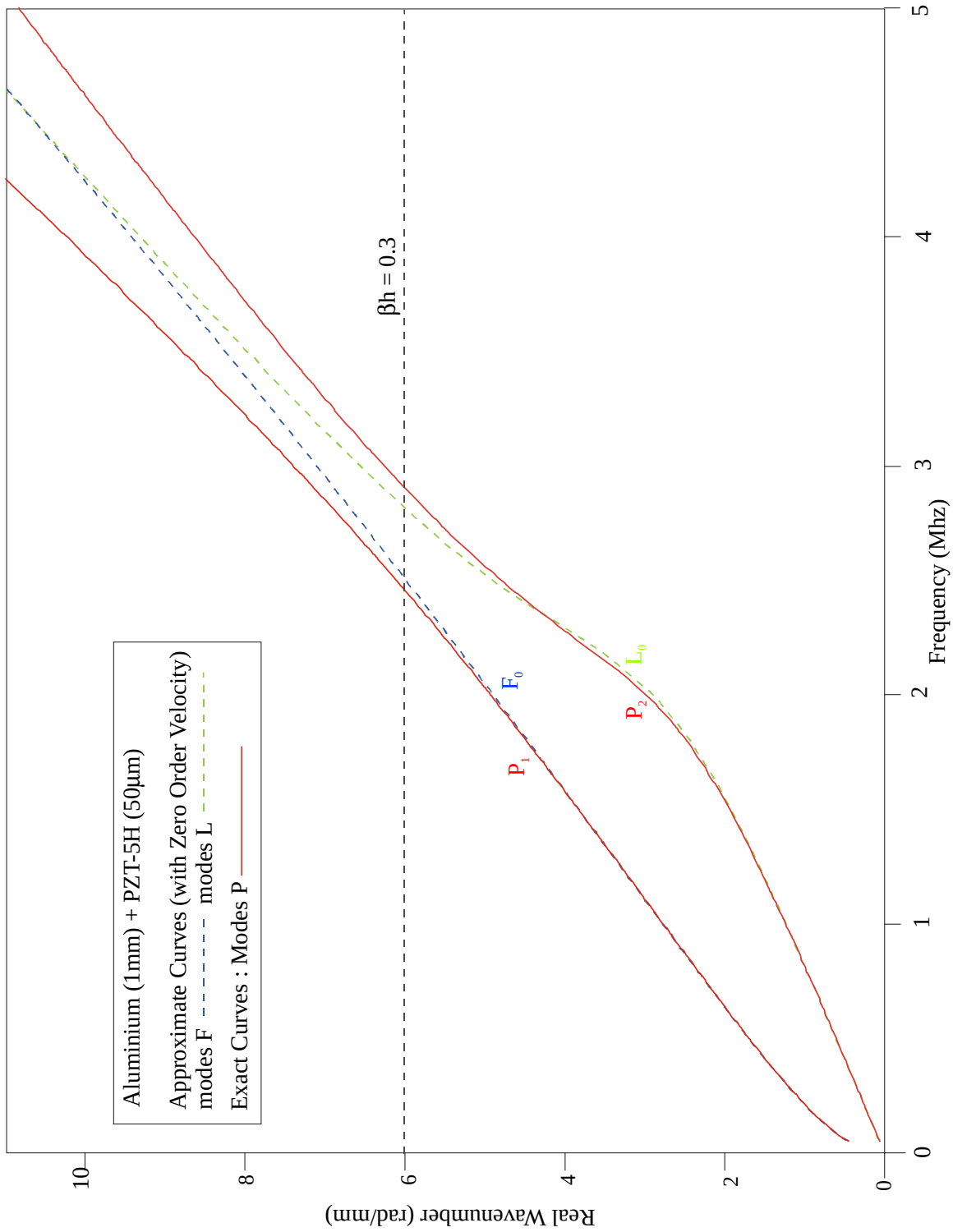

Figure 4.17 : Comparison between the exact wavenumber dispersion curves and the approximate wavenumber dispersion curves for the aluminium(1mm)/PZT(50µm) system. The approximate dispersions curves have been obtained using the zero order particle velocity amplitudes.

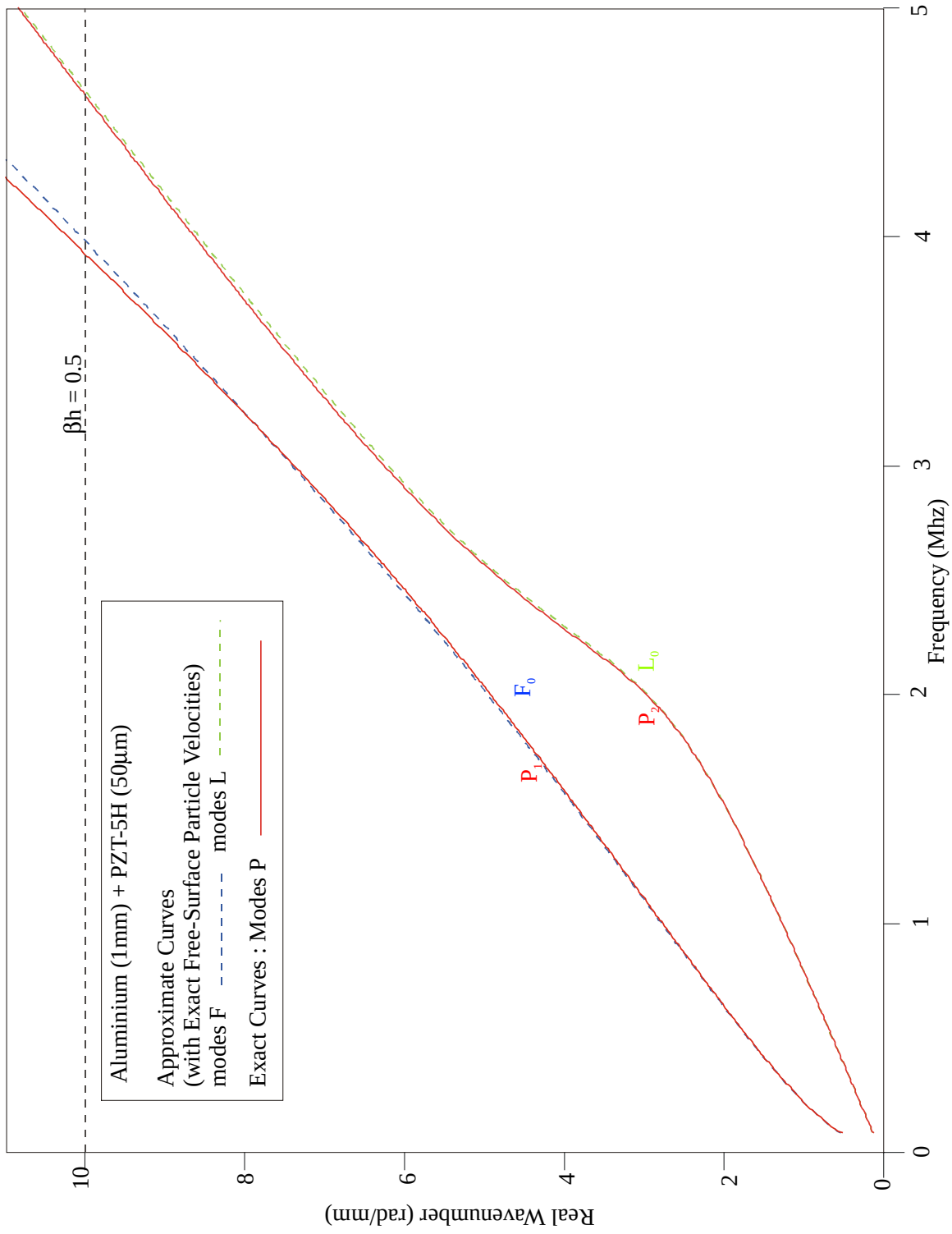

Figure 4.18 : Comparison between the exact wavenumber dispersion curves and the approximate wavenumber dispersion curves for the aluminium(1mm)/PZT(50µm) system. The approximate dispersions curves have been obtained using the exact free-surface particle velocity amplitudes.

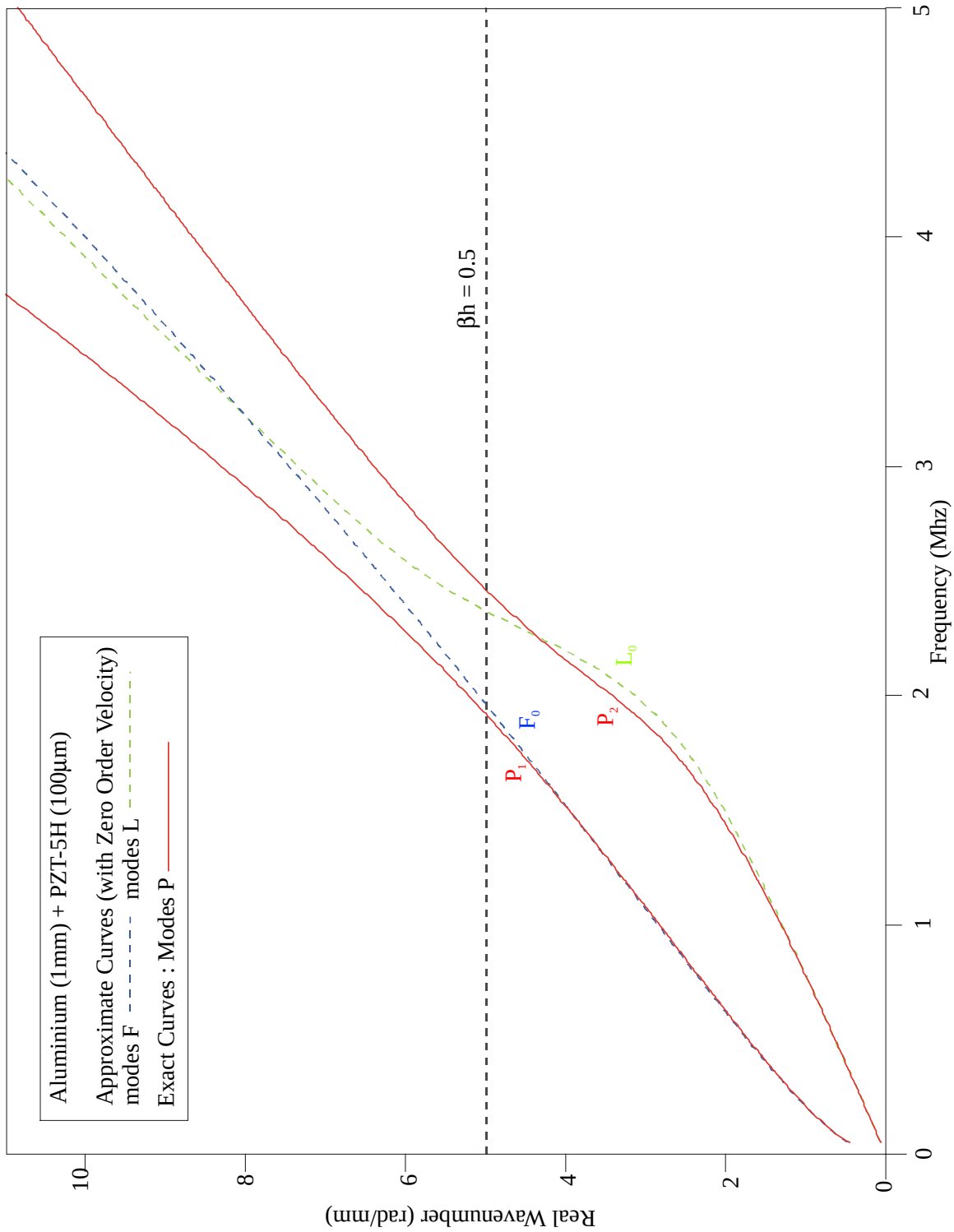

Figure 4.19 : Comparison between the exact wavenumber dispersion curves and the approximate wavenumber dispersion curves for the aluminium(1mm)/PZT(100µm) system. The approximate dispersions curves have been obtained using the zero order particle velocity amplitudes.

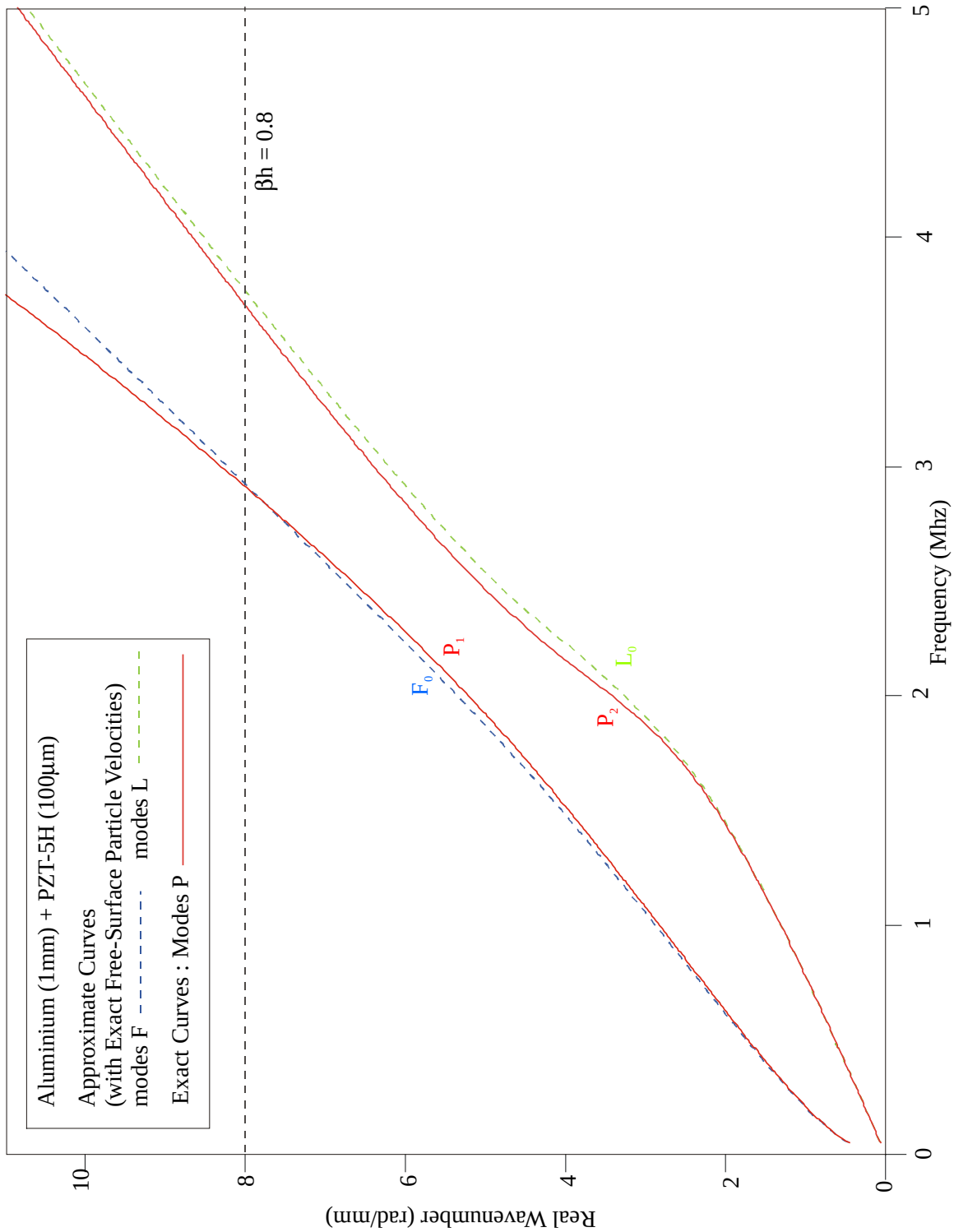

Figure 4.20 : Comparison between the exact wavenumber dispersion curves and the approximate wavenumber dispersion curves for the aluminium(1mm)/PZT(100µm) system. The approximate dispersion curves have been obtained using the exact free-surface particle velocity amplitudes.

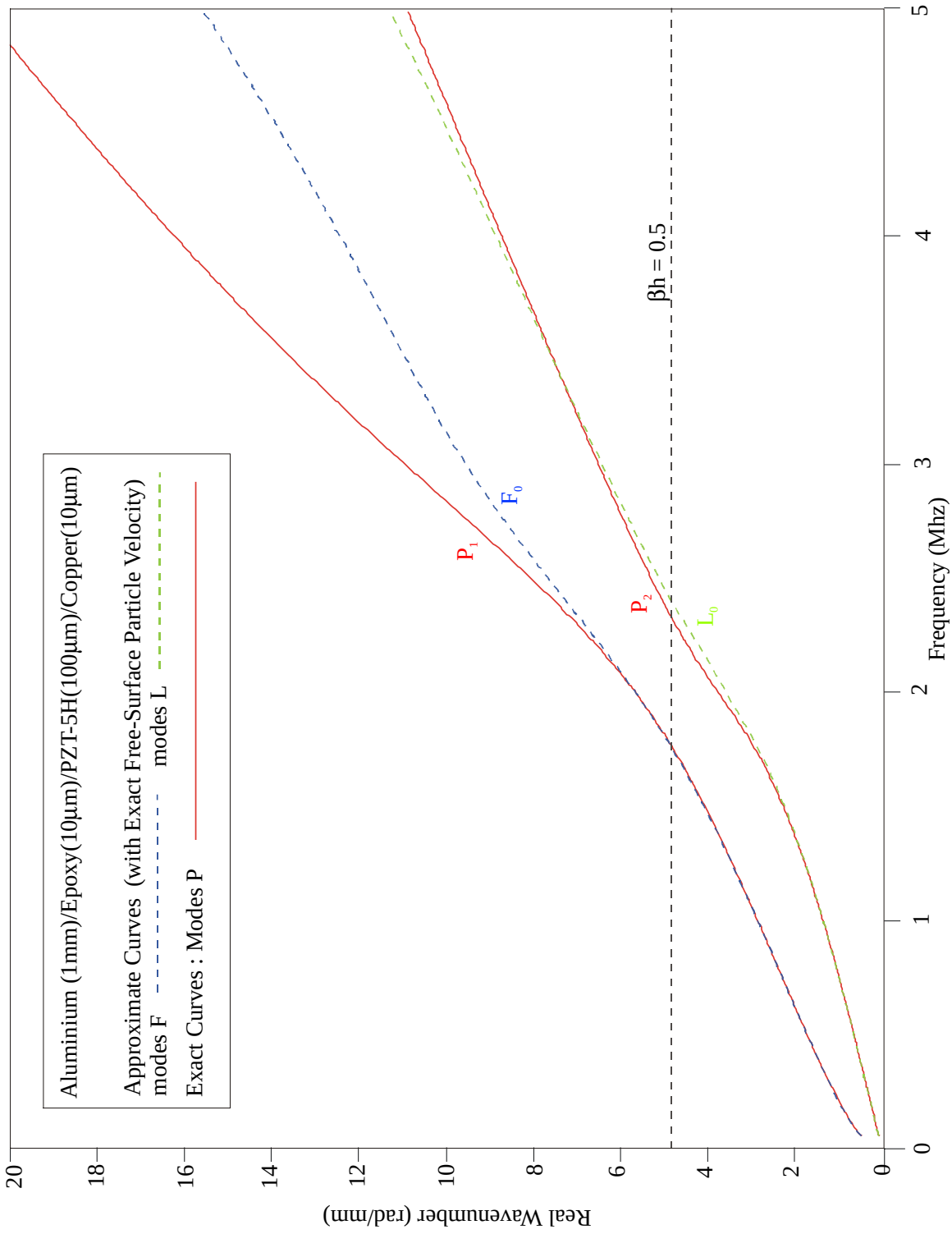

Figure 4.21 : Comparison between the exact wavenumber dispersion curves and the approximate wavenumber dispersion curves for the aluminium(1mm)/Epoxy (10µm)/PZT(100µm)/ Copper(10µm) system. The approximate dispersion curves have been obtained using the exact free-surface particle velocity amplitudes.

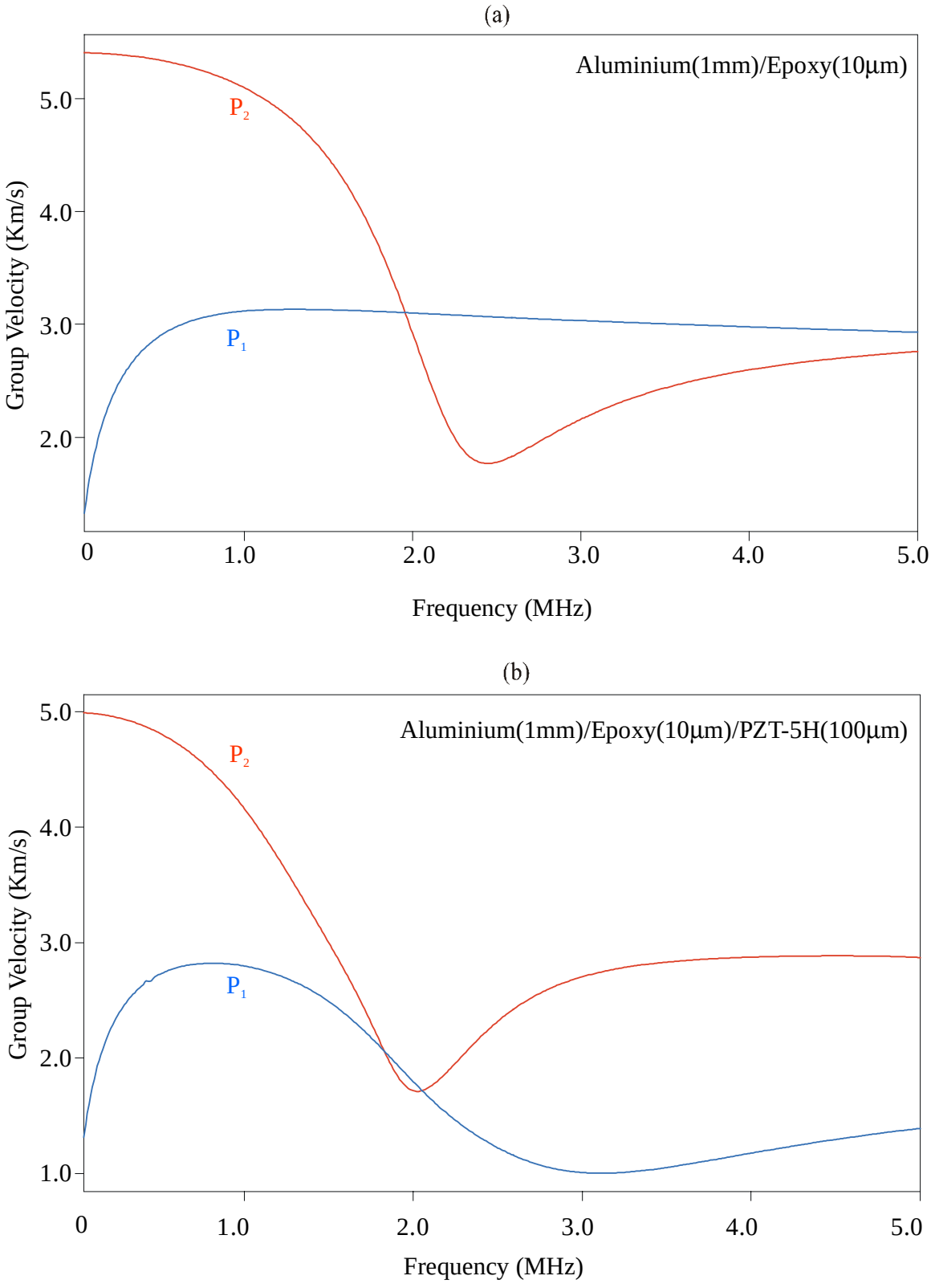

Figure 4.22 : (a) Exact group velocity dispersion curves for the Aluminium/Epoxy system. (b) Exact group velocity dispersion curves for the Aluminium/Epoxy/PZT-5H system.

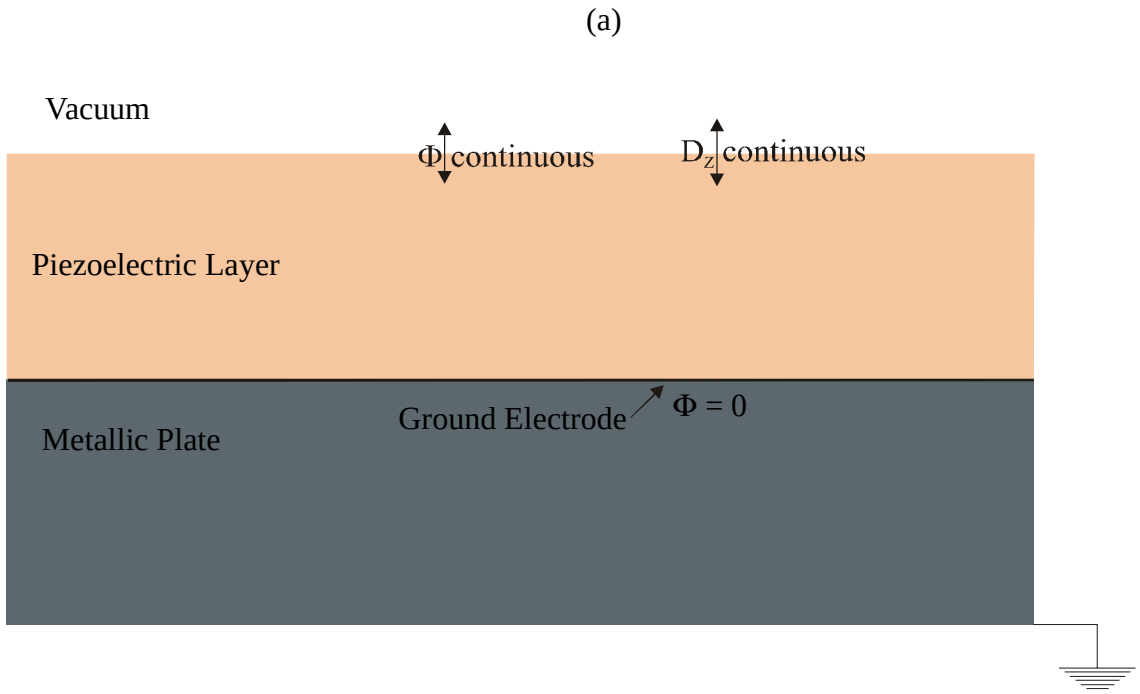

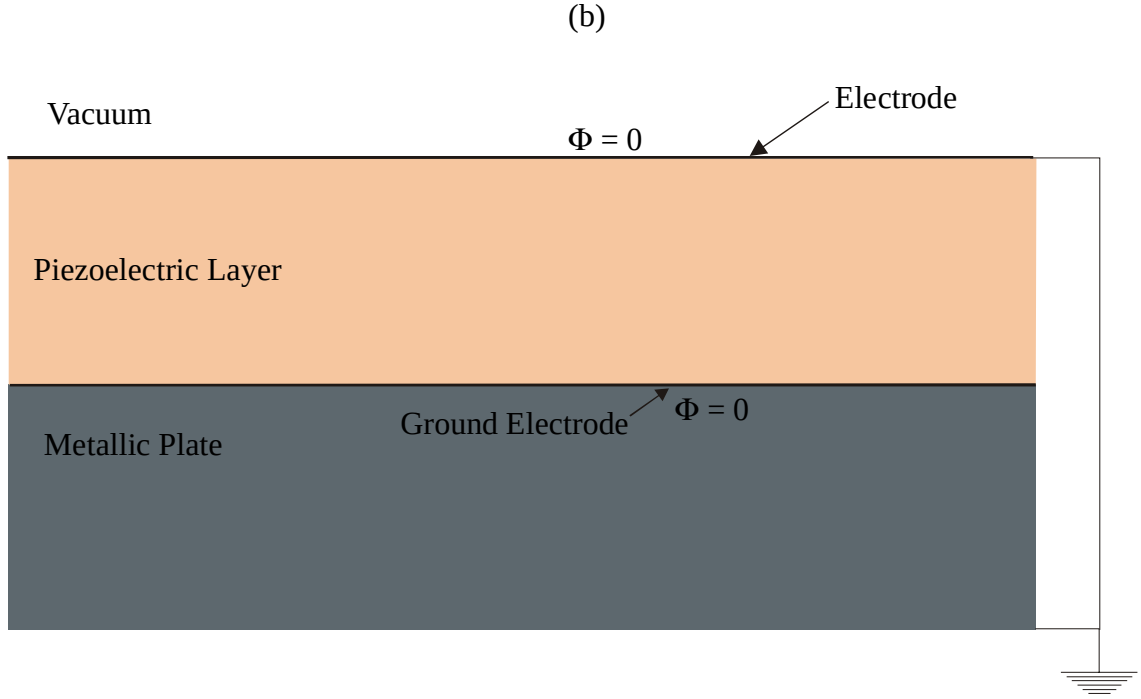

Figure 4.23 : Electrical boundary conditions in (a) the free-surface case, (b) the metallised case at the upper surface. In both cases the metal plate is grounded and the potential is zero at the interface.

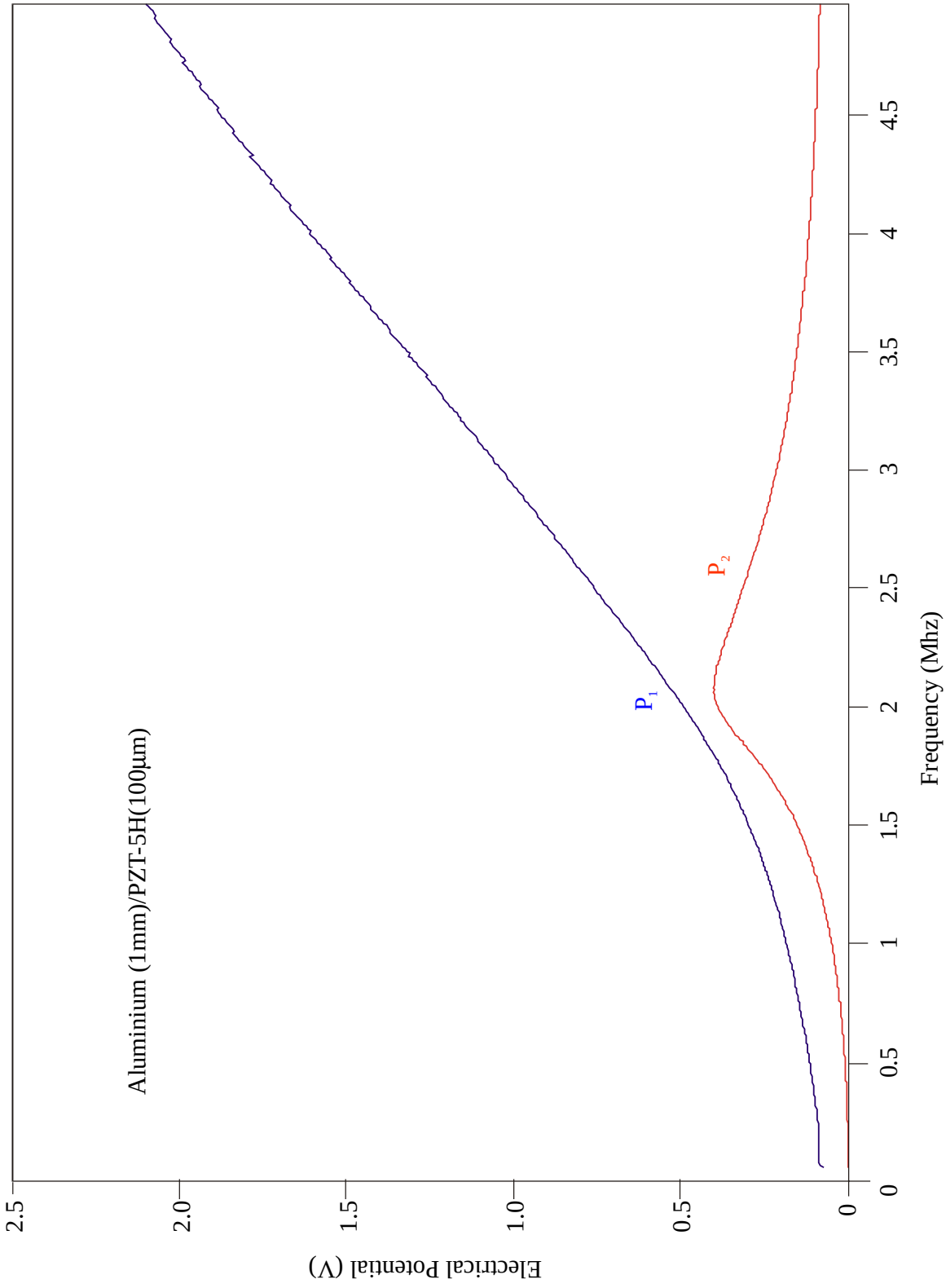

Figure 4.24 : Electric potential at the top surface of the PZT-5H layer.

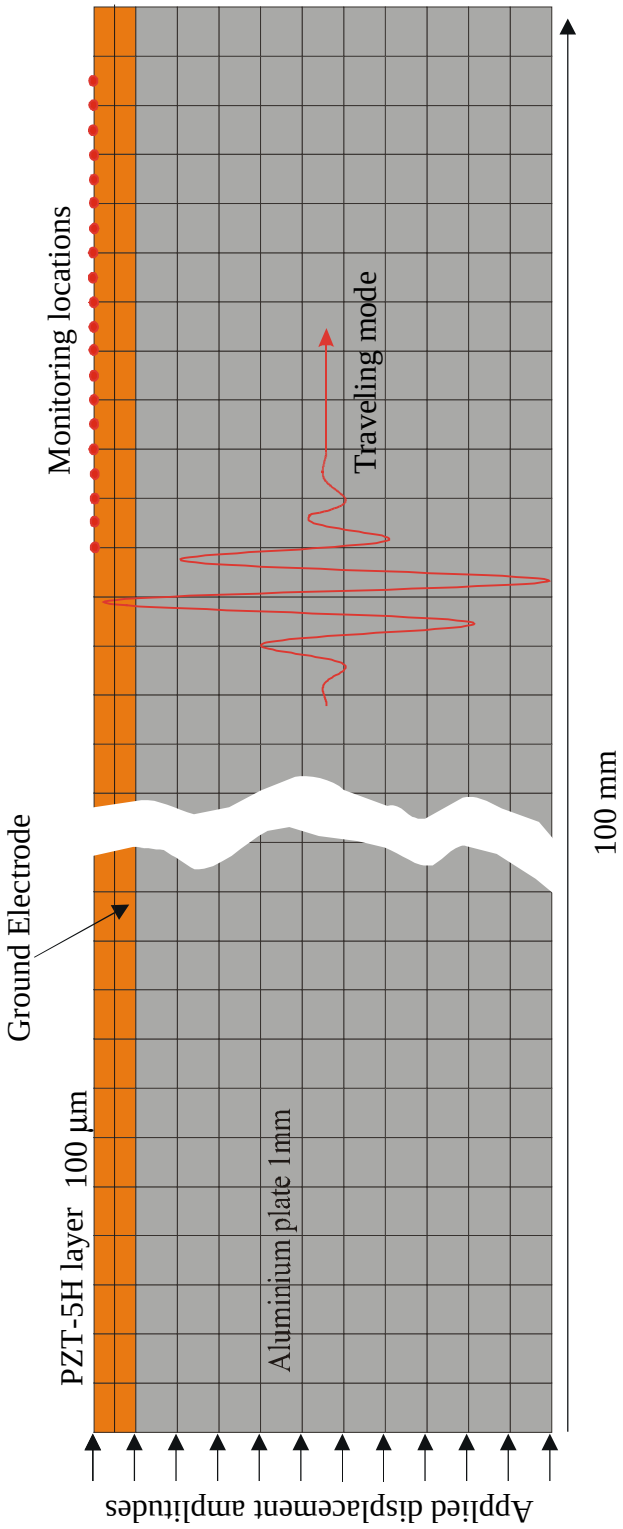

Figure 4.25 : Schematic diagram of the finite element model used to monitor the electric potential at the top surface of the PZT-5H layer.

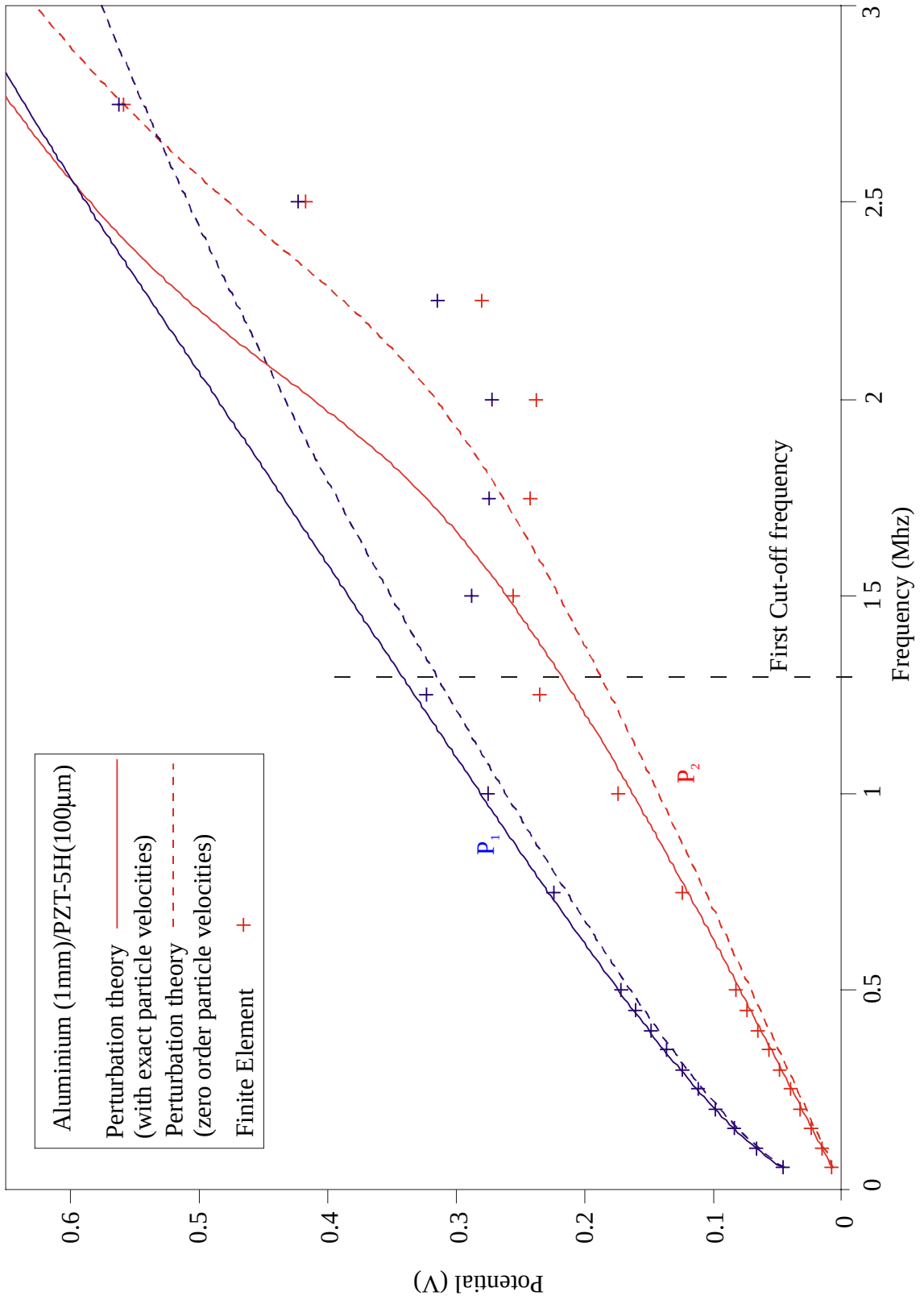

Figure 4.26 : Comparison between finite element predictions and perturbation theory calculations for the electric potential at the top surface of the PZT-5H layer, normalised to a wave amplitude of 1 nm in the direction of propagation. Dashed line curves were obtained using the particle velocities at the top of the aluminium plate alone and plain line curves were obtained using the particle velocities at the top of the PZT-5H layer.

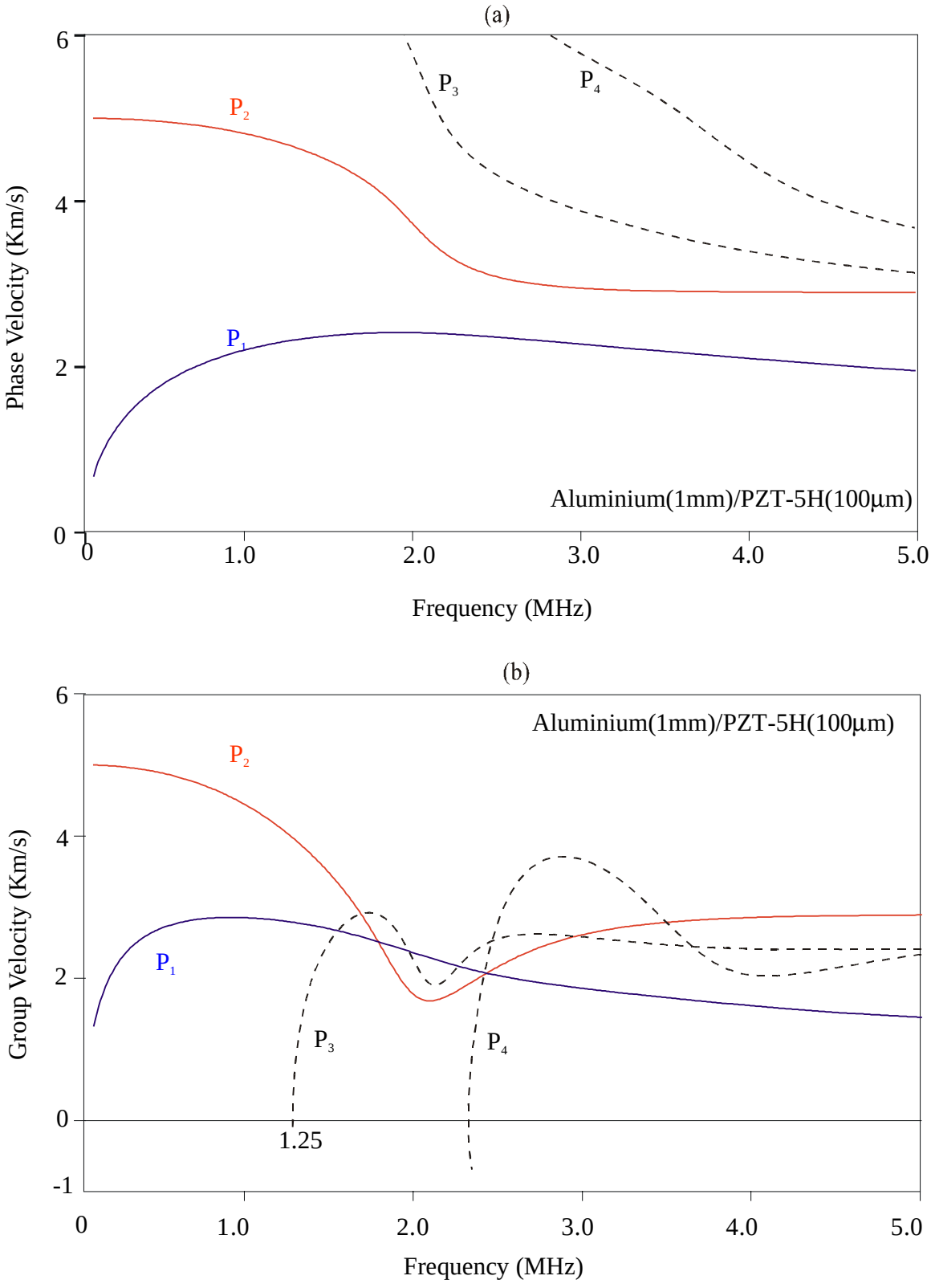

Figure 4.27 : (a) Exact phase velocity dispersion curves for the Aluminium/PZT-5H system. (b) Exact group velocity dispersion curves for the Aluminium/PZT-5H system showing the cut-off frequencies.

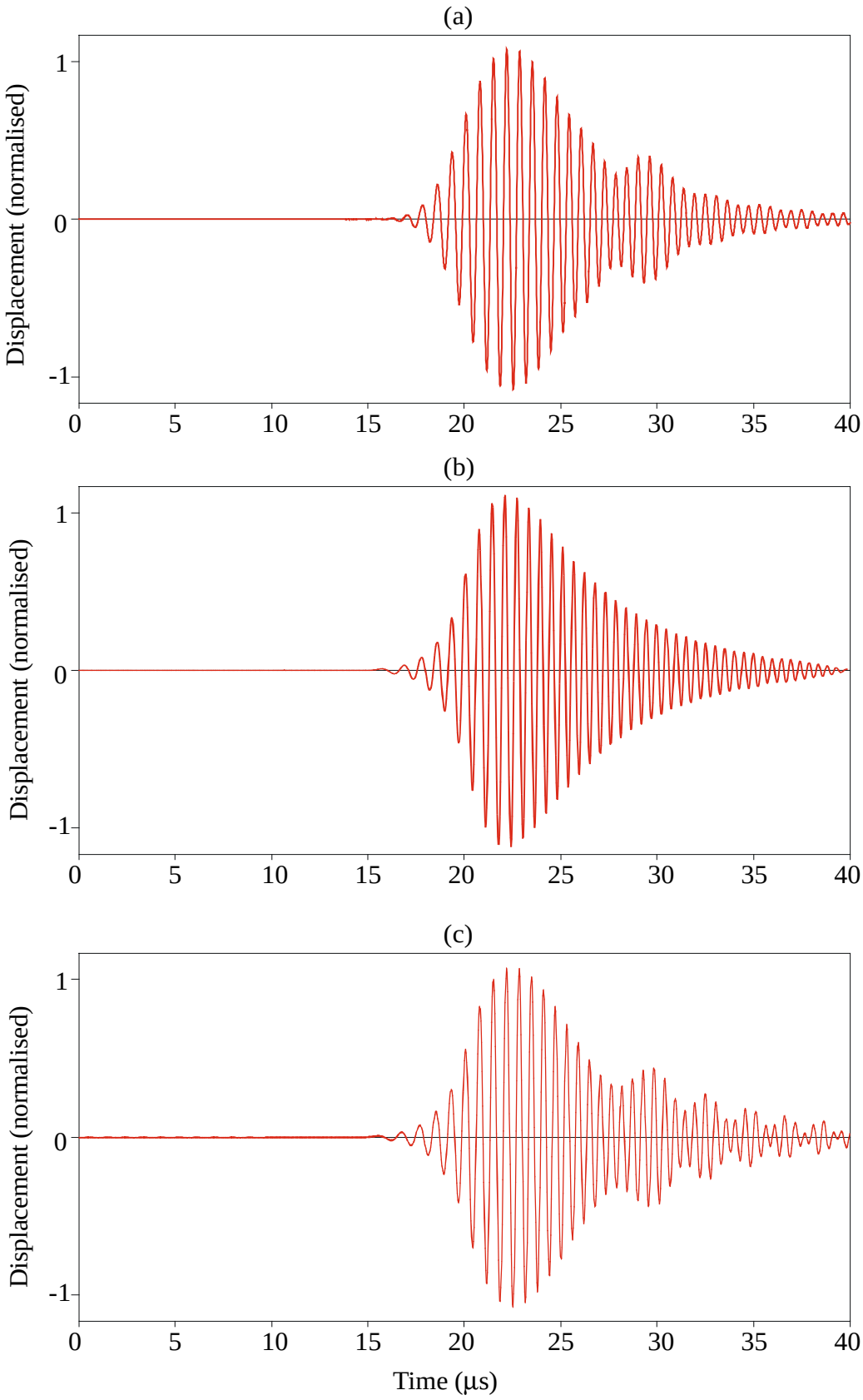

Figure 4.28 : Time domain traces of the inplane displacement of the mode P_2, at 1.5 MHz, after it has propagated over 67.5 mm. (a) Finite element prediction. (b) Simulation with the mode P_2 propagating alone. (b) Simulation with the modes P_2 and P_3 propagating together.

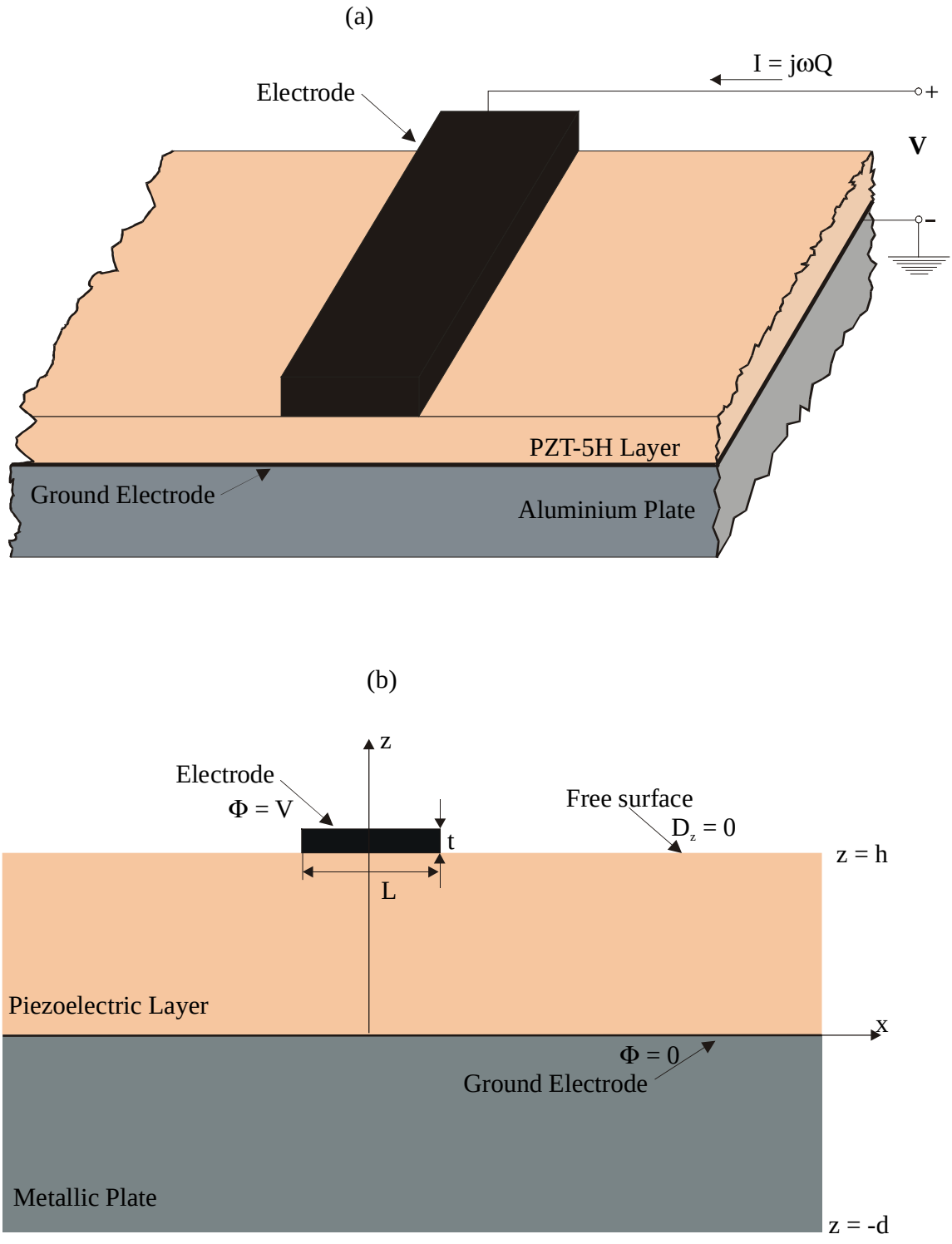

Figure 4.29 : Schematic diagram (a) of the transducer problem when a potential is applied at the top electrode. (b) Electrical boundary conditions and coordinate system.

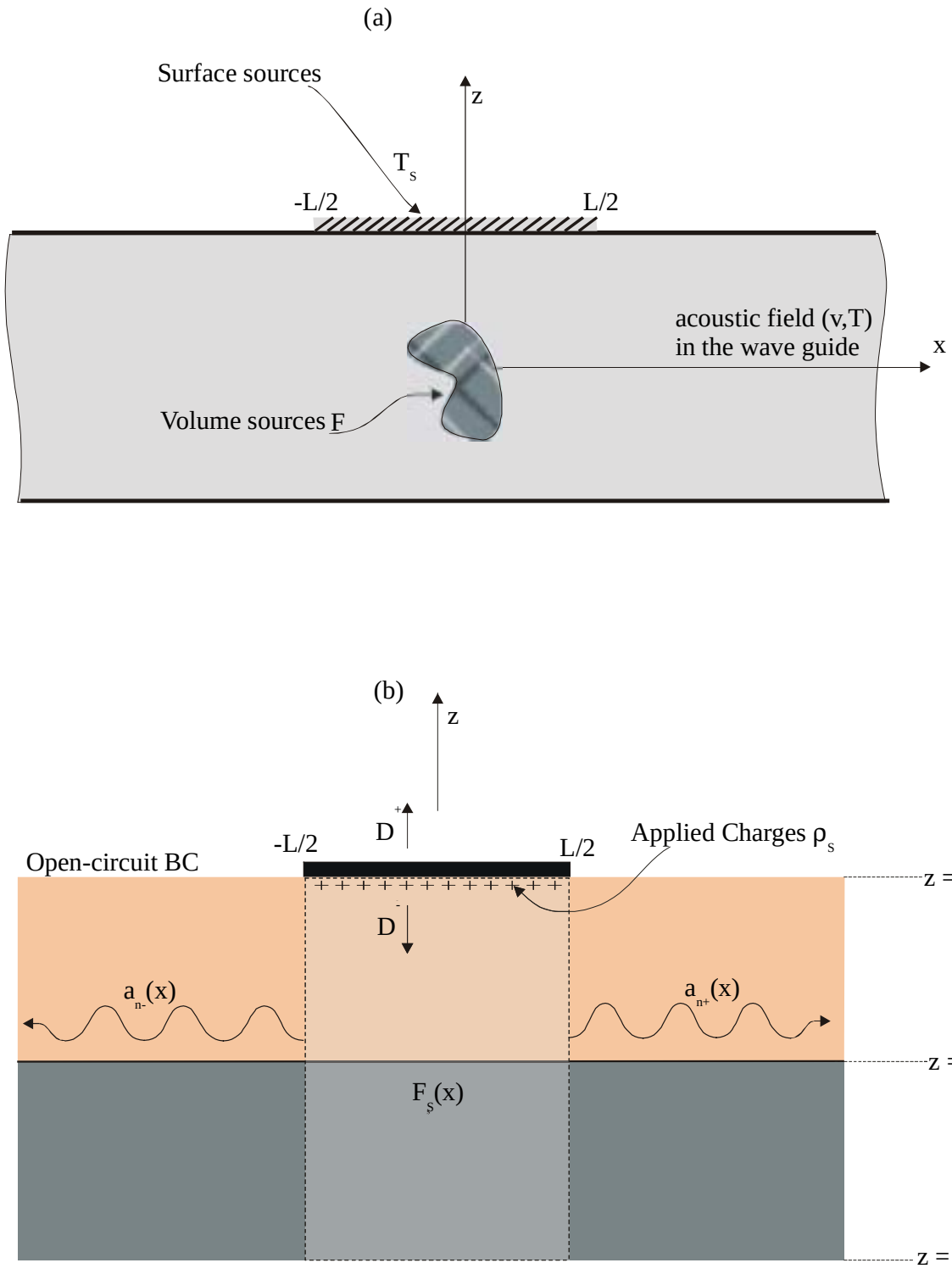

Figure 4.30 : Excitation of plate modes by (a) distributed surface tractions, (b) by electrical charges.

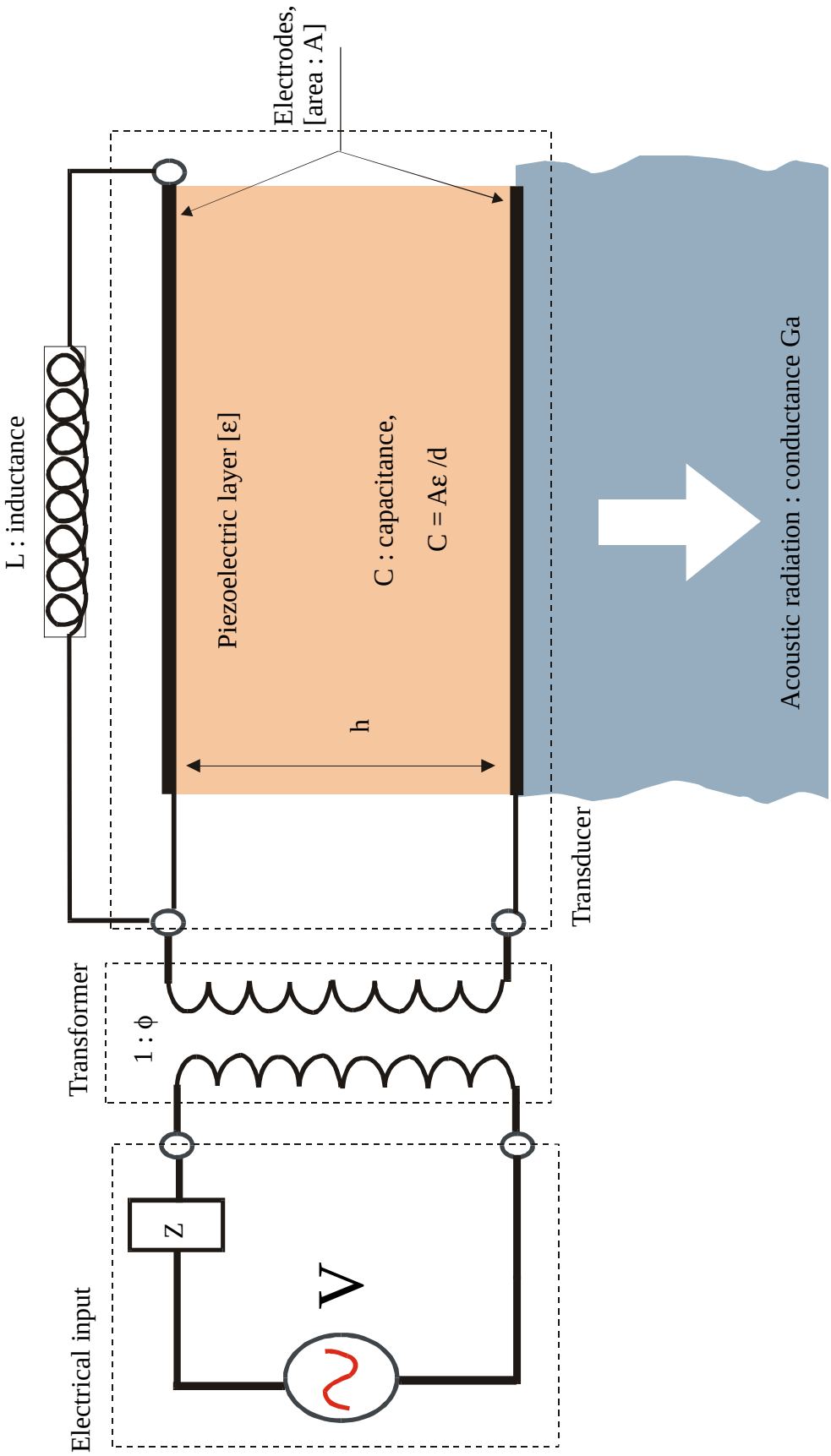

Figure 4.31 : Simplified representation of a bulk wave transducer without electrical and mechanical losses. The inductance is added to cancel the capacitance.

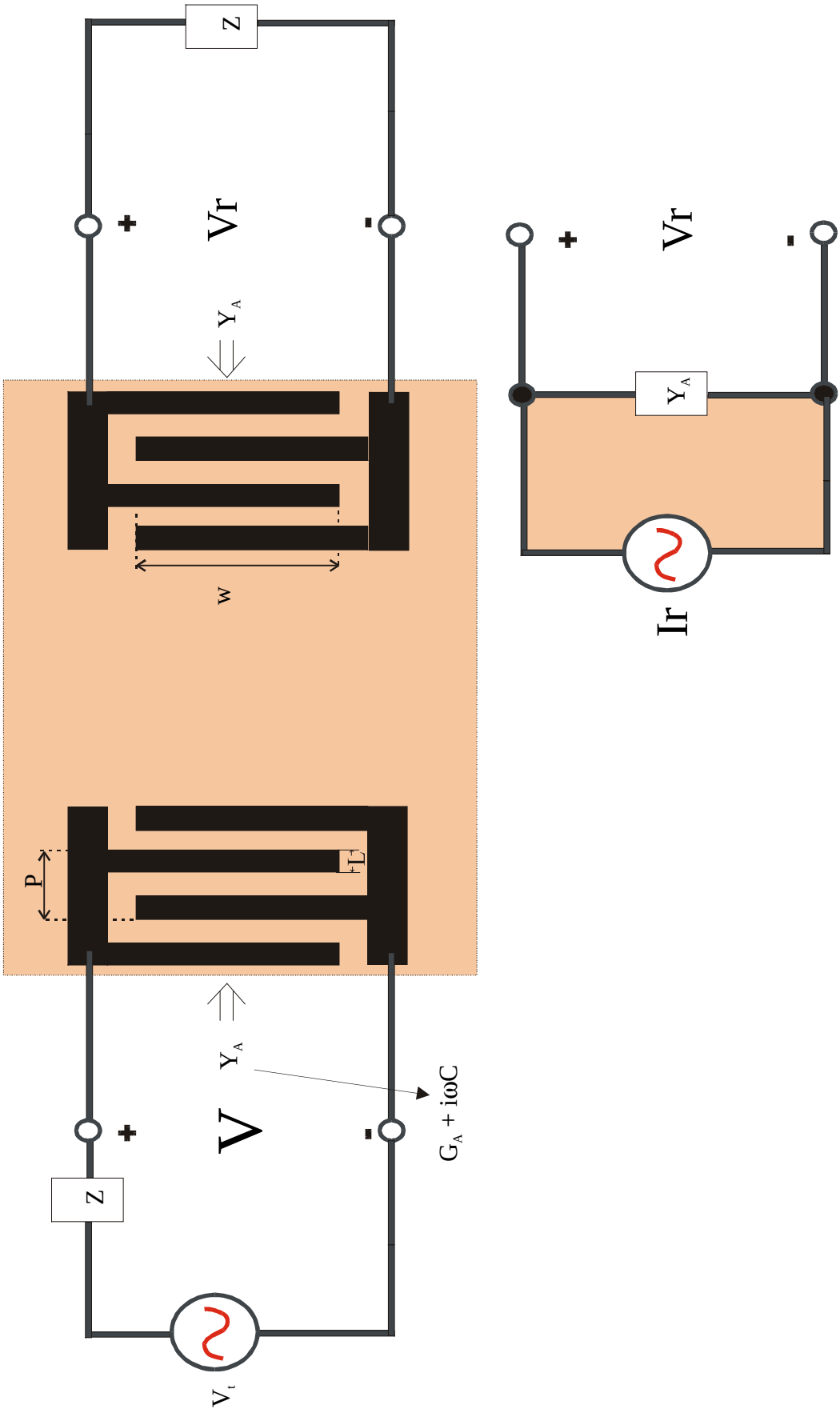

Figure 4.32 : Uniform interdigital electrode arrays and circuit interactions. The finger width is L and the spacing between two finger pair is L.

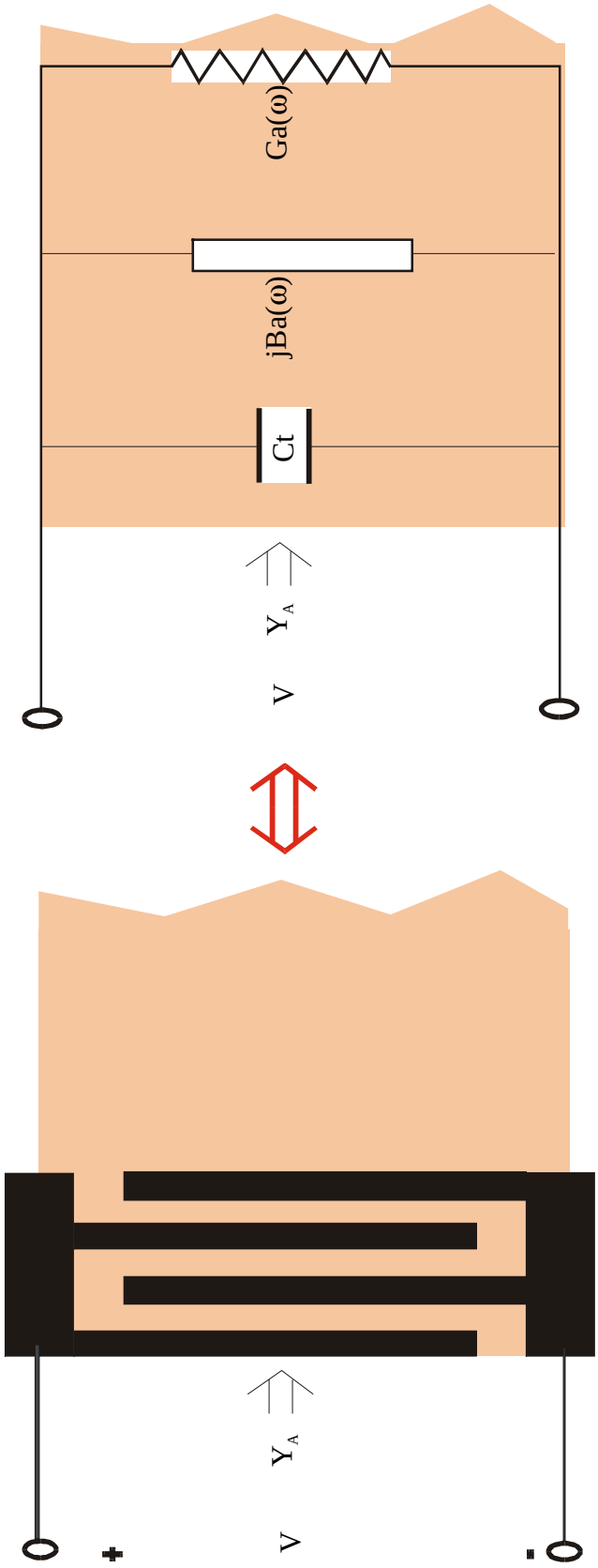

Figure 4.33 : Equivalent circuit for interdigital transducer.

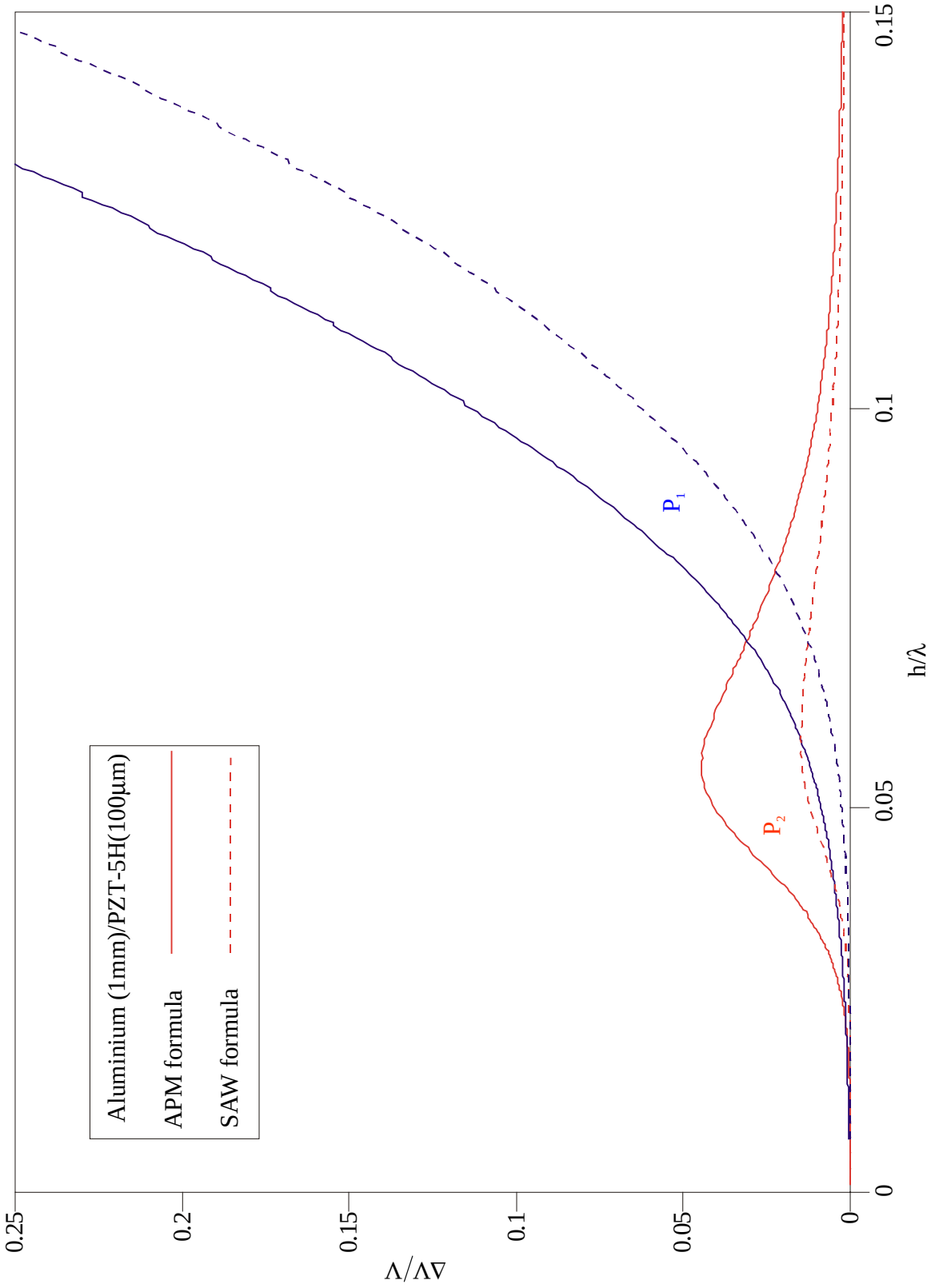

Figure 4.34 : $\Delta V/V$ for a PZT-5H thin layer (h= 0.1mm) on a grounded plane, as a function of the thickness to wavelength ratio, for the plate modes P1 and P2. $\Delta V/V$ calculated using the formula for APM in plain lines, $\Delta V/V$ calculated with the formula for SAW in dashed lines.

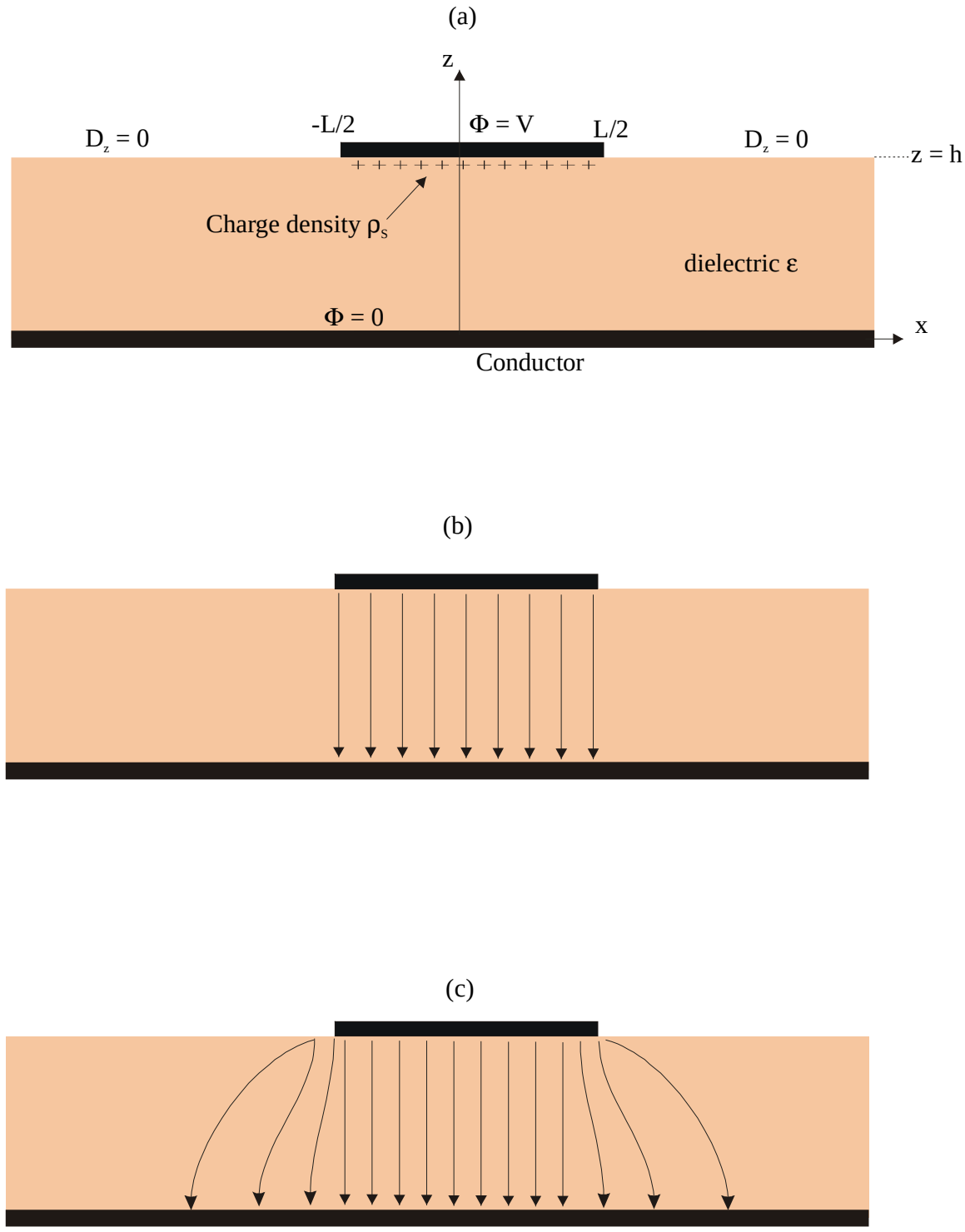

Figure 4.35 : (a) Microstrip structure, (b) cross-field approximation of the electric field, (c) electric field pattern showing the flux lines from the edge of the strip.

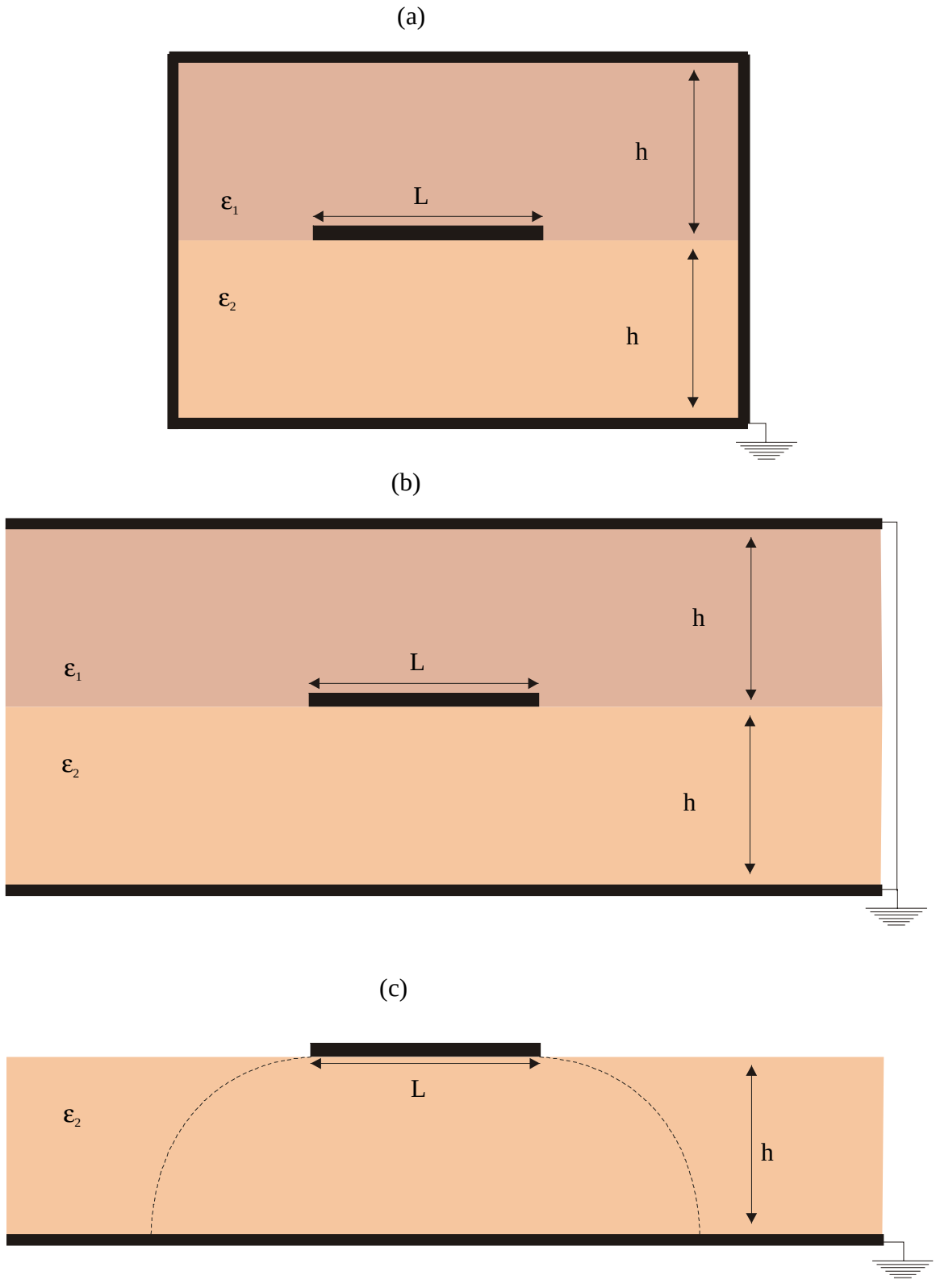

Figure 4.36 : Geometry of a single stripline between two different dielectric media surrounded with (a) a shielded box and (b) two infinite parallel ground planes. (c) Geometry of single stripline suspended over a ground plane.

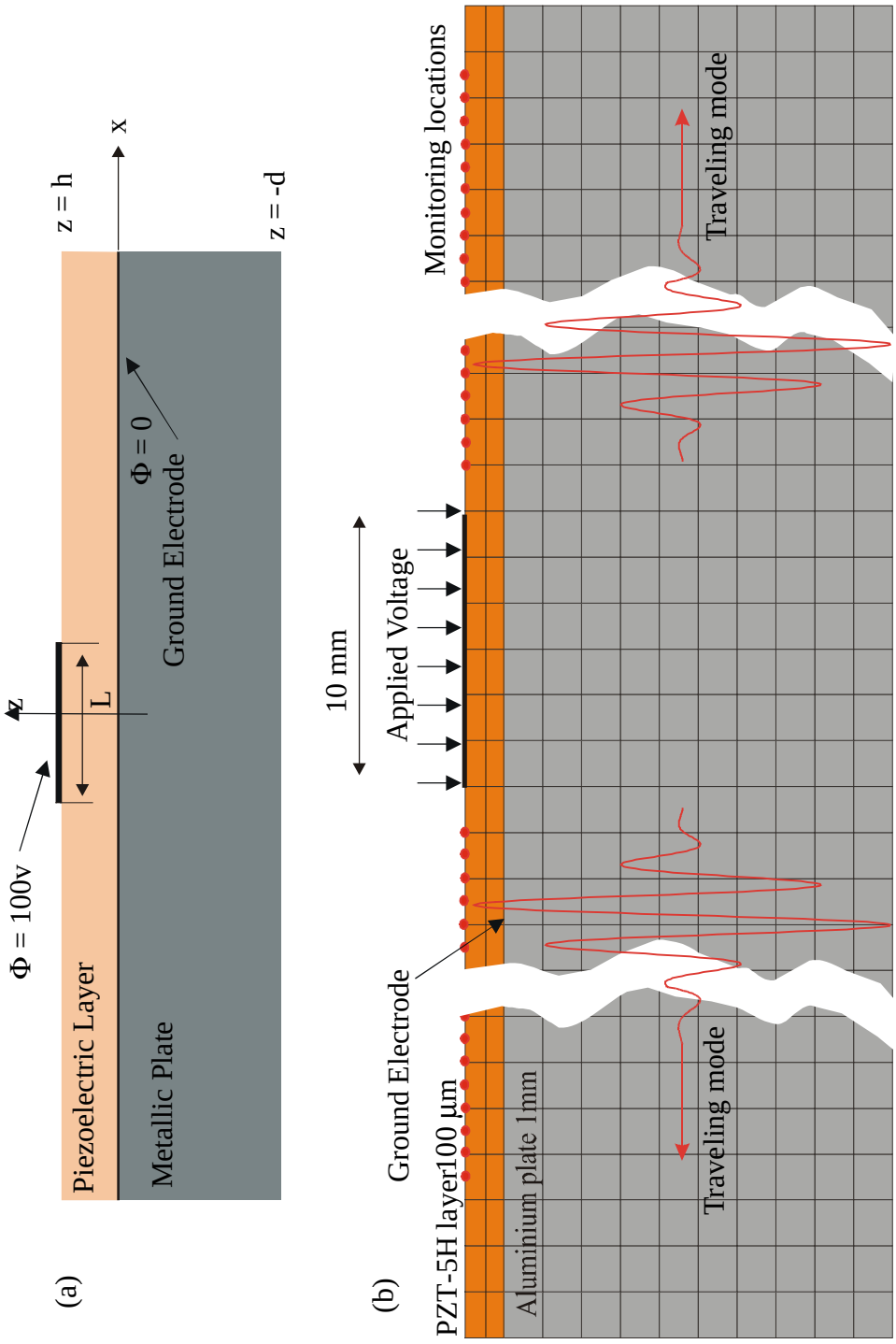

Figure 4.37 : Schematic diagram of the finite element model used to monitor the mechanical displacements in the x- and z-directions at the top surface of the PZT-5H layer when a voltage is applied at all nodes along a 10 mm long electrode.

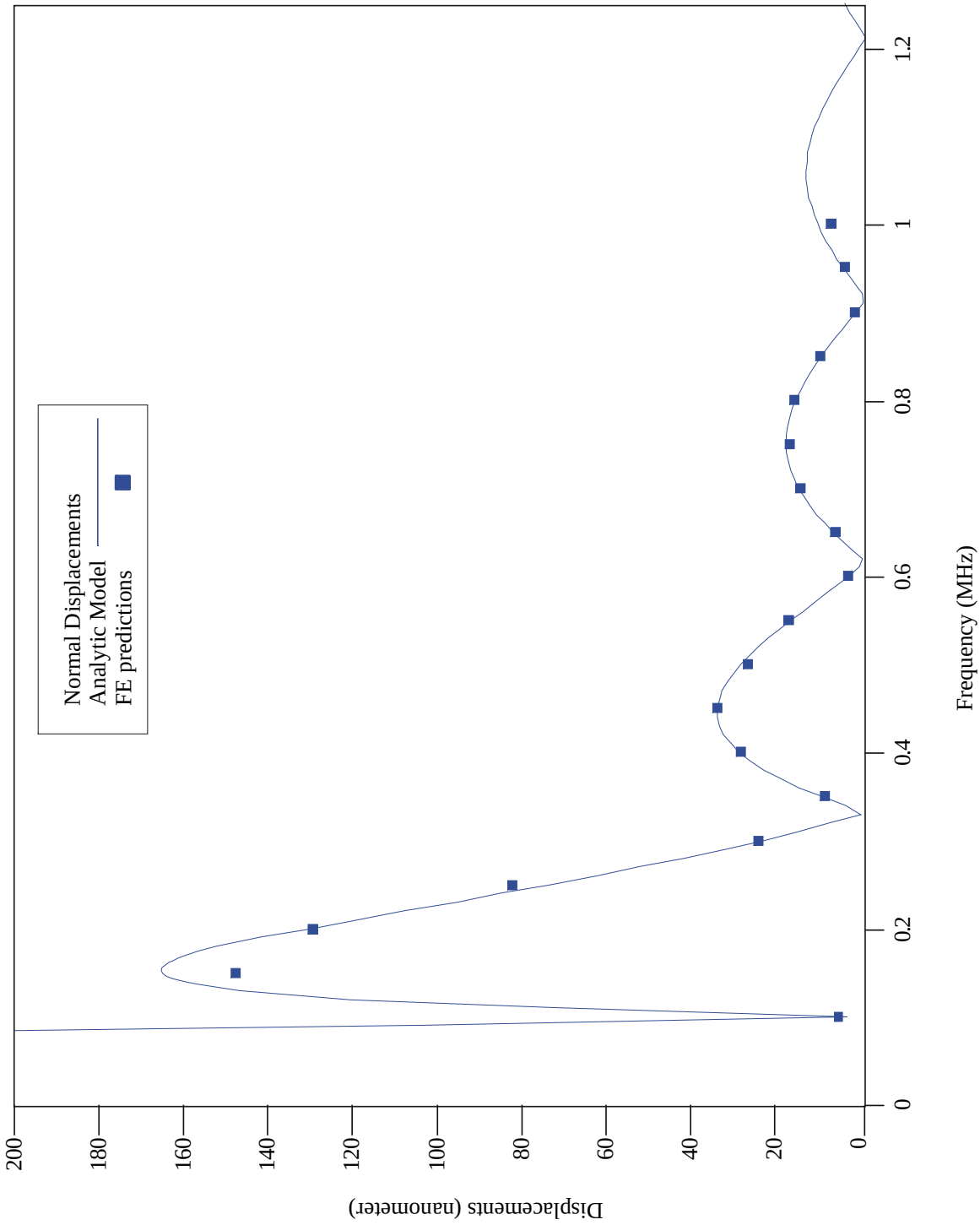

Figure 4.38 : Comparison between finite element predictions and normal mode amplitude calculations for the displacements at the top surface of the PZT-5H layer, in the normal (z) direction for the mode P_1 (lowest flexural mode).

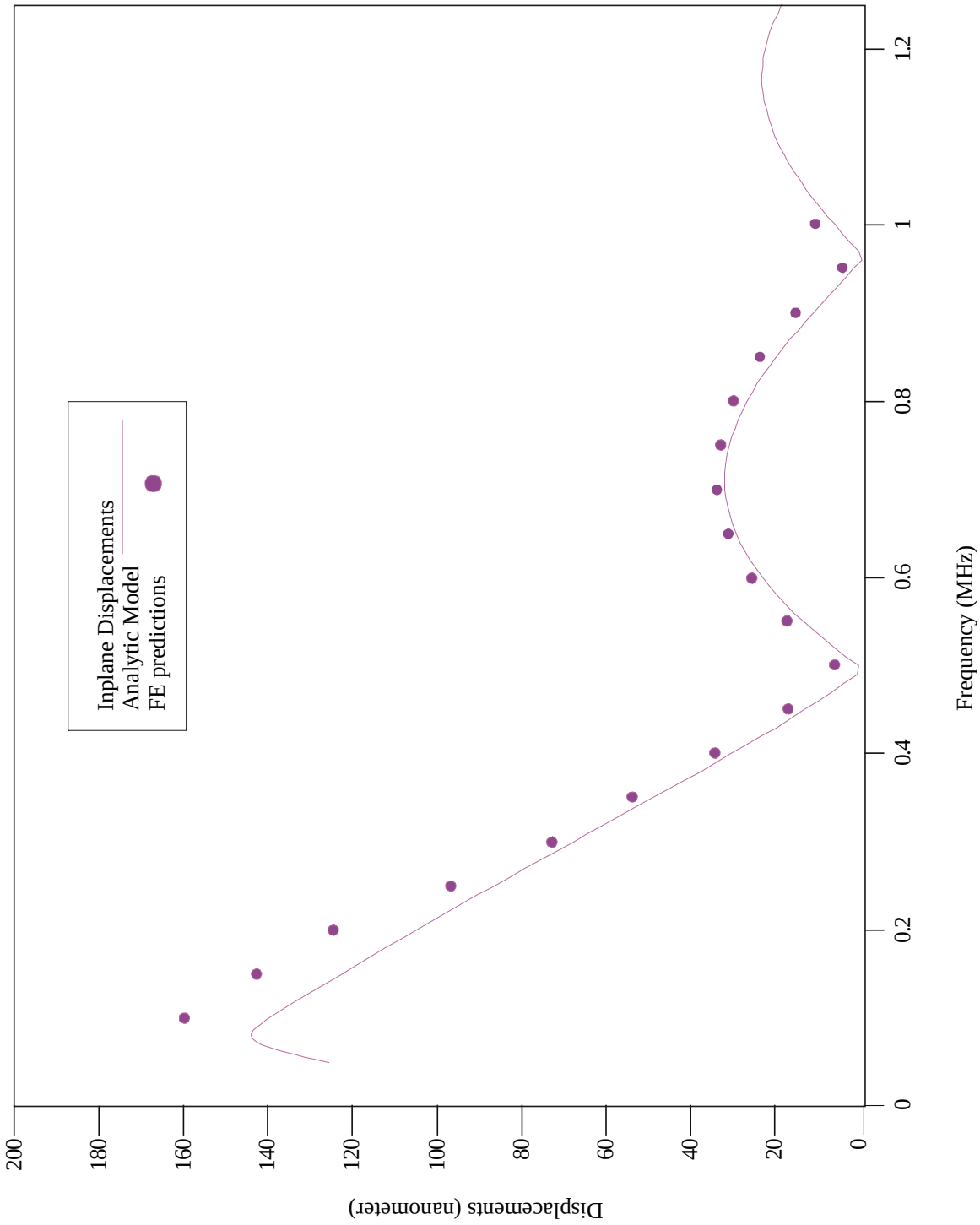

Figure 4.39 : Comparison between finite element predictions and normal mode amplitude calculations for the displacements at the top surface of the PZT-5H layer, in the inplane (x) direction for the mode P_2 (lowest longitudinal mode).

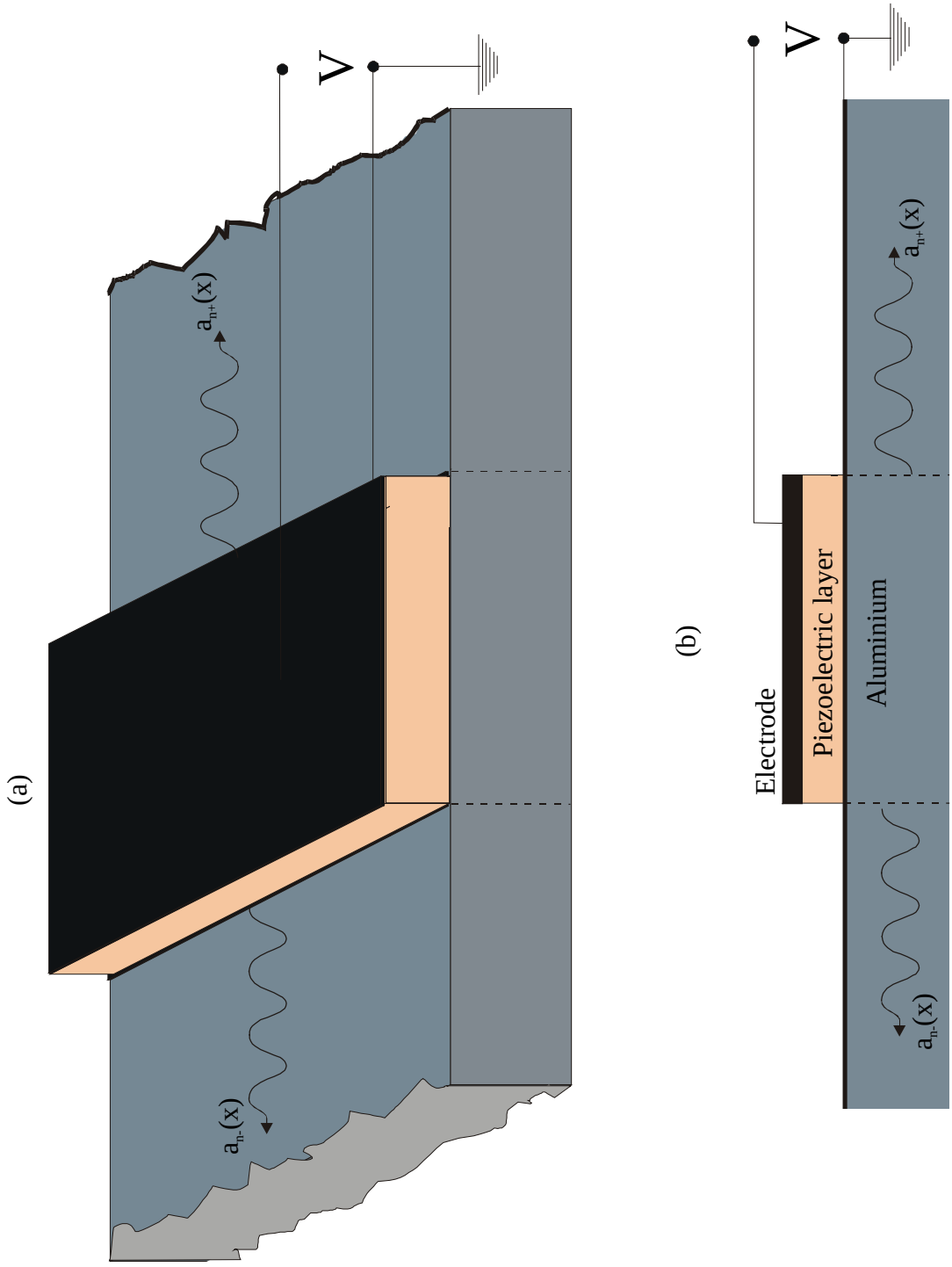

Figure 4.40 : Schematic representation of a single strip transducer. (b) Shows the cross section in the plane (xz) and the waves generated by the transducer.

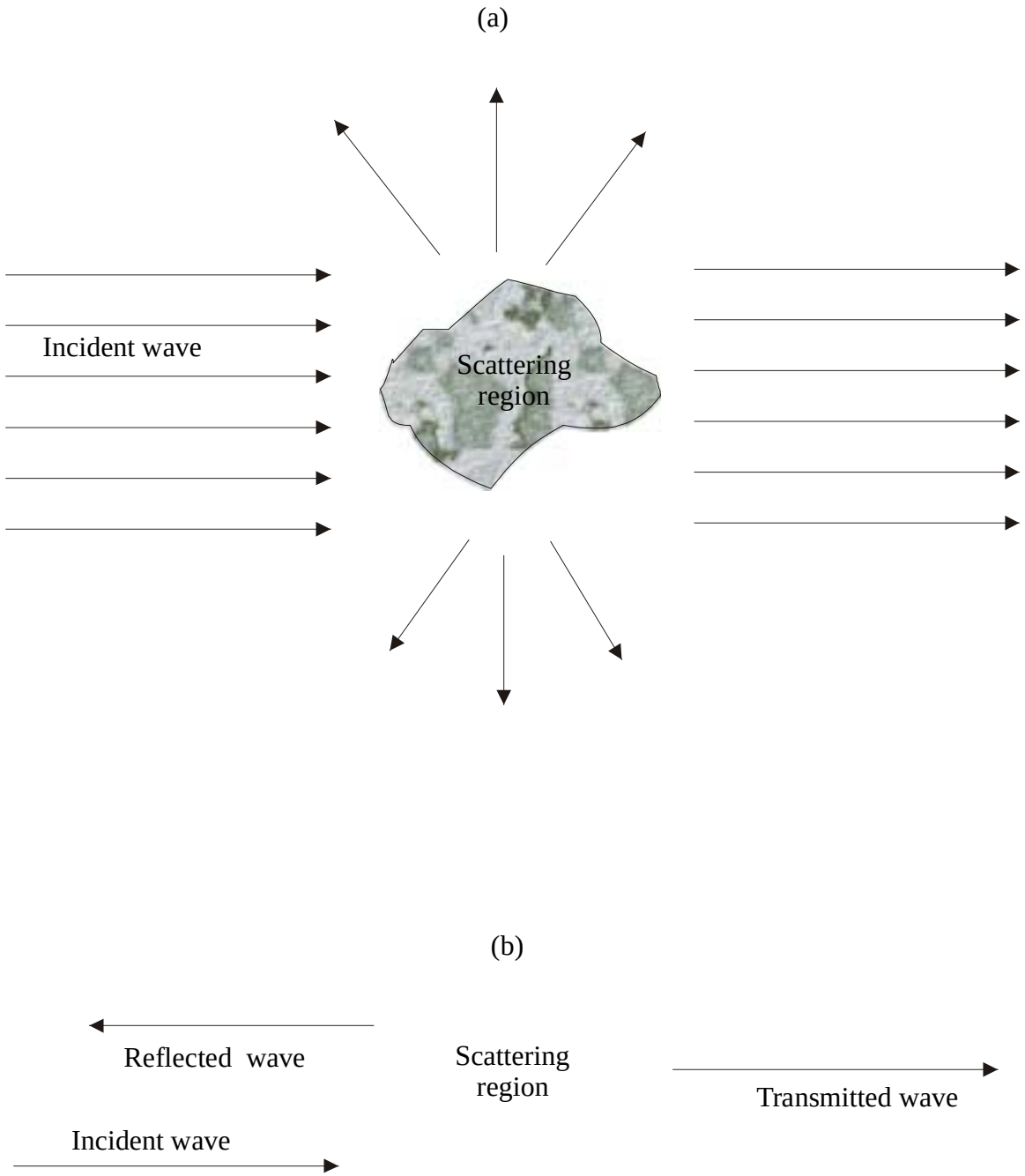

Figure 4.41 : (a) Schematic representation of incident and scattered wave, (b) Schematic representation of one-dimensional transmission-reflection problem

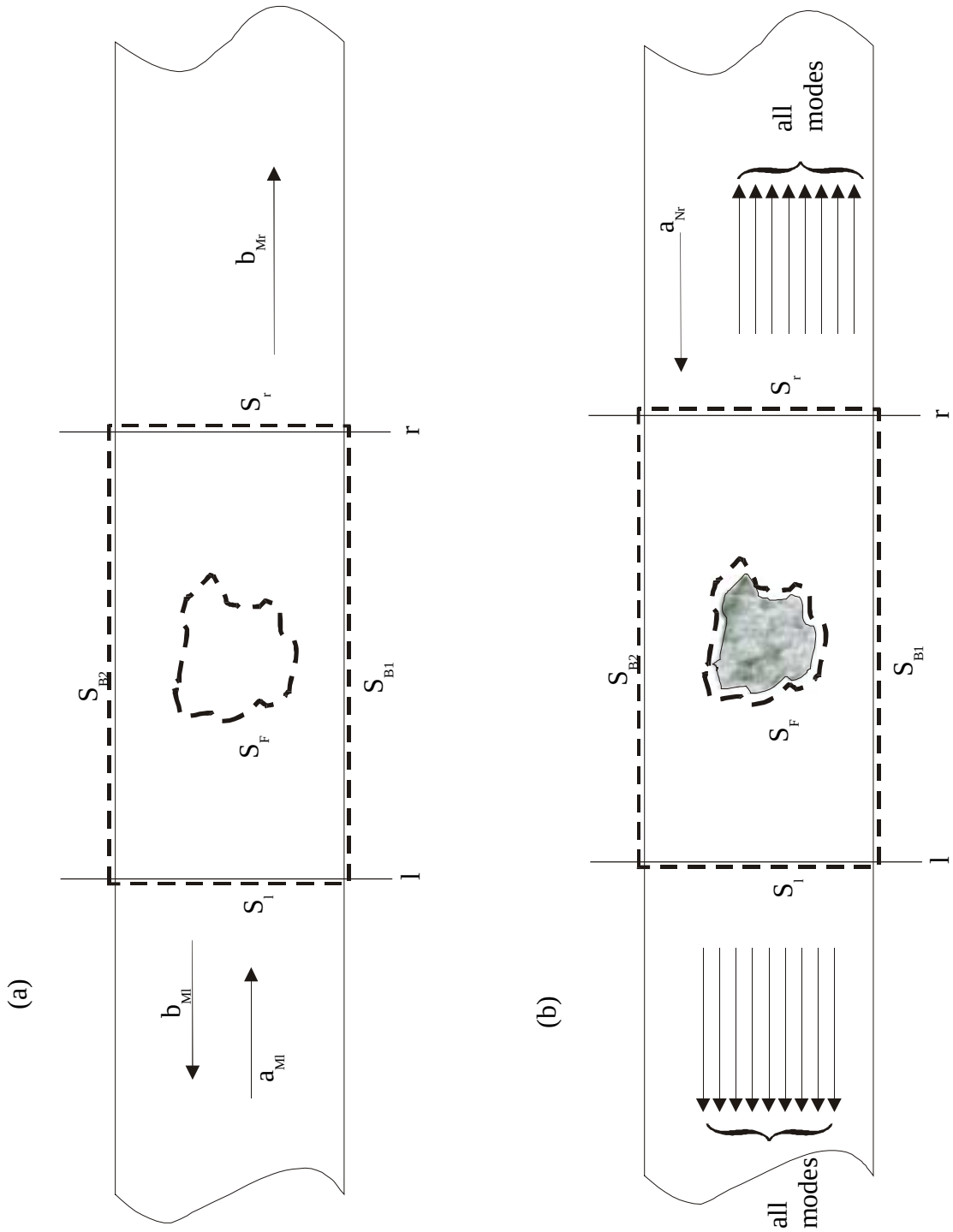

Figure 4.42 : Definition of S-parameters, (a) solution “1”, without the flaw, (b) solution “2”, with the flaw. (From Auld [4.7])

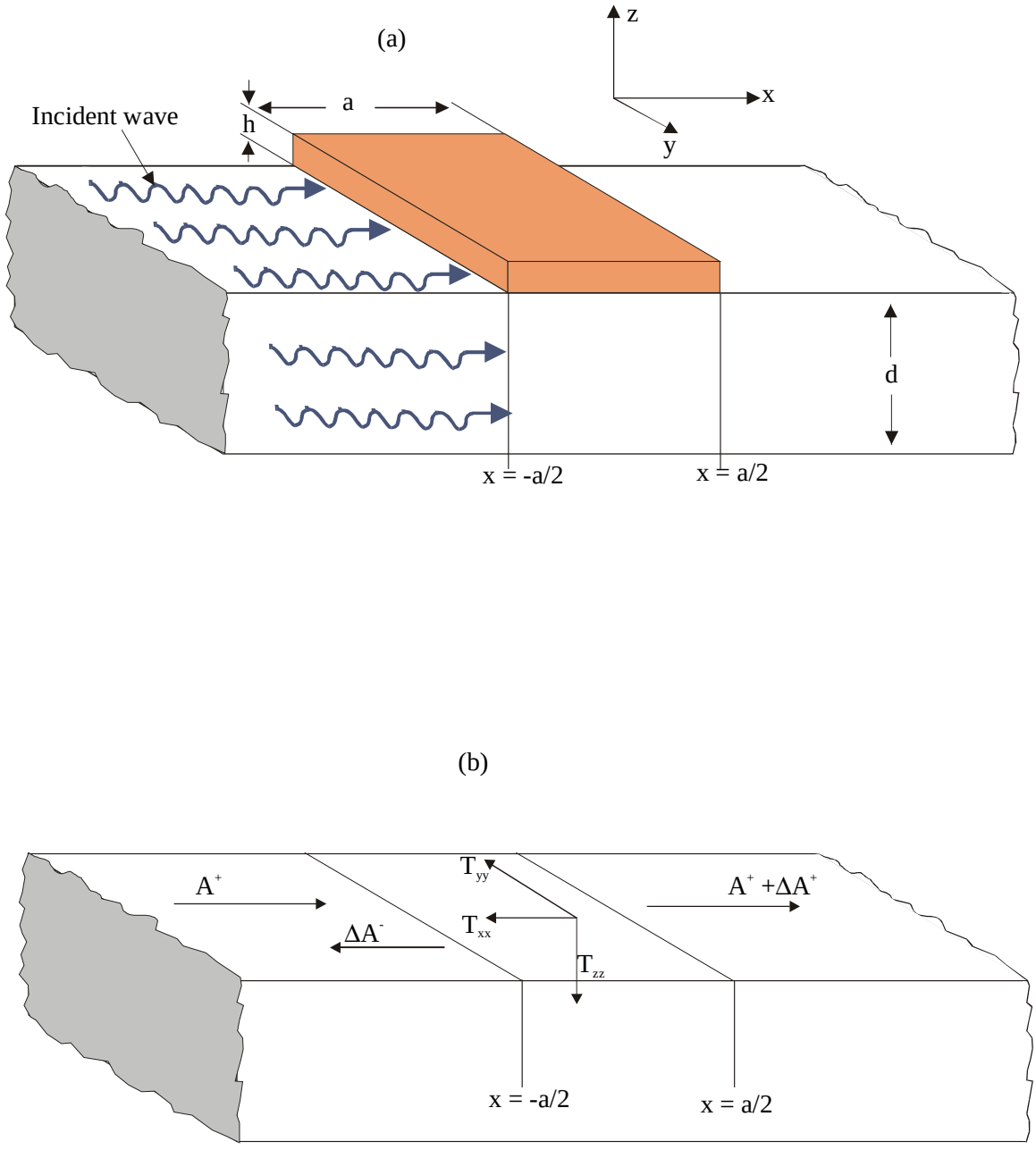

Figure 4.43 : Incident plate modes on a thin strip overlay. (b) Generation of scattered waves by the stress generated at the strip-substrate interface.

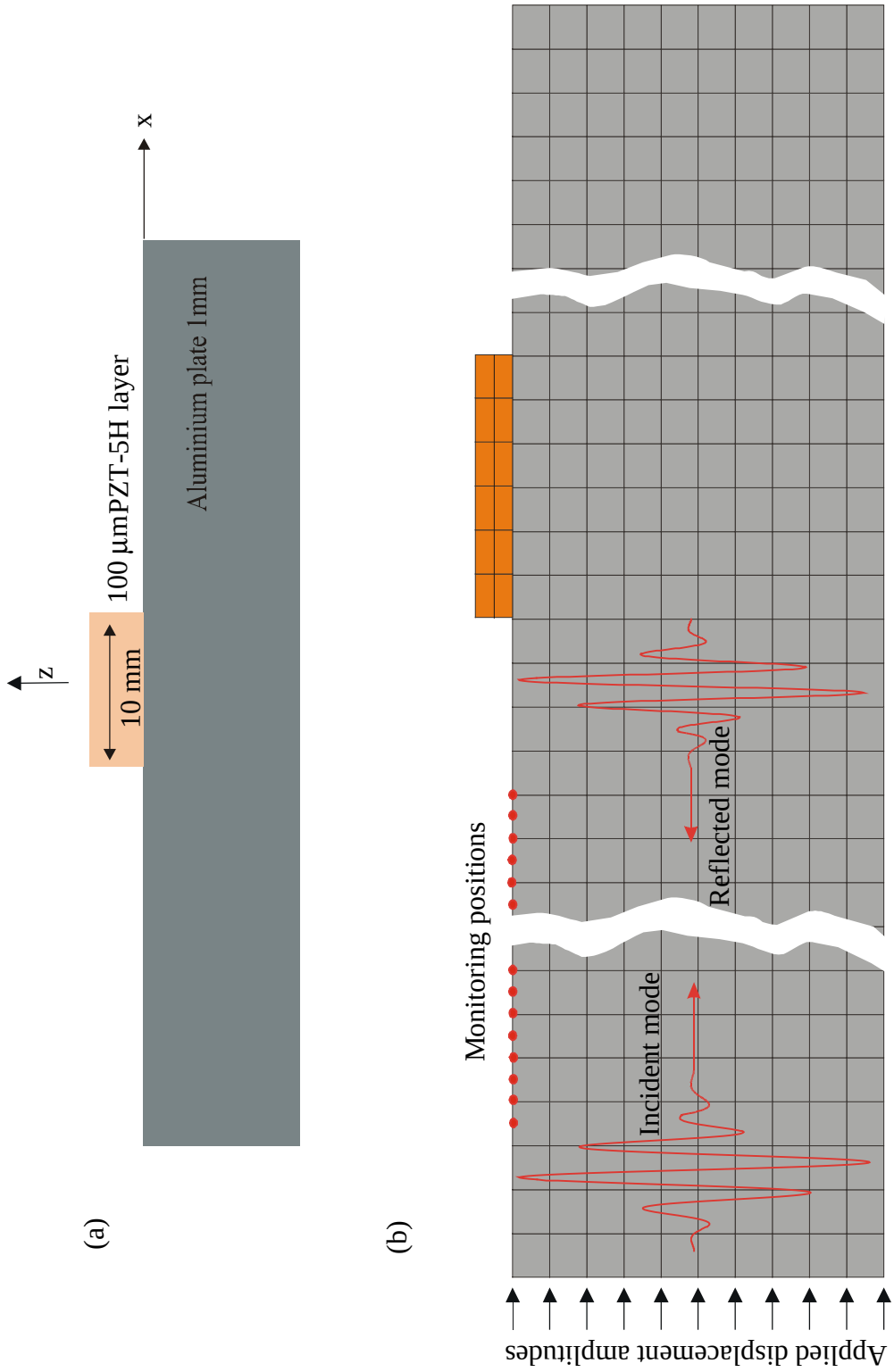

Figure 4.44 : Schematic diagram of the finite element model used to monitor the mechanical displacements in the x- and z-directions at the top surface of the PZT-5H layer for the modes reflected at a 10mm long electrode.

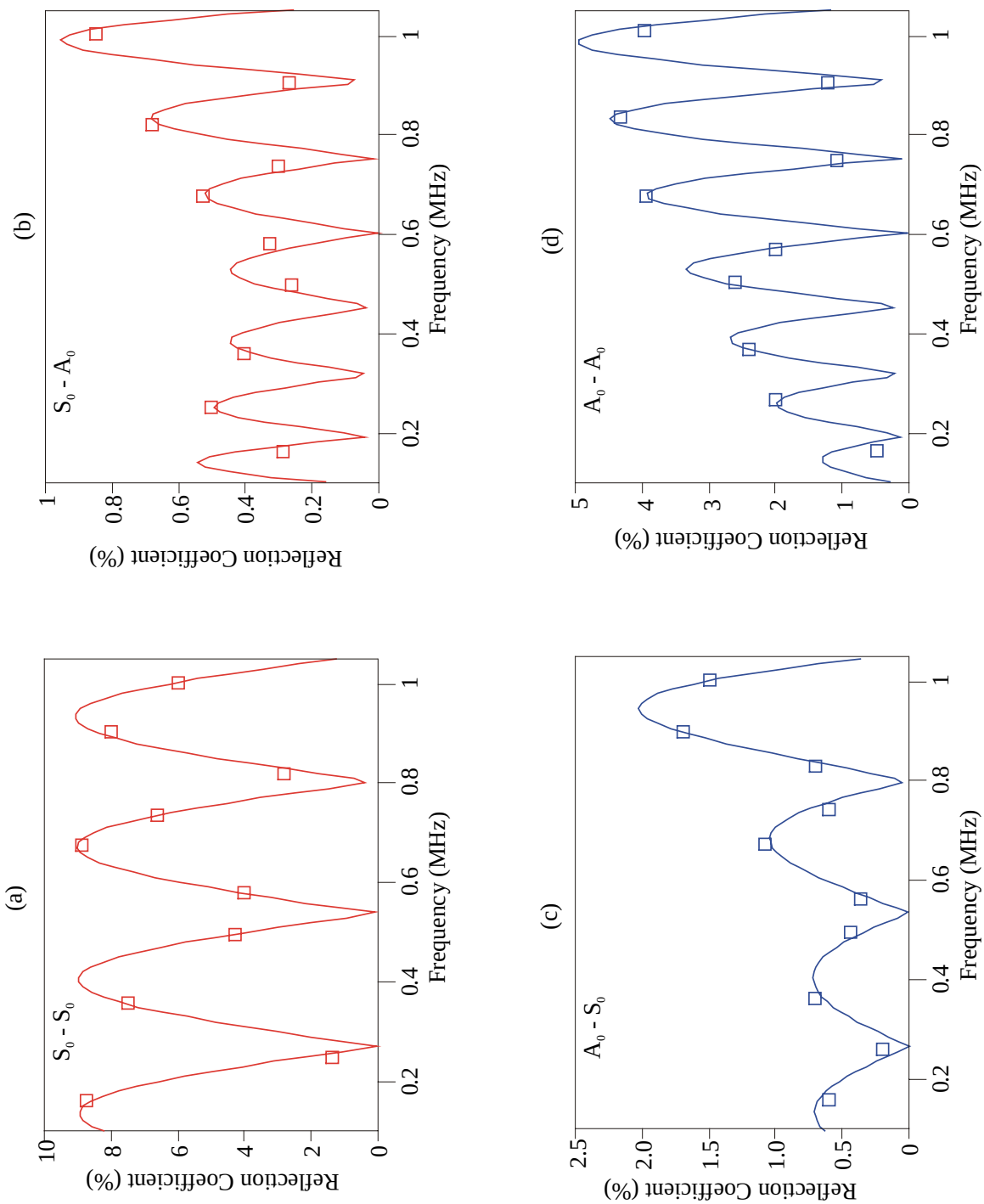

Figure 4.45 : Comparison between finite element predictions (empty square markers) and S-parameter calculations (plain curves) for the reflection coefficients of the mode S_0 into (a) the mode S_0, and into (b) A_0. Reflection coefficients for the mode A0 reflected into (c) S_0 and into (d) A_0.

Chapter 5

Interdigital Transducer for Acoustic Plate Modes

This Chapter, the last before we conclude, presents two direct applications of the analytic model developed in Chapter 4 and we use the FE program presented in Chapter 3 to validate some of the results. The first example is the single strip transducer. Since most of the intermediate calculations have been validated in Chapter 4, only the final result is presented and validated here. Following the single strip transducer, we apply our model to the IDT case. The amplitude of the waves and the impedance of the transducer are derived analytically and a preliminary analysis of a transmitter-receiver set-up is investigated both experimentally and using the FE model.

5.1 SINGLE STRIP

We have two concurrent motives to develop a model for single strip transducers. The first motive is in the perspective of the IDT model. IDTs, for both SAW and Lamb waves, can be seen as a series of “unit cells”. In SAW applications, a cell comprises two electrodes since, because of the absence of a ground plane, the electric field can develop only between two neighbouring electrodes. In plate mode applications, this motivation is partly removed since the main electric field is between the electrodes and the ground plane when the piezoelectric layer is thin. It is not our intention here to deny the existence of lateral electric fields between the electrodes but this lateral field is of second order compared to the through thickness one. Therefore IDTs for Lamb waves can be built as a series of single strip transducers. Hence building up a model for a strip transducer has already achieved most of the work to be done to build a model for IDTs. Moreover it is important to estimate the accuracy of the model on a simple pattern before adding extra assumptions and simplifications.

The second motivation is practical. It is concerned with the need to improve the design of bonded transducers in order to increase the amount of inplane motion generated over that of out-of-plane motion. Initial experiments carried out at Imperial College showed that PZT discs bonded to the surface of a plate generate mainly modes with large out-of-plane surface displacement. Unfortunately, the A_0 Lamb mode is not suitable for long-range inspection of liquid loaded and coated structures since it is very highly attenuative at low frequency-thickness products [5.1]. Figure 5.1 shows a plot of the attenuation of the first four Lamb modes in an aluminium plate immersed in water. It is seen that below the A_1 Lamb mode cut-off frequency, the S_0 Lamb mode is much less attenuated than the A_0 Lamb mode, and will therefore propagate over longer distances in coated or fluid loaded plate-like structures. This particular attribute of the S_0 Lamb mode, i.e. low coupling with surrounding media, is the main reason why the S_0 Lamb mode at low frequency-thickness products is a suitable candidate for long range inspection. The possibilities to improve the design of basic transducers are limited. One possibility is of course to use piezoelectric materials that will enhance the coupling in the inplane direction. This is a very well documented subject and for example Berlincourt [5.2] provided an extensive review of the characteristics of piezoelectric ceramics. Our model would however bring a further advantage since the interaction with the substrate is modelled. Varying the values of the piezoelectric constants in the model would allow multiple piezoelectric configurations to be tested and the relative amount of each generated mode could be compared. Once the piezoelectric material has been chosen, a further possibility to improve the transducer design to increase the coupling with the S_0 mode, is to vary the thickness of the adhesive bond. A study of the influence of the bond thickness on the relative amplitude of the A_0 and S_0 modes has been presented at the QNDE conference [5.3]. This study has been conducted using finite element models. Using the analytical model, each finite element case can be advantageously replaced by a model case with a finite epoxy thickness. Running the model takes few seconds on a desktop PC whereas each finite element case using the same computer took several hours, not counting the time necessary to process the output of the finite element program. The analytic model would not only reproduce the study in less time but would also bring insights on particular features which cannot be identified with the finite element models. In particular the modes in the transducer can be computed, with and without the scattering effect. This could prove to be extremely helpful in numerous situations.

5.1.1 PROBLEM STATEMENT

For these two reasons, we develop here a model for a single strip transducer in order to compute the ratio of the amplitude of the S_0 mode to the amplitude of the A_0 mode when a voltage is applied across the electrodes of a single strip transducer. The transducer is a 100μm thick piezoelectric plate, 10 mm long as shown in Figure 5.2. The electrode at the interface between the strip and the substrate is grounded and an AC voltage is applied at the top electrode. Due to the applied electric voltage, the piezoelectric layer is strained and motion is transmitted to the aluminium plate. On either side of the transducer Lamb waves travel. Because we operate the transducer below 1 MHz, only the S_0 and the A_0 modes can propagate in the plate away from the

transducer. The analytical results are validated with FE predictions. For simplicity the model presented in this section ignores the adhesive bond layer and the electrode is assumed to be infinitely thin. In the IDT model presented later, extra layers have been incorporated.

5.1.2 FULL TRANSDUCER MODEL

In Chapter 4, all the necessary calculations have been developed and validated separately. The dispersion curves for the aluminium plate and the dispersion curves for the substrate/piezoelectric layer system have been computed so that we know which modes propagate in the transducer and away from it. In section 4.6.2, the amplitude of the modes generated in the bilayered system have been accurately calculated, and in section 4.7 the scattering coefficients at the edges of the transducer have been calculated with good accuracy. However a step has been neglected that precludes form building the single strip transducer model directly from these results. Indeed when calculating the scattering coefficients we have been looking at a situation where a mode is incident at the transducer, and not the case where the wave is generated in the transducer and diffracted on its "way out".

5.1.2.1 Scattering Problem

The situation modelled in section 4.7 is depicted in Figure 5.3(a). The scattering of a Lamb mode at a strip can be described globally by five waves. A given wave "I" is incident at the left of the strip. Part of it is the reflected and part continues to propagate rightward. The waves reaching the other end of the transducer are also reflected and transmitted. The wave "R" represents the added effects of all the waves propagating leftward, due to the reflection of the incident wave but also to internal reflections and transmissions of the waves "A1" and "A2". The sum of all transmitted waves is the wave "T" and the reflections in the strip region can be described by two waves propagating in opposite directions, "A1" and "A2". The scattering coefficients calculated in section 4.7 give directly the reflection and transmission coefficient for each incident mode. However, when the transducer is acting as a transmitter, the incident waves are in the excitation region. To find the correct scattering coefficients in that situation, we can consider the situation depicted in Figure 5.3(b). Two waves a_{n-} and a_{n+} are travelling under the transducer. When they reach the edges of the transducer, they are reflected into a_{nR-} and a_{nR+} and also transmitted into a_{nT-} and a_{nT+}. It is clear that the situation in Figure 5.3(b) is very similar to that in Figure 5.3(a). Both situations are in fact the same if we consider the simple case where the amplitude of the incident wave in Figure 5.3(a) is equal to zero and if we add the contribution of the waves generated by the transmitter, a_{n+} and a_{n-}. We know those amplitudes from the transducer case with an infinite piezoelectric layer, solved in section 4.6.2. The amplitudes of the reflected waves inside the excitation region are then readily deduced form the former by adding the phase delays due to their extra distance of propagation. Detailed examples of similar calculations are given in [5.4, Vol. I, Chap. 6 & 8] for bulk waves. Eventually, knowing the amplitudes of the modes a_{n-} and a_{n+} and knowing the scattering parameters at the edges of the strip, the amplitudes of the modes a_{nT-} and a_{nT+} have been calculated.

5.1.2.2 Finite Element Validation

From the magnitudes of the reflections and mode conversions shown in Figure 4.45, it is not expected that the amplitude of the modes propagating away from the transducer are very different from those calculated in case when the layer was considered infinite. However we designed a series of FE models to validate this last stage of calculations. The models are basically the same as those used in the FE validation section 4.6.2.2. The only difference, as shown in Figure 5.4, is the limited size of the piezoelectric layer. This has been chosen to be 10mm long, the size of the electrode. The strip is placed in the middle of the plate. An AC voltage is applied at all the nodes along the top surface of the piezoelectric strip, using a Hanning windowed toneburst. The number of cycles has been chosen to be the best compromise between a very narrow band signal and too long a signal. In general 6 cycles have been used at the lowest frequencies, and that number has been increased up to 8 cycles at 1MHz. 18 models have been computed, from 150 kHz up to 1 MHz in 50 kHz steps. For each model, a series of 200 time histories have been recorded every 0.5mm. The length of the monitoring zone, 100mm corresponds to several wavelengths of each mode. The time histories have been recorded every 0.05 μs over 40 μs. For each model, a two-dimensional Fourier transform has been performed. The 2D-FFT technique allows us to separate each mode propagating in the model, and to identify its direction of propagation.

The ratio of the displacements of the S_0 mode to the displacements of the A_0 mode have been calculated. Figure 5.5 shows the magnitude of the ratio of the inplane displacements. As expected from the behaviour of the two fundamental modes, the ratio is greater than one since the S_0 mode has predominantly inplane motion and the A_0 mode is a bending mode with large normal motion and little compressional motion. The agreement between the normal mode theory and the FE predictions is good. The maxima in the curves are due to the amplitude of the A_0 mode approaching zero, as shown in Figure 4.38, and the ratio becomes ill-conditioned.

5.1.3 CONCLUSION

The single strip transducer is probably the most basic transducer design in rectangular coordinates. Its experimental use is certainly limited although its shape makes it very attractive if the transducer is to be embedded in the structure, for example in between two layers of a composite structure as described by Moulin [5.5]. Other geometries, such as platelet transducer [5.6] could also benefit from the model developed for a single strip. Our primary motivation in studying this particular design was to simplify the transducer as much as possible in order to be able to develop a model which we could test and validate easily. The finite element validations presented in the preceding section show that, despite the number of approximations used along the derivation of the analysis, our model can predict the behavior of a transducer attached to a waveguide with good accuracy. All the intermediate calculations have also been successfully validated what means that each step standing on his own can be used separately for any other purpose.

Starting from one strip transducer, we can now build an array of evenly separated strips. In the next section we will show how the calculations performed for a single strip can be used to analyze the behaviour of an array of strips.

5.2 INTERDIGITAL TRANSDUCER ON A METALLIC PLATE

Interdigital transducers are used in all practical surface-wave devices, and in many of them the performance of the transducer is the main factor determining the device performance. In recent years the IDT technology has been extended to other geometries and in particular to *smart structures* and NDT devices but the principles of operations are the same. The literature on the operation of IDTs for SAW is huge. Reference books on the subject are those from Morgan [5.7] and Mattews [5.8]. Dieulesaint [5.9] recently proposed a condensed although very complete review of the techniques used to model IDTs but the simpler descriptions proposed by Ristic [5.10] and Kino [5.11] are recommended for readers who are not familiar with these devices.

At Imperial College, my colleagues R. Monkhouse [5.12] and P. Wilcox [5.13] developed cheap and flexible PVDF transducers for the generation and detection of Lamb waves in large structures. These IDTs are different from the SAW ITDs because the piezoelectric film is very thin and bonded to a non-piezoelectric thin substrate. These works have been essentially directed toward the development and the practical design of the transducers. Wilcox studied in detail the behaviour of these transducers [5.14] in several experimental situations, and also developed a one-dimensional piezoelectric model [5.15]. The conclusion of his work was that the frequency response of these PVDF transducers restricted them to high order modes when used on structures thicker than 2mm. However it was clearly shown that they work very efficiently as transmitters and receivers of the A_0 mode in 1-2 mm thick plates with which we are concerned in this thesis. Using the model developed for single strip transducers, we will present here a simple model for the analysis of the behaviour of these transducers. It will be shown that in addition to being suitable for exciting and receiving the A_0 mode, they can also selectively generate the S_0 mode.

5.2.1 PLATE MODE EXCITATION BY INTERDIGITAL TRANSDUCERS

Interdigital transducers (IDTs) consist of uniformly spaced sets of strips, which are generally sufficiently long so that their electric fields may be closely approximated by the fields of an infinite periodic array. The operation of these devices is based on the launching and reception of waveguide modes by distributed transducers, each finger acting as a single strip transducer. Due to the electric potential applied on the electrodes, acoustic waves as well as electromagnetic waves are generated in the piezoelectric film. When the finger spacing is equal to half of the wavelength of the signal and the two electrodes of a single finger pair are driven differentially, the waves add constructively and the amplitude of the overall signal is the sum of the signals generated by each finger pair. It is well-known for SAW devices that for such transducers the frequency response may be expressed by simple consideration of an element factor describing the behaviour of a single finger or finger pair, and it is sufficient to know the element factor for the

case of a single finger at finite potential with all other fingers earthed, as a simple superposition of these terms will furnish the element factor for any electrode arrangement based on the infinite periodic array [5.16].

5.2.1.1 Application of the Single Strip Analysis to the Element Factor of an Interdigital Transducer

An even simpler technique can be applied to combine element factors to evaluate the response of a plate mode IDT made of a 100μm thick piezoelectric layer deposited on top of a 1mm aluminium substrate. Indeed in SAW devices the electric field lines are curves starting at one finger and ending at the neighbouring finger driven with an opposite voltage, whereas in a plate mode transducer device, the thickness of the piezoelectric layer is much smaller than the distance between neighbouring fingers, hence the main electric lines are vertical between the each finger and the ground electrode. An experimental study of a plate mode IDT made of interdigital electrodes on top of a PZT film deposited on a metallic substrate [5.17] showed that when a voltage is applied to the electrodes at the upper surface of the piezoelectric layer, the electric field under the electrodes is almost parallel to the normal direction, whilst in the gap between the electrodes the strength of electric field is much weaker. The ground electrode behaves like a mirror for the electric field, which results it in being concentrated under the electrodes. This difference in behaviour compared to SAW devices is due to the presence of the bottom electrode. For a given potential difference, the strength of the electric field depends on the distance between the electrodes. Typically in IDTs, the fingers are a quarter wavelength wide and the gap between the fingers is also equal to a quarter of the wavelength for which the transducer has been designed. Figure 5.7 shows the ratio of the quarter-wavelengths for the S_0 and A_0 modes of a 1mm thick aluminium plate to the thickness of the piezoelectric layer (100μm). This ratio is always above 4 below 1.5 MHz, and as high as 10 and 30 at 500 kHz for the A_0 and the S_0 modes respectively. Therefore the normal component of electric field under the electrodes is much larger than the transverse component between the electrodes. In PZT, this difference is increased further by the fact that the dielectric and piezoelectric constants associated with the normal electric field are larger than the constants associated with the transverse component of the electric field, as seen in Table 4.1. Therefore the grounded electrode serves to concentrate the rf fields in the piezoelectric layer, increasing the transducer impedance and the coupling to the acoustic wave. Comparison between the magnitudes of the curves in Figure 4.34 and values for the coupling of SAW given in the literature [5.4, Vol. II, Appendix 4] clearly shows that the coupling to the acoustic waves is much higher for the plate modes in a grounded piezoelectric layer than for surface waves propagating at the surface of a semi-infinite piezoelectric solid. This property has also been used to develop Rayleigh wave amplifiers [5.18]. Therefore we will approximate the capacitance of the IDT as being equal to the sum of the capacitance under each fingers and therefore, determining the impedance of an IDT transducer bonded to a metallic plate can be done in the same way as developed for a single strip transducer. Equations (4.87) and (4.88) in section 4.6.2.2 give the amplitudes of the modes propagating away from the transducer region and to evaluate them it is necessary to relate the electric displacement D_{Sz} to known quantities such as the applied voltage and current. As seen in section 4.6.3, knowledge of the modal

amplitudes give direct access to the radiation conductance of the transducer. The only problem that is therefore left for us to solve is to find the distribution of the electric fields due to the applied charges at the fingers of the IDT. This is a much more complex problem than the one-dimensional problem solved in section 4.6.4.1.

5.2.1.2 Electrical Field Spatial Distribution

To our knowledge the first paper in which the electrostatic problem, of determining the distributed charges due to a voltage applied to electrodes deposited on a piezoelectric substrate, is that of Coquin and Tiersten [5.19]. In this paper the conformal mapping technique was used to find the potential induced on the electrodes by SAW for an IDT system and also for a system of two identical electrodes. The electrical capacitance of an electrode pair was also calculated. In this paper, as in many other papers concerned only with SAW, the only capacitance is the transverse capacitance. In our thin piezoelectric layer configuration, the main capacitance is that between the electrode and the metallic substrate. Milsom [5.20] and Joshi [5.21] used the classic Green's function technique to solve the electrostatic problem. In this approach the charge distribution over each electrode is approximated by a function with unknown values at a number of discrete points. The problem is then reduced to solving an algebraic system of equations, the number of which being proportional to the number of electrodes and the number of discrete points; the more points the more accurate the calculations. Another technique to solve the electrostatic problem is the analytic function theory, which is based on the property that analytical functions are solutions of Laplace's equation. The problem is therefore reduced to finding the appropriate analytic function. It is a very elegant technique and a solution for IDTs has been given by Goryshnick [5.22]. Recent work by Biryukov [5.23] reports some of the early Russian results, and Peach [5.24] also proposed an analytical investigation of the electrostatic problem for a discrete number of electrode pairs.

The case of an infinite periodic structure of identical electrodes at alternating potentials has been treated by Joshi [5.25] and by Engan [5.26]. The solution proposed by Engan, which is very often referred to in IDT problems, is based on a Fourier series expansion. More details can be found in an earlier work from Chu [5.27] on the propagation of waves in helical waveguide where a similar boundary problem is solved. We used the same method as Engan to find the distribution of the electric field but because the boundary conditions in our problem are different from those for a SAW problem we had to redo all the calculations, starting right from the beginning. It must be pointed out that this analysis will involve rather long and complicated calculations. Most of them are developed in Appendix F and in this section we only present the principles and emphasise the differences between our solution and the well-know solutions for SAW. Therefore, readers who are ready to accept the validity of the solutions for SAW and also that the same IDTs developed for SAW do launch plate waves when the boundary conditions are changed may wish to omit the mathematical validation in the appendix.

The entire IDT problem is solved if we can obtain a relationship between $D_{Sz}(x,h)$, the electric displacement, and the applied voltage V. The electric

displacement can be written as the gradient of the potential (from Eq.(4.108) and Eq.(4.109)) and the potential obeys Laplace's equation in an insulator in absence of free charges. Therefore solving Laplace's equation for the potential gives the electric displacement and from it the amplitudes of the modes. At the upper surface of the piezoelectric layer, the alternation of the electrodes implies (for an infinite electrode array) that the boundary condition, at that plane z = h, is periodic, as shown in Figure 5.8(b)

$$\begin{cases} \Phi(x,h)=0 & \text{for} \quad d(1-a)/2<|x|<d/2 \\ \Phi(x,h)=V & \text{for} \quad 0<|x|<d(1-a)/2 \end{cases} \tag{5.1}$$

with

$$\begin{cases} \Phi(x+d,h)=-\Phi(x,h) \\ \Phi(x+2d,h)=\Phi(x,h) \end{cases} \tag{5.2}$$

It is this periodicity of the boundary condition that allows us to find an analytical solution to Laplace's equation. Indeed, the boundary condition being a periodic function in the variable x, the solution can be sought using the separation of variables technique and expanding the function of the x variable in Fourier series, the difficulty being in finding the coefficients F_m of the Fourier series. The reason why the solution for SAW, found by Engan [5.26], cannot be used here is that in this problem we have another boundary condition: the electric potential is zero at the grounded lower surface of the piezoelectric layer,

$$\Phi(x,0)=0 \tag{5.3}$$

This boundary condition not only changes the solution but even precludes using the same technique as that used for SAW problems. Indeed, although it is not clearly specified in Engan's paper, Engan's solution has been sought and developed for symmetric electrical boundary conditions: the electrode array is at the interface between two semi-infinite spaces, the crystal and the vacuum. In our particular problem the electric field is grounded at the interface between the piezoelectric layer and the metallic plate and therefore the problem is no longer geometrically symmetrical. The symmetry of the boundary conditions in the SAW problem has major consequences. Mathematically this implies that the Fourier coefficients F_m are the same in the crystal and in the vacuum but it also has a very important physical meaning, which we will discuss in the following section.

5.2.1.3 Shielding Problem

Let us imagine a typical SAW device configuration, with two different semi-infinite media above and below the electrodes. If the interface between the two media is assumed to be free electrically, than the electric fields must be continuous at the interface, that is, labelling the vacuum medium I and the piezoelectric medium, medium II,

$$D_z^I = D_z^{II} \tag{5.4}$$

$$\Phi^I\left(x, z=0\right) = \Phi^{II}\left(x, z=0\right) \tag{5.5}$$

where z is the direction normal to the interface. The divergence of the electric displacement is null in each medium and the continuity at the interface implies

$$\varepsilon_{xx}^I \frac{\partial \Phi^I}{\partial x} + \varepsilon_{xz}^I \frac{\partial \Phi^I}{\partial z} = \varepsilon_{xx}^{II} \frac{\partial \Phi^{II}}{\partial x} + \varepsilon_{xz}^{II} \frac{\partial \Phi^{II}}{\partial z} \tag{5.6}$$

and from Eq.(5.5) we have

$$\varepsilon_{xx}^I \frac{\partial \Phi}{\partial x} + \varepsilon_{xz}^I \frac{\partial \Phi}{\partial z} = \varepsilon_{xx}^{II} \frac{\partial \Phi}{\partial x} + \varepsilon_{xz}^{II} \frac{\partial \Phi}{\partial z} \tag{5.7}$$

and if $\varepsilon_{xz}^I = \varepsilon_{xz}^{II} = 0$, which is the case for all hexagonal crystals (and therefore for PZT ceramics), then the boundary interfacial condition imposes

$$\varepsilon_{xx}^I = \varepsilon_{xx}^{II} \tag{5.8}$$

and the solution obtained for z > 0 (medium I) is similar to the solution obtained for the region z < 0 (medium II). Hence the symmetry of the problem implies that the effect of the media is implicit. This symmetry of SAW devices is broken in the Lamb wave problem by the presence of an extra electrode (the ground electrode) and in order to solve the electrostatic problem in the same way as it has been done for SAW devices, it is necessary to "recreate" that symmetry. The simplest solution consists in introducing a shielding electrode, above the transducer, at a distance equal to the thickness of the piezoelectric layer, as shown in Figure 5.8(c). Resorting to this trick allows us to have a problem with symmetric electrical boundary conditions which we can now solve in the same way SAW problems were solved. This is done in Appendix F.

For an interdigital array of infinite length, the electric displacement is given by the Fourier representation

$$D_{Sz}(h, z) = \sum_{n=0}^{\infty} \varepsilon_p^T \coth\left(\gamma h \frac{\pi}{d}(2n+1)\right) F_{2n+1} \sin\left(\frac{\pi}{d}(2n+1) z\right) \tag{5.9}$$

with

$$\gamma = \beta_n \sqrt{\frac{\varepsilon_{xx}^T}{\varepsilon_{zz}^T}} \quad \text{and} \quad \varepsilon_p^T = \sqrt{\varepsilon_{zz}^T \varepsilon_{xx}^T} \tag{5.10}$$

and

$$F_{2n+1} = \frac{\pi V}{d}\frac{P_n\left(\cos(\pi a)\right)}{K\left(\sin(\pi a/2)\right)} \tag{5.11}$$

The coefficients F_m are the ratio of a Legendre polynomial P_n to an hyperbolic function K of first kind, and only the odd coefficients of the Fourier series are non null. Numerical values for both functions can be found in mathematical tables. Therefore the amplitude of the Lamb modes generated by the IDT is given by

$$\left|a_{n+}\right| = \frac{\omega\varepsilon_p^T\left|\Phi_{n+}^*\right|_{z=h}}{4P_{nn}}\left|\sum_{n=0}^{\infty}\coth\left(\gamma h\frac{\pi}{d}(2n+1)\right)F_{2n+1}\int_{-L/2}^{+L/2} j e^{-j\beta_n\xi}\sin\left(\frac{\pi}{d}(2n+1)\xi\right)d\xi\right| \tag{5.12}$$

The integral is given by [5.4]

$$\int_{-L/2}^{+L/2} e^{-j\beta_n\xi}\sin\left(\frac{\pi}{d}(2n+1)\xi\right)d\xi = jLe^{j\beta_n\xi}\left\{\begin{array}{l} e^{j(2n+1)(\pi L/2)}\dfrac{\sin\left(\beta_n+\dfrac{(2n+1)\pi}{d}\right)L}{\left(\beta_n+\dfrac{(2n+1)\pi}{d}\right)L} \\ -e^{-j(2n+1)(\pi L/d)}\dfrac{\sin\left(\beta_n-\dfrac{(2n+1)\pi}{d}\right)L}{\left(\beta_n-\dfrac{(2n+1)\pi}{d}\right)L}\end{array}\right\} \tag{5.13}$$

and near the fundamental resonance of the IDT, where

$$d \approx \lambda_n/2 \qquad \text{and} \qquad \beta_n \approx \pi/d \tag{5.14}$$

only the second term in Eq.(5.13), with n = 0, makes a significant contribution, therefore the amplitude of the positive travelling wave is

$$\left|a_{n+}\right| = \omega L\varepsilon_p^T\frac{\left|\Phi_{n+}^*\right|_{z=h}}{4P_{nn}}\left|\frac{\pi}{d}\frac{V}{K\left(\sin(\pi a/2)\right)}\coth\left(\gamma h\frac{\pi}{d}\right)\right|\left|\frac{\sin\left(\beta_n-\dfrac{\pi}{d}\right)L}{\left(\beta_n-\dfrac{\pi}{d}\right)L}\right| \tag{5.15}$$

and the number, N, of finger pairs in the transducers can be introduced using L = Nd.

5.2.2 RADIATION CONDUCTANCE OF THE TRANSDUCER

The calculations performed in Appendix F also provide two quantities much needed in the evaluation of the transducer performance, the capacitance of a single finger pair, and the radiation conductance. For a transducer with equal finger widths and

spacings, and for N pairs of fingers, the radiation conductance of the transducer is given by

$$R_a = \frac{16}{w\pi^2} Z_n \tag{5.16}$$

where w is the finger width in the direction perpendicular to the sagital plane. The model has been developed on the plane strain assumption, and therefore w is set to 1, but in the capacitance calculations it can be set to its actual value. This formula is very well known in SAW problems [5.4], [5.7], [5.8], [5.28], [5.29],[5.30] and the difference between the SAW and the plate modes comes in the form of the impedance,

$$Z_n = \frac{2}{\omega\left(\varepsilon_0 + \varepsilon_p^T \coth(\gamma h)\right)} \left| \frac{\Delta V_n}{V_n} \right| \tag{5.17}$$

and the capacitance of N finger pairs can be approximated, near the fundamental resonance, by

$$C_T = \frac{Nw\pi^3}{32}\left(\varepsilon_0 + \varepsilon_p^T \coth(\gamma h)\right) \tag{5.18}$$

In the case where the piezoelectric layer is extremely thin compared to the finger spacing, $\coth(\gamma h) \to 1/\gamma h$ and the capacitance is given by

$$C \approx 0.14 \varepsilon_{zz}^T \frac{dw}{h} \tag{5.19}$$

This compares with the use of the assumption that the field is uniform under the electrodes leading to the results

$$C = 0.125 \varepsilon_{zz}^T \frac{dw}{h} \tag{5.20}$$

Thus the approximation is reasonable.

5.3 EXPERIMENTAL VALIDATION AND FINITE ELEMENT INVESTIGATION

The amplitude of the mode generated by the IDT can be obtained using Eq.(5.15). This equation is very similar to that developed by Auld for SAW IDTs. For SAW the modal amplitude equation has been successfully validated [5.28]. Moreover the single strip model has been successfully checked in section 5.1, validating both the principle of the model and also the accuracy of the amplitude calculations for plate modes. Therefore rather than specifically validating Eq.(5.15) by designing a specific finite element model, we decided to compare the model predictions with experimental data.

In 1999 we conducted a study on a set of PVDF interdigital transducers, an emitter and a receiver optimised to generate and receive the mode S_0. Our primary interest was to investigate whether such transducers could generate predominantly inplane motion. Moreover we also wanted to validate some design ideas and investigate the degree of precision to which a complete finite element model could predict the real behaviour of such a *smart structure.* The test sample is depicted in Figure 5.9(a). Two interdigital transducers are deposited on a 1.2mm thick rectangular aluminium plate, 200 mm long and 70 mm wide. Both transducers comprise a single piezoelectric PVDF sheet and a pattern of 16 electrodes embedded in a thin layer of polyamide, each component being bonded using an epoxy based adhesive. The difference between the transducer used in transmission mode and the transducer used as a receiver lies in the shape of the electrodes. The emitter electrode pattern is apodised in the direction of propagation whereas the receiving electrodes are all of the same size. Normal mechanical displacements in between the emitter and the receiver have been measured using a Laser probe. We also measured displacement amplitude on the transducers themselves in order to have an insight on the generation process and also on the attenuation of the waves propagating underneath an IDT.

A finite element study has also been conducted using PZFlex at Strathclyde University before our finite element program FE77 was developed. The dimensions of finite element model, as shown in Figure 5.9(b), have been based on those of the sample. However modelling a 200 mm long plate would have multiplied uselessly the number of elements constituting the model. Hence the distance between the transducer was reduced to 30 mm and the plate does not extend behind the transducers. To avoid unwanted extra reflections from the end of the plate, absorbing boundaries have been used at each end of the aluminium plate.

5.3.1 PVDF MATERIAL CONSTANTS

An important issue when modelling PVDF based transducers is to find the mechanical, dielectric and piezoelectric constants of that material. Some are provided directly by the manufacturing companies and one can also find papers on bulk wave properties [5.31]. To date there seem to have been very few papers on the application of PVDF to surface or plate waves that also provide detailed material constants and, if they do, the data are unusable because of very specific conditions of application (very low temperatures or very high frequencies) [5.32]. There is a major difficulty in performing a theoretical analysis of plate wave propagation in PVDF (and in this sense a finite element model has the same requirements as a theoretical analysis): the very considerable amount of previous work on PVDF has been directed at the study of length expander and thickness longitudinal modes. Thus only a few crystal constants are available and we had to determine the others ourselves.

PVDF is orthorhombic. It has the symmetry properties of point group mm2 and thus has 18 independent constants: C_{11} C_{12} C_{13} C_{22} C_{23} C_{33} C_{44} C_{55} C_{66}, e_{31} e_{32} e_{33} e_{24} e_{15}, ε_{11} ε_{22} ε_{33} and the density ρ. Most of these constants are not experimentally accessible. In developing the set of data we have assumed that PVDF is isotropic in the plane perpendicular the axis of poling. This is similar to assuming that PVDF is a hexagonal

Z-cut crystal. Under these conditions we could reduce the number of independent constants by setting $C_{22} = C_{11}$, $C_{12} = C_{13} = C_{23}$, $C_{55} = C_{66}$, and $C_{44} = 0.5*(C_{11} - C_{12})$. When assuming that PVDF is hexagonal we implicitly assume that it is not uni-axially stretched. Fortunately measurements of longitudinal and shear waves velocities in the XY plane made at Imperial College proved that, at least on the sheets of PVDF we bought form AMP [5.34], this effect was not strong. Moreover since the model is two-dimensional any other assumption would have led to the same apparent conclusions. Also, comparing our measurements with data provided by ITAG we have assumed that the polymer used here is a low draw homopolymer. For our calculations, we have taken some of the constants provided by ITAG [5.33], AMP [5.34] and we have determined the others by matching theoretical data with our experimental values and our assumptions. The constants that we finally used are given in Table 5.1.

5.3.2 EXPERIMENTAL AND FINITE ELEMENT SETUP

Interdigital transducers are spatially selective, thus only certain modes can be excited by a given IDT. This selectivity is achieved when the electrode spacing matches the wavelength of a mode that can propagate in the structure. In the present case the structure is a 1.2mm thick aluminium plate and the modes that can exist and propagate in that plate can be predicted either analytically or using DISPERSE.

The interdigital transducer we used was designed to generate waves having 4mm wavelength, that is the width of a finger pair was set to 4mm. Since the wavelength is the ratio of the phase velocity to the frequency, there is at the most one frequency at which each mode will have a wavelength that will match the electrode spacing. Figure 5.10(a) shows the phase velocity dispersion curves of the first four Lamb modes for a 1.2 mm thick aluminium plate. It is seen that all four modes could be generated using a 4mm wavelength IDT at respectively 0.5 MHz, 1.3 MHz, 1.8 MHz and 2.4 MHz, for modes A_0, S_0, A_1 and S_1. However Figure 5.10(b) shows that the mode S_1 is very dispersive at 2.4 MHz and will not propagate over long distances. All other modes are in weakly dispersive regions and could be generated. Figure 5.10(c) shows the dispersion curves in a frequency versus wavenumber view.

The emitting transducer is driven with a 8 cycle rectangular toneburst at 1.3 MHz to generate the S_0 mode. Figure 5.11(a) shows the applied voltage time variation. Its frequency spectrum is shown in the diagram on the right. Since a rectangular window was used in the time domain, the frequency spectrum exhibits a number of side lobes. The highest sidelobe of a rectangular window is only 15dB down from the maximum of the spectrum which is a disadvantage but on the other hand the main lobe bandwidth is narrower than for any other window [5.35]. Figure 5.11(b) shows the charge variation with time on the 1st electrode and Figure 5.11(c) shows the time variation of the charge on the bottom electrode which in the case of a metal structure is the structure itself. This is displayed as a time-frequency plot in Figure 5.11(d).

For most metal substrates it is reasonable to assume infinite conductivity so that a static electric field cannot be maintained in the interior of the substrate. This field does exist in a perfect dielectric medium. It is seen in Figure 5.11(b) that the charge does not

go to zero instantaneously after the volatge drops down to zero and this could first be seen as an effect of bad conductivity of the electrodes. However in the FE model the voltage is not applied on the top of the electrodes but the electrodes are virtually defined at the interface between the copper electrodes and the PVDF layer. Hence the tail in Figure 5.11(b) is due to the presence of induced electric charges in the vicinity of the electrode in the piezoelectric layer. This pattern is indicative of resonace occuring in the IDT when the electrodes are not connected to any external electric circuit. During the time the voltage is applied, charges are present at the location of the electrodes. In this model the voltage is directly applied to the electrode. When the driving signal is switched off, the charges are in an unstable state. If there was a resistance, i.e. an electrical extrenal circuit, the charges would be dissipated, but since no electrical loss has been included in the model, the charges propagate back and forth between the electrodes with a frequency corresponding to the resonant frequency of the electrode pattern until they reach an equilibrium state or dissipate. When the excitation ends the system continues to oscillate. If there are no losses at all it will oscillate indefinitely.

The charge at the bottom electrode carries useful information about the nature of the piezoelectricaly stiffened acoustic waves that propagate within the piezoelectric layer. Going back to the assumption, used to derive the analytic model, that an interdigital transducer can be seen as a periodic succession of capacitors, during the time the IDT is driven, the presence of charges under the electrodes induces charges of the opposite signs on the bottom electrode. According to the sinusoidal variation of the applied voltage the charge distribution on the driven electrodes and on the bottom electrode vary periodically. When the excitation is switched off the standing wave is no longer sustained and separates into two waves that propagate in opposite directions. The signal shown in Figure 5.11(c) is the result of the interference between these two waves. These waves are piezoelectricaly stiffened acoustic waves whose properties depend on the crystalline symmetry of the piezoelectric material [5.4]. This interference pattern is highlighted in Figure 5.11(d) which shows a contour plot of the charge signal at the bottom electrode in time-frequency space. This time-frequency graph represents the power spectrum of the signal at a given time, that is a measurement of the energy at various frequencies at a given time. It can be seen that the maximum of each peak occurs at the same frequency which is 1.3 MHz. This means that the interfering waves have the same centre frequency which is the necessary condition for two waves travelling in opposite directions to combine to form a standing wave. Hence once the excitation is switched off two waves of centre frequency 1.3 MHz, having a wavelength matching the charge distribution on the top electrodes, i.e. 4 mm, travel in the aluminium plate.

5.3.3 PROCESSING OF THE FINITE ELEMENT RESULTS

In this model we were mainly concerned with mechanical results such as surface particle displacements in order to compare them with experimental values. The results have been grouped in 3 series, one for the surface particle displacements predicted and measured on the emitting transducer, one for the surface particle displacements predicted and measured on the plate itself between the transducers, and finally one

series for the surface particle displacements predicted and measured on the receiving transducer.

5.3.3.1 Transmitting IDT

Figure 5.12(a) to (d) show some examples of snapshot views at different times during the time when the excitation signal was applied to the transducer. The diagrams on the right of each snapshot show the part of the input voltage applied so far. Snapshots (a) and (b) show that the electrodes start to move as rigid bodies and as the pulse starts to be constituted significant motion starts to appear between the electrodes as shown in Figure 5.12(c) and (d). This is indicative of the formation of the travelling piezoelectricaly stiffened acoustic modes.

Figure 5.13(a) shows the absolute out-of-plane surface displacements measured using the laser interferometer on each electrode and between each electrode of the transmitting IDT. The electrodes have been numbered and can be related to Figure 5.8(a) It can be seen that the displacements are sometimes greater between the electrodes than on the electrodes. Also the displacement pattern is not symmetric with respect to the centre of transducer. This is due to poor signal-to-noise ratio due to low reflectivity of the polyamide and also, but less significantly, to the fact that the upper surface of the IDT is not perfectly flat.

Figure 5.13(b) shows the predicted out-of-plane surface displacements and direct comparison with the measured values is possible. Also dotted lines trace the electrode pattern so that it clearly appears that the maximum displacements occur on the electrodes while the displacements are a minimum between the electrodes. The even numbered electrode and the odd numbered electrodes were driven in opposite phase (+V and -V) but this does not make any difference since only absolute values of the displacements are plotted. The predicted values shown on Figure 5.13(b) have been obtained by first plotting snapshot views of the out-of-plane surface particle displacements at different times and then by extracting for each node the maximum displacement. It can be seen that the FE predictions are not symmetric with respect to the centre of transducer; symmetry would be expected since the IDT launches waves in both directions and the electrode pattern is geometrically symmetric. However at the scale of the finite elements constituting the model, the IDT is not symmetric since an even number of nodes has been used.

The mean value of the measured displacements is 2.54 nm and the mean value of the predicted displacements is 3.22 nm as seen in Figure 5.13(b). Considering the likely differences between the PVDF materials properties and the material constants defined in the FE model, that attenuation of the PVDF and epoxy have not been modelled and also considering that laser measurement accuracy is affected by the reflectivity of the surface when the magnitude of the displacements is of the order of the noise level, these results are surprisingly good.

5.3.3.2 Displacements at the Surface of the Plate.

The two transducers are 30 mm apart in the model and surface displacements in two directions were monitored at each surface node. Because of very slow propagation in the PVDF sheet the element size has to be as small as 0.05 mm making the time step very small also ($5.6\ 10^{-8}$ s). In order to perform 2 dimensional Fourier transforms in the in-plane and the out-of-plane directions and to obtain sufficient resolution to separate modes that could propagate in the aluminium plate, we have monitored the longest possible distance, i.e. 30mm, over a period of 30 μs. (a) shows a 3 dimensional view of the 2D-FFT performed in the direction normal to the plate. It can be seen that there is one major mode and traces of two other modes. The 2D view shown in (b) allows dispersion curves to be superimposed. The usual FFT transforms the time domain into the frequency domain. Performing a second FFT on the spatial data, i.e. along the monitored nodes, transforms the spatial domain into the wavenumber domain. Hence a 2D-FFT provides a view in the frequency-wavenumber plane and dispersion curves have to be traced in this plane (see Figure 5.9(c)) before being overlaid on the 2D-FFT view. In (b) it immediately appears that the main mode propagating in the plate is the S_0 mode. Modes A_0 and A_1 also propagate but with a very low amplitude.

2D-FFT are performed from a series of time traces monitored at different nodes along the direction of propagation of the waves. Figure 5.15(a) to (c) show time histories of the signal that propagates from the emitter toward the receiver at the surface of the plate, at different locations along that direction. The interference phenomena seen in these figures can be explained by the multi-mode propagation. Each mode propagates with a different group velocity and interferes constructively or destructively at different moments in time.

Experimental measurements of out-of-plane surface displacements have been done using the laser interferometer. Figure 5.16 shows the comparison between these measured absolute displacements and the maximum of each of the time traces monitored at each node between the emitter and the receiver. The absolute amplitude of the S_0 mode, calculated from Eq.(5.15) is also shown as a single line. It is very encouraging that the mean values from the experiments, finite element predictions and analytical calculations are within 0.3nm of each other, given the rough nature of the experiments and the number of simplifications made in the models.

5.3.3.3 Receiving IDT

The last series of measurement and predictions concern the receiving IDT. This one was passive and, in the finite element model was not connected to any electrical external circuit. Only mechanical degrees of freedom have been monitored.

Figure 5.17 shows snapshot view of the displacement measured at nodes along the receiver. Considering the group velocity of the S_0 mode, 7 to 8 μs should be the time needed for the S_0 mode to reach the receiver. In Figure 5.17(a) we see that the S_0 mode has been preceded by another signal. Figure 5.17(b) shows the arrival of the pulse. It is

clearly seen that the acoustic signal is preceded by an electromagnetic signal that activates the piezoelectric effect.

Figure 5.18(b) shows the displacements measured on and between the electrodes. It is seen that the amplitude decays from the first electrode (on the emitter side) toward the last electrode. Displacements are between 1 and 3 nanometers whereas they are between 1 and 5 nanometers on the emitting transducer (see Figure 5.13(b)). Also it is seen that displacements on the top of the receiver are 1 to 3 times larger than displacements on the plate, hence the receiver does not act only as an electro-mechanical converter but also as an amplifier.

Figure 5.18(a) shows the predicted surface displacements on and between the electrodes together with the measured displacements. Once again the mean value are very close and the shape of the predicted curve reproduces that of the measured curve. However the predictions are much sharper than the measurements. There are two explanations for that. First the laser spot has a dimension that is not negligible compared with the width of the electrodes, so no more than one or two measurements have been done on each electrode. Secondly, each electrode has been modelled with 15 nodes so the displacement distribution on each electrode is indicative of the charge density distribution underneath each electrode. At the edges of the electrode there is a concentration of the charges and the charge distribution follows the shape of a quadratic or cubic function of minimum magnitude at the middle of the electrode and maximum magnitude (theoretically infinite) on the sides. The FE predictions seem to show such a distribution.

In Figure 5.18(b) one can notice the small displacement measured on the first electrode whereas it is predicted to be very large. This is due to the fact that during the manufacturing process some adhesive spread beyond the transducer making measurements on the first and last electrodes very difficult.

It also can be seen in Figure 5.18(a) and in Figure 5.18(b) that the magnitude of the displacement decays dramatically along the transducer. Both measurements and predictions exhibit a large decay of the displacements. It is particularly interesting to notice that the material attenuation of PVDF and epoxy have not been modelled. Hence the decay of the predicted amplitude is only due to some internal phenomena. It is believed that internal scattering as well as mechanical and electrical loading (MEL) [5.7] are responsible for this decay. The analytical model we are developing should take these effects into account.

Figure 5.19 shows the predicted displacements at the upper surface of the IDT and the predicted displacements at the interface between the plate and the IDT. The amplification effect is still noticeable. The ratio at each node of the displacements at the upper surface to the displacements at the interface has been calculated and is shown on the same graph. This ratio is similar for each finger pair and is a maximum at the electrodes and minimum between the electrodes. Hence it is believed that this ratio is a representation of both the direct piezoelectric effect and the indirect piezoelectric effect. The average magnitude of this effect is 2.35. The effect is non zero between the electrodes and this is believed to be a representation of the coupling between the

electrodes, in other words each electrode does not act as an simple capacitor but the electric field is affected by the presence of neighbouring electrodes. This point is to be kept in mind when solving the receiver problem. The analytical model developed can easily be used to model the receiver, since there is a reciprocity relationship between the fields emitted by the transmitter and those received by the receiver. However the transmitter model has been developed on the assumption that each finger acts as a strip capacitor and the FE results show that this is not quite the case in a real receiver.

5.4 DISCUSSION

In the first part of this Chapter the single strip model has been validated very successfully. In the second part, an initial investigation of an IDT transmitter gave very encouraging agreement between finite element predictions, analytical analysis and experiments. However this was only a preliminary study and more work would be needed to validate thoroughly for their complex nature and to investigate different possible sources of errors. Previous studies of SAW devices showed that the phenomena that influence the behaviour of these devices can be classified into first-order and second-order effects [5.7]. For SAW, second-order effects have been shown to have limited effect on the overall performance of the transducer. However their probable existence in plate mode IDTs may explain the discrepancies between the analytical results, the experimental measurements and the finite element predictions.

The receiver case shown good agreement between finite element predictions and experiments, however an analytical model must still be developed for this case.

REFERENCES

[5.1] **Wilcox**, P. D., Cawley, P., and Lowe, M. J. S., "Lamb and SH Wave Transducer for the Inspection of Large Areas of Thick Plates", in Review of Progress in Quantitative NDE, eds. D.O. Thompson and D.E. Chimenti, American Institute of Physics, New York, Vol. 19, pp. 1049-1056, 2000.

[5.2] **Berlincourt**, D., Curran, D. R. Jaffe, H., "Piezoelectric and Piezomagnetic Materials", Physical Acoustics, Vol. I(A), ed. Masson, W. P., New York, Academic Press New York, pp. 169, 1964.

[5.3] **Marty**, P. N., Lowe M. J. S., and Cawley, P., "Finite Element Predictions of Guided Ultrasonic Wave Fields Generated by Piezoelectric Transducers", in Review of Progress in Quantitative NDE, eds. D.O. Thompson and D.E. Chimenti, American Institute of Physics, New York, Vol. 20, pp.1037 -1044, 2001.

[5.4] **Auld**, B. A., *Acoustic Fields and Waves In Solids*, Vol. II, 2nd ed., Robert E. Krieger Publishing Compagny, Malabar, Florida, 1990.

[5.5] **Moulin**, E., Assaad, J., Delebarre, C., Kaczmarek, H., and Balageas, D., "Piezoelectric Transducer Embedded in Composite Plate: Application to Lamb Wave Generation", J. Appl. Phys., Vol. 82, pp. 2049–2055, 1997.

[5.6] **Gachagan**, A., Reynolds, P. and Hayward, G., "McNab, A., "Construction and Evaluation of a New Generation of Flexible Ultrasonic Transducers", IEEE Ultrasonics Symposium, pp. 1-4, 1996.

[5.7] **Morgan**, D. P., *Surface-Wave Devices for Signal Processing*, Elsevier, Amsterdam, Oxford, New York, Tokyo, 1991.

[5.8] **Mattews**, H., *Surface Wave Filters*, John Wiley & Sons, New York, London, Sydney, Toronto, 1977.

[5.9] **Dieulesaint**, E. and Royer, D., *Elastic Waves in Solids*, 2nd edition, Chapter 7, John Wiley, 2000.

[5.10] **Ristic**, V. M., *Principles of Acoustic Devices*, Chapters 4 & 8, John Wiley & Sons, New York, London, Sydey, Toronto, 1983.

[5.11] **Kino**, G. S., *Acoustic Waves: Devices, Imaging and Analog Signal Processing*, Prentice Hall Inc., Englewood Cliffs, New Jersey, 1987.

[5.12] **Monkhouse**, R. S. C., Wilcox, P. D., and Cawley, P., "Flexible Interdigital PVDF Transducers for the Generation of Lamb Waves in Structures', Ultrasonics 1997.

[5.13] **Wilcox**, P., D., Monkhouse, R. S. C., Lowe, M. J. S. and Cawley, P., " The use of Huygens' Principle to Model the Acoustic Field from Interdigital Transducers", Review

of Progress in Quantitative NDE, eds. D.O. Thompson and D.E. Chimenti, Plenum Press, N. Y., Vol. 17, 1998.

[5.14] **Wilcox**, P. D., *Lamb Wave Inspection of Large Structures using Permanently Attached Transducers*, Ph.D. Thesis, University of London, (Imperial College, Mechanical engineering Department), 1998.

[5.15] **Wilcox**, P., D., Monkhouse, R. S. C., Cawley, P., Lowe, M. J. S. and Auld, B. A., "Development of a Computer Model for an Ultrasonic Polymer Film Transducer System", NDT & E International, Vol. 31(1), pp. 51-64, 1998.

[5.16] **Peach**, R. C., "A Normal Mode Expansion for Piezoelectric Plates and Certain of its Applications", IEEE Transaction on Ultrasonics, Ferroelectrics, and Frequency Control, Vol. 35, pp. 593-611, 1988.

[5.17] **De Cicco**, G., "Elastic Surface Wave Devices Based on Piezoelectric Thick Films", IEEE Ultrasonic Symposium Proceeding, pp. 281-285, 1993.

[5.18] **Kino**, G. S. and Reeder, T., "A Normal Mode Theory for Rayleigh Wave Amplifier", IEEE Transaction on Electron Devices, Vol. ED-18, pp. 909-919, 1971.

[5.19] **Coquin**, G. A. and Tiersten, H. F., "Analysis of the Excitation and Detection of Piezoelectric Surface Waves in Quartz By Means of Surface Electrodes", J. Acoustic. Soc. Am., Vol. 41, pp 921-939, 1966.

[5.20] **Milsom**, R. F., Reilly N. H. C., and Redwood, M., "Analysis of Generation and Detection of Surface and Bulk Acoustic Waves by Interdigital Transducers", IEEE Transaction on Sonics and Ultrasonics, Vol. SU-24, pp. 147-165, 1977.

[5.21] **Joshi**, S. G. and Jin, Y., "Excitation of ultrasonic Lamb Waves in Piezoelectric Plates", J. Appl. Phys., Vol. 69, pp. 8018-8024, 1991.

[5.22] **Goryshnik**, L. L. and Kondrat'ev, S. N., "Excitation of SAW by Interdigital Transducers", Sov. Phys.-Radio Eng. Electon., Vol 19(8), pp. 1719-1728, 1974.

[5.23] **Biryukov**, S. V. and Polevoi, V. G., "The Electrostatic Problem for the SAW Interdigital Transducers in an External Electric Field", IEEE Transaction on Ultrasonics, Ferroelectrics, and Frequency Control, Vol. 43(6), pp. 1150-1159, 1996.

[5.24] **Peach**, R. C., "A General Approach to the Electrostatic Problem of SAW interdigital Transducer", IEEE Transaction on Ultrasonics, Ferroelectrics, and Frequency Control, Vol. 28(2), pp. 96-105, 1981.

[5.25] **Joshi**, S. G. and White, R. M., "Excitation and Detection of Surface Elastic Waves in Piezoelectric Crystlas", J. Acoust. Soc. Am., Vol. 46(1), pp. 17-27, 1969.

[5.26] **Engan**, H., "Excitation of Elastic Surface Waves by Spatial Harmonics of Interdigital Transducers", IEEE Transaction on Electron Devices, Vol. ED16, pp. 1014-1017, 1969

[5.27] **Chu**, C. M., "Propagation of Waves in Helical Waveguide", J. Appl. Phys., Vol. 29(1), pp. 88-99, 1958.

[5.28] **Auld**, B. A. and Kino, G. S., "Normal Mode Theory for Acoustic Waves and its Application to the Interdigital Transducer", IEEE Transaction on Electron Devices, Vol. ED-18, pp. 898-908, 1971.

[5.29] **Kino**, G. S. and Wagers, R. S., "Theory of Interdigital Couplers on Non-Piezoelectric Substrates", J. Appl. Phys., Vol. 44, pp. 1480-1488, 1973.

[5.30] **Smith**, W. R. Gerard, H. M. Collins, J. H. Reeder, T. M., and Shaw, J., "Analysis of Interdigital Surface Wave Transducers by use of an Equivalent Circuit Model", IEEE Transaction on Microwave Theory and Techniques, Vol. 17, pp. 856-864, 1969.

[5.31] **Ohigashi**, H., "Electromechanical Properties of Polarized Polyvinylidene Fluoride Films studied by the Piezoelectric Resonance Method", J. Appl. Phys., 47(3), pp. 949-955, 1976.

[5.32] **Wagers**, R. S., "SAW Transduction on Silicon Substrates with PVF_2 Films", IEEE Ultrasonic Symposium Proceedings, 1979.

[5.33] **Ultrasonic & Acoustic Transducer Group**, "Sound measurements: Ultrasonic Adavances at Leeds University", Leeds University, One day meeting, 1996.

[5.34] **AMP** Incorporated web page. "Electromechanical Properties of PVDF" http://www.ampincorporated.com.

[5.35] **Randall**, R. B. and Tech, B. A., "Frequency Analysis - Application of B&K Equipement", Brüel & Kjaer.

TABLES

Stiffness (10^9 newton/ m^2)			
C_{11}	4.94	C_{33}	9.6
C_{12}	2.46	C_{44}	3.57
C_{13}	2.46	C_{55}	3.57
C_{23}	2.46	C_{66}	1.24
Piezoelectric Stress Constants (coulomb/m^2)		Relative Permittivity at Constant Strain $\varepsilon_0 = 8.854\ 10^{-12}$ farads/m	
e_{x5}	-0.207	ε_{xx}^T	12.4
e_{y4}	-0.207	ε_{yy}^T	12.4
e_{z1}	0.216	ε_{zz}^T	12.4
e_{z2}	0.216	Density (Kg/m^3)	
e_{z3}	-0.339	1100	

Table 5.1: Material parameters for PVDF.

FIGURES

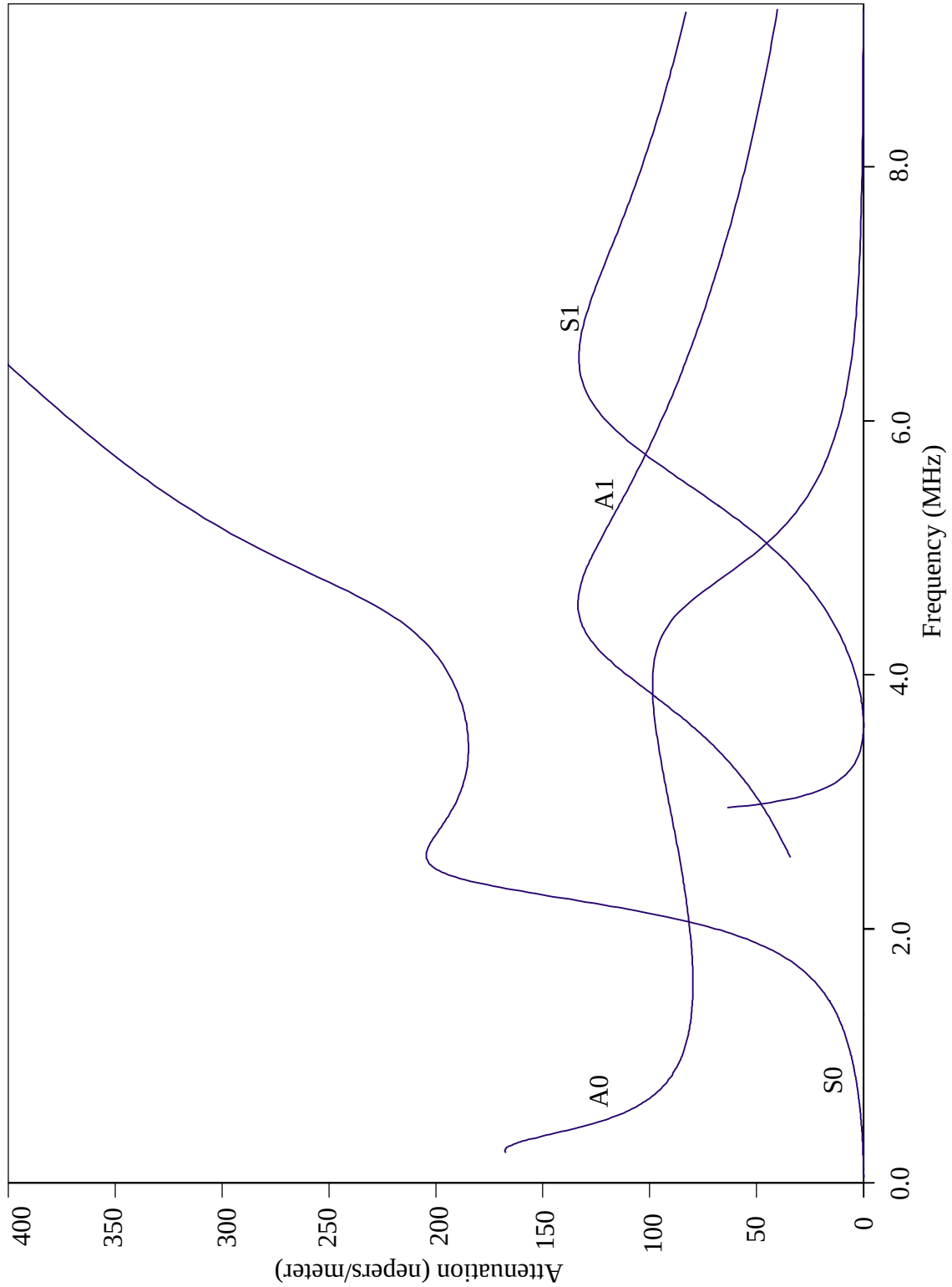

Figure 5.1 : Exact attenuation dispersion curves for a 1.2mm thick aluminium plate loaded with water on one face.

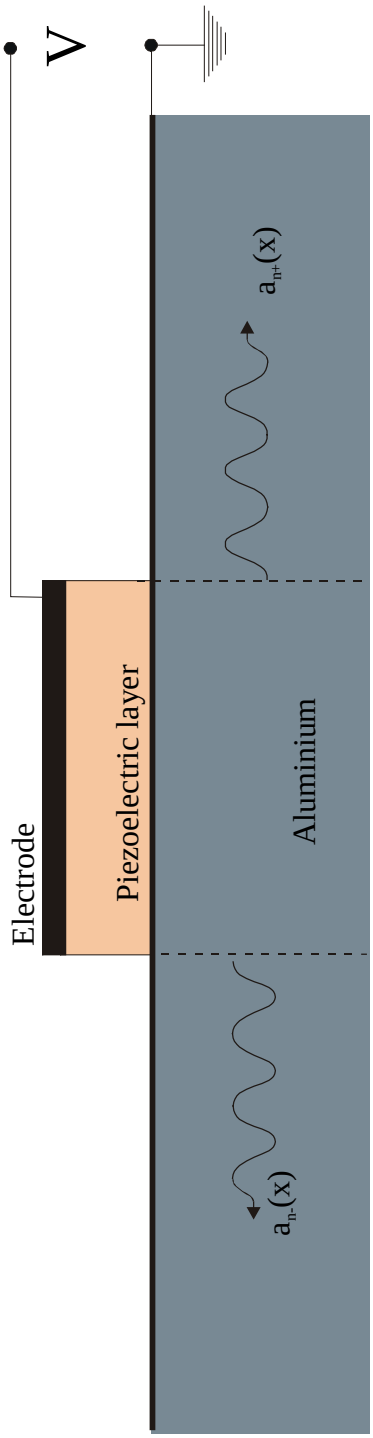

Figure 5.2 : Schematic representation of a single strip transducer. (b) Cross section in the plane (xz) and the waves generated by the transducer.

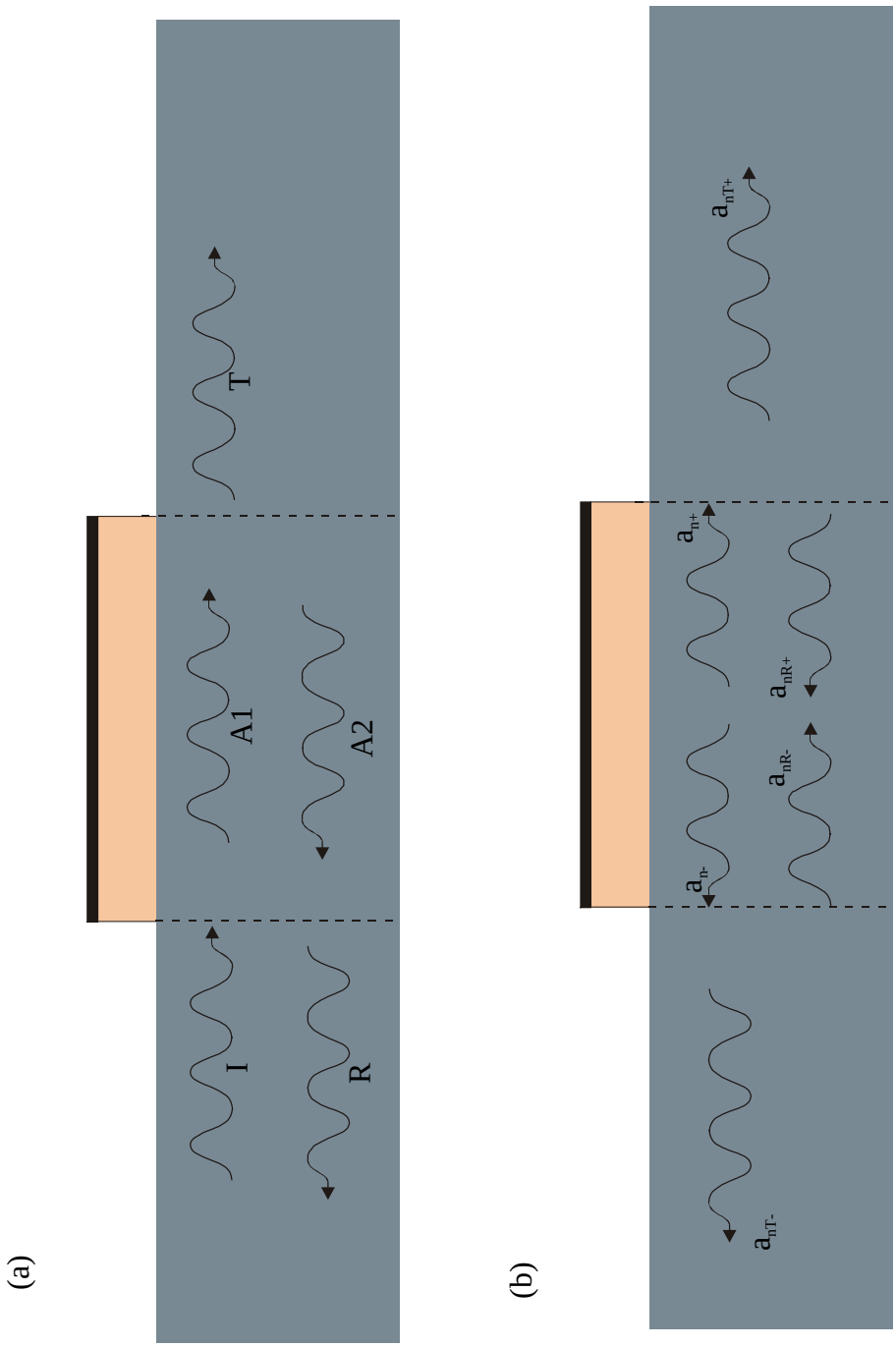

Figure 5.3 : (a) Reflection and transmission of Lamb modes at a single strip. (b) Scattering at a single strip transducer in transmitting mode.

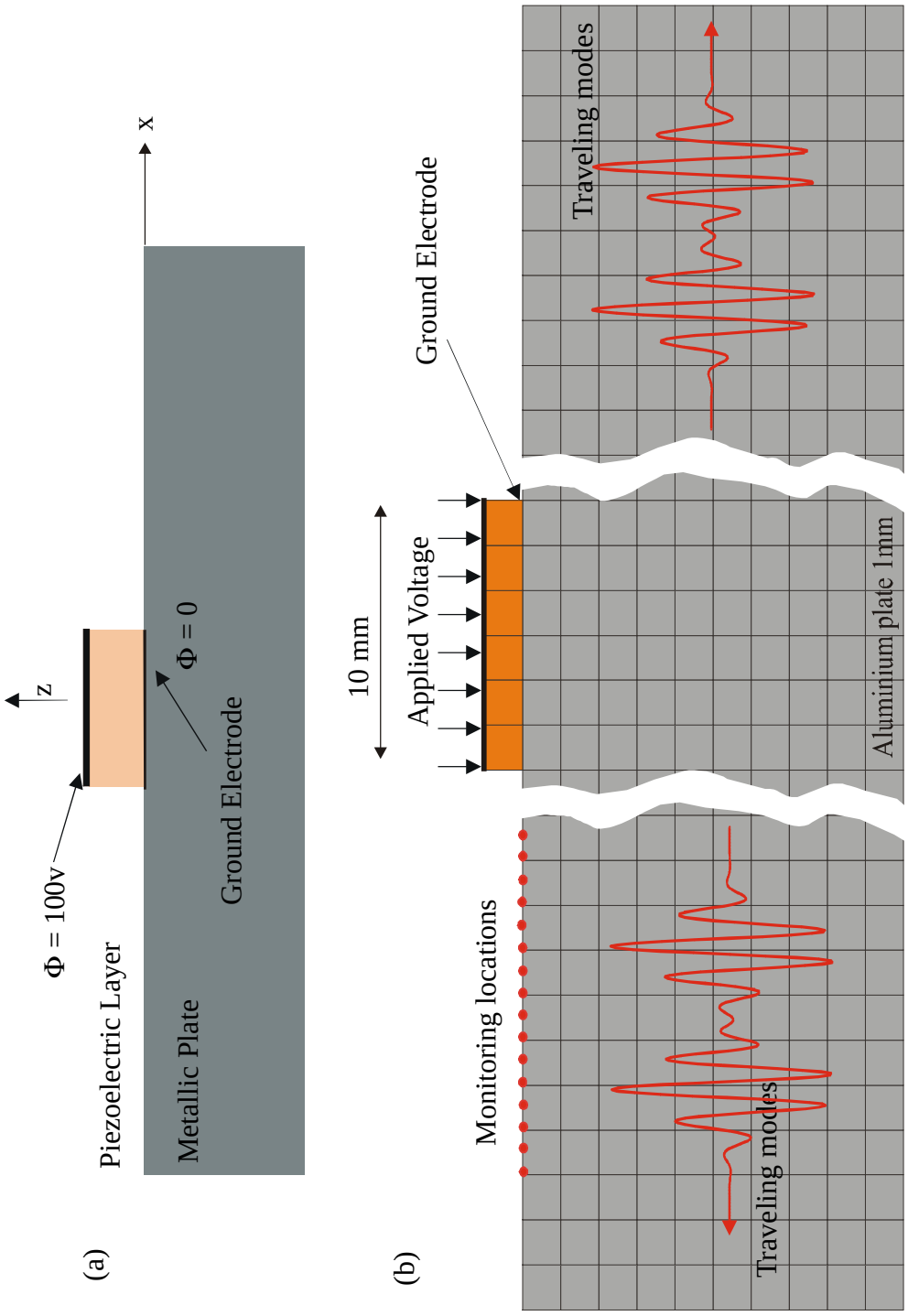

Figure 5.4 : Schematic diagram of the finite element model used to monitor the mechanical displacements in the x- and z-directions at the top surface of the PZT-5H layer for the modes reflected at a 10mm long electrode.

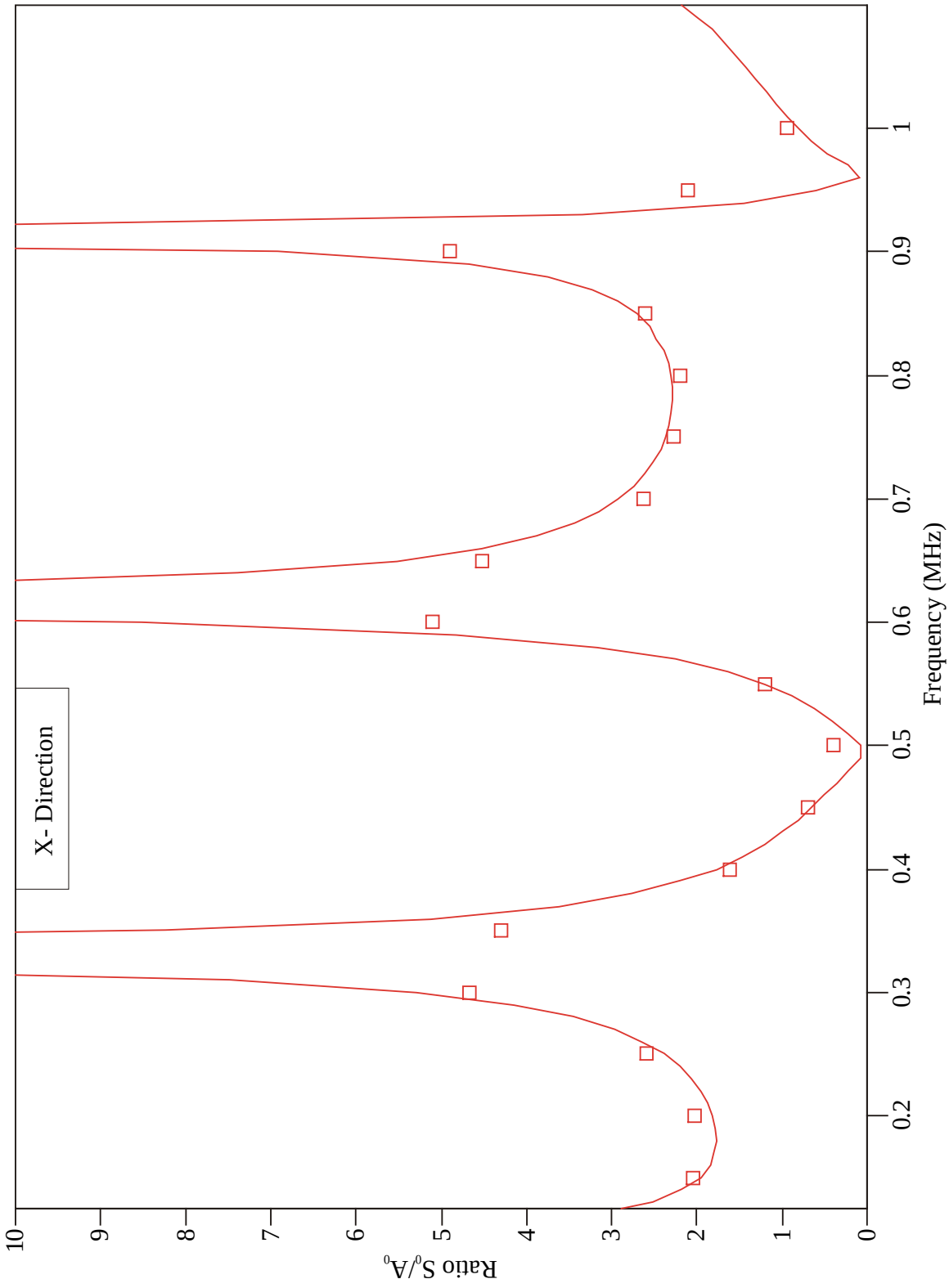

Figure 5.5 : Comparison between finite element predictions and normal mode amplitude calculations for the ratio of displacements of the S_0 mode to the displacement of the A_0 mode. The ratio S_0/A_0 is taken at the top surface of the aluminium plate and displacements are monitored in the inplane x-direction.

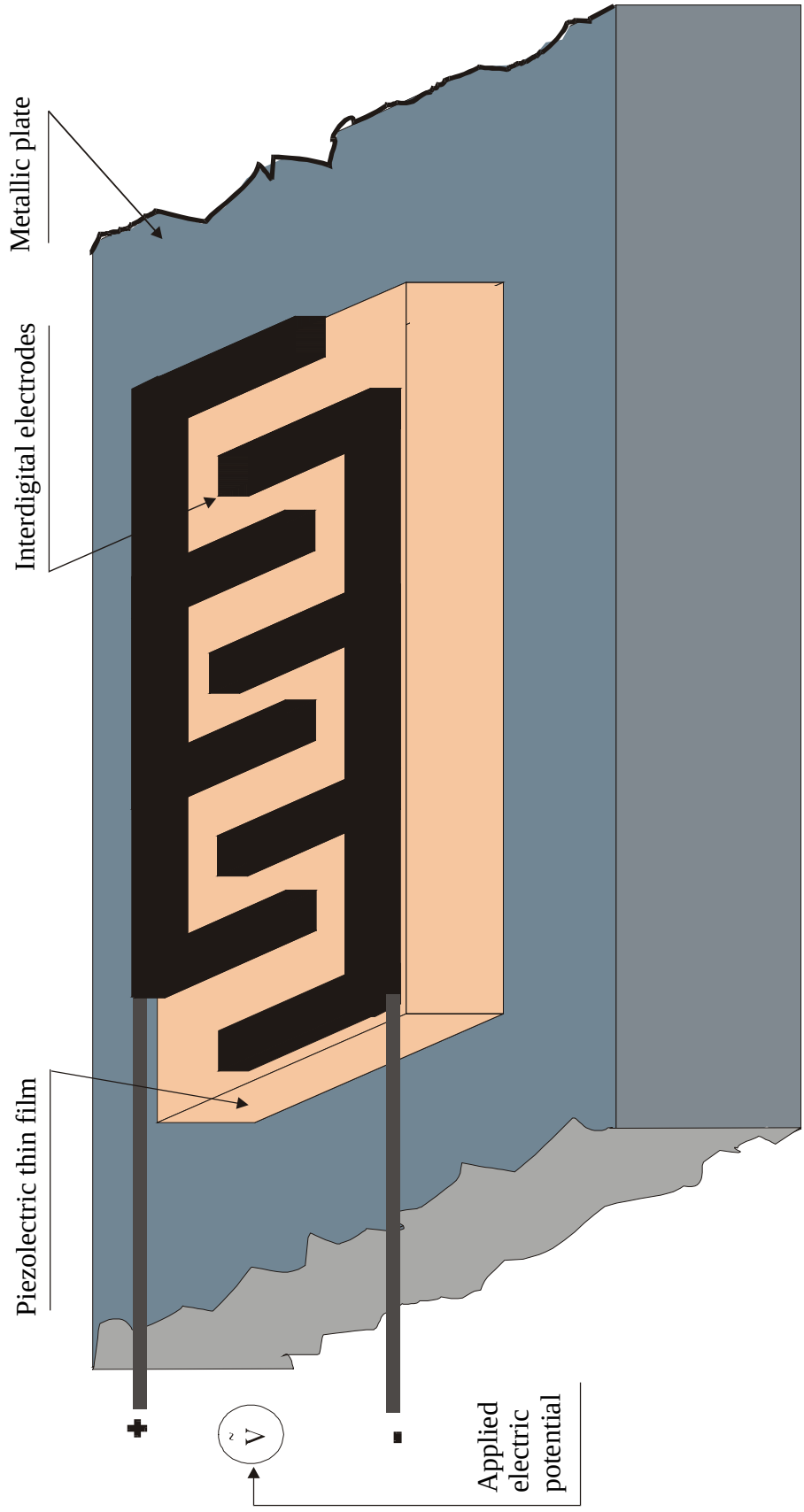

Figure 5.6 : Schematic diagram of an interdigital electrode transducer on a thin metallic plate.

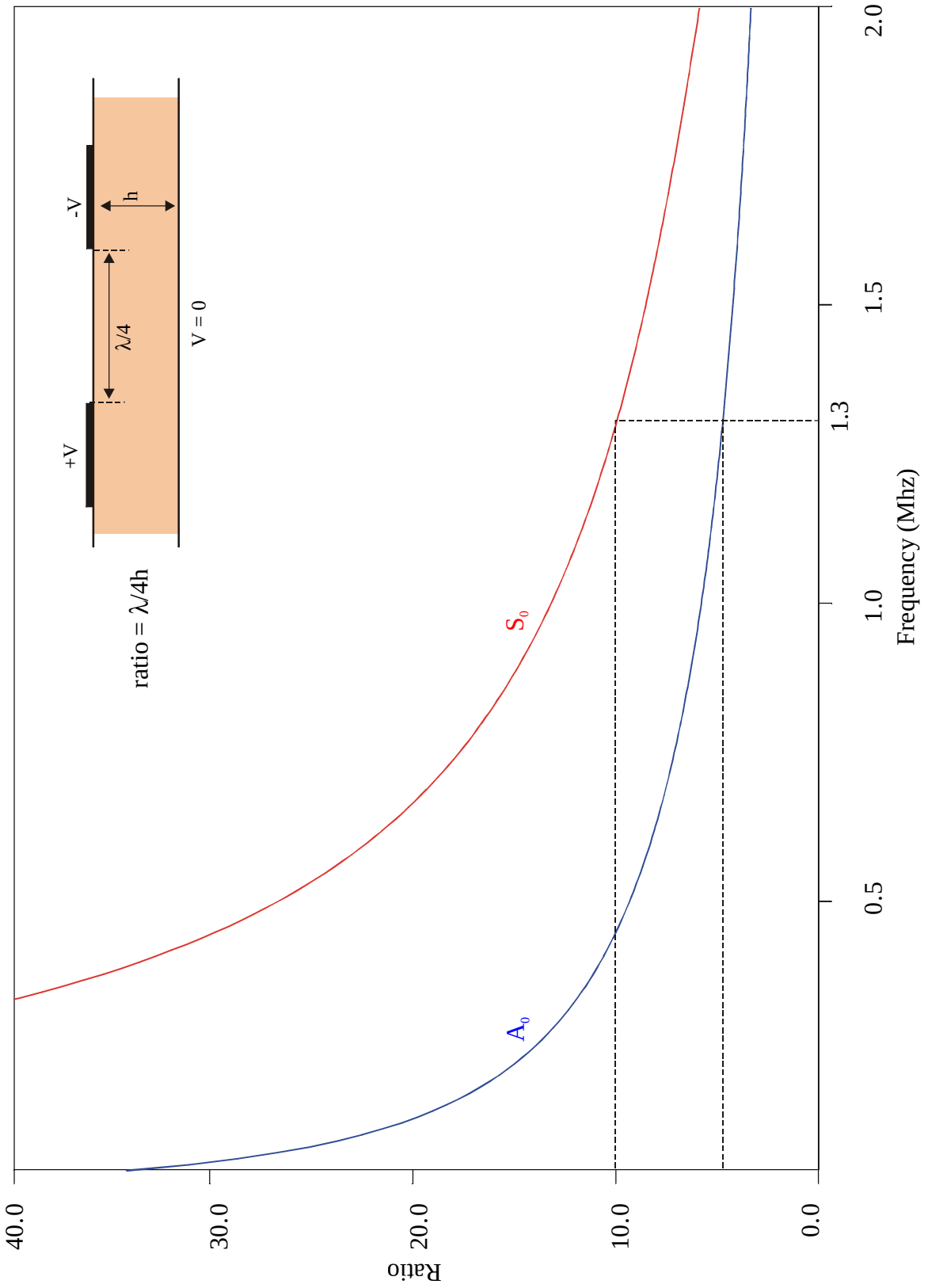

Figure 5.7 : Ratio of the quarter-wavelength to the piezoelectric layer thickness (100 mm) for the two fundamental modes.

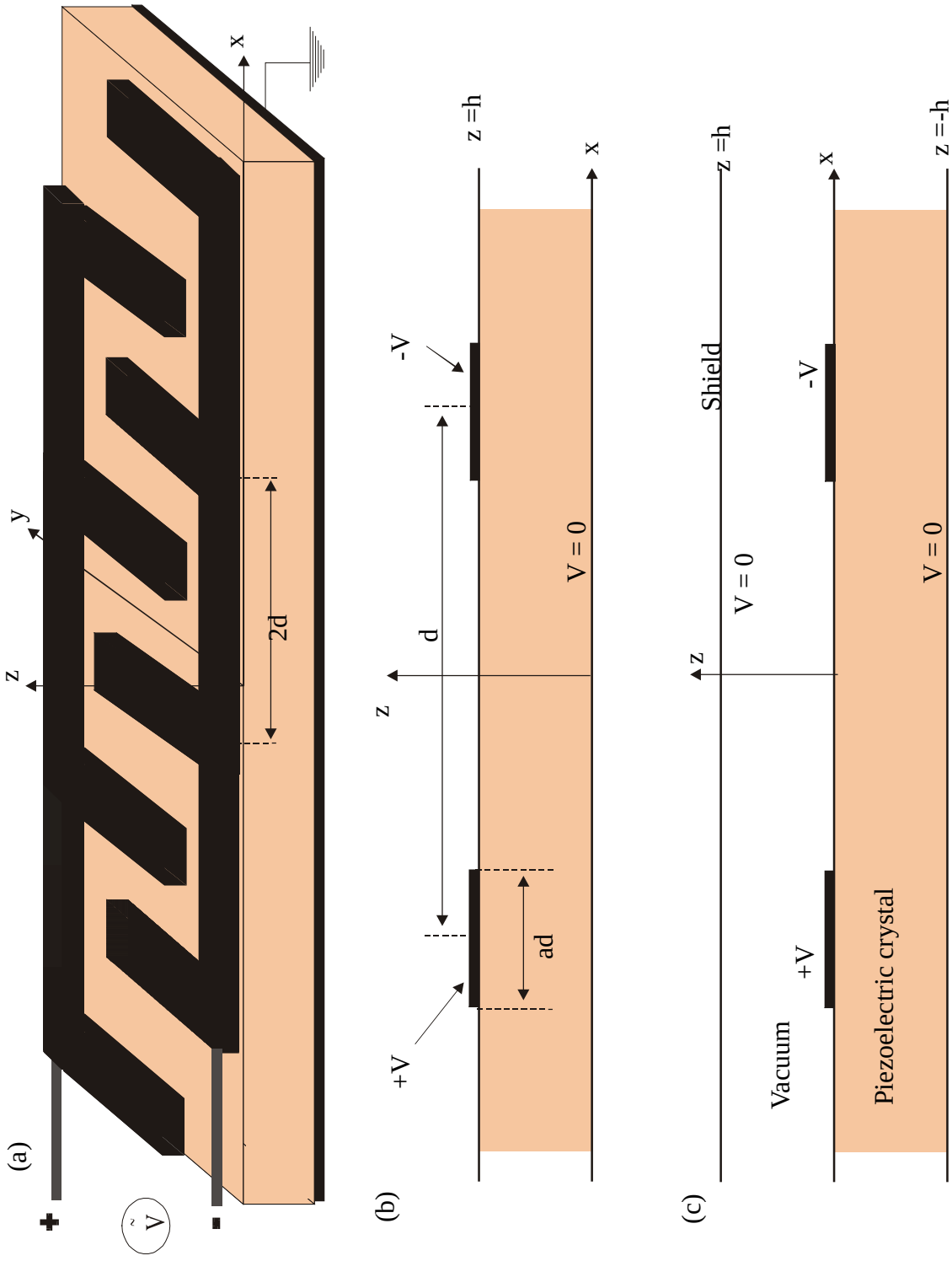

Figure 5.8 : Interdigital transducer. (a) Arrangement of the electrode array at the upper surface of the piezoelectric layer. (b) Boundary conditions for the elementary cell of the transducer. (c) Shielded configuration. In all figures the metallic plate is omitted.

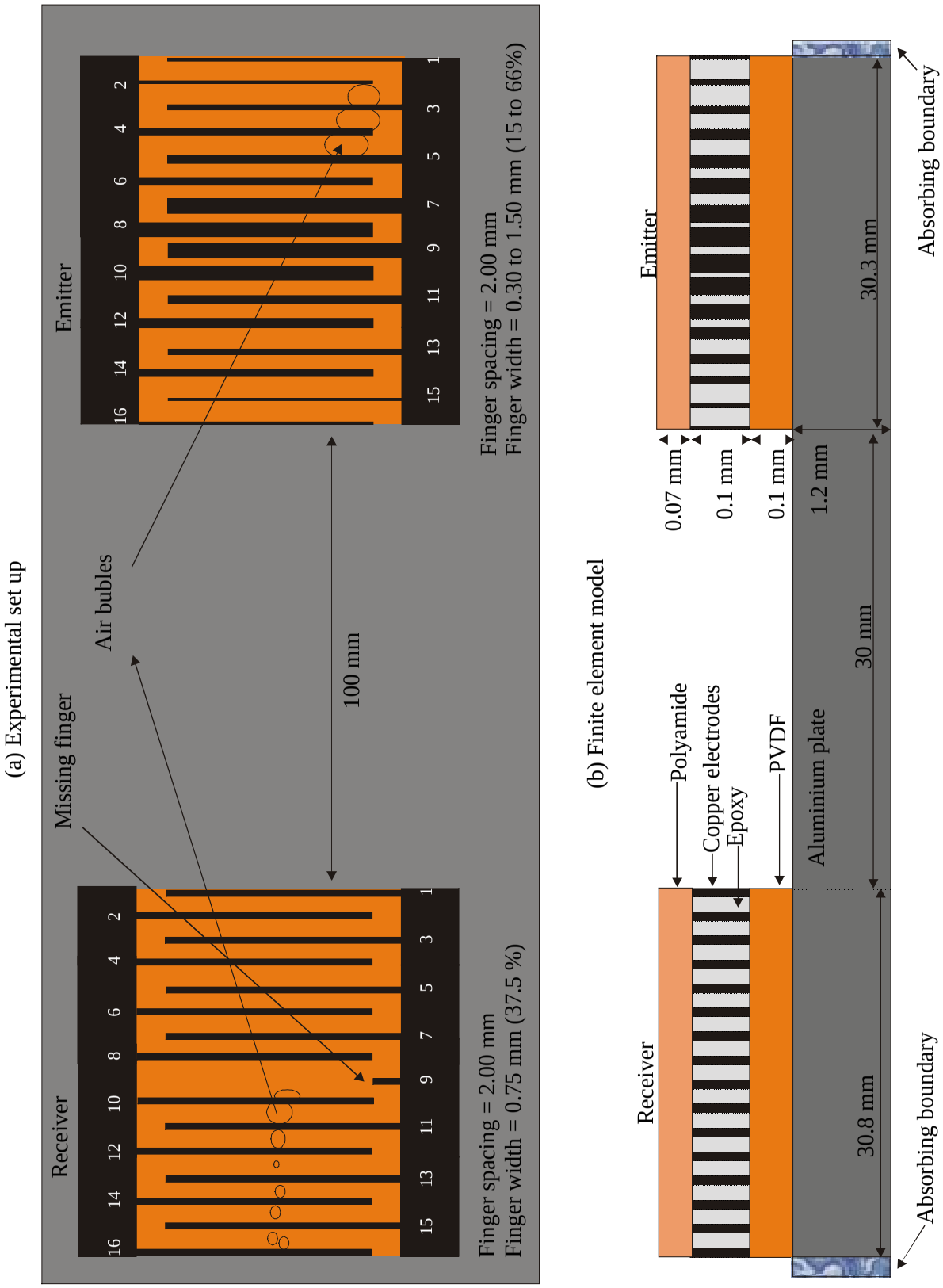

Figure 5.9 : Aluminium plate with two IDTs using PVDF piezoelectric layers and copper electrodes. (a) Shows the experimental set up. (b) Shows the Finite element model.

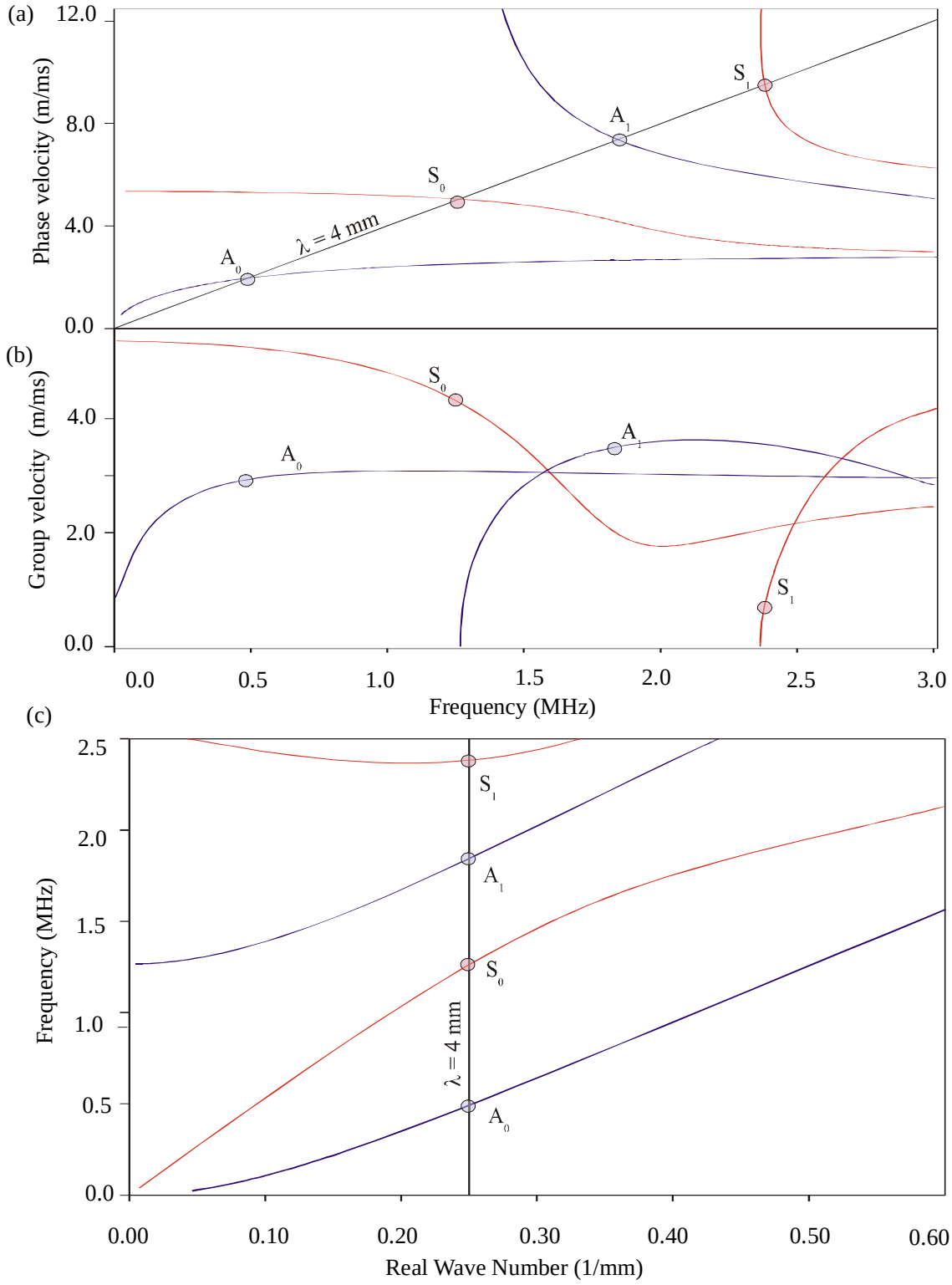

Figure 5.10 : Dispersion curves of the first four Lamb modes for a 1.2mm thick aluminium plate. a) Phase velocity dispersion curves, b) Group velocity dispersion curves and c) frequency versus real wavenumber curves

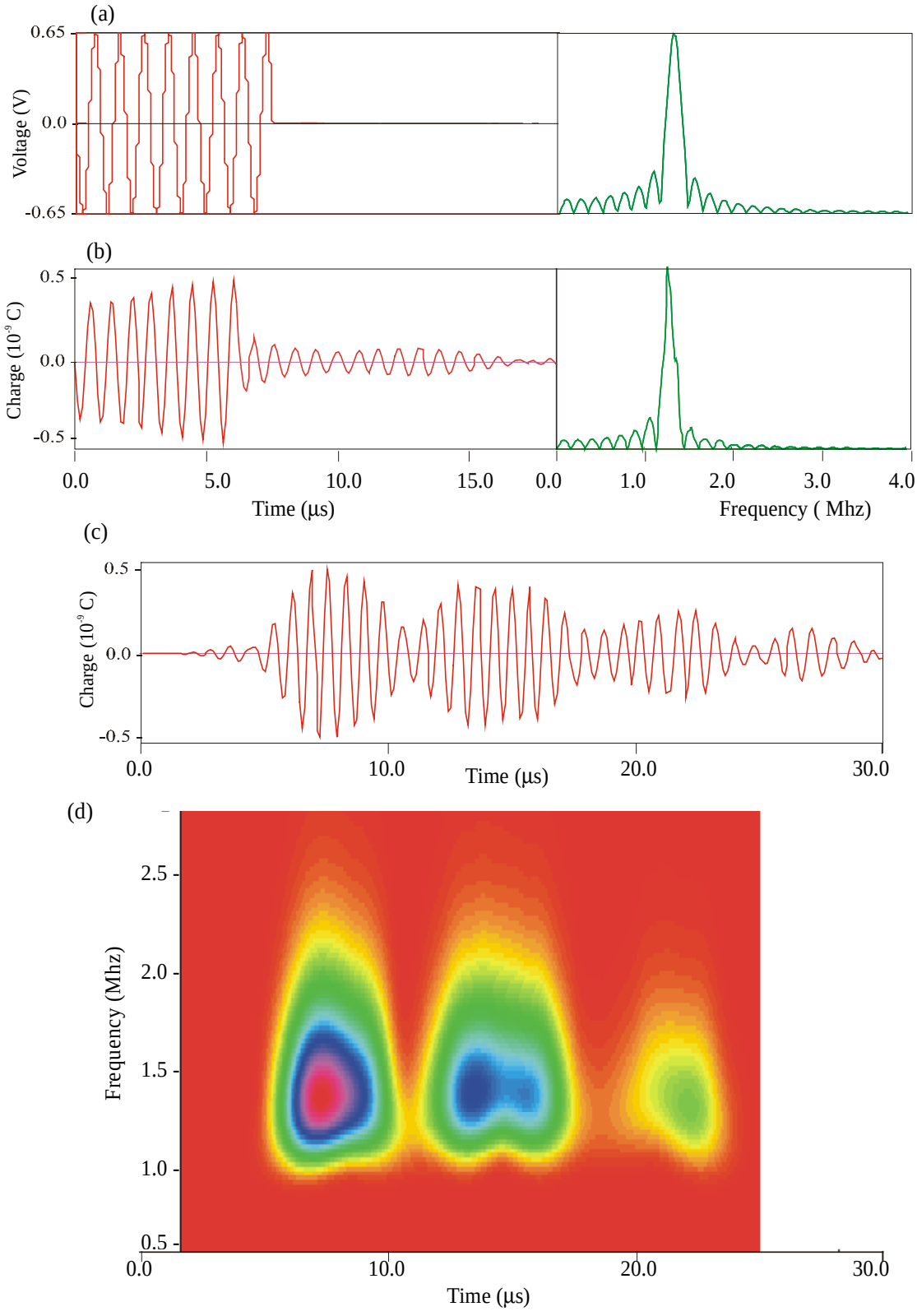

Figure 5.11 : (a) Input voltage signal, i.e. a 8 cycle sinusoidal toneburst of centre frequency 1.3 MHz. (b) Time evolution of the electrical charge distribution on the 1st electrode. The diagrams on the right show the frequency spectrum. (c) Average charge distribution on the grounded bottom electrode. (d) Time-frequency plot of the charge on the bottom electrode.

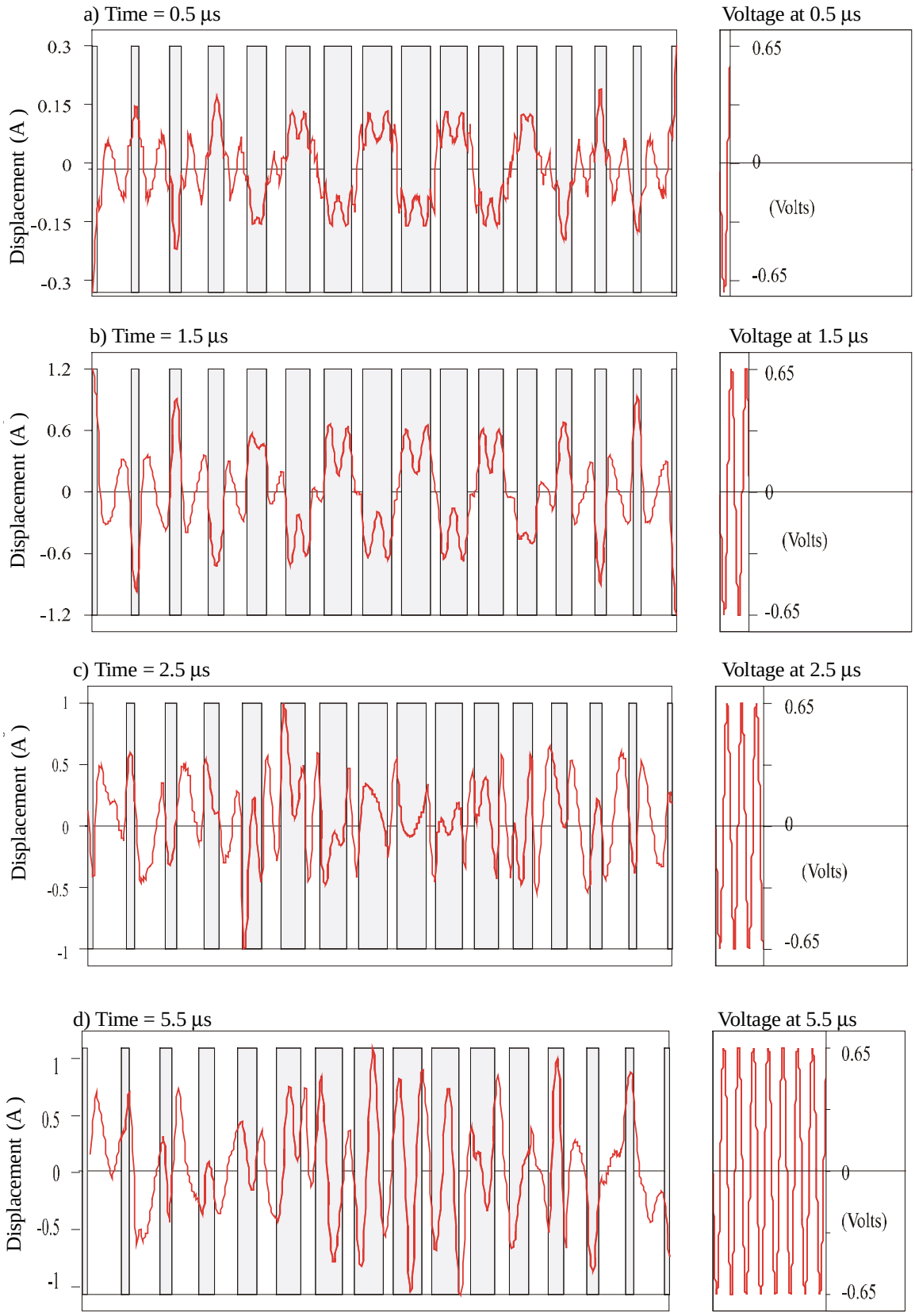

Figure 5.12 : Examples of snapshots of the normal displacements on the upper surface of the transmitting IDT at different moment in time during the application of the input signal. The electrode pattern is shown on each snapshots. Diagrams on the right of each snapshot show the part of the input voltage signal applied so far.

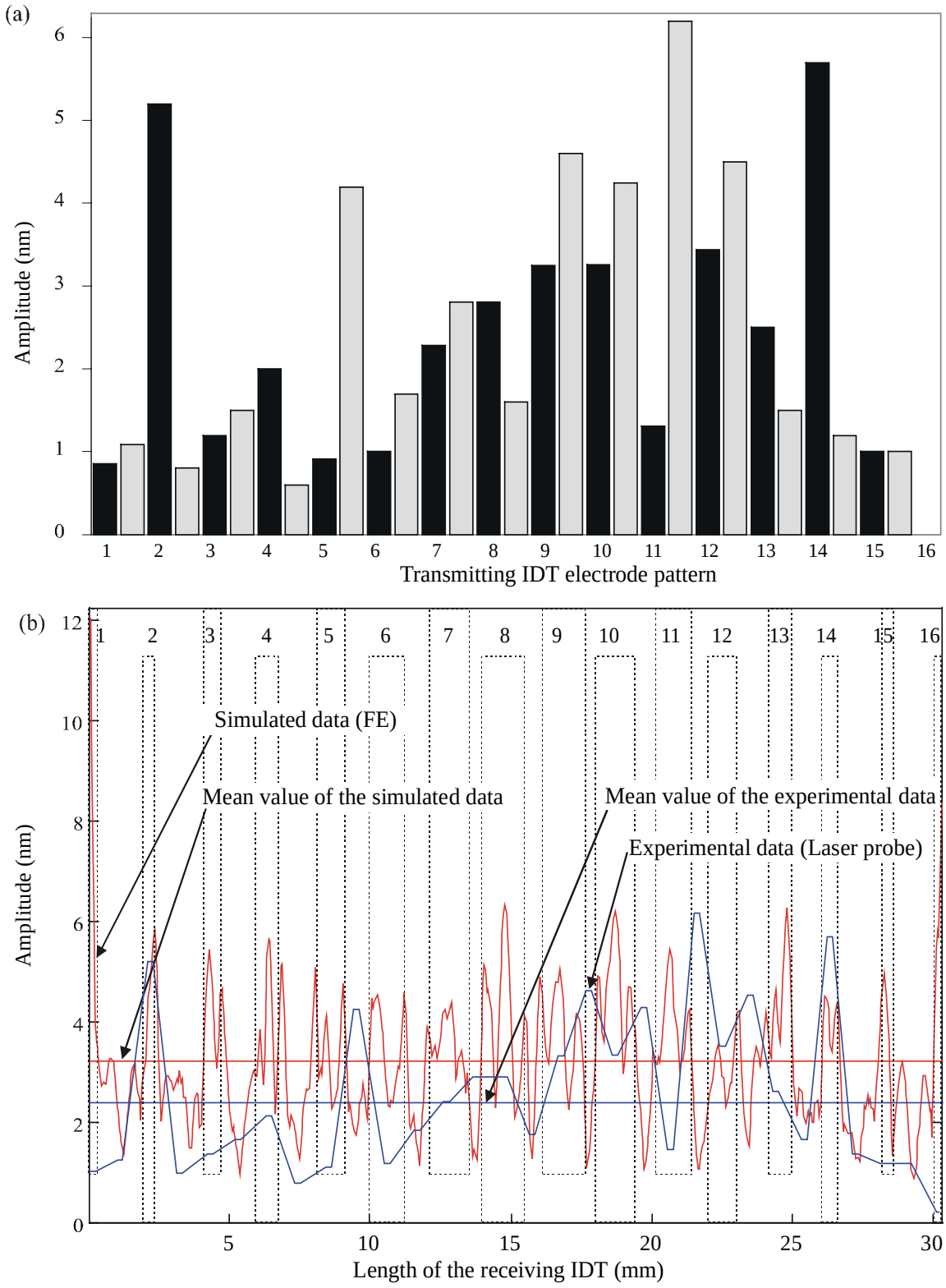

Figure 5.13 : Experimental and predicted out-of-plane displacements on the upper surface of the transmitting IDT. (a) Displacements measured experimentally using a laser probe on each of the electrode (black columns) and between them (gray columns). (b) Comparison between these experimental results and the displacements predicted using the finite element model. The apodised electrode pattern is superimposed.

(a)

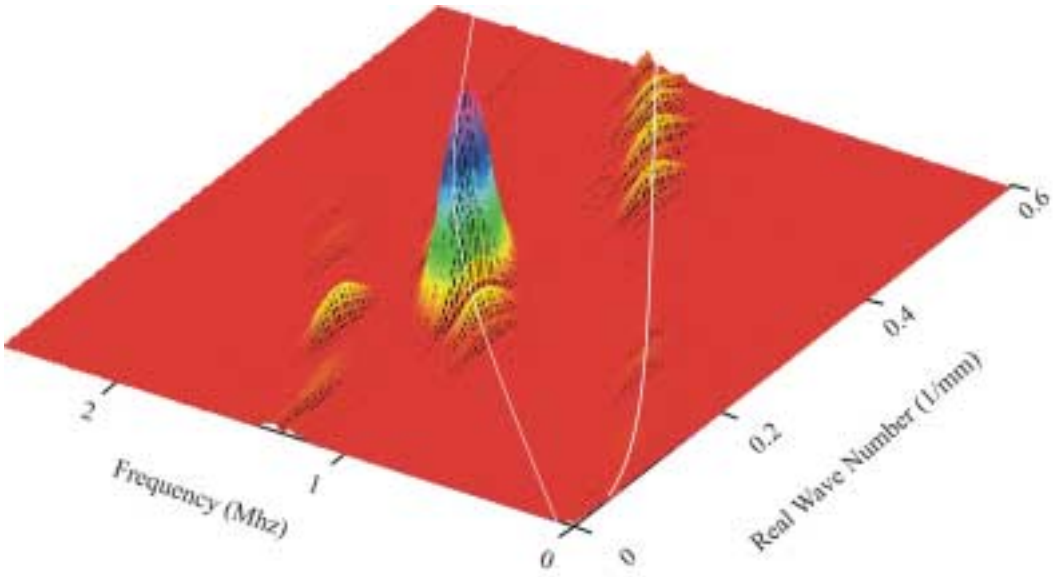

(b)

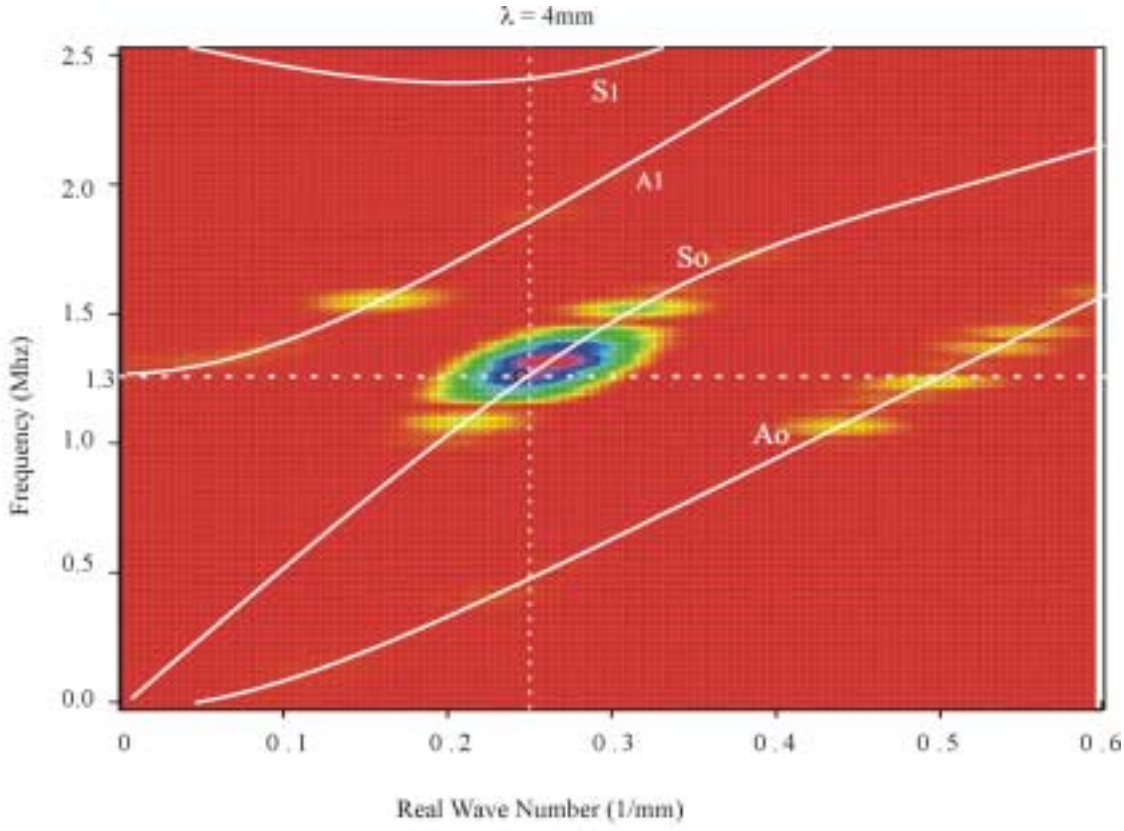

Figure 5.14 : Measurement of the normal displacement of Lamb modes propagating in a 1.2 mm thick aluminium plate. (a) Normalised 3D plot and (b) contour view of the 2D FFT results.

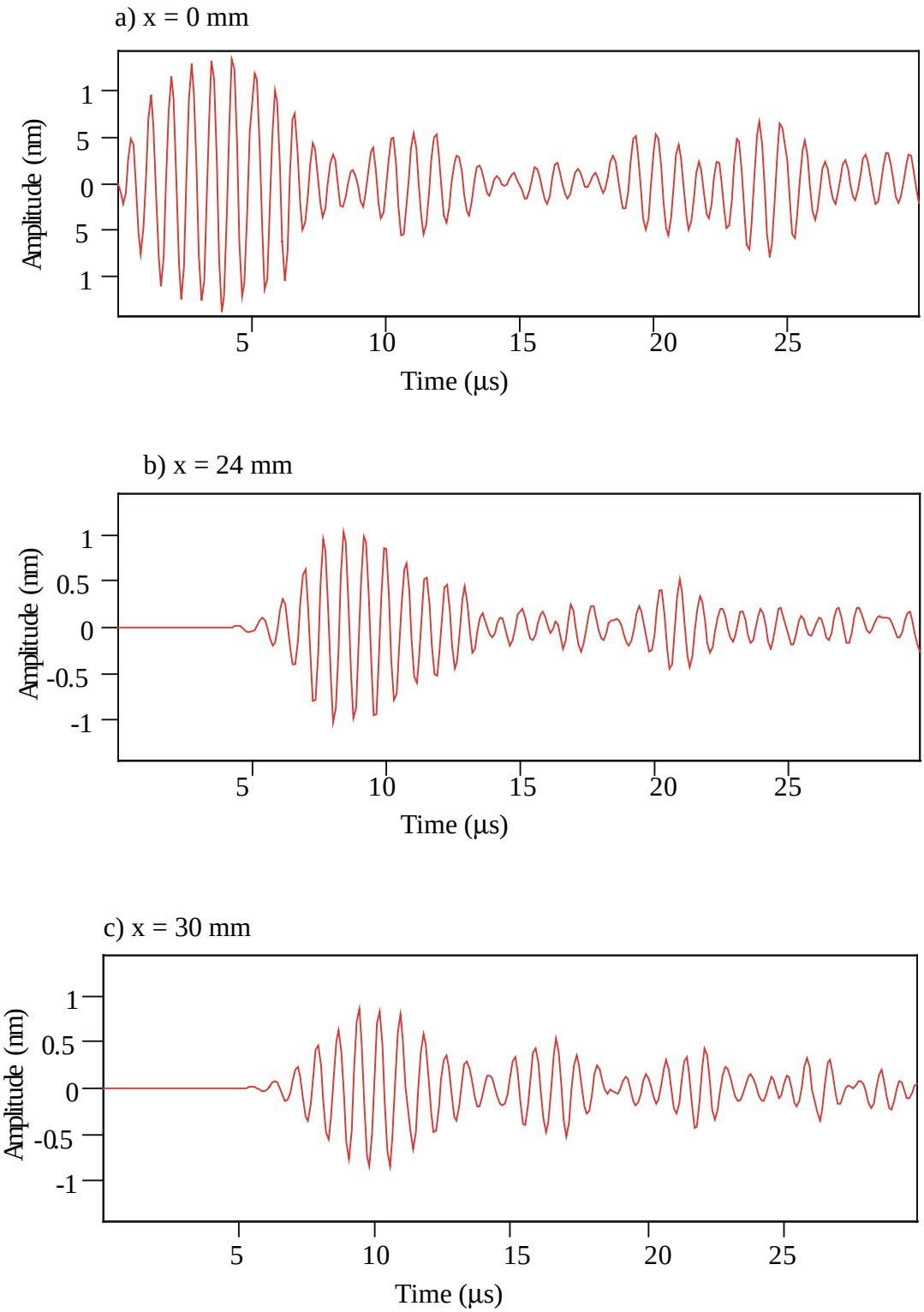

Figure 5.15 : (a), (b) and (c) out-of-plane surface displacements versus time for a 1.2mm thick aluminum plate at three different locations on the plate between the transmitter and the receiver.

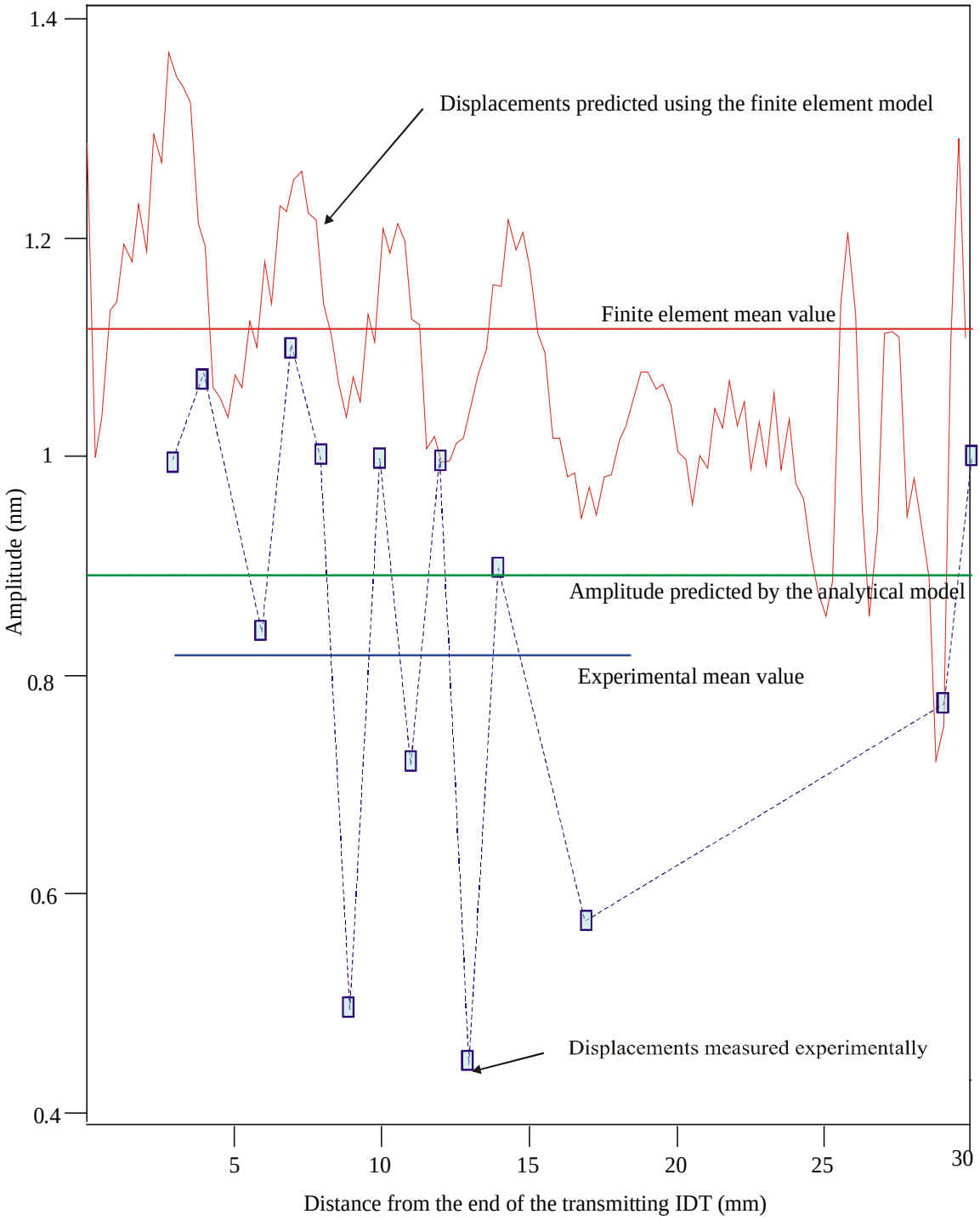

Figure 5.16 : Comparison of the out-of-plane surface displacements measured on the upper surface of the aluminium plate using a Laser probe with the out-of-plane surface displacements predicted using the finite element model and the absolute amplitude calculated from the analytical model. Experimental displacements have been measured every millimeter from 3 to 15mm and then at 17mm, 29mm and 30mm.

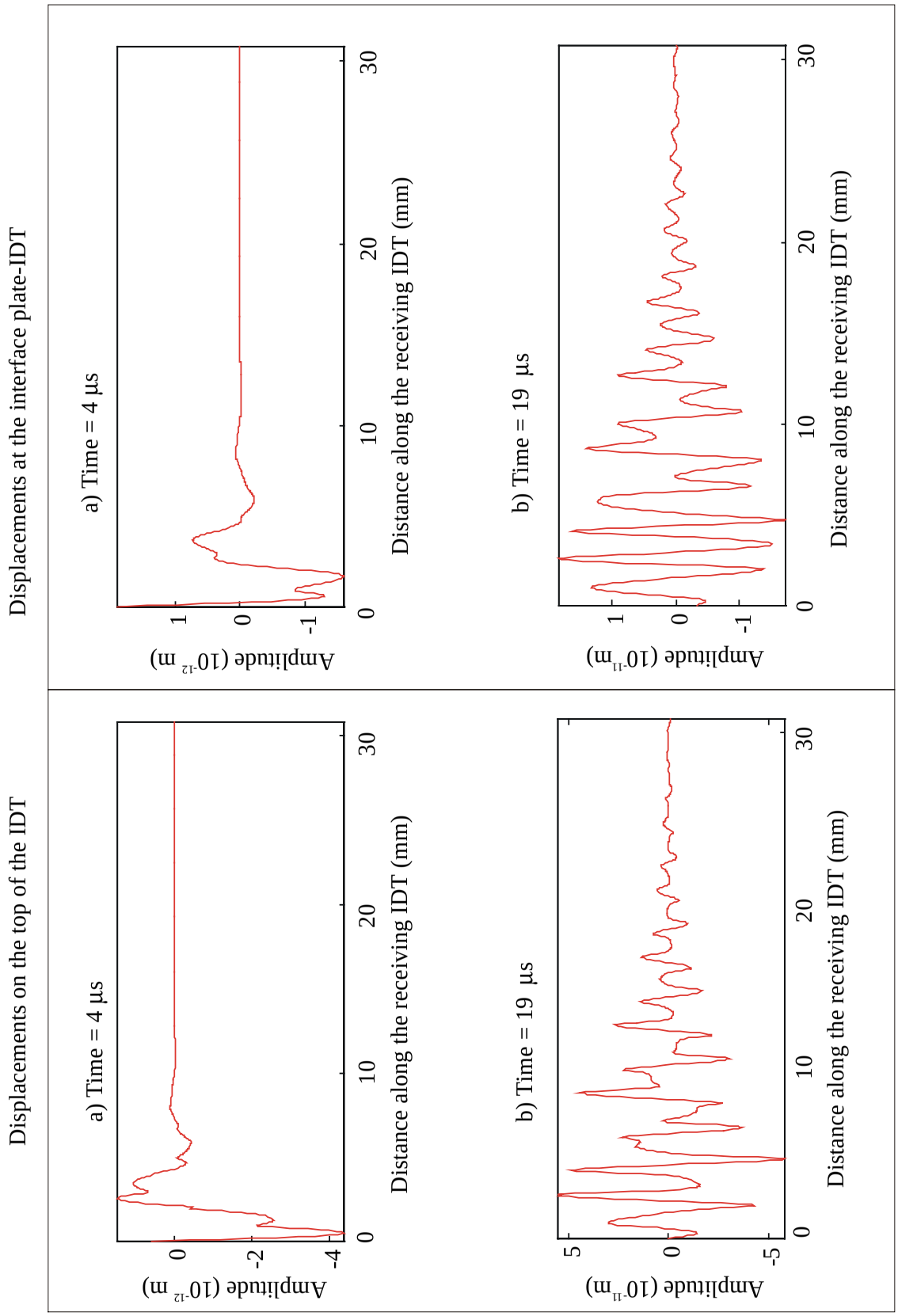

Figure 5.17 : Snapshots of the displacements at different times. The diagrams on the left show the simulated displacements at the upper surface of the receiving IDT. The diagrams on the right show the simulated displacements at the interface between the plate and the IDT.

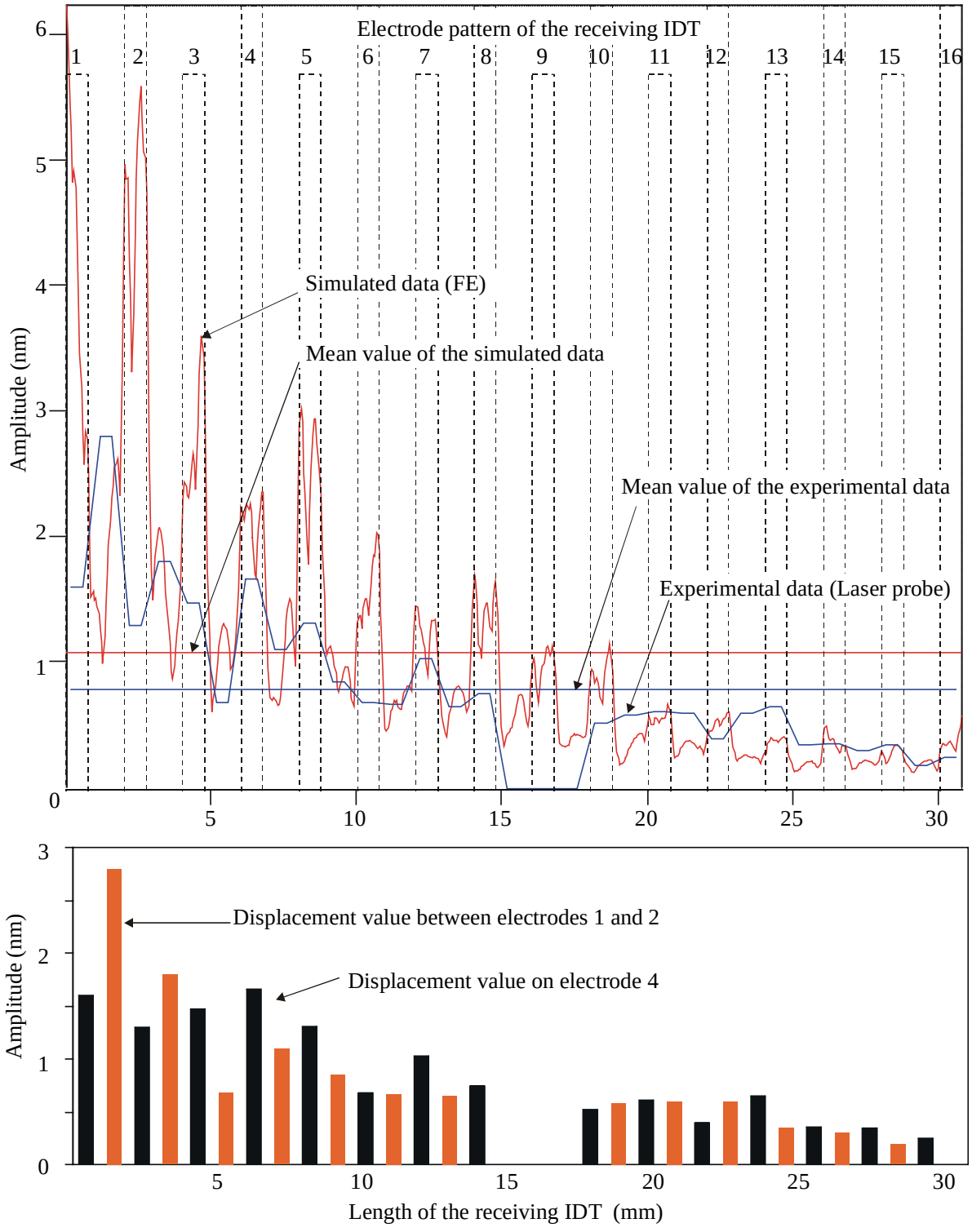

Figure 5.18 : (a) Comparison of the simulated and measured displacements at the upper surface of the receiving IDT. The mean value of each series is shown. (b) Displacements measured using a laser probe on the upper surface of the receiving IDT.

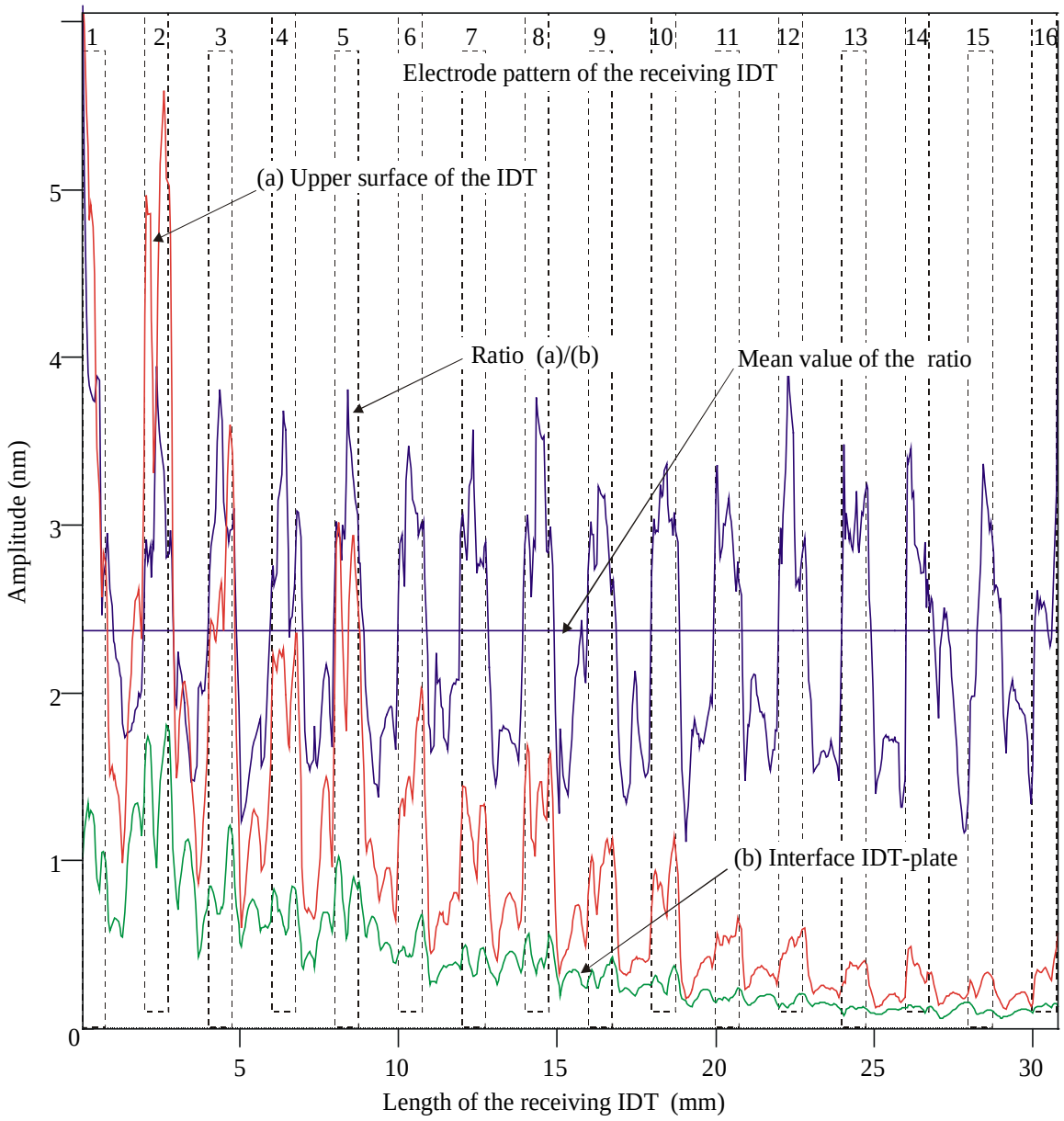

Figure 5.19 : Displacements simulated by Finite Element at the upper surface of the receiving IDT and at the interface between the plate and the receiving IDT. Their ratio is also shown, superposed on the electrode pattern of the receiving transducer.

Chapter 6

Conclusion

An analytical model for acoustic plate modes generated by piezoelectric transducers has been presented in this thesis. In this concluding chapter, a review of the thesis is presented which highlights the main findings. The interest in the model, along with its limitations, and some suggestions for future work are discussed. Lastly the main contributions of the thesis are summarised.

6.1 REVIEW OF THE THESIS

Chapter 1 described the motivation and set out the objectives of this work. The motivation was originally provided by a group of UK companies who required novel developments in *smart structure* applications. Among the solutions investigated were thin, permanently attached, interdigital transducers, designed to selectively generate Lamb waves in thin metallic structures. The thickness of the piezoelectric layer was in the range from few microns to 0.25 mm. These transducers being permanently attached to the structure under investigation could not be studied without considering their interaction with the structure and due to their geometries, one-dimensional models were not able to predict the amplitude of the Lamb waves excited by the transducer. Therefore there was a need for modelling tools. Two models have been developed, a finite element program and an analytical model. The main objective of both models was to take into account the electromechanical interaction between the electrical input and the guided waves. The different phases of the development of the tools and theories needed to investigate the behaviour of piezoelectric transducers were summarised in Chapter 1.

Lamb waves, which are the guided waves excited by the transducers have been reviewed in Chapter 2, where attention was focused on their modal properties. The model was built on two theories, the normal mode theory and the perturbation theory which have also been reviewed. Lastly, piezoelectricity and piezoelectric transducers were presented.

The development and validation of a finite element formulation that includes the piezoelectric effect alongside the dynamical matrix equation was described in Chapter 3. It was shown in detail how the equations of piezoelectricity were reduced to the well-known equation of structural dynamics, based on an adaptation of the condensation technique to the piezoelectric equations. Practical incorporation of these equations into an already existing finite element code was also discussed and practical examples were investigated and served as validation examples.

In Chapter 4, an analytical model has been developed on the basis of normal mode theory and perturbation methods. The structure of the model was detailed step by step and each of these steps was thoroughly validated using the finite element program. Firstly the mechanical influence of the transducer on the guided waves of the structure was studied. Secondly the electrical potential associated with the plate modes propagating in the transducer region was derived analytically. Then a first transducer model was derived, emphasising the differences with SAW transducers and a specific formulation for Lamb waves was developed. The third and last step was concerned with scattering coefficients. Calculation of the S-parameter for the fundamental Lamb modes at rectangular strips have been derived analytically and validated numerically.

Two applications of the finite element and of the analytical models have been presented in Chapter 5. The first example was a single strip transducer bonded to a 1mm thick aluminium plate. The amplitudes of the two Lamb waves generated by the transducer were predicted over a 1 MHz frequency range. The finite element and the analytical results were shown to be in good agreement with each other. The second application was concerned with the modelling of a practical interdigital transducer. A preliminary investigation has been carried out, first experimentally and then using the finite element and the analytical models. The theoretical investigation gave results very close to the experimental results concerning the amplitude of the generated modes, and several important features for the future design of IDT have been identified.

6.2 EVALUATION

Significant progress has been made on the understanding of the normal mode theory and the perturbation formalism. Electromagnetism and electrostatics have been studied and piezoelectric problems involving guided waves can now be approached from an electrical point of view without the use of over-simplified approximations.

6.2.1 FINITE ELEMENT MODEL

The implementation of the piezoelectric constitutive equations in the existing finite element program, FE77, has been performed. Excellent agreement has been found with a commercial package, PZFlex®. Several features have been identified using this finite element tool. In particular the electromechanical coupling of Lamb waves has been investigated. Although piezoelectric finite element packages already exist, only simple systems involving plate modes and piezoelectricity have been studied in the past. It has been shown that our finite element program is perfectly designed for the study of guided waves and presents several advantages over commercially available packages.

6.2.2 ANALYTICAL MODEL

Previous studies of the generation of Lamb waves by piezoelectric transducers have either used simplified models or very accurate but cumbersome solutions. Here a physical model has been developed. The solution procedure that we imagined is original in the sense that the model has been considered back to front, starting with the modal properties of the guided waves to be generated, and working out, step by step, all the coupling and transduction processes to eventually establish a relationship between the applied voltage and the amplitude of the modes.

The use of the normal mode formalism for the study of the excitation of Lamb waves is recent and has not been done for complex structures and most of our results are innovative. The use of the perturbation method for acoustic plate wave problems has been fully reviewed and it has also been shown how this method can be used for closely related problems, such as the propagation of guided waves in structures that cannot be modelled exactly.

All along the development of the model, our approach has been to break down complex problems into simple ones by using simplifying approximations. In particular this technique has been used to look at the scattering of Lamb waves at surface defects. A new and simple solution has been found that allows us to estimate with good accuracy the reflection coefficient of each Lamb mode, and also to predict the mode conversion of one mode into another one.

An analytical solution has been found for the case where the charges are applied uniformly over the surface of the transducer. Electrostatic solutions for the charge density on the electrodes of the transducer have been given for a thin and grounded piezoelectric layer mounted with either one single electrode or with an infinite array of evenly spaced electrodes. A new expression for the electromechanical coupling coefficient of the Lamb modes has been given in terms of the well-known $\Delta V/V$ coefficient, the fractional change in velocity when the surface on which the transducer is to be applied is short-circuited, originally developed for SAW.

6.2.3 WAVE AMPLITUDE AND TRANSDUCER PERFORMANCE

It was shown that the analytic model gives very good approximations of the amplitudes of the Lamb modes generated by a piezoelectric transducer. Using both the analytical model and the finite element program, we have appreciated some limitations of the actual design of permanently attached PVDF interdigital transducers. Preliminary results demonstrated the relative inefficiency of apodisation in the direction of propagation and also the influence of flaws due to the manufacturing process such as debonding and presence of inclusions (copper chips or air bubbles trapped between two electrodes). Eventually it was shown that cheap IDTs can generated predominantly the S_0 mode in thin structure.

6.3 SUMMARY OF MAIN CONTRIBUTIONS

The major contribution of this thesis is that a complete analytical model developed for permanently attached piezoelectric transducer has been shown to provide good predictions of the amplitude of the two fundamental Lamb modes generated by the transducers.

The structure of the model is original and novel in the way that it is has been developed starting from the modal properties of the Lamb modes of the structure and the influence of electrical sources has been added through successive perturbations. This model presents a great advantage over other models based on integral methods. It is very flexible and versatile. Many further developments can be considered.

In the development of this model, some theoretical points have been clarified and adapted to the specificity of Lamb waves.

In first place, it was demonstrated that the accuracy of the first order perturbation calculations for a thin overlay depends more on the mismatch between the acoustic impedances of the layer and the plate than on the conventionally used "βh" parameter. It was also shown that the first order expansions are more suitable than higher-order expansions as long as the exact particle velocities are used.

It was also shown that each plate mode has a different coupling parameter $\Delta V / V$, and this difference must be taken into account when designing a transducer. This formulation of the coupling parameter is novel and has been neglected in previous studies of the generation of Lamb waves using piezoelectric transducers.

The use of the perturbation theory for the prediction of scattering coefficients of Lamb waves at arbitrary flaws has been investigated and our results can be used directly for many different NDT applications.

It has been shown at some points thorough the development of the mechanical perturbation technique how results could be used in order to solve guided wave problems that have not yet been successfully solved.

6.4 FUTURE WORK

The future work on this project falls into two main categories. The first category involves direct improvement of the finite element and the analytical models, including the experimental applications. The second category involves the investigation of a new transducer design and also derivative uses of some calculations presented in this thesis for purposes other than transducer design. This section only attempts to address issues that have been mentioned at some point of this thesis but have not been developed to their full extent.

6.4.1 FINITE ELEMENT MODEL

A strong limitation in the present possibilities of the piezoelectric module of FE77 is the impossibility to model the influence of the external circuitry on the transducer. In the same way that mechanical mass and springs can be added locally it would be desirable to be able to attach resistances and inductances at some nodes. The use of resistances in particular would be extremely useful in order to provide a way out for the charges generated in the piezoelectric layer, and therefore avoid the ringing phenomenom observed in section 5.3.3. In addition to these electrical terminations, it would be desirable to be able to model electrical losses. The difficulty here is to adapt the time marching algorithm so that the damping matrix does not need to be inverted.

6.4.2 TRANSDUCER MODEL

6.4.2.1 Alternative Calculation

We mentioned at various stages of the development of the model, that the source function used to solve the normal mode amplitude equations is not unique and alternative forms of this source function can be used. An example of the use of the volume integral formulation (instead of the surface integral formulation) has been given at the scattering stage of the model. Using this technique for the transducer problem would allow us to solve the problem of piezoelectric transducers embedded in the structure. Such a study would be completely novel.

6.4.2.2 Second order effects

The analytical model for plate modes has been developed to take into account the first-order effects only. First-order effects are the piezoelectric coupling, the mechanical scattering at the edges of the transducer and the mechanical loading of the transducer. Second-order effects such as the electrical and mechanical scattering at each electrode, the beam diffraction due to the finite width of the transducer and also the presence of spurious modes have been quantified for SAW devices. Although our analytical model does not take these effects into account, its modular nature allows us to add extra effects in a relatively easy way. The charges under the electrodes act on the

piezoelectric wave in the same way that a thin overlay does on mechanical waves. Therefore the good agreement obtained for the mechanical scattering coefficients definitely warrants the development of electrical scattering coefficients. The problem of spurious modes is, in theory much more difficult to tackle, but recent works reported that a mode orthogonality relationship has been established for non-propagating Lamb modes. Starting from this, the model can be amended to account for the presence of these modes.

6.4.3 NEW TRANSDUCER DESIGNS

The IDT results indicate clearly that it is possible to design a transducer that would generate only the mode S_0. We believe that a cheap and powerful S_0 transducer can be manufactured by designing a clever electrode shape that would introduce a field modulation in a way similar to that of the IDT. Developing our model to investigate this new design can be done without undue effort since there is an extensive literature on the subject of electrode dicing and shaping.

6.4.4 SCATTERING CALCULATIONS

The results we obtain for the scattering parameters of the two fundamental Lamb modes are extremely encouraging and there is a real need in NDT for simple and efficient models capable of determining rapidly the magnitude of scattering at given defects. The first step in the future would be to run more validation cases in order to test the limits of the approximations, developing the calculations for complex defect shapes in order to establish a database of possible defect shapes. The analytical model provides almost immediate results which makes it extremely attractive compared to a finite element program. For a given surface defect, the scattering coefficients for all possible Lamb modes, at all frequencies can be extracted in less than a minute.

6.4.5 COUPLING OF THE ANALYTICAL MODEL AND THE FINITE ELEMENT PROGRAM

In this thesis we developed two different models, each having strong advantages and strong limitations. A perfect solution to almost all NDT problems would be to couple these models. The finite element program is far to slow too become a design tool. However if its use is restricted to small local areas, it could become extremely efficient. As seen in the analytical model, the amplitude of the modes generated by the transducer or at a scatterer can be found using the same equation, only the source function being different. This source function is basically the product of two fields, electrical or mechanical. It is the finding these fields that makes the problem difficult. The finite element program could therefore be used to predict for example the charge distribution at the electrodes or the displacements at the surface of the scatterer. These fields could then be fed back into the analytical model and the amplitude of the waves could be calculated immediately. This idea is not new, and we already considered coupling the program DISPERSE with our finite element package. However DISPERSE

is concerned only with free propagation and therefore computes only the dispersion properties of the modes and not their amplitudes. Our analytical model can do that.

Appendix A FE77 Input File

FE77 INPUT TEXT	COMMENTS
DATABASE 'Strip'	Open new database with name STRIP
BOOK new 'Metal_Book'	**Start mechanical book**
ATTRIBUTES 2-dimensional plane strain	2-Dimenasional model in plane strain conditions
GEOMETRY 'Metal_Plate'	Start defining the mesh geometry for the plate.
Regional Coordinates <x y 1 20> 0.0,0.0 100e-3,0.0 0.0,1e-3 100e-3,1e-3	Mesh defined in the plane xy. Defining the regions in 4 global positions(1,2,3,4)
Material ALUMINIUM Region QSTR 1,2,3,4 1000 10 Element QD04	Metal region made of aluminium Quadrilateral region made of 1000 (direction x) by 10 (in direction y) 4-noded square elements
ASSEMBLE Set stiffness Diagonal mass	Assemble Mass and Stiffness global matrices for the d.o.f of the first region (mechanical). Mass matrix is diagonalised.
BOOK new 'Piezo_Book' **ATTRIBUTES** 2-dimensional scalar	**Start Piezoelectric book** 2-D mesh for scalar d.o.f (potential ϕ)
GEOMETRY 'Piezo_Strip'	Start defining the mesh geometry for the strip.
Regional Coordinates <x y 1 20> 475e-4,1e-3 525e-4,1e-3 475e-4,3e-3 525e-4,3e-3	Mesh defined in the plane xy. Defining the regions with 4 points (x,y coordinates)
Material PZT_5H Region QSTR 1,2,3,4 50 20 Element QD04	Piezoelectric region made of PZT-5H Quadrilateral region of 50 (in direction x) by 20 (in direction y) 4-noded square elements
SUPPORT onplane 475e-4,10e-4 525e-4,10e-4 475e-4,30e-4 525e-4,30e-4	Set $\phi = 0$ at the interface between the PZT strip and the plate and at the top surface of the PZT strip, these 2 planes define 2 ground electrodes,

ASSEMBLE Capacitance	Assemble the capacitance matrix for this region
LOAD onplane VOLTAGE 200 475e-4,30e-4 525e-4,30e-4	Apply 200 volts along one of the supported electrode (define as a plane in the xy coordinates) The other electrode remains at potential zero (grounded electrode)
COUPLE 'metal_book' 'piezo_book'	**Couple the two books**
AWAVE	Call the time marching solution routine
Solution Central Difference	Using the Central difference algorithm
Step Time 0 13.0e-6 10.0e-09	Start time marching with 10 nano-sec time step for a total of 13 μs.
Step Cycle 0.9e6 5	Applying a 5-cycles toneburst at 0.9 MHz
Step Node 1 1, -1, V	Load is applied as a voltage toneburst to all nodes along the electrode defined in the Load module
Monitor 9501 x Monitor 9501 y	Monitoring results as displacements, At node 9,501 monitor x displacements At node 9,501 monitor y displacements *Displacements are saved in the database STRIP*
end job	**End the job at time 13 μs**

Appendix B Determination of the Stress Fields

The stress T and the particle velocity v fields in the piezoelectric film are found by expanding the fields as power series in the variable in the coordinate y normal to the upper free surface and keeping only the lower order terms. In calculating the stress in the film, the effect of piezoelectricity within the PZT-5H layer is neglected while the anisotropic nature of the crystal is included in the stress-strain relationship. Since the majority of the power flow in a plate mode is mechanical, neglecting the piezoelectric response of the crystal is not a seriously limiting approximation.

In the following we assume the plate modes to be harmonic, assuming propagation as $e^{i(\omega t-\beta x)}$. The starting equations are the equation of motion and the constitutive relation given in symbolic notations [4.7]:

$$\nabla.T=\rho\frac{\partial v}{\partial t} \tag{B.1}$$

$$\nabla_s v=\frac{\partial S}{\partial t} \tag{B.2}$$

$$S=s:T \tag{B.3}$$

where $[\nabla.]$ is the divergence operator for a second rank tensor and $[\nabla_s]$ is the symmetric gradient operator. In this problem we assume propagation occurs only in the sagittal plane (that is excluding SH waves) and along the direction z, therefore there is no displacement along the direction *y*. Therefore the operator for this problem simplifies to

$$[\nabla.]=\begin{bmatrix} \partial/\partial x & 0 & 0 & 0 & \partial/\partial z & 0 \\ 0 & 0 & 0 & \partial/\partial z & 0 & \partial/\partial x \\ 0 & 0 & \partial/\partial z & 0 & \partial/\partial x & 0 \end{bmatrix}=[\nabla_s]^T \tag{B.4}$$

Here we will treat a fairly general case, limiting the anisotropy of the crystals to only orthorhombic materials. The form of the stiffness and compliance matrices for anisotropic materials depends on the microscopic symmetry properties of the medium. If the medium itself is symmetric with respect to a particular transformation of coordinates, then the compliance and stiffness matrices must themselves be unchanged by the same transformation. Each crystal symmetry group is a *class* and various classes are grouped in *systems*. Orthorhombic systems have nine independent stiffness constants that reflect the fact that such lattices are unchanged only through 180 degrees rotations or mirror operations. The compliance matrix is

$$\begin{bmatrix} s_{11} & s_{12} & s_{13} & 0 & 0 & 0 \\ s_{12} & s_{22} & s_{23} & 0 & 0 & 0 \\ s_{13} & s_{23} & s_{33} & 0 & 0 & 0 \\ 0 & 0 & 0 & s_{44} & 0 & 0 \\ 0 & 0 & 0 & 0 & s_{55} & 0 \\ 0 & 0 & 0 & 0 & 0 & s_{66} \end{bmatrix} \tag{B.5}$$

In Eq.(B.1) to (B.3), T, S and s are used in their matrix representation. Substituting for the operators in Eq.(B.1) and Eq.(B.2) and multiplying out the equations, we obtain

$$-j\beta T_6 + \frac{\partial T_4}{\partial z} = 0 \tag{B.6}$$

$$-j\beta T_5 + \frac{\partial T_3}{\partial z} = -\rho\omega^2 u_3 \tag{B.7}$$

$$-j\beta T_1 + \frac{\partial T_5}{\partial z} = -\rho\omega^2 u_1 \tag{B.8}$$

$$-j\beta u_1 = S_1 \tag{B.9}$$

$$\frac{\partial u_3}{\partial z} = S_3 \tag{B.10}$$

$$-j\beta u_3 + \frac{\partial u_1}{\partial y} = S_5 \tag{B.11}$$

$$S_2 = S_4 = S_6 = 0 \tag{B.12}$$

where u_3 and u_1 are the displacements in the z and the x directions. Concerning the stress tensor, contracted notations have been used. $T_1 = T_{xx}$ and $T_3 = T_{zz}$ are the direct stresses in the directions x and z. $T_4 = T_{yz}$, $T_5 = T_{xz}$ and $T_6 = T_{xy}$ are the shear stresses. Equations (B.9)-(B.12) can be combined with the constitutive relationship Eq.(B.3), yielding the displacement in terms of the nonzero stresses:

$$\frac{\partial u_3}{\partial z} = \frac{s_{13}s_{22} - s_{12}s_{23}}{s_{22}} T_1 + \frac{s_{22}s_{33} - s_{23}s_{23}}{s_{22}} T_3 \tag{B.13}$$

$$-j\beta u_1 = \frac{s_{11}s_{22} - s_{12}s_{12}}{s_{22}} T_1 + \frac{s_{13}s_{22} - s_{23}s_{13}}{s_{22}} T_3 \tag{B.14}$$

$$-j\beta u_3 + \frac{\partial u_1}{\partial z} = s_{55} T_5 \tag{B.15}$$

From $S_2 = S_4 = S_6 = 0$, $T_4 = T_6 = 0$ and T_2 has been expressed in terms of T_1 and T_3:

$$T_2 = \frac{-s_{12}T_1 - s_{23}T_3}{s_{22}} \tag{B.16}$$

Equations (B.7), (B.8) and equations (B.13) to (B.16) form an homogeneous system in six unknowns. We substitute power series approximations for the stresses and particle displacements

$$T_I(z) = \sum_{n=0}^{m} \frac{1}{n!} T_I^{(n)} (y+h)^n$$
$$u_i(z) = \sum_{n=0}^{m} \frac{1}{n!} u_i^{(n)} (y+h)^n \qquad \text{where i = 1 or 3 and I=1,2,3 or 5} \tag{B.17}$$

Then by evaluating successive derivatives of the equation of motion and the constitutive relation at the upper surface *y=-h*, we obtain a set of recursive relations for the power series coefficients. These follow in Eqs.(B.18) to (B.23):

$$-j\beta T_5^{(n-1)} + T_3^{(n)} = -\rho\omega^2 u_3^{(n-1)} \tag{B.18}$$

$$-j\beta T_1^{(n-1)} + T_5^{(n)} = -\rho\omega^2 u_1^{(n-1)} \tag{B.19}$$

$$u_3^{(n)} = \frac{s_{13}s_{22} - s_{12}s_{23}}{s_{22}} T_1^{(n-1)} + \frac{s_{22}s_{33} - s_{23}s_{23}}{s_{22}} T_3^{(n-1)} \tag{B.20}$$

$$-j\beta u_1^{(n)} = \frac{s_{11}s_{22} - s_{12}s_{12}}{s_{22}} T_1^{(n)} + \frac{s_{13}s_{22} - s_{23}s_{13}}{s_{22}} T_3^{(n)} \tag{B.21}$$

$$-j\beta u_3^{(n-1)} + u_1^{(n)} = s_{55} T_5^{(n-1)} \tag{B.22}$$

$$T_2^{(n)} = \frac{-s_{12}T_1^{(n)} - s_{23}T_3^{(n)}}{s_{22}} \tag{B.23}$$

Making use of the boundary conditions at the upper surface, the power series coefficients can be expressed in terms of two unknowns, the particle displacements. Then the coefficients may be inserted into equations (B.18) to (B.23) to give the spatial variation of stress in the layer as a function of the particle displacements. We give here the details for the derivation of the stresses to first order only. The boundary conditions at the free surface of the layer are

$$T_3(-h) = 0 \tag{B.24}$$

$$T_5(-h) = 0 \tag{B.25}$$

and at first order, from Eq.(B.17) the non zero stresses in the layer are

$$T_1 = T_1^{(0)} + T_1^{(1)}(y+h) \qquad \text{for } 0 < z < h \qquad \text{(B.26)}$$

$$T_2 = T_2^{(0)} + T_2^{(1)}(z-h) \qquad \text{for } 0 < z < h \qquad \text{(B.27)}$$

$$T_3 = T_3^{(1)}(y+h) \qquad \text{for } 0 < z < h \qquad \text{(B.28)}$$

$$T_5 = T_5^{(1)}(y+h) \qquad \text{for } 0 < z < h \qquad \text{(B.29)}$$

From Eq.(B.18), the only nonzero coefficient for the normal stress in the layer, at first order, is

$$T_3^{(1)} = -\rho\omega^2 u_3(h) \qquad \text{(B.30)}$$

and then from Eq.(B.28) the normal stress in the layer, to first order is given as

$$T_3 = \left\{-\rho\omega^2(z-h)\right\} u_3(h) \qquad \text{(B.31)}$$

The shear stress coefficient at first order is found from equations (B.19) and (B.21), and from Eq.(B.29) the shear stress in the layer is given by

$$T_5 = \left\{\left(-\rho\omega^2 + \beta^2 \frac{s_{22}}{s_{11}s_{22} - s_{12}s_{12}}\right)(z-h)\right\} u_1(h) \qquad \text{(B.32)}$$

The inplane stress does not vanish at the upper surface so at first order two coefficients must be found. The zero-order coefficient comes from Eq.(B.21) posing n=0 and the first order coefficient comes from equations (B.21), (B.22) and (B.18) posing n=1. From Eq.(B.26) the inplane stress in the layer is given by

$$T_1 = \frac{s_{22}}{s_{11}s_{22} - s_{12}s_{12}} \begin{bmatrix} -u_1(h)\{j\beta\} \\ +u_3(h)\left\{\left(\beta^2 + \rho\omega^2 \frac{s_{13}s_{22} - s_{23}s_{13}}{s_{22}}\right)(z-h)\right\} \end{bmatrix} \qquad \text{(B.33)}$$

and eventually, from Eq.(B.23) the coefficients for the stress normal to the sagittal plane are found yielding

$$T_2 = \frac{-s_{12}}{s_{11}s_{22} - s_{12}^2} \begin{bmatrix} -u_1(h)\{j\beta\} \\ u_3(h)\left\{\left(\beta^2 + \rho\omega^2\left(\frac{-s_{11}s_{23}}{s_{12}} + \frac{s_{13}s_{22} - s_{23}s_{13} + s_{12}s_{23}}{s_{22}}\right)\right)(z-h)\right\} \end{bmatrix} \qquad \text{(B.34)}$$

Hence the stress fields are known to first order at the coordinate (z - h). It is noted that the stresses in the layer can all be predicted by knowledge of the layer material properties, the dispersion relation (β,ω) and the particle velocity amplitudes at the free surface (z = h) of the mode under consideration. These expressions have been developed for orthorhombic crystals. Most of the piezoelectric ceramics available on the market are made of hexagonal crystals which have a higher symmetry order than orthorhombic crystals. PZT-5H ceramics, before poling, are hexagonal systems of class 6mm which means that in addition to a 6-fold Z-axis it is also unchanged through mirror operations. Therefore the compliance matrix shows extra simplifications and only 6 constants are independent

$$\begin{bmatrix} s_{11} & s_{12} & s_{13} & 0 & 0 & 0 \\ s_{12} & s_{11} & s_{13} & 0 & 0 & 0 \\ s_{13} & s_{13} & s_{33} & 0 & 0 & 0 \\ 0 & 0 & 0 & s_{44} & 0 & 0 \\ 0 & 0 & 0 & 0 & s_{44} & 0 \\ 0 & 0 & 0 & 0 & 0 & s_{66} \end{bmatrix} \tag{B.35}$$

and the stresses to first order are

$$T_1 = \frac{s_{11}}{s_{11}^2 - s_{12}^2} \begin{bmatrix} -u_1(h)\{j\beta\} \\ +u_3(h)\left\{\left(\beta^2 + \rho\omega^2 \frac{s_{13}s_{11} - s_{13}^2}{s_{11}}\right)(z-h)\right\} \end{bmatrix} \tag{B.36}$$

$$T_2 = \frac{-s_{12}}{s_{11}^2 - s_{12}^2} \begin{bmatrix} -u_1(h)\{j\beta\} + \\ u_3(h)\left\{\left(\beta^2 + \rho\omega^2 s_{13}\left(\frac{-s_{11}}{s_{12}} + \frac{s_{11} + s_{12} - s_{13}}{s_{11}}\right)\right)(z-h)\right\} \end{bmatrix} \tag{B.37}$$

$$T_3 = \left\{-\rho\omega^2 (z-h)\right\} u_3(h) \tag{B.38}$$

$$T_5 = \left\{\left(-\rho\omega^2 + \beta^2 \frac{s_{11}}{s_{11}^2 - s_{12}^2}\right)(z-h)\right\} u_1(h) \tag{B.39}$$

If one supposes that the layer is made of an isotropic material, the coefficients in the matrix (B.35) simplifiy with $s_{33} = s_{11}$, $s_{13} = s_{12}$ and $s_{44} = s_{66}$ and then from

$$\frac{S_{11}}{S_{11}^2 - S_{12}^2} = \frac{4\mu(\lambda + \mu)}{\lambda + 2\mu} = \mu\left(1 + \frac{3\lambda + 2\mu}{\lambda + 2\mu}\right) \tag{B.40}$$

equations (B.38) and (B.39) become equivalent, but expressed in a different system of coordinates, to those given by Auld (Chapter 12 [4.7]) for the normal and shear stresses.

Appendix C Solution of the Poisson Equation

The electric displacement, for an insulator, obeys the Poisson equation

$$\nabla.\varepsilon^{T}.\nabla\Phi=\nabla.(d:T) \tag{C.1}$$

In the general case the permittivity matrix is fully populated but for most of the piezoelectric materials and in particular for PZT-5H it is a diagonal matrix

$$\varepsilon^{T}=\begin{bmatrix}\varepsilon_{xx}^{T} & 0 & 0\\ 0 & \varepsilon_{yy}^{T} & 0\\ 0 & 0 & \varepsilon_{zz}^{T}\end{bmatrix} \tag{C.2}$$

Therefore the left-hand side of Eq.(C.1), under plane strain conditions in the plane *xz*, develops as

$$\nabla.\varepsilon^{T}.\nabla\Phi=\varepsilon_{11}^{T}\frac{\partial^{2}\Phi}{\partial x^{2}}+\varepsilon_{33}^{T}\frac{\partial^{2}\Phi}{\partial z^{2}} \tag{C.3}$$

Similarly, for PZT-5H, the right-hand side of Eq. (C.1) develops into

$$\nabla.(d:T)=\frac{\partial(d_{x5}T_{5})}{\partial x}+\frac{\partial(d_{y4}T_{4})}{\partial y}+\frac{\partial(d_{z1}T_{1}+d_{z2}T_{2}+d_{z3}T_{3})}{\partial z} \tag{C.4}$$

since the piezoelectric strain matrix is

$$d=\begin{bmatrix}0 & 0 & 0 & 0 & d_{x5} & 0\\ 0 & 0 & 0 & d_{y4} & 0 & 0\\ d_{z1} & d_{z2} & d_{z3} & 0 & 0 & 0\end{bmatrix} \tag{C.5}$$

Hence the Poisson's equation for a PZT-5H layer in the *xz* plane is

$$\frac{\partial^{2}\Phi}{\partial z^{2}}-\beta^{2}\gamma^{2}\Phi=\frac{1}{\varepsilon_{33}^{T}}\left(\frac{\partial}{\partial x}d_{x5}T_{5}+\frac{\partial}{\partial z}d_{zI}T_{I}\right)\qquad 1\le I\le 3 \tag{C.6}$$

where summation over repeated indices is assumed. T_I are the three direct stresses and T_5 is the shear stress within the piezoelectric layer.

A general solution and a particular solution must be found to obtain a unique solution for this problem. Finding the particular solution of the Poisson equation can prove in

certain cases to be extremely difficult but in the present case the charge distribution, i.e. the right-hand side of Eq.(C.6), is known and moreover is of simple analytical form. In the general case where all orders are kept, the stresses are power series expansions and the general equation to solve is

$$\frac{\partial^2 \Phi}{\partial z^2} - \beta^2 \gamma^2 \Phi = \sum_{n=0}^{q} a(I,n) \frac{(z-h)^n}{n!} \tag{C.7}$$

where

$$a(I,n) = \frac{d_I}{\varepsilon_{33}^T} T_I^{(p)} \tag{C.8}$$

with

$$q = m-1, \quad p = n+1, \quad 0 \le n \le m-1 \quad \text{for } 1 \le I \le 3 \tag{C.9}$$

$$q = m, \quad p = n, \quad 0 \le n \le m \quad \text{for } I = 5 \tag{C.10}$$

and thus a particular solution to Eq.(C.6) is given by a power series whose coefficients must be determined

$$\Phi_p = \sum_{n=0}^{q} b(I,n) \frac{(z-h)^n}{n!} \tag{C.11}$$

By substituting Eq.(C.11) into Eq.(C.7) we obtain recursion relationships for each power of (z – h)

$$\frac{\partial \Phi}{\partial z} = \sum_{n=1}^{q} b(I,n) \frac{n(z-h)^{n-1}}{n!} \tag{C.12}$$

$$\frac{\partial^2 \Phi}{\partial z^2} = \sum_{n=2}^{q} b(I,n) \frac{n(n-1)(z-h)^{n-2}}{n!} \tag{C.13}$$

then from $\frac{n(n-1)}{n!} = \frac{1}{(n-2)!}$, Poisson's equation becomes

$$\sum_{n=0}^{q} \left(a(I,n) \frac{(z-h)^n}{n!} \right) = \sum_{n=2}^{q} \left(b(I,n) \frac{(z-h)^{n-2}}{(n-2)!} \right) - \gamma^2 \sum_{n=0}^{q} \left(b(I,n) \frac{(z-h)^n}{n!} \right) \tag{C.14}$$

and performing the index change r = n-2, this equation becomes

$$\sum_{r=0}^{q}\left(a(I,r)\frac{(z-h)^r}{r!}\right)=\sum_{r=0}^{q-2}\left(b(I,r+2)\frac{(z-h)^r}{r!}\right)-\gamma^2\sum_{r=0}^{q}\left(b(I,r)\frac{(z-h)^r}{r!}\right) \quad (C.15)$$

Thus the coefficients of the particular solution are

$$b(I,q)=\frac{-a(I,q)}{\gamma^2} \quad (C.16)$$

$$b(I,q-1)=\frac{-a(I,q-1)}{\gamma^2} \quad (C.17)$$

$$b(I,r)=\frac{-1}{\gamma^2}\left[a(I,r)-a(I,r+2)\right] \quad 0\le r\le q-2 \quad (C.18)$$

At first order, $m=1$, $q=1$ and

$$\begin{cases} b(I,0)=\dfrac{-a(I,0)}{\gamma^2} \\ b(I,1)=\dfrac{-a(I,1)}{\gamma^2} \end{cases} \quad (C.19)$$

and at second order

$$\begin{cases} b(I,0)=\dfrac{-1}{\gamma^2}\left(a(I,0)-b(I,2)\right) \\ b(I,1)=\dfrac{-a(I,1)}{\gamma^2} \\ b(I,2)=\dfrac{-a(I,2)}{\gamma^2} \end{cases} \quad (C.20)$$

with

$$a(I,0)=\frac{d_I}{\varepsilon_{33}^T}T_I^{(0)} \quad 1\le I\le 3 \quad (C.21)$$

$$a(I,1)=\frac{d_I}{\varepsilon_{33}^T}T_I^{(1)}+\frac{d_{x5}}{\varepsilon_{33}^T}T_5^{(0)} \quad 1\le I\le 3 \quad (C.22)$$

$$a(I,2)=\frac{d_I}{\varepsilon_{33}^T}T_I^{(2)}+\frac{d_{x5}}{\varepsilon_{33}^T}T_5^{(1)} \quad 1\le I\le 3 \quad (C.23)$$

Appendix D Electrical Boundary Perturbation

Here we derive a simple electrical perturbation calculation and show that the impedance of the normal modes generated in the bi-layered system by the applied electrical source can be evaluated by a simple measure of $\Delta V/V$. The system we are investigating here consists in a metallic substrate coated with a thin piezoelectric layer. Both the substrate and the layer are infinite in the direction of propagation. Since the metallic substrate is grounded the electrical problem reduces to that in the layer only. The bottom surface of the layer is grounded and let us assume that the electrical perturbation is the imposition of some electrical condition on the upper surface (z = h), and that this perturbation leaves the stress field in the layer unaffected. In this case the perturbation formula as given by Auld [4.7] is

$$\Delta\beta_n = j\frac{\left\{\Phi_n^*\left(j\omega D_n^{'}\right)+\Phi_n^{'}\left(j\omega D_n\right)^*\right\}.z\Big|_{z=h}}{4P_{nn}} \tag{D.1}$$

and relations between the perturbed electrical quantities $D_n^{'}$ and $\Phi_n^{'}$ and the known unperturbed quantities Φ_n and D_n on the plane z = h are needed. In the piezoelectric layer the electrical potential must satisfy Poisson's equation where the free charges are the piezoelectrically induced charges $\nabla.(d:T)$ as shown in Eq.(C.6). This is true for the potential in the unperturbed system and also for the potential in the perturbed system. Therefore because the equation is linear, this is also true for the difference between the perturbed and the unperturbed potential,

$$\Psi = \Phi' - \Phi \tag{D.2}$$

and if we assume that the stress in the layer are not affected by the perturbation, then substracting the Poisson equation for the perturbed system and that for the unperturbed system cancels the stress terms and the potential difference needs to satisfy only Laplace's equation,

$$\nabla.\varepsilon^T\nabla\Psi = 0 \tag{D.3}$$

A general solution to this equation, assuming that all quantities have a propagation term $e^{j\beta x}$ is

$$\Psi = \Psi(z)e^{-j\beta x} = \left(Ae^{-\gamma z} + Be^{\gamma z}\right)e^{-j\beta x} \tag{D.4}$$

where A and B are constants and

$$\gamma=\beta_n\sqrt{\frac{\varepsilon_{xx}^T}{\varepsilon_{zz}^T}} \tag{D.5}$$

when the dielectric tensor is diagonal which is the case of most piezo-ceramics such as PZT. From Eq.(D.2) the relationship between the perturbed and unperturbed quantities can be established as

$$\Phi'=\Psi+\Phi \tag{D.6}$$

$$D'=D-\varepsilon^T.\nabla\Psi \tag{D.7}$$

The problem now is to find the constants A and B that satisfy the perturbed electrical conditions. In both the perturbed and the unperturbed system the potential at the lower boundary of the layer is grounded so the potential is zero and from Eq.(D.4) we have

$$A+B=0 \tag{D.8}$$

and the potential difference is now given by

$$\Psi(z)=A\left(e^{-\gamma z}-e^{\gamma z}\right)=-2A\sinh(\gamma z) \tag{D.9}$$

Therefore the perturbed quantities at the upper boundary are

$$\Phi'(h)=\Phi(h)-2A\sinh(\gamma h) \tag{D.10}$$

$$D_z'(h)=D(h)+2A\beta_n\varepsilon_p^T\cosh(\gamma h) \tag{D.11}$$

where

$$\varepsilon_p^T=\sqrt{\varepsilon_{zz}^T\varepsilon_{xx}^T} \tag{D.12}$$

The constant A as yet not been determined but can be eliminated by expressing the normal displacements is term of the potentials and vice versa. Let us assume that the unperturbed problem has free electrical boundary condition at the upper surface, so that the electrical fields are continuous at that boundary. In the vacuum above the layer, the electrical unperturbed potential satisfies Laplace's equation and must vanish away from the interface,

$$\Phi=\Phi_n(z)e^{-j\beta x}=e^{\beta_n z}e^{-j\beta_n x} \qquad z>h \tag{D.13}$$

and the normal component of the electric displacement is

$$D_z=D_{nz}(z)e^{-j\beta x}=-\beta_n\varepsilon_0 e^{\beta_n z}e^{-j\beta_n x} \qquad z>h \tag{D.14}$$

Following Auld [4.7] we introduce an *electrical surface impedance* that is a convenient way to express the boundary condition

$$Z_E(h) = \left(\frac{\Phi(h)}{j\omega D_z(h)} \right) \tag{D.15}$$

For the unperturbed system, the free electrical boundary condition is then given by

$$Z_E(h) = \left(\frac{-1}{j\omega\beta_n\varepsilon_0} \right) \tag{D.16}$$

Now the electrical surface impedance of the perturbed boundary condition can be normalised to the unperturbed electrical surface impedance giving a relationship between the perturbed and the unperturbed electrical boundary conditions,

$$z_E^{'} = \frac{Z_E^{'}(h)}{\left|Z_E(h)\right|} = -j\beta_n\varepsilon_0 \left(\frac{\Phi^{'}(h)}{D_z^{'}(h)} \right) \tag{D.17}$$

Eliminating A from Eq.(D.11) and Eq.(D.10), and making use of the *electrical surface impedance* gives

$$\Phi^{'}(h) = -jz_E^{'} \left(\frac{\varepsilon_0 + \varepsilon_p^T \coth(\gamma h)}{\varepsilon_0 - jz_E^{'}\varepsilon_p^T \coth(\gamma h)} \right) \Phi(h) \tag{D.18}$$

and from Eq. (D.17)

$$D_z^{'}(h) = -\beta_n\varepsilon_0 \left(\frac{\varepsilon_0 + \varepsilon_p^T \coth(\gamma h)}{\varepsilon_0 - jz_E^{'}\varepsilon_p^T \coth(\gamma h)} \right) D_z(h) \tag{D.19}$$

The perturbed fields are expressed as a function of the unperturbed fields and of the electrical surface impedance. Substitution in the perturbation formula (D.1) gives

$$\frac{\Delta\beta_n}{\beta_n} = -\frac{\Delta V_n}{V_n} = \omega\varepsilon_0 \left(\frac{1 + jz_E^{'}(h)}{\varepsilon_0 - jz_E^{'}(h)\varepsilon_p^T \coth(\gamma h)} \right) \left(\varepsilon_0 + \varepsilon_p^T \coth(\gamma h) \right) \frac{\left|\Phi(h)\right|^2}{4P_{nn}} \tag{D.20}$$

and when the perturbation is due to an electrical short circuit on the boundary the velocity change is given by the short circuit perturbation

$$\left(\frac{\Delta V_n}{V_n} \right)_{SC} = \omega \left(\varepsilon_0 + \varepsilon_p^T \coth(\gamma h) \right) \frac{\left|\Phi(h)\right|^2}{4P_{nn}} \tag{D.21}$$

Equation (D.21) is derived from Eq.(D.20) by posing $z_E^{'} = 0$ which corresponds to a short circuit boundary condition. An open boundary condition would correspond to $z_E^{'} = \infty$. Defining a quantity Z_n with the dimension of an impedance

$$Z_n = \frac{\Phi_n(h)\Phi_n^*(h)}{2P_{nn}} \tag{D.22}$$

it follows that

$$Z_n = -\frac{2}{\omega\left(\varepsilon_0 + \varepsilon_p^T \coth(\gamma h)\right)}\left(\frac{\varepsilon_0 - jz_E^{'}(h)\varepsilon_p^T \coth(\gamma h)}{\varepsilon_0 + j\varepsilon_0 z_E^{'}(h)}\right)\frac{\Delta V_n}{V_n} \tag{D.23}$$

Thus the impedance of the piezoelectric modes is directly proportional to the quantity $\Delta V/V$, the relative change in acoustic phase velocity when an infinitesimally thin metal conductor shortcuts the upper surface of the piezoelectric layer. However it is not proportional to the frequency unlike in the traditional Rayleigh wave case.

Appendix E Interior Perturbation Approach to the S-Parameters

In this section we derive the S-parameters for Lamb waves incident at a groove using the *volume integral approach*. A groove is the "negative" of a strip and these calculations are in all points comparable to those carried out in section 4.7.2.1. The groove shape is a perfect rectangle, of constant depth h.

One viewpoint is to consider the groove as having caused a change in the boundary condition of the plate. Hence the perturbation is replaced by the unperturbed plate with changed boundary conditions, the Datta-Hunsinger boundary conditions, over the region of the groove. Alternatively, a groove can also be considered as an inhomogeneity in the plate waveguide. Consider a local inhomogeneity that has mass density ρ' and stiffness constant c'. In the following section the perturbed field will be denoted by a prime. An inhomogeneity is in the bulk of the material and it leaves the boundary conditions on the two surfaces of the plate waveguide unaffected. Such perturbations are called volume or interior perturbations. The known parameters in such perturbations are the material constants in the inhomogeneous region. A groove can be considered to be an inhomogeneity with ρ' = 0 and c' = 0, but the method remains valid for other values. The compliance and the density of the perturbed region are given by:

$$\begin{aligned} \rho'(z) &= \rho + \Delta\rho(z) \\ s'(z) &= s + \Delta s(z) \end{aligned} \tag{E.1}$$

In the absence of body forces, the perturbed field equations for time-harmonic fields yield the differential amplitude equation. This defines the scattered wave fields, which are driven by distributed "volume source" terms calculated from the zero-order fields. This forced wave equation can be solved by the normal mode method. Invoking ρ' = 0 and c' = 0, from Eq.(E.1), it can be shown that the differential amplitude equation reduces to

$$\left(\frac{\partial}{\partial z} + j\beta_n\right) a_n(x) = \frac{-j\omega h f_g(x)}{4P_{nn}} . \left[\rho v_n^*(0).v'(0) - S_n^*(0) : c : S'(0)\right] \tag{E.2}$$

where S is the strain tensor and : is the tensor product. To solve for the coefficient $a_n(x)$ of the scattered field, one needs to know the total scattered fields v'(0) and S'(0) in the previous equation. If an exact calculation for the perturbed problem is available, the perturbation calculation is unnecessary. Otherwise it is necessary to seek an approximate solution for the perturbed fields. This is always the central problem in employing the perturbation theory. Here we make the assumption that for shallow grooves the power carried by the incident wave is not depleted very much as it propagates through the groove perturbation. Since the coefficient of the incident wave

does not change very much from its initial value, we can also assume that the amplitudes of other modes do not build up to large values. Hence, we assume that v'(0) and T'(0) can be replaced by the known incident wave field v(0) and T(0). This perturbation assumption is reasonable as long as the right-hand side of Eq.(E.2) is small by virtue of a small value of *h*, the perturbation parameter.

Let us label the incident wave "M" by the scattered modes "N", so from Eq.(E.2) the amplitudes a_n and a_{n-} of the forward and backward travelling waves excited by sources in the perturbed region ($0 \le x \le w$) are given by,

$$a_{N+}(x) = e^{-j\beta_n z}\alpha_{N+}\int_0^w f(x)e^{-j(\beta_M - \beta_N)x}dx \tag{E.3}$$

$$a_{N-}(x) = -e^{j\beta_N x}\alpha_{N-}\int_0^w f(x)e^{-j(\beta_R + \beta_N)x}dx \tag{E.4}$$

where

$$\alpha_{N+} = \frac{-j\omega}{4P_{NN}}\left[\rho v_N^*(0).v_M(0) - S_M^*(0):c:S_M(0)\right] \tag{E.5}$$

$$\alpha_{N-} = \frac{j\omega}{4P_{NN}}\left[\rho v_{N-}^*(0).v_M(0) - S_{N-}^*(0):c:S_M(0)\right] \tag{E.6}$$

The simplest application is to calculate the amplitude of the reflected and transmitted part of the incident mode, therefore replacing $a_N(x)$ by $a_M(x)$, we obtain the scattered amplitudes travelling as

$$a_{M+}(x) = e^{-j\beta_M x}\alpha_{M+}w \qquad \text{for } x > w \tag{E.7}$$

$$a_{M-}(x) = -e^{j\beta_M x}\alpha_{M-}w\frac{\sin(\beta_M w)}{\beta_M w} \qquad \text{for } x < 0 \tag{E.8}$$

Therefore the reflection coefficient at x = 0 is

$$S_{11} = \frac{a_{M-}(0)}{a_M(0)} = -\alpha_{M-}\frac{\sin(\beta_M w)}{\beta_M w} \tag{E.9}$$

and the transmission coefficient from x = 0 to x = w is

$$S_{21} = 1 + \frac{a_{M+}(w)}{a_{M+}(0)} = (1 + w\alpha_{M+})e^{-j\beta_M w} \tag{E.10}$$

Appendix F Electric Field Spatial Distribution

Figure 5.8 shows the geometry of the transducer and the coordinate axes. The electrode fingers are sufficiently long so that the problem can be considered in two dimensions and plane strain conditions assumed. The thickness of the metal electrode is supposed to be negligible and we assume that the material is isotropic in the plane of the electrodes, i.e. the xy plane, what corresponds, for example, to a piezoelectric crystal of class 6mm or a piezoceramic whose axis of symmetry is parallel to the axis z, as it is the case for a Z-cut PZT ceramics and uniaxial PVDF sheets poled along the axis z. At the electrodes a sinusoidal voltage is applied:

$$V = v_0 e^{j(\omega t)} \tag{F.1}$$

and the boundary conditions, as shown in Figure 5.8(c), are

$$\Phi\left(x_1,0\right)=0 \tag{F.2}$$

$$\Phi\left(x_1,2h\right)=0 \tag{F.3}$$

$$\Phi(x_1,h) = 0 \quad \text{for} \quad \frac{d}{2}(1-a) < |x_1| < \frac{d}{2} \tag{F.4}$$

$$\Phi(x_1,h) = \frac{v_0}{2} \quad \text{for} \quad 0 < |x_1| < \frac{d}{2}(1-a) \tag{F.5}$$

with

$$\Phi(x_1 + d,h) = -\Phi(x_1,h) \tag{F.6}$$

$$\Phi(x_1 + 2d,h) = \Phi(x_1,h) \tag{F.7}$$

and in the quasistatic approximation the electric fields is the gradient of the electric potential Φ:

$$\Phi(x_i,t) = \Phi(x_i)e^{j(\omega t)} \text{ for } i = 1,2,3 \tag{F.8}$$

The electric displacement D in an insulator must satisfy Poisson's equation

$$\nabla.D = 0 \tag{F.9}$$

and assuming a small electromechanical coupling, the electric displacement is only due to the static electric field

$$D_i = \varepsilon_{ij}^S E_j = -\varepsilon_{ij}^S \frac{\partial \Phi}{\partial x_j} \quad \text{for i = 1,2,3} \tag{F.10}$$

Therefore the electric potential must satisfy Laplace's equation

$$\varepsilon_{ij}^S \frac{\partial^2 \Phi}{\partial x_i \partial x_j} = 0 \quad \text{for i = 1,2,3} \tag{F.11}$$

which in two dimensions in the plane (xz) and for a diagonal permittivity matrix can be simplified as

$$\varepsilon_{11}^S \frac{\partial^2 \Phi}{\partial x_1^2} + \varepsilon_{33}^S \frac{\partial^2 \Phi}{\partial x_3^2} = 0 \tag{F.12}$$

Solutions to Eq.(F.12) are sought in the form of

$$\Phi(x_1, x_3) = f(x_1) g(x_3) \tag{F.13}$$

leading to

$$\frac{f''}{f} = -\frac{\varepsilon_{33}^S}{\varepsilon_{11}^S} \frac{g''}{g} = -\chi^2 \tag{F.14}$$

where χ is a constant, pure real in order to allow the function f to be a periodic function of the variable x_1. This condition is imposed by the succession of electrodes in an infinite array as given by Eq.(F.6) and (F.7). Therefore the functions $f(x_1)$ and $g(x_3)$ are given by

$$\begin{aligned} f(x_1) &= F_1 \cos(\chi x_1) + F_2 \sin(\chi x_1) \\ g(x_3) &= G_1 \exp(-\gamma\chi x_3) + G_2 \exp(\gamma\chi x_3) \end{aligned} \tag{F.15}$$

with

$$\gamma = \sqrt{\frac{\varepsilon_{33}^S}{\varepsilon_{11}^S}} \tag{F.16}$$

The function $f(x_1)$ is anti-symmetric about x = 0 since the potential is alternatively positive and negative, therefore

$$f(0) = 0 \qquad \text{and} \qquad F_1 = 0 \tag{F.17}$$

Hence the potential is given by

$$\Phi(x_1, x_3) = F \sin(\chi x_1 + \delta)\left[G_1 \exp(-\gamma\chi x_3) + G_2 \exp(\gamma\chi x_3)\right] \tag{F.18}$$

where δ is a phase constant which must be determined. The periodic condition Eq.(F.6) on the potential can be also given as:

$$f(x_1 + d) = -f(x_1) \tag{F.19}$$

yielding the condition

$$2F\sin\left(\chi\left(x_1+\delta\right)+\chi\frac{d}{2}\right)\cos\left(\chi\frac{d}{2}\right)=0 \tag{F.20}$$

This condition restricts the allowed values for χ:

$$\chi_m = (2m+1)\frac{\pi}{d} \qquad m = 0, 1, 2,\ldots \tag{F.21}$$

and because the electric potential is the same in every period we can introduce

$$\delta = 0 \tag{F.22}$$

F.1 Modal Expansion to Satisfy the Boundary Conditions

The potential given by:

$$\Phi(x_1, x_3) = F\sin(\chi x_1)\left[G_1\exp(-\gamma\chi x_3)+G_2\exp(\gamma\chi x_3)\right] \tag{F.23}$$

does not satisfy all the boundary conditions and in particular the periodicity of the voltage at the plane z = h. A solution can be provided by an infinite number of solutions having the form as in Eq.(F.23) and satisfying the boundary conditions on the planes x = 0, $x = \pm d$, z = 0, z = 2h..

Eq.(F.21) shows that only the odd multiples of the basic periodicity d occur. Therefore the solution can be search as a Fourier expansion of any anti-symmetric function and, for example, in sine series. The superposition principle makes clear that any linear combination of the solution given by Eq.(F.23) is also a solution, therefore if we let A_m and B_m be arbitrary coefficients, a general solution is given by

$$\Phi(x_1, x_3) = \sum_{m=0}^{\infty}\sin(\chi_m x_1+\delta_m)\left[A_m\exp(-\gamma\chi_m x_3)+B_m\exp(\gamma\chi_m x_3)\right] \tag{F.24}$$

where χ_m has been assigned values such that the function $f(x_1)$ satisfies the conditions of symmetry in the variable x_1, what is similar to assign values such that a sine function is zero at the planes x = 0 and x = d. Now we want to adjust the coefficients A_m and B_m so that the boundary conditions at the plane z = h are satisfied.

The strength of the separation of variables technique is that it results in solutions that are orthogonal. To make use of this orthogonality property we first reformulate Eq.(F.24) in terms of hyperbolic functions:

$$\Phi(x_1, x_3) = \sum_{m=0}^{\infty} \sin(\chi_m x_1)\left[A_m \sinh(\gamma\chi_m x_3) + B_m \cosh(\gamma\chi_m x_3)\right] \quad \text{(F.25)}$$

and since the potential is zero at the plane z = 0, $B_m = 0$, and Eq.(F.25) becomes

$$\Phi(x_1, x_3) = \sum_{m=1}^{\infty} A_m \sin(\chi_m x_1)\sinh(\gamma\chi_m x_3) \quad \text{(F.26)}$$

To evaluate A_m, we first evaluate the potential at the electroded plane, z = h, and we use the orthogonality property of the sine functions. This is done by multiplying both sides of Eq.(F.26) by $\sin(\chi_p x_1)$ where p is an integer. Then we integrate both sides of the expression over the width of the system, yielding

$$\int_0^d \Phi(x_1, h)\sin(\chi_p x_1)dx_1 = \sum_{m=1}^{\infty} A_m \sinh(\gamma\chi_m h)\int_0^d \sin(\chi_m x_1)\sin(\chi_p x_1)dx_1 \quad \text{(F.27)}$$

The sine functions are orthogonal, therefore the integral

$$I = \int_0^d \sin(\chi_m x_1)\sin(\chi_p x_1)dx_1 \quad \text{(F.28)}$$

is zero unless p = m

$$\int_0^d \sin\left(\frac{2p+1}{d}\pi x_1\right)\sin\left(\frac{2m+1}{d}\pi x_1\right)dx_1 = \begin{cases} 0 & m \neq p \\ \frac{d}{2} & m = p \end{cases} \quad \text{(F.29)}$$

Thus all terms in the right hand side of Eq.(F.27) vanish, except for the term p = m. Of course "m" can be any integer and therefore we can solve Eq.(F.27) for the m^{th} coefficient and then replace p by m. the amplitude coefficient A_m is then given by

$$A_m = \frac{2}{d\sinh\left(\gamma\frac{2m+1}{d}\pi h\right)}\int_0^d \Phi(x_1, h)\sin\left(\frac{2m+1}{d}\pi x_1\right)dx_1 \quad \text{(F.30)}$$

The potential in vacuum outside the crystal may be written in a similar way with all the diagonal elements of the dielectric tensor replaced by ε_0. Since the potential must be continuous for x3 = h, the expression coefficients A_m must be the same for both media, as discussed in section 5.2.1.3. These constants are determined by the electric boundary conditions at the free surface. The tangential component of the electric field E_1 must be zero at the conductive electrodes and the normal electric displacement must be continuous between the electrodes. These two boundary conditions can be expressed in term of the electric potential as

$$-\frac{\partial\Phi(x_1,h)}{\partial x_1}=0 \qquad \text{for} \qquad \frac{d}{2}(1-a)<|x_1|<\frac{d}{2} \tag{F.31}$$

$$-\left.\frac{\partial\Phi(x_1,x_3)}{\partial x_3}\right|_{x_3=h}=\frac{v_0}{2} \qquad \text{for} \qquad 0<|x_1|<\frac{d}{2}(1-a) \tag{F.32}$$

These conditions lead to

$$\sum_{m=0}^{\infty}\frac{\pi}{d}(2m+1)A_m\ \sinh\left(\pi\gamma\frac{(2m+1)}{d}h\right)\cos\left(\frac{\pi}{d}(2m+1)x_1\right)=0 \qquad \text{for} \quad \frac{d}{2}(1-a)<|x_1|<\frac{d}{2} \tag{F.33}$$

$$\sum_{m=0}^{\infty}\frac{\pi}{d}(2m+1)\gamma A_m\ \cosh\left(\pi\gamma\frac{2m+1}{d}h\right)\sin\left(\frac{\pi}{d}(2m+1)x_1\right)=0 \qquad \text{for} \ \ 0<|x_1|<\frac{d}{2}(1-a) \tag{F.34}$$

Equations (F.33) and (F.34) are satisfied only if A_m is equal to the Legendre polynomial of first kind P_m [F.1], [F.2]. This part of the calculation is very similar to that carried out for SAW by Engand [5.26]. Following Engan, we can relate the coefficients A_m to the voltage applied at the electrodes, that is

$$v_0=2\Phi\left[x_1=\frac{d}{2}(1-a),h\right]=-\int_0^{\frac{d}{2}(1-a)}E_1(x_3=h)dx_1 \tag{F.35}$$

and we find

$$A_m=\frac{\pi V}{d}\frac{P_m\left(\cos(\pi a)\right)}{K\left(\sin(\pi a/2)\right)} \tag{F.36}$$

where the parameter $\sin(\pi a/2)$ as been introduced. This parameter, the modulus of the elliptic function K, is also the complementary modulus of the Legendre polynomial. It introduces the dependency of the coefficients A_m on the ratio "a" of the electrodes width to the half period "d". When the electrode width is equal to the inter-electrode gap (a = 0.5) all harmonics vanish except the first. Experiments on SAW carried out by Dieulesaint [5.9] show this analysis is true for low coupling constant materials such as PVDF but is no longer true for strongly piezoelectric materials such as PZT ceramics.

The derivations carried out by Engan [5.26] provide another quantity: the transducer capacitance. This may be found by calculating the total charge per unit length on the electrodes. This charge is separated into two charges on either sides of the electrodes. The charge on the crystal side is

$$Q = -2\int_{\frac{d}{2}(1-a)}^{\frac{d}{2}} D_3\left(x_3 = h^-\right)dx_1 \tag{F.37}$$

where the minus sign as a superscript of h indicates the electric displacement is calculated in the crystal. This yields

$$Q = \varepsilon_p \coth(\gamma h)\frac{K\left(\sin\frac{\pi a}{2}\right)}{K'\left(\sin\frac{\pi a}{2}\right)} \tag{F.38}$$

and including the charge on the vacuum side the total capacitance per unit width is given by

$$C = \left(\varepsilon_0 + \varepsilon_p^T \coth(\gamma h)\right)\frac{K\left(\sin\frac{\pi a}{2}\right)}{K'\left(\sin\frac{\pi a}{2}\right)} \tag{F.39}$$

[F.1] Engan, H., ELAB Report TE-91, Electronics Res. Lab., Norvegian Institute of Technology, Trondheim, Norway, 1967.

[F.2] Erdelyi, *Higher transcendental Functions*, Vol. 1, New York, McGraw-Hill, p.166., 1953.